

# **The Molecular Basis of Modern Marker Chemistry**

## **Part 1**

**By**

**Christopher J. von Ruhland M.Phil.**

**Submitted to the School of Chemistry, Cardiff University for the  
Degree of Doctor of Philosophy**

**October 2011**

## DECLARATION

This work has not been submitted in substance for any other degree or award at this or any other university or place of learning, nor is being submitted concurrently in candidature for any degree or other award.

Signed ..... (candidate)      Date .....

This thesis is being submitted in partial fulfillment of the requirements for the degree of PhD

Signed ..... (candidate)      Date .....

This thesis is the result of my own independent work/investigation, except where otherwise stated.

Other sources are acknowledged by explicit references. The views expressed are my own.

Signed ..... (candidate)      Date .....

I hereby give consent for my thesis, if accepted, to be available for photocopying and for inter-library loan, and for the title and summary to be made available to outside organisations.

Signed ..... (candidate)      Date .....

## **Acknowledgements**

Firstly, I would like extend my posthumous thanks to the late Dr. Geoff Newman who sadly died in February 2006. It was he who encouraged me to undertake a PhD and his incisiveness, breadth and depth of knowledge and expertise, sense of humour, and seemingly endless supply of anecdotes are sorely missed.

Secondly, I would like to thank my supervisors, Professor Pete Edwards and Dr. Ian Fallis, for proposing that I conduct my studies through the School of Chemistry and for their constant encouragement, advice and support throughout.

Within the School of Chemistry, I also wish to thank Dr. Ian Morgan for guiding me through the practical aspects of synthetic organic chemistry, Dr. Rob Jenkins for performing mass spectrometry and explaining the dark art that is MALDI-TOF, Dr. Angelo Amoroso and Dr. Simon Pope for their support and guidance when presented with sometimes odd 6-monthly reports, to everyone in the inorganic chemistry laboratory for creating such a welcoming and friendly atmosphere, and to the technical staff who keep everything going.

In the School of Medicine, I would like to thank Professor Bharat Jasani for his advice regarding the more esoteric aspects of marker amplification and Dr. Jan Hobot for his unswerving support during my studies. Were it not for these two fine gentlemen, Medical Microscopy Sciences would probably no longer exist, and much of the work presented here would have been impossible.

At the University Hospital of Wales, I would like to thanks Mrs. Susan Wozniak for providing immunohistochemically stained diagnostic control slides.

From JEOL UK Ltd, I would like to thank Dr. Larry Stoter for arranging access to a tomographic TEM and Dr. Andy Yarwood for his skill in the alignment of the tomographic tilt series. I would also like to thank Dr. Steve Holden of RAPRA for performing gel permeation chromatography and providing advice on the preparation of some challenging polymer samples.

I also wish to thank Dr. Steve Archibald of the Department of Chemistry, University of Hull and Dr. Simon Pope of the School of Chemistry, Cardiff University for agreeing to act as external and internal examiners respectively, for their identification of typographical errors and for their constructive criticisms of this thesis.

Finally, I would like to thank my two children, Zac and Eve, for their patience and understanding during my (seemingly endless) time spent in front of the computer.



<b>Table of Contents</b>	<b>Page</b>
<b>List of Abbreviations</b>	xii
<b>Abstract</b>	xvii
<b>Part 1</b>	
<b>Chapter 1</b>	
<b>Introduction</b>	
1 Introduction	2
1.1 An Apology from Biology	2
1.2 A Brief History of Microscopy	3
1.2.1 Early Lenses	3
1.2.2 Development of the Light Microscope	4
1.2.3 Development of the Electron Microscope	12
1.2.4 Interaction of Electrons with Matter	15
1.3 Biological Sample Preparation	17
1.3.1 Fixation	18
1.3.1.1 Chemical Fixation	19
1.3.1.2 Physical Fixation	21
1.3.2 Dehydration and Infiltration	23
1.3.3 Embedding Media	23
1.3.4 SEM Sample Preparation	25
1.3.5 Sectioning	26
1.4 Staining	26
1.4.1 Staining, Cytochemistry and Histochemistry	28
1.4.1.1 General Staining	29
1.4.1.2 Cytochemistry	29
1.4.1.3 Histochemistry	31
1.4.1.4 Immuno-techniques	36
1.4.1.4.1 Immunocytochemistry (ICC)	36
1.4.1.4.2 Immunohistochemistry (IHC)	37
1.4.2 Fluorescence <i>in situ</i> Hybridisation	45

1.4.3	Biochemical Techniques	47
1.4.4	Molecular Biology	47
1.4.5	Amplification Systems	47
1.4.5.1	Primary Probe Amplification	48
1.4.5.2	Target Retrieval	48
1.4.5.3	Reporter Amplification	48
1.4.5.4	Marker Amplification	51
1.4.6	Advantages and Disadvantages of Existing Markers	53
1.4.6.1	Fluorochromes	53
1.4.6.2	Metal Particles	53
1.4.6.3	Products of Enzyme Catalysed Reactions	53
1.4.7	Properties of an Ideal Marker	54
1.5	Summary	55
1.6	Structure and Aims of Thesis	56
1.7	References	58

## **Chapter 2**

### **Amplification of PolyDAB with Physical Developers**

2.1	Introduction	81
2.1.1	Intensification of PolyDAB with d-Block Metal Salts	82
2.1.2	Amplification of PolyDAB with Physical Developers	83
2.1.3	Amplification in Diagnostic Immunohistochemistry	84
2.1.3.1	Epstein-Barr Virus and LMP-1	85
2.1.3.2	T-cells and Granzyme B	86
2.1.3.3	Neurodegenerative Diseases and $\alpha$ -Synuclein	86
2.1.4	Amplification of Alkaline Phosphatase Markers	87
2.1.5	Model Systems	87
2.1.5.1	Dot Blot Model System	87
2.1.5.2	The Tonsil Tissue Model System	88
2.2	Materials	90
2.2.1	Reagents	90
2.2.2	Antibodies	91
2.2.3	Physical Developers	91

2.2.3.1	Gallyas' Physical Developer	92
2.2.3.2	Newman and Jasani's Physical Developer	92
2.2.4	Model Systems	93
2.2.5	Preparation of Vectabond-treated Slides	94
2.2.6	Selection of d-Block Metal Salts and Buffer Systems	94
2.3	Methods	94
2.3.1	Stability of d-Block Metal Salts in Solutions of DAB	94
2.3.2	Preparation of PVDF Membrane	95
2.3.3	Dot Blot Model System	95
2.3.3.1	Pre-polymerisation and Physical Developers	95
2.3.3.2	Post-polymerisation and Physical Developers	96
2.3.3.3	Sodium Sulfide Treatment and Physical Developers	96
2.3.3.4	Scoring System	96
2.3.3.5	Analytical Scanning Electron Microscopy	97
2.3.4	Tissue Model Systems	97
2.3.4.1	Tissue Preparation	97
2.3.4.2	Selection of Appropriate Antibody Dilutions	98
2.3.4.3	Immunocolloidal Gold	98
2.3.4.4	Counterstaining and Mounting	99
2.3.4.5	Immunohistochemical Evaluation of PolyDAB Amplification	99
2.3.4.6	Marker Amplification and Diagnostic Immunohistochemistry	100
2.3.5	Microscopic Examination and Digital Imaging	101
2.3.6	Alkaline Phosphatase Marker Amplification	101
2.4	Results	102
2.4.1	Stability of d-Block Metal Salts in Solutions of DAB	102
2.4.2	Dot Blot Model System	102
2.4.2.1	Pre-polymerisation and Amplification	102
2.4.2.1.1	Physical Developers Alone	102
2.4.2.1.2	Effects of Sulfide Treatment on Amplification	106
2.4.2.1.3	Nickel Concentration and Physical Developers	109

2.4.2.1.4 Nickel Concentration and Physical Developers – Effects of Sulfide Treatment	109
2.4.2.2 Post-polymerisation and Amplification	111
2.4.2.2.1 Physical Developers Alone	111
2.4.2.2.2 Effects of Sulfide Treatment on Amplification	113
2.4.2.3 Analytical Scanning Electron Microscopy	116
2.4.3 Tissue Model System	117
2.4.3.1 Selection of Appropriate Antibody Dilutions	117
2.4.3.2 Pre-polymerisation and Gallyas' Developers	122
2.4.3.3 Pre-polymerisation plus Sulfide and Physical Developers	122
2.4.3.4 Post-polymerisation and Gallyas' Developer	122
2.4.3.5 Post-polymerisation plus Sulfide and Physical Developers	123
2.4.4 Diagnostic Immunohistochemistry	130
2.4.5 Alkaline Phosphatase Marker Amplification	135
2.5 Discussion	136
2.6 Summary and Conclusions	147
2.7 References	149

## **Chapter 3**

### **Marker Amplification at the Limits of Sensitivity**

3.1 Introduction	163
3.2 Materials	165
3.2.1 Reagents	165
3.2.2 Physical Developers	165
3.2.2.1 Danscher's Developer	166
3.2.2.2 Hacker's Developer	166
3.3 Methods	167
3.3.1 Determination of the Limits of Sensitivity of the Colloidal Gold/Silver Method	167
3.3.2 Inhibition of Endogenous Enzymatic Activity	167
3.3.3 Determination of Sensitivity Limit for Peroxidase/DAB Au/Na <sub>2</sub> S/Silver	168

3.3.4	Reduction of Non-specific Complexing of Amplifying Reagents with Tissue	168
3.3.5	Suppression of Tissue Argyrophilia	169
3.3.6	Comparison of Physical Developers	169
3.3.7	Comparison of Secondary Antibody Conjugates	169
3.4	Results	171
3.4.1	Determination of the Limit of Sensitivity for the Colloidal Gold/Silver Method	171
3.4.2	Inhibition of Endogenous Enzymatic Activity	180
3.4.3	Determination of the Limit of Sensitivity for Peroxidase/DAB Au/Na <sub>2</sub> S/Silver	184
3.4.4	Reduction of Non-specific Complexing of Amplifying Reagents with Tissue	192
3.4.5	Suppression of Tissue Argyrophilia	201
3.4.6	Comparison of Physical Developers	204
3.4.7	Comparison of Secondary Antibody Conjugates	209
3.5	Discussion	215
3.6	Summary and Conclusions	218
3.7	References	219

## **Part 2**

### **Chapter 4**

#### **Electron Microscopic Immunohistochemistry and Analytical Electron Microscopical Tomography**

4.1	Introduction	225
4.1.1	Electron Tomography	227
4.1.2	Immunohistochemical Markers and Electron Opacity	228
4.1.3	Analytical Instrumentation	229
4.1.4	Analytical Electron Microscopical Tomography	230
4.1.5	Elemental Mapping	231
4.1.6	Choice of Section Substrate	232
4.1.7	Tissue Model Systems	235
4.2	Materials	236

4.2.1	Reagents	236
4.2.2	Model Systems	236
4.2.3	Antibodies	236
4.3	Methods	237
4.3.1	Choice of Section Substrate	237
4.3.2	Tissue Model Systems	237
4.3.2.1	Preparation of Paraffin Wax-embedded Sections for Preliminary Immunoelectron Microscopy	237
4.3.2.2	Preparation of Acrylic Resin-embedded Sections for Immunoelectron Microscopy	237
4.3.2.2.1	Resin Embedding	237
4.3.2.2.2	Microtomy and Ultramicrotomy	238
4.3.2.3	Immunohistochemical Staining	239
4.3.3	Scanning Electron Microscopy	240
4.3.4	Analytical Transmission Electron Microscopy	240
4.3.5	Electron Tomography	240
4.4	Results	241
4.4.1	Choice of Section Substrate	241
4.4.2	Scanning Electron Microscopy	241
4.4.2.1	Preliminary Studies in Paraffin Wax-embedded Sections	241
4.4.2.2	Resin Sections	244
4.4.3	Transmission Electron Microscopy	249
4.4.4	Analytical Transmission Electron Microscopy	257
4.4.5	Electron Tomography	260
4.5	Discussion	262
4.6	Summary and Conclusions	265
4.7	References	266

## **Chapter 5**

### **Halogenated Aromatic Diamine Polymers as Potential Markers for Analytical Electron Microscopical Tomography**

5.1	Introduction	273
5.1.1	Commercially Available Halogenated Aromatic Diamines	274

5.1.2	Synthesis of Halogenated Phenylene Diamines	274
5.1.3	Synthesis of Halogenated DAB	274
5.1.4	Selection of Suitable Substrates for Preliminary Dot Blot and Immunohistochemical Staining	276
5.2	Materials	277
5.2.1	Reagents	277
5.2.2	Tissue	277
5.3	Methods	278
5.3.1	Organic Synthesis	278
5.3.1.1	Characterisation of Intermediates and Final Products of Syntheses	278
5.3.1.2	Synthesis of Halogenated Phenylene 1,2-Diamines	278
5.3.1.2.1	1,2-Diamino-4-bromobenzene (4-Br-OPD)	278
5.3.1.2.2	1,2-Diamino-4-iodobenzene (4-I-OPD)	280
5.3.1.2.3	1,2-Diamino-4,5-dibromobenzene (4,5-diBr-OPD)	280
5.3.1.2.4	1,2-Diamino-4,5-diiodobenzene (4,5-diI-OPD)	282
5.3.1.3	Synthesis of Halogenated bis-Phenylene 1,2-Diamines	283
5.3.1.3.1	4,4'-(1,1,1,3,3,3-Hexafluoropropane-2,2-diyl) dibenzene-1,2-diamine (F6)	283
5.3.1.3.2	4,4'-Methanediyl dibenzene-1,2-diamine	285
5.3.1.3.3	6,6'-Dibromobiphenyl-3,3',4,4'-tetramine	286
5.3.1.3.3.1	Bromination of 4,4'-Dinitrobiphenyl	286
5.3.1.3.3.2	Nitration of 2,2'-Dibromobiphenyl	286
5.3.1.3.4	6,6'-Diiodobiphenyl-3,3',4,4'-tetramine	287
5.3.1.3.4.1	1-Methyl-2-iodo-4-nitrobenzene	287
5.3.1.3.4.2	1,3-Diiodo-2-methyl-4-nitrobenzene	287
5.3.1.3.4.3	1-Methy-2-iodo-4,5-dinitrobenzene	288
5.3.1.3.5	2,2'-Diiodo-4,4'-dinitrobiphenyl	288
5.3.2	Dot-blot Model System	288
5.3.3	Tissue Model System	289
5.3.3.1	Light Microscopy	289
5.3.3.2	Electron Microscopy	290
5.3.3.3	Analytical Electron Microscopy	290

5.4	Results	292
5.4.1	Dot Blot Model System	292
5.4.1.1	Choice of Dot Blot Substrate for Analytical SEM	292
5.4.1.2	Polymerisation of Halogenated Compounds on Dot Blots	292
5.4.1.3	Analytical Scanning Electron Microscopy	295
5.4.2	Tissue Model System	298
5.4.2.1	Light Microscopy	298
5.4.2.2	Analytical Scanning Electron Microscopy	308
5.4.2.3	Transmission Electron Microscopy	325
5.4.2.4	Analytical Transmission Electron Microscopy	333
5.5	Discussion	336
5.6	Summary and Conclusions	338
5.7	References	339

## **Chapter 6**

### **Electron Microscopical Visualisation of Fluorochromes**

6.1	Introduction	344
6.1.1	Model Systems	347
6.2	Materials	349
6.3	Methods	349
6.3.1	Model System	349
6.3.1.1	Homogeneous Model System	349
6.3.1.2	Tissue Model System	350
6.4	Results	351
6.4.1	Homogeneous Model System	351
6.4.1.1	DAB	351
6.4.1.1.1	Fluorescein	351
6.4.1.1.2	Tetramethylrhodamine	351
6.4.1.2	Newman and Jasani's Physical Developer	358
6.4.1.2.1	Fluorescein	358
6.4.1.2.2	Tetramethylrhodamine	358
6.4.1.3	Control Solutions	367
6.4.2	Tissue Model System	367



6.4.2.1	DAB	367
6.4.2.1.1	Fluorescein	367
6.4.2.1.2	Tetramethylrhodamine	367
6.4.2.2	Newman and Jasani's Physical Developer	372
6.4.2.2.1	Fluorescein	372
6.4.2.2.2	Tetramethylrhodamine	372
6.5	Discussion	376
6.6	Summary and Conclusions	379
6.7	References	380

## **Chapter 7**

### **Polymer Characterisation**

7.1	Introduction	386
7.2	Materials	386
7.3	Methods	387
7.3.1	Preparation of PolyDAB	387
7.3.1.1	Determination of Optimum Conditions for DAB Polymerisation	387
7.3.1.2	Determination of the Solubility of PolyDAB	387
7.3.1.3	Polymerisation of DAB in DMSO	387
7.3.1.4	Solubility of Wet PolyDAB in Polar Solvents	388
7.3.1.5	Solubility of Freeze-Dried PolyDAB in Polar Solvents	388
7.3.2	Characterisation of PolyDAB	389
7.3.2.1	IR Spectroscopy	389
7.3.2.2	MALDI-TOF	389
7.3.2.3	Gel Permeation Chromatography	390
7.3.2.4	$^1\text{H}$ , $^{13}\text{C}$ and $^{15}\text{N}$ NMR Spectroscopy	390
7.3.3	Synthesis of $^{15}\text{N}$ -labelled Biphenyl-3,3',4,4'-Tetramine (DAB)	390
7.4	Results	392
7.4.1	Preparation of PolyDAB	392
7.4.1.1	Determination of Optimum Conditions for DAB Polymerisation	392
7.4.1.2	Determination of the Solubility of PolyDAB	393

7.4.1.3	Polymerisation of DAB in DMSO	393
7.4.1.4	Solubility of Wet PolyDAB in Polar Solvents	393
7.4.1.5	Solubility of Freeze-dried PolyDAB in Polar Solvents	393
7.4.2	Characterisation of PolyDAB	393
7.4.2.1	Infra Red Spectroscopy	393
7.4.2.2	MALDI-TOF	394
7.4.2.3	Gel Permeation Chromatography	394
7.4.2.4	<sup>1</sup> H and <sup>13</sup> C NMR Spectroscopy	394
7.5	Discussion	395
7.6	Summary and Conclusions	399
7.7	References	400

## Chapter 8

### Additional Applications of Halogenated Aromatic Diamines

8.1	Introduction	402
8.2	Materials	404
8.3	Methods	404
8.3.1	Determination of the Sensitivity of Poly4,5-diCl-OPD	404
8.3.2	Inhibition of Horseradish Peroxidase	404
8.3.3	Fixation of Poly4,5-diCl-OPD	405
8.4	Results	406
8.4.1	Determination of the Sensitivity of Poly4,5-diCl-OPD	406
8.4.2	Inhibition of Horseradish Peroxidase	406
8.4.2.1	Preliminary Studies with DAB	406
8.4.2.1.1	H <sub>2</sub> O <sub>2</sub>	406
8.4.2.1.2	NaN <sub>3</sub>	416
8.4.2.1.3	NaCN	421
8.4.2.2	Studies with 4,5-diCl-OPD	427
8.4.2.2.1	Preliminary Studies of Inhibition with NaCN	427
8.4.2.2.2	Effects of HRP Inhibition with NaCN Following Re-incubation in Staining Solution	430
8.4.2.2.3	Determination of the Concentration of NaCN Required to Inhibit HRP for 60 Minutes	435

8.4.2.2.4 Effects of HRP Inhibition Following Re-incubation in Staining Solution containing 50 mM NaCN	439
8.4.3 Fixation of Poly4,5-diCl-OPD	444
8.5 Discussion	447
8.6 Summary and Conclusions	449
8.7 References	450

## **Chapter 9**

### **General Discussion and Conclusions**

9.1 General Discussion	453
9.2 Summary and Conclusion	460
9.3 References	461

## List of Abbreviations

ABC	avidin-biotin complex
ACTH	adrenocorticotrophic hormone
AEMT	analytical electron microscopical tomography
AP	alkaline phosphatase
BCIP	5-bromo-4-chloro-3-indolyl phosphate
br	broad
4-Br-OPD	1,2-diamino-4-bromobenzene
BSI	back-scattered imaging
CA	cellulose acetate
CARD	catalysed reporter deposition
CDCl <sub>3</sub>	deuterated chloroform
CHCA	$\alpha$ -cyano-4-hydroxycinnamic acid
CLEM	correlative light and electron microscopy
4-Cl-OPD	1,2-diamino-4-chlorobenzene
CPD	critical point drying
CTL	cytotoxic T-lymphocyte
d	doublet
DAB	biphenyl-3,3',4,4'-tetramine
DAB-PO <sub>4</sub>	0.05% w/v DAB in 100 mM sodium phosphate buffer pH 7.4
DAB-Tris	0.05% w/v DAB in 50 mM Tris/HCl buffer pH 7.6
DCM	dichloromethane
dd	doublet of doublets
ddH <sub>2</sub> O	double distilled water
3,5-diBr-OPD	1,2-diamino-3,5-dibromobenzene

4,5-diBr-OPD	1,2-diamino-4,5-dibromobenzene
4-F-OPD	1,2-diamino-4-fluorobenzene
4-F-5-Cl-OPD	1,2-diamino-4-fluoro-5-chlorobenzene
4,5-diCl-OPD	1,2-diamino-4,5-dichlorobenzene
2,5-diCl-PPD	1,4-diamino-2,5-dichlorobenzene
2,6-diCl-PPD	1,4-diamino-2,6-dichlorobenzene
3,4-diF-OPD	1,2-diamino-3,4-difluorobenzene
4,5-diF-OPD	1,2-diamino-4,5-difluorobenzene
4,5-diI-OPD	1,2-diamino-4,5-diiodobenzene
DMAP	4-dimethylaminopyridine
DMF	dimethylformamide
DMSO	dimethylsulfoxide
EBV	Epstein-Barr virus
EDS	energy dispersive spectrometry
EDX	energy dispersive X-ray spectrometry
EDTA	ethylenediamine tetraacetic acid
EELS	electron energy loss spectroscopy
EF	energy filtering
ESEM	environmental scanning electron microscope
F6	4,4'-(1,1,1,3,3,3-hexafluoropropane-2,2-diyl)dibenzene-1,2-diamine
4-F-OPD	1,2-diamino-4-fluorobenzene
GAM IgAP	goat anti-mouse Ig alkaline phosphatase conjugate
GAM IgCG5	goat anti-mouse Ig 5 nm colloidal gold conjugate
GAM IgFITC	goat anti-mouse Ig fluorescein isothiocyanate conjugate

GAM IgPC	goat anti-mouse Ig peroxidase conjugate
GAM IgTRITC	goat anti-mouse Ig tetramethylrhodamine isothiocyanate conjugate
GFP	green fluorescent protein
HABP	hyaluronic acid binding protein
H&E	haematoxylin and eosin
HRP	horseradish peroxidase
ICC	immunocytochemistry
Ig	immunoglobulin
IHC	immunohistochemistry
4-I-OPD	1,2-diamino-4-iodobenzene
kD	kiloDalton
LMP-1	late membrane protein-1
MALDI-TOF	matrix-assisted laser desorption ionisation time of flight
µg	microgram ( $10^{-6}$ g)
µm	micrometre ( $10^{-6}$ m)
µl	microlitre ( $10^{-6}$ l)
m	multiplet
ml	millilitre ( $10^{-3}$ l)
mM	milliMolar ( $10^{-3}$ Molar)
mmol	milliMole ( $10^{-3}$ Mole)
MTT	3-(4,5-dimethylthiazolyl-2)-2,5-diphenyl tetrazolium
NBT	nitro blue tetrazolium
0.3% Na <sub>2</sub> S	0.3% aqueous, neutralised sodium sulfide

NK	natural killer
ng	nanogram ( $10^{-9}$ g)
nm	nanometre ( $10^{-9}$ m)
OPD	1,2-diaminobenzene
PAS	periodic acid/Schiff
PEG	polyethylene glycol
PFA	paraformaldehyde
pm	picometres ( $10^{-12}$ m)
PBS/BSA	10mM phosphate buffer pH 7.4 containing 0.9% (w/v) NaCl and 0.6% (w/v) bovine serum albumin
PO <sub>4</sub>	phosphate
PO <sub>4</sub> buffer	100 mM phosphate buffer pH 7.3
ppm	parts per million
PVDF	polyvinylidene difluoride
RC	reconstituted cellulose
RT	room temperature
s	singlet
SEM	scanning electron microscope
SEMT	scanning electron microscopical tomography
SMA	smooth muscle actin
SPB	Sorenson's phosphate buffer (100 mM Na <sub>2</sub> HPO <sub>4</sub> /KH <sub>2</sub> PO <sub>4</sub> pH 7.4)
STEM	scanning transmission electron microscope
t	triplet

TBS/BSA	20 mM tris pH 7.4 containing 0.9% (w/v) NaCl and 0.6% (w/v) bovine serum albumin
td	triplet of doublets
TEM	transmission electron microscope
TFA	trifluoroacetic acid
THF	tetrahydrofuran
TriFMe-OPD	1,2-diamino-4-trifluoromethylbenzene
Tris	tris(hydroxymethyl)aminomethane
Tris buffer	50 mM Tris HCl buffer pH 7.6
TTEM	tomographic transmission electron microscope
TWB	Tris wash buffer
WDS	wavelength dispersive spectrometry
WDX	wavelength dispersive X-ray spectrometry



## Abstract

This thesis focuses on empirical investigations and refinements of immunohistochemical marker chemistry, to (1) gain insights into the rational design of novel amplifiable markers at the light microscopic level for (ultimately) single molecule detection, and (2) develop element-rich markers for use in analytical electron microscopical tomography (AEMT) to facilitate the 3-dimensional localisation of multiple target molecules at the ultrastructural level.

In Chapter 2, incorporation of d-block metals into polymerised 3,3',4,4'-tetraaminobiphenyl (polyDAB) was investigated; Ni(II), Pt(II), Pt(IV) and Au(III) complexes were shown to be the most effective catalysts of silver reduction from physical developers in membrane and tissue model systems. Treatment of d-block metal-polyDAB complexes with  $\text{Na}_2\text{S}_{(\text{aq})}$  increased both the range of catalytic complexes and catalytic activity. The most effective technique, employing Au(III) in combination with  $\text{Na}_2\text{S}$ , allowed previously invisible immunohistochemical deposits of polyDAB to be clearly seen in diagnostically relevant samples.

Chapter 3 refined this technique by manipulating reagent concentrations whilst suppressing tissue argyrophilia with  $\text{La(III)/H}_2\text{O}_2$ , increasing immunohistochemical sensitivity by an order of magnitude. Marker deposition and thus the degree of amplification were dependent on reagent quality and conjugate coupling method.

In Chapter 4, scanning and transmission electron microscopical examination of d-block metal-polyDAB complexes identified 8 that were demonstrable by back-scattered electron imaging of immunohistochemically stained tissue sections, including those of W(VI), Os(VIII), Pt(II) and Au(III). The majority were

detectable by energy dispersive X-ray analysis (EDX), but d-block metals were present in insufficient quantities for use in AEMT.

In Chapter 5, polymerised halogenated aromatic diamines and bis-diamines as markers for AEMT were investigated. Immunohistochemical polymerisation of these compounds resulted in deposits of varying properties and compositions. Of the 16 compounds studied, morphological criteria identified polymers of 1,2-diamino-4-bromobenzene and 1,2-diamino-4,5-diiodobenzene as suitable candidates; EDX indicated that the latter might be applicable to AEMT.

Chapter 6 investigated silver deposition from a physical developer by photoconversion, a process used to visualise fluorescent markers in the electron microscope. Photo-excitation of immunofluorescently-stained tissue sections in the presence of physical developer resulted in the selective deposition of silver at the immunopositive sites. This novel method, in combination with the traditional photoconversion techniques, has the potential to permit discrimination of multiple live-cell fluorescent markers by AEMT.

In Chapter 7, characterisation of polyDAB revealed the molecular weight to range from 600 to over 100,000; IR spectra were consistent with both indamine- or phenazine-like polymer structures. Poor solubility restricted further characterisation.

In Chapter 8, a fibrillary form of poly-1,2-diamino-4,5-dichlorobenzene demonstrated a dramatic improvement over polyDAB for immunohistochemistry, and indicated that novel markers based on living polymer technology would be of considerable benefit in biological/biomedical research and clinical diagnosis.

# **Chapter 1**

## **Introduction**

## **1 Introduction**

The identification and analysis of specific molecules in a variety of settings is an essential aspect of biological research and clinical diagnosis. One of the principle approaches for detecting biological molecules is the use of ‘reporter/marker’ systems; reporters detect them and markers visualise them.

Analytical techniques that employ such systems can be broadly divided into two categories; those that localise molecules of interest within whole organisms, slices of tissue (sections), or cultured cells, and those that analyse extracts thereof. The former includes light and electron microscopy, X-ray imaging, magnetic resonance imaging and positron emission tomography. The latter includes analytical biochemistry, molecular biology and the various ‘-omic’ sciences such as genomics, proteomics, glycomics etc.

### **1.1 An Apology from Biology**

Biological specimens, be they whole organisms, slices of tissue, or cultured cells, are extremely complex and delicate and thus present special challenges to the analytical scientist. From the physicist’s point of view, their properties are far from ideal; biological tissue is optically heterogeneous and cells, when in the living state, must be viewed in aqueous solution, thus limiting the resolution that can be obtained with the high quality lenses that optical physicists have spent so long perfecting. In addition, they are poor conductors of heat and electricity which puts constraints on certain aspects of tissue processing and the resolution that can be obtained in the electron microscope. The chemist, in turn, is faced with different problems; analytical techniques are frequently restricted by the requirement for aqueous solutions of (preferably) neutral pH and mild conditions. In addition, the

complexity of biological systems necessitates a large amount of empiricism once an analytical technique has been developed. To compound these problems, living cells react to their environment; the introduction of probably any substance into a living biological system will elicit a response, even though this may go unnoticed. In spite of these restrictions, considerable ingenuity has resulted in the accumulation of an enormous amount of knowledge regarding biological structure and function.

Microscopy represents part of a spectrum of imaging technologies whose resolution covers millimetres (positron emission tomography), tens of micrometres (X-ray and magnetic resonance imaging), micrometres ( $\mu\text{m}$ ) (light microscopy), nanometres (nm) (electron microscopy) and picometres (pm) (atomic force and scanning tunnelling microscopy).

With the development of ever more sophisticated technologies and the integration of existing ones for examining biological systems in their living, as well as their preserved state, considerable opportunities exist for developing novel chemistries to meet the new challenges.

## **1.2 A Brief History of Microscopy**

### **1.2.1 Early Lenses**

The earliest examples of convex lenses are rock crystal artefacts, discovered at Nineveh in Egypt, which have been dated to 2,600BCE (Barker, 1930). The ancient Greeks and Romans also possessed such artefacts but, like those of the Egyptians, it is uncertain whether they were used specifically for magnification, although it is unlikely that this property would have been overlooked.

The earliest known written description of the action of lenses is the 7 volume treatise, *Kitab al-Manazir* (Optics). Written in 1038 by the Arabian scholar Alhazen

Abu Ali al-Hasan Ibn Al-Haitham (figure 1.1), it described, amongst other subjects, the optical action of the eye and the mechanism of refraction. Its translation into Latin in 1270 greatly influenced the likes of Frances Bacon and Johannes Kepler.

### **1.2.2 Development of the Light Microscope**

The microscope can be defined as “a device by which one can make visible details of structure too minute to be seen with the unaided eye” (Hartley, 1993). Its invention, in about 1590, has been generally attributed to the Dutch spectacle makers, Hans and Zaccharias Janssen (figure 1.2). Early microscopes comprised either single, highly curved glass lenses or compound microscopes composed of several lenses. The former were small, portable and powerful whilst the latter afforded a much greater working distance, thus allowing specimens to be manipulated or dissected.

In 1665 Robert Hooke (figure 1.3) published *Micrographia*, a collection of 38 illustrations of specimens he had observed and in which he coined the term ‘cell’ (Hooke, 1665). *Micrographia* prompted the Dutch tradesman, Anthon van Leeuwenhoek (figure 1.4) to make his own simple, but powerful microscopes and thus to discover, for example, bacteria, free-living and parasitic microscopic protists, sperm cells and blood cells.

There followed an explosion of interest in the microscopical world that these instruments revealed, and over the following 200 years considerable improvements were made in microscope optics and design, such as the achromatic (1824), aplanatic (1827) and apochromatic (1879) lenses, and the water (1855) and homogeneous (1878) immersion lenses. Microscope design underwent similar developments, such as fine focus adjustment (1673), the concave illuminating



Figure 1.1. Alhazen Abu Ali al-Hasan  
Ibn Al-Haitham.



Figure 1.2. Zaccharias Janssen.  
Zaccharias Janssen



Figure 1.3. Robert Hooke.



Figure 1.4. Anthon van  
Leeuwenhoek.

mirror (1727), the substage condenser (1831) and the binocular eyepiece (1860) (Hartley, 1993).

In 1834, George Airy, the director of the Cambridge Observatory, published his observations on the diffraction of light from a point source (stars) (Airy, 1834) (figure 1.5). He observed that light did not produce a single point image, but a series of concentric rings, the Airy disc (figures 1.6).

In 1873, Ernst Abbe (figure 1.7) published the formal mathematical basis for optical microscopy and showed the diameter of the central peak of the Airy disc to be:

$$\frac{1.22\lambda}{n \sin \alpha}$$

where  $\lambda$  is the wavelength of light,  $\alpha$  is the half angle of acceptance of the lens and  $n$  is the refractive index of the medium between the object and the lens. Most importantly, he recognised that the limit to resolution was imposed, not by the design of lenses, but by the wavelength of light (Abbe, 1873).

When two point sources are brought closer and closer together such that their Airy discs overlap, there comes a point when they are so close that it may not be possible to state whether they are indeed separate objects i.e. that they can be resolved.

Lord Rayleigh established the arbitrary criterion that the point where the first minimum of one Airy disc coincided with the central maximum of the other should represent the resolving power of a lens system (Strutt, 1879) (figure 1.8). This distance,  $d$ , is thus:

$$d = \frac{0.61\lambda}{n \sin \alpha}$$





Figure 1.5. George Airy.



Figure 1.6. The Airy disc.



Figure 1.7. Ernst Abbe.

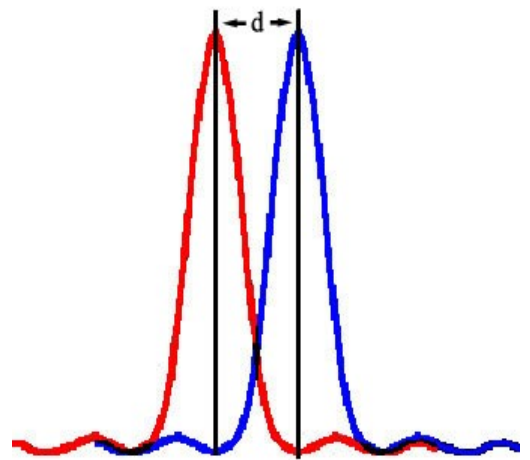


Figure 1.8. The Rayleigh Criterion.

Since visible light has a wavelength between 390 nm and 750 nm, using the shortest wavelength and the highest numerical aperture ( $n \sin\alpha$ ) lens, a theoretical resolution of 170 nm is possible. In practice, this is rarely, if ever, achieved.

With the resolution limit of the light microscope firmly established, attention was more fruitfully directed towards the production of image contrast and the optimisation of specimen preparation.

The invention of the phase contrast microscope, by Frits Zernike (figure 1.9) in 1935, permitted the high resolution examination of living, unstained biological tissue (which has little inherent contrast) by displaying phase differences in the light transmitted through the specimen as differences in amplitude (Zernike, 1935). Optical restrictions of the condenser and objective lenses, halo-like artefacts and specimen thickness limited resolution, but these problems were overcome by the development of differential interference contrast that exploited differences in the specimen's thickness and refractive index to produce differences in amplitude and colour (Normanski and Weill, 1954) (figure 1.10).

A lens's depth of field (the depth of sample that is in focus at any given time) is inversely proportional to  $(n \sin\alpha)^2$ , which places constraints on high resolution light microscopy; typically 0.2  $\mu\text{m}$  for a x100 oil-immersion objective lens. Thus, for a conventional 4  $\mu\text{m}$  thick section viewed under these conditions, 95% of the specimen is out of focus. This out of focus light contributes to the final image and compromises the spatial resolution that can be achieved.

Two techniques exist that overcome this problem, namely (1) thin sectioning and (2) confocal microscopy.

Cutting sections thinner than 0.5  $\mu\text{m}$  normally requires samples to be embedded in a hard resin, which restricts sample size for various practical reasons.



Figure 1.9. Fritz Zernike.



Figure 1.10. Georges Normanski.

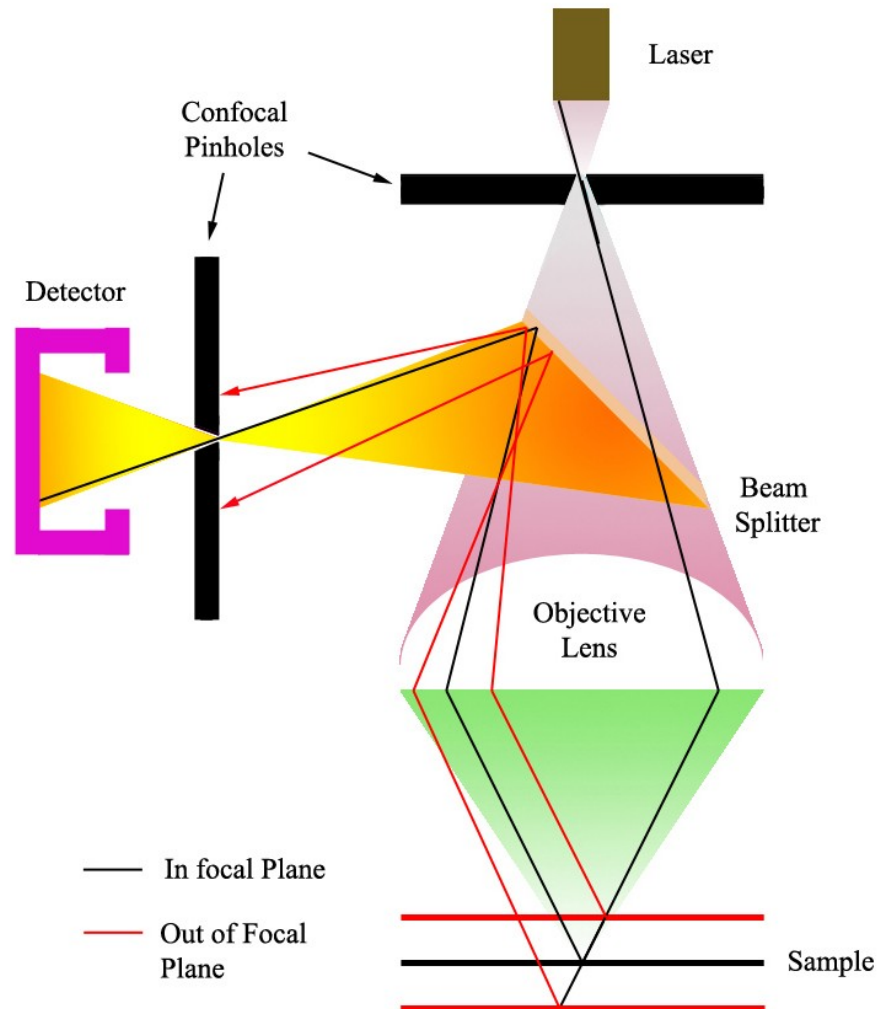


Figure 1.11. The principle of confocal microscopy.

In confocal microscopy, out of focus light is excluded with confocal pinholes (figure 1.11). The restricted view that this technique engenders is overcome by scanning the specimen with a point source of illumination. Scanning was originally achieved by moving either the specimen (Minsky, 1957) or the light source with a perforated spinning disc (Nipkow, 1884) in the tandem scanning microscope (Petran et al., 1968). Since most light is excluded with this technique, extremely bright sources are required such as mercury arc lamps as in later designs of the spinning disc system (Petran et al., 1985) or lasers in the confocal laser scanning microscope which uses mirrors to control beam movement (Brakenhoff 1979). These optical techniques have an absolute requirement for light derived from the specimen itself, and cannot exploit transmitted light, which puts constraints on their application. In the confocal's original manifestation, reflected light from the specimen itself formed the image, but modern biological confocal microscopy frequently collects light from fluorescent markers.

The most significant aspect of confocal microscopy is the facility for 3-dimensional reconstruction (figure 1.12) which is achieved by combining x-y scanning with controlled vertical movement of either the microscope stage or the objective lens (z-axis). It is this, in combination with rapid scanning technologies, which has been of particular importance for the study of dynamic events in living cells. Additional optical techniques are frequently incorporated into live cell studies, such as the determination of intramolecular conformational alterations or changes in intermolecular distance by Förster resonance energy transfer (Förster, 1948) or the measurement of diffusion rates within membranes using fluorescence recovery after photobleaching (Axelrod et al., 1976). More recently, fluorescent markers within cells have been localised at sub-diffraction resolutions using a variety of

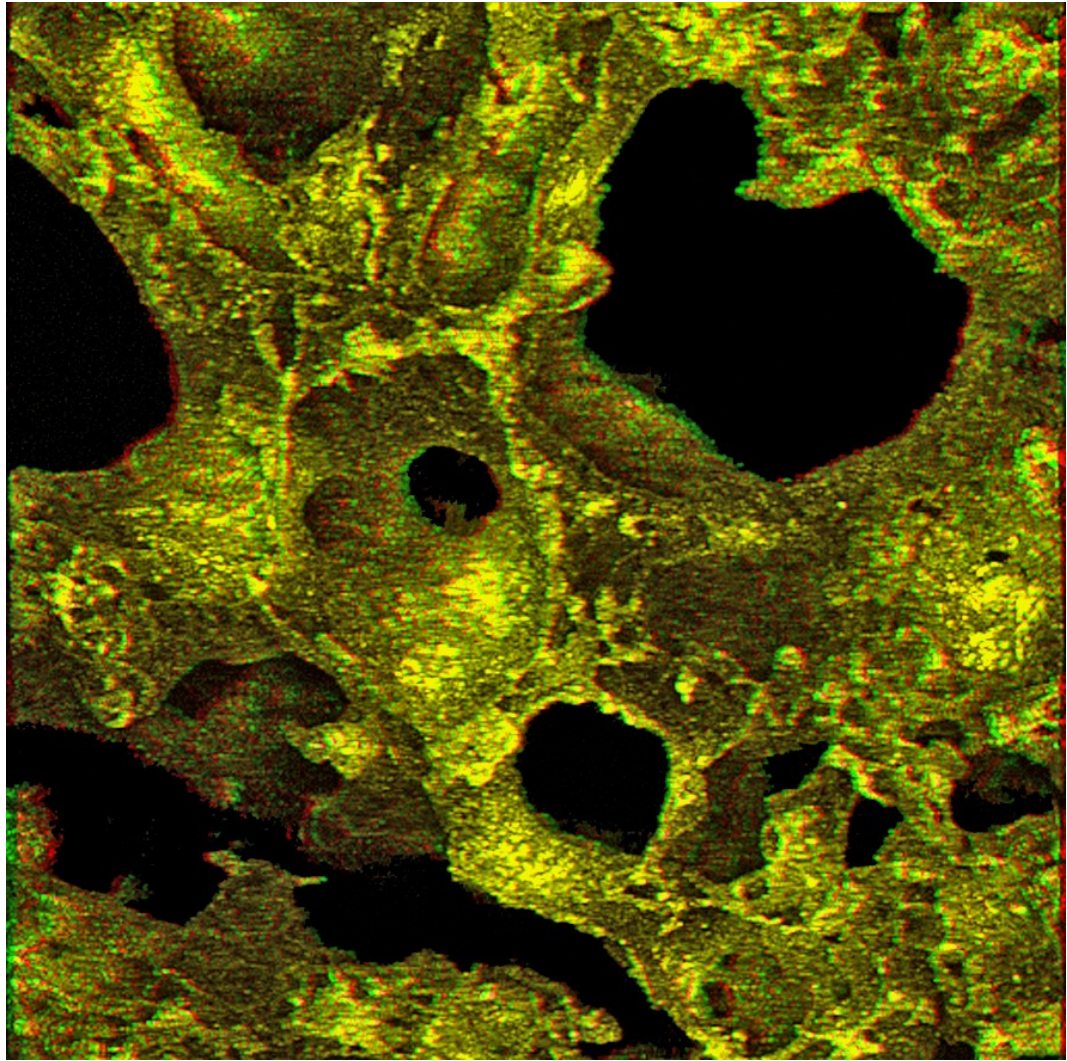


Figure 1.12. Red/green anaglyph reconstructed from a confocal image z-stack, collected in reflection mode, of a 90  $\mu\text{m}$  thick section of rat lung immunohistochemically stained for caveolin-1 and visualised with colloidal gold/silver. Requires red/green glasses.

techniques such as stimulated emission depletion microscopy (Donnert et al., 2006; Willig et al., 2006; Westphal et al., 2008), structured illumination microscopy (Gustafsson, 2000; 2005; Carlton et al., 2010), photoactivated localization microscopy (Betzig et al., 2006) and stochastic optical reconstruction microscopy (Rust et al., 2006). In none of these techniques, however, is it possible to directly visualise cellular structure at the same resolution.

Modern light microscopy, while allowing spectacular results to be achieved, is ultimately limited, in the broader sense, by the resolution limit imposed by visible light.

### 1.2.3 Development of the Electron Microscope

The theoretical description of the quantum nature of light by Max Planck in 1900, together with Niels Bohr's model of the atom in 1922, led Louis de Broglie (figure 1.13) to theorise that electrons also had wave-like characteristics (de Broglie, 1923), and that the wavelength was considerably less than that of light (de Broglie, 1925). If electrons, instead of light, could be used to form images, the resolution would be limited by the energy of the electron which is given by the equation:

$$\lambda = \frac{h}{mv}$$

where  $h$  is Planck's constant,  $m$  is the mass of the electron, and  $v$  is the electron's velocity. The accelerating voltage ( $V$ ) of the electron microscope, which determines the electron's momentum ( $mv$ ), is related to the wavelength of the electron according to the equation:

$$\lambda = \frac{h}{(2mV)^{1/2}}$$



Using this reasoning, Ernst Ruska (figure 1.14) and Max Knoll (figure 1.15) elaborated the first electron lens in 1931 and suggested the potential resolution of the electron microscope (Knoll and Ruska, 1932) which they subsequently constructed in 1933 (figure 1.16). The first practical transmission electron microscope (TEM), with a theoretical resolving power of 10 nm, was constructed at the University of Toronto by James Hillier and Albert F. Prebus in 1938, the same year as the first commercial machine was built by Siemens. Modern TEMs can easily achieve sub-nanometre resolution and the most advanced instruments have achieved a spatial resolution of 40 pm (Alem et al., 2011).

Since only the central area of the magnetic lens of the TEM is used, the instrument has a very small numerical aperture, typically 0.01 (compared to 1.4 for a x100 objective of a light microscope), resulting in a large depth of field; up to 1 mm at 80 kV. Aberration-corrected microscopes and scanning transmission electron microscopes (STEM) have much higher numerical apertures, and thus the depth of field is greatly reduced, often to a few nanometres. In the conventional TEM, the large depth of field is exploited in electron tomography, where relatively thick sections (500 nm or more) are rotated orthogonally to the beam axis to produce a series of images, and the 3-dimensional structure of the sample is reconstructed by back-projection (Crowther et al., 1970). In high resolution instruments, the small depth of field is exploited in an analogous way to confocal microscopy with the exception that out-of-focus information is removed from the through-focus series of digital images by various algorithms (Borisevich et al., 2006; Hovden et al., 2011).

The concept of the scanning electron microscope (SEM) was first proposed in 1935 (Knoll, 1935) and the first use of such an instrument for examining the surface of a solid object occurred in 1942 (Zworykin et al., 1942).



Figure 1.13. Louis de Broglie.

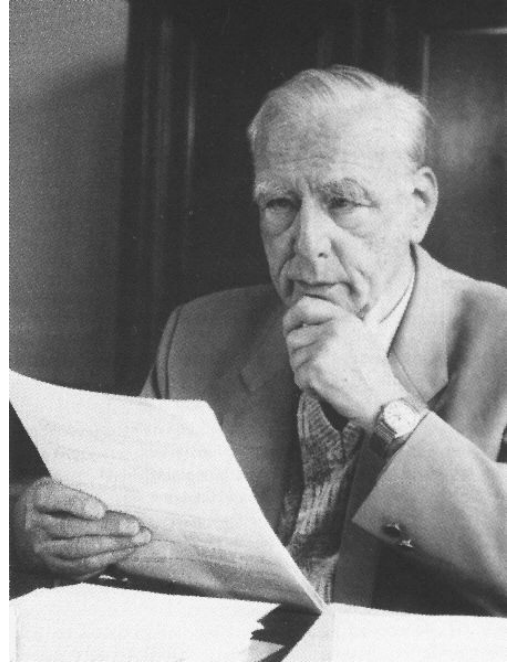


Figure 1.14. Ernst Ruska.



Figure 1.15. Max Knoll.

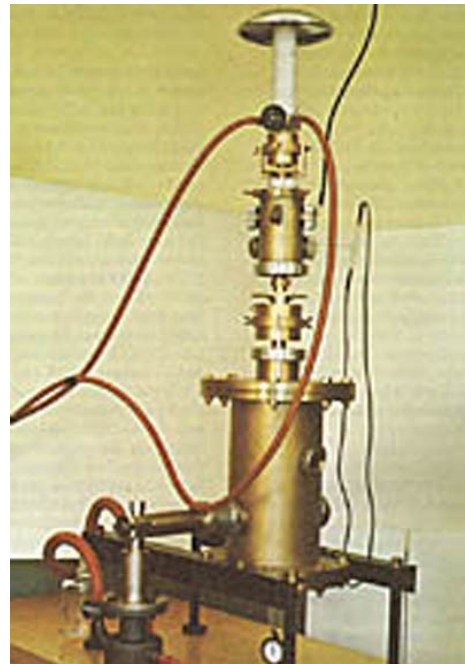


Figure 1.16. Knoll and Ruska's electron microscope.



The most remarkable aspect of the SEM was its ability to show three-dimensional structure (McMullan, 1953). Unlike the TEM, no image is formed anywhere within the SEM. Instead, the instrument employs lenses to de-magnify the electron beam to a finely focussed point which is scanned across the specimen. Electrons derived from the sample are detected, and the signal synchronised with a display screen. Spatial resolution is determined by both the diameter of the focussed beam, which is dependent upon the electron source, and the interaction volume from which signal-generating electrons are derived, the size of which is proportional to the energy of the electron beam and also to the composition of the material under observation (Goldstein et al., 2003).

Recently, scanning microscopes that use helium ions, rather than electrons, have been developed. The advantages of this technology are the small probe size, small interaction volume and brightness of the source (Ward et al., 2006; Postek and Vladoar, 2008). The instrument has been used primarily in the examination of materials (Rodenburg et al., 2010).

#### **1.2.4 Interaction of Electrons with Matter**

The interaction of high energy electrons with matter results in the production of a variety of signals that can give considerable information regarding the specimen's structure and composition. Electrons from the beam can undergo elastic scattering to provide specimen contrast in the TEM and also impart information regarding both the structure (electron diffraction) and atomic number contrast (back scattering). Inelastically scattered electrons that travel through the specimen in the TEM can provide information regarding both elemental composition and chemical

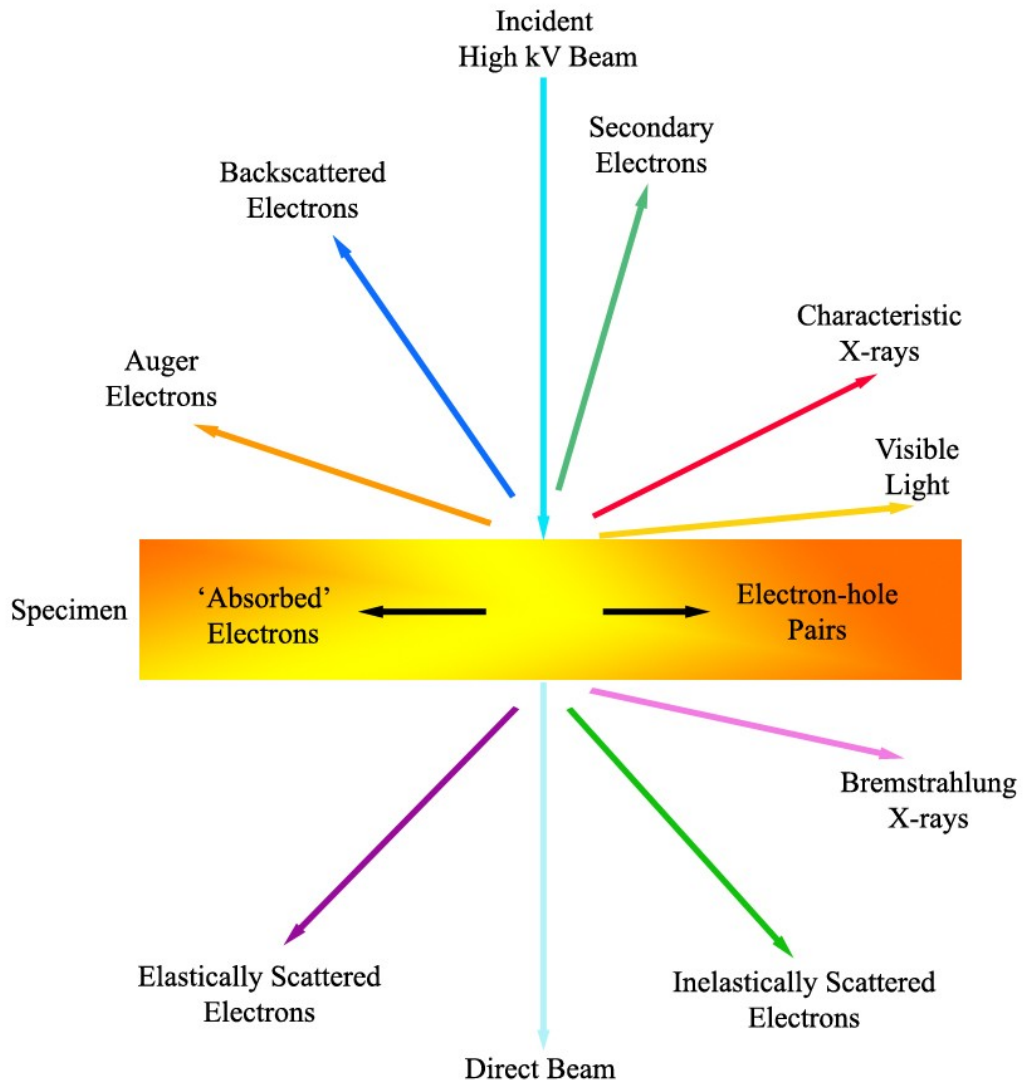


Figure 1.17. Interaction of high energy electrons with a thin specimen.

bonding (figure 1.17) (Williams and Carter, 1996; Goldstein et al., 2003). In addition, Bremsstrahlung X-rays (from the deceleration of electrons entering the sample) and characteristic X-rays (due to electron shell transitions following ejection of core electrons) are produced, the latter providing information regarding elemental composition. By scanning the beam across the specimen and analysing either characteristic X-rays or the energy loss of inelastically scattered electrons (Mekler et al., 1964), elemental maps can be produced. In the SEM, beam electrons impart some of their energy to eject low energy electrons (secondary electrons) from the conductance layer to provide information regarding surface topology.

### **1.3 Biological Sample Preparation**

Judged by the quality of the preparations used as basis for many investigations, the importance of technical process is not fully appreciated. The value of the results obtained from any microscopical study is directly dependent upon the quality of the techniques employed in preparing the material (McClung, 1929).

Living cells can be observed from smears on glass-slides or from tissue culture in Petri dishes, but resolution is poor. It is much improved if the tissue has the same refractive index ( $n$ ) as that of the glass lens with which it is viewed. In order to achieve this, the tissue or cells are placed on glass slides and mounted under thin slivers of glass (coverslips) in a clear substance (mountant) with the same refractive index as glass. The highest resolution is achieved when the air gap between the coverslip and the microscope lens is excluded with a drop of fluid (immersion oil) again having the same refractive index as glass.

One of the earliest mountants was the resinous plant extract, Canada Balsam. Its use required cells and tissue to be dehydrated and 'cleared' (clearing is the increase in refractive index that results from many commonly employed solvents that are miscible with both dehydrating solvents and mountants and which results in the tissue becoming more transparent). Live cells reacted very badly to such treatment, becoming shrunken and severely distorted. It became clear that tissue, cells and their contents required preservation by 'fixation', a method designed to stop all cellular processes immediately before they can react to subsequent treatments. In theory, fixation may be defined as the instantaneous, perfect preservation of tissue structure and chemistry. Further, the perfectly preserved cell structure should be prevented from changing whilst the tissue is processed for microscopic examination. In practice, this ideal is rarely achieved, and, in some cases, undesirable.

Even when mounted correctly, whole cells and tissues still lack clarity because of the limited depth of focus of glass lenses, and thin sections are often required to study the interior cellular structure. Before sectioning can be achieved the tissue must be embedded in a suitable matrix to provide mechanical support; the harder the matrix, the thinner the sections that can be prepared.

### **1.3.1 Fixation**

Fixation of tissue is a vast and complicated subject. Innumerable techniques have been devised, many of which have their own specialised applications and devotees. By 1958 it was estimated that over 200 chemical fixatives containing formaldehyde existed (Baker, 1958). Two broad approaches to fixation have predominated. Chemical fixation precipitates or cross-links native constituents into

insoluble derivatives whilst physical fixation, usually very rapid freezing, immobilises cell constituents without causing chemical change.

#### **1.3.1.1 Chemical Fixation**

Common precipitating fixatives include organic solvents such as acetone, chloroform, methanol and ethanol that rapidly precipitate protein and some other cellular constituents. Organic solvents may damage cells by contortion of structures and extraction of substances. Lipids are especially at risk of extraction, in particular from cell membranes that are rich in saturated and unsaturated lipid.

Cross-linking fixatives include the low molecular weight aldehydes, such as formaldehyde and glutaraldehyde, which cross-link proteins without precipitating them, and certain heavy metal compounds. Formaldehyde in neutral buffered aqueous solution (usually 4% w/v) is the most commonly used fixative for light microscopy. Its fixative properties were first noted in 1893 during assessment of its potential as a bactericide (Blum, 1893). Formaldehyde penetrates rapidly into tissue and cross-links mainly proteins. Much of the understanding of formaldehyde fixation is based on model systems (Fraenkel-Conrat et al., 1947; Fraenkel-Conrat and Olcott, 1948a; 1948b), and there remains considerable uncertainty as to its exact mechanism of action in tissue. Fixation must continue for at least 22 hours before permanent methylene bridges are formed (Fox et al., 1985) and the great histologist, Lillie, insisted that 48 hours was the minimum requirement for adequate fixation (Lillie, 1965).

There is, unfortunately, considerable confusion in the literature regarding the preparation of formaldehyde solutions. Traditionally, such solutions were prepared by simple dilution of formalin (water saturated with formaldehyde gas) in neutral

buffer, 100 mM phosphate being the most common. Alternatively, paraformaldehyde (PFA) was dissolved in water by reflux and the diluted solution stored over marble chips (to remove formic acid), often for many months, to ensure depolymerisation (Dr. Geoff Newman, Medical Microscopy Sciences, Cardiff University, personal communication). More recently, the use of freshly prepared dilute solutions of PFA has become commonplace, based on the belief that depolymerisation is immediate and complete. Indeed, simple solution has been used as a judge of this (Helander, 2000). This practice appears to have arisen from the preparation of formalin from trioxane (Richardson, 1961), its subsequent misnaming as PFA (Robertson et al., 1963; Glauert, 1975), and the unsupported assertion that solution of PFA leads to immediate depolymerisation (Glauert, 1975). Studies regarding the depolymerisation of PFA in aqueous solution are few, but suggest that the concentration of formaldehyde (as methylene glycol) in freshly prepared solutions is quite low (Hallbeck, 1957) and that equilibration times following dilution of concentrated solutions can be many hours (Le Botlan et al., 1983).

In 1963 glutaraldehyde was identified as the best primary fixative for electron microscopy (Sabatini et al., 1963). In contrast to formaldehyde, glutaraldehyde penetrates tissue slowly (approximately 0.5 mm in 3 hours at room temperature) but irreversibly cross-links almost instantaneously. Further studies introduced mixtures of aldehydes, the most popular being formaldehyde and glutaraldehyde (Karnovsky, 1965).

Another popular chemical fixative is osmium tetroxide, which is used almost exclusively for electron microscopy. Its value as a fixative was noted in 1927 (Strangeways and Canti, 1927) and it was used as the sole fixative in early electron

microscopic studies (Palade, 1952). Osmium tetroxide, like glutaraldehyde, penetrates tissue slowly. Now it is usually employed as a secondary fixative following aldehyde fixation. Its main value has been to improve the preservation of unsaturated lipids (Riemersma, 1968) and to increase tissue contrast in the electron microscope.

Uranyl acetate is a less frequently employed, though no less useful, fixative than osmium tetroxide. It is used either as a secondary fixative after primary aldehyde fixation (Ryter et al., 1958) or as a tertiary fixative/pre-embedding stain after aldehyde and osmium (Farquhar and Palade, 1965) and probably acts by stabilising the phospholipids of cell membranes (Silva et al., 1968).

Chemical fixation, while allowing a broad range of staining techniques to be employed, has a number of undesirable side effects, such as tissue shrinkage (Sabatini et al., 1963; Eisenberg and Mobley, 1975), the lowering or loss of biological activity (Sabatini et al., 1963; Ericsson and Biberfel, 1967) and/or antigenic reactivity (Hancock et al., 1982) and the rearrangement of cellular structure (Hobot et al., 1985) following loss of membrane permeability (Woldringh, 1973).

### **1.3.1.2 Physical Fixation**

Even when good vitreous samples are available, however, there remains a major difficulty in locating and unequivocally identifying specific areas of interest for study in the cryo-EM. The inherently low contrast of frozen-hydrated samples, combined with their beam sensitivity, makes it difficult to find regions of interest without destroying them; this severely limits the benefit of an otherwise powerful technique for answering biological questions (Schwartz, 2007).

Rapid freezing techniques are not strictly acts of fixation but rather physical immobilisation. Freezing generates its own artefacts which usually revolve around the formation of ice crystals, resulting in loss of structure and cellular content. For light microscopy, such artefacts are tolerable if histology is urgently required e.g. diagnosis during surgery or if tissue reactivity is paramount such as the demonstration of enzyme activity. In these circumstances, freezing is achieved by plunging the specimen into isopentane cooled with dry ice.

For high resolution light microscopy, or electron microscopy, more elaborate techniques are required, namely the formation of vitreous ice i.e. ice which has no discernable crystalline structure in the electron microscope. Specimens must be very small, typically  $0.1 - 0.2 \text{ mm}^3$  due to the poor thermal conductivity of biological material. Freezing can be achieved by slamming the specimen onto a liquid nitrogen pre-cooled polished copper block or plunging it into liquid nitrogen pre-cooled liquid propane. Vitreous ice, and thus good ultrastructural preservation, is achieved to a depth of approximately  $6 \text{ }\mu\text{m}$ . Proprietary high pressure freezing systems are also available which claim to produce vitreous ice to a depth of  $200 \text{ }\mu\text{m}$ , but  $30 \text{ }\mu\text{m}$  is probably more realistic (Dr. Jan Hobot, Medical Microscopy Sciences, Cardiff University, personal communication) and such systems are very expensive.

The water content of the tissue now acts as the embedding matrix, allowing sections to be cut in the micrometre range, for light microscopy, or in the nanometre range for transmission electron microscopy. Frozen sections still require chemical fixation to prevent loss of structure or substance when the section is thawed for subsequent staining. Frozen, hydrated sections may be observed directly in the transmission electron microscope if a suitable freeze-stage is available to keep them frozen in the heat of the electron beam, but contrast is very poor and the



thickness of the specimen is restricted, usually to a maximum of about 0.5  $\mu\text{m}$ , limiting their use in electron tomography.

### **1.3.2 Dehydration and Infiltration**

The majority of embedding media are insoluble in water and dehydration is usually required. This is achieved by passing the specimen through a gradient of organic solvents, usually ethanol or acetone (typically 30%, 50%, 70%, 90% and finally 100%), the intention being to gently remove the water and avoid osmotic shock (distortion and contraction of cells that occurs if tissue is plunged into high concentrations of organic solvents).

The dehydrating solvent is often replaced with a suitable intermediate solvent which is miscible with both the dehydrating solvent and the embedding medium. An alternative to full dehydration is partial dehydration to 70% organic solvent which markedly increases the tissue's sensitivity to reporters (Newman et al., 1982; 1983a) and can be employed with certain hydrophilic embedding media.

Once suitably dehydrated, the sample is infiltrated with several changes of the embedding medium to ensure complete removal of the dehydrating agent.

### **1.3.3 Embedding Media**

Paraffin wax, which was introduced in the late 19<sup>th</sup> century by Edwin Klebs, remains the most popular tissue embedding medium for light microscopy. The intermediate solvent is usually xylene. Other embedding media have been used including celloidin (Peterfi 1921), gelatine (Oakley, 1937) agar (Friedland, 1951) and ester waxes (Steedman, 1960).

For TEM, much thinner sections are required (typically 70 nm) and harder

embedding substances are essential. The early embedding resins were based on methacrylate (Newman et al., 1949), but these were unstable in the electron beam and prone to uneven polymerisation and shrinkage. By the time that these problems had been addressed (Kushida, 1961a; 1961b), the beam stable epoxy resins (Craig et al., 1962; Glauert, 1965; Spurr, 1969) had become firmly established and remain the most popular embedding media today. The epoxy resins are hydrophobic and almost impervious to aqueous stains unless these are strongly alkaline. Sections can be 'etched' for immunohistochemistry (Bendayan and Zollinger, 1983), but the procedures are deleterious to tissue reactivity and staining is often poor with high, non-specific background staining. In many cases, specific staining techniques are applied pre-embedding, which can limit the specimen's usefulness for other applications.

The problems associated with epoxy resins have been largely circumvented by the introduction of acrylic resins such as the lowicryls (Kellenberger et al., 1980) and the LR resins (Newman et al., 1983a). These resins are beam stable and, most importantly, hydrophilic. This latter property not only allows partial dehydration of tissue but also post-embedding staining with almost any technique without the need to etch. The lowicryls have the added advantage of permitting low temperature (below  $-35^{\circ}\text{C}$ ) embedding techniques for cryoimmobilised or very lightly fixed tissue (Newman and Hobot, 2001). In addition, their composition is published and thus their properties can be manipulated to meet specific requirements (Carlemalm et al., 1982; Acetarin et al., 1986).

#### 1.3.4 SEM Sample Preparation

Preparation for scanning electron microscopy rarely requires embedding, since biological SEM is primarily concerned with surface features. The specimen is fully dehydrated as above and an additional step of critical point drying (CPD) is introduced (Anderson, 1951). CPD replaces the dehydrating solvent with liquid carbon dioxide under high pressure. Once exchange is complete, the temperature is raised above the critical point and gaseous carbon dioxide is slowly withdrawn. Hexamethyldisilazane has been proposed as a cheap alternative to CPD (Nation, 1983), since it requires no specialised high pressure equipment, relying solely on solvent evaporation. Since biological tissue has poor thermal and electrical conductivity, the specimen is finally coated in a thin (5-50 nm) layer of metal (e.g. gold, platinum, chromium) to minimise beam damage and accumulation of electrical charge which impairs image quality. It is this layer of metal that provides secondary electrons for imaging. Alternatively, the specimen may be coated in carbon to allow X-ray microanalysis or back-scattered electron imaging to be performed.

The invention of the environmental SEM (Danilatos, 1981), which employed differential pumping to achieve an hydrated atmosphere within the specimen chamber of the instrument, obviated the need to dehydrate and coat samples. Its principle biological application has been the observation of unfixed samples in their hydrated state, such as plant cells (Pope and Scheetz, 1990), carrots (Thiel and Donald, 1998), bacteria (Bergmans et al., 2005) and yeast (Ren et al., 2008). All these organisms, however, possess cell walls that confer protection to the adverse effects of the electron beam. In contrast, considerable damage occurs to animal cells when they are subjected to similar conditions (Kirk et al., 2009).

### **1.3.5 Sectioning**

Tissue sections are cut on a microtome or cryostat, for paraffin embedded or frozen sections respectively, and collected onto glass slides. 4 µm thick sections are usually preferred since this ensures that the internal structures of all but the smallest cells are available for staining and examination. For subsequent staining, wax is removed by simply reversing the dehydration process (rehydration). Epoxy resin sections require etching if anything other than the simplest staining technique is required, but acrylic sections can be stained directly. For electron microscopy, ultramicrotomes (for resin-embedded samples) and cryoultramicrotomes (for frozen samples) are used and the specimen is collected on a thin metal grid which confers mechanical support as well as thermal and electrical conductivity.

## **1.4 Staining**

The method of staining, once having taken root in the animal histologist, grew and grew, till to be an histologist became practically synonymous with being a dyer, with the difference, that the professional dyer knew what he was about, while the histologist, with few exceptions, did not know, nor does he to the present day (Mann, 1902).

This rather caustic remark may perhaps have been true in the latter part of the 19<sup>th</sup> century, but innumerable publications concerning the mechanism of staining since that time attest to the detailed understanding of the vast majority of staining techniques. With the widespread introduction of high throughput, automated staining systems and staining kits, the latter part of Mann's comment may well become true once again, since it is no longer necessary to understand the

mechanism of staining, nor indeed the function of the individual components. All that is required is to mix solution A with solution B.

Most biological tissue has insufficient inherent colour or electron opacity (capacity to scatter beam electrons) to allow it to be conveniently examined in the light or electron microscope respectively. To overcome these limitations, the inherent optical properties of biological tissue have been exploited to great effect, but it is not only more convenient to impart colour/electron opacity to biological tissue but often considerably more useful, since additional information regarding morphology and composition can be elucidated.

Staining at the light microscopic level has been traditionally regarded as a variety of dyeing using natural or synthetic coloured organic reagents. The development of increasingly sophisticated staining techniques has led to a revision of this perception such that it may now be defined as “any means of conferring a colour reaction on tissue elements and their stainable contents, metabolic, functional or pathological” (Conn, 1977). Its application to electron microscopy merely requires the substitution of ‘differential electron opacity’ for ‘colour’.

The first deliberate use of stains for microscopical examination dates back to 1714 when van Leeuwenhoek used saffron to improve the visibility of muscle fibres, but it was not until the 1860’s that staining with, for example, the boxwood extract haematoxylin, and aniline dyes became widespread. Today, a vast number of stains and staining techniques are available for illustrating various tissue components (Conn, 1977; Drury and Wallington, 1980; Culling et al., 1985; Hayat, 1993).

Staining can be performed before embedding (pre-embedding) or after (post-embedding).

#### **1.4.1 Staining, Cytochemistry and Histochemistry**

General staining techniques are those where the underlying mechanism of staining was not known, or at least poorly understood, at the time of their invention. In contrast, cytochemical and histochemical techniques employ a specific chemical reaction to illustrate a particular cellular component or process. The definitions for these two major cellular analytical techniques, cytochemistry and histochemistry, have changed over the preceding century as technologies have advanced, and new disciplines developed. Even today, considerable confusion exists regarding exact definitions, particularly when applied to immunostaining techniques. Cytochemistry originally referred to the biochemical analysis of cells, and included such techniques as morphometry, electrophoresis and quantitative estimation of enzyme activity from tissue extracts (Glick, 1961), but these techniques developed into separate subjects e.g. cytometry and biochemistry. Histochemistry has been defined as “a borderline field between histology, analytical chemistry or biochemistry” (Gomori, 1952) or “the identification, localisation and quantification, in cells and tissues and by chemical or physical tests, of specific substances, reactive groups and enzyme catalysed activities” (Pearse, 1972). A practical distinction might be based on whether whole cells/tissues or sections are being examined, but this becomes imprecise when thick sections (>20 µm thick) containing whole cells are the subject of investigation.

For the purpose of this thesis, cytochemistry and histochemistry will be defined as the performance of chemical reactions on whole cells/tissue and on sections (irrespective of their thickness) respectively.

#### **1.4.1.1 General Staining**

By far the most popular general staining technique, at least in animal tissue, is haematoxylin and eosin (H&E) (figure 1.18). Haematoxylin is one of the earliest histological stains (Waldeyer, 1863) and is used, principally, to illustrate cell nuclei by virtue of its affinity for the basic histone proteins of chromatin. A vast array of formulations have been developed to improve intensity and fastness of colour, and by 1954 over 120 had been catalogued (Gray, 1954). Toluidine blue is frequently employed as a morphological stain for thin (0.35  $\mu\text{m}$ ) sections of resin embedded material for light microscopy (figure 1.19) (Richardson et al., 1960). In cytology, the polychromatic Papanicolaou's stain is widely used to discriminate a variety of cell types in smear preparations, and is of particular value in screening for cervical cancer (Papanicolaou and Traut, 1941).

#### **1.4.1.2 Cytochemistry**

Living cells present special challenges for the microscopist since the plasma membrane represents a significant barrier to the introduction of reporters and markers into the cell's interior. Low molecular weight dyes can often freely penetrate living cells for tracking cell movement (Merrilees et al., 1995) and illustrating the distribution of organelles (Plasek and Sigler, 1996) and ion-sensitive proteins have been internalised using liposomes (Dormer et al., 1977). For the detection of proteins, this problem has been largely overcome by molecular biological techniques. These techniques frequently use viral vectors to introduce genes into the target cell or organism that encode the protein of interest, with an additional amino acid sequence that encodes either a fluorescent protein tag, or acts as a reporter. Expression of this hybrid protein is believed to reflect the behaviour

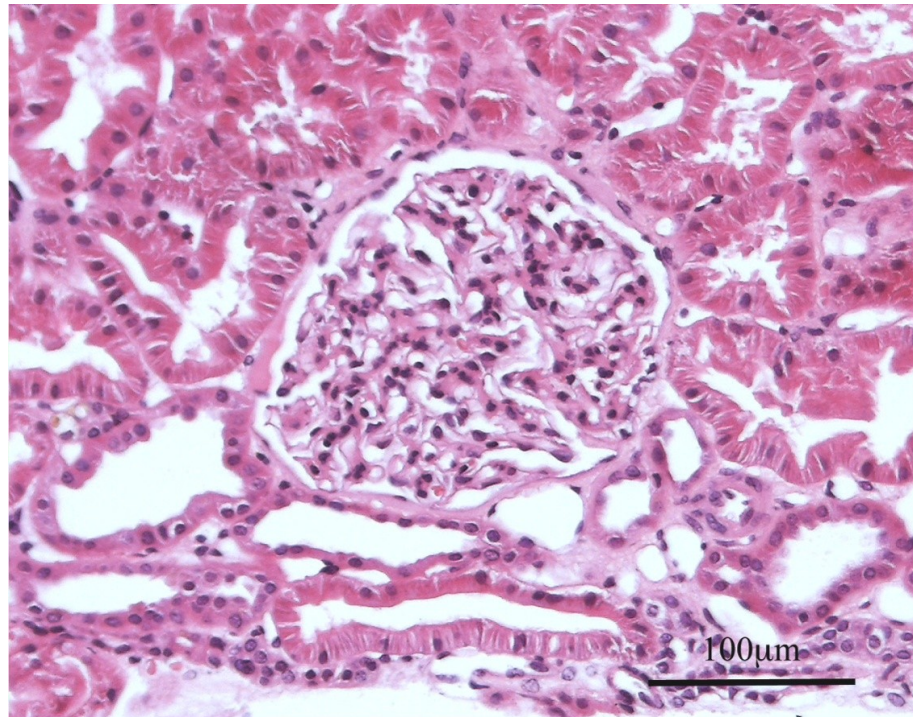


Figure 1.18. 4 μm thick section of paraffin wax-embedded kidney stained with haematoxylin and eosin.

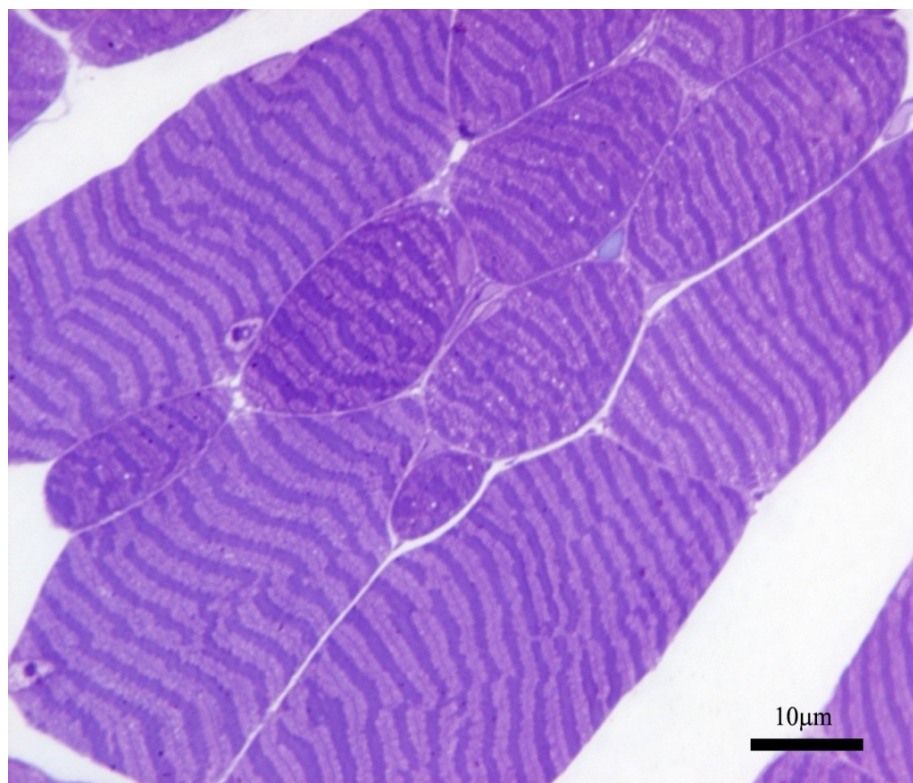


Figure 1.19. 0.35 μm thick section of LR White-embedded abdominal muscle stained with toluidine blue.



and distribution of its native counterpart. Fluorescent proteins include green fluorescent protein (GFP) (Chalfie et al., 1994) and its derivatives. Concern regarding the size of GFP and its potential to interfere with the normal functioning of the protein has led to the development of short peptide tags that act as coordination hosts for fluorogenic ligands e.g. tetracycline and its respective biarsenical ligand (Adams et al., 2002).

At the electron microscopic level, very few cytochemical techniques have been employed, since it is rare that whole cells are examined, principally because of their thickness. In the SEM, the distribution of cellular peroxidase and acid phosphatase has been successfully demonstrated (Soligo et al., 1983). Techniques for visualising fluorochromes in the electron microscope exploit the early observation that they can, upon excitation, induce the polymerisation of biphenyl-3,3',4,4'-tetramine (3,3'-diaminobenzidine, or DAB) which is then rendered electron-opaque by treatment with osmium tetroxide (Maranto, 1982). Such preparations are invariably examined by thin section following either resin embedding or rapid freezing.

#### **1.4.1.3 Histochemistry**

The complexity and specificity of these methods range from the staining of broad classes of compounds with similar physicochemical properties to highly specific and complex techniques that illustrate single molecular species.

Anionic sites, such as the complex acidic polysaccharides of gut secretory cells, can be visualised with cationic dyes such as the copper phthalocyanin, Alcian blue (figure 1.20) (Steedman, 1950). In this case, the reporter and marker are the same.

Tissue carbohydrates can be demonstrated by selective oxidation with periodic acid to yield dialdehydes (reporter) and visualised with Schiff stain (pararosaniline)

(marker) in the periodic acid-Schiff (PAS) stain (figure 1.21) (Hotchkiss, 1948). The electron microscopical equivalent of this technique uses a secondary reporter, thiocarbohydrazide, to form an electron-opaque marker complex with osmium (Seligman et al., 1965) or silver (Theiry, 1967; Neiss, 1988). The latter technique has also been modified for light microscopic examination of thin resin sections (figure 1.22) (von Ruhland and Newman, 2001).

More specific techniques for demonstrating carbohydrates exploit the affinity of a group of (predominantly) plant proteins called lectins for specific complex carbohydrate residues. Ricin, for example, is derived from the seed of the castor oil plant *Ricinus communis* and occurs in two forms, designated RCA<sub>60</sub> and RCA<sub>120</sub>, which bind strongly to N-acetyl-D-galactosamine and terminal  $\beta$ -D-galactosyl residues respectively (Nicholson et al., 1974). Highly specific carbohydrate binding proteins exist that can identify single complex carbohydrates, such as hyaluronic acid binding protein (HABP) (figure 1.23) (Dsouza and Datta, 1985).

The high specificity of other reporter/target interactions have been exploited such as the detection of tissue antibodies by their respective antigens (Coons et al., 1955) and the localisation of enzyme substrates by using the enzyme as the reporter.

These reporters can be visualised by linking them to a variety of markers such as fluorochromes or colloidal gold, or marker generating systems such as enzymes. Enzymes may be visualised directly by their action upon a substrate analogue, which results in the production of a marker. More frequently, however, the product of the enzyme catalysed reaction is linked to a separate marker generating reaction; the demonstration of tissue alkaline phosphatase serves to illustrate this principle.

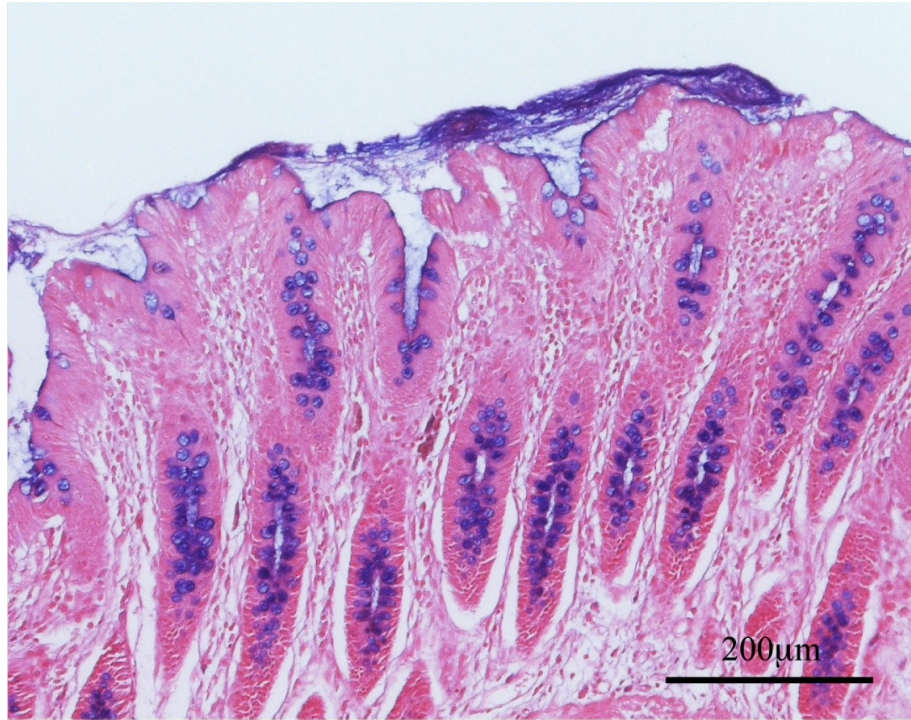


Figure 1.20. 4  $\mu\text{m}$  thick section of paraffin wax-embedded colon. Goblet cells stained with Alcian blue. Eosin counterstain.



Figure 1.21. 4  $\mu\text{m}$  thick section of paraffin wax-embedded peritoneum. Basement membrane of blood vessels stained with PAS. Cell nuclei stained with haematoxylin.



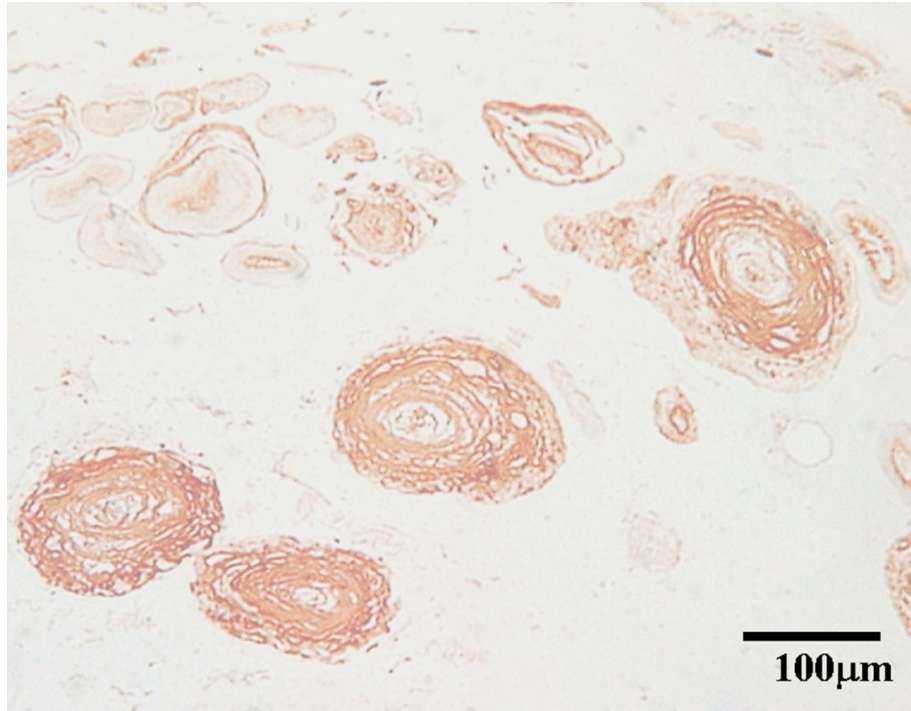


Figure 1.22. 0.35  $\mu\text{m}$  thick section of LR White-embedded peritoneum. Sclerotic blood vessels stained with periodic acid-thiocarbohydrazide-silver proteinate-silver enhancement.



Figure 1.23. 0.35  $\mu\text{m}$  thick section of LR White-embedded fibrotic peritoneum stained for hyaluronic acid with HABP-colloidal gold conjugate and silver amplification. Sirius red counterstain.

Early techniques, using phosphate esters of simple organic compounds such as  $\beta$ -glycerphosphate as the enzyme substrate, employed calcium salts to precipitate the phosphate (reporter) that was released following enzymatic hydrolysis. The precipitate was visualised by substitution with either silver(I) and subsequent photoreduction to metallic silver (marker), or with cobalt(II) followed by conversion to black cobalt sulfide (marker) (Gomori, 1939). Later techniques employed reactions that formed insoluble azo dyes with the organic product, such as  $\beta$ -naphthyl phosphate (substrate) with  $\alpha$ -naphthyl diazonium chloride (Menten et al., 1944) or with  $\alpha$ -naphthyl diazonium naphthalene-1,5-disulphonate (Manheimer and Seligman, 1948), or exploited the chromogenic dimerisation of indolyl (Seligman et al., 1954) or its halogenated derivatives (Horowitz et al., 1966), either alone or coupled to the reduction of tetrazoliums (McGadey, 1970). More recently, the early techniques of phosphate precipitation have been revisited and modified, such as conversion of cobalt phosphate to its ferricyanide followed by intensification with osmium (Hanker, 1979) or precipitation of phosphate with cerium, conversion to the perhydroxide followed by catalytic polymerisation and deposition of DAB for light (Halbhuber et al., 1988) or electron microscopy (Halbhuber et al., 1991). Recently, fluorogenic substrates have become available for increasing signal strength (Huang et al., 1993).

The application of these principles together with considerable ingenuity has allowed a vast range of tissue enzymes to be visualised and localised at both the light and electron microscopic levels (Pearce, 1972; Hanker, 1979).

#### **1.4.1.4 Immuno-techniques**

Immuno-techniques are specialised histochemical methods which exploit the high specificity of antibodies for their respective antigens. These techniques overcome the fact that different proteins, with a few notable exceptions, e.g amyloid and reticulin, react in an identical manner with conventional histochemical staining techniques. Antibodies are proteins, and thus no different. They can be visualised indirectly, however, by attaching a marker to them (labelling or conjugating). The enormous number of antibodies now available makes this approach impractical, since application dictates the choice of marker. It is more efficient and convenient to use indirect methods. The simplest technique uses a labelled secondary antibody (secondary reporter). More complex techniques use bridge systems and polymeric secondary reporters.

##### **1.4.1.4.1 Immunocytochemistry (ICC)**

Antibodies, labelled with R salt (2,3,6- $\beta$ -naphtholdisulphonate) coupled via diazotised benzidine, were first used at the London Hospital, U.K. in 1934, demonstrating that they could be indirectly visualised without adversely compromising their immunoreactivity. Importantly, the significance of diluting the antibody to overcome non-specific staining was also noted (Marrack, 1934). Marrack labelled the surface of his cells, but nowadays, it is often desirable to visualise internal cellular components. Since antibodies are large molecules (150kD), they do not penetrate the cell membrane and it is necessary to permeabilise cells by treating them with organic solvents (Fujiwara and Pollard, 1976) or detergents such as saponin (Ohtsuki et al., 1978), but structural preservation is severely compromised (Wassler et al., 1987).

Given the poor structural preservation that inevitably accompanies techniques that facilitate ICC of whole cells, it is not surprising that no TEM studies appear to have been conducted on these preparations. In contrast, many studies have exploited the SEM where interest is centred primarily on surface phenomena. Given the complex topography of cell surfaces, ease of identification, rather than electron opacity, has determined the choice of markers (Molday and Maher, 1980). The earliest markers were latex spheres (Lo Buglio et al.; 1972, Molday et al., 1974), but these have been superseded by colloidal gold (Horisberger et al., 1975) since it is easily visualised using backscattered electron imaging. The possibility of using marker generating systems, particularly enzymes, has also been suggested. Horseradish peroxidase (HRP) has been used to polymerise DAB, which has been subsequently identified based on morphological criteria (Ward et al., 1973). A refinement of this idea, involving the modification of DAB with a suitable element to facilitate identification using analytical electron microscopy has also been suggested (Chandler, 1973) but this was never examined, probably because of the success of the colloidal gold technique.

#### **1.4.1.4.2 Immunohistochemistry (IHC)**

In 1941, Marrack's seminal work was repeated by Albert Coons who increased signal strength by labelling antibodies with the fluorochrome, anthracene (Coons et al., 1941) and subsequently with fluorescein to detect antigens in tissue sections for the first time (Coons et al., 1942). The simultaneous detection of several antigens was achieved with the multiple immunofluorescence technique in which each antibody was labelled with a different fluorochrome (Clayton, 1954). Problems with tissue autofluorescence prompted the development of an alternative to fluorescein,

tetramethylrhodamine (Hiramoto et al., 1958). Both fluorescein and tetramethylrhodamine remained the most popular fluorochromes until the development of more photostable compounds such as the cyanine dyes (Mujumdar et al., 1989), Alexa dyes (Panchuk-Voloshina et al., 1999) (figure 1.24) and semiconductor Quantum Dots (Bruchez et al., 1998). The major advantages of fluorochromes over the products of enzyme-catalysed reactions are the ease of multiple labelling and their applicability to confocal microscopy. With the exception of Quantum Dots (Giepmans et al., 2005), the low electron opacity of fluorochromes has restricted their application to light microscopy.

Early studies examining the applicability of enzymes to deposit markers in an IHC setting focussed on HRP and acid phosphatase conjugates. The latter gave better localisation, but were unstable and difficult to prepare. In addition, unwanted affinity of acid phosphatase for cell nuclei was also observed (Nakane and Pierce, 1967). HRP conjugates, although producing less well defined staining, were much more stable (Avrameas and Uriel, 1966; Nakane and Pierce, 1967).

Alkaline phosphatase conjugates were introduced in 1971 (Engvall and Perlman, 1971). The most commonly used substrate is the halogenated indolyl phosphate, 5-bromo-4-chloro-3-indolyl phosphate (BCIP) which, following hydrolysis, undergoes tautomerization and oxidative dimerisation to indigo white (in alkaline solution). This is coupled to the reduction of nitro blue tetrazolium (NBT) to its formazan (figures 1.25 and 1.26). Fluorescent substrates have also been synthesised (Larison et al., 1993; 1994; 1995).



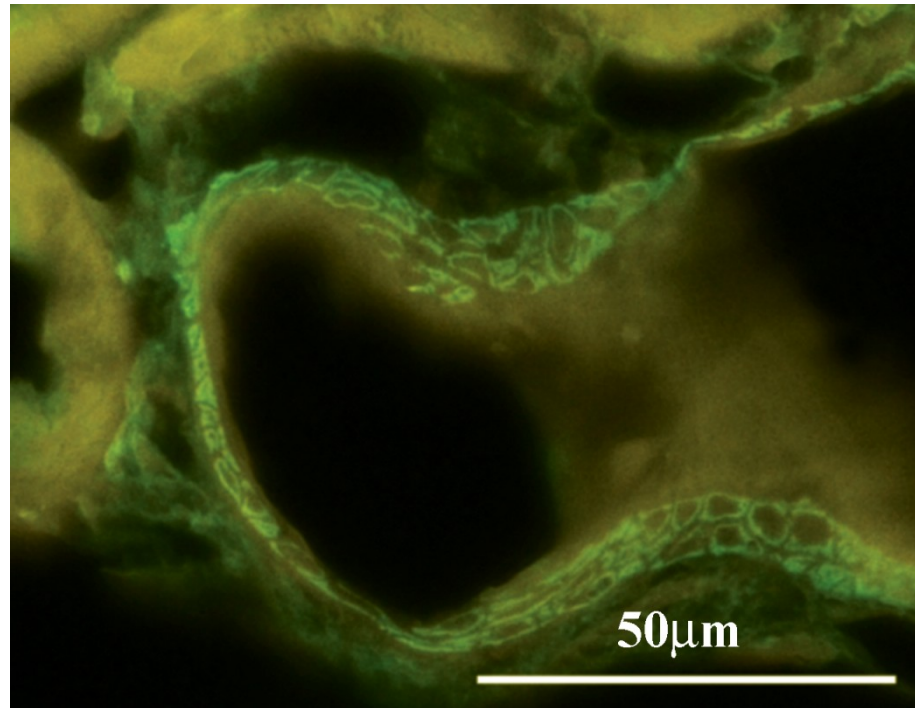


Figure 1.24. 4  $\mu\text{m}$  thick section of paraffin wax-embedded arteriole immunohistochemically stained for smooth muscle actin and visualised with Alexa 488.

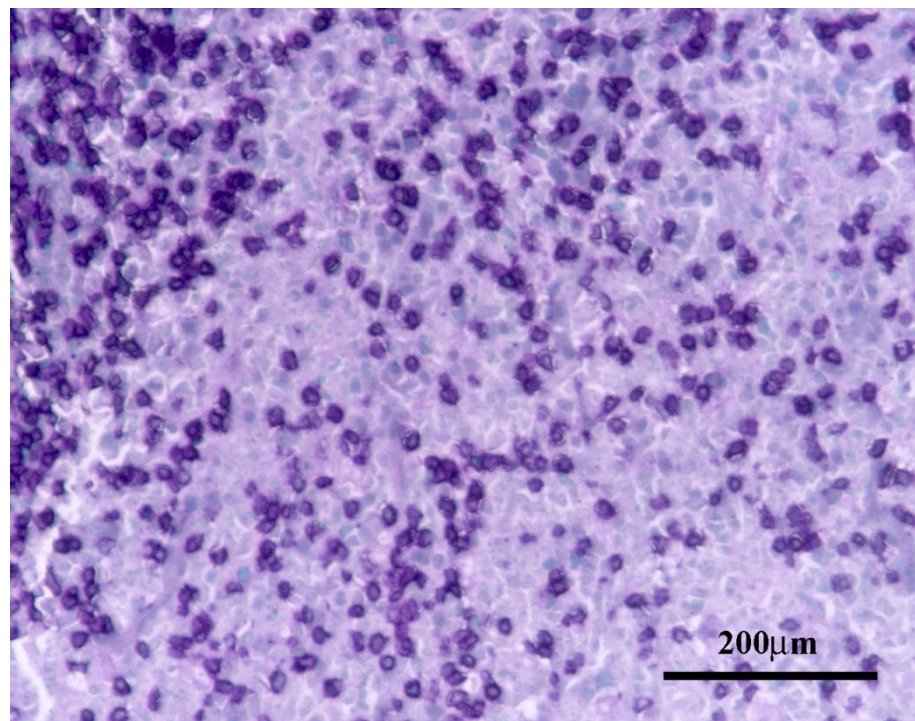


Figure 1.25. 4  $\mu\text{m}$  thick section of paraffin wax-embedded tonsil. Lymphocytes immunohistochemically stained for CD45RO and visualised with alkaline phosphatase conjugate and BCIP/NBT.

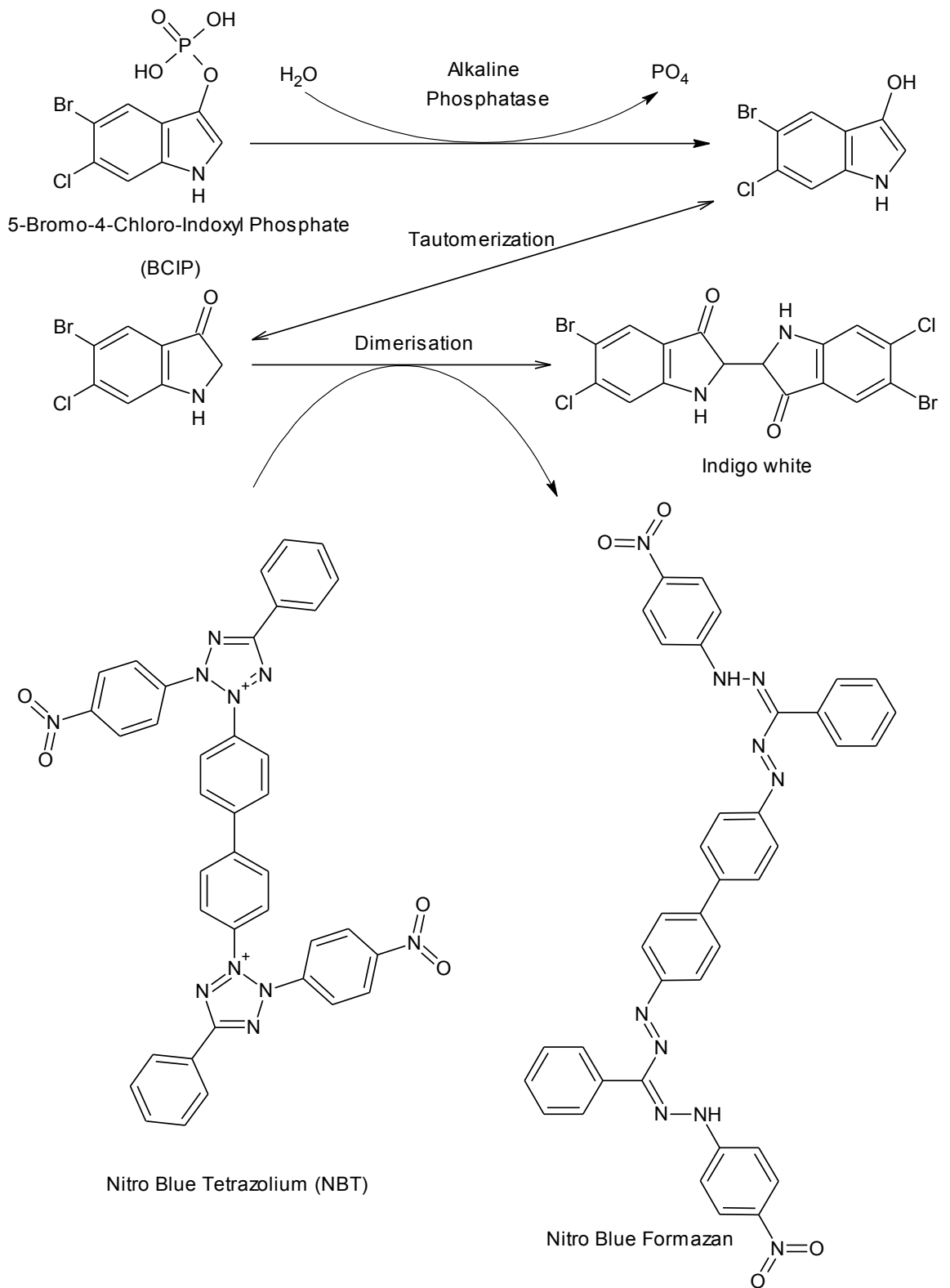


Figure 1.26. Mechanism underlying the histochemical demonstration of alkaline phosphatase using BCIP/NBT

The most popular enzyme conjugate for IHC, however, is HRP. The enzyme has been extensively studied and the catalytic mechanism, involving an unusual Fe(IV) oxyferryl intermediate, has been elucidated (Veitch, 2004) (figure 1.27). In immunohistochemical staining, reduction of the substrate, hydrogen peroxide, is coupled to the oxidative polymerisation of DAB (Seligman et al., 1968) to yield a red-brown deposit (figure 1.28). This marker, polyDAB, is permanent and insoluble in all solvents used in histological preparation. The poor solubility of polyDAB, while being one of its great strengths in immunohistochemistry, has hindered its characterisation. The few attempts that have been performed have yielded limited data, and both the mechanism of polymerisation and the nature of the final polymer remain speculative (Seligman et al., 1968; Cammer and Moore, 1973; Litwin, 1979) (figure 1.29). Like alkaline phosphatase, fluorescent HRP substrates have also been developed (Krieg and Halbhuber, 2004).

Other enzyme conjugates have been advocated where endogenous phosphatase or peroxidase activity is problematic, namely glucose oxidase (Stage and Avrameas, 1976) and  $\beta$ -galactosidase (Tanimori et al., 1983). These have not received significant interest because of their limited commercial availability. The use of colloidal gold labelled antibodies was suggested for light microscopical IHC (Gu et al., 1981) but the cost of reagents made this approach impractical.

A number of strategies have been employed to impart electron opacity to antibodies for IHC in the TEM, including labelling with ferritin (Singer, 1959), mercury (Pepe, 1961), uranium (Sternberger et al., 1963) and iodine (Mekler et al., 1964), but these have been superseded by metal particles, principally colloidal gold (Faulk and Taylor, 1971) (figure 1.30) which can be prepared in a number of sizes, allowing multiple immunolabelling (Horisberger and Rosset, 1977) (figure 1.31).

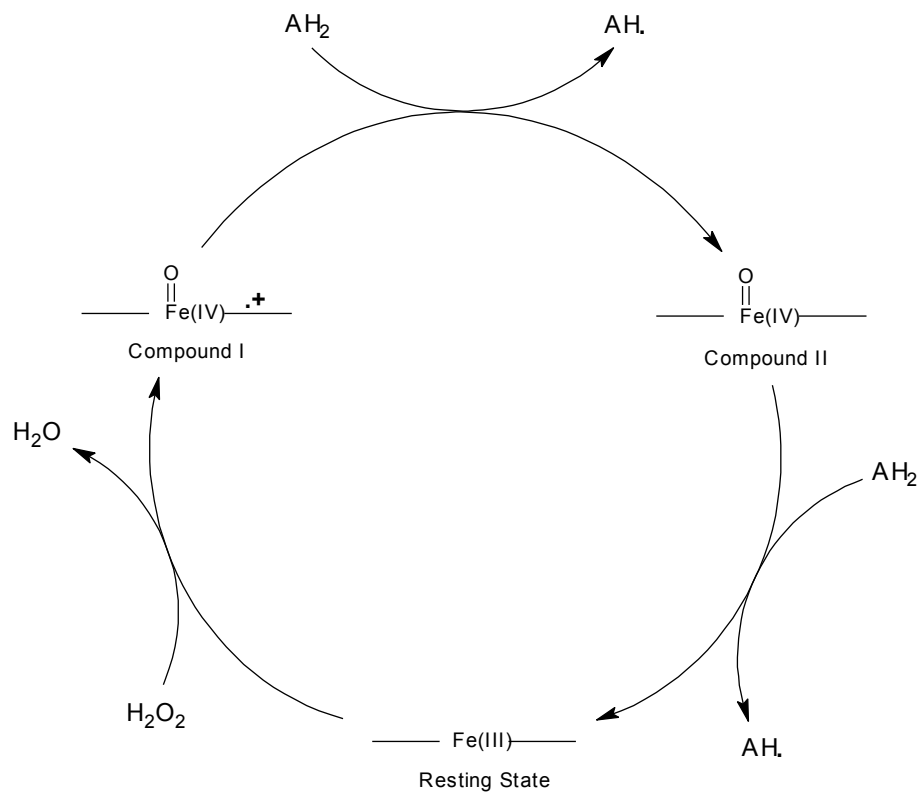


Figure 1.27. The horseradish peroxidase catalytic cycle.

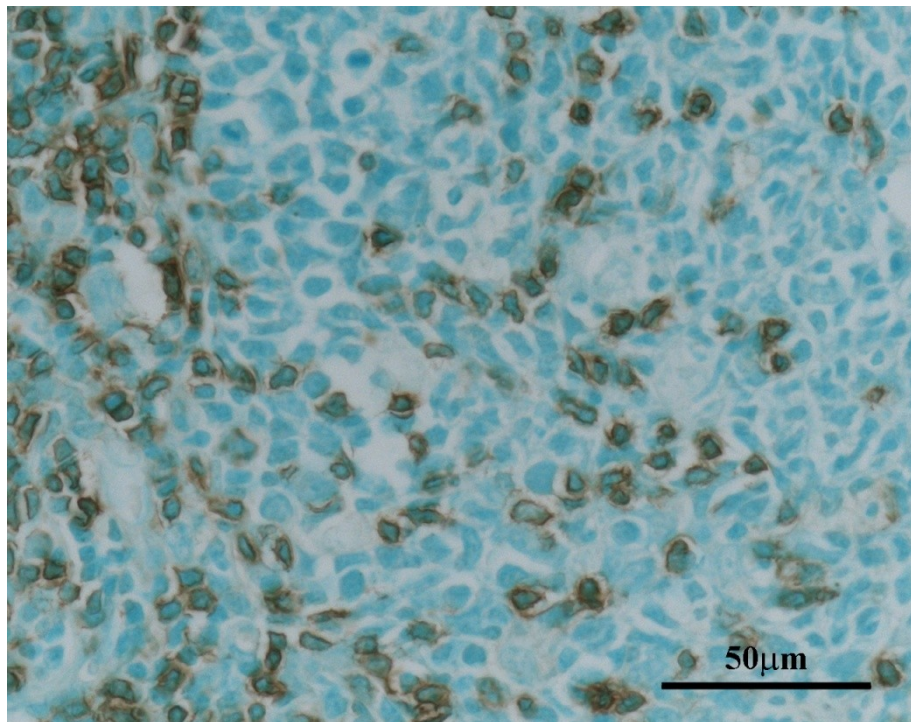


Figure 1.28. 4  $\mu\text{m}$  thick section of paraffin wax-embedded tonsil. Lymphocytes immunohistochemically stained for CD45RO using HRP conjugate and  $\text{H}_2\text{O}_2/\text{DAB}$ .

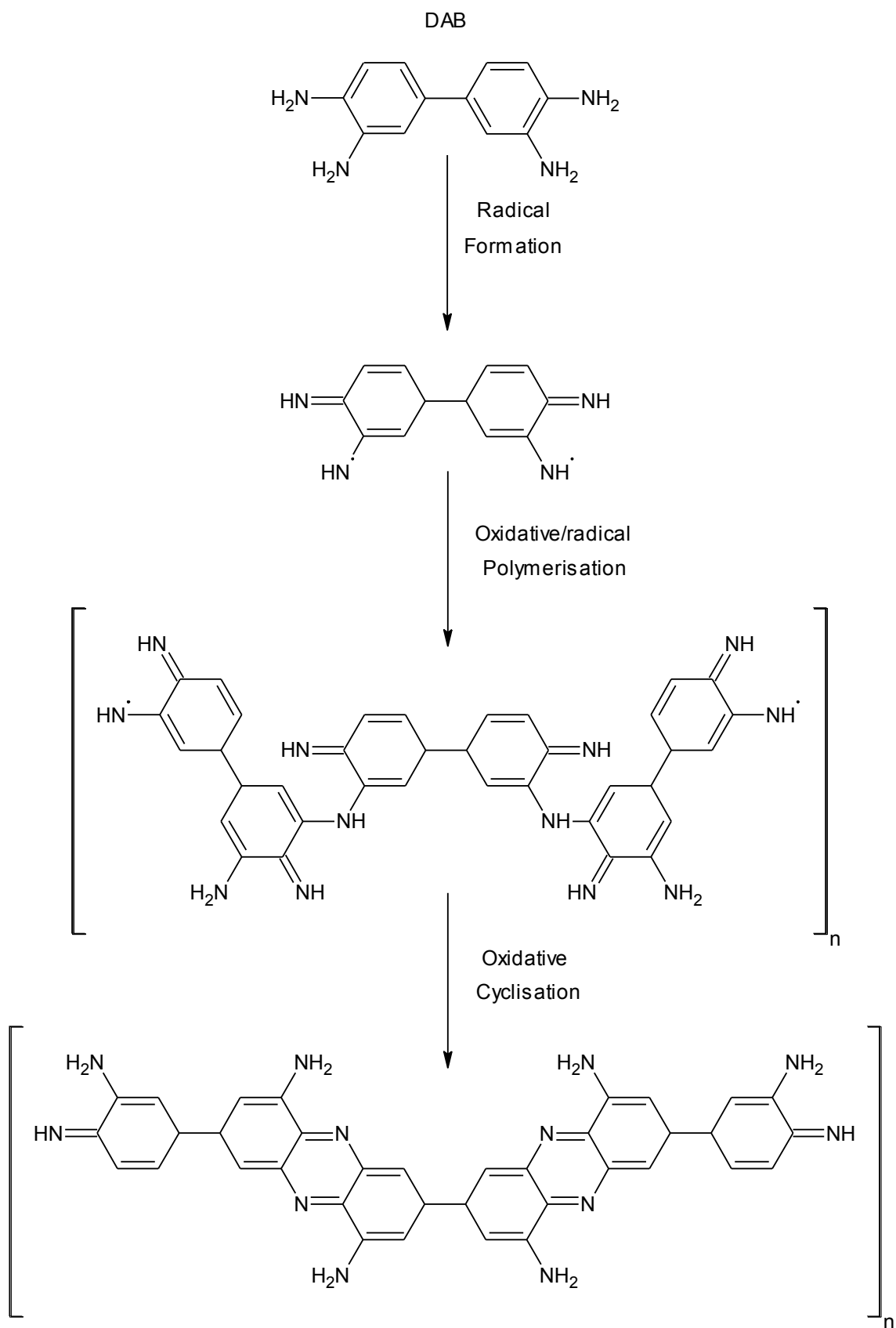


Figure 1.29. Suggested mechanism for the polymerisation of DAB.

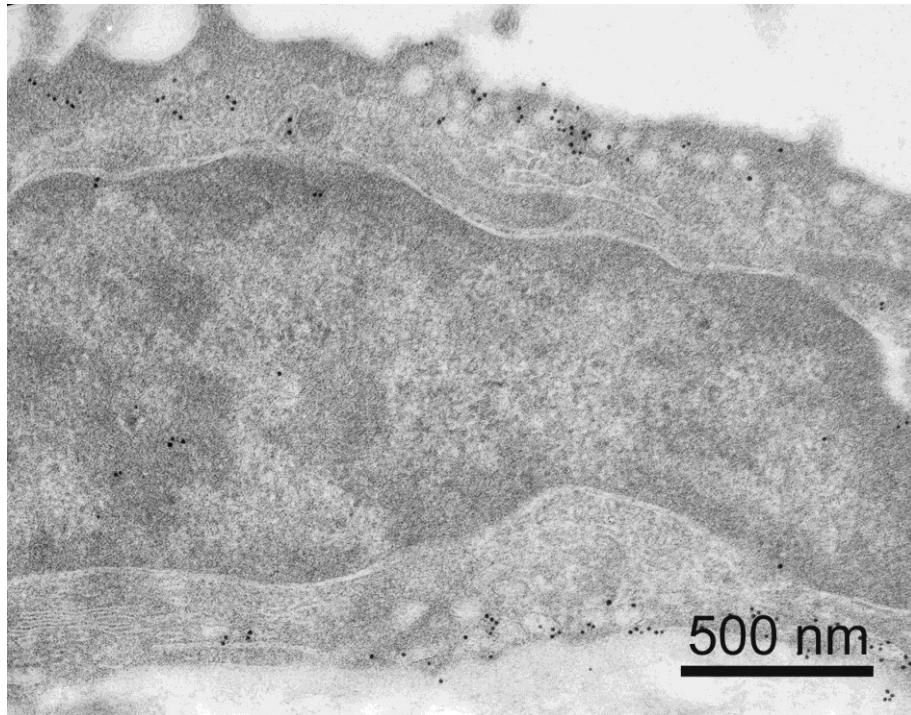


Figure 1.30. 80 nm thick section of LR White-embedded pleural mesothelial cell immunohistochemically stained for caveolin-1 using 10 nm colloidal gold. Uranyl acetate counterstain.

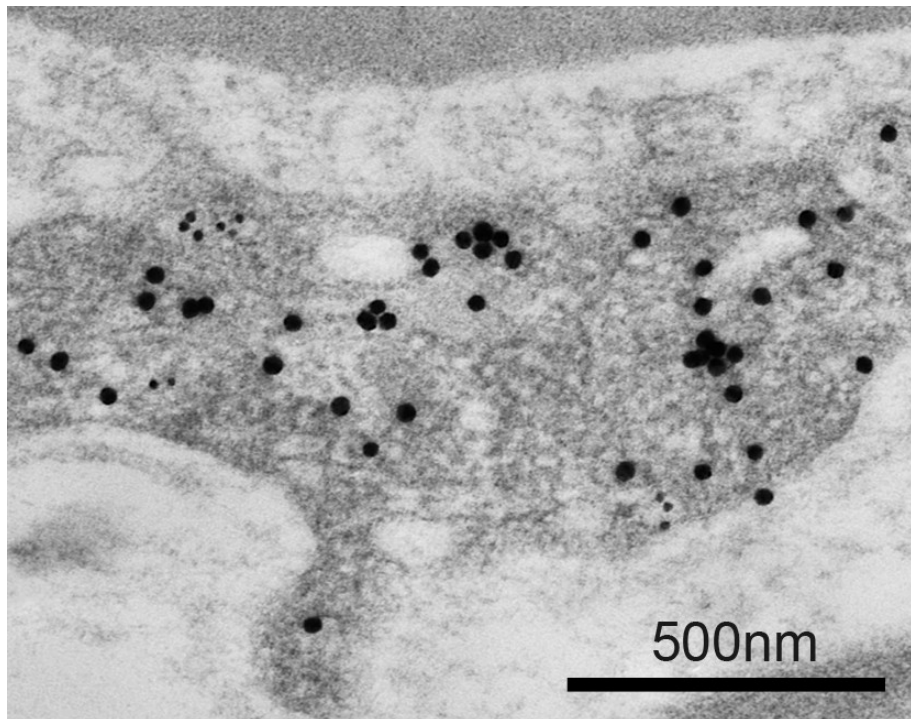


Figure 1.31. 80 nm thick section of LR White-embedded blood vessel. Vascular endothelial cell immunohistochemically stained for caveolin-1 (5 nm) and vimentin (20 nm) using colloidal gold. Uranyl acetate counterstain.



More recently, Nanogold™, a 1.4 nm gold particle, (Hainfeld, 1992; Hainfeld and Furuya, 1992) has been developed to overcome the tissue-penetration problem of traditional preparations of colloidal gold, which are usually produced between 5 nm and 20 nm.

The potential of horseradish peroxidase for IHC in the TEM has received some interest, since polyDAB is easily made electron-opaque with osmium (Graham and Karnovsky, 1966) and gold salts (Newman et al., 1983b) (figure 1.32). In addition, polyDAB-gold can be demonstrated using X-ray microanalysis (Siegesmund et al., 1979), suggesting the possibility of multiple labelling using different enzyme conjugates. It has also been suggested that HRP conjugates can penetrate resin sections (Newman and Hobot, 1987), raising the intriguing possibility of applying this technology to electron tomography.

Attempts to visualise alkaline phosphatase products in the electron microscope have met with little interest because of their obscurity (Hanker, 1979) or complexity (Halbhuber et al., 1991).

The requirement for markers that could be visualised at both the light and electron microscopic levels was recognised early on, and led to the development of antibodies that were doubly labelled with mercury and fluorescein (Pepe, 1961) or ferritin and fluorescein (Hsu et al., 1963). The modern equivalent is Nanogold™ and fluorescein (Powell et al., 1997; 1998).

#### **1.4.2 Fluorescence *in-situ* Hybridisation**

Nucleic acid in tissue is often double stranded but can be denatured to single strands. A complementary single stranded nucleic acid polymer will therefore act as

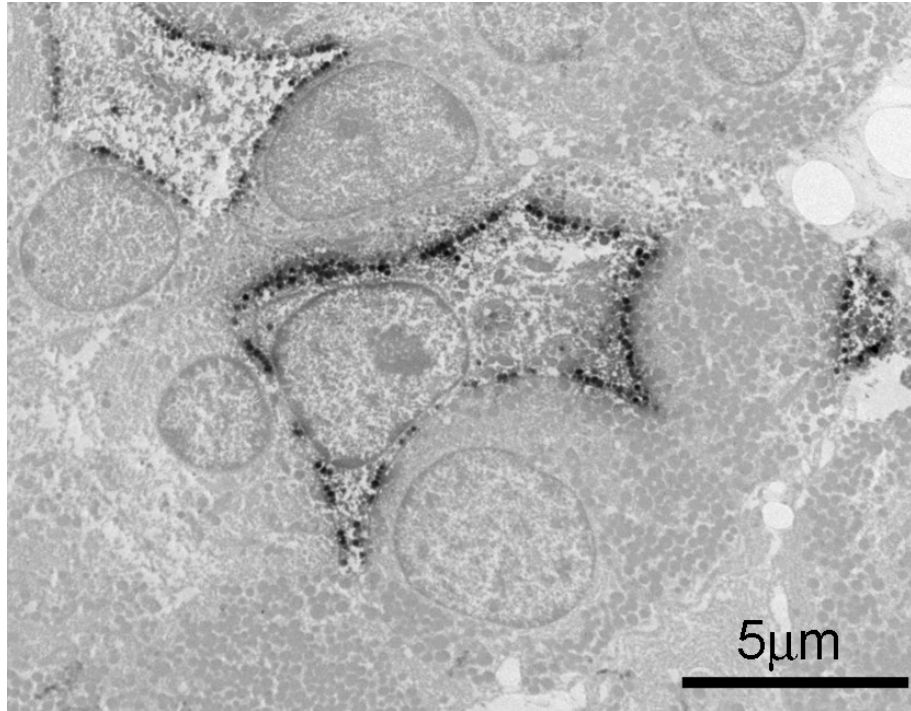


Figure 1.32. 80 nm thick section of LR White-embedded pituitary. Corticotroph immunohistochemically stained for adrenocorticotrophic hormone and visualised with HRP and H<sub>2</sub>O<sub>2</sub>/DAB followed by gold(III) chloride. No counterstain.



a reporter. The marker system, when attached to the reporter sequence, is usually either an enzyme, shown by a histochemical reaction, or a fluorochrome. Immunohistochemical techniques are frequently used to localise labels attached to single stranded probes.

### **1.4.3 Biochemical Techniques**

Biochemical analysis of cell and tissue extracts can involve techniques that are analogous to immunohistochemistry. Extracts are separated and immobilised electrophoretically (Western blotting) and the components identified with immuno-techniques. The most frequently employed reporter/marker system was alkaline phosphatase and BCIP (Knecht and Dimond, 1984) or BCIP and NBT (Blake et al., 1984). This system has been largely superseded by chemiluminescent technologies.

### **1.4.4 Molecular Biology**

Separation and analysis of specific nucleic acid sequences is performed in an analogous process to Western blotting. The reporter molecules are not antibodies, as in Western blotting, but complementary nucleic acid sequences that bind with very high specificity. The molecular biological equivalent of Western blotting is Southern blotting (for DNA) (Southern, 1974; 1975) and Northern blotting for (RNA) (Alwine et al., 1979). Markers are similar to those used for Western blotting.

### **1.4.5 Amplification Systems**

The theoretical ideal of any reporter/marker system is single molecule detection. In reality, this would require considerable signal amplification, even for

macromolecules. A number of approaches have been developed that are by no means mutually exclusive.

#### **1.4.5.1 Primary Probe Amplification**

This is the selection and/or production of primary probes that have a greater affinity or avidity for their respective target molecules. This has been particularly important in the immunohistochemical staining of aldehyde-fixed samples, since antibodies are raised against unmodified antigens or their fragments, and it is thus serendipitous that they recognise fixed antigens.

#### **1.4.5.2 Target Retrieval**

Many target molecules in a solid sample, such as a tissue section, are inaccessible to primary probes due to the presence of surrounding tissue structures, or are unrecognisable as a result of covalent modification by chemical fixatives. These restrictions have been largely overcome, by enzymatic digestion (Huang et al., 1976) and microwave heating (Shi et al., 1991) respectively. Microwave treatment of tissue sections has been particularly beneficial in rendering antigens more recognisable by their respective antibodies and thus increasing the range of substances that can be visualised.

#### **1.4.5.3 Reporter Amplification**

The simplest form of reporter amplification is the use of secondary antibodies since more than one can attach to each primary antibody. Successive layers could potentially be constructed, but such a technique would rapidly become prohibitively expensive. A more efficient technique is the introduction of multidentate bridging

molecules such as the avidin-biotin complex (ABC). This technique uses the protein avidin (from egg white) or, more commonly, streptavidin (from *Streptomyces avidinii*) which can bind up to four biotin molecules. Biotinylated markers or enzymes form the final layer (Guesdon et al., 1979; Hsu et al., 1981).

Catalysed reporter deposition (CARD) employs labelled (e.g. biotinylated) enzyme substrates as binding sites for additional reporters (e.g. ABC). This technique was originally developed for biochemical analysis in immunoassays (Bobrow et al., 1989) and membrane (dot blot) immunoassays (Bobrow et al., 1991) using soluble or insoluble chromogenic markers respectively. Immunocytochemical/histochemical applications frequently use biotinylated tyramide (Hunyady et al., 1996). Recent techniques include deposition of fluorochromes such as europium chelates (de Haas et al., 1996). Proprietary polymeric systems increase signal strength by covalently attaching numerous markers or enzymes to a polymer backbone which is, in turn, attached to a reporter molecule (figure 1.33).

Reporter amplification has the capacity to generate very large quantities of signal. Problems arise where multilayered systems are employed since reagents are applied in excess to ensure saturation of all available specific sites. Non-specific background staining inevitably results and this increases with each successive layer. Additional problems include the limited tissue penetration of polymeric systems, steric hindrance, and the presence of 'specific-unwanted' sites within tissue such as endogenous biotin. To overcome these problems, the complexity of the reporter system can be reduced to just the primary reporter and secondary reporter conjugate followed by marker amplification.

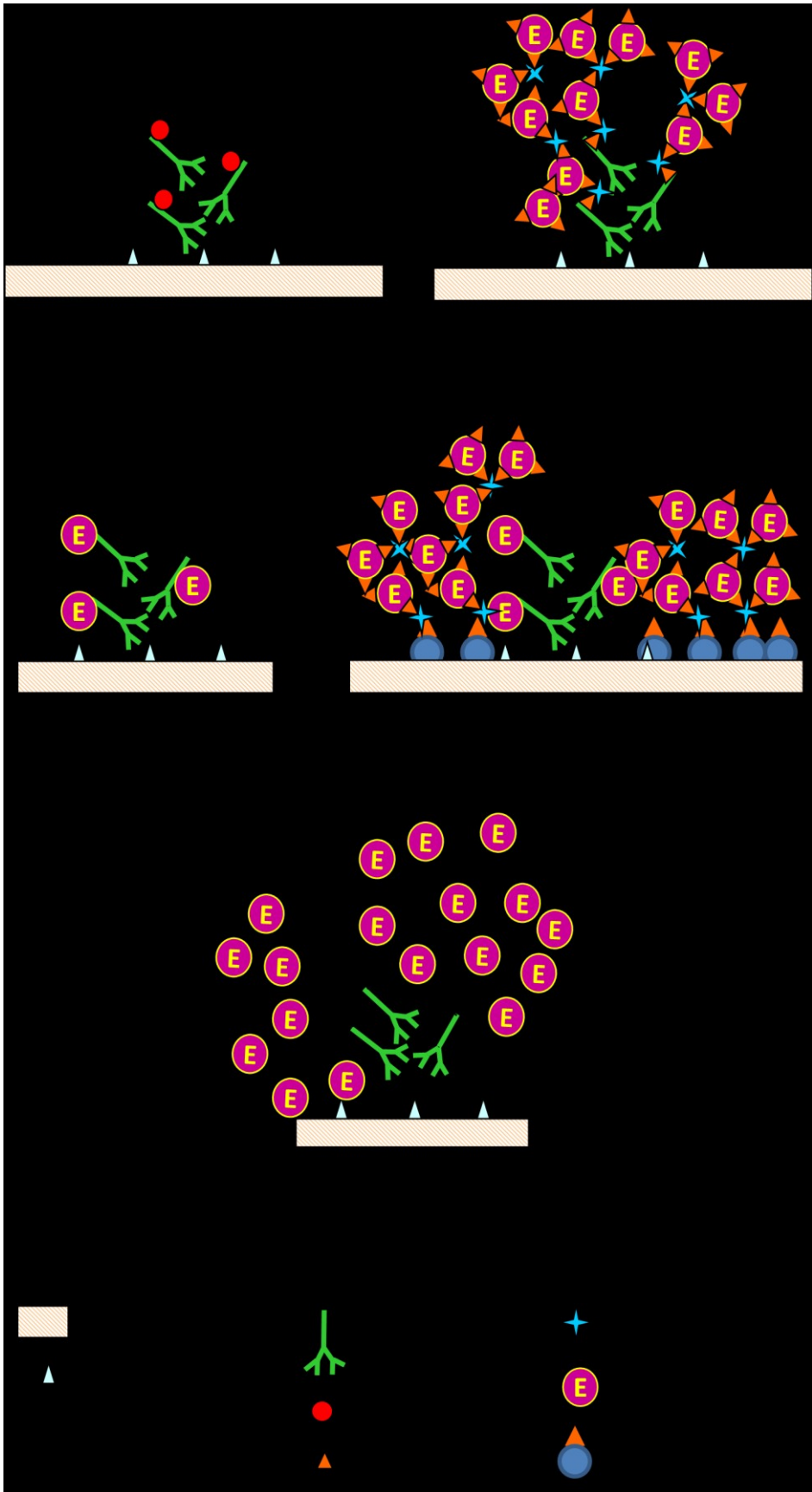


Figure 1.33. Principles of reporter amplification.

#### 1.4.5.4 Marker Amplification

One of the most successful techniques for amplifying markers is physical development (Newman and Jasani, 1998b). This process is analogous to photographic development where the photo-reduced silver grains in the undeveloped negative or photographic paper catalyse the reduction of silver ions, derived from the photographic emulsion, in the presence of a reducing agent (the photographic developer). Physical development combines ionic silver and the reducing agent in the same final solution. Light insensitive physical developers, which are convenient for laboratory use, prevent light catalysed reduction of silver by colloidal protection (Gallyas, 1979) or complexing (Newman and Jasani, 1998a). There are a number of commercial physical developers available as well as published formulations (Gallyas, 1979; Danscher, 1981; Newman and Jasani, 1998a).

Colloidal gold can be seen directly in the light microscope, but it is more usual to amplify this poor signal by exploiting its capacity to reduce silver from physical developers (Danscher, 1981; Holgate et al., 1983). A similar principle is used to visualise Nanogold™ particles (Hainfeld and Furuya, 1992).

PolyDAB can also be amplified by physical developers, either alone (Gallyas et al., 1982), or following complexing with d-block metals (Przepiorka and Myerson, 1986; Gallyas and Merchenthaler, 1988; Green et al., 1989; Mullink et al., 1992) and their sulfides (Newman et al., 1983c) (figure 1.34). Halhuber's technique for alkaline phosphatase (Halhuber et al., 1988), which ultimately results in the polymerisation of DAB, could be amplified by techniques that are applied to peroxidase but the method is extremely complicated and has received little interest.

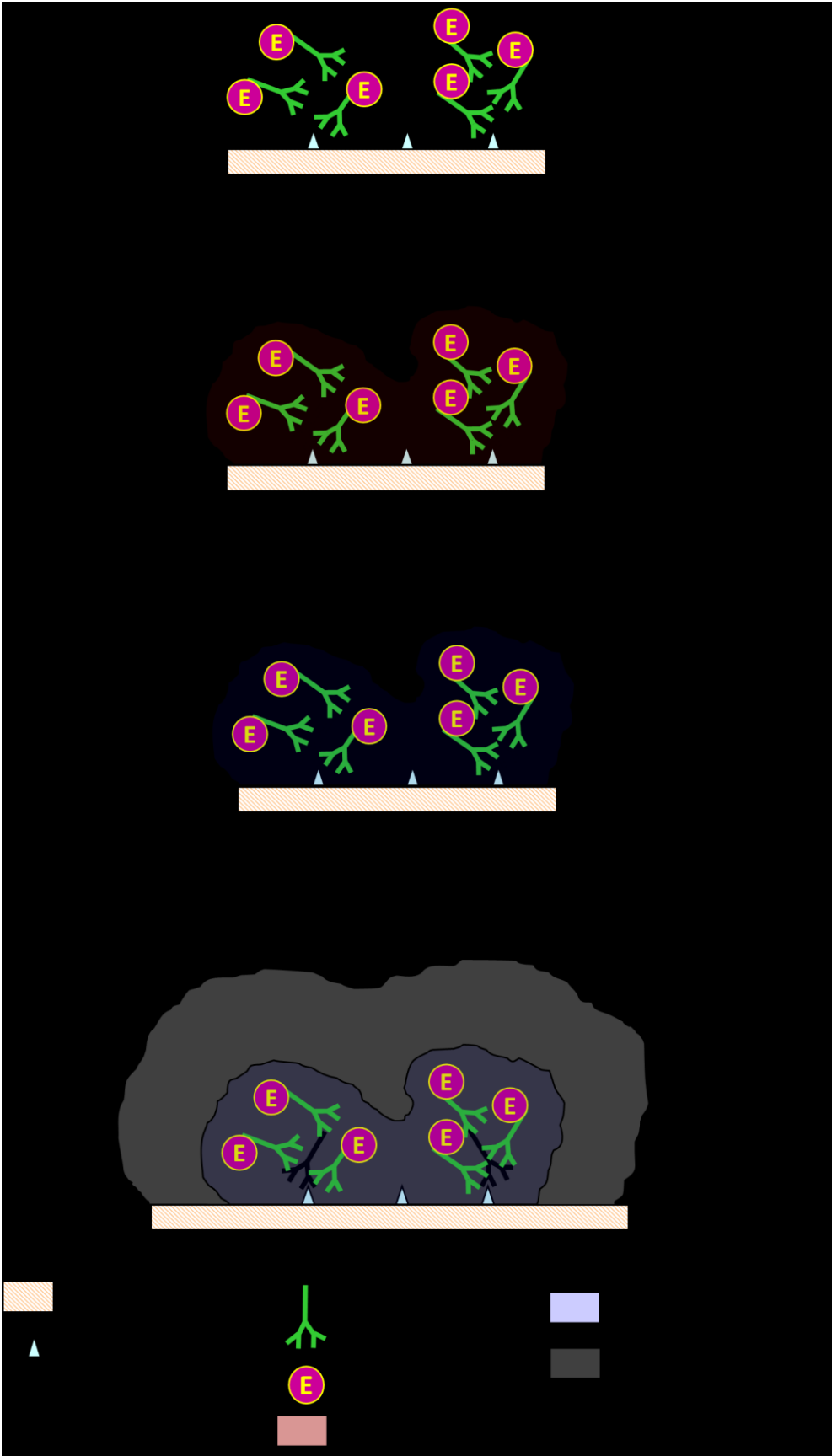


Figure 1.34. Principle of marker amplification.

## **1.4.6 Advantages and Disadvantages of Existing Markers**

### **1.4.6.1 Fluorochromes**

Fluorochromes offer high signal to noise and are of considerable importance in live cell studies. In addition, they can be easily visualised by confocal microscopy allowing 3-dimensional and 4-dimensional (+ time) studies. Their main drawback has been the instability of fluorescently labelled preparation which was first observed in 1942 (Coons et al., 1942), although modern developments such as quantum dots has largely overcome this. In addition, no conventional fluorescent counterstains exist and fluorescence produces free radicals that can damage cells. Furthermore, autofluorescence is a serious problem of aldehyde-fixed tissue and, with the exception of the quantum dots, fluorochromes are not directly visible in the electron microscope.

### **1.4.6.2 Metal Particles**

The particulate nature of colloidal gold facilitates its recognition in the EM and it is easily amplified with physical developers. Tissue penetration is poor and labelling density varies inversely with particle size. This latter feature renders any attempt at quantitation highly dubious.

Nanogold™ particles were developed to overcome the penetration problems of colloidal gold but they difficult to see, even in the electron microscope, are hard to amplify and are expensive.

### **1.4.6.3 Products of Enzyme Catalysed Reactions**

PolyDAB is permanent and easily intensified with certain d-block metals. It can be easily made electron-opaque and amplified with physical developers. In

addition, its allegedly diffuse nature (compared with metal particles) has been exploited in electron tomography (Geuze et al., 2003). There are, however, numerous disadvantages of the peroxidase/DAB system. Peroxidases and pseudo-peroxidases (e.g. catalase) are endogenous to many tissues and the substrate, hydrogen peroxide, is common to many biological systems. In addition, a number of non-enzymatic catalysts of the reaction exist, such as endogenous metals (Sayre et al., 2000) and haem proteins (Schmid et al., 1989). Suppression of endogenous enzymatic activity is frequently detrimental to tissue reactivity and suppression of endogenous non-enzymatic activity is extremely difficult (Schmid et al., 1989). Furthermore, the reaction does not proceed beyond approximately 3 minutes due to deposition of the product, making quantitation difficult, the substrates are hazardous, poorly defined regarding impurities (DAB) and unstable. Finally, as has been mentioned earlier, little is known about the polymerisation of DAB, nor of the co-ordination chemistry of the product, polyDAB.

Alkaline phosphatase is not significantly affected by product inhibition hence quantitation is a possibility. Endogenous activity is easily suppressed (van Belle, 1972) and the enzyme's wide substrate specificity allows considerable opportunities for novel chemistry. Current products (mainly formazans) have a tendency to diffuse during tissue dehydration and mounting, and are completely dissolved by prolonged exposure to organic solvents such as ethanol. They cannot be amplified at present, nor easily made electron-opaque.

#### **1.4.7 Properties of an Ideal Marker**

An ideal marker should be finely localised and strongly adherent to the target, clearly visible, even at low concentrations, and be stoichiometrically related to



primary reporter density. It should be specific to the reporter system and have no affinity for non-target substances. It should be compatible with biological systems and insoluble in aqueous solution and/or organic solvents such as ethanol, xylene and histological mountants. The marker should be chemically stable, amplifiable and electron-opaque, or easily rendered so. None of the currently available marker systems fulfil all the above criteria.

## **1.5 Summary**

Marker chemistry has been developed on a largely empirical basis and the occurrence of additional properties, such as the capacity to facilitate amplification, or electron opacity is often serendipitous. Modern requirements, such as the demonstration of biological molecules in low copy number at the light microscopic level and the 3-D visualisation of multiple markers in a tomographic EM setting, present exciting new challenges.

Of the various amplification systems, outlined above, enzymes are currently the most suitable, since they provide a mechanism for generating large amounts of marker. The choice is restricted, however, by their high quality commercial availability. While alkaline phosphatase offers the greatest opportunity for novel marker chemistry, the properties of the HRP reaction product, polyDAB, have much to commend it. Unfortunately, almost nothing is known about its chemistry; the description of its structure is based solely on infrared spectroscopy (Seligman et al., 1968) and little is known about its behaviour as a coordination host. The elucidation of this information could provide useful insights into the design of novel enzyme substrates that will ultimately be of benefit to diagnostic histopathology.

The visualisation of multiple markers in tomographic electron microscopy can, in principle, be realised by exploiting the analytical capabilities of the instrument and employing markers that contain sufficient quantities of specific element to facilitate ease of discrimination by energy filtering techniques, or that minimise X-ray signal acquisition time.

Paradoxically, the requirement for high resolution microscopy has come, not from pathologists and cell biologists, but from molecular biologists and biochemists, who have finally recognised the limitations of the light microscope and require the higher resolution that is afforded by the electron microscope.

Unfortunately, the prominence of molecular biology and the ‘-omic’ sciences over the last few decades has been accompanied by a concomitant reduction in interest in electron microscopy. As a result, much expertise has been lost and considerable confusion and ignorance exists. For example, the technology that is frequently employed for electron microscopy is either outdated (1960s) e.g. pre-embedding immunocytochemistry/histochemistry, osmium post-fixation and epoxy resin embedding, or is perceived to require the most complex procedures and expensive equipment i.e. the various cryo techniques.

Novel markers should, ideally, be simple to use and not require complex preparative procedures or expensive equipment to observe them, and thus be as broadly applicable as possible.

## **1.6 Structure and Aims of the Thesis**

This thesis is divided into two parts. Part 1 examines the amplification of polyDAB with physical developers at the light microscopic level and comprises Chapter 2, an empirical investigation of the interaction of d-block metal salts with

polyDAB in both a pre- and post-polymerisation setting, with a view to determining which combinations are powerful catalysts of silver reduction and thus which might have some utility in diagnostic histopathology, and Chapter 3, in which these studies are further refined to determine the practical limits of sensitivity of the peroxidase/DAB system.

In Part 2 the investigation focuses on the development of markers for use in analytical electron microscopical tomography. Chapter 4 applies the results of chapter 2 in an electron microscopical setting with a view to developing immunohistochemical markers based on polyDAB-metal complexes. These studies are extended to halogenated aromatic diamines and bis-diamines as enzyme substrates in Chapter 5, and techniques for visualising fluorochromes in the electron microscope are explored in Chapter 6. Chapter 7 describes a limited characterisation of polyDAB with a view to understanding its behaviour and thus indicating fruitful directions for rational marker design. Chapter 8 briefly explores alternative applications of halogenated aromatic diamines, and Chapter 9 is a general discussion of the results of the experimental chapters.

## 1.7 References

- ABBE, E. 1873. zur Theorie des microskops und der microskopische bilder zeugung. *Schultz's Archives*, 9, 413-468.
- ACETARIN, J. D., CARLEMALM, E. & VILLIGER, W. 1986. Developments of new lowicryl resins for embedding biological specimens at even lower temperatures. *Journal of Microscopy-Oxford*, 143, 81-88.
- ADAMS, S. R., CAMPBELL, R. E., GROSS, L. A., MARTIN, B. R., WALKUP, G. K., YAO, Y., LLOPIS, J. & TSIEN, R. Y. 2002. New biarsenical ligands and tetracysteine motifs for protein labeling in vitro and in vivo: Synthesis and biological applications. *Journal of the American Chemical Society*, 124, 6063-6076.
- AIRY, G. B. 1834. On the diffraction of an object-glass with circular aperture. *Transactions of the Cambridge Philosophical Society*.
- ALEM, N., YAZYEV, O. V., KISIELOWSKI, C., DENES, P., DAHMEN, U., HARTEL, P., HAIDER, M., BISCHOFF, M., JIANG, B., LOUIE, S. G. & ZETTL, A. 2011. Probing the out-of-plane distortion of single point defects in atomically thin hexagonal boron nitride at the picometer scale. *Physical Review Letters*, 106, 126102.
- ALWINE, J. C., KEMP, D. J., PARKER, B. A., REISER, J., RENART, J., STARK, G. R. & WAHL, G. M. 1979. Detection of specific RNAs or specific fragments of DNA by fractionation in gels and transfer to diazobenzyloxymethyl paper. *Methods in Enzymology*, 68, 220-242.
- ANDERSON, T. F. 1951. Techniques for the preservation of three-dimensional structure in preparing specimens for the electron microscope. *Transactions of the New York Academy of Sciences*, 13, 130-134.
- AVRAMEAS, S. & URIEL, J. 1966. [Method of antigen and antibody labelling with enzymes and its immunodiffusion application]. *Comptes Rendus Hebdomadaires des Seances de l'Academie des Sciences - D: Sciences Naturelles*, 262, 2543-2545.

- AXELROD, D., KOPPEL, D. E., SCHLESSINGER, J., ELSON, E. & WEBB, W. W. 1976. Mobility measurement by analysis of fluorescence photobleaching recovery kinetics. *Biophysical Journal*, 16, 1055-1069.
- BAKER, J. R. 1958. *Principles of Biological Microtechnique*, London, Methuen and Company.
- BARKER, W. B. 1930. 'The Nineveh lens'. *British Journal of Physiological Optics*, 4, 4-6.
- BENDAYAN, M. & ZOLLINGER, M. 1983. Ultrastructural-localization of antigenic sites on osmium-fixed tissues applying the protein a-gold technique. *Journal of Histochemistry & Cytochemistry*, 31, 101-109.
- BERGMANS, L., MOISIADIS, P., VAN MEERBEEK, B., QUIRYNEN, M. & LAMBRECHTS, P. 2005. Microscopic observation of bacteria: review highlighting the use of environmental SEM. *International Endodontic Journal*, 38, 775-788.
- BETZIG, E., PATTERSON, G. H., SOUGRAT, R., LINDWASSER, O. W., OLENYCH, S., BONIFACINO, J. S., DAVIDSON, M. W., LIPPINCOTT-SCHWARTZ, J. & HESS, H. F. 2006. Imaging intracellular fluorescent proteins at nanometer resolution. *Science*, 313, 1642-1645.
- BLAKE, M. S., JOHNSTON, K. H., RUSSELL-JONES, G. J. & GOTSCHLICH, E. C. 1984. A rapid, sensitive method for detection of alkaline phosphatase-conjugated anti-antibody on Western blots. *Analytical Biochemistry*, 136, 175-179.
- BLUM, F. 1893. Der formaldehyd als hartungsmittel. *Zeitschrift fur Wissenschaftliche Mikroskopie*, 10, 314.
- BOBROW, M. N., HARRIS, T. D., SHAUGHNESSY, K. J. & LITT, G. J. 1989. Catalyzed reporter deposition, a novel method of signal amplification. Application to immunoassays. *Journal of Immunological Methods*, 125, 279-285.

- BOBROW, M. N., SHAUGHNESSY, K. J. & LITT, G. J. 1991. Catalyzed reporter deposition, a novel method of signal amplification. II. Application to membrane immunoassays. *Journal of Immunological Methods*, 137, 103-112.
- BORISEVICH, A. Y., LUPINI, A. R. & PENNYCOOK, S. J. 2006. Depth sectioning with the aberration-corrected scanning transmission electron microscope. *Proceedings of the National Academy of Sciences of the United States of America*, 103, 3044-3048.
- BRUCHEZ, M., MORONNE, M., GIN, P., WEISS, S. & ALIVISATOS, A. P. 1998 Semiconductor nanocrystals as fluorescent biological labels. *Science*, 281, 2013-2016.
- CAMMER, W. & MOORE, C. L. 1973. Oxidation of 3,3'-diaminobenzidine by rat liver mitochondria. *Biochemistry*, 12, 2502-2509.
- CARLEMALM, E., GARAVITO, R. M. & VILLIGER, W. 1982. Resin development for electron microscopy and an analysis of embedding at low temperature. *Journal of Microscopy-Oxford*, 126, 123-143.
- CARLTON, P. M., BOULANGER, J., KERVRANN, C., SIBARITA, J.-B., SALAMERO, J., GORDON-MESSER, S., BRESSAN, D., HABER, J. E., HAASE, S., SHAO, L., WINOTO, L., MATSUDA, A., KNER, P., UZAWA, S., GUSTAFSSON, M., KAM, Z., AGARD, D. A. & SEDAT, J. W. 2010. Fast live simultaneous multiwavelength four-dimensional optical microscopy. *Proceedings of the National Academy of Sciences of the United States of America*, 107, 16016-16022.
- CHALFIE, M., TU, Y., EUSKIRCHEN, G., WARD, W. & PRASHER, D. 1994. Green fluorescent protein as a marker for gene expression. *Science*, 263, 802-805.
- CHANDLER, J. A. The use of wavelength dispersive X-ray microanalysis in cytochemistry. *In*: WISSE, E., DAEMS, W. TH., MOLENAAR, L. AND VON DUIJN, P., ed. *Electron Microscopy and Cytochemistry*, 1973 Drienerlo, The Netherlands. North Holland Publishing Company, 203-222.

- CLAYTON, R. M. 1954. Localization of embryonic antigens by antisera labelled with fluorescent dyes. *Nature*, 174, 1059.
- CONN, H. J. 1977. *Biological Stains*, Baltimore, Williams and Wilkins Company.
- COONS, A. H., CREECH, H. J. & JONES, R. N. 1941. Immunological properties of an antibody containing a fluorescent group. *Proceedings of the Society for Experimental Biology and Medicine*, 47, 200-202.
- COONS, A. H., CREECH, H. J., JONES, R. N. & BERLINER, E. 1942. The demonstration of pneumococcal antigen in tissue by the use of fluorescent antibody. *Journal of Immunology*, 45, 159-170.
- COONS, A. H., LEDUC, E. H. & CONNOLLY, J. M. 1955. Studies on antibody production. I. A method for the histochemical demonstration of specific antibody and its application to a study of the hyperimmune rabbit. *Journal of Experimental Medicine*, 102, 49-60.
- CRAIG, E. L., GREIDER, M. H. & FRAJOLA, W. J. 1962. An embedding technique for electron microscopy using EPON 812. *Journal of Cell Biology*, 12, 190-194.
- CROWTHER, R. A., DE ROSIER, D. J. & KLUG, A. 1970. The reconstruction of a three-dimensional structure from projections and its application to electron microscopy. *Proceedings of the Royal Society of London Series a-Mathematical and Physical Sciences*, 317, 319-340.
- CULLING, C. F. A., ALLISON, R. T. & BARR, W. T. 1985. *Cellular pathology techniques*, London, Butterworth.
- DANILATOS, G. D. 1981. Design and construction of an atmospheric or environmental SEM .1. *Scanning*, 4, 9-20.
- DANSCHER, G. 1981. Localization of gold in biological tissue - a photochemical method for light and electron-microscopy. *Histochemistry*, 71, 81-88.

- DE BROGLIE, L. 1923. Radiation - waves and quanta. *Comptes rendus de l'Académie des Sciences*, 177, 507-510.
- DE BROGLIE, L. 1925. Recherches sur la theorie des quanta. (Researches on the theory of quanta.). *Annales de Physiques*, 3, 22-128.
- DE HAAS, R. R., VERWOERD, N. P., VAN DER CORPUT, M. P., VAN GIJLSWIJK, R. P., SIITARI, H. & TANKE, H. J. 1996. The use of peroxidase-mediated deposition of biotin-tyramide in combination with time-resolved fluorescence imaging of europium chelate label in immunohistochemistry and in situ hybridization. *Journal of Histochemistry & Cytochemistry*, 44, 1091-1099.
- DONNERT, G., KELLER, J., MEDDA, R., ANDREI, M. A., RIZZOLI, S. O., LUEHRMANN, R., JAHN, R., EGGELING, C. & HELL, S. W. 2006. Macromolecular-scale resolution in biological fluorescence microscopy. *Proceedings of the National Academy of Sciences of the United States of America*, 103, 11440-11445.
- DORMER, R. L., CAMPBELL, A. K. & NEWMAN, G. R. 1977. Studies on entrapment of calcium-activated photoprotein obelin and carbonic-anhydrase in liposomes and their interaction with isolated adipocytes. *Biochemical Society Transactions*, 5, 1151-1154.
- DRURY, R. A. B. & WALLINGTON, E. A. 1980. *Carleton's histological techniques*, Oxford, Oxford University Press.
- DSOUZA, M. & DATTA, K. 1985. Evidence for naturally-occurring hyaluronic-acid binding-protein in rat-liver. *Biochemistry International*, 10, 43-51.
- EISENBERG, B. R. & MOBLEY, B. A. 1975. Size changes in single muscle fibers during fixation and embedding. *Tissue & Cell*, 7, 383-387.
- ENGVALL, E. & PERLMAN, P. 1971. Enzyme-linked immunosorbent assay (ELISA). Quantitative assay of immunoglobulin G. *Immunochemistry*, 8, 871-874.



- ERICSSON, J. L. & BIBERFEL.P 1967. Studies on aldehyde fixation - fixation rates and their relation to fine structure and some histochemical reactions in liver. *Laboratory Investigation*, 17, 281-298
- FARQUHAR, M. G. & PALADE, G. E. 1965. Cell junctions in amphibian skin. *Journal of Cell Biology*, 26 263-291.
- FAULK, W. P. & TAYLOR, G. M. 1971. An immunocolloid method for the electron microscope. *Immunochemistry*, 8, 1081-1083.
- FÖRSTER, T. 1948. Zwischenmolekulare energiewanderung und fluoreszenz. *Annalen Der Physik*, 2, 55-75.
- FOX, C. H., JOHNSON, F. B., WHITING, J. & ROLLER, P. P. 1985. Formaldehyde fixation. *Journal of Histochemistry & Cytochemistry*, 33, 845-853.
- FRAENKEL-CONRAT, H., BRANDON, B. & OLCOTT, H. 1947. The reaction of formaldehyde with proteins, IV: participation of indole groups: gramicidin. *Journal of Biological Chemistry*, 168, 99-118.
- FRAENKEL-CONRAT, H. & OLCOTT, H. 1948a. Reaction of formaldehyde with proteins, VI: crosslinking of amino groups with phenol, imidazole, or indole groups. *Journal of Biological Chemistry*, 174, 827-843.
- FRAENKEL-CONRAT, H. & OLCOTT, H. 1948b. The reaction of formaldehyde with proteins, V: crosslinking between amino and primary amide or guanidyl groups. *Journal of the American Chemical Society*, 70, 673-684.
- FRIEDLAND, L. M. 1951. A note on frozen section technic. *American Journal of Clinical Pathology*, 21, 797.
- FUJIWARA, K. & POLLARD, T. D. 1976. Fluorescent-antibody localisation of myosin in cytoplasm, cleavage furrow, and mitotic spindle of human cells. *Journal of Cell Biology*, 71, 848-875.
- GALLYAS, F. 1979. Light insensitive physical developers. *Stain Technology*, 54, 173-175.

- GALLYAS, F., GORCS, T. & MERCHENTHALER, I. 1982. High-grade intensification of the end-product of the diaminobenzidine reaction for peroxidase histochemistry. *Journal of Histochemistry & Cytochemistry*, 30, 183-184.
- GALLYAS, F. & MERCHENTHALER, I. 1988. Copper-H<sub>2</sub>O<sub>2</sub> oxidation strikingly improves silver intensification of the nickel diaminobenzidine (Ni-Dab) end-product of the peroxidase reaction. *Journal of Histochemistry & Cytochemistry*, 36, 807-810.
- GEUZE, H. J., MURK, J. L., STROOBANTS, A. K., GRIFFITH, J. M., KLEIJMEER, M. J., KOSTER, A. J., VERKLEIJ, A. J., DISTEL, B. & TABAK, H. F. 2003. Involvement of the endoplasmic reticulum in peroxisome formation. *Molecular Biology of the Cell*, 14, 2900-2907.
- GIEPMANS, B. N. G., DEERINCK, T. J., SMARR, B. L., JONES, Y. Z. & ELLISMAN, M. H. 2005. Correlated light and electron microscopic imaging of multiple endogenous proteins using Quantum dots. *Nature Methods*, 2, 743-749.
- GLAUERT, A. M. 1965. *The fixation and embedding of biological specimens*, Oxford, Blackwell Scientific Publications.
- GLAUERT, A. M. 1975. *Fixation, dehydration and embedding of biological specimens*, Amsterdam, North Holland Publishing Company.
- GOLDSTEIN, J., NEWBURY, D., JOY, D., LYMAN, C., ECHLIN, P., LIFSHIN, E., SAWYER, L. & MICHAEL, J. 2003. *Scanning electron microscopy and X-ray microanalysis*, New York, Kluwer Academic/Plenum Press.
- GOMORI, G. 1939. Microtechnical demonstration of phosphatase in tissue sections. *Proceedings of the Society for Experimental Biology and Medicine*, 42, 23 - 26.

- GRAHAM, R. C. & KARNOVSKY, M. J. 1966. The early stages of absorption of injected horseradish peroxidase in the proximal tubules of mouse kidney: ultrastructural cytochemistry by a new technique. *Journal of Histochemistry and Cytochemistry*, 14, 291-302.
- GRAY, P. 1954. *The microtome's formulary and guide*, London, Constable and Co. Ltd.
- GREEN, M. A., SVILAND, L., MALCOLM, A. J. & PEARSON, A. D. J. 1989. Improved methods for immunoperoxidase detection of membrane antigens in frozen sections. *Journal of Clinical Pathology*, 42, 875-880.
- GU, J., DEMEY, J., MOEREMANS, M. & POLAK, J. M. 1981. Sequential use of the PAP and immunogold staining methods for the light microscopical double staining of tissue antigens - its application to the study of regulatory peptides in the gut. *Regulatory Peptides*, 1, 365-374.
- GUESDON, J. L., TERNYNCK, T. & AVRAMEAS, S. 1979. Use of avidin-biotin interaction in immunoenzymatic techniques. *Journal of Histochemistry & Cytochemistry*, 27, 1131-1139.
- GUSTAFSSON, M. G. L. 2000. Surpassing the lateral resolution limit by a factor of two using structured illumination microscopy. *Journal of Microscopy-Oxford*, 198, 82-87.
- GUSTAFSSON, M. G. L. 2005. Nonlinear structured-illumination microscopy: Wide-field fluorescence imaging with theoretically unlimited resolution. *Proceedings of the National Academy of Sciences of the United States of America*, 102, 13081-13086.
- HAINFELD, J. F. 1992. Site-specific cluster labels. *Ultramicroscopy*, 46, 135-144.
- HAINFELD, J. F. & FURUYA, F. R. 1992. A 1.4-nm gold cluster covalently attached to antibodies improves immunolabeling. *Journal of Histochemistry & Cytochemistry*, 40, 177-184.

- HALBHUBER, K. J., GOSSRAU, R., MOLLER, U., HULSTAERT, C. E., ZIMMERMANN, N. & FEUERSTEIN, H. 1988. The cerium perhydroxide-diaminobenzidine (Ce-H<sub>2</sub>O<sub>2</sub>-DAB) procedure. New methods for light microscopic phosphatase histochemistry and immunohistochemistry. *Histochemistry*, 90, 289-297.
- HALBHUBER, K. J., HULSTAERT, C. E., GERRITS, P., MOLLER, U. & KALICHARAN FEUERSTEIN, D. H. 1991. Cerium as amplifying agent - An improved cerium-perhydroxide-DAB-nickel (Ce/Ce-H<sub>2</sub>O<sub>2</sub>-DAB-Ni) method for the visualization of cerium phosphate in resin sections. *Cellular & Molecular Biology*, 37, 295-307.
- HALLBECK, R. E. 1957. Depolymerization of paraformaldehyde. *Jour Amer Soc Sugar Beet Technol*, 9, 313-315.
- HANCOCK, W. W., BECKER, G. J. & ATKINS, R. C. 1982. A comparison of fixatives and immunohistochemical techniques for use with monoclonal antibodies to cell surface antigens. *American Journal of Clinical Pathology*, 78, 825-831.
- HANKER, J. S. 1979. Osmiophilic reagents in electronmicroscopic histocytochemistry. *Progress in Histochemistry & Cytochemistry*, 12, 1-85.
- HARTLEY, W. G. 1993. *The Light Microscope. It's Use and Development.*, Oxford, Senecio Publishing Company.
- HAYAT, M. A. 1993. *Stains and cytochemical methods*, New York, Plenum Press.
- HELANDER, K. G. 2000. Formaldehyde prepared from paraformaldehyde is stable. *Biotechnic & Histochemistry*, 75, 19-22.
- HIRAMOTO, R., ENGEL, K. & PRESSMAN, D. 1958. Tetramethylrhodamine as immunohistochemical fluorescent label in the study of chronic thyroiditis. *Proceedings of the Society for Experimental Biology & Medicine*, 97, 611-614.

- HOBOT, J. A., VILLIGER, W., ESCAIG, J., MAEDER, M., RYTER, A. & KELLENBERGER, E. 1985. Shape and fine-structure of nucleoids observed on sections of ultrarapidly frozen and cryosubstituted bacteria. *Journal of Bacteriology*, 162, 960-971.
- HOLGATE, C. S., JACKSON, P., COWEN, P. N. & BIRD, C. C. 1983. Immunogold silver staining - New method of immunostaining with enhanced sensitivity. *Journal of Histochemistry & Cytochemistry*, 31, 938-944.
- HOOKE, R. 1665. *Micrographia, or, Some physiological descriptions of minute bodies made by magnifying glasses*, London, John Martyn and James Allestry.
- HORISBERGER, M. & ROSSET, J. 1977. Colloidal gold, a useful marker for transmission and scanning electron microscopy. *Journal of Histochemistry & Cytochemistry*, 25, 295-305.
- HORISBERGER, M., ROSSET, J. & BAUER, H. 1975. Colloidal gold granules as markers for cell surface receptors in the scanning electron microscope. *Experientia*, 31, 1147-1149.
- HOROWITZ, J. P., CHAU, J., NOEL, M., DONATTI, J. T. & FREISLER, J. 1966. Substrates for cytochemical demonstration of enzyme activity. II. Some dihalo-3-indoyl phosphates and sulphates. *Journal of Medical Chemistry*, 9, 449.
- HOTCHKISS, R. D. 1948. A microscopical reaction resulting in the staining of polysaccharide structures in fixed tissue preparations. *Archives of Biochemistry*, 16, 131-141.
- HOVDEN, R., XIN, H. L. & MULLER, D. A. 2011. Extended depth of field for high-resolution scanning transmission electron microscopy. *Microscopy and Microanalysis*, 17, 75-80.
- HSU, K. C., RIFKIND, R. A. & ZABRISKIE, J. B. 1963. Fluorescent, electron microscopic, and immunoelectrophoretic studies of labeled antibodies. *Science*, 142, 1471-1473.

- HSU, S. M., RAINE, L. & FANGER, H. 1981. Use of avidin-biotin-peroxidase complex (ABC) in immunoperoxidase techniques - a comparison between ABC and unlabeled antibody (PAP) Procedures. *Journal of Histochemistry & Cytochemistry*, 29, 577-580.
- HUANG, S., MINASSIAN, H. & MORE, J. D. 1976. Application of immunofluorescent staining on paraffin sections improved by trypsin digestion. *Laboratory Investigation*, 35, 383-390.
- HUANG, Z. J., YOU, W. M., HAUGLAND, R. P., PARAGAS, V. B., OLSON, N. A. & HAUGLAND, R. P. 1993. A novel fluorogenic substrate for detecting alkaline phosphatase activity insitu. *Journal of Histochemistry & Cytochemistry*, 41, 313-317.
- HUNYADY, B., KREMPELS, K., HARTA, G. & MEZEY, E. 1996. Immunohistochemical signal amplification by catalyzed reporter deposition and its application in double immunostaining. *Journal of Histochemistry & Cytochemistry*, 44, 1353-1362.
- KARNOVSKY, M. J. 1965. A formaldehyde-glutaraldehyde fixative of high osmolarity for use in electron microscopy. *Journal of Cell Biology*, 27, 137A.
- KELLENBERGER, E., CARLEMALM, E., VILLIGER, W., ROTH, J. & GARAVITO, R. M. 1980. Low denaturation embedding for electron microscopy of thin sections. Waldkraiburg, Germany: Chemische Werke Lowi GmbH.
- KIRK, S. E., SKEPPER, J. N. & DONALD, A. M. 2009. Application of environmental scanning electron microscopy to determine biological surface structure. *Journal of Microscopy-Oxford*, 233, 205-224.
- KNECHT, D. A. & DIMOND, R. L. 1984. Visualisation of antigenic proteins on western blots. *Analytical Biochemistry*, 136, 180-184.
- KNOLL, M. 1935. Aufladepotential und sekundäremission elektronenbestrahlter körper. *Zeitschrift für Technische Physik*, 16, 467-475.

- KNOLL, M. & RUSKA, E. 1932. Das elektronenmikroskop. (The electron microscope.). *Zeitschrift fur Physik*, 78, 318-339.
- KRIEG, R. & HALBHUBER, K. J. 2004. Novel oxidative self-anchoring fluorescent substrates for the histochemical localization of endogenous and immunobound peroxidase activity. *Journal of Molecular Histology*, 35, 471-487.
- KUSHIDA, H. 1961a. A new embedding method for ultrathin sectioning using a methacrylate resin with three dimensional polymer structure. *Journal of Electron Microscopy*, 10, 194-199.
- KUSHIDA, H. 1961b. A styrene-methacrylate resin embedding method for ultrathin sectioning. *Journal of Electron Microscopy*, 10, 16-19.
- LARISON, K. D., BREMILLER, R., PARAGAS, V., SINGER, V., NALEWAY, J. J. & HAUGLAND, R. P. 1993. New fluorogenic alkaline phosphatase substrate used with standard immunohistochemical methods to characterize zebrafish retinal antigens. *Faseb Journal*, 7, A1085.
- LARISON, K. D., BREMILLER, R., PARAGAS, V., SINGER, V., NALEWAY, J. J. & HAUGLAND, R. P. 1994. Elf - a new fluorogenic alkaline phosphatase substrate for immunohistochemical applications. *Faseb Journal*, 8, A903.
- LARISON, K. D., BREMILLER, R., WELLS, K. S., CLEMENTS, I. & HAUGLAND, R. P. 1995. Use of a new fluorogenic phosphatase substrate in immunohistochemical applications. *Journal of Histochemistry & Cytochemistry*, 43, 77-83.
- LE BOTLAN, D. J., MECHIN, B. G. & MARTIN, G. J. 1983. Proton and C-13 nuclear magnetic resonance spectroscopy of formaldehyde in water. *Analytical Chemistry*, 55, 587-591.
- LITWIN, J. A. 1979. Histochemistry and cytochemistry of 3,3'-diaminobenzidine. A review. *Folia Histochemica Et Cytobiologica*, 17, 3-28.
- LILLIE, R. D. 1965. *Histopathologic technic and practical histochemistry*, New York, McGraw-Hill Book Company.

- LO BUGLIO, A. F., RINEHART, J. J. & BALCERZEK, S. P. 1972. A new immunologic marker for scanning electron microscopy. *In: JOHARI, O. & CORWIN, I. (eds.) Scanning electron microscopy*. Chicago: ITT Research Institute.
- MANHEIMER, L. H. & SELIGMAN, A. M. 1948. Improvement in the method for the histochemical demonstration of alkaline phosphatase and its use in a study of normal and neoplastic tissues. *Journal of the National Cancer Institute*, 9, 181-199.
- MANN, G. 1902. *Physiological Histology*, Oxford, Clarendon Press.
- MARANTO, A. R. 1982. Neuronal mapping: a photooxidation reaction makes Lucifer yellow useful for electron microscopy. *Science*, 217, 953-955.
- MARRACK, J. 1934. Nature of antibodies. *Nature*, 133, 292-293.
- MCCLUNG, C. E. 1929. *Handbook of Microscopical Technique*, New York, Hoeber.
- MCGADEY, J. 1970. A tetrazolium method for non-specific alkaline phosphatase. *Histochemie*, 23, 180-184.
- MCMULLAN, D. 1953. An improved scanning electron microscope for opaque specimens. *Proceedings of the Institution of Electrical Engineers*, 100 Part II 245-249.
- MEKLER, L. B., KLIMENKO, S. M., DOBREZOV, G. E., NAUMOVA, V. K., HOFFMAN, Y. P. & ZHDANOV, V. M. 1964. Cytochemical and immunochemical analysis at the electron microscopy level: Obtaining contrasting antibodies by use of iodine. *Nature.*, 203, 717-719.
- MENTEN, M. L., JUNGE, J. & GREEN, M. H. 1944. A coupling histochemical azo dye test for alkaline phosphatase in the kidney. *Journal of Biological Chemistry*, 153, 471-477.
- MERRILEES, M. J., BEAUMONT, B. W. & SCOTT, L. J. 1995. Fluoroprobe quantification of viable and non-viable cells in human coronary and internal thoracic arteries sampled at autopsy. *Journal of Vascular Research*, 32, 371-377.



- MINSKY, M. 1957. *Confocal Scanning Microscope*. U.S.A. patent application.
- MOLDAY, R. S., DREYER, W. J., REMBAUM, A. & YEN, S. P. 1974. Latex spheres as markers for studies of cell surface receptors by scanning electron microscopy. *Nature*, 249, 81-82.
- MOLDAY, R. S. & MAHER, P. 1980. A review of cell surface markers and labelling techniques for scanning electron microscopy. *Histochemical Journal*, 12, 273-315.
- MUJUMDAR, R. B., ERNST, L. A., MUJUMDAR, S. R. & WAGGONER, A. S. 1989. Cyanine dye labeling reagents containing isothiocyanate groups. *Cytometry*, 10, 11-19.
- MULLINK, H., VOS, W., JIWA, M., HORSTMAN, A., VANDERVALK, P., WALBOOMERS, J. M. M. & MEIJER, C. 1992. Application and comparison of silver intensification methods for the diaminobenzidine and diaminobenzidine nickel end-product of the peroxidation reaction in immunohistochemistry and insitu hybridization. *Journal of Histochemistry & Cytochemistry*, 40, 495-504.
- NAKANE, P. K. & PIERCE, G. B., JR. 1967. Enzyme-labeled antibodies for the light and electron microscopic localization of tissue antigens. *Journal of Cell Biology*, 33, 307-318.
- NATION, J. L. 1983. A new method using hexamethyldisilazane for preparation of soft insect tissues for scanning electron microscopy. *Stain Technology*, 58, 347-351.
- NEISS, W. F. 1988. Enhancement of the periodic acid-schiff (PAS) and periodic acid-thiocarbohydrazide-silver proteinate (PA-TCH-SP) reaction in LR White sections. *Histochemistry*, 88, 603-612.
- NEWMAN, G. R. & HOBOT, J. A. 1987. Modern acrylics for post - embedding immunostaining techniques. *Journal of Histochemistry and Cytochemistry*, 35, 971-981.

- NEWMAN, G. R. & HOBOT, J. A. 2001. *Resin microscopy and on-section immunocytochemistry*, Springer-Verlag.
- NEWMAN, G. R. & JASANI, B. 1998a. Silver development in microscopy and bioanalysis: A new versatile formulation for modern needs. *Histochemical Journal*, 30, 635-645.
- NEWMAN, G. R. & JASANI, B. 1998b. Silver development in microscopy and bioanalysis: Past and present. *Journal of Pathology*, 186, 119-125.
- NEWMAN, G. R., JASANI, B. & WILLIAMS, E. D. 1982. The preservation of ultrastructure and antigenicity. *Journal of Microscopy*, 127, RP5-RP6.
- NEWMAN, G. R., JASANI, B. & WILLIAMS, E. D. 1983a. A simple post-embedding system for the rapid demonstration of tissue antigens under the electron microscope. *Histochemical Journal*, 15, 543-555.
- NEWMAN, G. R., JASANI, B. & WILLIAMS, E. D. 1983b. Metal compound intensification of the electron density of diaminobenzidine. *Journal of Histochemistry & Cytochemistry*, 31, 1430-1434.
- NEWMAN, G. R., JASANI, B. & WILLIAMS, E. D. 1983c. The visualization of trace amounts of diaminobenzidine (DAB) polymer by a novel gold-sulfide-silver method. *Journal of Microscopy-Oxford*, 132, RP1-RP2.
- NEWMAN, J. B., BORYSKO, E. & SWERDLOW, M. 1949. New sectioning techniques for light and electron microscopy. *Science*, 110, 66-68.
- NICHOLSON, G. L., BLAUSTEIN, J. & ETZLER, M. E. 1974. Characterisation of two plant lectins from *Ricinus communis* and their quantitative interaction with a murine lymphoma. *Biochemistry* 13 196-204.
- NIPKOW, P. 1884. Germany patent application.
- NORMASKI, G. & WEILL, A. R. 1954. Sur l'observation des figures de croissance des cristaux par les methodes interferentielles a des ondes. *Bulletin de la Societe Francaise Mineralogie et de Cristallographie*, 77, 840-868.

- OAKLEY, C. L. 1937. Frozen sections of eyes. *Journal of Pathology and Bacteriology*, 44, 365-368.
- OHTSUKI, I., MANZI, R. M., PALADE, G. E. & JAMIESON, J. D. 1978. Entry of macromolecular tracers into cells fixed with low concentrations of aldehydes. *Biologie Cellulaire*, 31, 119-126.
- PALADE, G. E. 1952. A study of fixation for electron microscopy. *Journal of Experimental Medicine*, 95 285-298.
- PANCHUK-VOLOSHINA, N., HAUGLAND, R. P., BISHOP-STEWART, J., BHALGAT, M. K., MILLARD, P. J., MAO, F., LEUNG, W.-Y. & HAUGLAND, R. P. 1999. Alexa dyes, a series of new fluorescent dyes that yield exceptionally bright, photostable conjugates. *Journal of Histochemistry & Cytochemistry*, 47, 1179-1188.
- PAPANICOLAOU, G. N. & TRAUT, H. F. 1941. The diagnostic value of vaginal smears in carcinoma of the uterus. *American Journal of Obstetrics and Gynecology*, 42, 193-206.
- PEARCE, A. G. E. 1972. *Histochemistry. Theoretical and Applied*, Churchill Livingstone.
- PEPE, F. A. 1961. The use of specific antibody in electron microscopy. I. Preparation of mercury-labeled antibody. *Journal of Biophysical & Biochemical Cytology*, 11, 515-520.
- PETTRAN, M., HADRAVSKY, M., BENES, J. & KUCERA, R. 1985. The tandem scanning reflected light microscope. Part 1 - the principle, and its design. *Proceedings of the Royal Microscopical Society*, 20, 125-129.
- PETTRAN, M., HADRAVSKY, M., EGGER, M. D. & GALAMBOS, R. 1968. Tandem scanning reflected-light microscope. *Journal of the Optical Society of America*, 58, 661-664.

- PLASEK, J. & SIGLER, K. 1996. Slow fluorescent indicators of membrane potential: A survey of different approaches to probe response analysis. *Journal of Photochemistry and Photobiology B-Biology*, 33, 101-124.
- POPE, R. & SCHEETZ, R. W. 1990. Dynamic events related to humidity changes on botanical samples imaged with the environmental SEM. *Scanning*, 12, I38-I40.
- POSTEK, M. T. & VLADAR, A. E. 2008. Helium ion microscopy and its application to nanotechnology and nanometrology. *Scanning*, 30, 457-462.
- POWELL, R. D., HALSEY, C. M. R. & HAINFELD, J. F. 1998. Combined fluorescent and gold immunoprobes: Reagents and methods for correlative light and electron microscopy. *Microscopy Research and Technique*, 42, 2-12.
- POWELL, R. D., HALSEY, C. M. R., SPECTOR, D. L., KAURIN, S. L., MCCANN, J. & HAINFELD, J. F. 1997. A covalent fluorescent-gold immunoprobe: Simultaneous detection of a pre-mRNA splicing factor by light and electron microscopy. *Journal of Histochemistry & Cytochemistry*, 45, 947-956.
- PRZEPIORKA, D. & MYERSON, D. 1986. A single-step silver enhancement method permitting rapid diagnosis of cytomegalovirus-infection in formalin-fixed, paraffin-embedded tissue-sections by insitu hybridization and immunoperoxidase Detection. *Journal of Histochemistry & Cytochemistry*, 34, 1731-1734.
- REN, Y., DONALD, A. M. & ZHANG, Z. 2008. Investigation of the morphology, viability and mechanical properties of yeast cells in environmental SEM. *Scanning*, 30, 435-442.
- RICHARDSON, K. C. 1961. Formalin-osmium tetroxide fixation of nuclei, tracts or discrete regions in the central nervous system for electron microscopy. *Anatomical Record*, 139, 333.

- RICHARDSON, K. C., JARETT, L. & FINKE, E. H. 1960. Embedding in epoxy resins for ultrathin sectioning in electron microscopy. *Stain Technology*, 35, 313-323.
- RIEMERSMA, J. C. 1968. Osmium tetroxide fixation of lipids for electron microscopy. A possible reaction mechanism. *Biochimica et Biophysica Acta*, 152, 718-727.
- ROBERTSON, J. D., STAGE, D. E. & BODENHEIMER, T. S. 1963. Ultrastructure of mauthner cell synapses and nodes in goldfish brains. *Journal of Cell Biology*, 19, 159-199.
- RODENBURG, C., LIU, X., JEPSON, M. A. E., ZHOU, Z., RAINFORTH, W. M. & RODENBURG, J. M. 2010. The role of helium ion microscopy in the characterisation of complex three-dimensional nanostructures. *Ultramicroscopy*, 110, 1178-1184.
- RUST, M. J., BATES, M. & ZHUANG, X. 2006. Sub-diffraction-limit imaging by stochastic optical reconstruction microscopy (STORM). *Nature Methods*, 3, 793-795.
- RYTER, A., KELLENBERGER, E., BIRCHANDERSEN, A. & MAALOE, O. 1958. [Electron microscopic study on plasmas containing desoxyribonucleic acid. I. Nucleoids of actively growing bacteria.]. *Zeitschrift fur Naturforschung - Teil B - Anorganische Chemie, Organische Chemie, Biochemie, Biophysik, Biologie*, 13B, 597-605.
- SABATINI, D. D., BENSCH, K. G. & BARNETT, R. J. 1963. Cytochemistry and electron microscopy. The preservation of cellular ultrastructure and enzymatic activity by aldehyde fixation. *Journal of Cell Biology*, 17, 19-58.
- SAYRE, L. M., PERRY, G., HARRIS, P. L. R., LIU, Y. H., SCHUBERT, K. A. & SMITH, M. A. 2000. In situ oxidative catalysis by neurofibrillary tangles and senile plaques in Alzheimer's disease: A central role for bound transition metals. *Journal of Neurochemistry*, 74, 270-279.

- SCHMID, K. W., HITTMAIR, A., SCHMIDHAMMER, H. & JASANI, B. 1989. Non-deleterious inhibition of endogenous peroxidase activity (EPA) by cyclopropanone hydrate - a definitive approach. *Journal of Histochemistry & Cytochemistry*, 37, 473-477.
- SCHWARTZ, C. L., SARBASH, V. I., ATAULLAKHANOV F. I., MCINTOSH, J. R. & NICASTRO, D. 2007. Cryo-fluorescence microscopy facilitates correlations between light and cryo-electron microscopy and reduces the rate of photobleaching. *Journal of Microscopy*, 227, 99-109.
- SELIGMAN, A. M., HANKER, J. S., WASSERKRUG, H., DMOCHOWSKI, H. & LATZOFF, L. 1965. Histochemical demonstration of some oxidised macromolecules with thiocarbohydrazide (TCH) or thiosemicarbazide (TSH) and osmium tetroxide. *Journal of Histochemistry and Cytochemistry*, 13, 629-639.
- SELIGMAN, A. M., HEYMAN, H. & BARNETT, R. J. 1954. The histochemical demonstration of alkaline phosphatase activity with indoxyl phosphate. *Journal of Histochemistry and Cytochemistry*, 2, 441-442.
- SELIGMAN, A. M., KARNOVSKY, M. J., WASSERKRUG, H. L. & HANKER, J. S. 1968. Nondroplet ultrastructural demonstration of cytochrome oxidase activity with a polymerising osmiophilic reagent, diaminobenzidine (DAB). *Journal of Cell Biology*, 38, 1-14.
- SHI, S. R., KEY, M. E. & KALRA, K. L. 1991. Antigen retrieval in formalin-fixed, paraffin-embedded tissues - an enhancement method for immunohistochemical staining based on microwave-oven heating of tissue sections. *Journal of Histochemistry & Cytochemistry*, 39, 741-748.
- SIEGISMUND, K. A., YORDE, D. E. & DRAGEN, R. 1979. A quantitative immunoperoxidase procedure employing energy dispersive X-ray analysis. *Journal of Histochemistry & Cytochemistry*, 27, 1226-1230.
- SILVA, M. T., GUERRA, F. C. & MAGALHAES, M. M. 1968. The fixative action of uranyl acetate in electron microscopy. *Experientia*, 24 1074.

- SINGER, S. J. 1959. Preparation of an electron-dense antibody conjugate. *Nature*, 183, 1523-1524.
- SOLIGO, D., POZZOLI, E., NAVA, M. T., POLLI, N., LAMBERTENGHIDELILIERI, G. & DEHARVEN, E. 1983. Cytochemical methods for the backscattered electron imaging mode of scanning electron-microscopy - further applications to the study of human-leukemic cells. *Scanning Electron Microscopy*, 1795-1802.
- SOUTHERN, E. M. 1974. An improved method for transferring nucleotides from electrophoresis strips to thin layers of ion-exchange cellulose. *Analytical Biochemistry*, 62, 317-318.
- SOUTHERN, E. M. 1975. Detection of specific sequences among DNA fragments separated by gel electrophoresis. *Journal of Molecular Biology*, 98, 503-517.
- SPURR, A. R. 1969. A low-viscosity epoxy resin embedding medium for electron microscopy. *Journal of Ultrastructure Research*, 26, 31-43.
- STAGE, D. E. & AVRAMEAS, S. 1976. Detection of anti-TNP antibody-forming cells (AFC) with TNP-enzyme and TNP-Fab anti-enzyme conjugates. *Journal of Immunological Methods*, 10, 105-118.
- STEEDMAN, H. F. 1950. Alcian Blue 8GS: A new stain for mucin. *Quarterly Journal of Microscopical Sciences*, 91, 447-449.
- STEEDMAN, H. F. 1960. Ester wax 1960: a histological embedding medium. *Quarterly Journal of Microscopical Science*, 101, 459-462.
- STERNBERGER, L. A., DONATTI, J. T. & WILSON, C. E. 1963. Electron microscopic study on specific protection of isolated *Bordetella Bronchiseptica* antibody during exhaustive labelling with uranium. *Journal of Histochemistry and Cytochemistry*, 11, 48-58.
- STRANGWAYS, T. S. P. & CANTI, R. G. 1927. The living cell in vitro as shown by dark-ground illumination and the changes induced in such cells by fixing reagents. *Quarterly Journal of Microscopical Sciences*, 71, 1-14.

- STRUTT, J. W. I. L. R. 1879. Investigations in optics, with special reference to the spectroscope. *Philosophical Magazine*, VIII 261, 403 and 477
- TANIMORI, H., ISHIKAWA, F. & KITAGAWA, T. 1983. A sandwich enzyme-immunoassay of rabbit immunoglobulin-G with an enzyme labeling method and a new solid support. *Journal of Immunological Methods*, 62, 123-131.
- THEIRY, J.-P. 1967. Mise en évidence des polysaccharides sur coupes fines en microscopie électronique. *Journal of Microscopy (Paris)*, 6, 987-1018.
- THIEL, B. L. & DONALD, A. M. 1998. In situ mechanical testing of fully hydrated carrots (*Daucus carota*) in the environmental SEM. *Annals of Botany*, 82, 727-733.
- VAN BELLE, H. 1972. Kinetics and inhibition of alkaline phosphatases from canine tissues. *Biophysica et Biochimica Acta*, 289, 158-168.
- VEITCH, N. C. 2004. Horseradish peroxidase: a modern view of a classic enzyme. *Phytochemistry*, 65, 249-259.
- VON RUHLAND, C. J. & NEWMAN, G. R. 2001. A cytochemical method for visualising blood vessels selectively in semithin LR White sections. *Histochemical Journal*, 33, 433-435.
- WALDEYER, H. W. G. 1863. Untersuchungen über den Ursprung und den Verlauf des Achsenzylinders bei wirbellosen und Wirbeltieren, sowie über dessen Endverhalten in der quergestreiften Muskelfaser. *Zeitschrift für rationelle Medizin*, 20, 193-256.
- WARD, B. W., NOTTE, J. A. & ECONOMOU, N. P. 2006. Helium ion microscope: A new tool for nanoscale microscopy and metrology. *Journal of Vacuum Science & Technology B*, 24, 2871-2874.
- WARD, H. A., YAMANA, S., PIHL, E. & NAIRN, R. C. 1973. Ultrastructural localisation of antilymphocyte globulin on viable lymphocytes by immunoperoxidase technique. *Immunology*, 23, 61-68.



- WASSLER, M., JONASSON, I., PERSSON, R. & FRIES, E. 1987. Differential permeabilisation of membranes by saponin treatment of isolated rat hepatocytes - release of secretory proteins. *Biochemical Journal*, 247, 407-415.
- WESTPHAL, V., RIZZOLI, S. O., LAUTERBACH, M. A., KAMIN, D., JAHN, R. & HELL, S. W. 2008. Video-rate far-field optical nanoscopy dissects synaptic vesicle movement. *Science*, 320, 246-249.
- WILLIAMS, D. B. & CARTER, C. B. 1996a. *Transmission electron microscopy: a textbook for material scientists*, New York, Plenum Press.
- WILLIG, K. I., RIZZOLI, S. O., WESTPHAL, V., JAHN, R. & HELL, S. W. 2006. STED microscopy reveals that synaptotagmin remains clustered after synaptic vesicle exocytosis. *Nature*, 440, 935-939.
- WOLDRINGH, C. L. 1973. Effects of cations on the organisation of the nucleoplasm in *Escherichia coli* prefixed with osmium tetroxide or glutaraldehyde. *Cytobiologie*, 8, 97-111.
- ZERNIKE, F. 1935. Das phasenkontrastverfahren bei der mikroskopischen beobachtung. *Zeitschrift für Technische Physik*, 16, 454-457.
- ZWORYKIN, V. A., HILLIER, J. & SNYDER, R. L. 1942. A scanning electron microscope. *ASTM Bulletin*, 117, 15-23.

# **Chapter 2**

## **The Amplification of PolyDAB with Physical Developers**

## 2.1 Introduction

The requirement for demonstrating ever smaller quantities of target molecules in biological research and clinical diagnosis has led to the development of a number of powerful techniques, namely (1) primary probe amplification, (2) target retrieval, (3) reporter amplification and (4) marker amplification.

The first three have been much more easily incorporated into high throughput, automated laboratories since standardisation, and hence quality control, are easily achieved by manipulating concentrations of reagents or staining times. Marker amplification, in contrast, requires observation of the final staining procedure to identify the appropriate endpoint of the reaction i.e. where background staining just starts to arise.

Intensification and amplification are two terms that have been used interchangeably for describing techniques that increase marker visibility. For the purpose of this thesis, a distinction will be drawn between the two, namely that intensification involves manipulation of the marker's optical properties (usually extinction coefficient and/or absorption spectrum), whereas amplification involves the deposition of additional marker at the site of the initial reaction.

The former is usually achieved by either modifying the marker once it has been deposited e.g. the conversion of the pale blue cobalt phosphate substitution product of tissue alkaline phosphatase activity to black cobalt sulfide (Gomori, 1939) or by incorporating additional chromogenic components into the reaction mixture, such as the coupling of tetrazolium reduction to indolyl dimerisation for the histochemical demonstration of tissue non-specific esterases (McGadey, 1967).

The latter usually exploits catalytic properties of the initial marker to facilitate localised deposition of secondary marker. An early example is the cobalt-sulfide-

silver technique (Tyrer and Bell, 1974) which combined the cobalt-sulfide method for visualising neurones (Pitman et al., 1972) with the observation, by the German chemist Timm, that sulfides were much more powerful catalysts of silver reduction than their non-sulfide counterparts (Timm, 1958). This development facilitated the observation of the finest neurones that were previously almost impossible to distinguish against the background tissue.

The 'Timm reaction', described above, was subsequently applied in a number of histochemical contexts and was further refined to selectively demonstrate metals in biological tissue (Danscher, 1981a; 1984, Danscher and Stoltenberg, 2006). It was the exploitation of this latter technique, for specifically visualising gold in biological tissue (Danscher, 1981b), that led to the development of the successful immunocolloidal gold-silver method (Holgate et al., 1983). Prior to this, both primary antibodies and secondary antibody-colloidal gold conjugates needed to be applied in high concentrations for the colloidal gold marker to be directly visible (Gu et al., 1981). It is, however, the peroxidase/DAB system that has received the greatest interest in terms of both intensification and amplification. The probable reason for this is that the reaction, while rapid, is subject to product inhibition, unlike alkaline phosphatase.

### **2.1.1 Intensification of PolyDAB with d-Block Metal Salts**

In the late 1970s and early 1980s, the effects of d-block metal compounds on the appearance of polyDAB was recognised and exploited in light microscopy to produce either an intensification of colour (Hanker et al., 1979), or a profound colour change (Adams, 1977; 1981; Hancock, 1982). These observations prompted

further studies to evaluate this phenomenon, albeit to a limited extent (Hsu and Soban, 1982; Scopsi and Larsson, 1986).

### **2.1.2 Amplification of PolyDAB with Physical Developers**

The observation that polyDAB could catalyse silver reduction from a physical developer (Gallyas et al., 1982) led to the examination of this phenomenon following polymerisation of DAB in the presence of d-block metal salts (Przepiorka and Myerson, 1986; Gallyas and Merchenthaler, 1988; Green et al., 1989; Mullink et al., 1992).

The high affinity of polyDAB for  $\text{Au(III)Cl}_4^-$  (Siegesmund et al., 1979) in combination with the Timm reaction led to the development of the powerful gold-sulfide-silver amplification technique (Newman et al., 1983b). In none of these studies, however, was an extensive range of commercially available d-block metal salts systematically explored.

Any investigation of the interaction of d-block metal compounds with polyDAB is complicated by the availability of innumerable d-block metal complexes. In addition, the absence of either detailed chemistry concerning the polymerisation of DAB or its interaction with d-block metal salts renders such studies necessarily empirical. Furthermore, some d-block metal salts are either insoluble or unstable in aqueous solutions, or are radioactive. Finally, DAB needs to be strongly buffered at neutral pH for it to work successfully as a histochemical marker and some d-block metal salts are incompatible with these solutions, such as the chlorides of copper and palladium with Tris buffered DAB (Hsu and Soban, 1982).

Some d-block metal salts will be stable, albeit at very low concentrations, with DAB in neutral buffered solutions and can therefore be included in the reaction (pre-polymerisation). Some of those salts, which are not tolerated by such solutions of DAB, will react with the polymerised product after the reaction is complete (post-polymerisation), and some will do both.

### **2.1.3 Amplification in Diagnostic Immunohistochemistry**

Since the demonstration of the potential value of immunohistochemical staining in diagnostic pathology (Pearse and Bussolati, 1970), it has become an invaluable tool for both the diagnosis and staging of a wide variety of diseases (Mason and Gatter, 1987; Idikio, 2010). In particular, it provides predictive information regarding the progression of breast cancers and thus informs the delivery of appropriate therapy (Walker, 2008).

Marker amplification has enjoyed a number of successes in diagnostic immunohistochemistry, such as the demonstration of the thyroid stimulating hormone receptor on normal thyroid follicular cells (Schmid and Jasani, 1987), and both the oestrogen receptor in breast tumours (Gee et al., 1991) and Epstein-Barr virus DNA in lymph nodes (Mullink et al., 1992) in paraffin wax-embedded tissue, but has received progressively less interest over the last two decades due to the greater ease with which target retrieval and reporter amplification have been incorporated into high through-put, automated laboratories. There remain, however, a number of instances where additional amplification still has some utility, namely (1) where antigenic concentration is low and, even with the full power of target retrieval and reporter amplification, positivity is uncertain, and (2) where immunopositive events are rare and could be easily overlooked. Examples of

the former include the Epstein-Barr virus antigen, LMP-1 and the T-cell enzyme, granzyme B. An example of the latter is  $\alpha$ -synuclein, a marker of neurodegenerative disease.

#### **2.1.3.1 Epstein-Barr Virus and LMP-1**

Epstein-Barr virus (EBV) is a human herpes virus that occurs, asymptotically, in 90% of the human population. Initial inoculation results in infected cells, probably B-lymphocytes (antigen-producing cells), entering a lytic phase where viruses are produced and released by budding of the cell membrane. Following this, infected B-lymphocytes enter a latent phase where proliferation occurs, the condition manifesting as mononucleosis, which occurs in 50% of individuals that are infected during adolescence and early adulthood (Pai and Khanna, 2001; Young, 2001; Rickinson, 2002). It is also associated with a number of B-cell cancers, including Burkitt's lymphoma (Levy and Henle, 1966; Henle et al., 1968), some cases of Hodgkin's lymphoma (Johansson et al., 1970), and lymphoid tumours that can arise in immunosuppressed patients (Nalesnik, 1990) as well as epithelial cell cancers such as nasopharyngeal carcinoma (Henle and Henle, 1970).

The EBV-derived latent membrane protein, LMP-1, is essential to the induction and maintenance of B-lymphocyte transformation and proliferation (Wang et al., 1985; Kaye et al., 1993) and thus provides a useful target for immunohistochemical staining. Comparisons with alternative techniques, such as *in situ* hybridisation of EBV early RNAs and polymerase chain reaction (Lauritzen et al., 1994; Fanaian et al., 2009), have suggested that IHC is the least sensitive.

### **2.1.3.2 T-cells and Granzyme B**

Cytotoxic T-lymphocytes (CTLs) and natural killer (NK) cells induce apoptosis and lysis in target cells such as those infected with viruses and those of allografts. Cytoplasmic granules within CTLs and NK cells contain a variety of cytolytic molecules including perforin (Lichtenheld et al., 1988), proteoglycans (Schmidt et al., 1985) and serine esterases (Hameed et al., 1988), the latter often being referred to as granzymes. The production of antibodies to granzyme B facilitated the immunohistochemical demonstration of CTLs in tissue (Hameed et al., 1991) which has been of predictive value in acute allograft rejection (Israelbiet et al., 1993; Legrosmaida et al., 1994; D'Errico et al., 2003).

### **2.1.3.3 Neurodegenerative Diseases and $\alpha$ -Synuclein**

The principle histological features of the common neurodegenerative diseases are the presence of proteinaceous deposits that occur both between cells, as plaques, and as cytoplasmic inclusions. In Alzheimer's disease, the most common neurodegenerative disorder, intercellular plaques are composed predominantly of amyloid (Margolis, 1959; Terry et al., 1964). Intracellular inclusions, in the form of neurofibrillary tangles, consist of tau protein (Brion et al., 1985). In Parkinson's disease, and a number of rarer conditions, the defining histological feature is the presence of intracellular Lewy bodies which are composed mainly of  $\alpha$ -synuclein (Spillantini et al., 1997). Synucleins are found in abundance in the brain, but their function is poorly understood;  $\alpha$ - and  $\beta$ -synucleins are concentrated in the nerve terminal and may be involved in the control of vesicular transport processes (Goedert, 2001), whereas  $\gamma$ -synuclein is found mainly in peripheral and sensory



nerves, throughout the nerve cell body and may be involved in microtubule function (Zhang et al., 2011).

#### **2.1.4 Amplification of Alkaline Phosphatase Markers**

The literature appears to contain no references to alkaline phosphatase (AP) marker amplification. The reason is probably two-fold, namely (1) AP is not appreciably inhibited by its insoluble products and (2) the commonly employed immunohistochemical AP marker, NBT formazan, (McGadey, 1970), has not been reported to form metal complexes, discouraging investigation with subsequent application by either physical development alone or in a Timm-style reaction. A number of formazans do, however, form d-block metals complexes such as diphenylthiocarbazone (dithizone) and its di- $\beta$ -naphthyl analogue (Oesper and Klingenberg, 1948; Nineham, 1955). In addition, the observation that the formazan of 3-(4,5-dimethylthiazolyl-2)-2,5-diphenyl tetrazolium (MTT) formed more insoluble complexes with nickel, cobalt and copper (Hunter and Roberts, 1941), prompted its successful application in a histochemical setting (Pearse, 1957).

#### **2.1.5 Model Systems**

##### **2.1.5.1 Dot Blot Model System**

Prior to an investigation of polyDAB amplification in an immunohistochemical setting, it is convenient to conduct preliminary studies in a simpler model system, since this avoids the necessity of cutting, rehydrating and immunohistochemically staining tissue sections. Polyvinylidene difluoride (PVDF) membrane is used extensively in Western and Northern blotting techniques, for immobilising electrophoretically separated proteins and nucleic acids respectively, by virtue of hydrophobic

interactions (Pluskal et al., 1986). Its high retention of these polymers makes it an ideal substrate for immobilising antibody-enzyme conjugates for subsequent marker deposition and amplification experiments.

#### **2.1.5.2 The Tonsil Tissue Model System**

One of the most commonly used tissue models for developing novel immunohistochemical marker systems is palatine tonsil, since routine tonsillectomy has ensured its regular supply. The paired palatine tonsils are part of a group of secondary lymphoid organs that form a ring around the pharynx; the Waldeyer-Pirogov tonsillar ring (Waldeyer, 1884) or pharyngeal lymphoid ring. The tonsils are composed of a surface layer of epithelial cells that invaginates to form the lymphoepithelium of the tonsillar crypts, sub-epithelial lymphoid tissue, composed of lymphoid follicles and interfollicular regions, and supporting connective tissue (figure 2.1). The lymphoepithelium has a honeycomb of epithelial cells filled mainly with lymphocytes. Continuous with this is the mantle zone where T-cells are found. B-cell maturation occurs in the follicles (figure 2.2). The tonsils provide the first line of defence against oral and inhaled bacteria and viruses (Perry and Whyte, 1998).

Of the many lymphocyte antigens that can be demonstrated in the tonsil, CD45 represents a particularly good target, since it constitutes up to 10% of the lymphocyte cell surface (Thomas and Lefrancois, 1988). CD45 is a receptor-like protein tyrosine phosphatase which occurs in a number of isoforms, and controls cellular sensitivity to external stimuli by altering the relative threshold of response. Perturbation of this function may contribute to autoimmunity, immunodeficiency, and malignancy (Hermiston et al., 2003). The 8 isoforms of CD45 result from alternative slicing of the 3 exons, labelled A, B, and C (Streuli et al., 1987).

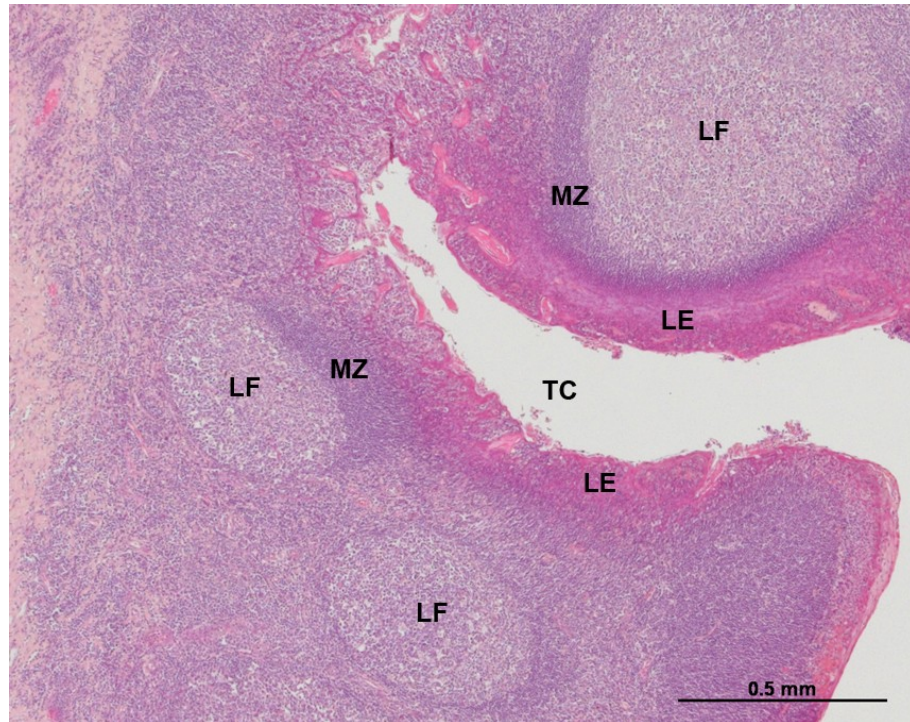


Figure 2.1. Low power image of a 4  $\mu$ m thick section of paraffin wax-embedded human palatine tonsil, stained with H&E, showing lymphoepithelium (LE), tonsillar crypt (TC), lymphoid follicles (LF) and mantle zone (MZ).

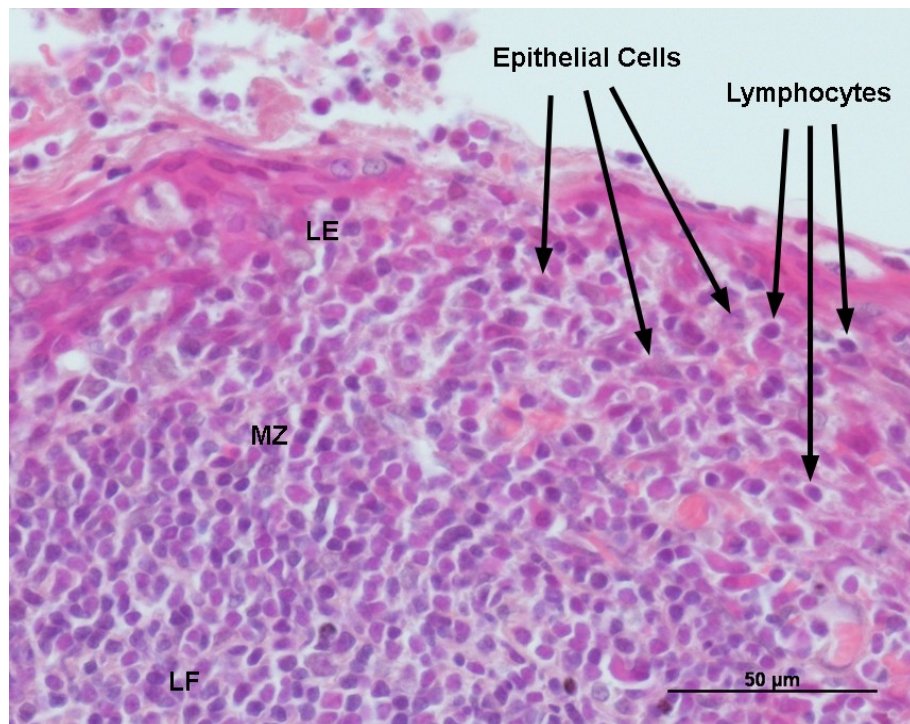


Figure 2.2. High power image of the same section, showing lymphoepithelium (LE), lymphoid follicles (LF) and mantle zone (MZ).

## 2.2 Materials

### 2.2.1 Reagents

All reagents were of analytical grade.  $\text{Na}_2\text{S}$ ,  $\text{Ni(II)Cl}_2 \cdot 6\text{H}_2\text{O}$  and  $\text{Mn(II)Cl}_2 \cdot 4\text{H}_2\text{O}$  were purchased from BDH (Lutterworth, Leicestershire, U.K.).  $\text{Cu(II)Cl}_2 \cdot 2\text{H}_2\text{O}$ , sodium acetate, glacial acetic acid, Triton X-100, hydroquinone, tris(hydroxymethyl)aminomethane (Tris), citric acid, sodium citrate, sodium thiosulfate, pyrogallol, polyethylene glycol (PEG), glycerol, ethanol and xylene were purchased from Fisher Scientific (Loughborough, Leicestershire, U.K.). 3,3'-diaminobenzidine tetrahydrochloride (DAB) (5-bromo-4-chloro-3-indolyl phosphate (BCIP), 3-(4,5-dimethylthiazolyl-2)-2,5-diphenyl tetrazolium (MTT),  $\text{Sc(III)Cl}_3 \cdot 6\text{H}_2\text{O}$ ,  $\text{Y(III)Cl}_3 \cdot 6\text{H}_2\text{O}$ ,  $\text{La(III)Cl}_3 \cdot 7\text{H}_2\text{O}$ ,  $\text{V(III)Cl}_3$ ,  $\text{Cr(II)Cl}_2$ ,  $\text{Cr(III)Cl}_3 \cdot 6\text{H}_2\text{O}$ ,  $\text{H}_3\text{PMo(IV)}_{12}\text{O}_{40} \cdot \text{hydrate}$  ( $x\text{H}_2\text{O}$ ),  $\text{H}_3\text{PW(IV)}_{12}\text{O}_{40} \cdot x\text{H}_2\text{O}$ ,  $\text{Na}_2\text{W(VI)O}_4 \cdot 2\text{H}_2\text{O}$ ,  $\text{Re(III)Cl}_3$ ,  $\text{Fe(II)Cl}_2 \cdot 4\text{H}_2\text{O}$ ,  $\text{Fe(III)Cl}_3 \cdot 6\text{H}_2\text{O}$ ,  $\text{Ru(III)Cl}_3$ ,  $\text{K}_3\text{Ru(III)Cl}_6$ ,  $\text{K}_2\text{Os(IV)Cl}_6$ ,  $\text{Co(II)Cl}_2 \cdot 6\text{H}_2\text{O}$ ,  $\text{Rh(III)Cl}_3 \cdot x\text{H}_2\text{O}$ ,  $\text{Ir(IV)Cl}_4 \cdot x\text{H}_2\text{O}$ ,  $\text{K}_3\text{Ir(III)Cl}_6$ ,  $\text{K}_2\text{Ir(IV)Cl}_6$ ,  $\text{K}_2\text{Pd(II)Cl}_4$ ,  $\text{K}_2\text{Pd(IV)Cl}_6$ ,  $\text{K}_2\text{Pt(II)Cl}_4$ ,  $\text{K}_2\text{Pt(VI)Cl}_6$ ,  $\text{Ag(I)NO}_3$ ,  $\text{NaAu(III)Cl}_4$  and  $\text{Zn(II)Cl}_2$  were purchased from Sigma-Aldrich (Poole, Dorset, U.K.).  $\text{Os(VIII)O}_4$  was purchased from TAAB Laboratories (Aldermaston, Berkshire, and U.K.). Chlorides of titanium, zirconium, hafnium, niobium, and tantalum were omitted from the study due to insolubility or instability in aqueous solution. Chlorides of cadmium and mercury were omitted because of toxicity. Technetium was omitted, as it is radioactive. Target retrieval solution, Tris wash buffer, Dako antibody diluent, peroxidase block were purchased from Dako (Ely,

Cambridgeshire, U.K.), Haematoxylin was purchased from Menarini Diagnostics (Wokingham, Berkshire, U.K.).

### **2.2.2 Antibodies**

Mouse monoclonal anti-CD45Ro (clone UCHL-1), goat anti-mouse immunoglobulin (Ig) HRP conjugate (GAM IgPC) and goat anti-mouse Ig alkaline phosphatase conjugate (GAM IgAP) were purchased from Autogen Bioclear (Calne, Wiltshire, U.K.). Goat anti-mouse Ig – 5nm colloidal gold conjugate (GAM IgCG5) was prepared in-house by Dr. Jan Hobot (Slot and Geuze, 1985). Mouse anti-LMP-1, anti-granzyme B and Envision detection system (including DAB+ chromagen and substrate buffer) were supplied by Dako (Ely, Cambridgeshire, U.K.). Mouse monoclonal anti- $\alpha$ -synuclin was purchased from Novocastra Laboratories Ltd (Newcastle upon Tyne, U. K.).

### **2.2.3 Physical Developers**

The two physical developers that were chosen for use in the amplification of polyDAB were those of Gallyas, and Newman and Jasani (Gallyas, 1979; Newman and Jasani, 1998), since their compositions have been published, they are both easy to prepare, both are light insensitive and are thus suitable for use under ordinary laboratory conditions. All glassware used for preparing and storing solutions was cleaned sequentially with chromic acid (20% w/v potassium dichromate in 20% sulfuric acid), 0.1M HCl and double distilled water (ddH<sub>2</sub>O). In both preparations, solution of each component was ensured prior to addition of the next.

### **2.2.3.1 Gallyas' Physical Developer**

Gallyas' physical developer was prepared for use at a final pH of 5.0.

#### **Solution A**

11.25 g sodium acetate trihydrate was dissolved in 150 ml ddH<sub>2</sub>O and 1.875 ml glacial acetic acid added with stirring. 0.25 g Ag(I)NO<sub>3</sub> was added followed by 7.5 ml 1% Triton X-100. The resulting solution was made up to 200 ml with ddH<sub>2</sub>O and stored at 4°C.

#### **Solution B**

5% (w/v) sodium(VI)tungstate in ddH<sub>2</sub>O (stored at RT)

#### **Solution C** (prepared immediately prior to use)

0.8% hydroquinone in ddH<sub>2</sub>O.

The three solutions are combined in order in the ratio of 8:1:1, immediately before use (Gallyas, 1979).

### **2.2.3.2 Newman and Jasani's Physical Developer**

The two components of Newman and Jasani's physical developer have a shelf lives of at least 10 years when stored at 4°C (von Ruhland and Jasani, 2010) and are thus conveniently prepared as 1 litre solutions.

#### **Silver stock solution**

181.5 g Tris base was dissolved in 750 ml ddH<sub>2</sub>O followed by 3.0 g Ag(I)NO<sub>3</sub> and glacial acetic acid added to a final pH of 7.4. The solution was made up to 1 l with ddH<sub>2</sub>O and stored at 4°C.

#### **Reducer stock solution**

The reducer stock is prepared initially as two solutions.

### **Solution A**

5.25 g citric acid monohydrate was dissolved in 350 ml ddH<sub>2</sub>O and 5.00 g anhydrous sodium sulfite added, followed by 1.25 g sodium thiosulfate pentahydrate, 15.00 g pyrogallol and 100.00 g polyethylene glycol 1500. Sodium citrate dihydrate was added to produce a final pH of 5.0 and the solution made up to 500 ml with ddH<sub>2</sub>O.

### **Solution B**

100 ml glycerol was mixed with 400 ml ethanol.

The two solutions were thoroughly mixed and stored at 4°C.

Both silver and reducer stock solutions were stored for 1 week at 4°C, each topped up to 1 l with ddH<sub>2</sub>O, and filtered through Whatman No 1 filter paper. The two solutions were combined in equal volumes immediately prior to use (Newman and Jasani, 1998).

#### **2.2.4 Model Systems**

Immobilon P PVDF membrane was purchased from Millipore Ltd (Watford, Hertfordshire, U.K.).

Anonymised human tonsil for preliminary investigations was acquired, with consent, from routine tonsillectomy prior to the introduction of the Human Tissue Act (2004). Control pathological tissue for diagnostic immunohistochemical staining (tonsil from routine tonsillectomy, lymphoid tissue from Stage 4 Hodgkin's lymphoma, brain tissue from Alzheimer's disease) was supplied by the Department of Histopathology, University Hospital of Wales.

### **2.2.5 Preparation of Vectabond-treated Slides**

To ensure adhesion of tissue sections to the glass microscope slides during the prolonged immunohistochemical staining and subsequent amplification procedures, glass slides required pre-treatment. Slides were immersed in acetone for 5 minutes followed by a further 5 minutes in Vectabond reagent (Vector Laboratories, Peterborough, U.K.) diluted  $1/10$  in acetone. After a 30 second wash in ddH<sub>2</sub>O, slides were air-dried.

### **2.2.6 Selection of d-Block Metal Salts and Buffer Systems**

For ease of comparison with published data, only d-block metal chlorides were investigated. The exceptions were osmium(VIII)tetroxide (which has been used extensively for rendering polyDAB electron dense) phosphotungstic acid, phosphomolybdic acid (the former having some affinity for polyDAB (Newman et al., 1983a) and both of which have been used in histological staining techniques), and silver(I)nitrate (the halides being photolabile).

The investigation was limited to the two main buffering systems with which DAB is commonly employed, namely 100 mM Sorensen's phosphate pH 7.4 and 50 mM Tris HCl pH 7.6.

## **2.3 Methods**

### **2.3.1 Stability of d-Block Metal Salts in Solutions of DAB**

Metal salts were added, at a final concentration of 1 mM, to 0.05% DAB in either 100 mM phosphate buffer pH 7.3 (DAB-PO<sub>4</sub>) (Adams, 1977) or 50 mM Tris HCl buffer pH 7.6 (DAB-Tris) (Hanker et al., 1979) plus 0.005% H<sub>2</sub>O<sub>2</sub>. After three minutes, solutions were examined, and those metal salts that caused any cloudiness



or precipitate to appear (classified as unstable), were excluded from the subsequent study. Those metal salts that caused no obvious change in the appearance of the solution (classified as stable) were used in subsequent experiments.

### **2.3.2 Preparation of PVDF Membrane**

PVDF membrane was wetted by immersion in methanol for 5 minutes followed by thorough washing in ddH<sub>2</sub>O. Whatman No. 1 filter paper was soaked in ddH<sub>2</sub>O and surplus water removed by pressing dry filter paper onto it. 3.5 x 1 cm wetted membrane was placed on the filter paper and excess water removed by applying dry filter paper as described above. Double dilutions of GAM IgPC, such that dots were produced that were just visible at the third doubling dilution, from  $1/50,000$  to  $1/1,600,000$  in ddH<sub>2</sub>O were applied as 2  $\mu$ l droplets to the membrane (Newman and Jasani, 1998). All incubations and washes were performed in 30 ml polystyrene weighing boats (Fisher Scientific, Loughborough, Leicestershire, U. K.) containing 10 ml of reagent.

### **2.3.3 Dot Blot Model System**

#### **2.3.3.1 Pre-polymerisation and Physical Developers**

d-Block metal salts were added, to a final concentration of 1 mM, to either DAB-PO<sub>4</sub> or DAB-Tris. Dot blots of GAM IgPC were immediately placed in each of the solutions and incubated for three minutes. Following thorough washing in ddH<sub>2</sub>O, the preparations were placed directly into either Gallyas' or Newman and Jasani's physical developer.

Nickel salts have been used at much higher concentrations in DAB-Tris than any other metal (Hancock, 1982; 1984; Tago et al., 1986; Lanciego et al., 1997; Tajima et al., 2000; Gonzalo et al., 2001). To further investigate this phenomenon, dot blots were prepared, as described above, from Tris buffered DAB solutions containing 1, 5, 20 or 100 mM Ni(II)Cl<sub>2</sub> and incubated for 10 minutes in developer.

#### **2.3.3.2 Post- polymerisation and Physical Developers**

Dot blots were incubated for 3 minutes in DAB-Tris, thoroughly washed in ddH<sub>2</sub>O, and immersed for five minutes in 2.5 mM solutions of the d-block metal salts. Dot blots were thoroughly washed in ddH<sub>2</sub>O and incubated in physical developer for ten minutes.

#### **2.3.3.3 Sodium Sulfide Treatment and Physical Developers**

Dot blots were prepared as for 2.3.3.1. and 2.3.3.2., above, immersed in 0.3% aqueous, neutralised Na<sub>2</sub>S (0.3% Na<sub>2</sub>S) for 2 minutes, thoroughly washed in ddH<sub>2</sub>O and incubated in physical developer for ten minutes.

#### **2.3.3.4 Scoring System**

Intensification and amplification of dot blots was scored on a scale of 0 to 6. A score of 0 indicated no amplification and scores of 1 to 6 indicated amplification of the first (<sup>1</sup>/<sub>50,000</sub>) to the last (<sup>1</sup>/<sub>1,600,000</sub>) dot. Those metal salts that produced strong amplification of polyDAB with low background were chosen for subsequent immunohistochemical evaluation.

### **2.3.3.5 Analytical Scanning Electron Microscopy**

In a preliminary examination to determine which metal salts formed complexes with polyDAB, dot blots were prepared as above with GAM IgPC diluted  $1/50,000$ . PolyDAB was polymerised in the presence of d-block metal salts, or the salts applied post-polymerisation according to sections 2.3.3.1. and 2.3.3.2 respectively. Samples were air dried, attached to 32 mm diameter aluminium stubs with double-sided sticky tape, carbon coated in an Edwards E306A vacuum coater (Edwards, Crawley, West Sussex, U.K.) and examined in a JEOL 840A scanning electron microscope (JEOL UK Ltd, Welwyn Gardens City, Herts., U.K.) in back-scattered electron imaging (BSI) mode and analysed with an INCA X-cite energy dispersive X-ray spectrometer (Oxford Instruments, Abingdon, Oxon., U.K.) under the following conditions:

Accelerating voltage: 20 kV Probe current:  $10^{-8}$  amps Magnification x 25

Working distance: 15 mm Count time: 50 seconds Processing dead time < 10%

### **2.3.4 Tissue Model System**

#### **2.3.4.1 Tissue Preparation**

For preliminary studies, human tonsil was fixed by immersion for 24 hours in 4% formaldehyde + 0.2% glutaraldehyde in 100 mM Sorensen's phosphate buffer pH 7.4, dehydrated through graded ethanol, cleared in xylene and embedded in paraffin wax.

Serial 4  $\mu$ m sections were cut on an RM2155 motorised microtome (Leica Microsystems (UK) Ltd, Milton Keynes, Bucks., U.K.) and dried onto Vectabond-treated slides at 50°C.

Pre-cut sections of 10% neutral buffered formalin-fixed, paraffin wax-embedded diagnostic control tissue were supplied by the Department of Histopathology, University Hospital of Wales.

#### **2.3.4.2 Selection of Appropriate Antibody Dilutions**

Sections were de-waxed in xylene, and rehydrated through graded ethanol. Suppression of endogenous peroxidatic activity with methanolic H<sub>2</sub>O<sub>2</sub> (Streefkerk, 1972) was omitted since this was found to reduce the immunohistochemical response by at least 1 doubling dilution of primary antibody, making direct comparison with immunocolloidal gold staining unreliable.

Following 10 minutes equilibration in 20 mM Tris pH 7.4 containing 0.9% NaCl and 0.6% bovine serum albumin (TBS/BSA), sections were incubated for 90 minutes in mouse monoclonal anti-CD45 Ro in doubling dilutions from 1/1000 to 1/16,000 with TBS/BSA to determine an appropriate titre such that the subsequent level of metal-free immunohistochemical staining was just visible. After 3 x 1 minute washes in TBS/BSA, sections were incubated for a further hour in 1/150 GAM Ig PC in TBS/BSA. Sections were washed for 1 minute in TBS/BSA and 2 x 1 min in 50 mM Tris-HCl pH 7.6 followed by a 3 minute incubation in DAB-Tris.

#### **2.3.4.3 Immunocolloidal Gold**

To provide a standard against which polyDAB amplification could be compared, sections were immunohistochemically stained with 1/4000 (chosen according to 2.3.4.2., above) anti-CD45Ro as above followed by an hour incubation in GAM IgCG5. Following thorough washing in ddH<sub>2</sub>O, sections were fixed for 5

minutes with 0.5% glutaraldehyde in 100 mM phosphate buffer pH 7.3. After washing in ddH<sub>2</sub>O, residual aldehyde groups were blocked for 10 minutes in 0.75 M Tris acetate pH 7.5. Surplus solution was removed, and sections immersed in either Gallyas' or Newman and Jasani's physical developer and the reaction observed microscopically. The reaction was terminated by thorough washing in ddH<sub>2</sub>O.

#### **2.3.4.4 Counterstaining and Mounting**

All sections were lightly counterstained by immersion in 0.02% methyl green for 2 minutes, dehydrated through graded ethanol, cleared in xylene and mounted in Gurr's neutral mountant.

#### **2.3.4.5 Immunohistochemical Evaluation of PolyDAB Amplification**

Following thorough washing with either 100 mM phosphate buffer pH 7.3 or 50 mM Tris buffer pH 7.6, GAM Ig PC labelled sections were incubated with DAB-PO<sub>4</sub> or DAB-Tris plus metal salts respectively, or metals applied post-polymerisation. After thorough washing in ddH<sub>2</sub>O, sections were immersed in physical developer, with or without 2 minute pre-treatment with 0.3% Na<sub>2</sub>S, and the reaction observed microscopically.

Silver intensification of specific staining was continued until the time point when non-specific staining first became apparent.

#### 2.3.4.6 Marker Amplification and Diagnostic Immunohistochemistry

Tissue from Stage 4 Hodgkin's lymphoma, tonsil, and brain from Alzheimer's disease were immunostained for (a) the Epstein-Barr virus protein, LMP-1 (low concentration antigen), (b) the cytotoxic T-cell enzyme, granzyme B (low concentration antigen), and (c)  $\alpha$ -synuclein, a diagnostic indicator of neurodegenerative disease (rare event) respectively.

4  $\mu$ m thick tissue sections on Superfrost Plus slides were rehydrated and immunostained according to the standard schedule used by the Department of Histopathology, University Hospital of Wales, Cardiff. Briefly, rehydrated sections were subjected to high pressure antigen retrieval with target retrieval solution for 1 minute at 125°C, 20 psi in a Decloaking Chamber (Biocare Medical, Concord, California, U.S.A.). Immunohistochemical staining was performed in an Autostainer Plus (Dako, Ely, Cambridgeshire, U.K.). Following washing with ddH<sub>2</sub>O and Tris wash buffer (TWB), sections were incubated for 45 minutes in primary antibody (all diluted  $1/_{20}$  with Dako antibody diluent), washed with TWB and treated with peroxidase block for 5 minutes. After a further wash in TWB, sections were incubated in Envision detection system for 30 minutes. Sections were washed again in TWB and developed with DAB+ chromagen (diluted  $1/_{50}$  with substrate buffer) with or without amplification. Sections were lightly counterstained for 1 minute with haematoxylin, blued in tap water, dehydrated and mounted. For amplification, immunohistochemically stained sections were incubated in 2.5 mM NaAu(III)Cl<sub>4</sub> for 5 minutes, washed thoroughly in ddH<sub>2</sub>O, incubated for a further 2 minutes in 0.3% Na<sub>2</sub>S, washed in ddH<sub>2</sub>O and treated with Newman and Jasani's physical developer for 10 minutes and counterstained as above.

### **2.3.5 Microscopic Examination and Digital Imaging**

Sections were examined on an Olympus BX51 microscope (Olympus Optical Co. (U.K.) Ltd, London, U.K.) in bright field mode and digital photomicrographs captured with a Zeiss Axiocam and Axiovision software (Carl Zeiss Vision GmbH, Hallbergmoos, Germany). Images were processed with Adobe Photoshop (Adobe Systems Incorporated, San Jose, California, U.S.A.).

### **2.3.6 Alkaline Phosphatase Marker Amplification**

Dot blots were prepared with doubling dilutions of GAM IgAP from  $1/500$  to  $1/16,000$  as described above. Dot blots were incubated for 30 minutes in 100 mM glycine buffer pH 9.0 containing 200  $\mu\text{g/ml}$  BCIP and 400  $\mu\text{g/ml}$  MTT. For both pre- and post- reduction studies,  $\text{Ni(II)Cl}_2$ ,  $\text{Co(II)Cl}_2$  and  $\text{Cu(II)Cl}_2$  were used at 10 mM (Pearse, 1957). Dot blots were incubated in the physical developers with and without pre-treatment with sodium sulfide as described above.

## 2.4 Results

### 2.4.1 Stability of d-Block Metal Salts in Solutions of DAB

Of the 31 d-block metal salts investigated, 19 were stable (as defined in section 2.3.1) in both DAB-PO<sub>4</sub> and DAB-Tris, and a further 6 were stable in DAB-PO<sub>4</sub> only. Ni(II)Cl<sub>2</sub> was stable in DAB-Tris up to at least 100 mM. In contrast, the other DAB-Tris-stable d-block metal salts could only be added up to a final concentration of 1 mM. Results are summarised in Table 2.1.

### 2.4.2 Dot Blot Model System

Dot blots produced with DAB alone could be clearly seen at GAM IgPC dilutions of <sup>1</sup>/<sub>50,000</sub> and <sup>1</sup>/<sub>100,000</sub>, and only just seen at <sup>1</sup>/<sub>200,000</sub> (figure 2.3a).

#### 2.4.2.1 Pre-polymerisation and Amplification

##### 2.4.2.1.1 Physical Developers Alone

Of the 25 d-block metal salts that were compatible with DAB-PO<sub>4</sub>, only 3 produced dot blots that could be intensified with Gallyas' physical developer, namely Co(II)Cl<sub>2</sub>, Ni(II)Cl<sub>2</sub> (figure 2.3b and c) and K<sub>2</sub>Pt(II)Cl<sub>4</sub>. The remaining salts produced either no discernable increase in signal (dot blot) intensity (16/24) or caused an increase in background (PVDF membrane) staining only (5/24). In contrast, no intensification occurred in any of the dot blots following treatment with Newman and Jasani's developer. In addition, the blue-black colour of the dots produced by solutions containing either Ni(II)Cl<sub>2</sub> or Co(II)Cl<sub>2</sub> was rapidly lost. Only one metal compound, K<sub>2</sub>Os(IV)Cl<sub>6</sub>, caused an increase in background staining. A similar pattern was observed in dot blots produced from d-block metal salts in DAB-Tris. Results are summarised in tables 2.2 and 2.3.



Table 2.1. Stability of d-block metal salts in DAB-PO<sub>4</sub> and DAB-Tris.

Metal	DAB-PO <sub>4</sub>	DAB-Tris	Metal	DAB-PO <sub>4</sub>	DAB-Tris
Sc(III)Cl <sub>3</sub>	✓	✓	Os(VIII)O <sub>4</sub>	×	×
Y(III)Cl <sub>3</sub>	✓	✓	Co(II)Cl <sub>2</sub>	✓	×
La(III)Cl <sub>3</sub>	✓	✓	Rh(III)Cl <sub>3</sub>	✓	✓
V(III)Cl <sub>3</sub>	✓	✓	K <sub>3</sub> Ir(III)Cl <sub>6</sub>	✓	✓
Cr(II)Cl <sub>2</sub>	✓	✓	K <sub>2</sub> Ir(IV)Cl <sub>6</sub>	✓	✓
Cr(III)Cl <sub>3</sub>	✓	✓	Ir(IV)Cl <sub>4</sub>	✓	✓
H <sub>3</sub> PMo(IV) <sub>12</sub> O <sub>40</sub>	✓	×	Ni(II)Cl <sub>2</sub>	✓	✓
Na <sub>2</sub> W(VI)O <sub>4</sub>	✓	×	K <sub>2</sub> Pd(II)Cl <sub>4</sub>	×	×
H <sub>3</sub> PW(IV) <sub>12</sub> O <sub>40</sub>	✓	×	K <sub>2</sub> Pd(IV)Cl <sub>6</sub>	×	×
Mn(II)Cl <sub>2</sub>	✓	✓	K <sub>2</sub> Pt(II)Cl <sub>4</sub>	✓	✓
Re(III)Cl <sub>3</sub>	✓	✓	K <sub>2</sub> Pt(IV)Cl <sub>6</sub>	✓	✓
Fe(II)Cl <sub>2</sub>	✓	×	Cu(II)Cl <sub>2</sub>	×	×
Fe(III)Cl <sub>3</sub>	✓	×	Ag(I)NO <sub>3</sub>	✓	✓
Ru(III)Cl <sub>3</sub>	✓	✓	NaAu(III)Cl <sub>4</sub>	×	×
K <sub>3</sub> Ru(III)Cl <sub>6</sub>	×	×	Zn(II)Cl <sub>2</sub>	✓	✓
K <sub>2</sub> Os(IV)Cl <sub>6</sub>	✓	✓			

Table 2.2. Amplification of dot blots from DAB-PO<sub>4</sub>-metal salt combinations with Gallyas' or Newman and Jasani's developers.

Metal	Gallyas		Newman & Jasani	
	Foreground	Background	Foreground	Background
Sc(III)Cl <sub>3</sub>	0	0	0	0
Y(III)Cl <sub>3</sub>	0	0	0	0
La(III)Cl <sub>3</sub>	0	0	0	0
V(III)Cl <sub>3</sub>	0	0	0	0
Cr(II)Cl <sub>2</sub>	0	0	0	0
Cr(III)Cl <sub>3</sub>	0	0	0	0
H <sub>3</sub> PMo(IV) <sub>12</sub> O <sub>40</sub>	0	0	0	0
Na <sub>2</sub> W(VI)O <sub>4</sub>	0	0	0	0
H <sub>3</sub> PW(IV) <sub>12</sub> O <sub>40</sub>	0	0	0	0
Mn(II)Cl <sub>2</sub>	0	0	0	0
Re(III)Cl <sub>3</sub>	0	0	0	0
Fe(II)Cl <sub>2</sub>	0	0	0	0
Fe(III)Cl <sub>3</sub>	0	++	0	0
Ru(III)Cl <sub>3</sub>	0	++	0	0
K <sub>3</sub> Ru(III)Cl <sub>6</sub>	-	-	-	-
K <sub>2</sub> Os(IV)Cl <sub>6</sub>	0	+	0	++
Os(VIII)O <sub>4</sub>	-	-	-	-
Co(II)Cl <sub>2</sub>	+	0	0	0
Rh(III)Cl <sub>3</sub>	0	0	0	0
K <sub>3</sub> Ir(III)Cl <sub>6</sub>	0	++++	0	0
K <sub>2</sub> Ir(IV)Cl <sub>6</sub>	0	0	0	0
Ir(IV)Cl <sub>4</sub>	0	0	0	0
Ni(II)Cl <sub>2</sub>	++++++	0	0	0
K <sub>2</sub> Pd(II)Cl <sub>4</sub>	-	-	-	-
K <sub>2</sub> Pd(IV)Cl <sub>6</sub>	-	-	-	-
K <sub>2</sub> Pt(II)Cl <sub>4</sub>	++++++	+++	0	0
K <sub>2</sub> Pt(IV)Cl <sub>6</sub>	0	+++++	0	0
Cu(II)Cl <sub>2</sub>	-	-	-	-
Ag(I)NO <sub>3</sub>	0	0	0	0
NaAu(III)Cl <sub>4</sub>	-	-	-	-
Zn(II)Cl <sub>2</sub>	0	0	0	0

Table 2.3. Amplification of dot blots from DAB-Tris-metal salt combinations with Gallyas' or Newman and Jasani's developers.

Metal	Gallyas		Newman & Jasani	
	Foreground	Background	Foreground	Background
Sc(III)Cl <sub>3</sub>	0	0	0	0
Y(III)Cl <sub>3</sub>	0	0	0	0
La(III)Cl <sub>3</sub>	0	0	0	0
V(III)Cl <sub>3</sub>	0	0	0	0
Cr(II)Cl <sub>2</sub>	0	0	0	0
Cr(III)Cl <sub>3</sub>	0	0	0	0
H <sub>3</sub> PMo(IV) <sub>12</sub> O <sub>40</sub>	-	-	-	-
Na <sub>2</sub> W(VI)O <sub>4</sub>	-	-	-	-
H <sub>3</sub> PW(IV) <sub>12</sub> O <sub>40</sub>	-	-	-	-
Mn(II)Cl <sub>2</sub>	0	0	0	0
Re(III)Cl <sub>3</sub>	0	0	0	0
Fe(II)Cl <sub>2</sub>	-	-	-	-
Fe(III)Cl <sub>3</sub>	-	-	-	-
Ru(III)Cl <sub>3</sub>	0	++	0	0
K <sub>3</sub> Ru(III)Cl <sub>6</sub>	-	-	-	-
K <sub>2</sub> Os(IV)Cl <sub>6</sub>	0	+	0	++
Os(VIII)O <sub>4</sub>	-	-	-	-
Co(II)Cl <sub>2</sub>	-	-	-	-
Rh(III)Cl <sub>3</sub>	0	0	0	0
K <sub>3</sub> Ir(III)Cl <sub>6</sub>	0	0	0	0
K <sub>2</sub> Ir(IV)Cl <sub>6</sub>	0	0	0	0
Ir(IV)Cl <sub>4</sub>	0	+++	0	0
Ni(II)Cl <sub>2</sub>	++++++	0	0	0
K <sub>2</sub> Pd(II)Cl <sub>4</sub>	-	-	-	-
K <sub>2</sub> Pd(IV)Cl <sub>6</sub>	-	-	-	-
K <sub>2</sub> Pt(II)Cl <sub>4</sub>	++++++	++	0	0
K <sub>2</sub> Pt(IV)Cl <sub>6</sub>	0	+++++	0	0
Cu(II)Cl <sub>2</sub>	-	-	-	-
Ag(I)NO <sub>3</sub>	0	0	0	0
NaAu(III)Cl <sub>4</sub>	-	-	-	-
Zn(II)Cl <sub>2</sub>	0	0	0	0

#### 2.4.2.1.2 Effects of Sulfide Treatment on Amplification

Following treatment with 0.3% Na<sub>2</sub>S, dot blots from DAB-PO<sub>4</sub> solutions containing Co(II)Cl<sub>2</sub> were further intensified by Gallyas' developer (figure 2.3d). Those from solutions containing Ni(II)Cl<sub>2</sub> produced less intensification than before Na<sub>2</sub>S treatment (figure 2.3e), and those from solutions containing K<sub>2</sub>Pt(II)Cl<sub>4</sub> showed greatly increased background staining. Dot blots from 3 additional metal salt solutions were amplified, namely K<sub>3</sub>Ir(III)Cl<sub>6</sub>, K<sub>2</sub>Ir(IV)Cl<sub>6</sub> and Ag(I)NO<sub>3</sub>.

In the case of DAB-Tris, Ni(II)Cl<sub>2</sub> gave a similar result, but a notable improvement was seen in the case of Ag(I)NO<sub>3</sub>, and Rh(III)Cl<sub>3</sub> produced some intensification over background. In contrast, K<sub>3</sub>Ir(III)Cl<sub>6</sub> and K<sub>2</sub>Ir(IV)Cl<sub>6</sub> produced higher background than signal.

The remaining metal salts produced either no discernable increase in dot blot intensity (13/25 (DAB-PO<sub>4</sub>), 11/19 (DAB-Tris)) or in increased background staining only (5/25 (DAB-PO<sub>4</sub>), 4/19 (DAB-Tris)).

For DAB-PO<sub>4</sub>, Newman and Jasani's developer produced amplification of NiCl<sub>2</sub> that was comparable to that produced by Gallyas' developer. Dot blots from solutions containing Co(II)Cl<sub>2</sub>, Ag(I)NO<sub>3</sub> (figure 2.3f), Fe(II)Cl<sub>2</sub> and K<sub>2</sub>Pt(II)Cl<sub>4</sub> were also amplified, but background staining was elevated to varying degrees. Similar results were observed for Ni(II)Cl<sub>2</sub> and Ag(I)NO<sub>3</sub> in DAB-Tris, although background staining was absent.

No change was seen in most salts (12/25 (DAB-PO<sub>4</sub>), 11/19 (DAB-Tris)) while some (8/25 (DAB-PO<sub>4</sub>), 8/19 (DAB-Tris)) had higher background than signal. Results are summarised in tables 2.4 and 2.5.

Table 2.4. Amplification of dot blots from DAB-PO<sub>4</sub>-metal salt combinations plus sulfide with Gallyas' and Newman or Jasani's developers.

Metal	Gallyas		Newman & Jasani	
	Foreground	Background	Foreground	Background
Sc(III)Cl <sub>3</sub>	0	0	0	0
Y(III)Cl <sub>3</sub>	0	0	0	0
La(III)Cl <sub>3</sub>	0	0	0	0
V(III)Cl <sub>3</sub>	0	0	0	0
Cr(II)Cl <sub>2</sub>	0	0	0	0
Cr(III)Cl <sub>3</sub>	0	0	0	0
H <sub>3</sub> PMo(IV) <sub>12</sub> O <sub>40</sub>	0	0	0	0
Na <sub>2</sub> W(VI)O <sub>4</sub>	0	0	0	0
H <sub>3</sub> PW(IV) <sub>12</sub> O <sub>40</sub>	0	0	0	0
Mn(II)Cl <sub>2</sub>	0	0	0	0
Re(III)Cl <sub>3</sub>	0	0	0	0
Fe(II)Cl <sub>2</sub>	0	++++	++++	0
Fe(III)Cl <sub>3</sub>	0	+	+	+
Ru(III)Cl <sub>3</sub>	0	0	0	++++++
K <sub>3</sub> Ru(III)Cl <sub>6</sub>	-	-	-	-
K <sub>2</sub> Os(IV)Cl <sub>6</sub>	0	0	0	++++
Os(VIII)O <sub>4</sub>	-	-	-	-
Co(II)Cl <sub>2</sub>	+++++	+++	+++	0
Rh(III)Cl <sub>3</sub>	0	++	++	+
K <sub>3</sub> Ir(III)Cl <sub>6</sub>	+	0	0	++++++
K <sub>2</sub> Ir(IV)Cl <sub>6</sub>	+++	0	0	0
Ir(IV)Cl <sub>4</sub>	++++	+++	+++	++
Ni(II)Cl <sub>2</sub>	++++	+++	+++	0
K <sub>2</sub> Pd(II)Cl <sub>4</sub>	-	-	-	-
K <sub>2</sub> Pd(IV)Cl <sub>6</sub>	-	-	-	-
K <sub>2</sub> Pt(II)Cl <sub>4</sub>	++++	+++	+++	++++++
K <sub>2</sub> Pt(IV)Cl <sub>6</sub>	0	0	0	++++++
Cu(II)Cl <sub>2</sub>	-	-	-	-
Ag(I)NO <sub>3</sub>	+++++	+++++	+++++	++
NaAu(III)Cl <sub>4</sub>	-	-	-	-
Zn(II)Cl <sub>2</sub>	0	0	0	0

Table 2.5. Amplification of dot blots from DAB-Tris-metal salt combinations plus sulfide with Gallyas' or Newman and Jasani's developers.

Metal	Gallyas		Newman & Jasani	
	Foreground	Background	Foreground	Background
Sc(III)Cl <sub>3</sub>	0	0	0	0
Y(III)Cl <sub>3</sub>	0	0	0	0
La(III)Cl <sub>3</sub>	0	0	0	0
V(III)Cl <sub>3</sub>	0	0	0	0
Cr(II)Cl <sub>2</sub>	0	0	0	0
Cr(III)Cl <sub>3</sub>	0	0	0	0
H <sub>3</sub> PMo(IV) <sub>12</sub> O <sub>40</sub>	-	-	-	-
Na <sub>2</sub> W(VI)O <sub>4</sub>	-	-	-	-
H <sub>3</sub> PW(IV) <sub>12</sub> O <sub>40</sub>	-	-	-	-
Mn(II)Cl <sub>2</sub>	0	0	0	0
Re(III)Cl <sub>3</sub>	0	0	0	0
Fe(II)Cl <sub>2</sub>	-	-	-	-
Fe(III)Cl <sub>3</sub>	-	-	-	-
Ru(III)Cl <sub>3</sub>	0	+++++	0	+++++
K <sub>3</sub> Ru(III)Cl <sub>6</sub>	-	-	-	-
K <sub>2</sub> Os(IV)Cl <sub>6</sub>	0	+++++	0	+++++
Os(VIII)O <sub>4</sub>	-	-	-	-
Co(II)Cl <sub>2</sub>	-	-	-	-
Rh(III)Cl <sub>3</sub>	+++	++	++	++++
K <sub>3</sub> Ir(III)Cl <sub>6</sub>	0	+++++	0	++++
K <sub>2</sub> Ir(IV)Cl <sub>6</sub>	+++	++++	+++	++++
Ir(IV)Cl <sub>4</sub>	+++	++++	+++	++++
Ni(II)Cl <sub>2</sub>	+++	0	+++	0
K <sub>2</sub> Pd(II)Cl <sub>4</sub>	-	-	-	-
K <sub>2</sub> Pd(IV)Cl <sub>6</sub>	-	-	-	-
K <sub>2</sub> Pt(II)Cl <sub>4</sub>	++++	+++++	+++	++++
K <sub>2</sub> Pt(IV)Cl <sub>6</sub>	0	+++++	0	+++++
Cu(II)Cl <sub>2</sub>	-	-	-	-
Ag(I)NO <sub>3</sub>	+++++	0	+++++	0
NaAu(III)Cl <sub>4</sub>	-	-	-	-
Zn(II)Cl <sub>2</sub>	0	0	0	0

#### **2.4.2.1.3 Nickel Concentration and Physical Developers**

Slight increases in the intensity of the dot blots, compared to the metal free control, were observed prior to physical developer treatment. These changes were most pronounced in dot blots from solutions containing 20 mM and 100 mM Ni(II)Cl<sub>2</sub>.

Gallyas' developer produced a dramatic and progressive increase in staining intensity with increasing concentrations of Ni(II)Cl<sub>2</sub> (figure 2.4a and b). Again, Newman and Jasani's developer caused rapid loss of the blue-black colour from the dots and no amplification occurred.

#### **2.4.2.1.4 Nickel Concentration and Physical Developers - Effects of Sulfide Treatment**

Following treatment with 0.3% Na<sub>2</sub>S and amplification with Gallyas' physical developer, only at the highest concentration of Ni(II)Cl<sub>2</sub> were all dots visible, and these were less intensely stained than the corresponding set without sulfide treatment. In addition, background staining was slightly elevated (figure 2.4c and d).

Following amplification with Newman and Jasani's developer of sulfide treated samples, all dots were clearly visible at 5 mM Ni(II)Cl<sub>2</sub> (figure 2.4e). At 20 mM and 100 mM Ni(II)Cl<sub>2</sub>, dots were more strongly stained at higher concentration of peroxidase, and more weakly stained at lower peroxidase concentration, than the corresponding dots produced by 5 mM Ni(II)Cl<sub>2</sub> (figure 2.4f). Results are summarised in table 2.6.

Table 2.6. Effects of Ni(II)Cl<sub>2</sub> concentration, with and without subsequent sulfide treatment, on subsequent amplification with Gallyas' or Newman and Jasani's developers.

[Ni(II)Cl <sub>2</sub> ]	Gallyas		Newman & Jasani	
	Foreground	Background	Foreground	Background
1 mM	++++	0	0	0
5 mM	++++	0	0	0
20 mM	+++++	0	0	0
100 mM	++++++	0	0	+

	+ 0.3% Na <sub>2</sub> S		+ 0.3% Na <sub>2</sub> S	
	Foreground	Background	Foreground	Background
1 mM	++	0	++	+
5 mM	+++	0	++++++	+
20 mM	++++	0	+++++	+
100 mM	+++++	+	+++++	+



## 2.4.2.2 Post-polymerisation and Amplification

### 2.4.2.2.1 Physical Developers Alone

In sharp contrast to the results of the pre-polymerisation experiments, the application of d-block metal salts to polyDAB produced a far greater range (11/31 cf. 3/19) of dot blots that were amplifiable with Gallyas' developer. The most striking results were with the platinum salts that produced maximal intensification, and no background, within 1 minute (figure 2.5a). The remaining 9 salts required the full 10 minutes, and 5 had elevated background staining as well. Of the remainder, treatment with Gallyas' developer in 16 had no effect, and in 4, background staining only. Interestingly, neither  $\text{Ni(II)Cl}_2$  nor  $\text{Co(II)Cl}_2$  produced any visible increase in the intensity of the dot blots either before or after physical development.

Newman and Jasani's physical developer produced similar results, albeit of a lesser range than was observed with Gallyas' developer. 4 metal salt-treated dot blots ( $\text{NaAu(III)Cl}_4$ ,  $\text{K}_2\text{Os(V)Cl}_6$ , and  $\text{Os(VIII)O}_4$ ) were moderately amplified whilst the remainder produced either no discernable increase in signal or background intensity (24/31), equal increases in both (2/31) or increased background only (1/31). Of particular note was the failure of platinum or iridium salts to facilitate amplification, as seen with Gallyas' developer. Results are summarised in table 2.7.

Table 2.7. Amplification of dot blots, following post-polymerisation application of metal salts, with Gallyas' or Newman and Jasani's developers.

Metal	Gallyas		Newman & Jasani	
	Foreground	Background	Foreground	Background
Sc(III)Cl <sub>3</sub>	0	0	0	0
Y(III)Cl <sub>3</sub>	0	0	0	0
La(III)Cl <sub>3</sub>	0	0	0	0
V(III)Cl <sub>3</sub>	+	0	0	0
Cr(II)Cl <sub>2</sub>	0	0	0	0
Cr(III)Cl <sub>3</sub>	0	0	0	0
H <sub>3</sub> PMo(IV) <sub>12</sub> O <sub>40</sub>	0	0	0	0
Na <sub>2</sub> W(VI)O <sub>4</sub>	0	0	0	0
H <sub>3</sub> PW(IV) <sub>12</sub> O <sub>40</sub>	0	0	0	0
Mn(II)Cl <sub>2</sub>	0	0	0	0
Re(III)Cl <sub>3</sub>	0	+++++++	0	+++++++
Fe(II)Cl <sub>2</sub>	0	0	0	0
Fe(III)Cl <sub>3</sub>	0	0	0	0
Ru(III)Cl <sub>3</sub>	0	+++++++	0	0
K <sub>3</sub> Ru(III)Cl <sub>6</sub>	+	+++++++	0	0
K <sub>2</sub> Os(IV)Cl <sub>6</sub>	0	0	++	+
Os(VIII)O <sub>4</sub>	+++++++	++	++	+
Co(II)Cl <sub>2</sub>	0	0	0	0
Rh(III)Cl <sub>3</sub>	+	0	0	0
K <sub>3</sub> Ir(III)Cl <sub>6</sub>	0	0	0	0
K <sub>2</sub> Ir(IV)Cl <sub>6</sub>	+++++++	+++	0	0
Ir(IV)Cl <sub>4</sub>	+++++++	+++	0	0
Ni(II)Cl <sub>2</sub>	0	0	0	0
K <sub>2</sub> Pd(II)Cl <sub>4</sub>	++	0	+	+
K <sub>2</sub> Pd(IV)Cl <sub>6</sub>	+	0	+	+
K <sub>2</sub> Pt(II)Cl <sub>4</sub>	+++++++		0	0
K <sub>2</sub> Pt(IV)Cl <sub>6</sub>	+++++++	0	0	0
Cu(II)Cl <sub>2</sub>	0	0	0	0
Ag(I)NO <sub>3</sub>	0	+	0	0
NaAu(III)Cl <sub>4</sub>	+++++++	++	+++	+
Zn(II)Cl <sub>2</sub>	0	0	0	0

#### 2.4.2.2.2 Effects of Sulfide Treatment on Amplification

With Gallyas' developer, sulfide treatment promoted increased amplification in 11/31 of the dot blots, 2 having shown no propensity for amplification prior to sulfide treatment ( $\text{Cu(II)Cl}_2$  and  $\text{K}_3\text{Ir(III)Cl}_6$ ). Furthermore, the background staining that occurred with  $\text{NaAu(III)Cl}_4$  in the absence of sulfide treatment was abolished without any apparent loss of foreground. Conversely, the intense staining seen following  $\text{K}_2\text{Pt(II)Cl}_4$  alone was not improved with sulfide treatment; background staining was worsened (figure 2.5b). The remaining metal salts produced either no obvious increase in dot blot or background intensity (10/31), higher background than foreground (6/31) or increased background only (3/31).

With Newman and Jasani's developer,  $\text{Na}_2\text{S}$  increased not only the intensity of amplification ( $\text{NaAu(III)Cl}_4$  (figure 2.5c)), but also the range of polyDAB-metal 'complexes' that could be amplified ( $\text{Fe(II)Cl}_2$ , (figure 2.5d)  $\text{Cu(II)SO}_4$  (figure 2.5e),  $\text{Ag(I)NO}_3$ ,  $\text{K}_2\text{Pt(IV)Cl}_6$ ). The remaining metal salts produced either no increase in dot blot or background staining (18/31), higher background than foreground, e.g.  $\text{K}_2\text{Pd(IV)Cl}_4$  (figure 2.5f) (5/31) or an equal increase in both (1/31). Results are summarised in table 2.8.

The rapid loss of the blue-black colour associated with dot blots that were produced from solutions containing cobalt or nickel, following immersion in Newman and Jasani's developer, together with the failure of this developer to produce the striking results seen with the post-polymerisation application of platinum in conjunction with Gallyas' developer prompted an investigation to determine which component(s) of Newman and Jasani's developer were responsible for these discrepant observations.

Table 2.8. Amplification of dot blots following post-polymerisation application of metal salt and sulfide with Gallyas' or Newman and Jasani's developers.

Metal	Gallyas		Newman & Jasani	
	Foreground	Background	Foreground	Background
Sc(III)Cl <sub>3</sub>	0	0	0	0
Y(III)Cl <sub>3</sub>	0	0	0	0
La(III)Cl <sub>3</sub>	0	0	0	0
V(III)Cl <sub>3</sub>	+++	0	0	0
Cr(II)Cl <sub>2</sub>	0	0	0	0
Cr(III)Cl <sub>3</sub>	0	0	0	0
H <sub>3</sub> PMo(IV) <sub>12</sub> O <sub>40</sub>	0	0	0	0
Na <sub>2</sub> W(VI)O <sub>4</sub>	0	0	0	0
H <sub>3</sub> PW(IV) <sub>12</sub> O <sub>40</sub>	0	0	0	0
Mn(II)Cl <sub>2</sub>	0	0	0	0
Re(III)Cl <sub>3</sub>	0	++++++	0	++++++
Fe(II)Cl <sub>2</sub>	++++++	++++++	+++++	+
Fe(III)Cl <sub>3</sub>	0	+++	+	++++
Ru(III)Cl <sub>3</sub>	0	++++++	0	0
K <sub>3</sub> Ru(III)Cl <sub>6</sub>	+	++++++	0	0
K <sub>2</sub> Os(IV)Cl <sub>6</sub>	++	++++++	0	++
Os(VIII)O <sub>4</sub>	++++++	+++++	++++	+++
Co(II)Cl <sub>2</sub>	+++	++++++	0	0
Rh(III)Cl <sub>3</sub>	+++	0	0	0
K <sub>3</sub> Ir(III)Cl <sub>6</sub>	+++	+	0	0
K <sub>2</sub> Ir(IV)Cl <sub>6</sub>	+++++	++	0	0
Ir(IV)Cl <sub>4</sub>	+++++	+	0	+
Ni(II)Cl <sub>2</sub>	0	0	0	0
K <sub>2</sub> Pd(II)Cl <sub>4</sub>	++++++	+++	++	++++
K <sub>2</sub> Pd(IV)Cl <sub>6</sub>	+++	++++++	++++++	++++
K <sub>2</sub> Pt(II)Cl <sub>4</sub>	++++++	+	0	0
K <sub>2</sub> Pt(IV)Cl <sub>6</sub>	+++++	0	+	0
Cu(II)Cl <sub>2</sub>	++++++	+	++++++	0
Ag(I)NO <sub>3</sub>	+++	++++++	++++++	++
NaAu(III)Cl <sub>4</sub>	++++++	0	++++++	0
Zn(II)Cl <sub>2</sub>	0	0	0	0

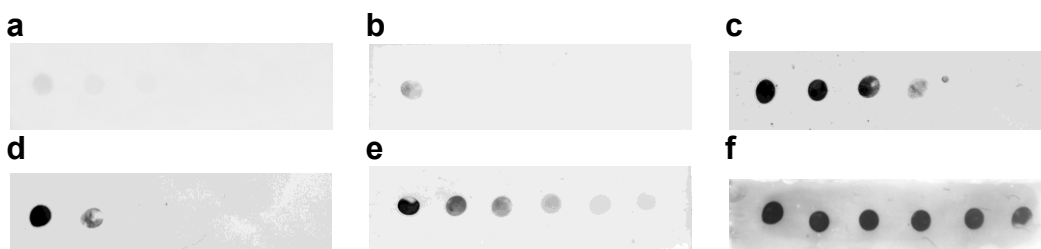


Figure 2.3. Representative dot blots from pre-polymerisation experiments. DAB alone (a), Co(II) + Gallyas' developer (b), Ni(II) + Gallyas' developer (c), Co(II) + Na<sub>2</sub>S + Gallyas' developer (d), Ni(II) + Na<sub>2</sub>S + Gallyas' developer (e), and Ag(I) + Na<sub>2</sub>S + Newman and Jasani's developer (f).

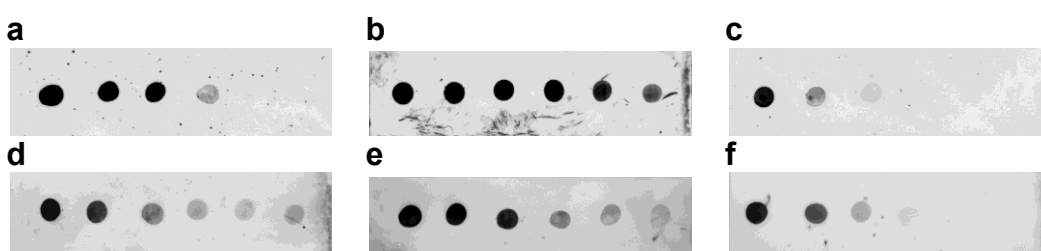


Figure 2.4. Representative dot blots from Ni(II) concentration experiments. 5 mM Ni(II) + Gallyas' developer (a), 100 mM Ni(II) + Gallyas' developer (b) 5 mM Ni(II) + Na<sub>2</sub>S + Gallyas' developer (c), 100 mM Ni(II) + Na<sub>2</sub>S + Gallyas' developer (d), 5 mM Ni(II) + Na<sub>2</sub>S + Newman and Jasani's developer (e) and 100 mM Ni(II) + Na<sub>2</sub>S + Newman and Jasani's developer (f).

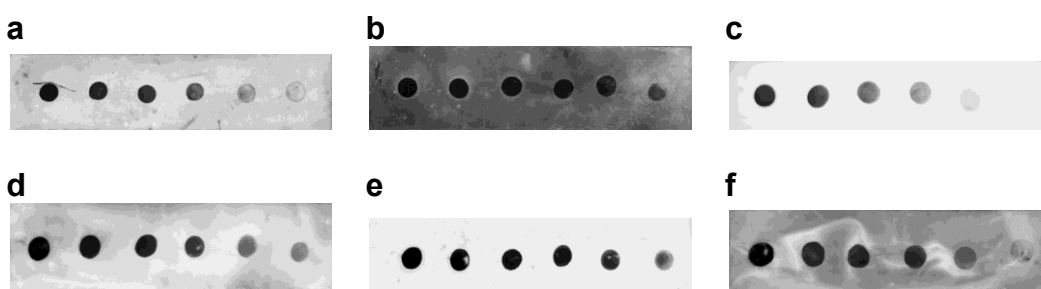


Figure 2.5. Representative dot blots from post-polymerisation experiments. Pt(II) + Gallyas' developer (a), Pt(II) + Na<sub>2</sub>S + Gallyas' developer (b), Au(III) + Na<sub>2</sub>S + Newman and Jasani's developer (c) Fe(II) + Na<sub>2</sub>S + Newman and Jasani's developer (d), Cu(II) + Na<sub>2</sub>S + Newman and Jasani's developer (e) and Pd(IV) + Na<sub>2</sub>S + Newman and Jasani's developer (f).

By preparing solutions that omitted each of the various components in turn, and observing the loss of colour from dot blots containing either Ni(II)Cl<sub>2</sub> or Co(II)Cl<sub>2</sub>, it was found that colour loss was due partly to the citrate buffer of the reducer solution, but mainly due to the reducing agent, pyrogallol. A similar effect was achieved with 1% neutral EDTA, suggesting that metal salt extraction, rather than chemical alteration (e.g. reduction by pyrogallol) of polyDAB was the cause. Attempts to subsequently reintroduce either Ni(II)Cl<sub>2</sub> or Co(II)Cl<sub>2</sub> by immersing the dot blots in solutions of up to 100 mM of the salts for 10 minutes failed to produce any colour change.

Since platinum loss could not be visualised directly, dot blots were immersed for up to 10 minutes in the various preparations of Newman and Jasani's developer, thoroughly washed, and then immersed in Gallyas' developer. In contrast to Ni(II)Cl<sub>2</sub> and Co(II)Cl<sub>2</sub>, platinum was rapidly extracted by sodium sulphite, a component of the reducer solution. Loss of platinum occurred in less than 10 seconds.

#### **2.4.2.3 Analytical Scanning Electron Microscopy**

The PVDF membrane of the dot blots provided a useful control for preliminary examination by BSI, since it appeared brighter than the surrounding adhesive tape due to the presence of fluorine and thus its higher average atomic number composition.

The vast majority of dot blots showed no increased brightness, and those that did contained d-block metals that were restricted to the second and third row.

Even with a high probe current and long dwell time, very few dot blots produced measurable X-ray signals; only 4 from pre-polymerisation and 5 in the

post-polymerisation experiments (figures 2.6 and 2.7 respectively). Quantitation was not possible, since the nitrogen peak (0.3924 KeV) due to polyDAB was obscured within the broad carbon peak of both the membrane and carbon coating (0.2774 KeV). Results are summarised in table 2.9.

### **2.4.3 Tissue Model System**

From the results above, d-block metal salts that facilitated the strongest amplification and lowest background were selected for testing on tissue sections. Those to be amplified with Gallyas' developer were 1) pre-polymerisation; Ni(II)Cl<sub>2</sub> at 1, 5, 20 and 100 mM in DAB-Tris, 2) pre-polymerisation with sulfide; Ag(I)NO<sub>3</sub> in DAB-Tris, Co(II)Cl<sub>2</sub>, and K<sub>3</sub>Ir(III)Cl<sub>6</sub> in DAB-PO<sub>4</sub>, 3) post-polymerisation; K<sub>2</sub>Pt(II)Cl<sub>4</sub>, K<sub>2</sub>Pt(IV)Cl<sub>6</sub> and 4) post-polymerisation with sulfide; V(III)Cl<sub>3</sub>, Fe(II)Cl<sub>2</sub>, Cu(II)Cl<sub>2</sub>, Rh(III)Cl<sub>3</sub>, and NaAu(III)Cl<sub>4</sub>. Those to be amplified with Newman and Jasani's developer, all following treatment with Na<sub>2</sub>S, were 1) pre-polymerisation; Ni(II)Cl<sub>2</sub> at 5, 20 and 100 mM and Ag(I)NO<sub>3</sub> in DAB-Tris, and Co(II)Cl<sub>2</sub>, in DAB-PO<sub>4</sub> and 2) post-polymerisation; Cu(II)Cl<sub>2</sub>, Fe(II)Cl<sub>2</sub>, Au(III)Cl<sub>3</sub> and NaAu(III)Cl<sub>4</sub>.

#### **2.4.3.1 Selection of Appropriate Antibody Dilutions**

The primary antibody dilution that produced immunohistochemical staining that was just visible was  $1/4000$  (figure 2.8a).

Table 2.9. Summary of results from back-scattered electron imaging and X-ray microanalysis.

Metal	Pre-polymerisation DAB-PO4		Pre-polymerisation DAB-Tris		Post-polymerisation	
	BSI	X-ray	BSI	X-ray	BSI	X-ray
Sc(III)Cl <sub>3</sub>	x	x	x	x	x	x
Y(III)Cl <sub>3</sub>	x	x	x	x	x	x
La(III)Cl <sub>3</sub>	x	x	x	x	x	x
V(III)Cl <sub>3</sub>	x	x	x	x	x	x
Cr(II)Cl <sub>2</sub>	x	x	x	x	x	x
Cr(III)Cl <sub>3</sub>	x	x	x	x	x	x
H <sub>3</sub> PMo(IV) <sub>12</sub> O <sub>40</sub>	✓	✓	-	-	x	x
Na <sub>2</sub> W(VI)O <sub>4</sub>	✓	✓	-	-	✓	✓
H <sub>3</sub> PW(IV) <sub>12</sub> O <sub>40</sub>	x	x	✓	x	x	x
Mn(II)Cl <sub>2</sub>	x	x	x	x	x	x
Re(III)Cl <sub>3</sub>	x	x	x	x	x	x
Fe(II)Cl <sub>2</sub>	x	x	-	-	x	x
Fe(III)Cl <sub>3</sub>	x	x	-	-	x	x
Ru(III)Cl <sub>3</sub>	x	x	x	x	x	x
K <sub>3</sub> Ru(III)Cl <sub>6</sub>	x	x	x	x	x	x
K <sub>2</sub> Os(IV)Cl <sub>6</sub>	x	x	✓	x	x	x
Os(VIII)O <sub>4</sub>	-	-	-	-	✓	x
Co(II)Cl <sub>2</sub>	x	x	x	x	x	x
Rh(III)Cl <sub>3</sub>	x	x	x	x	✓	✓
Ir(IV)Cl <sub>4</sub>	x	x	x	x	x	x
K <sub>3</sub> Ir(III)Cl <sub>6</sub>	x	x	x	x	x	x
K <sub>2</sub> Ir(IV)Cl <sub>6</sub>	x	x	x	x	x	x
Ir(VI)Cl <sub>4</sub>	✓	x	✓	x	✓	x
Ni(II)Cl <sub>2</sub>	x	✓	x	x	x	x
Ni(II)Cl <sub>2</sub> 5 mM	-	-	x	x	x	x
Ni(II)Cl <sub>2</sub> 20 mM	-	-	x	x	x	x
Ni(II)Cl <sub>2</sub> 100 mM	-	-	x	x	x	x
K <sub>2</sub> Pd(II)Cl <sub>4</sub>	-	-	-	-	✓	✓
K <sub>2</sub> Pd(IV)Cl <sub>6</sub>	-	-	-	-	✓	✓
K <sub>2</sub> Pt(II)Cl <sub>4</sub>	✓	x	✓	✓	✓	x



$\text{K}_2\text{Pt(IV)Cl}_6$	x	x	✓	x	✓	x
$\text{Cu(II)Cl}_2$	x	x	-	-	x	x
$\text{Ag(I)NO}_3$	x	x	-	-	x	x
$\text{NaAu(III)Cl}_4$	-	-	-	-	✓	✓
$\text{Zn(II)Cl}_2$	x	x	x	x	x	x

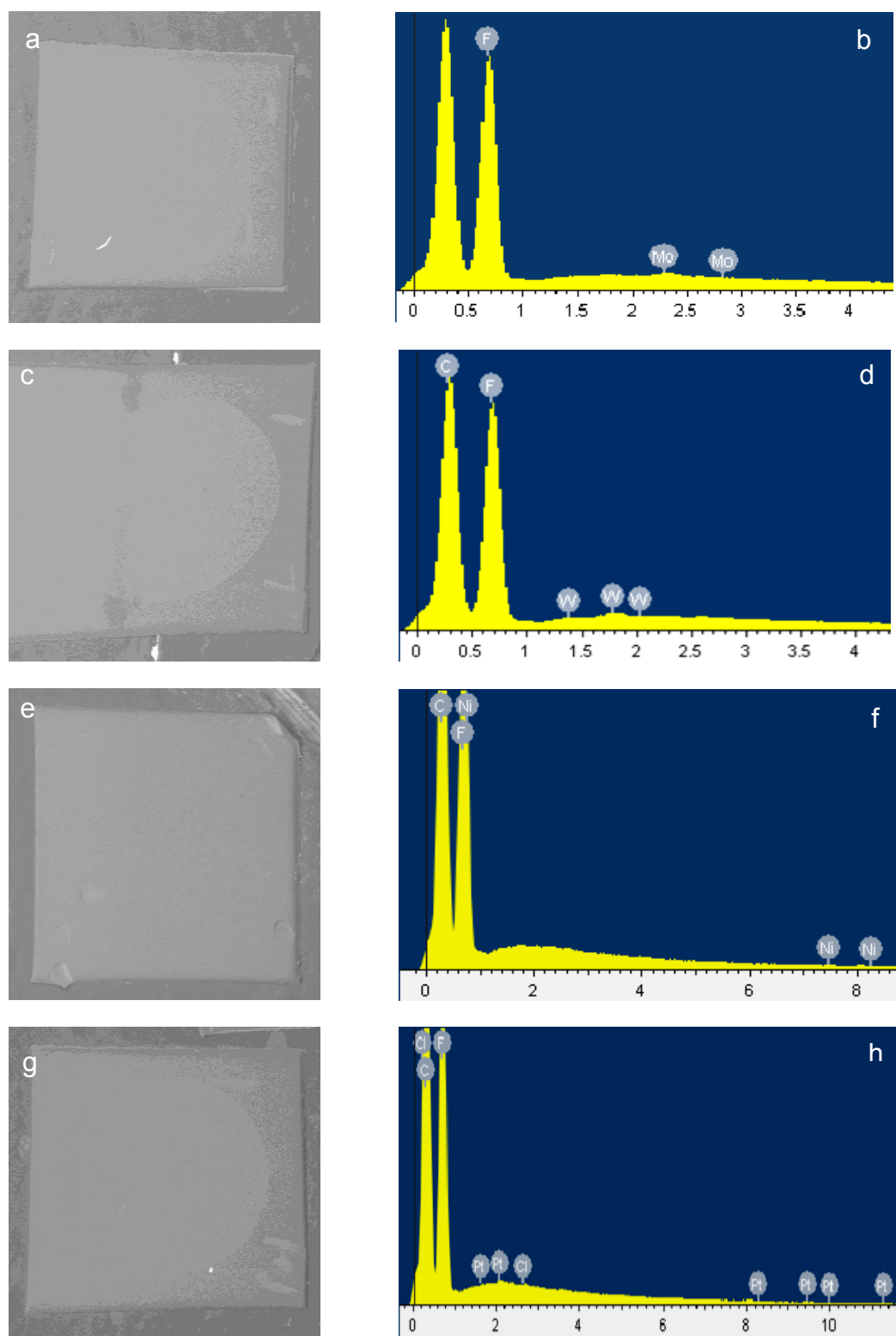


Figure 2.6. Back-scattered electron images and corresponding X-ray emission spectra of pre-polymerisation dot blots of  $\text{H}_3\text{PMo(IV)}_{12}\text{O}_{40}$  (a and b) and  $\text{NaW(VI)O}_4$  (c and d) from DAB- $\text{PO}_4$ , and  $\text{Ni(II)Cl}_2$  (e and f) and  $\text{K}_2\text{Pt(II)Cl}_4$  (g and h) from DAB-Tris.

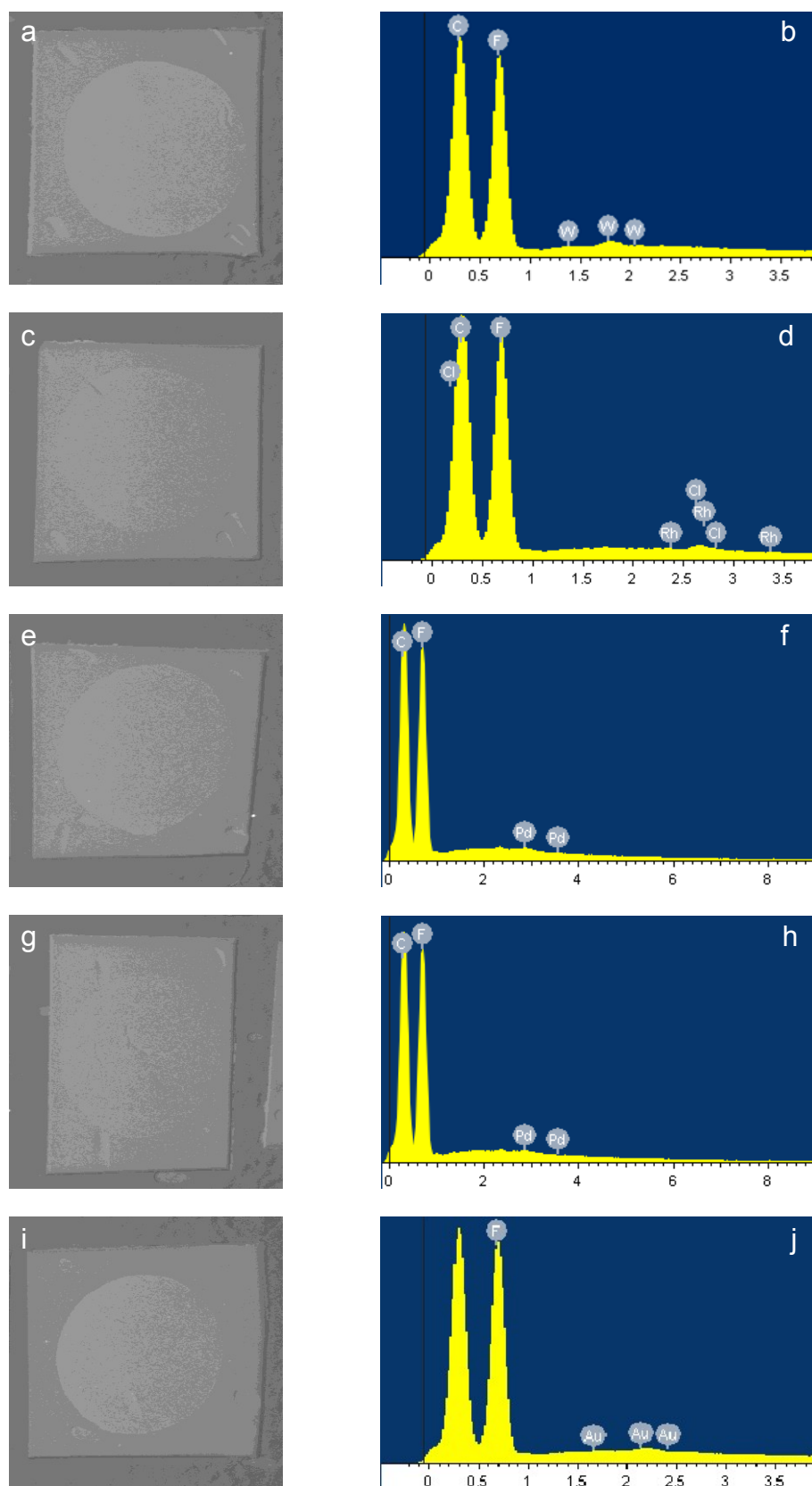


Figure 2.7. Back-scattered electron images and corresponding X-ray emission spectra of post-polymerisation dot blots.  $\text{Na}_2\text{W(VI)O}_4$  (a and b),  $\text{Rh(III)Cl}_3$  (c and d),  $\text{K}_2\text{Pd(II)Cl}_4$  (e and f)  $\text{K}_2\text{Pd(IV)Cl}_6$  (G and h) and  $\text{NaAu(III)Cl}_4$  (i and j).

#### **2.4.3.2 Pre-polymerisation with Gallyas' Developer**

Ni(II)Cl<sub>2</sub> showed a slight concentration dependent increase in maximal staining intensity and a more marked concentration dependent decrease in staining time. At the highest concentration (100 mM) (figure 2.8b), background staining was slightly elevated.

#### **2.4.3.3 Pre-polymerisation plus Sulfide and Physical Developers**

With Gallyas' developer, Ag(I)NO<sub>3</sub> produced increased specific staining with little general background, although erythrocyte (red blood cell) staining was dramatically increased. Only slight amplification was seen with either Co(II)Cl<sub>2</sub>, or K<sub>3</sub>Ir(III)Cl<sub>6</sub>.

With Newman and Jasani's developer, Ag(I)NO<sub>3</sub> produced the strongest response (figure 2.8c). In contrast to Gallyas' developer, no significant erythrocyte staining was observed. Ni(II)Cl<sub>2</sub> produced similar, albeit reduced, specific amplification compared with Gallyas' developer. Co(II)Cl<sub>2</sub> produced a greater amplification than was seen following Gallyas' developer, but background staining was high.

#### **2.4.3.4 Post- polymerisation and Gallyas' Developer**

Dramatic amplification was seen with both platinum salts which, like the dot blots, were both maximally amplified in just 1 minute (figure 2.9a).

#### 2.4.3.5 Post- polymerisation plus Sulfide and Physical Developers

With Gallyas' developer, amplification was observed with  $\text{NaAu(III)Cl}_4$ ,  $\text{V(III)Cl}_3$  (figure 2.9b) and, to a slightly lesser extent,  $\text{Rh(III)Cl}_3$ .  $\text{K}_3\text{Ir(III)Cl}_6$  produced little intensification whereas  $\text{Cu(II)Cl}_2$  produced increased background staining which rapidly overwhelmed the slight increase in specific staining intensity.

Of the three metal salts tested with Newman and Jasani's developer, only  $\text{NaAu(III)Cl}_4$  produced any intensification (figure 2.9c).  $\text{Fe(II)Cl}_2$  produced an almost immediate and dramatic increase in background staining which made observation of any specific amplification impossible.  $\text{Cu(II)Cl}_2$  produced similar results to those seen with Gallyas' developer (figure 2.9d).

Visualisation of immunocolloidal gold required 20 minutes in Gallyas', and 30 minutes in Newman and Jasani's (figure 2.9e) developers, respectively. Background staining was restricted to erythrocytes in the case of Gallyas' developer, but none was seen with Newman and Jasani's. Results are summarised in table 2.10.

Table 2.10 Summary of immunohistochemical amplification with Gallyas' and Newman and Jasani's physical developers arranged in order of strength and specificity (signal minus background)

Metal	Application and Developer	Time (minutes)	Signal - Background
Colloidal Gold	Newman and Jasani	30	6
NaAu(III)Cl <sub>4</sub> + Na <sub>2</sub> S	Post-, Newman and Jasani	8	6
K <sub>2</sub> Pt(II)Cl <sub>4</sub>	Post-, Gallyas	1	5
K <sub>2</sub> Pt(IV)Cl <sub>6</sub>	Post-, Gallyas	1	5
NaAu(III)Cl <sub>4</sub> + Na <sub>2</sub> S	Post-, Gallyas	6	5
V(III)Cl <sub>3</sub> + Na <sub>2</sub> S	Post-, Gallyas	10	5
Ag(I)NO <sub>3</sub> + Na <sub>2</sub> S	Pre-, Newman and Jasani	13.5	5
Colloidal Gold	Gallyas	20	4
Ni(II)Cl <sub>2</sub> 100 mM	Pre-, Gallyas	4	4
Ni(II)Cl <sub>2</sub> 20 mM	Pre-, Gallyas	6	4
Ni(II)Cl <sub>2</sub> 5 mM	Pre-, Gallyas	8.5	4
Rh(III)Cl <sub>3</sub> + Na <sub>2</sub> S	Post-, Gallyas	10	4
Ni(II)Cl <sub>2</sub> 1 mM	Pre-, Gallyas	10	3
Ag(I)NO <sub>3</sub> + Na <sub>2</sub> S	Pre-, Gallyas	10	3
Ni(II)Cl <sub>2</sub> 100 mM + Na <sub>2</sub> S	Pre-, Newman and Jasani	5.5	2
Co(II)Cl <sub>2</sub> + Na <sub>2</sub> S	Pre-, Newman and Jasani	7.5	2
Ni(II)Cl <sub>2</sub> 20 mM + Na <sub>2</sub> S	Pre-, Newman and Jasani	8	2
Ni(II)Cl <sub>2</sub> 5 mM + Na <sub>2</sub> S	Pre-, Newman and Jasani	11	2
Co(II)Cl <sub>2</sub> + Na <sub>2</sub> S	Pre-, Gallyas	3	1
K <sub>3</sub> Ir(III)Cl <sub>6</sub>	Pre-, Gallyas	10	1
Na <sub>2</sub> S	Post-, Newman and Jasani	13.5	1
Cu(II)Cl <sub>2</sub> + Na <sub>2</sub> S	Post-, Newman and Jasani	6.5	-2
Cu(II)Cl <sub>2</sub> + Na <sub>2</sub> S	Post-, Gallyas	1.5	-2
Fe(II)Cl <sub>2</sub> + Na <sub>2</sub> S	Post-, Newman and Jasani	1	-6

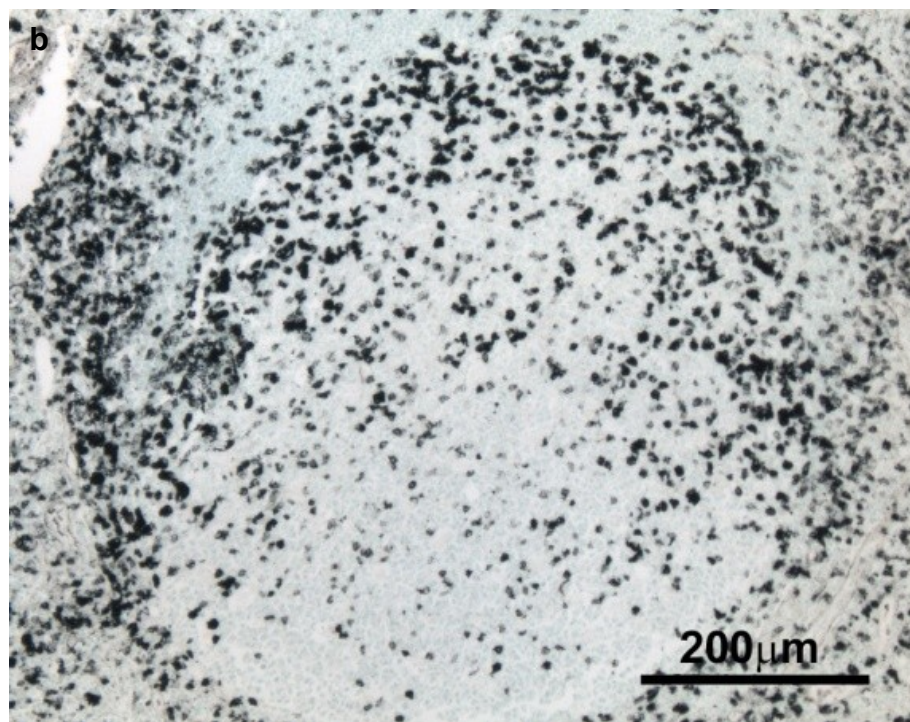
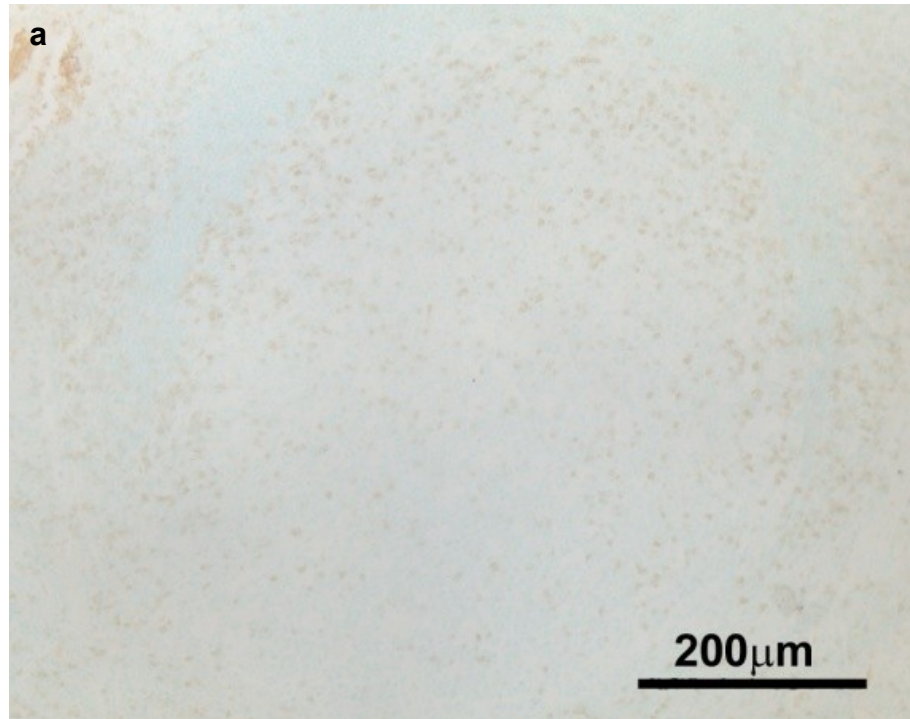


Figure 2.8. 4 μm thick paraffin wax-embedded tonsil immunohistochemically stained for CD45Ro with metals applied pre-polymerisation; DAB alone (a), 100 mM Ni(II) + Gallyas' developer (b).



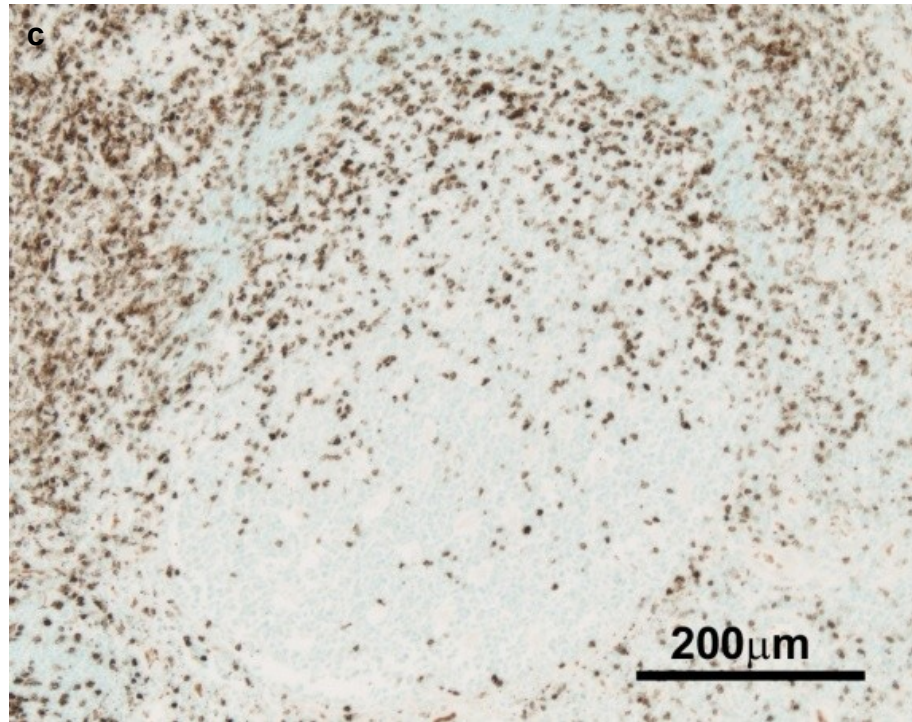


Figure 2.8 (continued). 4 μm thick paraffin wax-embedded tonsil immunohistochemically stained for CD45Ro with metal applied pre-polymerisation; Ag(I) + Na<sub>2</sub>S + Newman and Jasani's developer (c).



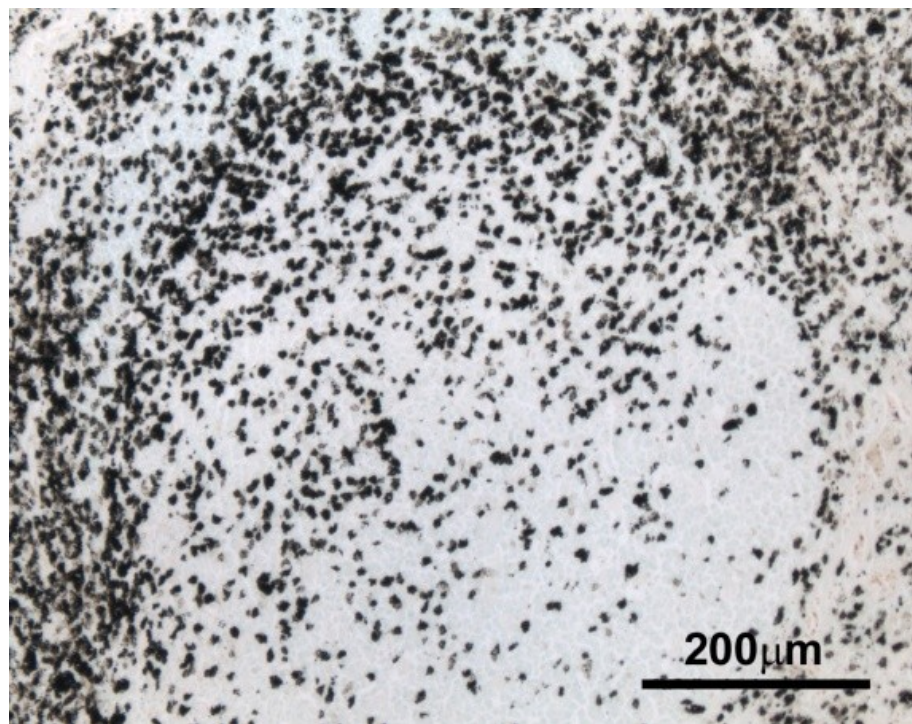
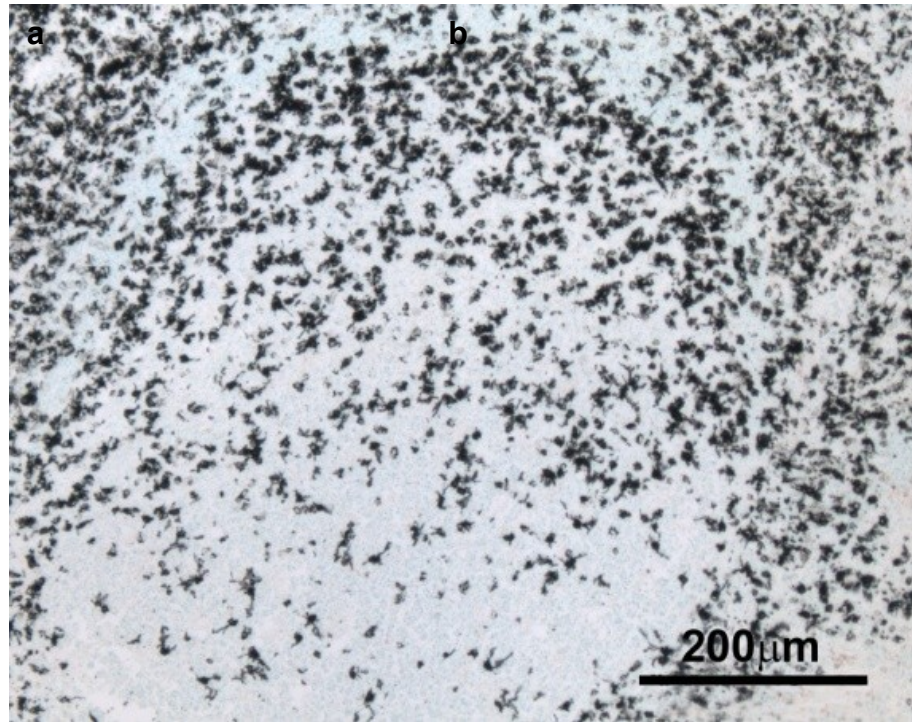


Figure 2.9. 4  $\mu\text{m}$  thick paraffin wax-embedded tonsil immunohistochemically stained for CD45Ro with metals applied post-polymerisation; Pt(II) + Gallyas' developer (1 minute) (a) V(III) +  $\text{Na}_2\text{S}$  + Gallyas' developer (b).



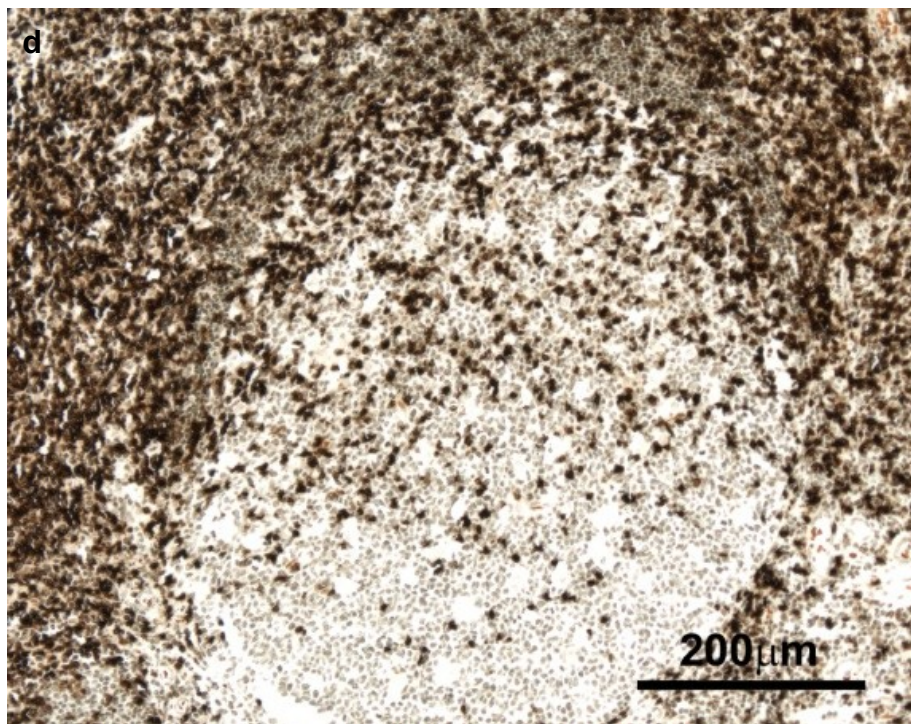
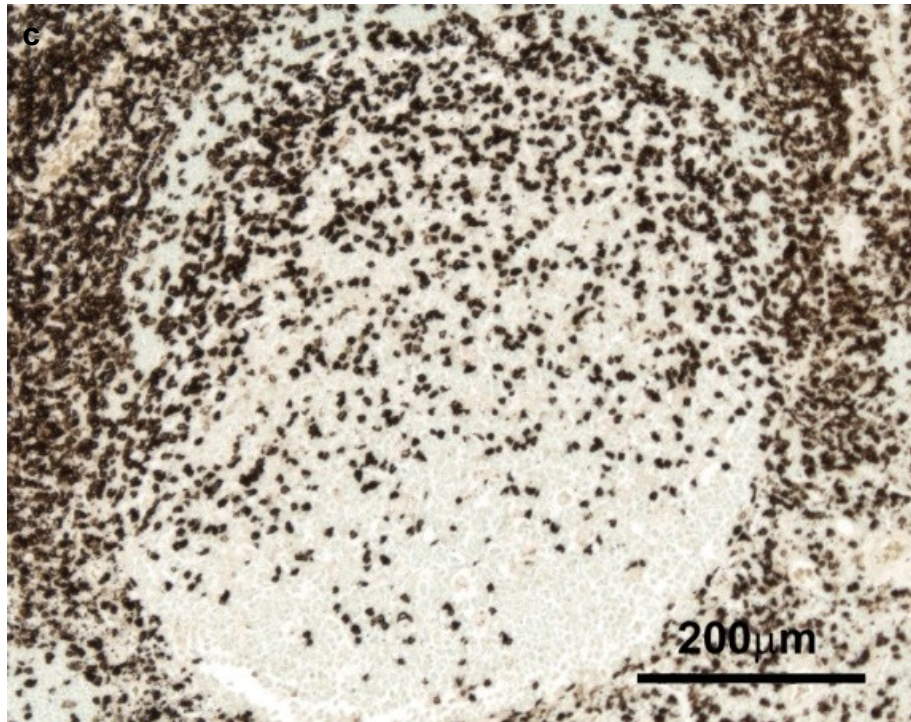


Figure 2.9 (continued). 4  $\mu\text{m}$  thick paraffin wax-embedded tonsil immunohistochemically stained for CD45Ro with metals applied post-polymerisation; Au(III) + Na<sub>2</sub>S + Newman and Jasani's developer (c), Cu(II) + Na<sub>2</sub>S + Newman and Jasani's developer (d).

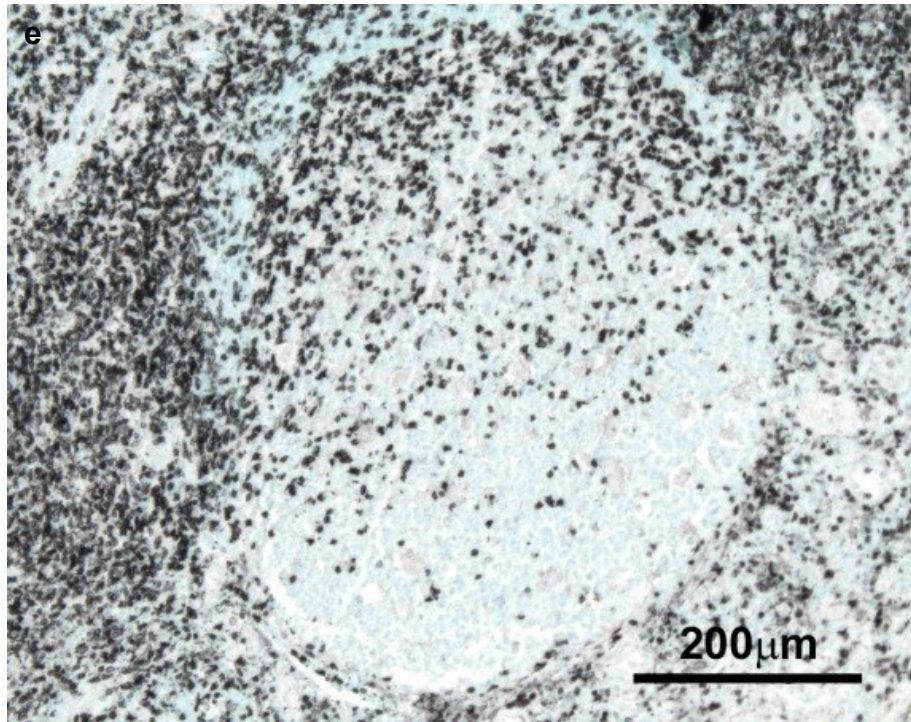


Figure 2.9 (continued). 4 μm thick paraffin wax-embedded tonsil immunohistochemically stained for CD45Ro and colloidal gold + Newman and Jasani's developer (e).

#### 2.4.4 Diagnostic Immunohistochemistry

In Hodgkin's lymphoma tissue sections immunostained for LMP-1, marker intensity was generally weak, even with both antigen retrieval and reporter amplification (figure 2.10a). Marker amplification using  $\text{NaAu(III)Cl}_4 + \text{Na}_2\text{S} +$  Newman and Jasani's developer resulted in dramatic improvements in visible signal strength together with the demonstration of additional positively stained sites which were previously below the detection limit of the conventional method (figure 2.10b).

Marker intensity in control tonsil tissue that had been immunostained for granzyme B was barely discernable, even though, as with LMP-1 staining, target retrieval and reporter amplification had been employed (figure 2.11a). Following marker amplification, immunopositive sites were clearly seen, as were additional sites that were previously invisible (figure 2.11b).

In control Alzheimer's brain sections,  $\alpha$ -synuclein-positive cells could be clearly seen at higher power, although staining in some cases was weak (figure 2.12a). Marker amplification resulted in all immunopositive sites becoming clearly visible (figure 2.12b). At lower power, positive sites in control sections could just be discerned (figure 2.12c). Staining intensity was markedly increased following marker amplification, and allowed positively stained cells to be clearly identified (figure 2.12d).



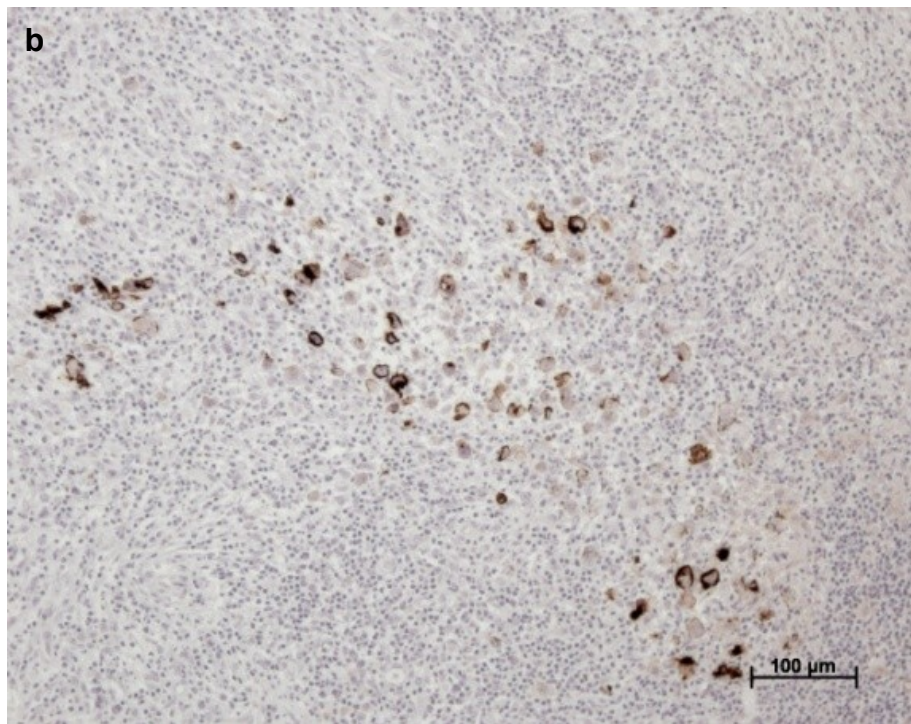
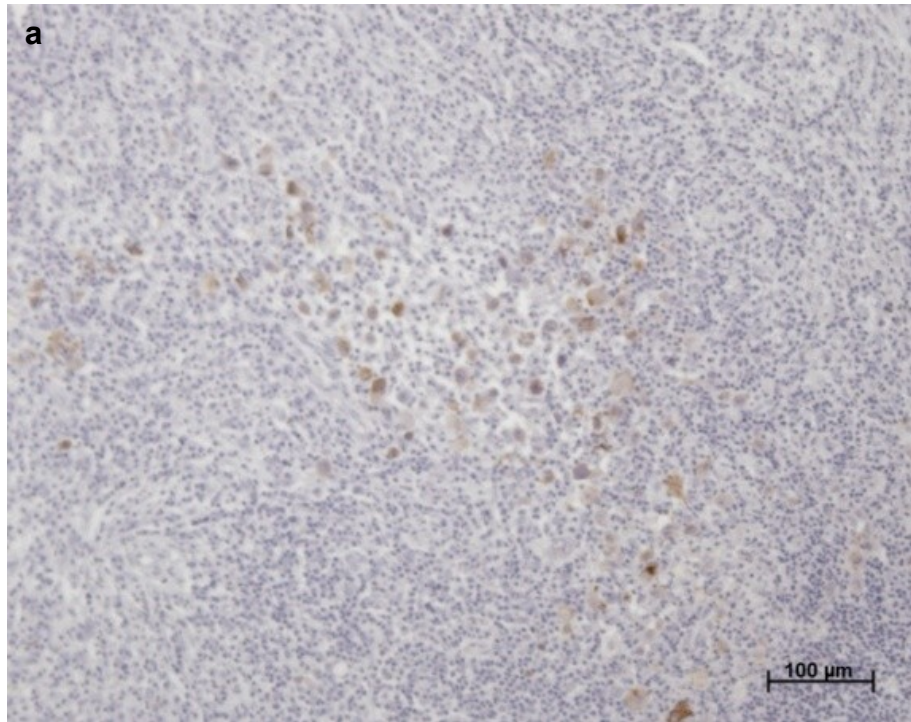


Figure 2.10. 4 μm thick paraffin wax-embedded stage 4 Hodgkin's lymphoma tissue immunohistochemically stained for LMP-1 (a) and after marker amplification (b).

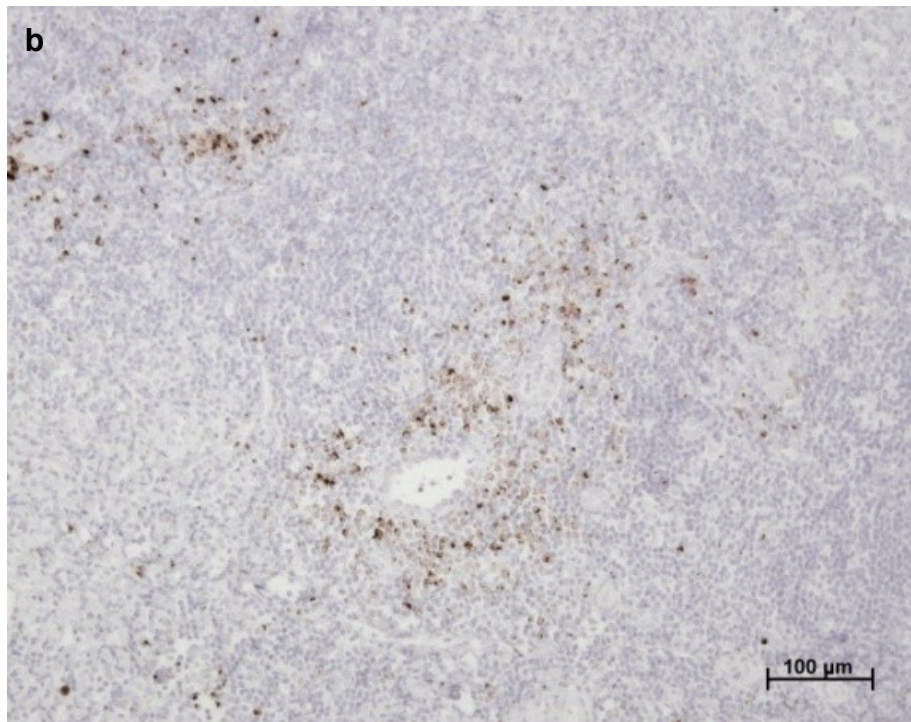
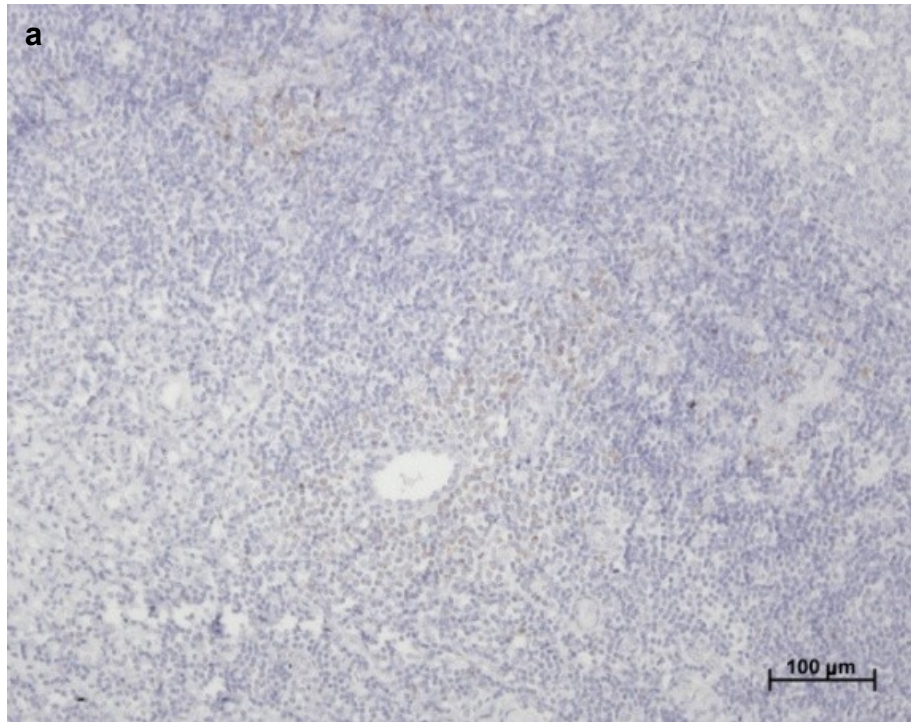


Figure 2.11. 4 μm thick paraffin wax-embedded tonsil immunohistochemically stained for granzyme B (a) and following marker amplification (b).



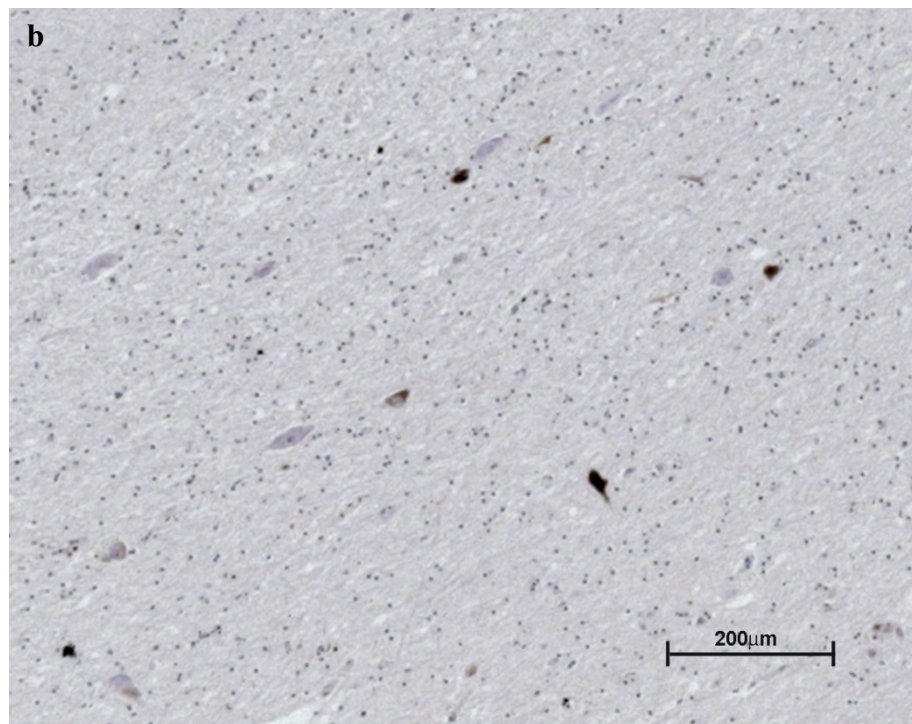
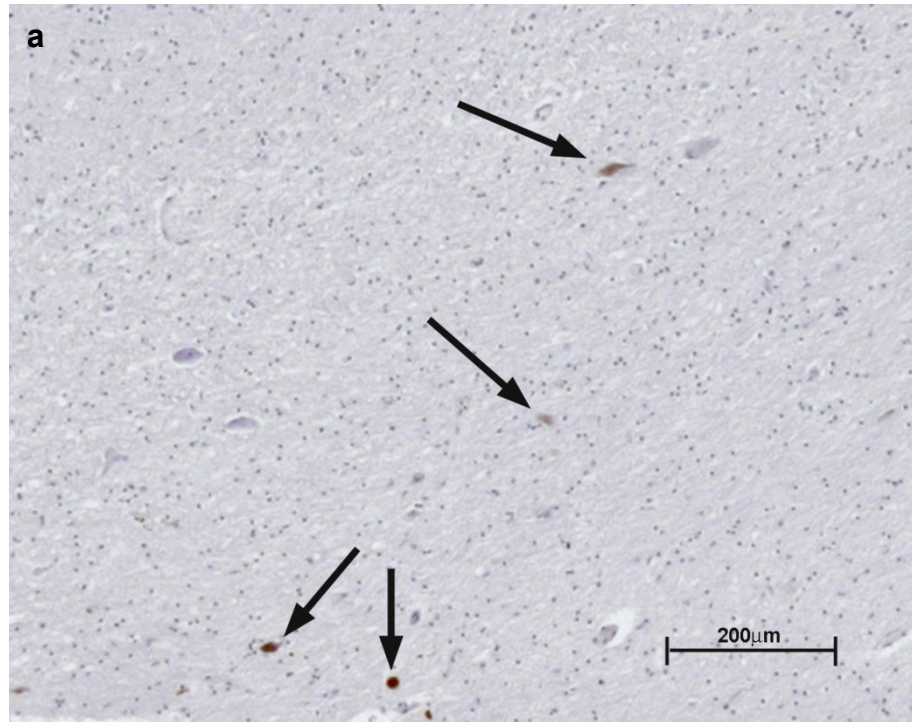


Figure 2.12. Higher power images of 4  $\mu\text{m}$  thick paraffin wax-embedded brain tissue from Alzheimer's disease immunohistochemically stained for  $\alpha$ -synuclein, showing clearly visible and faint staining (arrows) (a) and following marker amplification (b).

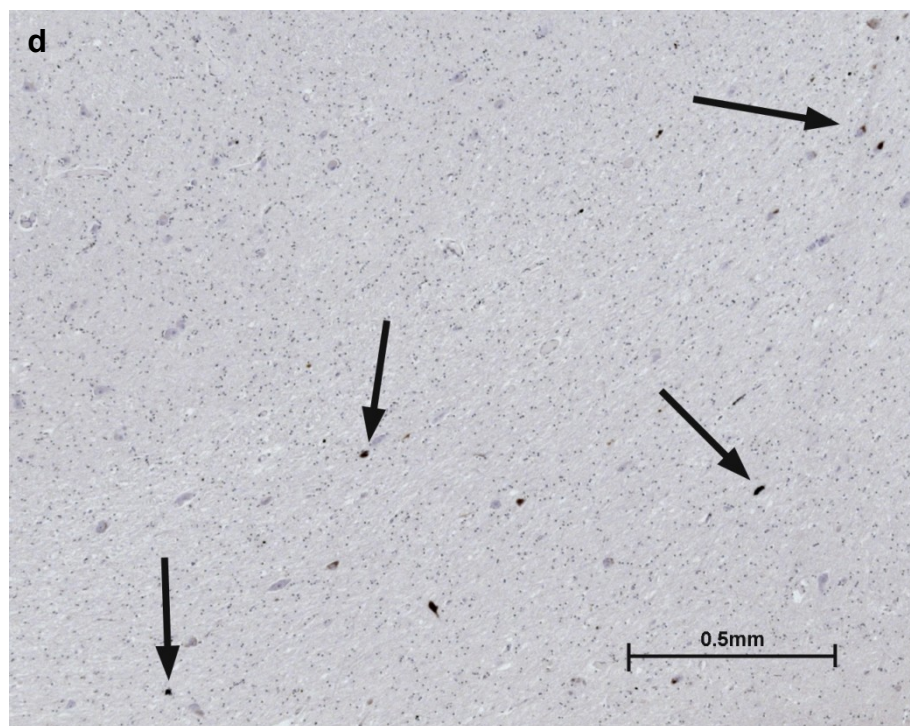
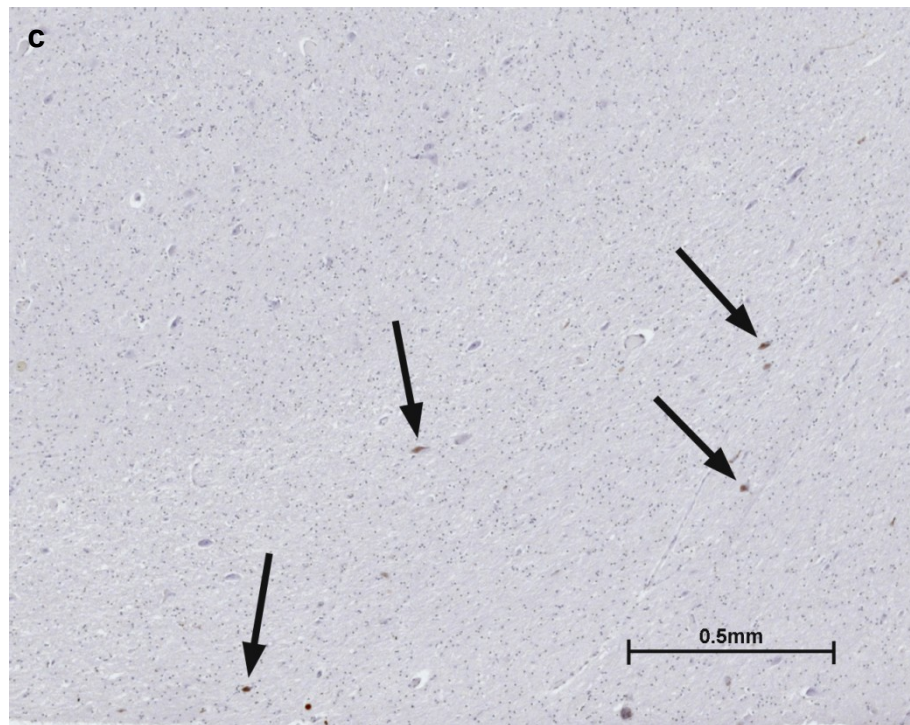


Figure 2.12 (continued). Lower power images of 4  $\mu$ m thick paraffin wax-embedded brain tissue from Alzheimer's disease immunohistochemically stained for  $\alpha$ -synuclein, showing visible staining (arrows) (c) and following marker amplification, showing more intense immunopositive sites (arrows) (d).



#### **2.4.5 Alkaline Phosphatase Marker Amplification**

In the absence of metal salts, dots were magenta in colour. In the presence of cobalt, nickel and copper salts, blue dots were produced under both pre- and post-reduction conditions. Neither Gallyas', nor Newman and Jasani's developer succeeded in amplifying any of the dot blot preparations.

Treatment with sodium sulfide instantly caused both the dots and the membrane to turn black. To further investigate this reaction to sulfide treatment, MTT was replaced with nitro blue tetrazolium (NBT). Treatment with sodium sulfide produced identical results.

## 2.5 Discussion

In preliminary dot blot experiments, amplification of polyDAB combined with a number of d-block metal salts in both a pre- and post-polymerisation setting, with or without subsequent treatment with  $\text{Na}_2\text{S}$ , was achieved by both Gallyas' and Newman & Jasani's physical developers, and allowed previously invisible amounts of marker to be clearly seen.  $\text{Na}_2\text{S}$  treatment not only increased the range of polyDAB-metal salts that could be amplified but, in general, also increased the degree of amplification.

The best results, which were subsequently evaluated in the immunohistochemical model, were those that involved the post-polymerisation application of d-block metal salts, usually in combination with  $\text{Na}_2\text{S}$ .

Of groups 3 to 6, only  $\text{V(III)Cl}_3$  catalysed silver reduction in the post-polymerisation setting, and only with Gallyas' developer after  $\text{Na}_2\text{S}$  treatment. In addition, it performed much better in the tissue model system than the result from the dot blot experiment suggested. It was not, however, demonstrable by either BSI or EDX. In contrast,  $\text{H}_3\text{PMo(IV)}_{12}\text{O}_{40}$ ,  $\text{Na}_2\text{W(VI)O}_4$  and  $\text{H}_3\text{PW(IV)}_{12}\text{O}_{40}$  were all detectable by these methods in some settings, yet none of them catalysed silver reduction. Phosphotungstic acid has previously been reported to increase the electron opacity of polyDAB in a post-polymerisation setting (Newman et al., 1983a) at a similar concentration (1%, 3.4 mM) to that used here (2.5 mM), but was not detectable by BSI or X-ray analysis in the post-polymerisation setting.

Group 7 metals either did not catalyse silver reduction ( $\text{Mn(II)Cl}_2$ ), or produced widespread background staining of the dot blots ( $\text{Re(III)Cl}_3$ ) and were not investigated in the tissue model. Neither metal was demonstrable by BSI or EDX.

The general effect of Group 8 metals was to elevate non-specific background staining of the dot blots. The only exceptions were the combination of Fe(II)Cl<sub>2</sub>, either pre-polymerisation with DAB-PO<sub>4</sub> or post-polymerisation, followed by Na<sub>2</sub>S and Newman and Jasani's developer, or the post-polymerisation application of Os(VIII)O<sub>4</sub> followed by Gallyas' developer. In the case of Fe(II)Cl<sub>2</sub>, the promising results of the dot blots were not, however, replicated in the tissue model system where widespread background staining occurred within seconds. Only the osmium compounds were detectable by BSI, and then only a faint increase in dot blot brightness was seen.

Group 9 metals performed poorly in the pre-polymerisation experiments and, like those of Group 8, tended to increase background staining. Co(II)Cl<sub>2</sub> produced encouraging results when combined with Na<sub>2</sub>S and Newman & Jasani's developer, but results from the tissue model system were disappointing. Cobalt(II) has received considerably less attention in the literature than nickel(II), even though it was the first metal to be incorporated into polyDAB for light microscopical applications (Adams, 1977). A probable explanation for this is that the most commonly employed buffer for DAB is Tris, and cobalt(II) appears to be unstable in this system. In the post-polymerisation setting, no change in the colour of polyDAB was observed following incubation in Co(II)Cl<sub>2</sub>, nor was any reduction of silver noted, even after Na<sub>2</sub>S treatment. In contrast, both Rh(III)Cl<sub>3</sub> and the iridium salts produced moderate amplification following Na<sub>2</sub>S treatment, but only with Gallyas' developer. In the immunohistochemical model, Rh(III)Cl<sub>3</sub> performed moderately well whereas the only iridium salt (K<sub>3</sub>Ir(III)Cl<sub>6</sub>) that was tested produced rather poor results compared with what had been observed in the dot blot model.

Dramatic improvements in staining intensity and specificity were observed with Group 10 metals, compared to previous groups. The stability of high concentrations of Ni(II)Cl<sub>2</sub> in DAB-Tris was both remarkable and unique. In the dot blot model, sensitivity increased with nickel(II) concentrations up to 20 mM in combination with Gallyas' developer, but this was not reflected in the immunohistochemical model where increasing concentrations of nickel(II) reduced the endpoint time, but did not appear to improve sensitivity. A similar pattern was observed with Newman and Jasani's developer, but there was a requirement for Na<sub>2</sub>S treatment, and intensity of staining was less. The blue/black colour of dot blots produced by Ni(II)Cl<sub>2</sub> in the pre-polymerisation experiments, like Co(II)Cl<sub>2</sub>, was lost following incubation in Newman & Jasani's developer, and was caused, primarily, by the reducing agent, pyrogallol and, to some extent, by the reducer buffer, citrate. This extractive effect could be replicated by EDTA, suggesting that it was not necessarily due to reduction by pyrogallol. Surprisingly, neither cobalt(II) nor nickel(II) appeared to be re-introduced into extracted polyDAB, as indicated by colour change. Similarly, neither salt promoted amplification in the post-polymerisation setting. Ni(II)Cl<sub>2</sub> in DAB-PO<sub>4</sub>, but not in DAB-Tris was detected by EDX. The reason for this is unclear, since results from the amplification experiments suggested that greater amounts would be present at the higher concentrations of nickel(II) that were included in DAB-Tris combinations. It is, however, possible that nickel(II) was also deposited as its phosphate in the DAB-PO<sub>4</sub> mixture in addition to catalytic quantities in polyDAB, although similar results were not observed for cobalt(II). Both compounds might also have altered the nature of the final product during the polymerisation process, rendering it more catalytic, which might explain why both

nickel(II) and cobalt(II) salts could be successfully employed pre-polymerisation, but not post-polymerisation. Nickel(II) salts (either Ni(II)Cl<sub>2</sub> or Ni(II)(NH<sub>4</sub>)<sub>2</sub>SO<sub>4</sub>) have been used at concentrations of 1 mM (Hsu and Soban, 1982), 10 mM (Lanciego et al., 1997; Gonzalo et al., 2001), 40 mM (Tajima et al., 2000) and 63 mM (Hancock, 1982; 1984) or over a range of 0.25 – 126 mM (Tago et al., 1986) and it surprising that similar nickel(II) concentrations have not been employed in combination with physical developers. Where subsequent amplification has been applied, nickel(II) salts have not been used in excess of about 4 mM (Przepiorka and Myerson, 1986; Gallyas and Merchenthaler, 1988; Merchenthaler et al., 1989; Frigo et al., 1991; Mullink et al., 1992).

The two palladium compounds could only be employed in the post-polymerisation setting and promoted only slight amplification with physical developers alone, even though both could be detected by BSI and EDX. Amplification following Na<sub>2</sub>S treatment resulted in unacceptably high background staining and they were not tested in the tissue model system.

The platinum salts produced the most dramatic results of all in both the dot blot and immunohistochemical model systems when used in combination with Gallyas' developer. Amplification was so rapid that it was almost uncontrollable; the difference between the end point of signal amplification and the appearance of background staining was a matter of seconds. Surprisingly, treatment with Na<sub>2</sub>S had little beneficial effect and tended to worsen background staining. The presence of both compounds could, in general, be demonstrated by BSI, but were not so easily detectable by EDX. K<sub>2</sub>Pt(II)Cl<sub>4</sub> and K<sub>2</sub>Pt(IV)Cl<sub>6</sub> have been used to increase the electron opacity of polyDAB in both a pre- (Hiraoka and Hirai, 1992; 1995) and post-polymerisation setting (de Bruijn et al., 1986) respectively. Both studies

reported detectable levels of platinum at non-specific sites by EDX, which may explain the background staining observed with  $\text{K}_2\text{Pt(II)Cl}_4$  in the pre-polymerisation experiments. The absence of background staining observed in the post-polymerisation results may reflect differences in protocols; de Bruijn et al (1986) applied  $\text{K}_2\text{Pt(IV)Cl}_6$  as a 10% (219 mM) solution in 10% HCl, whereas in this study, the salt was applied as a simple 2.5 mM aqueous solution.

Group 11 metals produced similarly dramatic and intense amplification of polyDAB as that seen with the Group 10 metals. The post-polymerisation treatment of polyDAB with copper(II)chloride in combination with  $\text{Na}_2\text{S}$  gave very encouraging results in the dot blot model, but this was not reproduced in the immunohistochemical model, where rapid and widespread background staining occurred, similar to that seen with  $\text{Fe(II)Cl}_2$ . The suppression of tissue autofluorescence with copper(II)sulfate alone (Schnell et al., 1999), and both tissue autofluorescence (Kelly, 2010) and argyrophilia (Gallyas and Wolff, 1986) by copper(II)sulfate in combination with hydrogen peroxide suggests the widespread existence of copper(II) binding sites.

Silver(I)nitrate performed far better in a pre-polymerisation than in a post-polymerisation setting, but appeared to have an absolute requirement for  $\text{Na}_2\text{S}$  to be demonstrable with either developer. This may explain why polyDAB alone was not intensified by either developer in this study. Silver(I), from either developer, might interact with polyDAB, but not in such a way, or in sufficient quantities to be amplifiable. PolyDAB has been intensified with silver either as part of a physical developer (Gallyas et al., 1982; Gorcs et al., 1986) or in related silver staining techniques such as silver methanamine (Rodriguez et al., 1984) or ammoniacal

silver (Quinn and Graybiel, 1996). Metallic silver has been deposited directly by HRP in the enzyme metallography technique and has shown dramatically improved staining intensity when compared with clearly visible polyDAB (Hainfeld et al., 2002). No obvious metallic silver deposit was observed in the pre-polymerisation experiments involving silver(I)nitrate. Since the composition of the reagents that are used in the enzyme metallographic process have not been published it is not possible to account for these discrepancies.

$\text{NaAu(III)Cl}_4$ , following treatment with  $\text{Na}_2\text{S}$  produced excellent results with both developers, and was much more controllable than the platinum salts discussed above. It was the only metal in the group to be demonstrable by both BSI and EDX. The affinity of polyDAB for gold(III) salts was first noted in 1979 (Siegesmund et al., 1979) and was subsequently advocated as a replacement for osmium(VIII) as a means of rendering polyDAB electron opaque (Newman et al., 1983a).  $\text{NaAu(III)Cl}_4$  has been investigated previously with both Gallyas' (Newman et al., 1983b; Scopsi and Larsson, 1986; Green et al., 1989) and Newman and Jasani's developer (Newman and Jasani, 1998).

$\text{Zn(II)Cl}_2$ , the only representative of the group 12 metals, failed to catalyse silver reduction either alone, or following treatment with  $\text{Na}_2\text{S}$ . Zinc(II) in tissue can be demonstrated by the sulfide-silver technique (Danscher and Stoltenberg, 2006), but it presumably does not complex with DAB in appreciable quantities.

The most surprising feature of the pre-polymerisation experiments was how few d-block metal salts promoted silver amplification. With Gallyas' developer, only three salts produced any response at all, and Newman and Jasani's, developer gave negative results across the whole range. The failure of the latter developer to

perform as well as the former was due to the metal-extracting properties of some of its components, namely pyrogallol, citrate and sulfite.

The majority of metal salts were stable in both DAB-PO<sub>4</sub> and DAB-Tris at a final concentration of 1 mM. The instability of some d-block metal salts, namely copper(II) and palladium(II) has been noted previously (Hsu and Soban, 1982). Interestingly, these authors found cobalt(II) and iron(III), but not silver(I), to be stable in DAB-Tris, results that conflict with the findings here. In a detailed study of the d-block metal catalysed polymerisation of DAB in Tris buffer, Litwin found both copper(II) and cobalt(II) and, to a lesser extent, iron(III) and manganese(II) to be powerful catalysts (Litwin, 1982) and thus unsuitable for use in the pre-polymerisation setting. Similar effects were observed here, with the exception of manganese(II), which probably reflected both sub-optimal pH and concentration for this reaction.

Treatment with Na<sub>2</sub>S probably has two effects, namely increasing the catalytic activity of bound metal (Timm, 1958) and differentiation. The former effect has been used to advantage previously both at the light (Newman et al., 1983b) and electron microscopic levels (Smiley and Goldman-Rakic, 1993). The differentiating effect of Na<sub>2</sub>S has been observed previously with gold(III) salts (Newman and Jasani, 1998) and explains the difference in catalytic activity of polyDAB from nickel(II) containing solutions with Gallyas' developer, with or without Na<sub>2</sub>S treatment; proportionately more nickel(II) was dissolved by Na<sub>2</sub>S at lower concentrations of nickel(II) than at higher concentrations. Differences in the catalytic activity of polyDAB-metal complexes presumably reflect a balance between the two. Whether metal are completely converted to their respective



sulfides and are simply immobilised as insoluble products in polyDAB, or remain partly co-ordinated to polyDAB is unclear.

Analytical SEM examination of dot blots revealed a number of metals that had formed complexes with polyDAB. In addition, there was general agreement between BSI and EDX. BSI is a qualitative technique that relies on average atomic number for contrast. Consequently, it is less sensitive to low concentrations of low atomic number elements than to higher ones, which might explain the lack of contrast imparted to dot blots by the first row elements. EDX is both qualitative and quantitative and does not suffer from the same restrictions, but suffers, particularly in the SEM, from a high background Bremsstrahlung radiation at the lower energy ranges. Quantitation was not possible since the nitrogen peak of polyDAB was obscured by the broad carbon peak of both the membrane and the conductive carbon coating. Some separation of these peaks might have been achieved by increasing processing time, but this would have been at the expense of sensitivity, and acquisition time would have been considerably extended.

Accurate diagnosis in a busy histopathological setting ideally requires positive staining to be unequivocal. In the majority of cases where immunohistochemical staining is required, this is achieved by both target retrieval and reporter amplification techniques. There exist, however, a small number of cases where these are still inadequate to demonstrate clear positivity, and additional amplification is required. The application of the most powerful marker amplification technique to diagnostically relevant samples resulted in both the clarification of immunopositivity and the revelation of additional positivity that was below the visible detection limit of the conventional system. In a busy diagnostic setting, these former sites could be easily overlooked, leading to false diagnosis. In

addition, the detection of additional immunopositive sites might have implications for both diagnosis and subsequent treatment. Where immunopositive cells were visible before marker amplification, but present in low numbers and sparsely distributed i.e. in the control Alzheimer's brain sample, marker amplification made these positive sites much more easily visible and had the potential to facilitate rapid evaluation of large areas of tissue at low magnification.

Interest in marker amplification has diminished as a consequence of developments in target retrieval and reporter amplification, since these have lent themselves more readily to automation and thus widespread application, particularly in diagnostic laboratories and industry. Such techniques are not without their own problems, however. Target retrieval must be tailored to each antigen, making the establishment of standardised procedures difficult. In addition, it has been noted to increase false positive results due to biotin or biotin-like molecules (Kim et al., 2002). As the number of layers used in reporter amplification is increased, to detect ever smaller quantities of antigen, background staining may become an inevitable problem since each successive layer is applied in excess to ensure maximal detection of the previous layer. While polymeric conjugates overcome this to a certain extent, steric hindrance associated with such macromolecular structures might compromise sensitivity. The tyramide amplification technique represents another powerful method for detecting low concentrations of antigen but its widespread introduction has been confounded by problems such as non-specific background staining (Freedman and Maddox, 2001), uneven staining or paradoxical overstaining (Mengel et al., 1999).

Unlike other detection systems, marker amplification has the flexibility to be employed once the marker has been deposited, if required e.g. where positivity is

uncertain. Furthermore, fresh sections do not have to be cut and stained since the technique can be applied to the stained section, thus saving time and labour. An additional advantage of this is that archival tissue sections can be revisited.

The complexity of the techniques precludes their widespread use in routine laboratories, and considerable simplification is required. An understanding of both the co-ordination chemistry of polyDAB and the mechanistic chemistry underlying the amplification reaction would aid the rational design of novel amplifiable markers. Co-ordination complexes of aromatic amines and diamines have been described, such as those of 1,2-diaminobenzene and Ni(II) (Pank and Jun, 2005) (figure 2.13a) or Cr(III) (Redshaw et al, 1992) (figure 2.13b) or benzidine and Co(II) (Topacli and Topacli, 2003) (figure 2.13c). There was no obvious evidence of complex formation in solutions that remained stable in the presence of DAB, such as colour change, even though this was particularly evident post-polymerisation in a number of cases, notably Ni(II) and Co(II). What little co-ordination chemistry of polyDAB that exists is largely speculative; it has been suggested that the bonding of  $\text{Pt(IV)Cl}_6^{2-}$  to polyDAB at low pH (<0.3) is via electrostatic bonds to protonated amines (de Bruijn et al, 1986) (figure 2.13e). A more plausible structure might be that based on the Pt(II)-phenazine compounds of Siedle et al (1985), where the metal centre is directly co-ordinated to the nitrogen ligand (figure 2.13e). Both indamine and phenazine structures that are suggested to occur in polyDAB (Seligman et al, 1968) could thus act as ligands for d-block metals.

The failure of the alkaline phosphatase (AP) marker, MTT-metal, to catalyse silver reduction from either developer was unexpected in view of the success of the DAB experiments. Presumably, the co-ordination chemistry of the formazan-metal complex renders it non-catalytic.

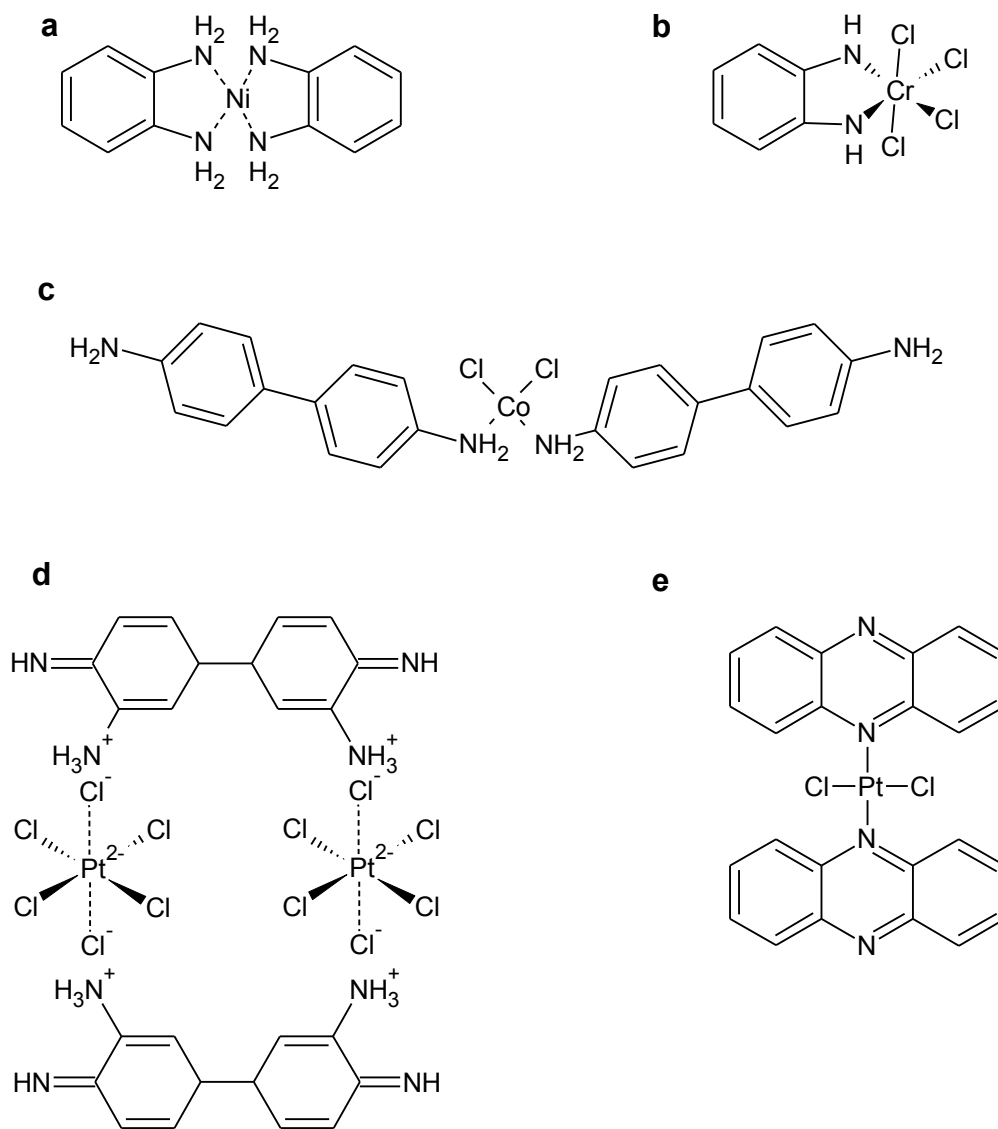


Figure 2.13. Co-ordination complexes of aromatic amines, diamines, polyDAB and phenazine. Bis(1,2-diaminobenzene)Ni(II) (a), 1,2-diaminobenzene Cr(III)Cl<sub>4</sub> (b), bis(3,3'-diaminobiphenyl)Co(II)Cl<sub>2</sub> (c), polyDAB-Pt(IV)Cl<sub>6</sub><sup>2-</sup> complex (d) and (phenazine)<sub>2</sub>-Pt(II)Cl<sub>2</sub> complex (e).

The coordination chemistry of a number of metal-formazan complexes have been described, such as those of with Fe(II), Ni(II), Cu(II) or Pd(II) centres, which adopt the form  $ML_2$  with bidentate ligands (Siedle and Pignolet, 1980; Gilroy et al., 2008; Pervova et al., 2010,) and those with Fe(III) or Co(III) centres, which form  $ML_3$  complexes with tetradentate ligands (Gilroy et al., 2008). Whether MTT adopts similar complexes remains to be determined, since this might provide useful insights into the mechanism of metal-catalysed silver reduction. The non-specific reaction to  $Na_2S$  was also surprising, particularly the blackening of the PVDF membrane which was presumably relatively free of formazan. Bound tetrazolium, which would probably be barely visible, may react with  $Na_2S$  to yield the black product and, given the identical response of NBT, this may be a common reaction of tetrazoliums.

## **2.6 Summary and Conclusions**

The main advantages of the peroxidase/DAB system are the rapidity of product formation and the permanence of the marker, polyDAB. It is probably for these two reasons alone that it has become and remained the marker of choice for immunohistochemistry at the light microscopic level. The main weakness of the system is product inhibition, and it is this that has necessitated the development of the various intensification and amplification procedures.

Amplification of polyDAB combined with a number of d-block metal salts in both a pre- and post-polymerisation setting, with or without subsequent treatment with sodium sulfide, was achieved by both Gallyas' and Newman and Jasani's physical developers, and allowed previously invisible amounts of marker to be

clearly seen. Na<sub>2</sub>S treatment not only increased the range of polyDAB-metal salts that could be amplified but, in general, also increased the degree of amplification.

With the notable exception of V(III)Cl<sub>3</sub>, those metal compounds that formed catalytic complexes with polyDAB were restricted to groups 8 – 11. Of these, metals in groups 10 and 11 were particularly powerful and, generally, resulted in the greatest specificity of reactivity.

Current marker amplification technology is too complex to be introduced into high-throughput automated procedures and suffers from a number of additional weaknesses namely:

- (1) The silver reagent of Gallyas' developer has a relatively short shelf life (about 3 months) and the reducer (hydroquinone) must be freshly prepared each time.
- (2) Newman and Jasani's developer, while considerably more stable than Gallyas', contains components, such as citrate and pyrogallol, which appear to extract almost all metals from polyDAB.
- (3) Na<sub>2</sub>S, which is an essential pre-treatment for Newman and Jasani's developer to work optimally, is unstable and has a pungent smell.
- (4) The choice and application of metal and silver developer requires experience and expertise.

This chapter has focussed on the histological application of marker amplification yet the technology described above could equally well be applied in other contexts, particularly those that seek to visualise molecules on membranes e.g. Western blotting. Under these conditions, many of the problems associated with tissue, mentioned above, no longer pertain and the use of, for example, platinum salts with Gallyas' developer or copper(II) + Na<sub>2</sub>S with Newman and Jasani's developer might well produce more superior results than hitherto obtained.

## 2.7 References

- ADAMS, J. C. 1977. Technical considerations on the use of horseradish peroxidase as a neuronal marker. *Neuroscience*, 2, 141-145.
- ADAMS, J. C. 1981. Heavy-metal intensification of DAB-based HRP reaction-product. *Journal of Histochemistry & Cytochemistry*, 29, 775.
- BRION, J. P., PASSAREIRO, H., NUNEZ, J. & FLAMENTDURAND, J. 1985. Immunological detection of Tau protein in neurofibrillary tangles of Alzheimer's disease. *Archives of Biology*, 96, 229-235.
- D'ERRICO, A., CORTI, B., PINNA, A. D., ALTIMARI, A., GRUPPIONI, E., GABUSI, E., FIORENTINO, M., BAGNI, A. & GRIGIONI, W. F. 2003. Granzyme B and perforin as predictive markers for acute rejection in human intestinal transplantation. *Transplantation Proceedings*, 35, 3061-3065.
- DANSCHER, G. 1981a. Histochemical demonstration of heavy metals - a revised version of the sulfide silver method suitable for both light and electron-microscopy. *Histochemistry*, 71, 1-16.
- DANSCHER, G. 1981b. Localization of gold in biological tissue - a photochemical method for light and electron microscopy. *Histochemistry*, 71, 81-88.
- DANSCHER, G. 1984. Autometallography - a new technique for light and electron microscopic visualization of metals in biological tissues (gold, silver, metal sulfides and metal selenides). *Histochemistry*, 81, 331-335.
- DANSCHER, G. & STOLTENBERG, M. 2006. Autometallography (AMG) - Silver enhancement of quantum dots resulting from (1) metabolism of toxic metals in animals and humans, (2) in vivo, in vitro and immersion created zinc-sulphur/zinc-selenium nanocrystals, (3) metal ions liberated from metal implants and particles. *Progress in Histochemistry and Cytochemistry*, 41, 57-139.
- DE BRUIJN, W. C., VAN DER MEULEN, J., BREDEROO, P. & DAEMS, W. T. 1986. Pt-staining of peroxidatic reaction products at the ultrastructural level. *Histochemistry*, 84, 492-500.

- FANAIAN, N. K., COHEN, C., WALDROP, S., WANG, J. & SHEHATA, B. M. 2009. Epstein-Barr Virus (EBV)-Encoded RNA: Automated in-situ hybridization (ISH) compared with manual ISH and immunohistochemistry for detection of EBV in pediatric lymphoproliferative disorders. *Pediatric and Developmental Pathology*, 12, 195-199.
- FREEDMAN, L. J. & MADDOX, M. T. 2001. A comparison of anti-biotin and biotinylated anti-avidin double-bridge and biotinylated tyramide immunohistochemical amplification. *Journal of Neuroscience Methods*, 112, 43-49.
- FRIGO, B., SCOPSI, L., PATRIARCA, C. & F., R. 1991. Silver enhancement of nickel-diaminobenzidine as applied to single and double immunoperoxidase staining. *Biotechnic & Histochemistry*, 66, 159-167.
- GALLYAS, F. 1979. Light insensitive physical developers. *Stain Technology*, 54, 173-175.
- GALLYAS, F., GORCS, T. & MERCHENTHALER, I. 1982. High grade intensification of the end product of the diaminobenzidine reaction for peroxidase histochemistry. *Journal of Histochemistry & Cytochemistry*, 30, 183-184.
- GALLYAS, F. & MERCHENTHALER, I. 1988. Copper-H<sub>2</sub>O<sub>2</sub> oxidation strikingly improves silver intensification of the nickel diaminobenzidine (Ni-DAB) end product of the peroxidase reaction. *Journal of Histochemistry & Cytochemistry*, 36, 807-810.
- GALLYAS, F. & WOLFF, J. R. 1986. Metal-catalyzed oxidation renders silver intensification selective - applications for the histochemistry of diaminobenzidine and neurofibrillary changes. *Journal of Histochemistry & Cytochemistry*, 34, 1667-1672.
- GEE, J. M. W., AMSELGRUBER, W. M., JASANI, B. & NICHOLSON, R. I. 1991. Use of the dinitrophenyl hapten sandwich staining procedure (DHSS) to localize estrogen receptors in paraffin-embedded tissues. *Journal of Histochemistry & Cytochemistry*, 39, 1659-1670.



- GILROY, J. B., PATRICK, B. O., MCDONALD, R. & HICKS, R. G. 2008. Transition metal complexes of 3-cyano- and 3-nitroformazans. *Inorganic Chemistry*, 47, 1287-1294.
- GOEDERT, M. 2001. Alpha-synuclein and neurodegenerative diseases. *Nature Reviews Neuroscience*, 2, 492-501.
- GOMORI, G. 1939. Microtechnical demonstration of phosphatase in tissue sections. *Proceedings of the Society for Experimental Biology and Medicine*, 42, 23 - 26.
- GONZALO, N., MORENO, A., ERDOZAIN, M. A., GARCIA, P., VAZQUEZ, A., CASTLE, M. & LANCIEGO, J. L. 2001. A sequential protocol combining dual neuroanatomical tract-tracing with the visualization of local circuit neurons within the striatum. *Journal of Neuroscience Methods*, 111, 59-66.
- GORCS, T. J., LERANTH, C. & MACLUSKY, N. J. 1986. The use of gold-substituted silver-intensified diaminobenzidine (DAB) and non-intensified DAB for simultaneous electron microscopic immunoperoxidase labeling of tyrosine hydroxylase and glutamic acid decarboxylase immunoreactivity in the rat medial preoptic area. *Journal of Histochemistry & Cytochemistry*, 34, 1439-1447.
- GREEN, M. A., SVILAND, L., MALCOLM, A. J. & PEARSON, A. D. J. 1989. Improved methods for immunoperoxidase detection of membrane antigens in frozen sections. *Journal of Clinical Pathology*, 42, 875-880.
- GU, J., DEMEY, J., MOEREMANS, M. & POLAK, J. M. 1981. Sequential use of the PAP and immunogold staining methods for the light microscopical double staining of tissue antigens - its application to the study of regulatory peptides in the gut. *Regulatory Peptides*, 1, 365-374.
- HAINFELD, J. F., EISEN, R. N., TUBBS, R. R. & D., P. R. 2002. Enzymatic metallography: A simple new staining method. *Microscopy and Microanalysis*, 8, 926-917.

- HAMEED, A., LOWREY, D. M., LICHTENHELD, M. & PODACK, E. R. 1988. Characterization of 3 serine esterases isolated from human IL-2-activated killer cells. *Journal of Immunology*, 141, 3142-3147.
- HAMEED, A., TRUONG, L. D., PRICE, V., KRUEHNBUEHL, O. & TSCHOPP, J. 1991. Immunohistochemical localization of granzyme-B antigen in cytotoxic cells in human tissues. *American Journal of Pathology*, 138, 1069-1075.
- HANCOCK, M. B. 1982. DAB-nickel substrate for the differential immunoperoxidase staining of nerve fibers and fiber terminals. *Journal of Histochemistry & Cytochemistry*, 30, 578-578.
- HANCOCK, M. B. 1984. Visualization of peptide-immunoreactive processes on serotonin-immunoreactive cells using 2-color immunoperoxidase staining. *Journal of Histochemistry & Cytochemistry*, 32, 311-314.
- HANKER, J. S., AMBROSE, W. W., JAMES, C. J., MANDELKORN, J., YATES, P. E., GALL, S. A., BOSSEN, E. H., FAY, J. W., LASZLO, J. & MOORE, J. O. 1979. Facilitated light microscopic cytochemical diagnosis of acute myelogenous leukemia. *Cancer Research*, 39, 1635-1639.
- HENLE, G., HENLE, W. & DIEHL, V. 1968. Relation of Burkitt's tumor-associated herpes-type virus to infectious mononucleosis. *Proceedings of the National Academy of Sciences of the United States of America*, 59, 94-101.
- HENLE, W. & HENLE, G. 1970. Evidence for a relation of Epstein-Barr virus to Burkitt's lymphoma and nasopharyngeal carcinoma. *Bibliotheca haematologica*, 706-713.
- HERMISTON, M. L., XU, Z. & WEISS, A. 2003. CD45: A critical regulator of signaling thresholds in immune cells. *Annual Review of Immunology*, 21, 107-137.
- HIRAOKA, T. & HIRAI, K. I. 1992. Platinum-diaminobenzidine reaction and its contribution to the quantitation of cytochrome oxidase activity. *Journal of Electron Microscopy*, 41, 127-129.

- HIRAOKA, T. & HIRAI, K. I. 1995. Cytochrome oxidase activity of individual mitochondrion as quantified by platinum-diaminobenzidine reaction with energy-dispersive X-Ray analyzer. *Acta Histochemica Et Cytochemica*, 28, 247-254.
- HOLGATE, C. S., JACKSON, P., COWEN, P. N. & BIRD, C. C. 1983. Immunogold silver staining - new method of immunostaining with enhanced sensitivity. *Journal of Histochemistry & Cytochemistry*, 31, 938-944.
- HSU, S. M. & SOBAN, E. 1982. Color modification of diaminobenzidine (DAB) precipitation by metallic ions and its application for double immunohistochemistry. *Journal of Histochemistry & Cytochemistry*, 30, 1079-1082.
- HUNTER, L. & ROBERTS, C. B. 1941. The Azo - group as a chelating group. Part V. Metallic derivatives of arylazo - oximes and formazyl compounds. *Journal of the Chemical Society*, 823 - 826.
- IDIKIO, H. A. 2010. Immunohistochemistry in diagnostic surgical pathology: contributions of protein life-cycle, use of evidence-based methods and data normalization on interpretation of immunohistochemical stains. *International Journal of Clinical and Experimental Pathology*, 3, 169-176.
- ISRAELBIET, D., LEGROSMAIDA, S., CLEMENT, M. V., CARNOT, F., REYNAUD, P. & SASPORTES, M. 1993. Perforin and granzyme B expression in alveolar lymphocytes is associated to severe acute lung rejection (ALR). *American Review of Respiratory Disease*, 147, A262.
- JOHANSSON, B., KLEIN, G., HENLE, W. & HENLE, G. 1970. Epstein-Barr virus (EBV)-associated antibody patterns in malignant lymphoma and leukemia.1. Hodgkin's disease. *International Journal of Cancer*, 6, 450-462.
- KAYE, K. M., IZUMI, K. M. & KIEFF, E. 1993. Epstein-Barr virus latent membrane protein 1 is essential for B lymphocyte growth transformation. *Proceedings of the National Academy of Sciences of the United States of America*, 90, 9150-9154.

- KELLY, S. 2010. *The Optimisation of Immunohistochemical Marker Amplification*.  
Bachelor of Science, University of Wales Institute, Cardiff.
- KIM, S. H., JUNG, K. C., SHIN, Y. K., LEE, K. M., PARK, Y. S., CHOI, Y. L.,  
OH, K. I., KIM, M. K., CHUNG, D. H., SONG, H. G. & PARK, S. H. 2002.  
The enhanced reactivity of endogenous biotin-like molecules by antigen  
retrieval procedures and signal amplification with tyramine. *Histochemical  
Journal*, 34, 97-103.
- LANCIEGO, J. L., GOEDE, P. H., WITTER, M. P. & WOUTERLOOD, F. G.  
1997. Use of peroxidase substrate Vector VIP for multiple staining in light  
microscopy. *Journal of Neuroscience Methods*, 74, 1-7.
- LAURITZEN, A. F., HORDING, U. & NIELSEN, H. W. 1994. Epstein-Barr  
virus and Hodgkin's disease - A comparative immunological, in-situ  
hybridization, and polymerase chain-reaction study. *Acta Pathologica  
Microbiologica et Immunologica Scandinavica*, 102, 495-500.
- LEGROSMADA, S., SOULIE, A., BENVENUTI, C., WARGNIER, A.,  
VALLEE, N., BERTHOU, C., GUILLET, J., SASPORTES, M. & SIGAUX,  
N. 1994. Granzyme-B and perforin can be used as predictive markers of acute  
rejection in heart transplantation. *European Journal of Immunology*, 24, 229-233.
- LEVY, J. A. & HENLE, G. 1966. Indirect immunofluorescence tests with sera  
from African children and cultured Burkitt lymphoma cells. *Journal of  
Bacteriology*, 92, 275-&.
- LICHTENHELD, M. G., OLSEN, K. J., LU, P., LOWREY, D. M., HAMEED,  
A., HENGARTNER, H. & PODACK, E. R. 1988. Structure and function of  
human perforin. *Nature*, 335, 448-451.
- LITWIN, J. A. 1982. Transition metal-catalysed oxidation of 3,3'-  
diaminobenzidine (DAB) in a model system. *Acta Histochemica*, 71, 111-117.

- MARGOLIS, G. 1959. Senile cerebral disease - a critical survey of traditional concepts based upon observations with newer technics. *Laboratory Investigation*, 8, 335-370.
- MASON, D. Y. & GATTER, K. C. 1987. The role of immunohistochemistry in diagnostic pathology. *Journal of Clinical Pathology*, 40, 1042-1054.
- McGADEY, J. 1967. Modified indoxyl acetate technique for the histochemical demonstration of non-specific esterases in mouse testis. *J Med Lab Technol*, 24, 126-128.
- MCGADEY, J. 1970. A tetrazolium method for non-specific alkaline phosphatase. *Histochemie*, 23, 180-184.
- MENGEL, M., WERNER, M. & VON WASIELEWSKI, R. 1999. Concentration dependent and adverse effects in immunohistochemistry using the tyramine amplification technique. *Histochemical Journal*, 31, 195-200.
- MERCHENTHALER, I., STANKOVICS, J. & GALLYAS, F. 1989. A highly sensitive one-step method for silver intensification of the nickel diaminobenzidine end-product of peroxidase reaction. *Journal of Histochemistry & Cytochemistry*, 37, 1563-1565.
- MULLINK, H., VOS, W., JIWA, M., HORSTMAN, A., VANDERVALK, P., WALBOOMERS, J. M. M. & MEIJER, C. 1992. Application and comparison of silver intensification methods for the diaminobenzidine and diaminobenzidine nickel end-product of the peroxidation reaction in immunohistochemistry and insitu hybridization. *Journal of Histochemistry & Cytochemistry*, 40, 495-504.
- NALESNIK, M. A. 1990. Involvement of the gastrointestinal tract by Epstein-Barr virus associated post-transplant lymphoproliferative disorders. *American Journal of Surgical Pathology*, 14, 92-100.

- NEWMAN, G. R. & JASANI, B. 1998. Silver development in microscopy and bioanalysis: A new versatile formulation for modern needs. *Histochemical Journal*, 30, 635-645.
- NEWMAN, G. R., JASANI, B. & WILLIAMS, E. D. 1983a. Metal compound intensification of the electron density of diaminobenzidine. *Journal of Histochemistry & Cytochemistry*, 31, 1430-1434.
- NEWMAN, G. R., JASANI, B. & WILLIAMS, E. D. 1983b. The visualization of trace amounts of diaminobenzidine (DAB) polymer by a novel gold-sulfide-silver method. *Journal of Microscopy-Oxford*, 132, RP1-RP2.
- NINEHAM, A. W. 1955. The chemistry of the formazans and tetrazolium salts. *Chemical Reviews*, 55, 355-482.
- NORTON, A. J., RAMSAY, A. D., SMITH, S. H., BEVERLEY, P. C. L. & ISAACSON, P. G. 1986. Monoclonal-antibody (UCHL-1) that recognizes normal and neoplastic T-cells in routinely fixed tissues. *Journal of Clinical Pathology*, 39, 399-405.
- OESPER, R. E. & KLINGENBERG, J. J. 1948. The synthesis and properties of di-2,4-dimethylphenylthiocarbazone. *Journal of Organic Chemistry*, 13, 309 - 312.
- PAI, S. & KHANNA, R. 2001. Role of LMP-1 in immune control of EBV infection. *Cancer Biology*, 11, 445-460.
- PARK, S. AND JUN, K. 2005. Synthesis and properties of phenylenediamine nickel complexes. *Journal of Industrial and Engineering Chemistry*, 11, 883-886.
- PEARSE, A. G. E. 1957. Intracellular localisation of dehydrogenase systems using monotetrazolium salts and metal chelation of their formazans. *Journal of Histochemistry and Cytochemistry*, 5, 515-527.
- PEARSE, A. G. E. & BUSSOLATI, G. 1970. Immunofluorescence studies of the distribution of gastrin cells in different clinical states. *Gut*, 11, 646-648.

- PERRY, M. & WHYTE, A. 1998. Immunology of the tonsils. *Immunology Today*, 19, 414-421.
- PERVOVA, I. G., SLEPUKHIN, P. A., ZAIDMAN, A. V., LIPUNOVA, G. N. & LIPUNOV, I. N. 2010. Nickel(II) and iron(II) complexes with 1-(2(4)-chlorophenyl)benzothiazolylformazans. *Russian Journal of Coordination Chemistry*, 36, 213-219.
- PITMAN, R. M., TWEEDLE, C. D. & COHEN, M. J. 1972. Branching of central neurons - intracellular cobalt injection for light and electron microscopy. *Science*, 176, 412-414.
- PLUSKAL, M. G., PRZEKOP, M. B., KAVONIAN, M. R., VECOLI, C. & HICKS, D. A. 1986. Immobilon PVDF transfer membrane - a new membrane substrate for western blotting of proteins. *Biotechniques*, 4, 272-283.
- PRZEPIORKA, D. & MYERSON, D. 1986. A single-step silver enhancement method permitting rapid diagnosis of cytomegalovirus infection in formalin-fixed, paraffin-embedded tissue sections by insitu hybridization and immunoperoxidase detection. *Journal of Histochemistry & Cytochemistry*, 34, 1731-1734.
- QUINN, B. & GRAYBIEL, A. M. 1996. A differentiated silver intensification procedure for the peroxidase-diaminobenzidine reaction. *Journal of Histochemistry & Cytochemistry*, 44, 71-74.
- REDSHAW, R., WILKINSON, G, HUSSAIN-BATES, B., AND HURSTHOUSE, M. 1992. o-Phenylenediamine and related complexes of chromium, vanadium and manganese. *Journal of the Chemical Society, Dalton Transactions*. 1803-1811.
- RICKINSON, A. 2002. Epstein-Barr virus. *Virus Research*, 82, 109-113.

- RODRIGUEZ, E. M., YULIS, R., PERUZZO, B., ALVIAL, G. & ANDRADE, R. 1984. Standardization of various applications of methacrylate embedding and silver methenamine for light and electron microscopy immunocytochemistry. *Histochemistry*, 81, 253-263.
- SCHMID, K. W. & JASANI, B. 1987. Light microscope demonstration of TSH specific binding sites on rat thyroid follicular cell surface. *Journal of Histochemistry & Cytochemistry*, 35, 1023-1023.
- SCHMIDT, R. E., MACDERMOTT, R. P., BARTLEY, G., BERTOVICH, M., AMATO, D. A., AUSTEN, K. F., SCHLOSSMAN, S. F., STEVENS, R. L. & RITZ, J. 1985. Specific release of proteoglycans from human natural killer cells during target lysis. *Nature*, 318, 289-291.
- SCHNELL, S. A., STAINES, W. A. & WESSENDORF, M. W. 1999. Reduction of lipofuscin-like autofluorescence in fluorescently labeled tissue. *Journal of Histochemistry & Cytochemistry*, 47, 719-730.
- SCOPSI, L. & LARSSON, L. I. 1986. Increased sensitivity in peroxidase immunocytochemistry - a comparative study of a number of peroxidase visualization methods employing a model system. *Histochemistry*, 84, 221-230.
- SELIGMAN, A. M., KARNOVSKY, M. J., WASSERKRUG, H. L. & HANKER, J. S. 1968. Nondroplet ultrastructural demonstration of cytochrome oxidase activity with a polymerising osmiophilic reagent, diaminobenzidine (DAB). *Journal of Cell Biology*, 38, 1-14.
- SIEDLE, A. R. & PIGNOLET, L. H. 1980. Formazanylpalladium compounds. Synthesis and structure of bis(1,3,5-tri-p-tolylformazanyl) palladium. *Inorganic Chemistry*, 19, 2052-2056.
- SEDLE, A. R., MANN, K. R., BOHLING, D. A., FILIPOVICH, G., TOREN, P. E., PALENSKY, F. J., NEWMARK, R. A., DUERST, R. W., STEBBINGS, W. L. MISHMASH, H. E. and MELANCON, K. 1985. Redox, ligand-exchange, oligomerization, and hydrosilation chemistry of *trans*-dichloro(ethylene)(phenazine)platinum. *Inorganic Chemistry*, 24, 2216-2223.



- SIEGESMUND, K. A., YORDE, D. E. & DRAGEN, R. 1979. A quantitative immunoperoxidase procedure employing energy dispersive x-ray analysis. *Journal of Histochemistry & Cytochemistry*, 27, 1226-1230.
- SLOT, J. W. & GEUZE, H. J. 1985. A new method of preparing gold probes for multiple-labeling cytochemistry. *European Journal of Cell Biology*, 38, 87-93.
- SMILEY, J. F. & GOLDMAN-RAKIC, P. S. 1993. Silver-enhanced diaminobenzidine-sulfide (SEDS): a technique for high-resolution immunoelectron microscopy demonstrated with monoamine immunoreactivity in monkey cerebral cortex and caudate. *Journal of Histochemistry & Cytochemistry*, 41, 1393-1404.
- SPILLANTINI, M. G., SCHMIDT, M. L., LEE, V. M. Y., TROJANOWSKI, J. Q., JAKES, R. & GOEDERT, M. 1997. Alpha-synuclein in Lewy bodies. *Nature*, 388, 839-840.
- STREEFKERK, J. G. 1972. Inhibition of erythrocyte pseudoperoxidase activity by treatment with hydrogen peroxide following methanol. *Journal of Histochemistry & Cytochemistry*, 20, 829-831.
- STREULI, M., HALL, L. R., SAGA, Y., SCHLOSSMAN, S. F. & SAITO, H. 1987. Differential usage of 3 exons generates at least 5 different messenger RNAs encoding human leukocyte common antigens. *Journal of Experimental Medicine*, 166, 1548-1566.
- STREULI, M., MORIMOTO, C., SCHRIEBER, M., SCHLOSSMAN, S. F. & SAITO, H. 1988. Characterization of CD45 and CD45R monoclonal-antibodies using transfected mouse cell lines that express individual human leukocyte common antigens. *Journal of Immunology*, 141, 3910-3914.
- TAGO, H., KIMURA, H. & MAEDA, T. 1986. Visualization of detailed acetylcholinesterase fiber and neuron staining in rat brain by a sensitive histochemical procedure. *Journal of Histochemistry & Cytochemistry*, 34, 1431-1438.

- TAJIMA, Y., KAWASAKI, M., OHNO, J., KUSAMA, K., MARUYAMA, S. & KATO, K. 2000. Comparative image analysis of EGF immunoreaction in rat submandibular gland using 3,3'-diaminobenzidine with metal enhancer substrate. *Biotechnic & Histochemistry*, 75, 15-18.
- TERRY, R. D., WEISS, M. & GONATAS, N. K. 1964. Ultrastructural studies in Alzheimer's pre-senile dementia. *American Journal of Pathology*, 44, 269-297.
- THOMAS, M. L. & LEFRANCOIS, L. 1988. Differential expression of the leucocyte-common antigen family. *Immunology Today*, 9, 320-326.
- TIMM, F. 1958. Zur histochemie der schwermetalle. Das sulfidsilberverfahren. *Deutsche Zeitschrift fur die Gesamte Gerichtliche Medizin*, 46, 706-711.
- TOPACLI, C. AND TOPACLI, A. 2003. Semi-empirical infrared spectra simulations of benzidine and its metal chloride complexes. *Journal of Molecular Structure*. 658, 9-15.
- TYRER, N. M. & BELL, E. M. 1974. Intensification of cobalt-filled neuron profiles using a modification if Timm's sulfide-silver method. *Brain Research*, 73, 151-155.
- VON RUHLAND, C. J. & JASANI, B. 2010. The amplification of polymerized diaminobenzidine with physical developers: sensitizing effects of transition metal salts and sulphide. *Journal of Microscopy-Oxford*, 238, 111-122.
- WALDEYER, W. 1884. Ueber den lymphatischen Apparat des Pharynx. *Deutsche Medizinische Wochenschrift*, 10, 313.
- WALKER, R. A. 2008. Immunohistochemical markers as predictive tools for breast cancer. *Journal of Clinical Pathology*, 61, 689-696.
- WANG, D., LIEBOWITZ, D. & KIEFF, E. 1985. An EBV membrane protein expressed in immortalized lymphocytes transforms established rodent cells. *Cell*, 43, 831-840.

YOUNG, L. S. 2001. LMP1 structure and signal transduction. *Cancer Biology*, 11, 435-444.

ZHANG, H., KOUADIO, A., CARTLEDGE, D. & GODWIN, A. K. 2011. Role of gamma-synuclein in microtubule regulation. *Experimental Cell Research*, 317, 1330-1339.

# **Chapter 3**

## **Marker Amplification at the Limits of Sensitivity**

### 3.1 Introduction

The ultimate test of any amplification system is its ability to perform as well, or better, than the most sensitive system currently available. When applied to tissue model systems, the practical limit of sensitivity of a particular amplification procedure is indicated by the highest primary antibody dilution at which positivity can be unequivocally identified. This is analogous to circumstances where exceptionally small amounts of target molecule are present and considerable amplification is required, thus prolonged times in the physical developer become essential. In these circumstances, a number of factors become particularly important, namely (1) endogenous enzymatic and non-enzymatic catalytic activity, (2) unwanted reactions of other amplifying reagents with tissue components (3), tissue argyrophilia, (4) self-nucleation of the physical developer, and (5) the affinities/avidities of antibody conjugates.

Given the widespread application of the peroxidase-DAB system, it is not surprising that considerable attention has been given to the suppression of both enzymatic (peroxidase, catalase etc.) and non-enzymatic (haem proteins, metals) peroxidase-like activity in tissue. Such activities are commonly overcome by application of aqueous or methanolic solutions of  $H_2O_2$  (van Duijn, 1957; Streefkerk, 1972), aqueous solutions of azide or phenylhydrazine (Straus, 1972), or combination thereof (Li et al, 1987). Such reagents can be deleterious to the immunohistochemical reactivity of the tissue and are used at low concentrations.

Complexing of d-block metal compounds to tissue components has been noted (Newman et al, 1983; de Bruijn et al. 1986), but has received little attention in the context of marker amplification (Newman and Jasani, 1998). At low concentrations

of polyDAB, selectivity can be improved by reducing the concentrations of both NaAu(III)Cl<sub>4</sub> and Na<sub>2</sub>S (Dr. Geoff Newman, personal communications).

Argyrophilia have been extensively studied by the Hungarian neurobiologist, Ferenc Gallyas, who sub-divided the process into three categories based on physicochemical considerations, namely Type I; the reduction of silver(I) by catalytic and reducing groups of the tissue, Type II; the reduction of silver(I) by a soluble reducing agent that is catalysed by compounds that have been deposited in the tissue by staining techniques, or as a result of a physiological or pathological process, and Type III; the reduction of silver(I) in the presence of a soluble reducing agent under the influence of catalytic tissue groups (Gallyas, 1979a; 1979b; 1982a; 1982b; 2008). It has recently been shown that suppression of tissue argyrophilia using copper(II)/H<sub>2</sub>O<sub>2</sub> (Gallyas and Merchenthaler, 1988) is incompatible with the sulfide/silver amplification technique, but La(III)/H<sub>2</sub>O<sub>2</sub>, in contrast, has some utility in this regard (Kelly, 2010).

Self-nucleation within physical developer solutions is, initially, a light-catalysed reaction that results in the reduction of silver(I). The resulting sub-microscopic particles of metallic silver catalyse further reduction of silver(I) until the particles become visible (i.e. greater than approximately 200 nm), and this defines the bench-life of the developer. The light-catalysed reaction can be suppressed by including colloidal protectants such as gum arabic (Danscher, 1981b) or sodium tungstate (Gallyas, 1979c) in the developer, or by complexing the silver(I) with Tris (Newman and Jasani, 1998) or citrate (Hacker et al, 1990).

A number of techniques for preparing antibody-enzyme conjugates have been devised, but the most popular are the two-step glutaraldehyde (Avrameas and Uriel, 1966) and periodate (Nakane and Kawaoi, 1974) techniques. The former is

considered the less deleterious of the two, with respect to antibody affinity and enzymatic activity (Boorsma et al, 1976). Colloidal gold conjugates are prepared by adsorption of the antibody onto the metal particle surface (Hayat, 1989).

## **3.2 Materials**

### **3.2.1 Reagents**

Mouse monoclonal anti-CD45 Ro (clone UCHL-1) was purchased from Autogen Bioclear (Calne, Wiltshire, U.K.). Goat anti-mouse Ig HRP conjugates (GAM IgPC) were supplied by Autogen Bioclear (Calne, Wiltshire, U.K.), Sigma-Aldrich (Poole, Dorset, U.K.) and Dako (Ely, Cambridgeshire, U.K.). Envision™ was supplied by Dako (Ely, Cambridgeshire, U.K.). Silver(I)acetate, silver(I)lactate and 90% lactic acid were supplied by Fisher Scientific (Loughborough, Leicestershire, U.K.). Gum arabic was purchased from BDH (Lutterworth, Leicestershire, U.K.). All other reagents were purchased from suppliers listed in section 2.2.1.

### **3.2.2 Physical Developers**

Gallyas' and Newman and Jasani's physical developers were prepared according to section 2.2.3 of the previous chapter. Two further developers were employed, since both have been specifically designed to visualise metal sulfides in tissue, namely Danscher's silver lactate developer (Danscher, 1981a) and Hacker's silver acetate developer (Hacker et al, 1990).

### **3.2.2.1 Danscher's Developer**

#### **Solution A**

100 g of gum arabic was dissolved over 5 days in 200 ml ddH<sub>2</sub>O and filtered through a 0.2 µm pore syringe filter.

#### **Solution B**

3.15 ml of 50% sodium lactate and 6 ml of 90% lactic acid were dissolved, mixed, and made up to 100 ml in ddH<sub>2</sub>O.

#### **Solution C**

0.85 g hydroquinone was dissolved in 15 ml ddH<sub>2</sub>O just before use.

#### **Solution D**

0.12 g silver(I)lactate was dissolved in 15 ml ddH<sub>2</sub>O and protected from light by wrapping the vial in tin foil.

The developer was prepared by mixing 60 ml of solution A, 10 ml of solution B and 15 ml of solution C, followed by 15 ml solution D. The solution was poured into a Coplin jar in a light-tight water bath at 26°C (Danscher, 1981a).

### **3.2.2.2 Hacker's Developer**

#### **Solution A**

Solution A was prepared freshly each time. 100 mg silver(I)acetate was dissolved in ddH<sub>2</sub>O to a final volume of 50 ml and filtered through a 0.2 µm pore syringe filter.



## **Solution B**

25.5 g citric acid and 23.5 g trisodium citrate  $2\text{H}_2\text{O}$  were dissolved in ddH<sub>2</sub>O to a final volume of 100 ml and adjusted to pH 3.8 with citric acid. Immediately before use, 500 mg hydroquinone was dissolved in the buffer.

The developer was prepared by mixing solutions A and B in the ratio of 1:2 immediately before use (Hacker et al, 1990).

## **3.3 Methods**

### **3.3.1 Determination of the Limits of Sensitivity of the Colloidal Gold/Silver Method**

Tonsil sections were immunohistochemically stained and developed with silver as in section 2.3.4.3., above, with approximately logarithmic dilutions of the primary antibody ( $1/5,000$ ,  $1/10,000$ ,  $1/20,000$ , etc. down to  $1/1,000,000$ ). The highest dilution of the primary antibody where positivity could be unequivocally identified was chosen as the standard against which polyDAB amplification was compared.

### **3.3.2 Inhibition of Endogenous Enzymatic Activity**

In preliminary experiments, tissue sections were pre-treated with either 50 mM phenylhydrazine in 50 mM phosphate buffer pH 7.3 at 37°C for 1 hour (Straus, 1972), 50 mM phenylhydrazine in 50 mM phosphate buffer pH 7.3 at 37°C for 10 minutes + 0.0003% H<sub>2</sub>O<sub>2</sub> for 20 minutes (Jasani et al, 1986; Wynford-Thomas et al, 1986), 0.1% sodium azide + 0.3% H<sub>2</sub>O<sub>2</sub> for 10 minutes (Li et al, 1987), methanol for 20 minutes + 0.025% H<sub>2</sub>O<sub>2</sub> in PBS 20 minutes (Streefkerk, 1972), or 0.02 M

HCl for 20 minutes (Liu et al, 2006), followed by immunohistochemical staining using the colloidal gold/silver method as in section 2.3.4.3, above, with UCHL-1 at  $1/50,000$ ,  $1/100,000$  and  $1/200,000$  to determine the effects of inhibitors on immunohistochemical reactivity.

In a further experiment, endogenous enzymatic inhibition was repeated followed by incubation in DAB-PO<sub>4</sub> for 3 minutes and subsequent treatment with 2.5 mM NaAu(III)Cl<sub>4</sub>, 0.3% Na<sub>2</sub>S and Newman and Jasani's developer for 10 minutes, as in section 2.3.4.5., above.

The treatment that least effected immunohistochemical sensitivity and maximally suppressed endogenous enzymatic activity was selected for subsequent evaluation using the peroxidase/DAB system.

### **3.3.3 Determination of Sensitivity Limit for Peroxidase/DAB Au/Na<sub>2</sub>S/Silver**

Following inhibition of endogenous enzymatic activity with 0.02 M HCl for 20 minutes, as determined in the previous section, tissue sections were immunohistochemically stained with UCHL-1 from  $1/1000$ , to  $1/20,000$  followed by GAM Ig PC and DAB-PO<sub>4</sub>, with or without subsequent amplification with 2.5 mM NaAu(III)Cl<sub>4</sub> + 0.3% Na<sub>2</sub>S + Newman and Jasani's developer, as above.

### **3.3.4 Reduction of Non-specific Complexing of Amplifying Reagents with Tissue**

Following inhibition of endogenous enzymatic activity and immunohistochemical staining with UCHL-1 at  $1/10,000$ , sections were incubated in NaAu(III)Cl<sub>4</sub> at 2.5 mM, 1 mM, 0.3 mM and 0.1 mM and in Na<sub>2</sub>S at 0.3%, 0.1%,

0.03% and 0.01% followed by treatment with Newman and Jasani's developer. The concentrations of NaAu(III)Cl<sub>4</sub> and Na<sub>2</sub>S that produced the strongest signal and minimal background staining were chosen for subsequent experiments.

### **3.3.5 Suppression of Tissue Argyrophilia**

Following immunohistochemical staining with UCHL-1 at  $1/_{20,000}$  and  $1/_{50,000}$  as above, sections were treated with 10 mM La(III)Cl<sub>3</sub> for 1 hour followed by 3% H<sub>2</sub>O<sub>2</sub> for 10 minutes post-DAB polymerisation (Kelly, 2010) prior to amplification using 0.3 mM gold/0.1% sulfide and physical development.

### **3.3.6 Comparison of Physical Developers**

Following immunohistochemical staining as above, with UCHL-1 at  $1/_{20,000}$  and  $1/_{50,000}$ , and Santa Cruz GAM IgPC, sections were developed with either Newman and Jasani's, Gallyas', Danscher's or Hacker's developers. In the case of Danscher's developer, the progress of amplification could not be followed under daylight conditions so sections were removed from the developer at 5 minute intervals, washed thoroughly in distilled water, and examined under the light microscope before being returned to the developer if further amplification was indicated. Where overstaining occurred, silver deposits were differentiated with 0.5% potassium ferricyanide, and the process observed microscopically.

### **3.3.7 Comparison of Secondary Antibody Conjugates**

The antibody used to prepare the colloidal gold conjugate was not available as a peroxidase conjugate (Sigma-Aldrich personal communications), so direct comparison was not possible. A Sigma-Aldrich peroxidase conjugate, linked by the

periodate method, was chosen for comparison with the Santa Cruz antibody to determine whether any differences existed between commercial sources. In addition, a peroxidase conjugate from Dako, prepared by the glutaraldehyde method was also examined. All conjugates were applied at  $1/150$  in PBS/BSA and immunohistochemical staining performed as above.

In a further experiment, a proprietary polymeric conjugate, Envision™, was employed to determine whether any differences in sensitivity might be due to the final amounts of polyDAB deposited. Such conjugates are composed of several peroxidase enzymes covalently attached to a polyethylene glycol backbone which, in turn, is covalently attached to several antibodies (Dako, personal communication). Envision™ was applied as a  $1/10$  of the stock solution in 10mM phosphate buffer pH 7.4 containing 0.9% (w/v) NaCl and 0.6% (w/v) bovine serum albumin (PBS/BSA)

PBS/BSA since this was found to produce lower background staining than the undiluted proprietary formulation. Immunohistochemical staining was performed as above, except that UCHL-1 was used at  $1/50,000$ ,  $1/100,000$ ,  $1/200,000$  and  $1/500,000$ .

In a final experiment, the peroxidase conjugates were diluted to a final IgG concentration of  $1\mu\text{g/ml}$  and further diluted  $1/2$ ,  $1/5$ ,  $1/10$ ,  $1/20$ ,  $1/50$  etc. to  $1/1000$  and 2  $\mu\text{l}$  drops applied to PVDF membrane and incubated for 3 minutes in DAB- $\text{PO}_4$  as in section 2.3.2., to determine whether any differences existed in enzymatic activity.

### **3.4. Results**

#### **3.4.1 Determination of the Limit of Sensitivity for the Colloidal Gold/Silver Method**

Clear and unequivocal immunopositive staining could be seen at primary antibody dilutions as low as  $1/100,000$  at low magnification (x 10 objective) (figure 3.1a, c, e, g and i), and down to  $1/500,000$  at higher magnification (x 40 objective) (figure 3.1b, d, f, h, j, l and n), although the number of immunopositive cells was considerable reduced. At  $1/1,000,000$  UCHL-1, it was not possible to identify positive cells with any certainty (figure 3.1o and p). Development time increased with primary antibody dilution and only the slightest argyrophilic reaction, involving erythrocytes, was noted with Newman and Jasani's developer. UCHL-1 at  $1/500,000$  was chosen as the standard against which polyDAB amplification was to be compared.

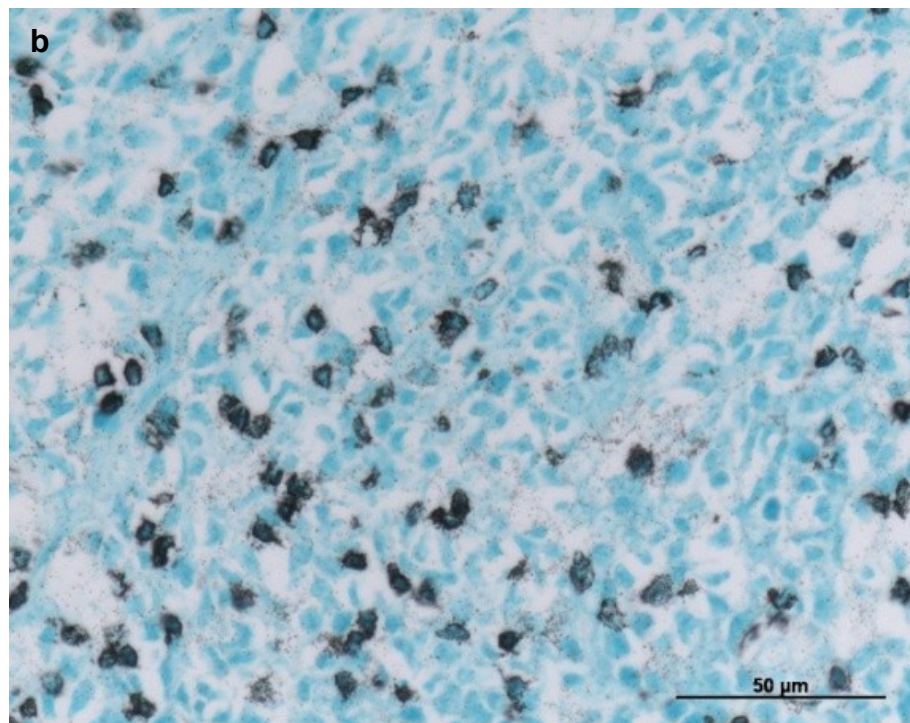
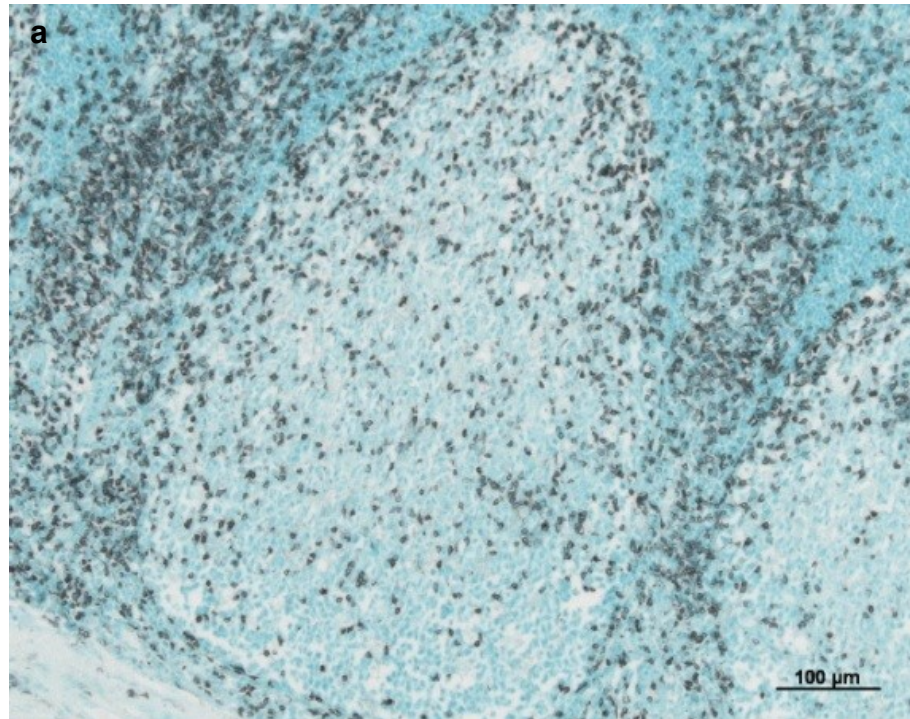


Figure 3.1. 4 μm thick sections of paraffin wax-embedded human tonsil immunohistochemically stained with UCHL-1 and GAM Ig CG5 followed by Newman and Jasani's developer. UCHL-1 at  $1/500$ .  
Low magnification (a) and high magnification (b).



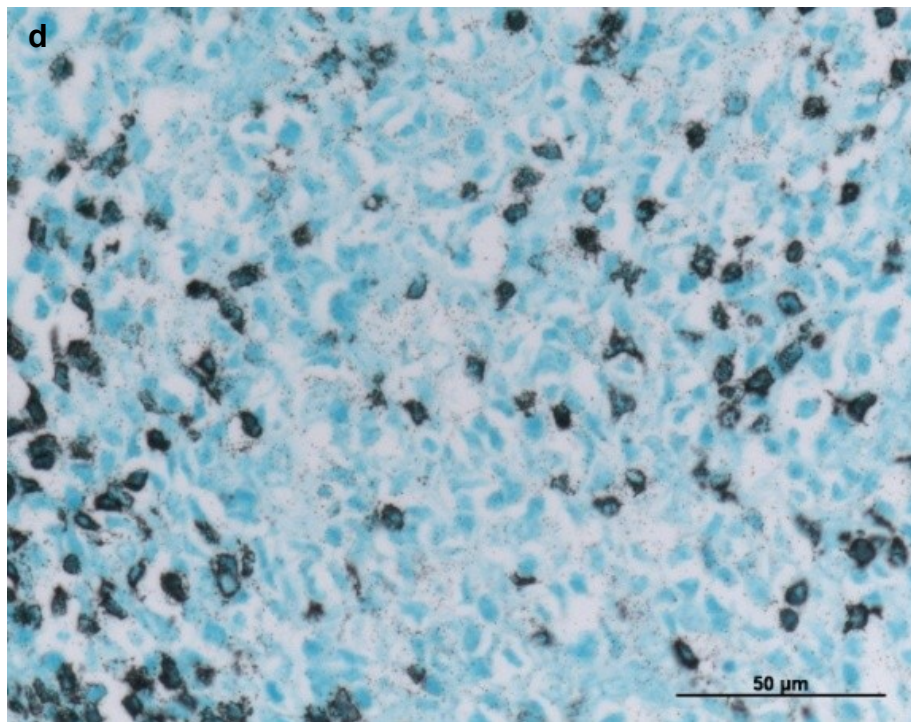
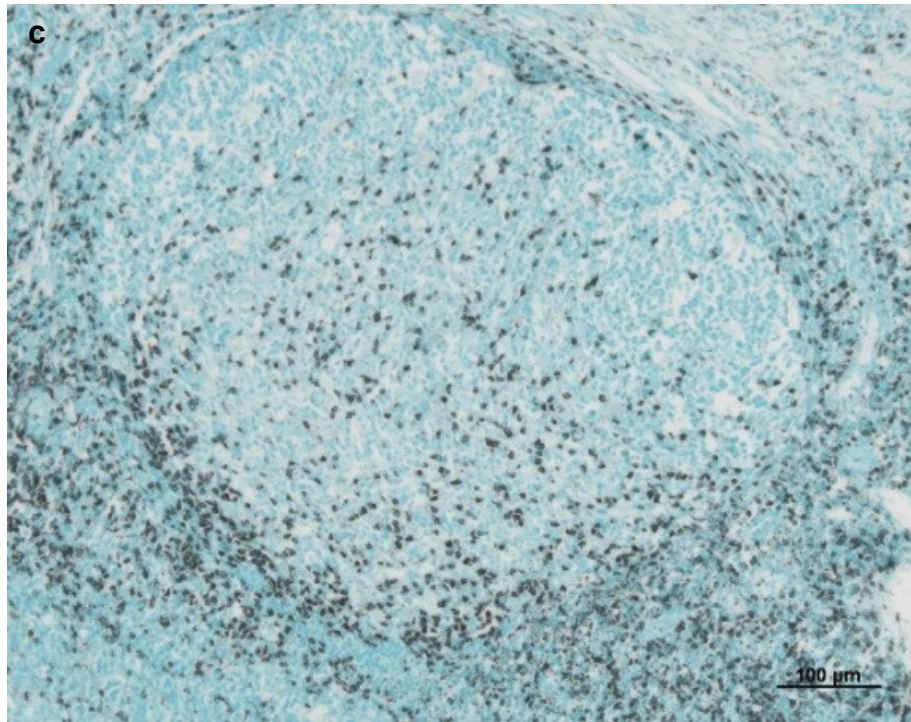


Figure 3.1 (continued). 4 μm thick sections of paraffin wax-embedded human tonsil immunohistochemically stained with UCHL-1 and GAM Ig CG5 followed by Newman and Jasani's developer. UCHL-1 at  $1/10,000$ .  
Low magnification (c) and high magnification (d).

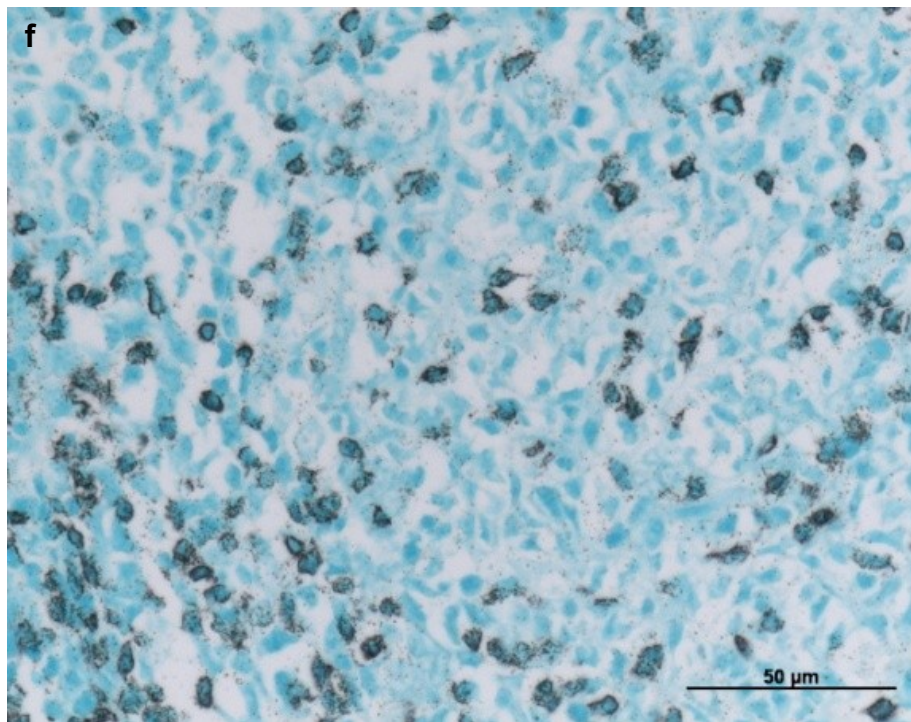
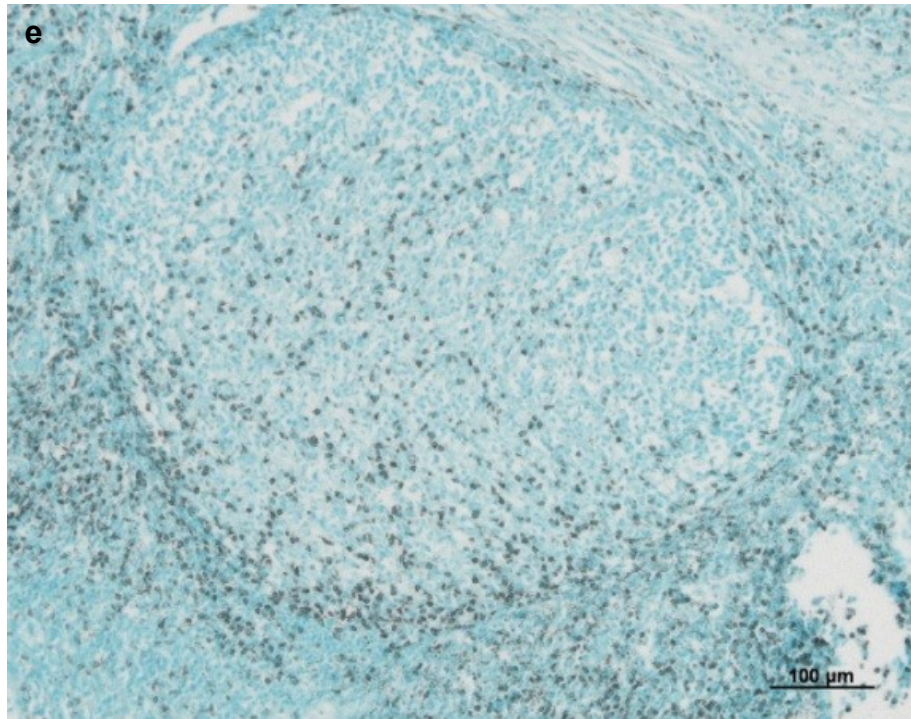


Figure 3.1 (continued). 4 μm thick sections of paraffin wax-embedded human tonsil immunohistochemically stained with UCHL-1 and GAM Ig CG5 followed by Newman and Jasani's developer. UCHL-1 at  $1/20,000$ .  
Low magnification (e) and high magnification (f).



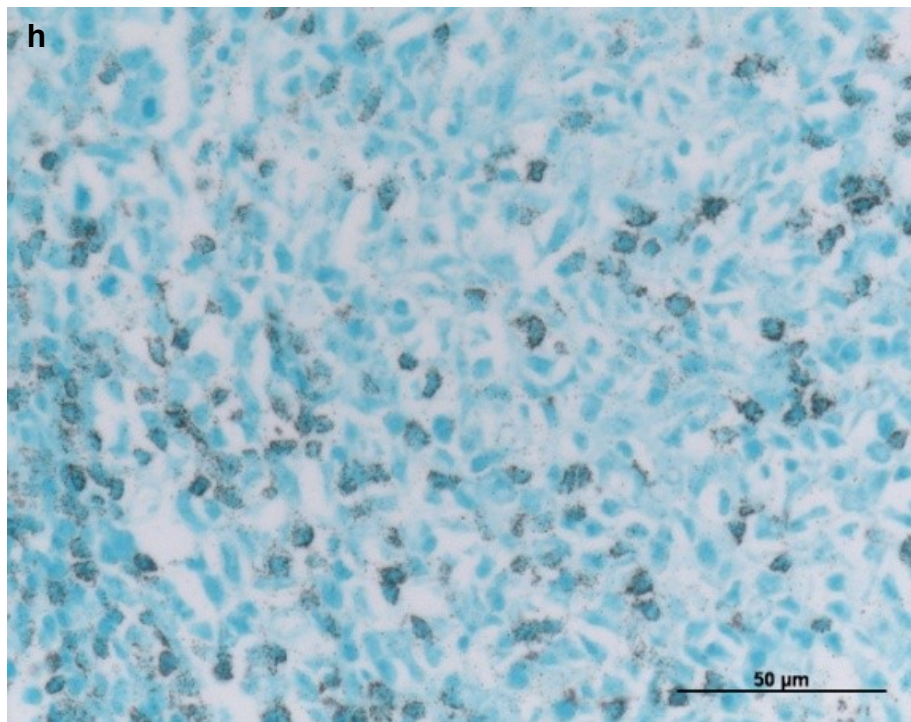
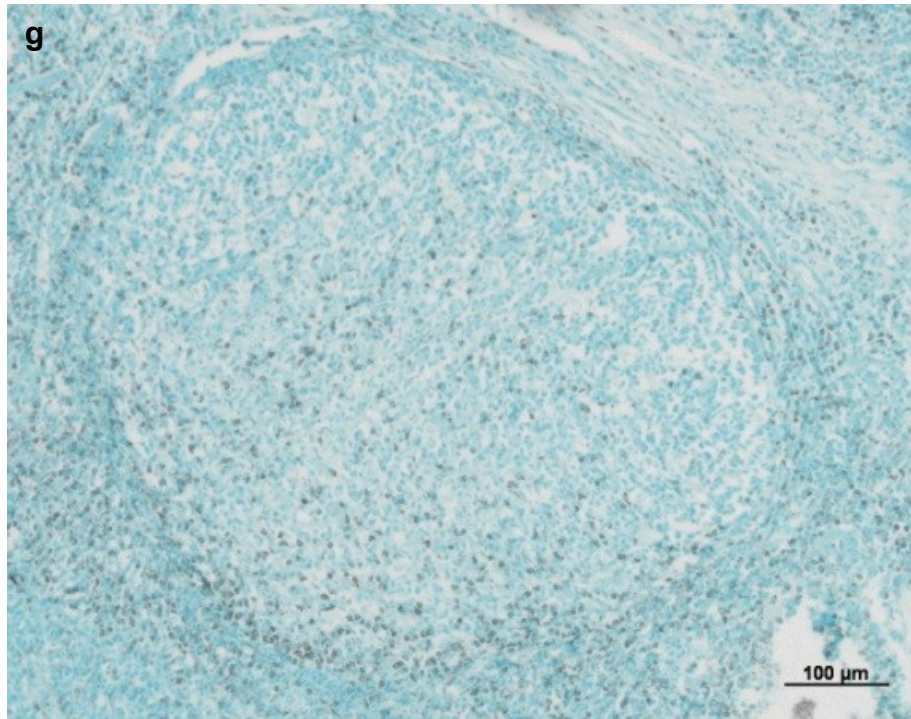


Figure 3.1 (continued). 4 μm thick sections of paraffin wax-embedded human tonsil immunohistochemically stained with UCHL-1 and GAM Ig CG5 followed by Newman and Jasani's developer. UCHL-1 at  $1/50,000$ .  
Low magnification (g) and high magnification (h).

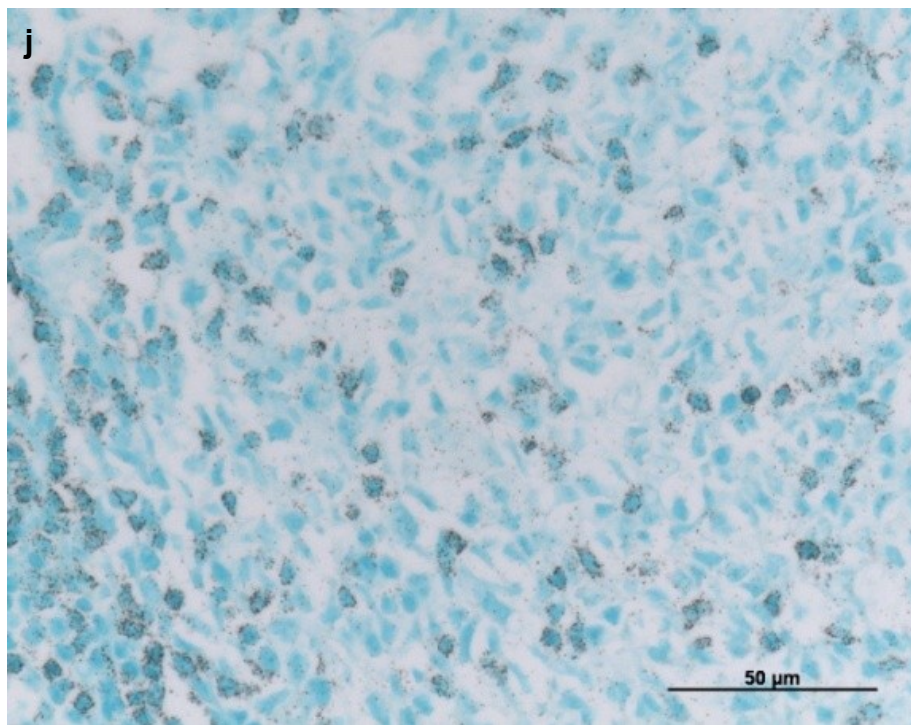
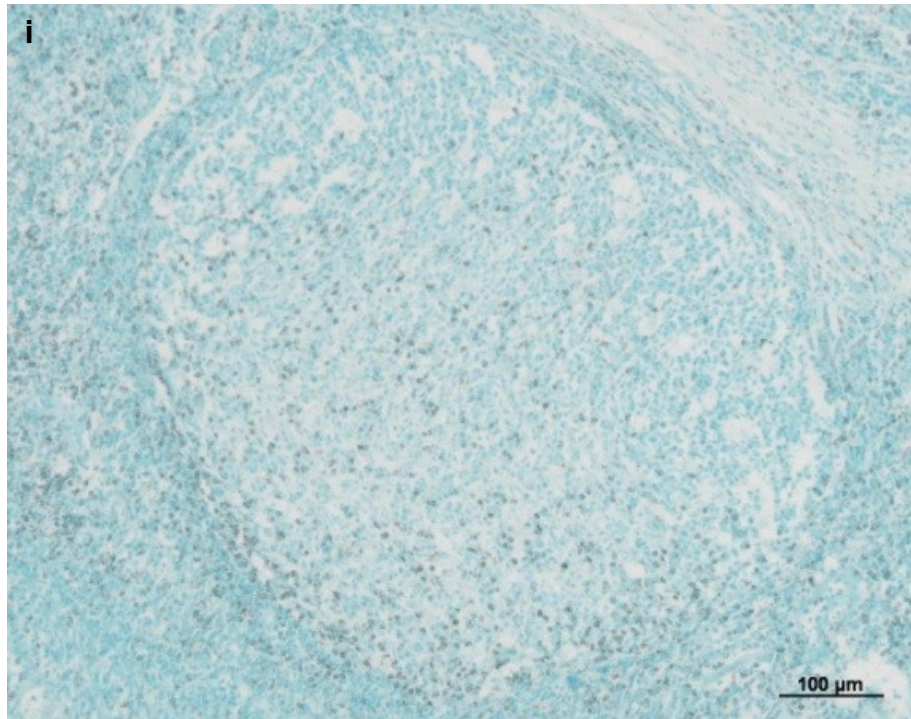


Figure 3.1 (continued). 4 μm thick sections of paraffin wax-embedded human tonsil immunohistochemically stained with UCHL-1 and GAM Ig CG5 followed by

Newman and Jasani's developer. UCHL-1 at  $1/100,000$ .

Low magnification (i) and high magnification (j).



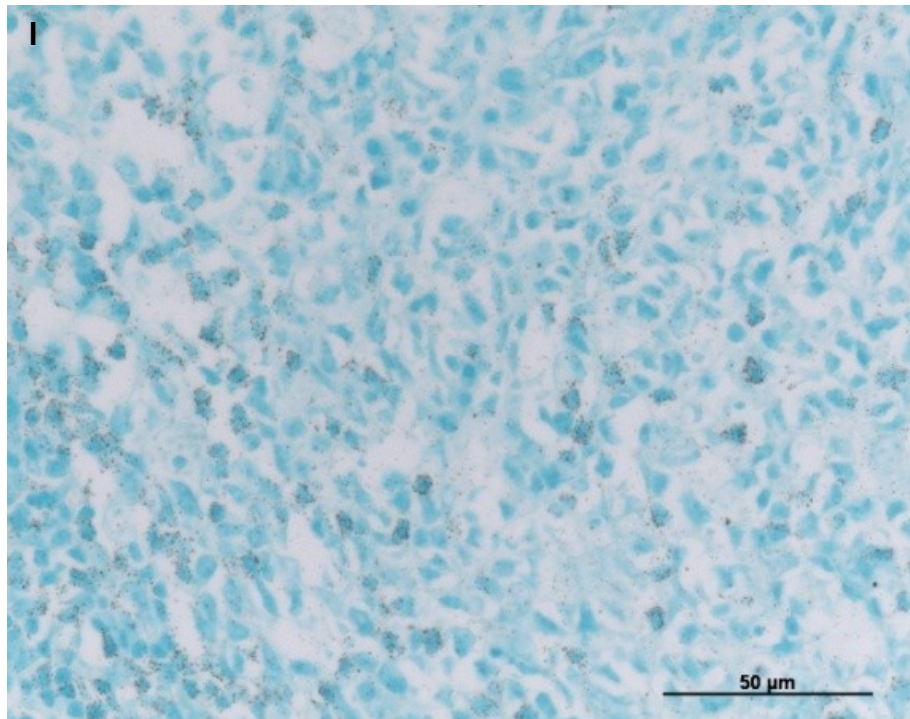
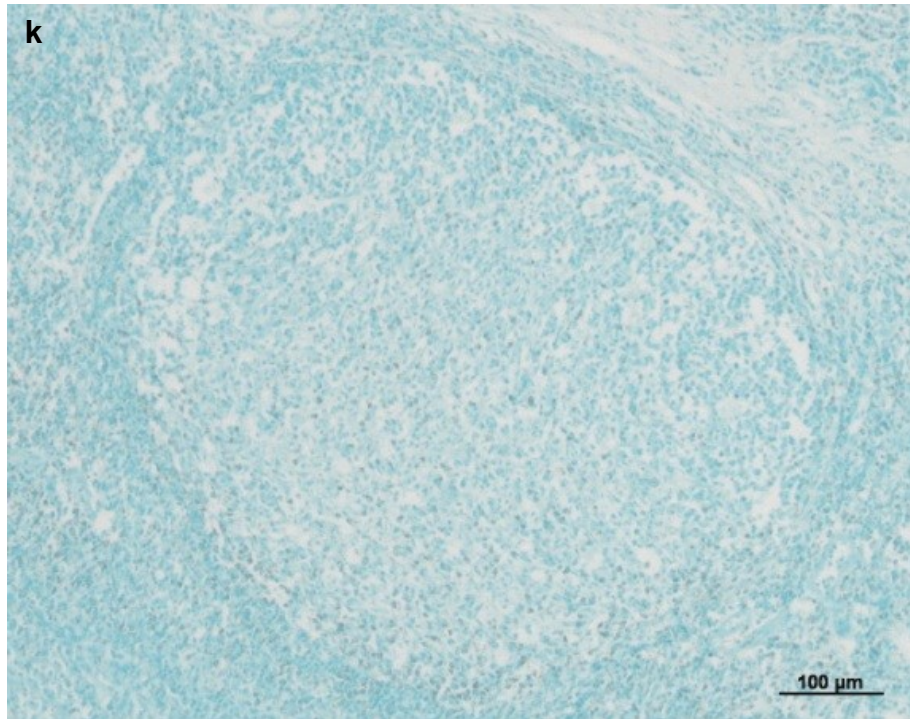


Figure 3.1 (continued). 4 μm thick sections of paraffin wax-embedded human tonsil immunohistochemically stained with UCHL-1 and GAM Ig CG5 followed by Newman and Jasani's developer. UCHL-1 at  $1/200,000$ .  
Low magnification (k) and high magnification (l).

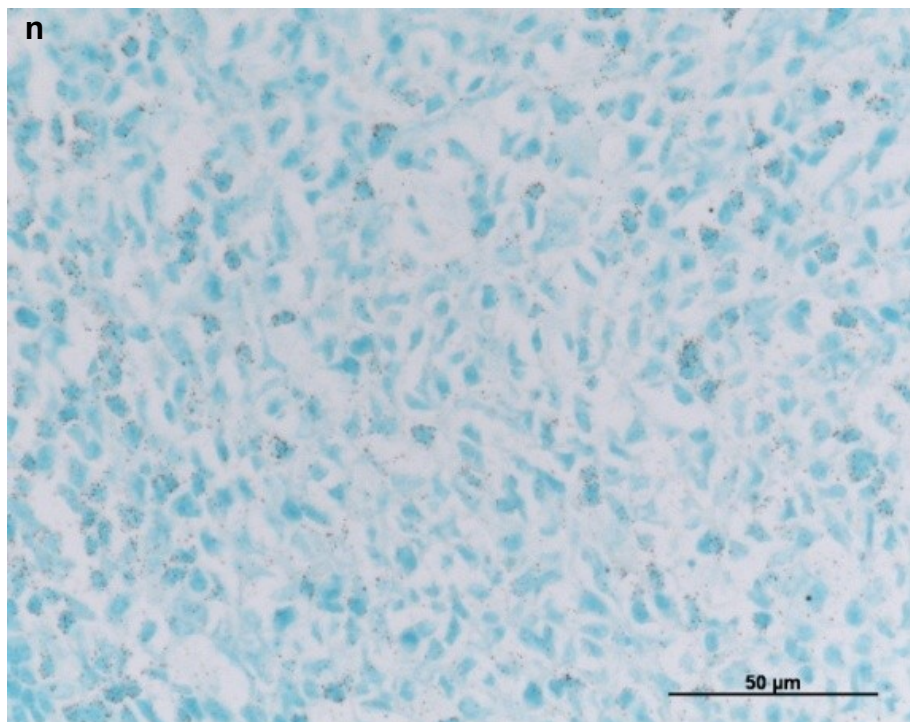
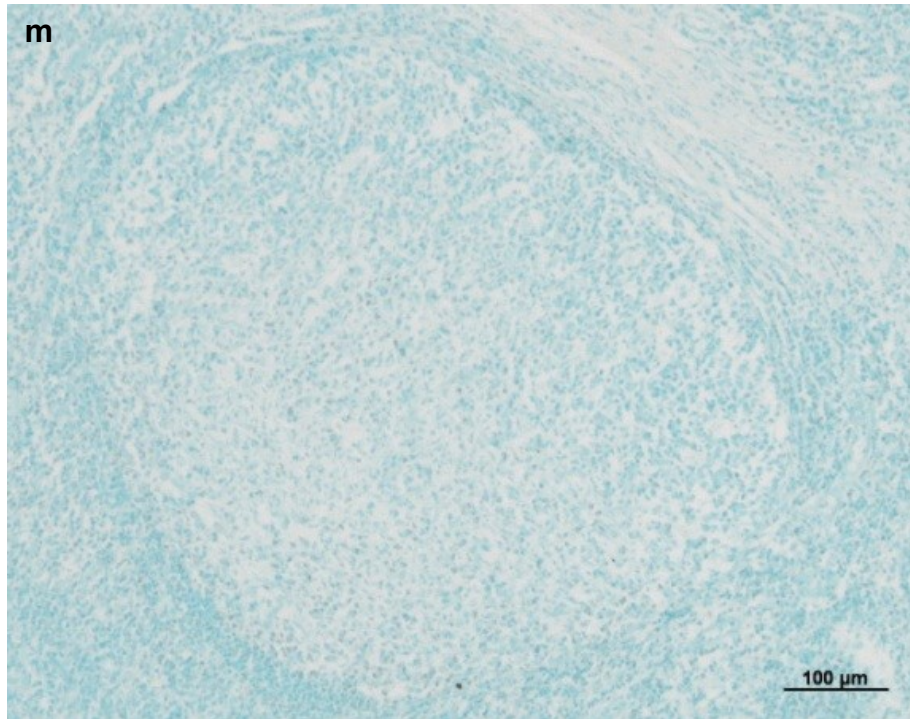


Figure 3.1 (continued). 4 μm thick sections of paraffin wax-embedded human tonsil immunohistochemically stained with UCHL-1 and GAM Ig CG5 followed by Newman and Jasani's developer. UCHL-1 at  $1/500,000$ .  
Low magnification (m) and high magnification (n).



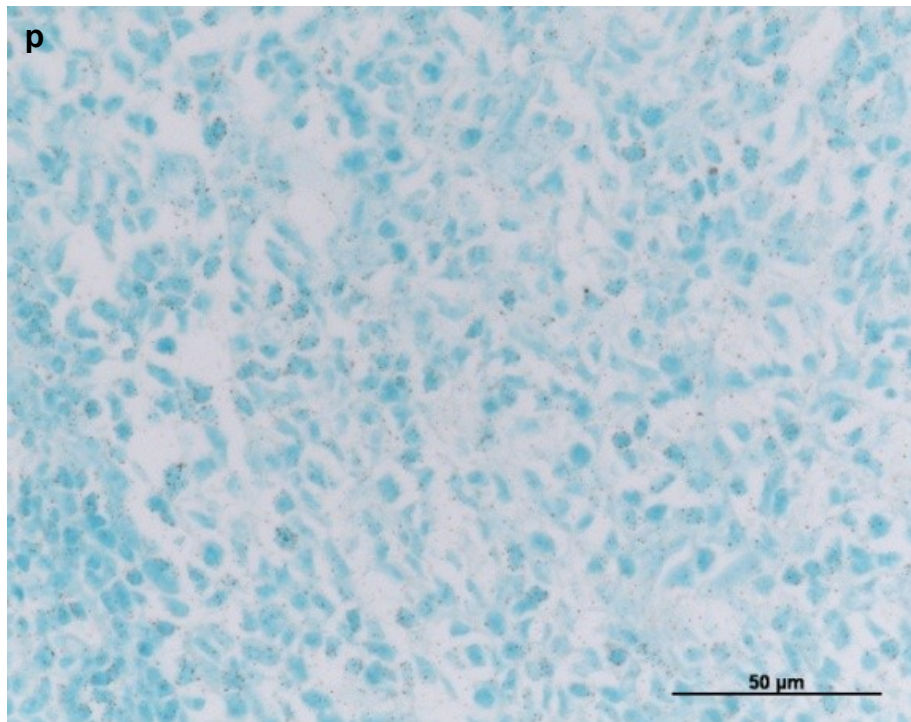
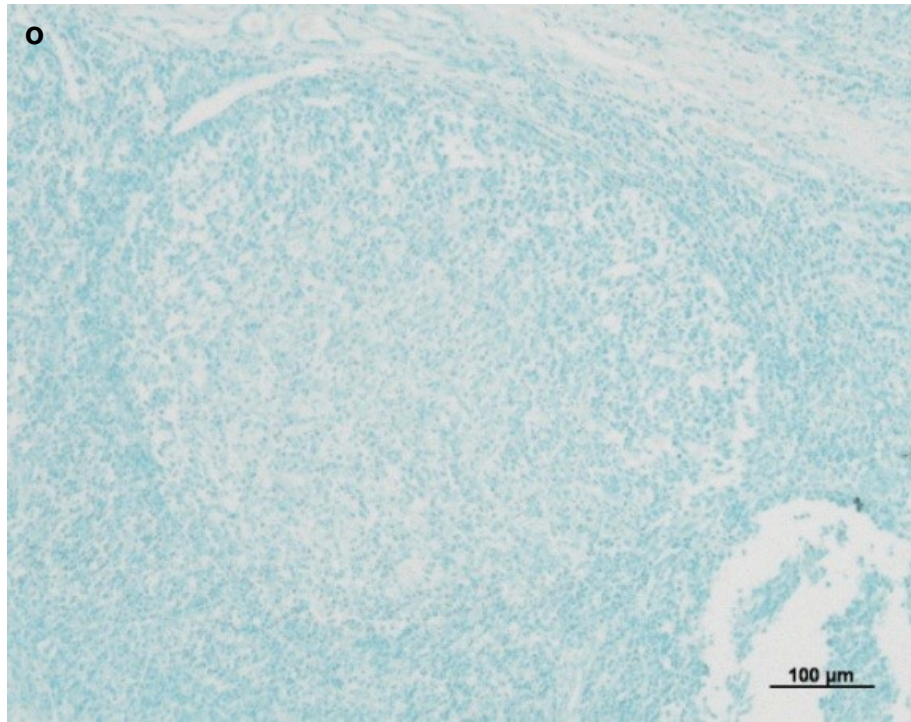


Figure 3.1 (continued). 4 μm thick sections of paraffin wax-embedded human tonsil immunohistochemically stained with UCHL-1 and GAM Ig CG5 followed by Newman and Jasani's developer. UCHL-1 at  $1/1,000,000$ .  
Low magnification (o) and high magnification (p).

### 3.4.2 Inhibition of Endogenous Enzymatic Activity

No effect of any of the inhibitors on the immunohistochemical responsiveness of the tissue was seen.

In the absence of inhibitors, staining following DAB/Au/Na<sub>2</sub>S/silver occurred predominantly in erythrocytes and, to a lesser extent, collagen (figure 3.2a). Following inhibition with phenylhydrazine, either alone (figure 3.2b) or in combination with H<sub>2</sub>O<sub>2</sub> (figure 3.2c), or with azide + H<sub>2</sub>O<sub>2</sub> (figure 3.2d), erythrocyte staining was abolished, but intense staining of vascular endothelium occurred. In the case of phenylhydrazine alone, collagen staining was also elevated. Both methanol + H<sub>2</sub>O<sub>2</sub> (figure 3.2e) and HCl treatment (figures 3.2f) reduced the staining of erythrocytes and collagen, methanol + H<sub>2</sub>O<sub>2</sub> being slightly better, although a slight endothelial staining was evident. 0.02 M HCl was chosen for simplicity of application.

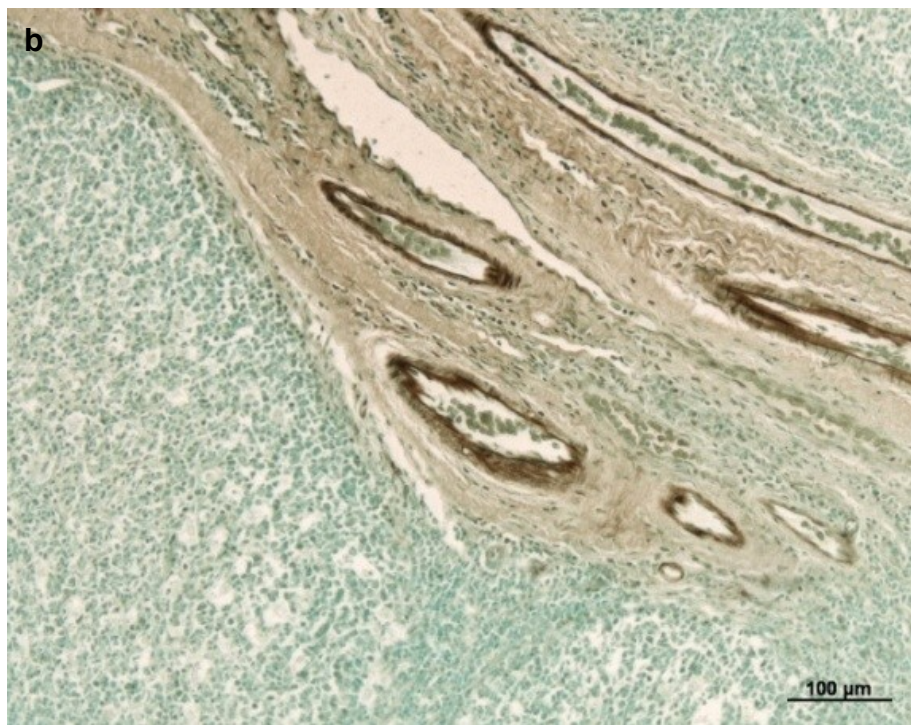
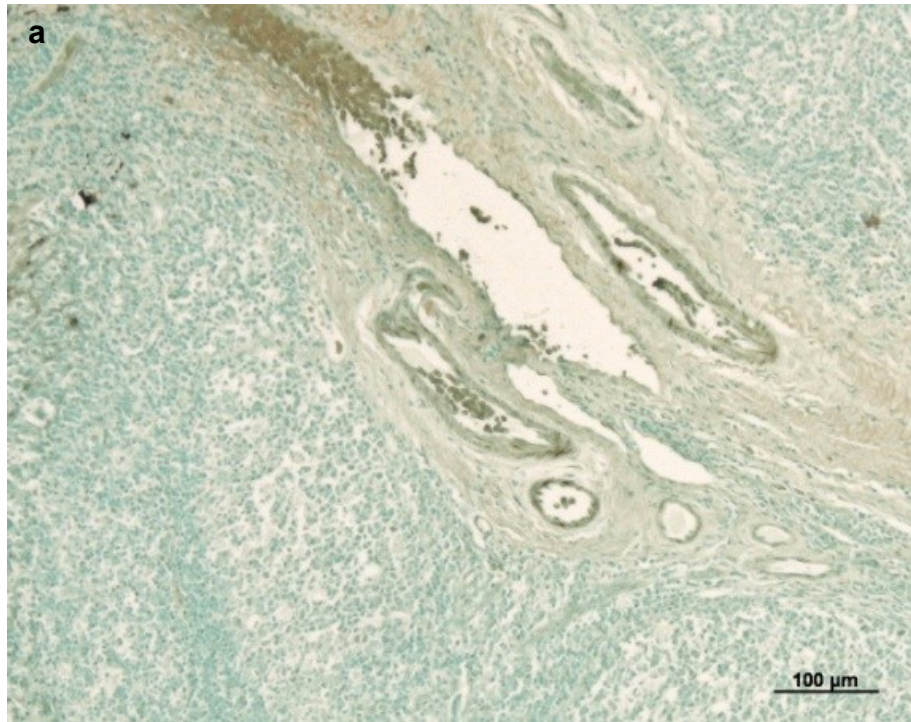


Figure 3.2. 4  $\mu\text{m}$  thick sections of paraffin wax-embedded human tonsil. Effects of endogenous peroxidase inhibitors on subsequent treatment with 2.5 mM  $\text{NaAu(III)Cl}_4 + 0.3\% \text{Na}_2\text{S} + \text{Newman and Jasani's developer}$ . No inhibitors (a) and 50 mM phenylhydrazine (b).



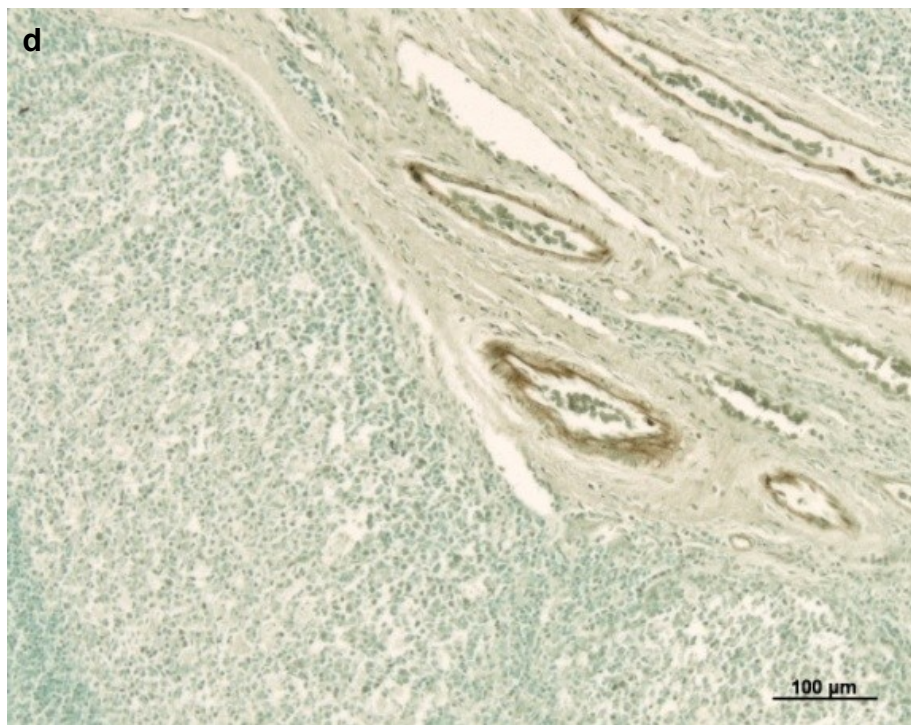
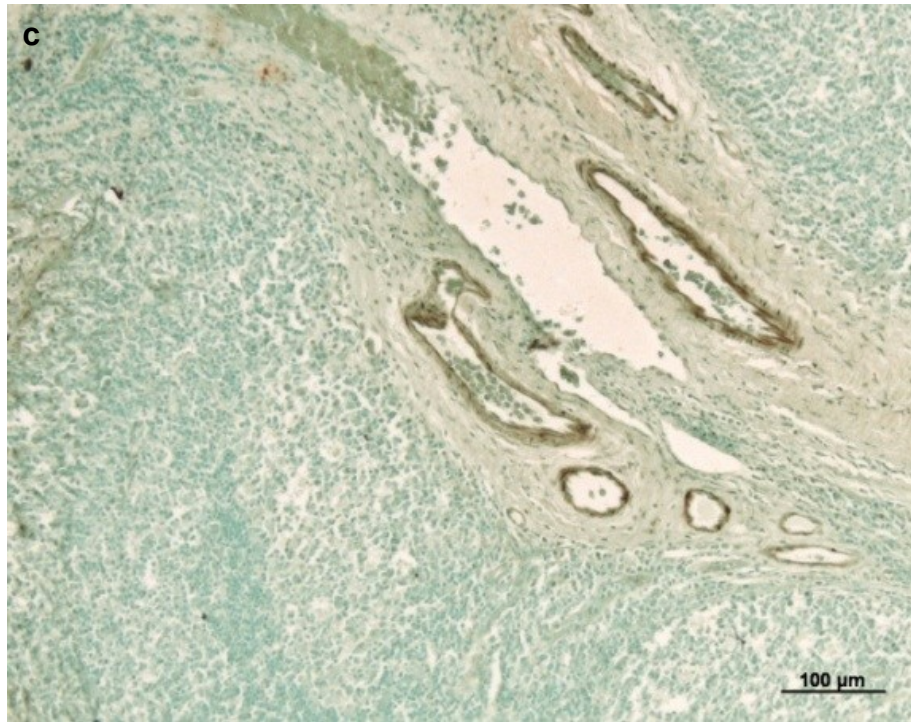


Figure 3.2 (continued). 4  $\mu\text{m}$  thick sections of paraffin wax-embedded human tonsil. Effects of endogenous peroxidase inhibitors on subsequent treatment with 2.5 mM  $\text{NaAu(III)Cl}_4$  + 0.3%  $\text{Na}_2\text{S}$  + Newman and Jasani's developer. 50 mM phenylhydrazine + 0.0003%  $\text{H}_2\text{O}_2$  (c) and 0.1%  $\text{NaN}_3$  + 0.3%  $\text{H}_2\text{O}_2$  (d).



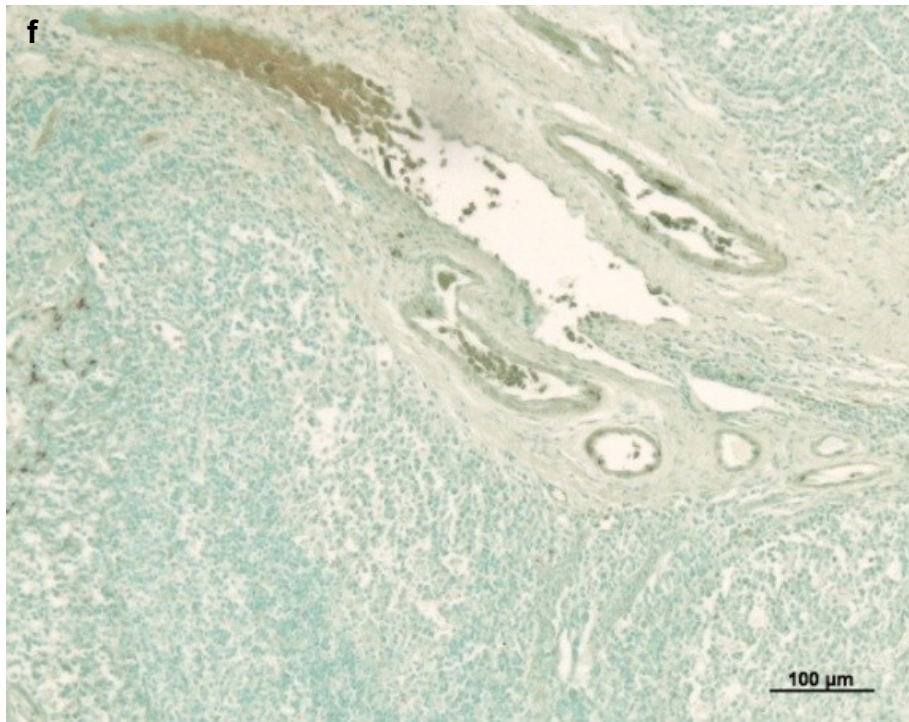
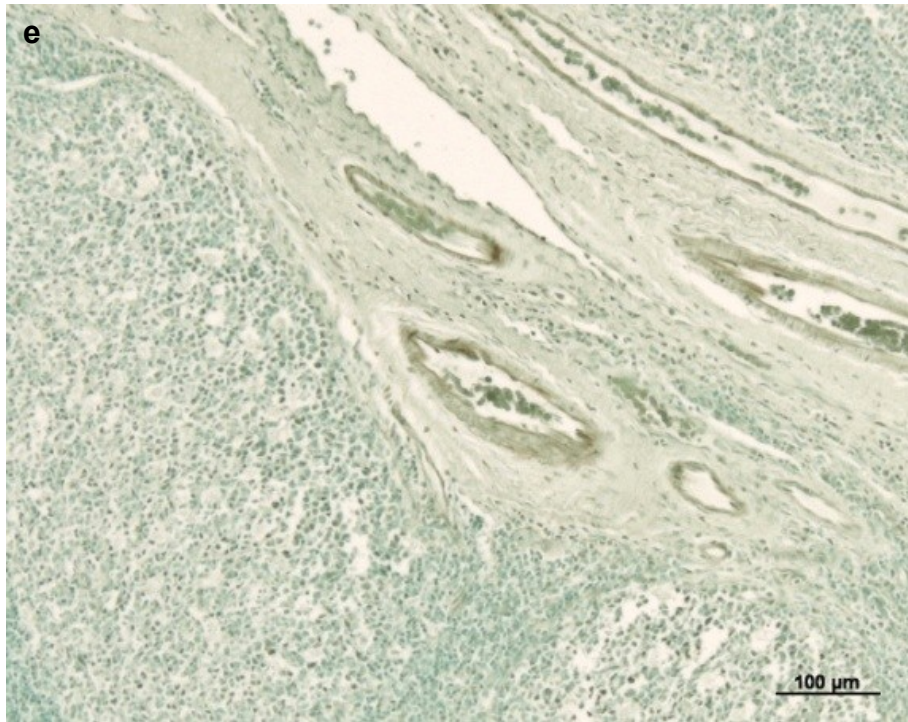


Figure 3.2 (continued). 4  $\mu\text{m}$  thick sections of paraffin wax-embedded human tonsil. Effects of endogenous peroxidase inhibitors on subsequent treatment with 2.5 mM  $\text{NaAu(III)Cl}_4$  + 0.3%  $\text{Na}_2\text{S}$  + Newman and Jasani's developer. Methanol + 0.025%  $\text{H}_2\text{O}_2$  in PBS (e) and 0.02 M HCl (f).

### **3.4.3 Determination of the Limit of Sensitivity for Peroxidase/DAB Au/Na<sub>2</sub>S/Silver**

In the absence of amplification, immunopositivity could be clearly seen at both low (x 10 objective) and high (x 40 objective) magnification at  $1/1000$  and  $1/2000$  (figure 3.3a – d) but only seen at high magnification at  $1/5,000$  UCHL-1 (figure 3.3f). No staining could be seen at  $1/10,000$  (figure 3.3g and h). Following amplification with 2.5 mM NaAu(III)Cl<sub>4</sub>, 0.3% Na<sub>2</sub>S and Newman and Jasani's developer, immunopositivity was clear at  $1/5000$  (figure 3.4a and b) and  $1/10,000$  (figure 3.4c and d), but at  $1/20,000$  background staining prevented unequivocal identification of immunopositive sites (figure 3.4e and f).

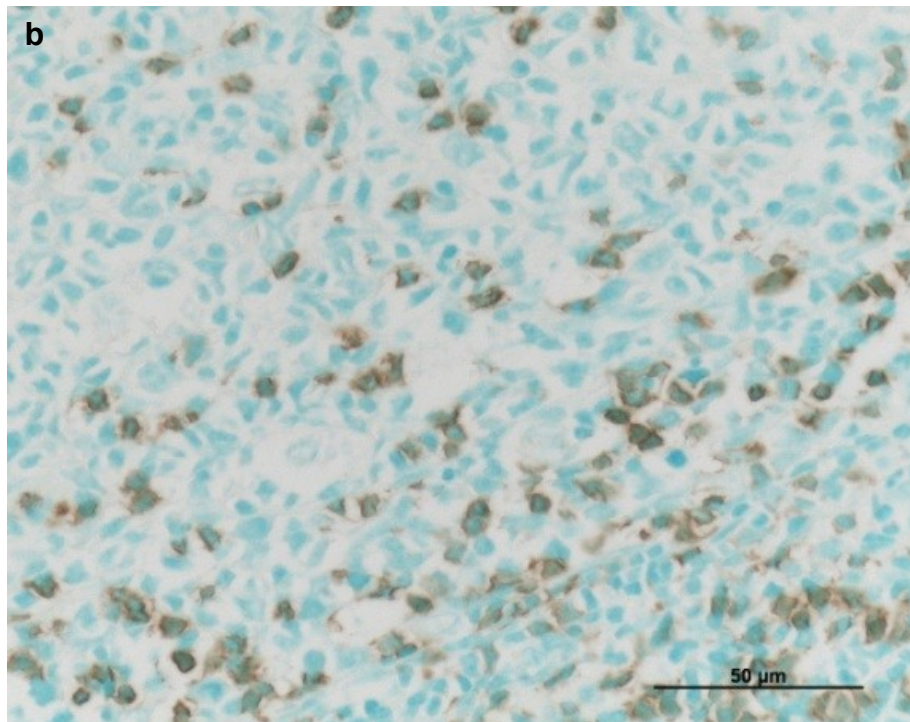
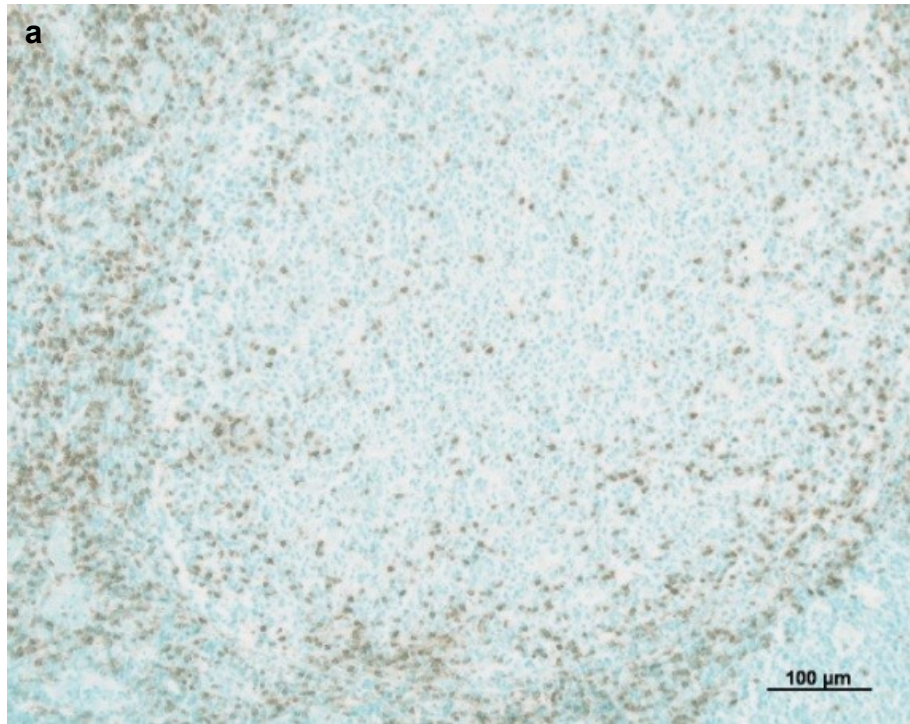


Figure 3.3. 4 μm thick sections of paraffin wax-embedded human tonsil immunohistochemically stained with UCHL-1 and GAM Ig PC and DAB-PO<sub>4</sub>.

UCHL-1 at  $1/_{1,000}$ . Low magnification (a) and high magnification (b).



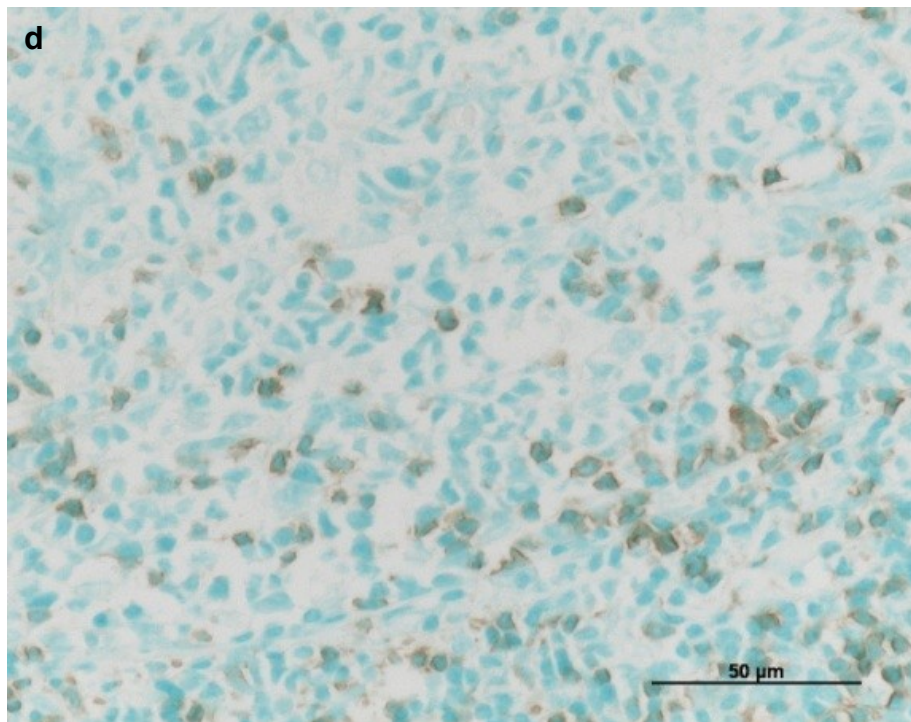
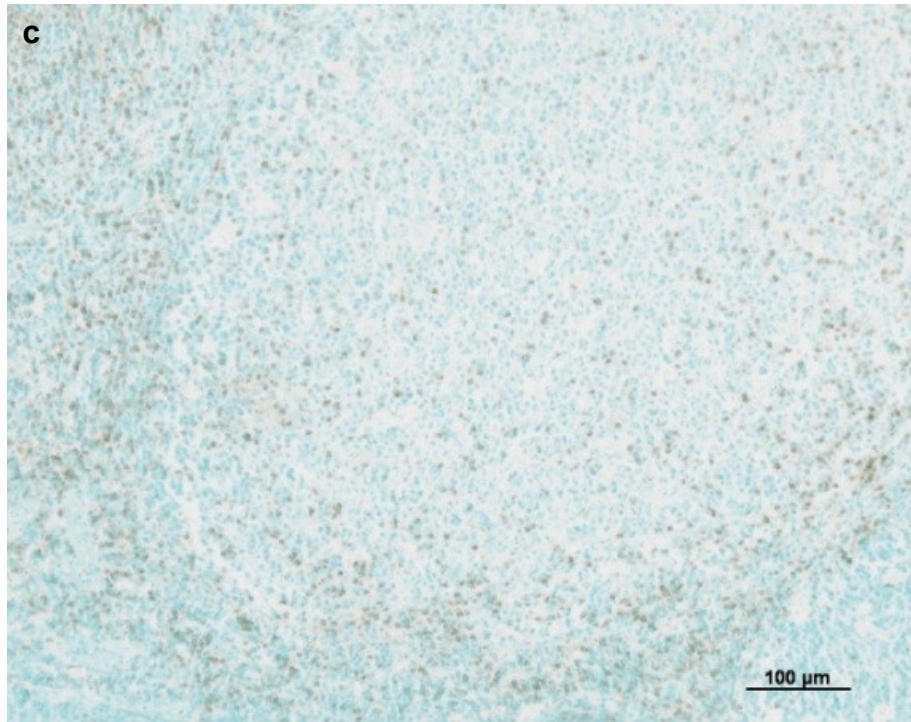


Figure 3.3 (continued). 4 μm thick sections of paraffin wax-embedded human tonsil immunohistochemically stained with UCHL-1 and GAM Ig PC and DAB-PO<sub>4</sub>.

UCHL-1 at  $1/2,000$ . Low magnification (c) and high magnification (d).

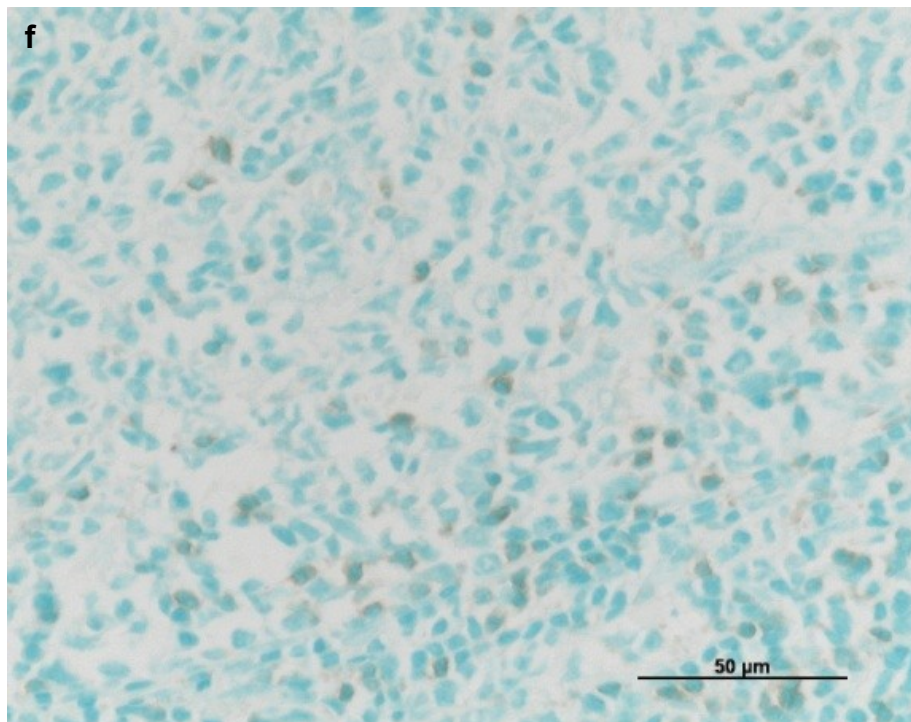
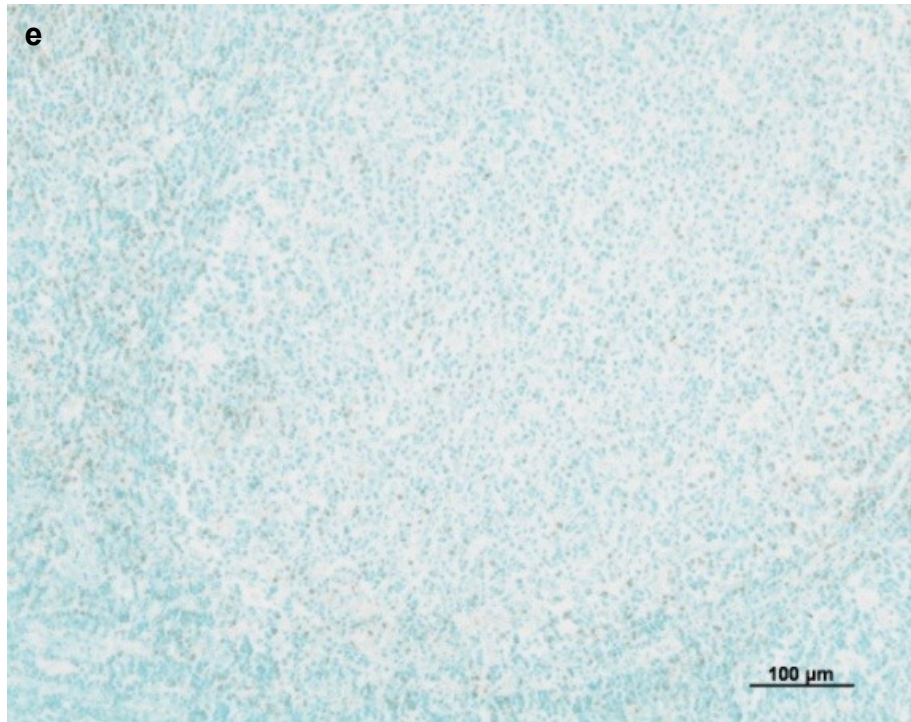


Figure 3.3 (continued). 4 μm thick sections of paraffin wax-embedded human tonsil immunohistochemically stained with UCHL-1 and GAM Ig PC and DAB-PO<sub>4</sub>.

UCHL-1 at  $1/5,000$ . Low magnification (e) and high magnification (f).



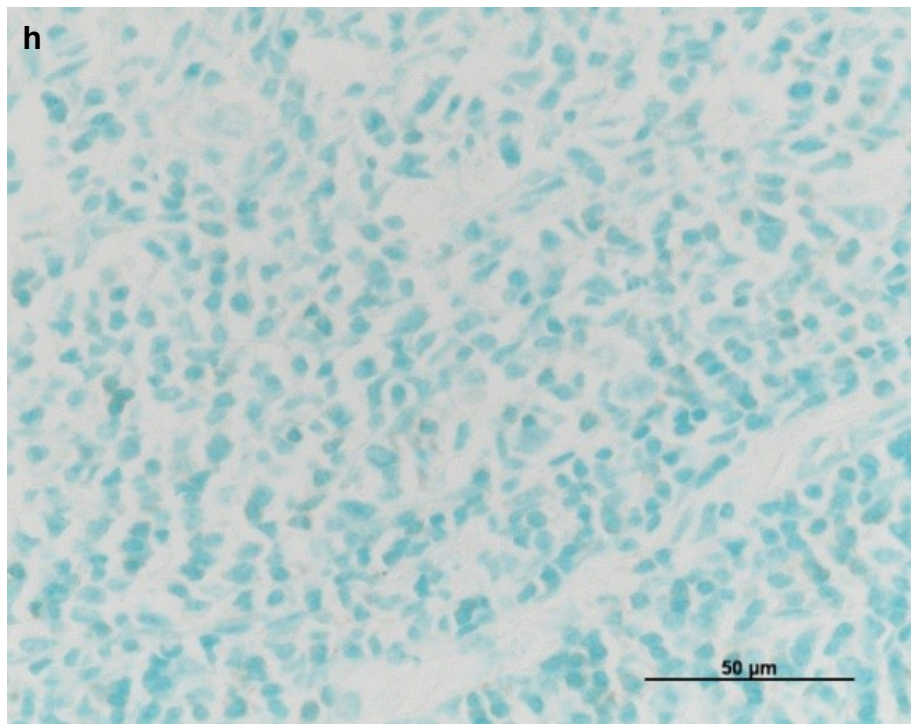
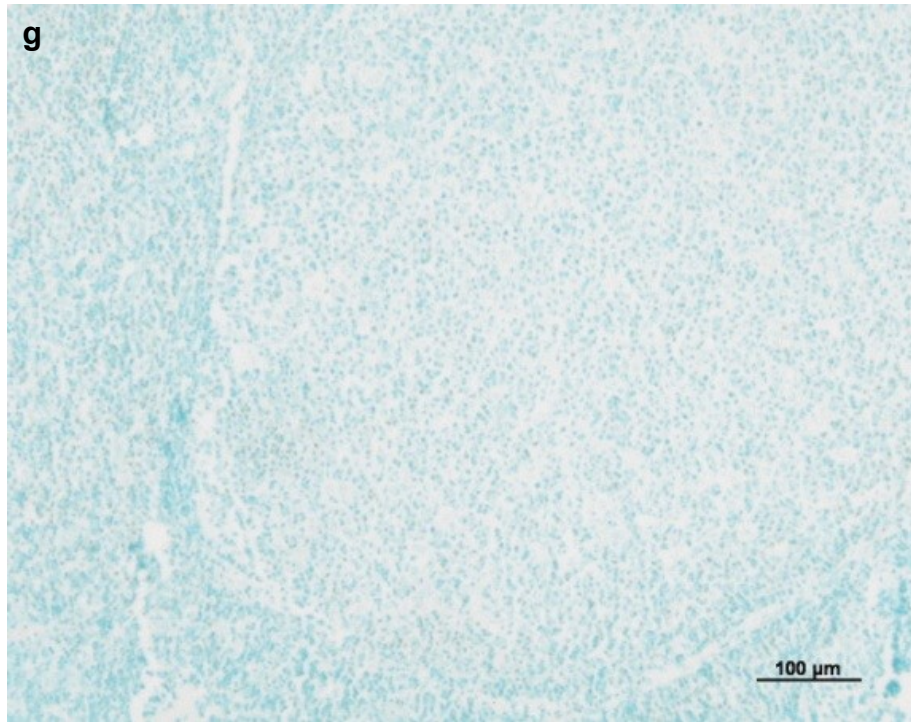


Figure 3.3 (continued). 4 μm thick sections of paraffin wax-embedded human tonsil immunohistochemically stained with UCHL-1 and GAM Ig PC and DAB-PO<sub>4</sub>.

UCHL-1 at  $1/10,000$ . Low magnification (g) and high magnification (h).

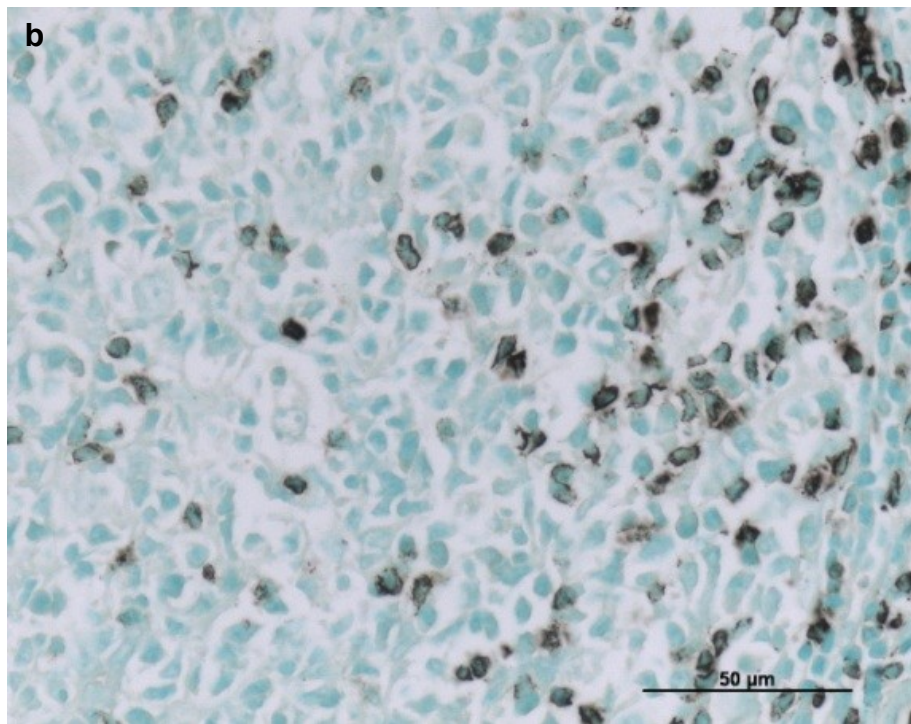
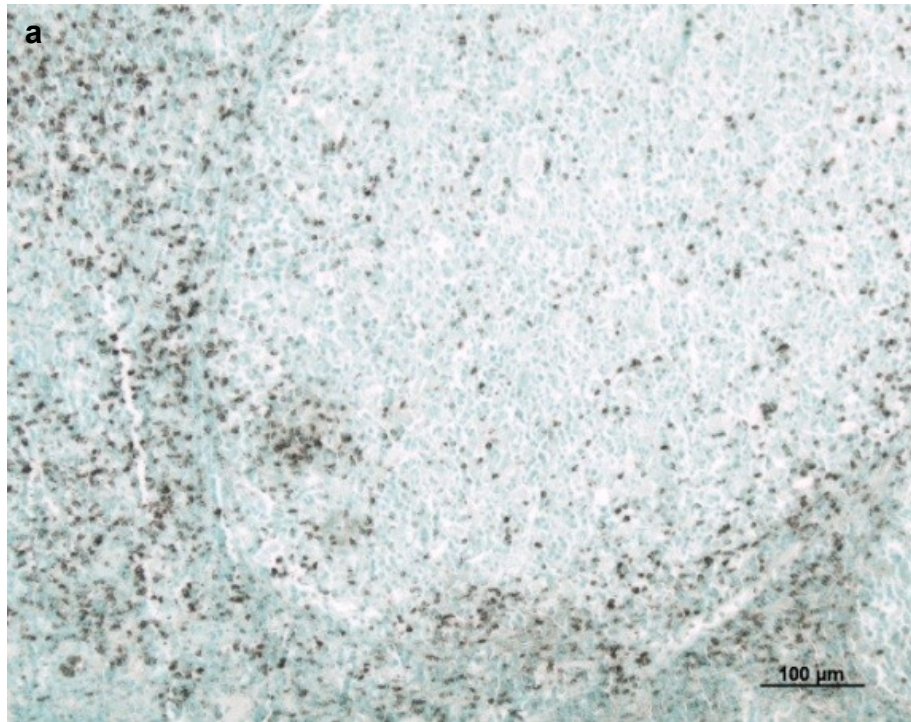


Figure 3.4. 4  $\mu\text{m}$  thick sections of paraffin wax-embedded human tonsil immunohistochemically stained with UCHL-1 and GAM Ig PC and DAB- $\text{PO}_4$  followed by 2.5 mM  $\text{NaAu(III)Cl}_4$  and 0.3%  $\text{Na}_2\text{S}$ . UCHL-1 at  $1/5,000$ .

Low magnification (a) and high magnification (b).



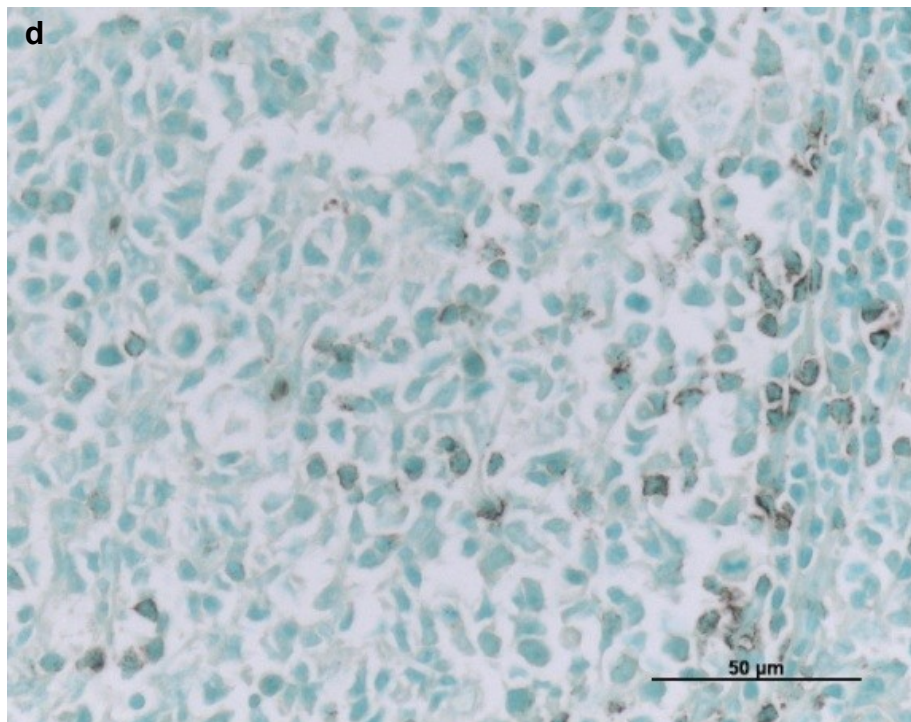
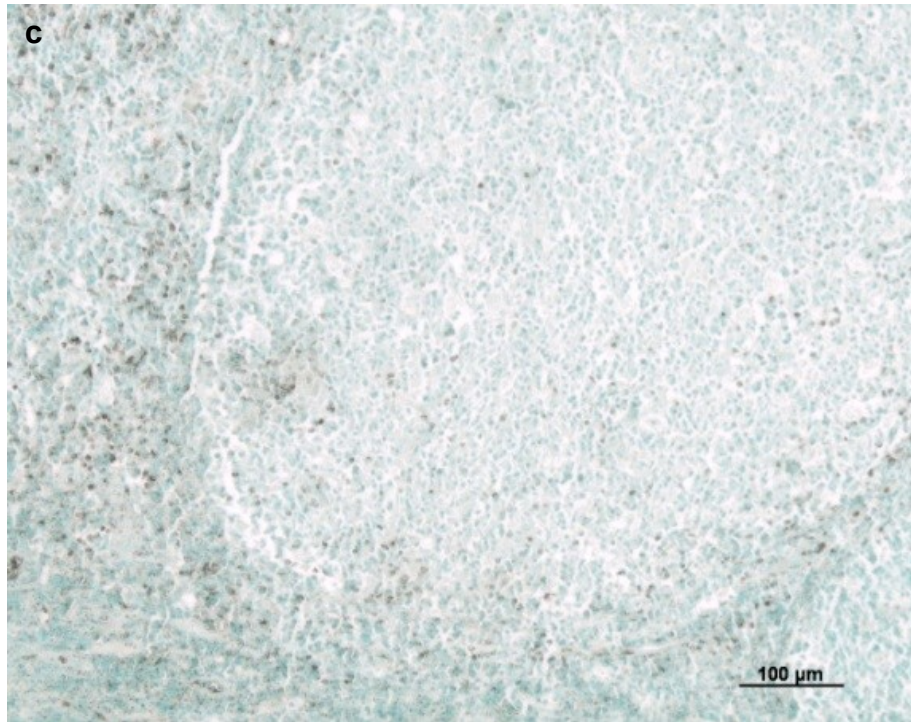


Figure 3.4 (continued). 4  $\mu\text{m}$  thick sections of paraffin wax-embedded human tonsil immunohistochemically stained with UCHL-1 and GAM Ig PC and DAB-PO<sub>4</sub> followed by 2.5 mM NaAu(III)Cl<sub>4</sub> and 0.3% Na<sub>2</sub>S. UCHL-1 at  $1/10,000$ .  
Low magnification (c) and high magnification (d).



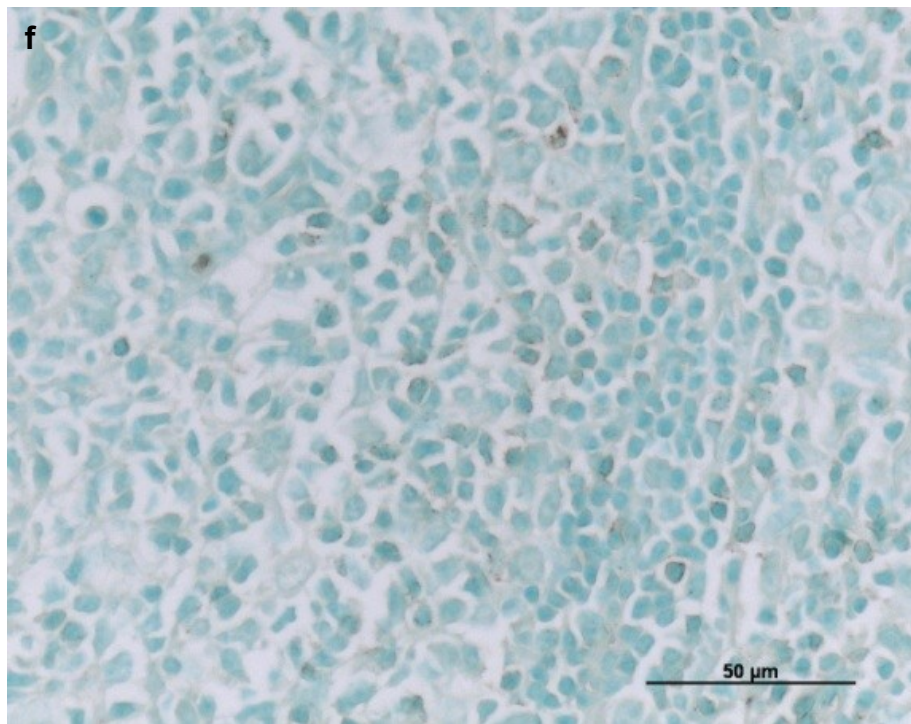
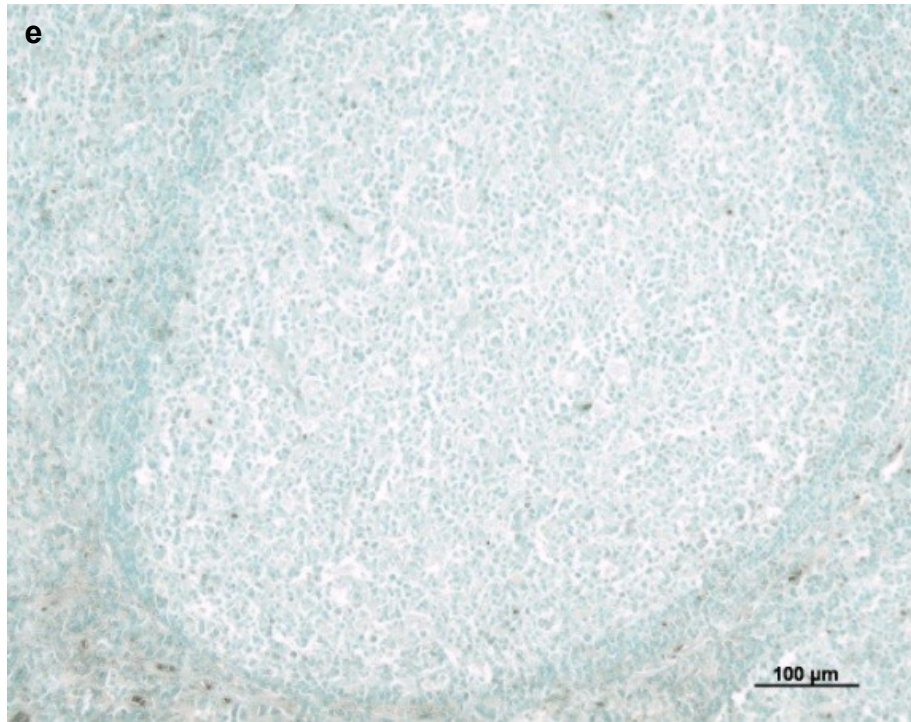


Figure 3.4 (continued). 4  $\mu\text{m}$  thick sections of paraffin wax-embedded human tonsil immunohistochemically stained with UCHL-1 and GAM Ig PC and DAB-PO<sub>4</sub> followed by 2.5 mM NaAu(III)Cl<sub>4</sub> and 0.3% Na<sub>2</sub>S. UCHL-1 at  $1/_{20,000}$ .  
Low magnification (e) and high magnification (f).

#### 3.4.4 Reduction of Non-specific Complexing of Amplifying Reagents with Tissue

At 2.5 mM NaAu(III)Cl<sub>4</sub>, the best result was seen with 0.3% Na<sub>2</sub>S (figure 3.5a), signal strength declining and background staining increasing as the concentration of Na<sub>2</sub>S was reduced (figure 3.5b – d). At 1 mM NaAu(III)Cl<sub>4</sub>, a similar pattern was seen, although both signal strength and background were reduced (figure 3.5e – h) When NaAu(III)Cl<sub>4</sub> was applied at 0.3 mM, faint staining with high background was seen following 0.3% Na<sub>2</sub>S (figure 3.5i), but lowering the concentration of Na<sub>2</sub>S to 0.1% dramatically improved signal strength without elevating background (figure 3.5j). At lower concentrations of Na<sub>2</sub>S, signal strength progressively fell (figure 3.5k) and background staining increased (figure 3.5l). At the lowest concentration of NaAu(III)Cl<sub>4</sub>, positivity could be seen at all concentrations of Na<sub>2</sub>S, but in all cases, a fine granular background was present. In addition, positive sites were also granular in appearance (figure 3.5m – p).

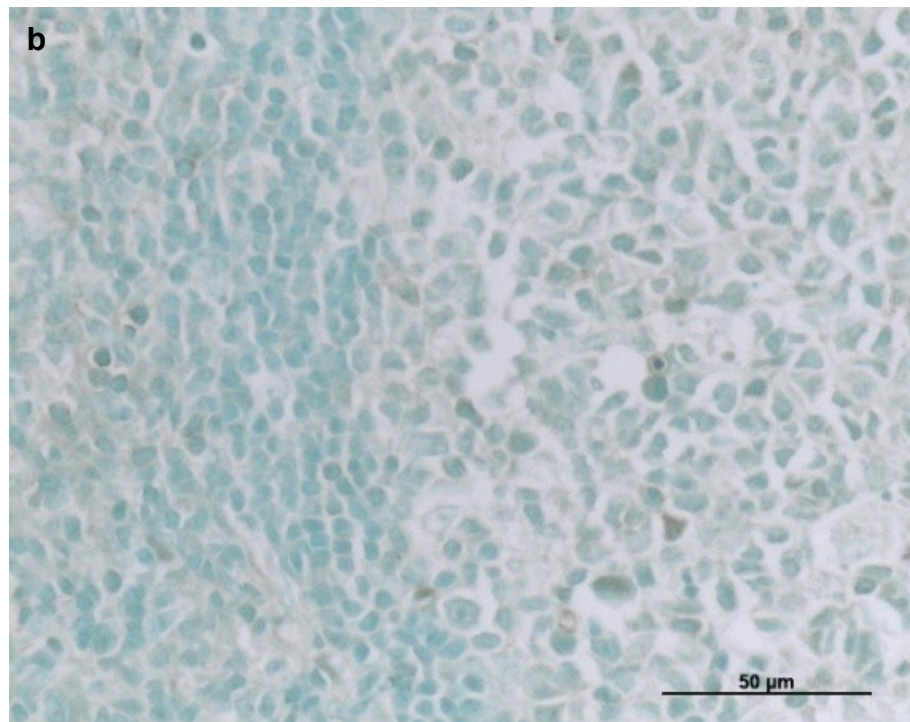
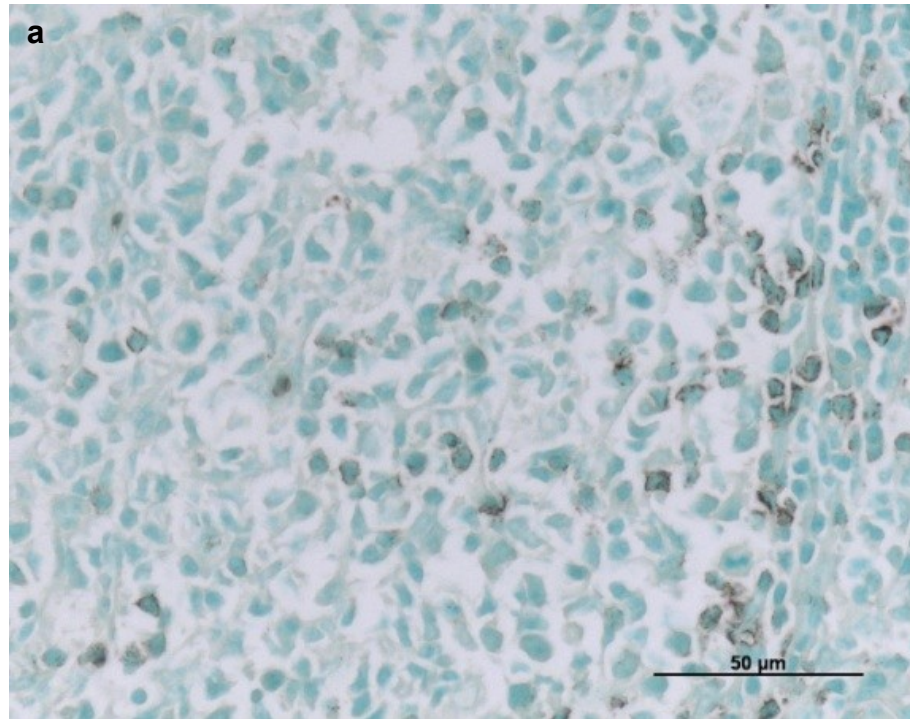


Figure 3.5. 4  $\mu\text{m}$  thick sections of paraffin wax-embedded human tonsil immunohistochemically stained with  $1/_{10,000}$  UCHL-1 and GAM Ig PC/DAB- $\text{PO}_4$  followed by 2.5 mM  $\text{NaAu(III)Cl}_4$  and  $\text{Na}_2\text{S}$  at 0.3% (a) and 0.1% (b).



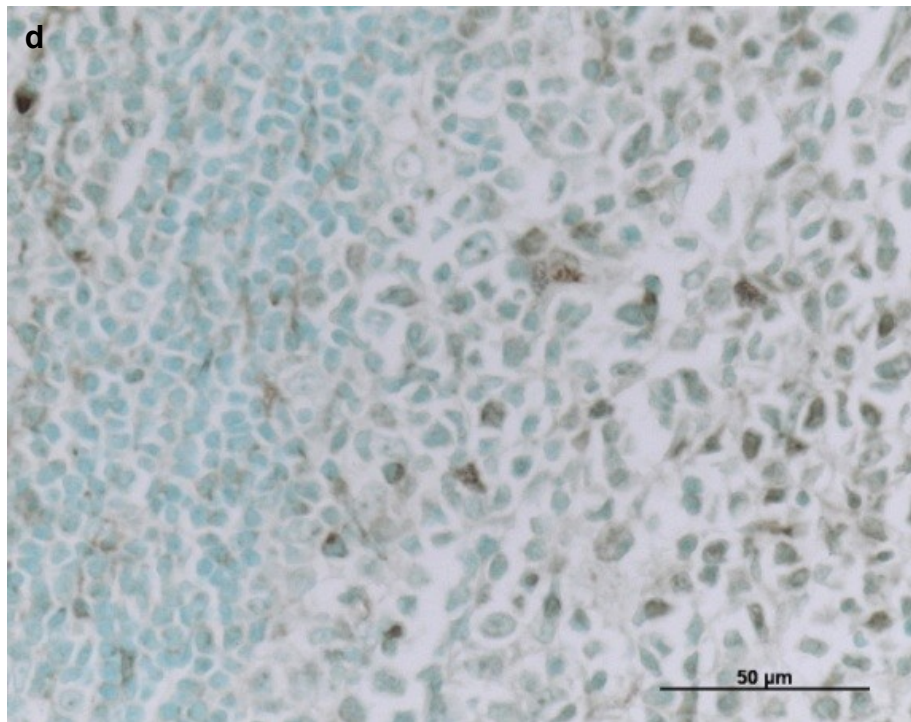
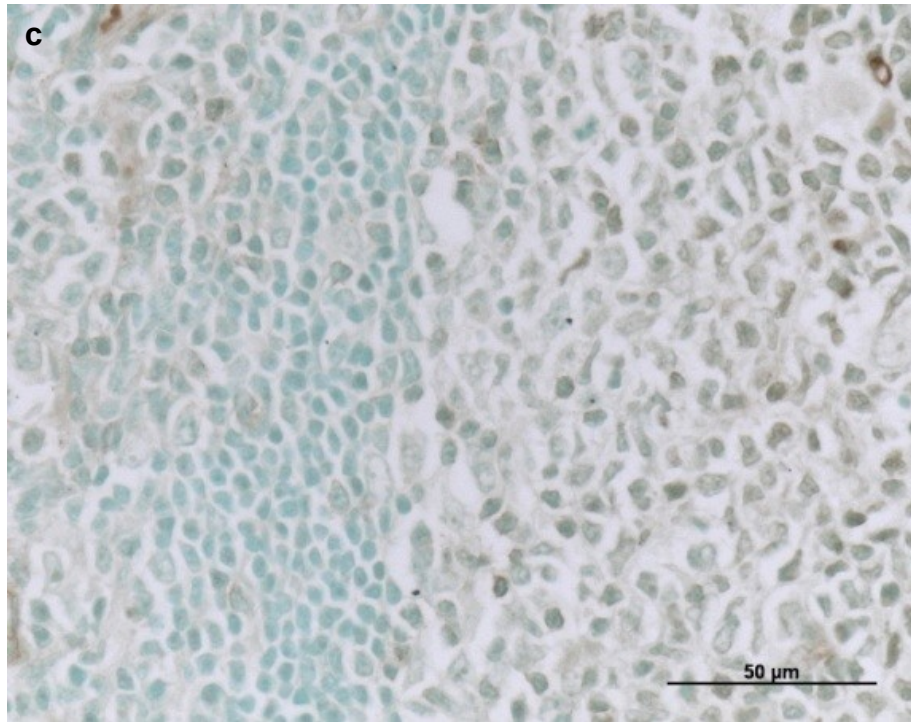


Figure 3.5 (continued). 4 μm thick sections of paraffin wax-embedded human tonsil immunohistochemically stained with  $1/10,000$  UCHL-1 and GAM Ig PC/DAB-PO<sub>4</sub> followed by 2.5 mM NaAu(III)Cl<sub>4</sub> and Na<sub>2</sub>S at 0.03% (c) and 0.01% (d).

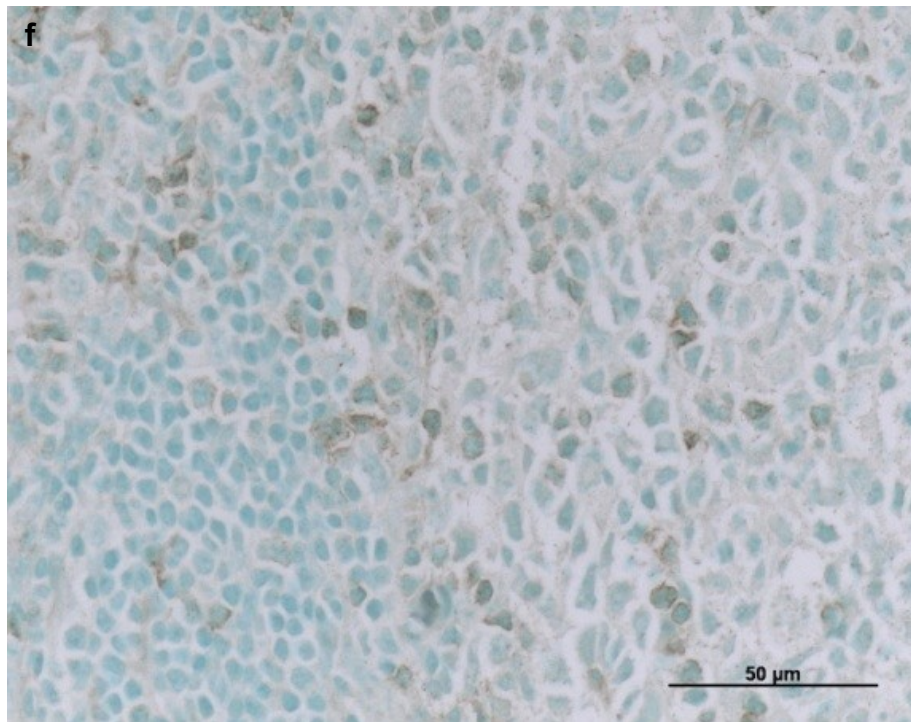
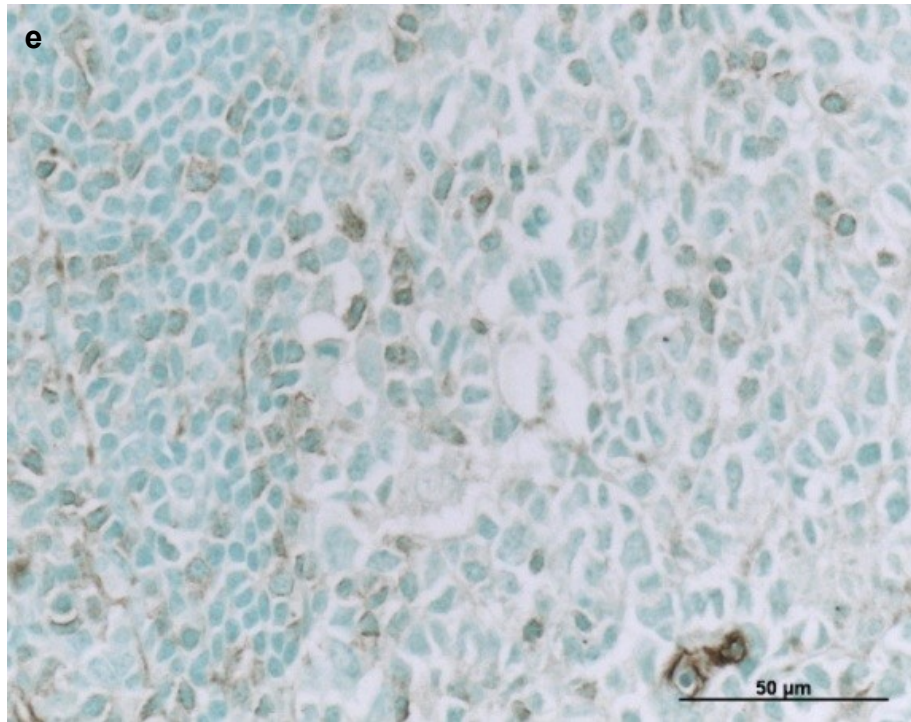


Figure 3.5 (continued). 4 μm thick sections of paraffin wax-embedded human tonsil immunohistochemically stained with  $1/10,000$  UCHL-1 and GAM Ig PC/DAB-PO<sub>4</sub> followed by 1 mM NaAu(III)Cl<sub>4</sub> and Na<sub>2</sub>S at 0.3% (e), 0.1% (f).



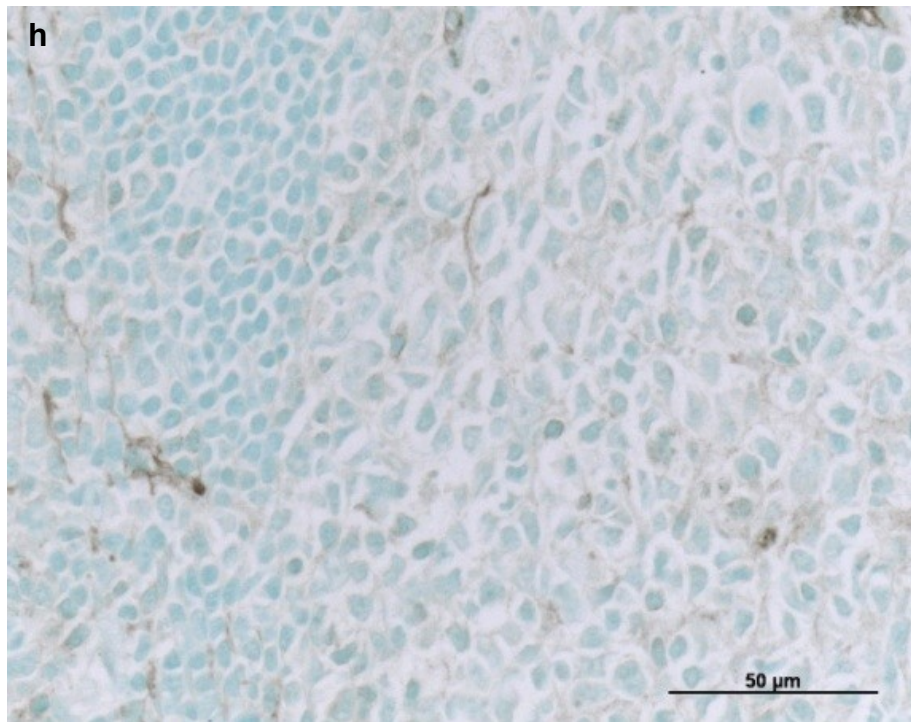
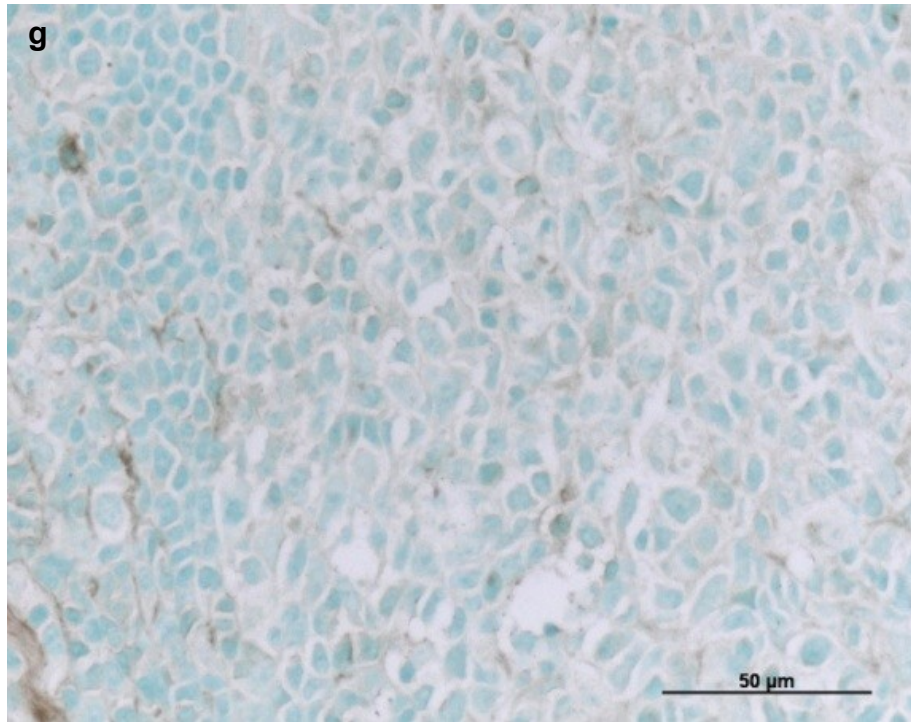


Figure 3.5 (continued). 4  $\mu\text{m}$  thick sections of paraffin wax-embedded human tonsil immunohistochemically stained with  $1/10,000$  UCHL-1 and GAM Ig PC/DAB- $\text{PO}_4$  followed by 1 mM  $\text{NaAu(III)Cl}_4$  and  $\text{Na}_2\text{S}$  at 0.03% (g) and 0.01% (h).

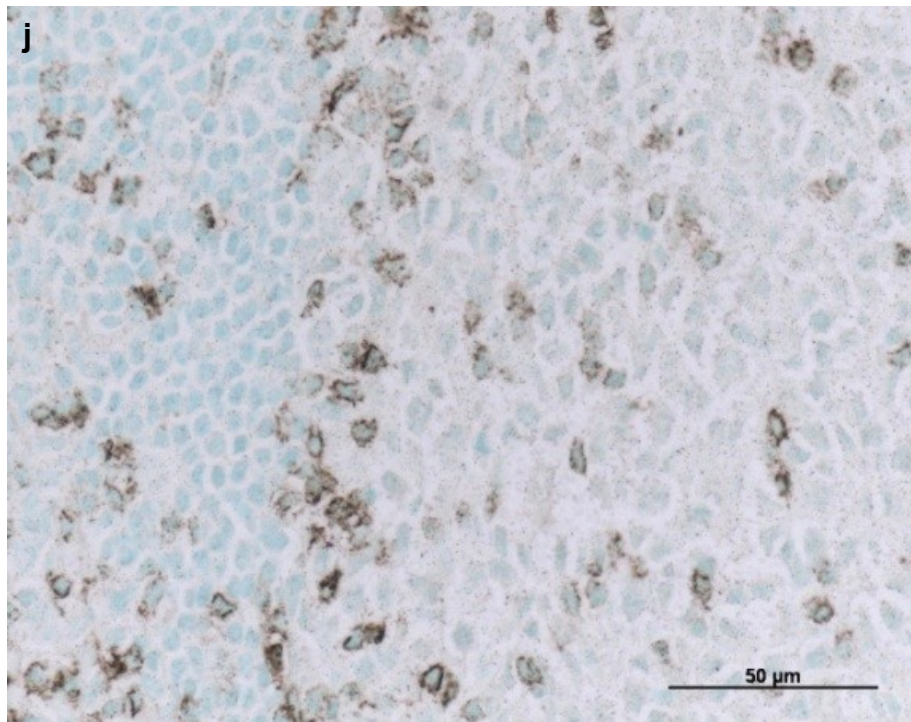
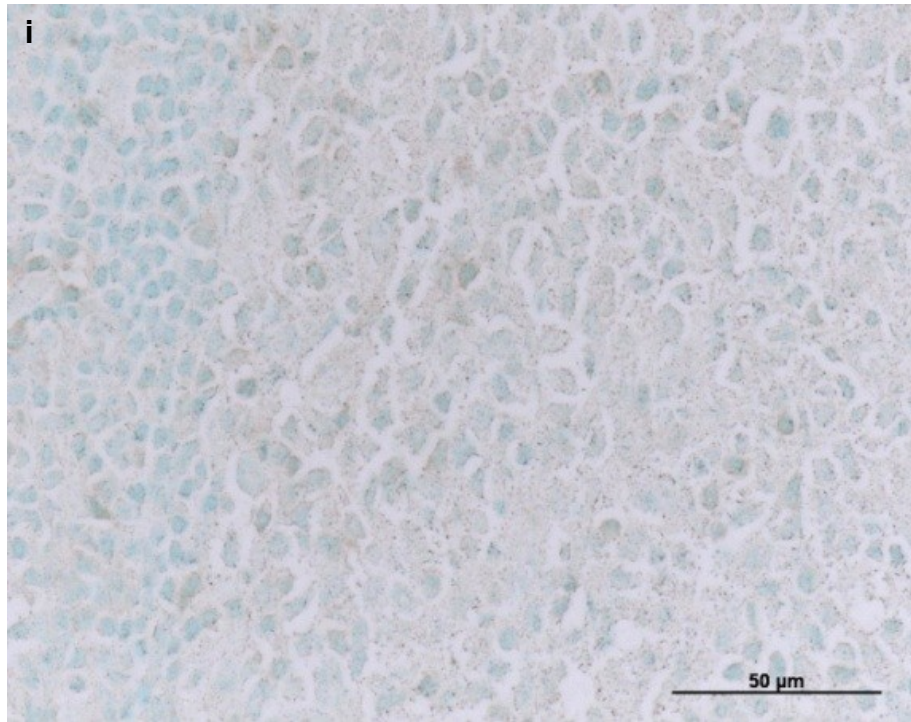


Figure 3.5 (continued). 4 μm thick sections of paraffin wax-embedded human tonsil immunohistochemically stained with  $1/_{10,000}$  UCHL-1 and GAM Ig PC/DAB-PO<sub>4</sub> followed by 0.3 mM NaAu(III)Cl<sub>4</sub> and Na<sub>2</sub>S at 0.3% (i) and 0.1% (j).



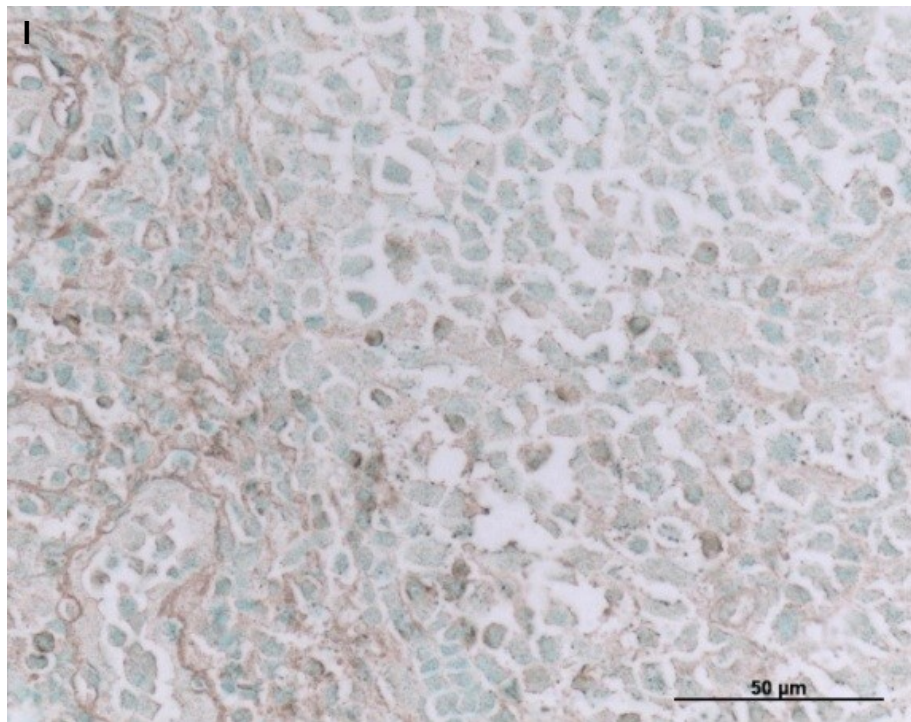
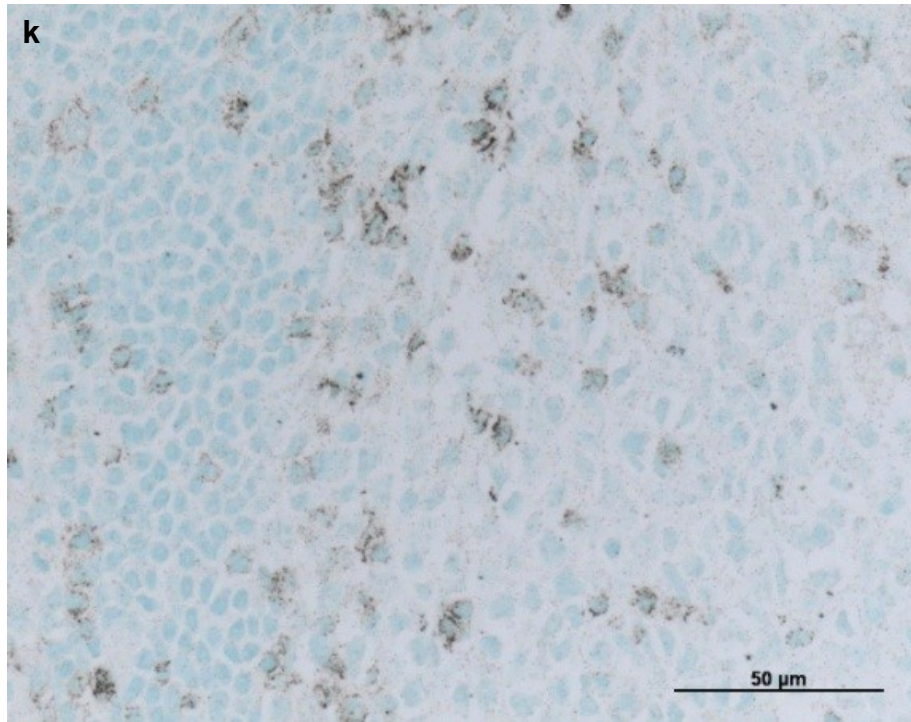


Figure 3.5 (continued). 4 μm thick sections of paraffin wax-embedded human tonsil immunohistochemically stained with  $1/_{10,000}$  UCHL-1 and GAM Ig PC/DAB-PO<sub>4</sub> followed by 0.3 mM NaAu(III)Cl<sub>4</sub> and Na<sub>2</sub>S at 0.03% (k) and 0.01% (l).



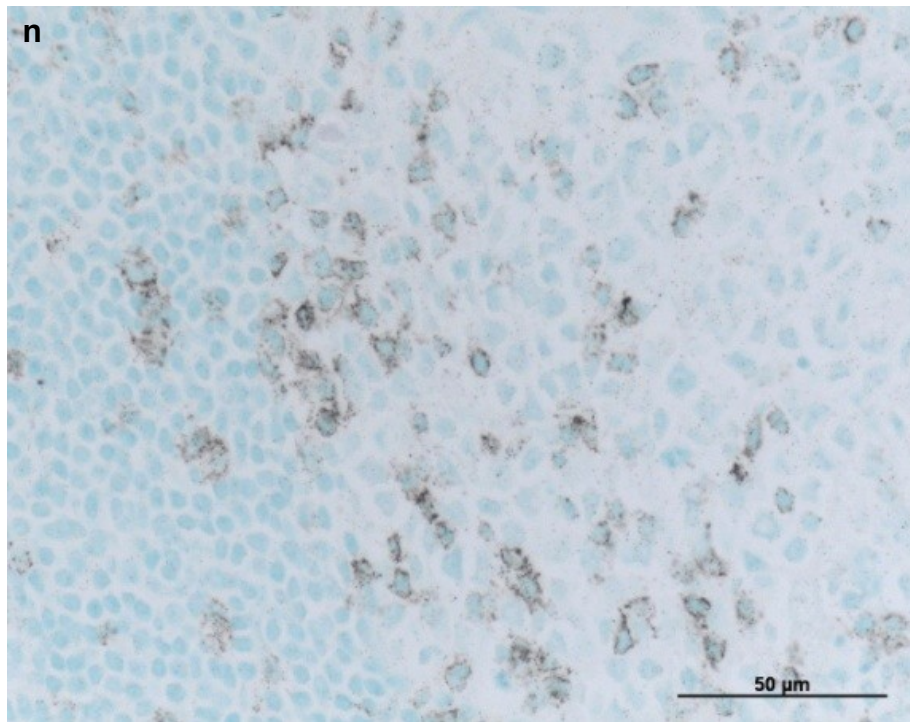
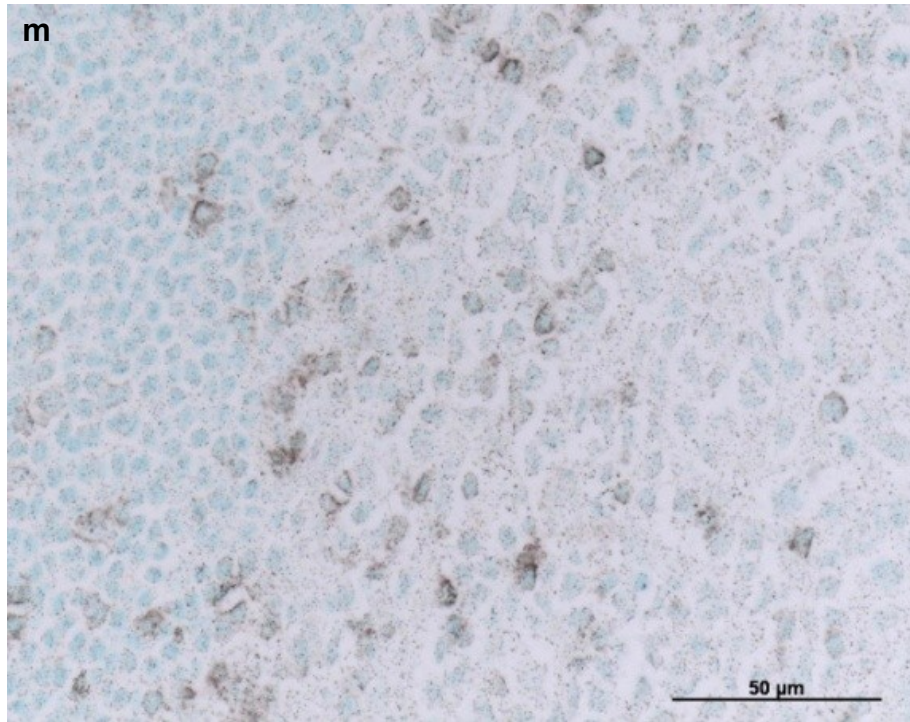


Figure 3.5 (continued). 4 μm thick sections of paraffin wax-embedded human tonsil immunohistochemically stained with  $1/_{10,000}$  UCHL-1 and GAM Ig PC/DAB-PO<sub>4</sub> followed by 0.1 mM NaAu(III)Cl<sub>4</sub> and Na<sub>2</sub>S at 0.3% (m), 0.1% (n).

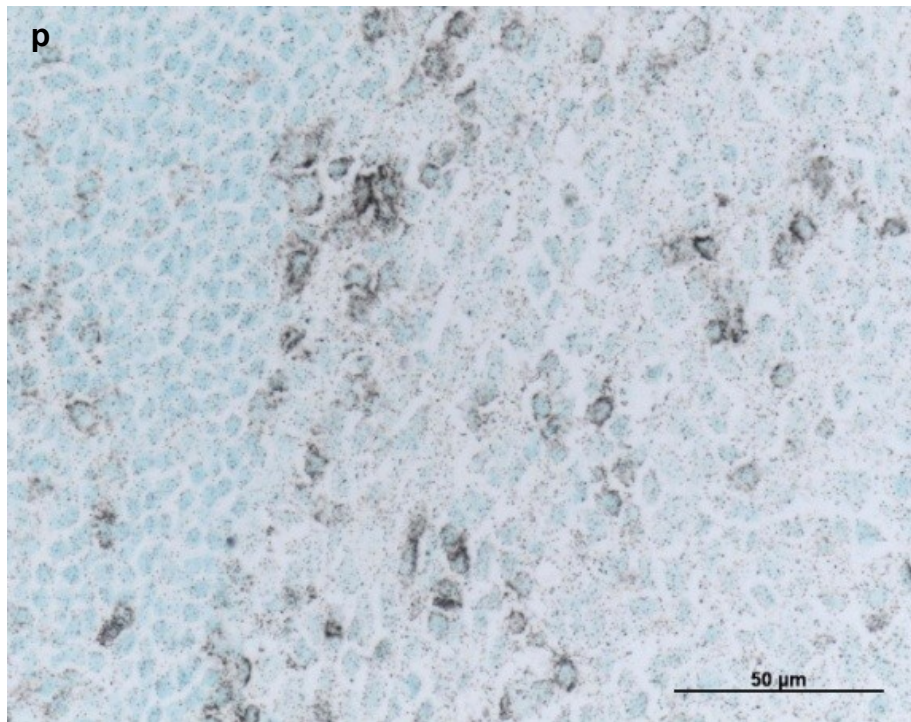
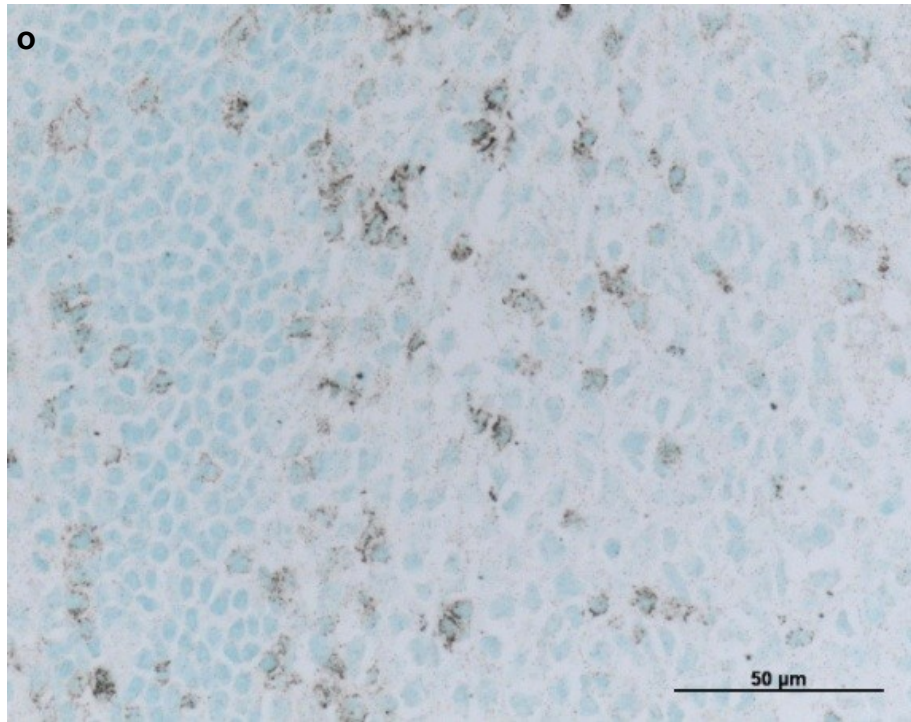


Figure 3.5 (continued). 4  $\mu\text{m}$  thick sections of paraffin wax-embedded human tonsil immunohistochemically stained with  $1/_{10,000}$  UCHL-1 and GAM Ig PC/DAB- $\text{PO}_4$  followed by 0.1 mM  $\text{NaAu(III)Cl}_4$  and  $\text{Na}_2\text{S}$  at 0.03% (o) and 0.01% (p).

### 3.4.5 Suppression of Tissue Argyrophilia

Post-DAB polymerisation treatment with 10 mM La(III)Cl<sub>3</sub> followed by 3% H<sub>2</sub>O<sub>2</sub> extended the development time and resulted in an improvement in immunohistochemical signal intensity such that staining, which could only be seen at <sup>1</sup>/<sub>20,000</sub> in its absence (figure 3.6a and b), could now be clearly seen at <sup>1</sup>/<sub>50,000</sub> (figure 3.6c and d).



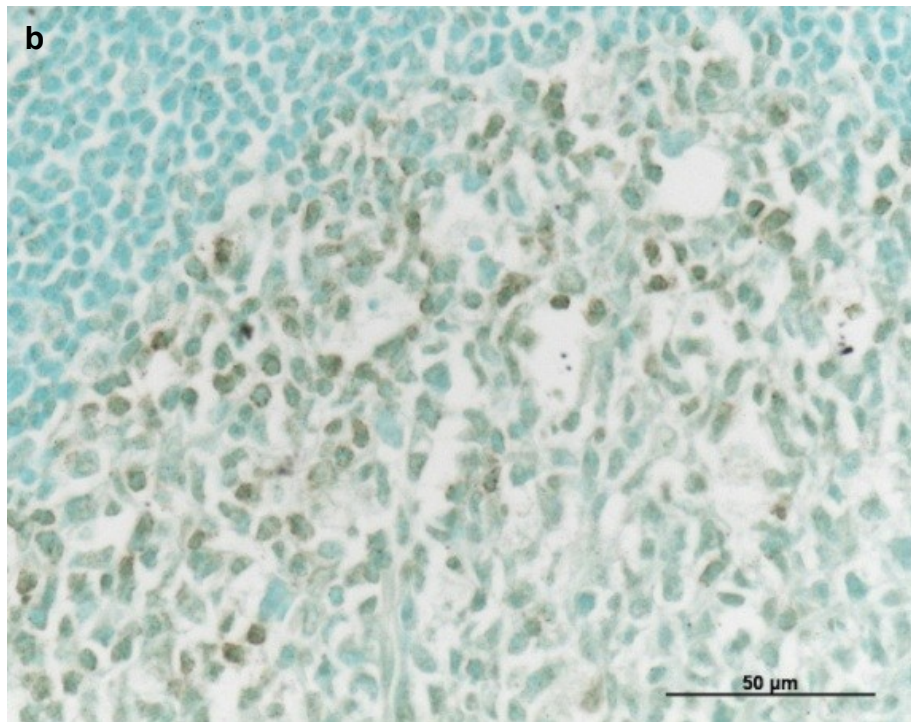
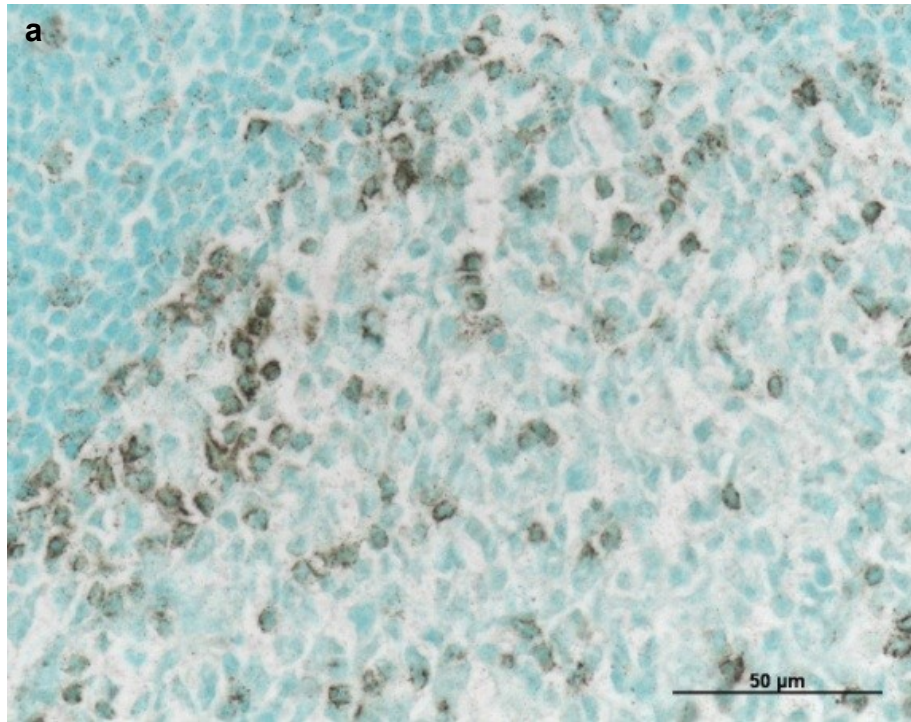


Figure 3.5. 4  $\mu\text{m}$  thick sections of paraffin wax-embedded human tonsil immunohistochemically stained for CD45Ro. Effects of suppression of tissue argyrophilia with 10 mM  $\text{LaCl}_3$  followed by 3%  $\text{H}_2\text{O}_2$  on amplification with 0.3 mM  $\text{NaAu(III)Cl}_4$  + 0.1%  $\text{Na}_2\text{S}$  + Newman and Jasani's developer. UCHL-1 at  $1/20,000$  (a) and  $1/50,000$  (b) without suppression.

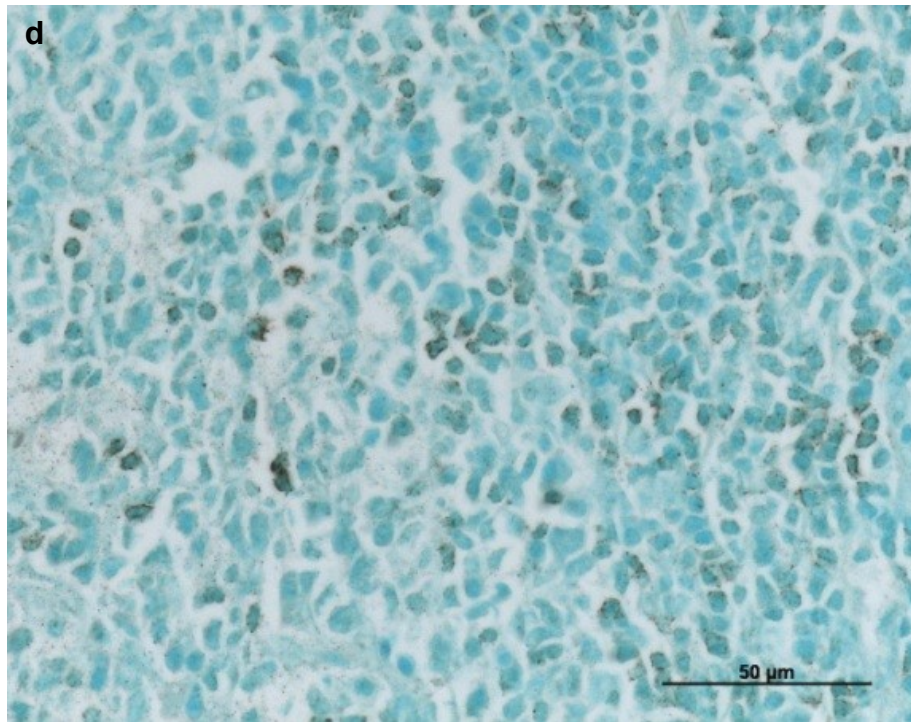
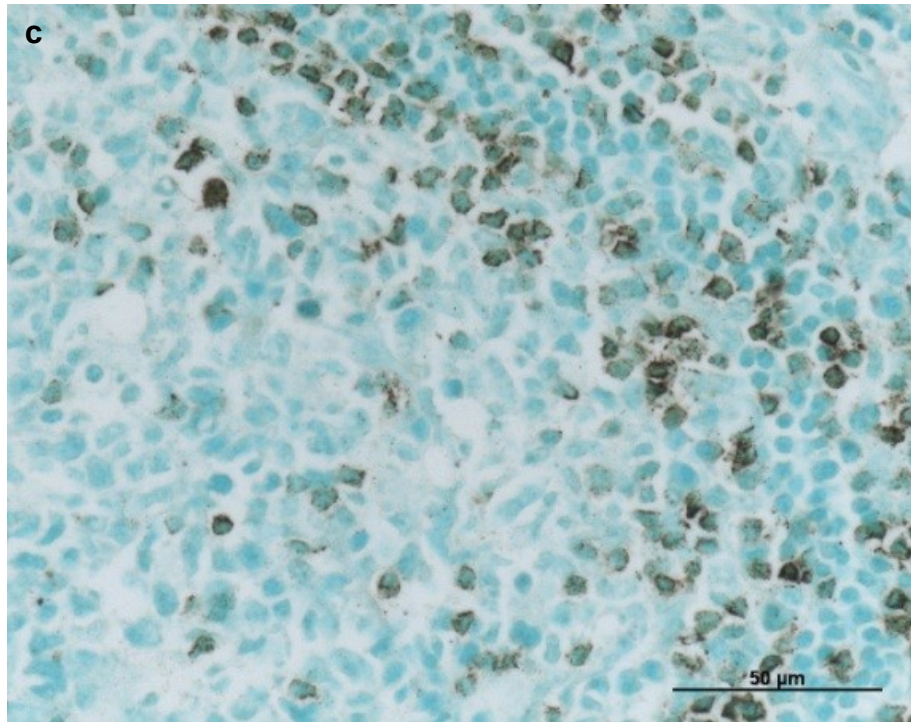


Figure 3.5 (continued). 4  $\mu$ m thick sections of paraffin wax-embedded human tonsil immunohistochemically stained for CD45Ro. Effects of suppression of tissue argyrophilia with 10 mM  $\text{LaCl}_3$  followed by 3%  $\text{H}_2\text{O}_2$  on amplification with 0.3 mM  $\text{NaAu(III)Cl}_4$  + 0.1%  $\text{Na}_2\text{S}$  + Newman and Jasani's developer. UCHL-1 at  $1/20,000$  (c) and  $1/50,000$  (d) with suppression.

### 3.4.6 Comparison of Physical Developers

As previously shown, Newman and Jasani's developer was able to reveal immunopositivity at UCHL-1 dilutions of both  $1/20,000$  and  $1/50,000$  (figure 3.7a and b). Gallyas' developer did not achieve the same level of amplification as Newman and Jasani's, mainly due to problems of self-nucleation, which resulted in the appearance of numerous particles in the developer solution (figure 3.7c and d). Danscher's developer was extremely powerful, and background staining was clearly evident at both UCHL-1 concentrations after just 5 minutes (compared with 27 and 32 minutes for Newman and Jasani's developer for UCHL-1 at  $1/20,000$  and  $1/50,000$ , respectively). Inspection of the sections revealed clear positivity at  $1/20,000$  UCHL-1, and differentiation with 0.5% potassium ferricyanide to remove the background staining was able to demonstrate positivity at  $1/50,000$  as well (figure 3.7e and f). Hacker's developer did not suffer the problems of self-nucleation that occurred with Gallyas' developer, but was only able to reveal positivity at  $1/20,000$  UCHL-1 (figure 3.7g and h).



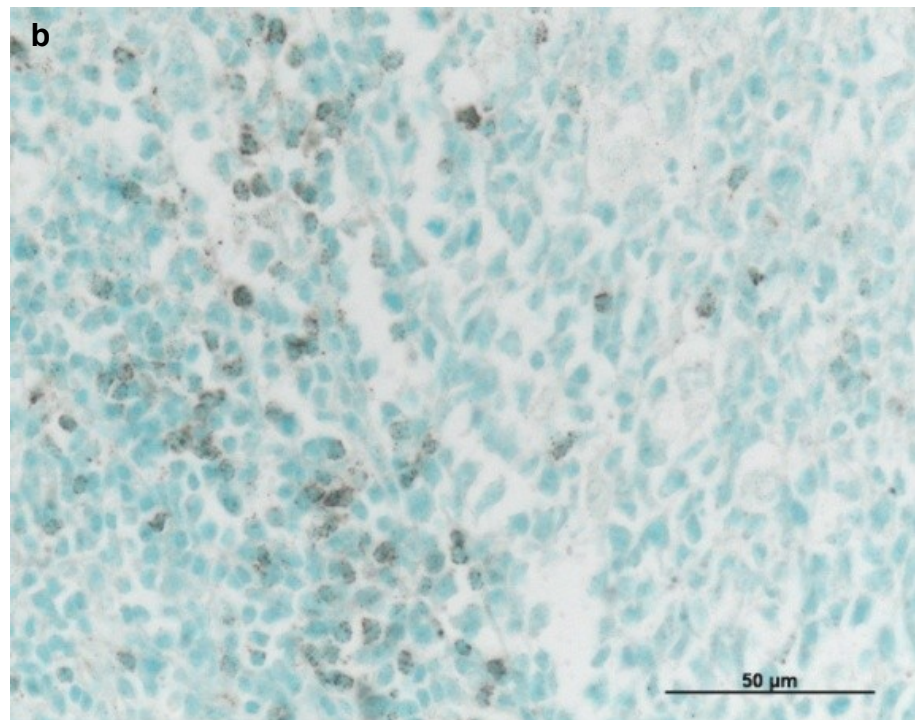
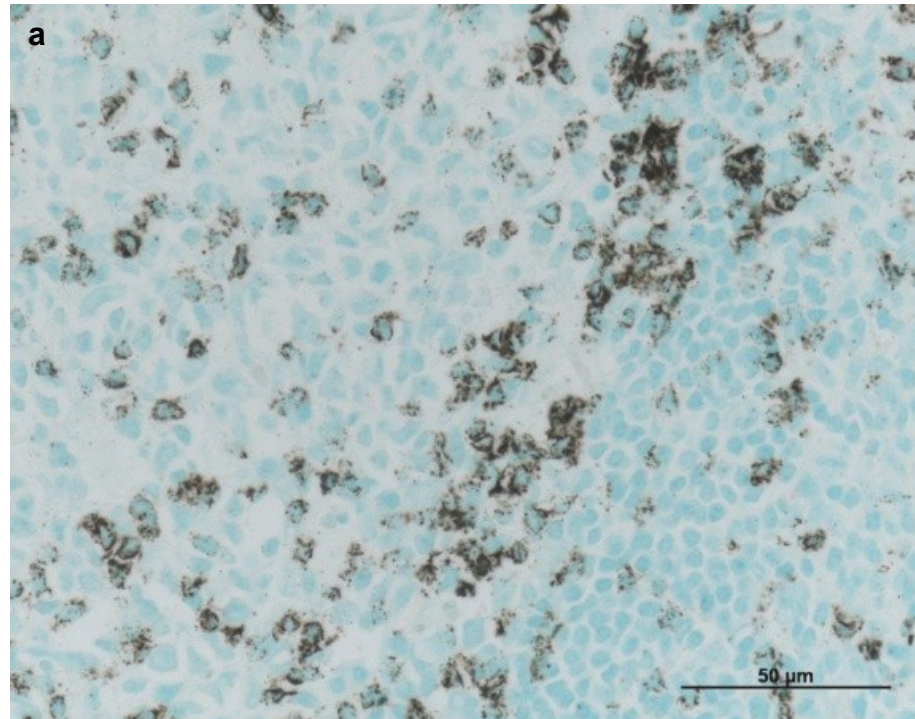


Figure 3.7. 4 μm thick sections of paraffin wax-embedded human tonsil immunohistochemically stained for CD45Ro. Comparison of physical developers on amplification. Newman and Jasani's developer, with UCHL-1 at  $1/20,000$  (a) and  $1/50,000$  (b).

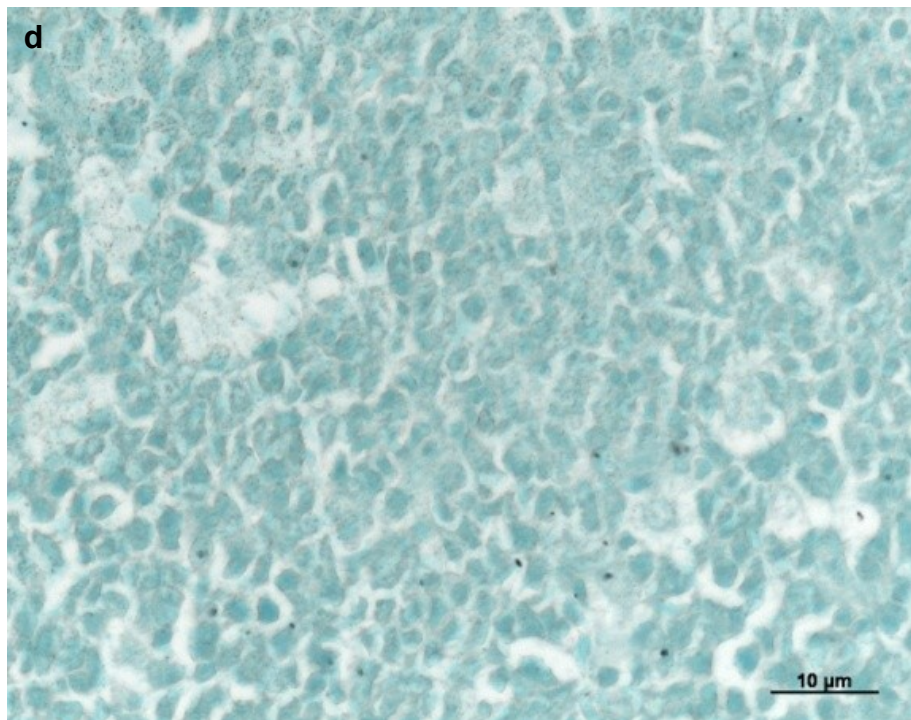
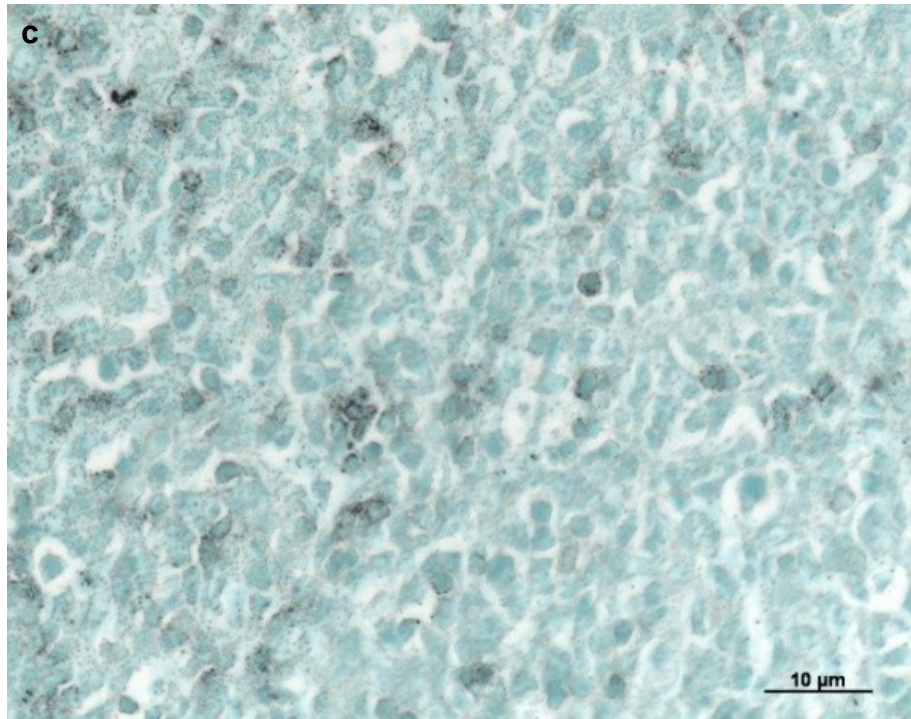


Figure 3.7 (continued). 4 μm thick sections of paraffin wax-embedded human tonsil immunohistochemically stained for CD45Ro. Comparison of physical developers on amplification. Gallyas' developer, with UCHL-1 at  $1/20,000$  (c) and  $1/50,000$  (d).



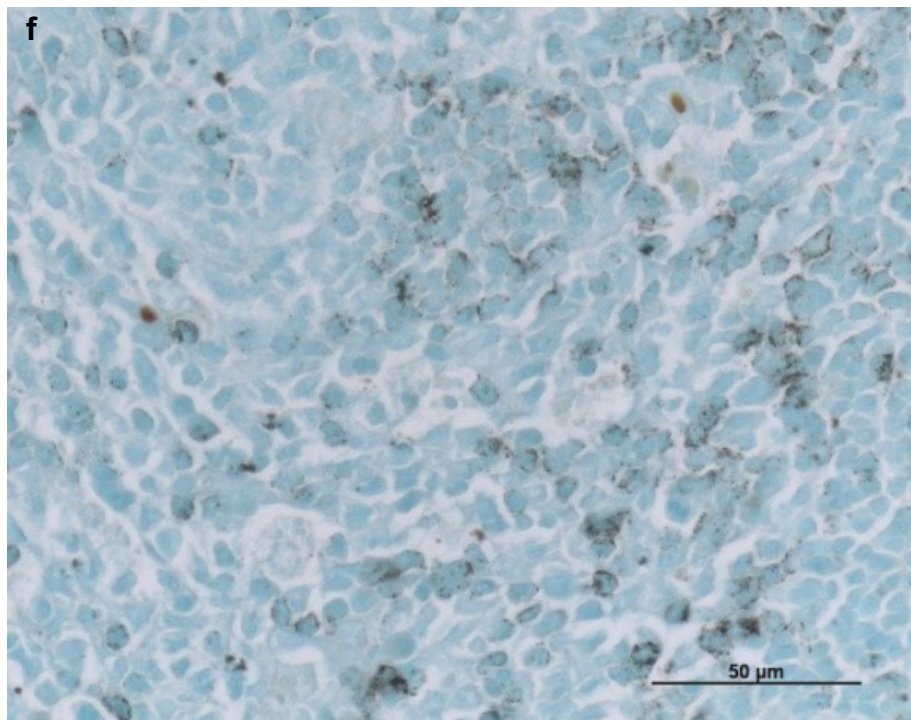
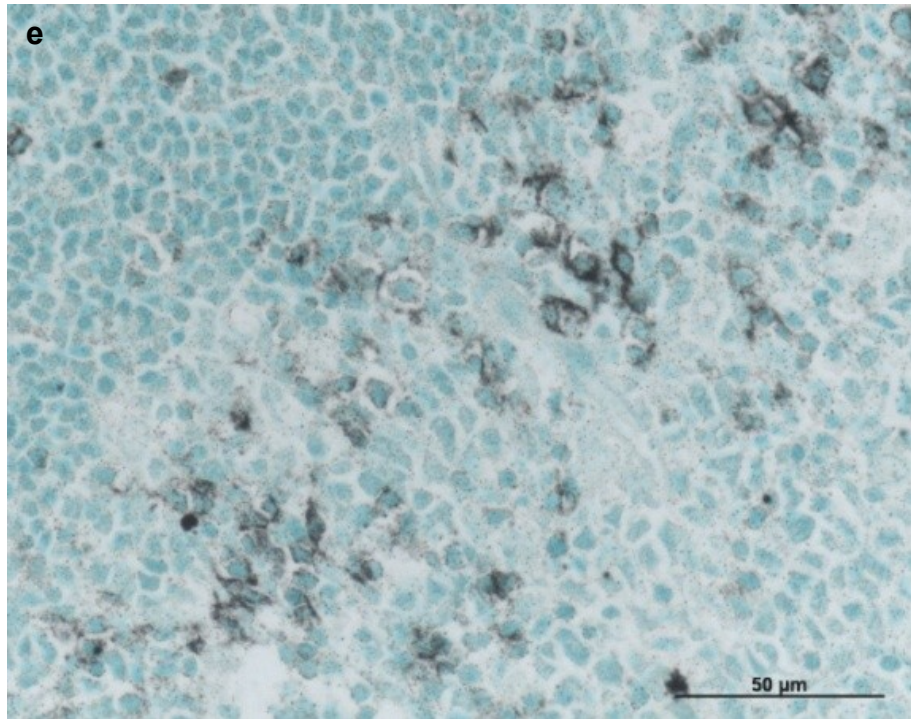


Figure 3.7 (continued). 4 μm thick sections of paraffin wax-embedded human tonsil immunohistochemically stained for CD45Ro. Comparison of physical developers on amplification. Danscher's developer, with UCHL-1 at  $1/20,000$  (e) and  $1/50,000$  (f).

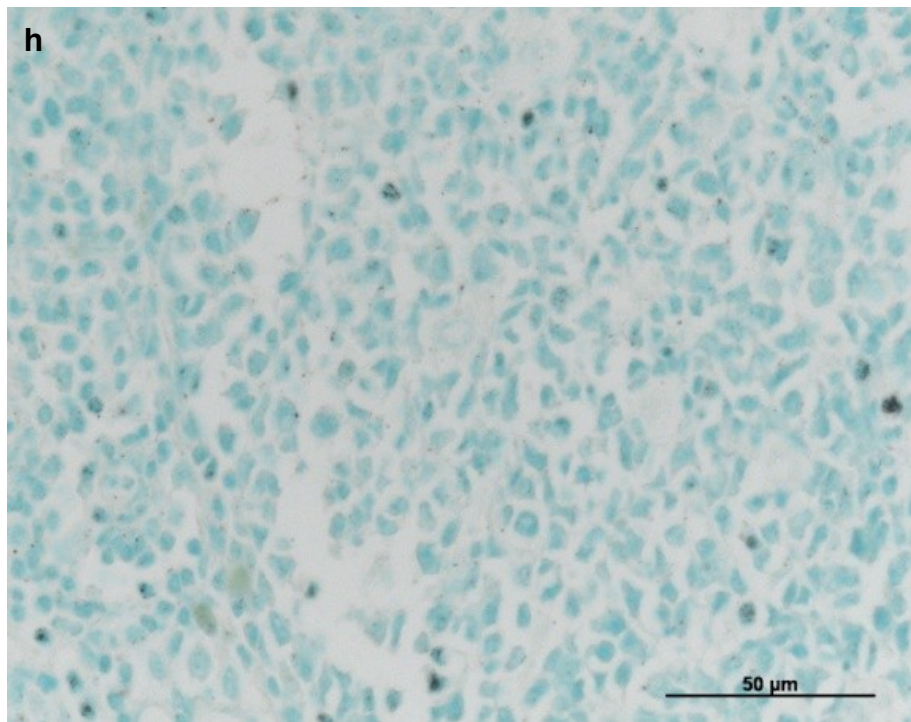
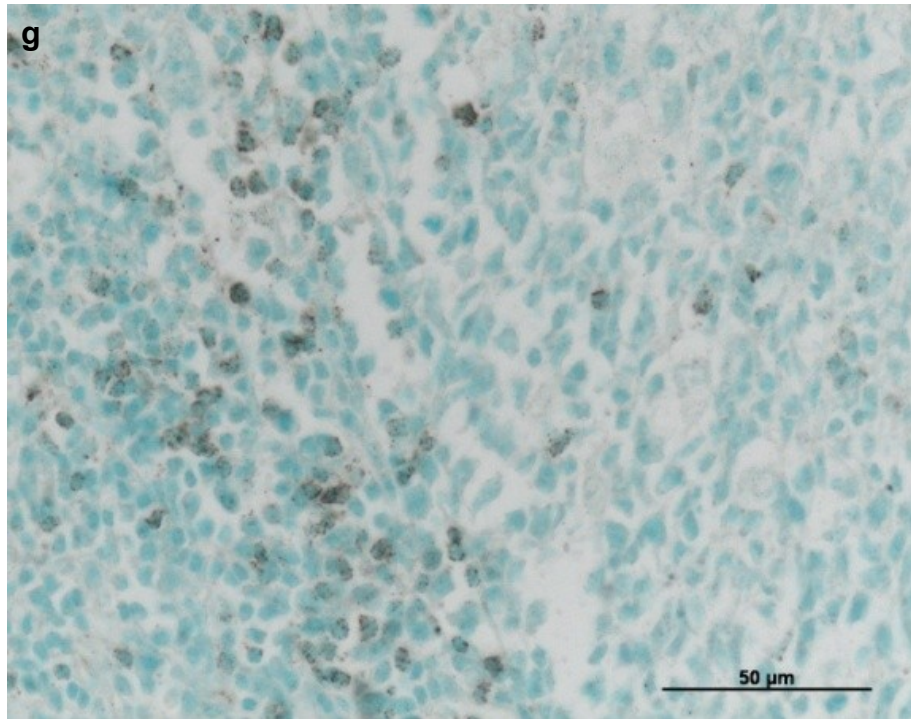


Figure 3.7 (continued). 4 μm thick sections of paraffin wax-embedded human tonsil immunohistochemically stained for CD45Ro. Comparison of physical developers on amplification. Hacker's developer, with UCHL-1 at  $1/20,000$  (g) and  $1/50,000$  (h).

### 3.4.7 Comparison of Secondary Antibody Conjugates

Compared to the Santa Cruz peroxidase conjugate, the Sigma-Aldrich conjugate performed poorly. While staining with the Santa Cruz conjugate could be clearly seen at both  $1/_{20,000}$  and  $1/_{50,000}$  UCHL-1 (figure 3.8a and b), staining with the Sigma-Aldrich conjugate could only just be seen at  $1/_{10,000}$  and at  $1/_{20,000}$ , not at all (figure 3.8c and d). The Dako conjugate, performed the worst of all, with positivity being visible at  $1/_{2,000}$  and barely visible at  $1/_{5,000}$  (figure 3.8e and f). Using the Envision™ system, UCHL-1 at dilutions of  $1/_{50,000}$  and  $1/_{100,000}$  could be clearly seen, although staining was finely granular in the latter case. (figure 3.8g and h).

In dot blot preparations, dot blots produced by the Santa Cruz conjugate could be detected at all concentrations down to 5 ng/ml (figure 3.9a and b), and those produced by the Dako peroxidase conjugate, down to 10 ng/ml IgG (figure 3.9c and d). Those produced by the Sigma conjugate could be seen only down to 50 ng/ml (figure 3.9e).



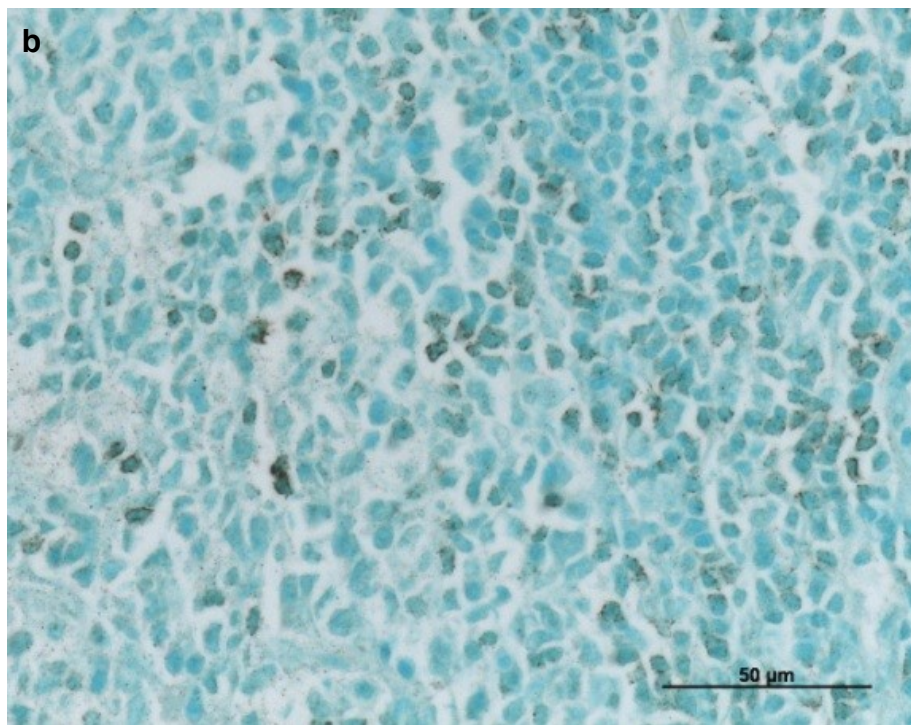
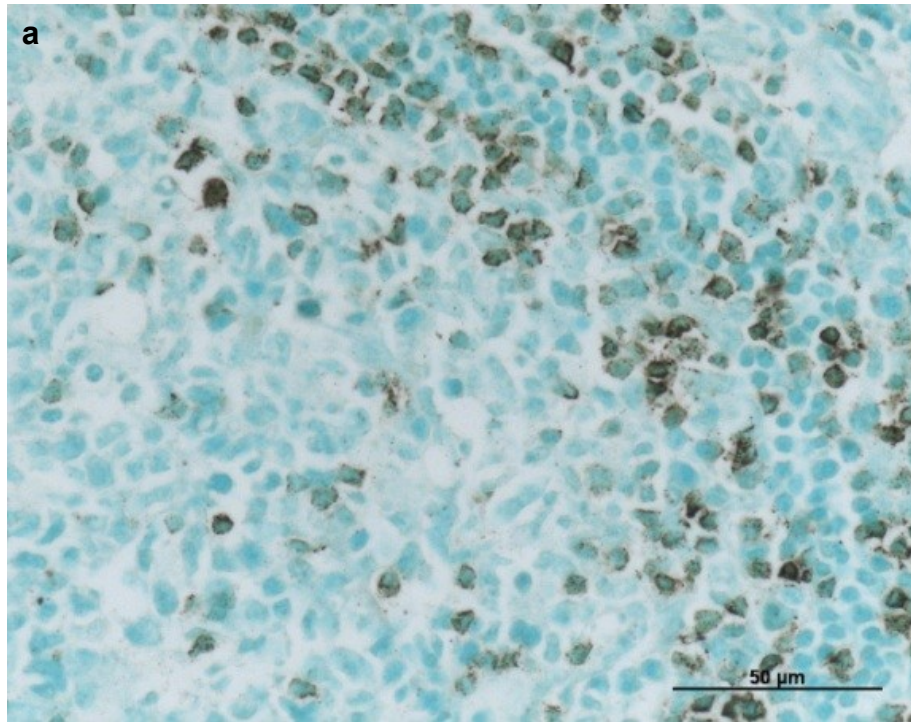


Figure 3.8. 4 μm thick sections of paraffin wax-embedded human tonsil immunohistochemically stained for CD45Ro. Comparison of secondary antibody conjugates. Santa Cruz peroxidase conjugate with UCHL-1 at  $1/20,000$  (a) and  $1/50,000$  (b).

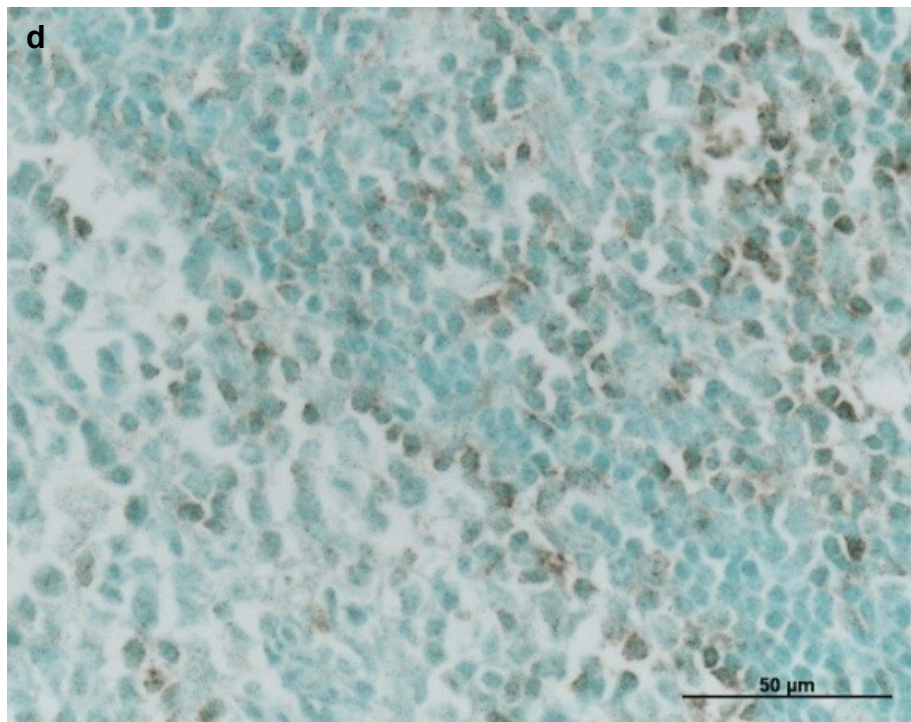
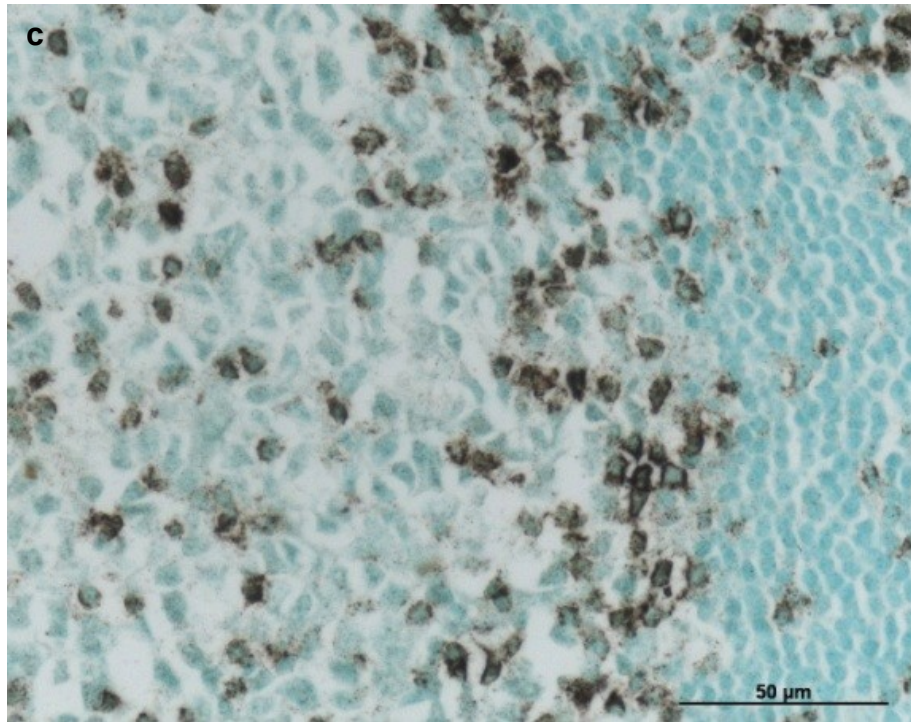


Figure 3.8 (continued). 4 μm thick sections of paraffin wax-embedded human tonsil immunohistochemically stained for CD45Ro. Comparison of secondary antibody conjugates. Sigma Aldrich peroxidase conjugate with UCHL-1 at  $1/5,000$  (c) and

$1/10,000$  (d).



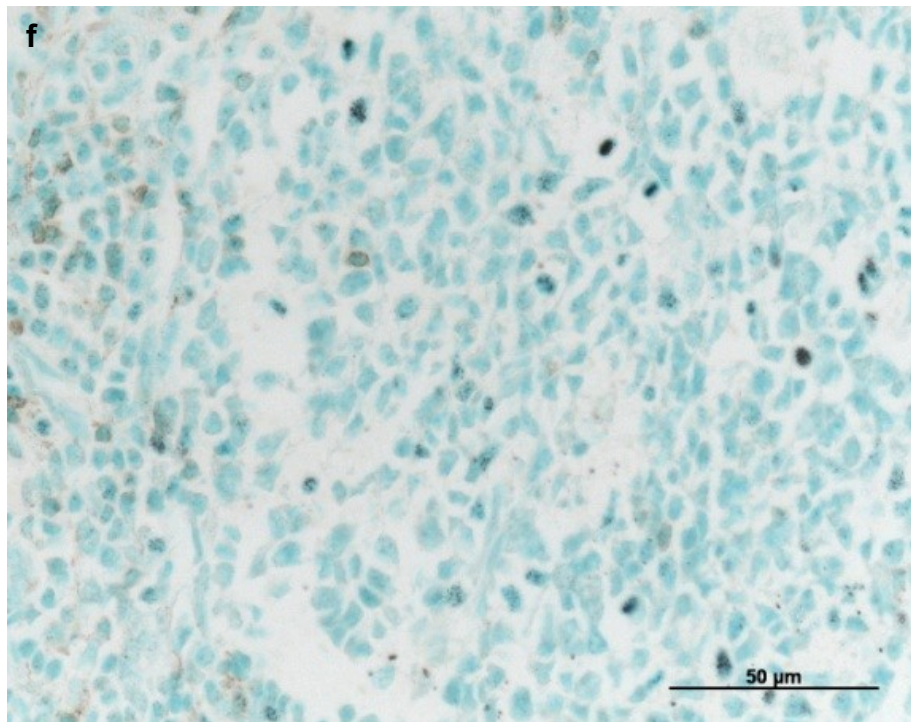
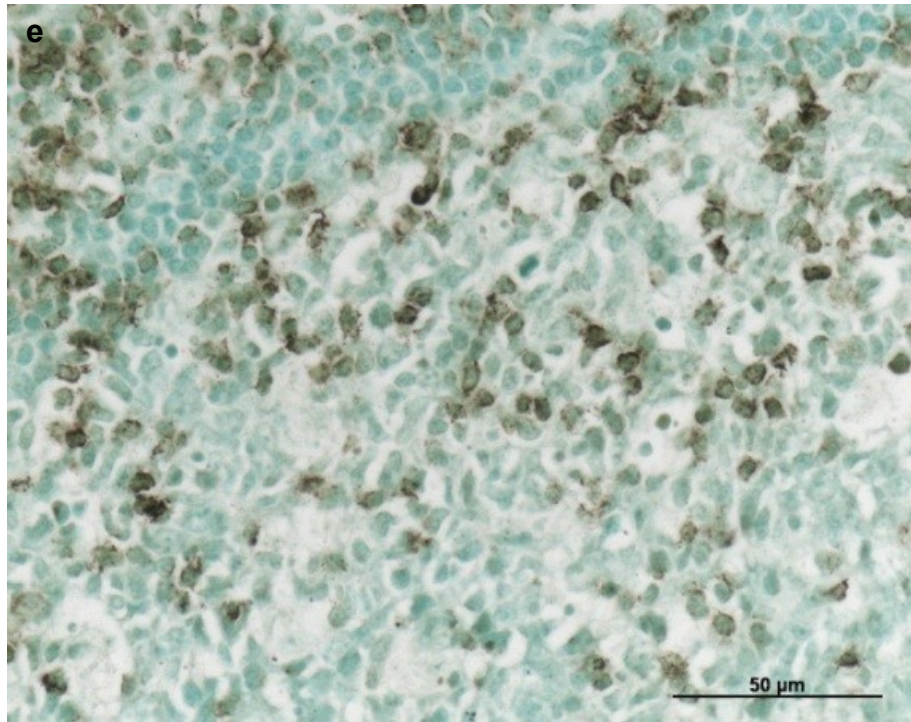


Figure 3.8 (continued). 4  $\mu\text{m}$  thick sections of paraffin wax-embedded human tonsil immunohistochemically stained for CD45Ro. Comparison of secondary antibody conjugates. Dako peroxidase conjugate with UCHL-1 at  $1/2,000$  (e) and  $1/5,000$  (f).

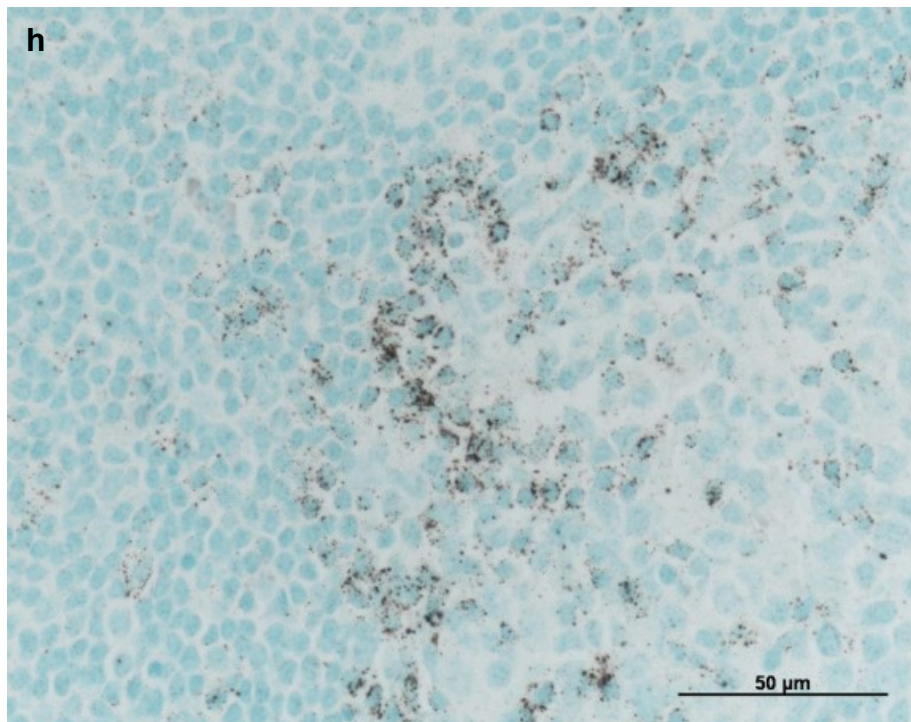
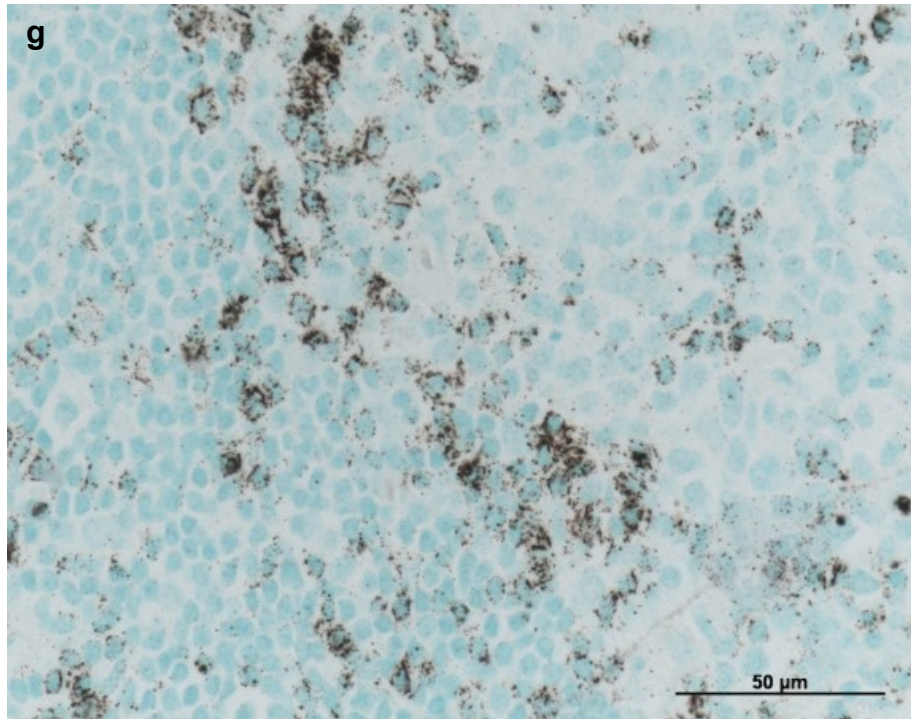


Figure 3.8 (continued). 4 μm thick sections of paraffin wax-embedded human tonsil immunohistochemically stained for CD45Ro. Comparison of secondary antibody conjugates. Dako Envision™ peroxidase conjugate with UCHL-1 at  $1/50,000$  (g) and  $1/100,000$  (h).



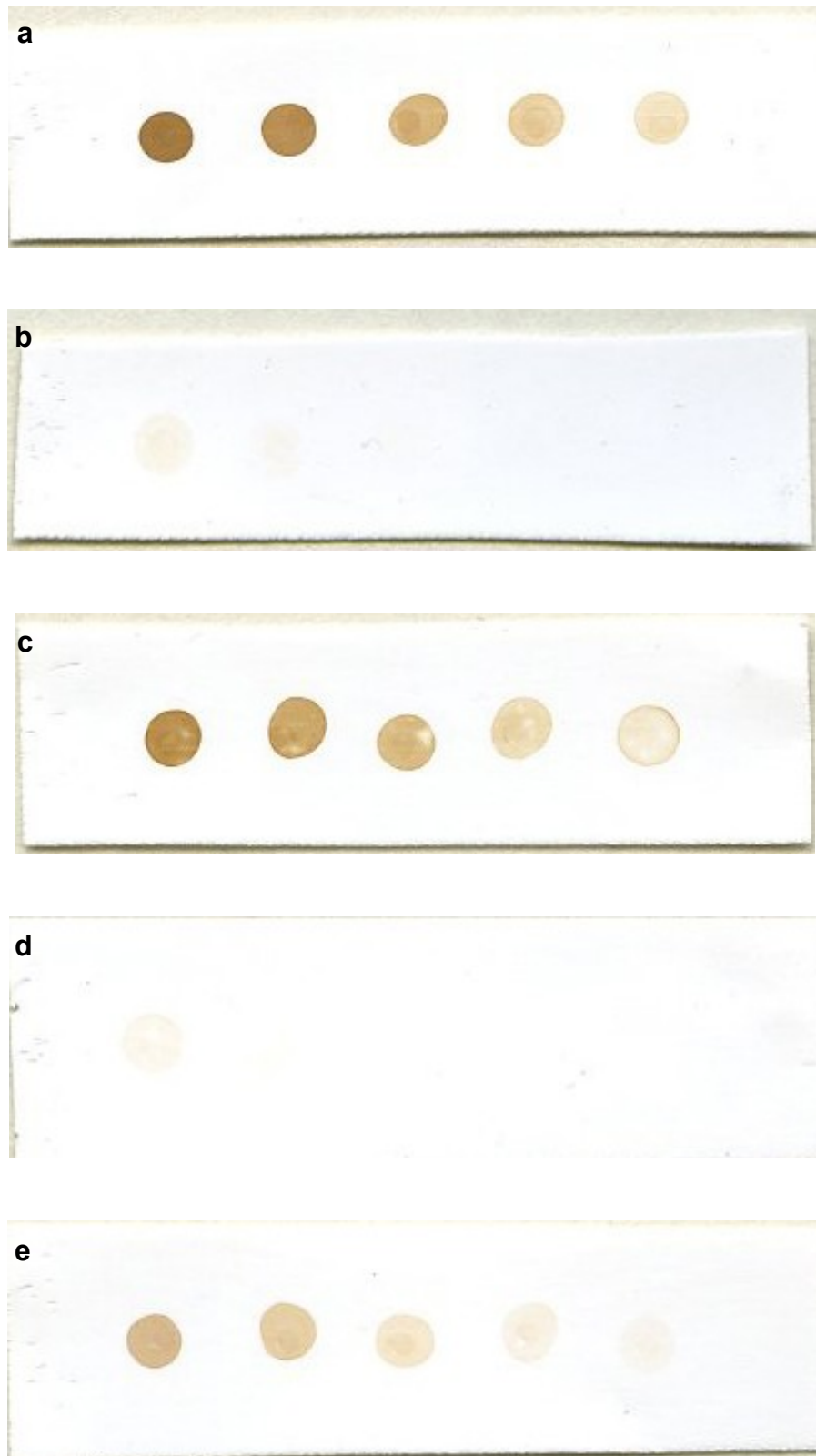


Figure 3.9. Dot blots of peroxidase conjugates logarithmically diluted from 1  $\mu\text{g}/\text{ml}$  to 1  $\text{ng}/\text{ml}$ . Santa Cruz (a and b), Dako (c and d) and Sigma (e).

### 3.5 Discussion

At the limits of immunohistochemical sensitivity, as defined in these studies by the colloidal gold/silver method, a number of factors became particularly important where the amplification of polyDAB was concerned, namely (1) the choice of endogenous peroxidase inhibitor, (2) the concentrations of amplifying reagents, (3) tissue argyrophilia, (4) the choice of physical developer, and (5) the choice of peroxidase conjugate.

None of the endogenous peroxidase inhibitors caused any obvious reduction in immunohistochemical sensitivity, but treatment of tissue sections with either phenylhydrazine or azide followed by gold/sulfide/silver resulted in an unexpected staining of vascular endothelium and the reason for the specificity of this reaction is unclear.

Reductions of the concentrations of both tetrachloraurate and sulfide lowered background staining such that immunohistochemical sensitivity was improved by one doubling dilution. A further improvement was observed when tissue argyrophilia was suppressed by metal-catalysed oxidation with La(III)/H<sub>2</sub>O<sub>2</sub>. The increase in development time, as noted by Gallyas (Gallyas and Wolff, 1986), permitted much smaller quantities of polyDAB to be seen, such that sensitivity was extended to  $1/50,000$  of the primary antibody, representing a five-fold improvement over the original technique.

Gallyas' developer might have been able to achieve the same level of amplification as Newman and Jasani's, had self-nucleation not been such a problem. Different preparations, made over the course of several years, have revealed Gallyas' developer to be somewhat capricious in this regard. The power of Danscher's developer, which has been specifically formulated for revealing the

presence of trace metals in tissue sections following their conversion to sulfides (Danscher, 1981a), was apparent when gross overstaining occurred after just 5 minutes. Examination of the sections revealed immunopositivity, and the subsequent removal of background staining by differentiation in potassium ferricyanide allowed it to be clearly seen. Greater control over development might be achieved by lowering the concentration of reducing agent. Hacker's developer in contrast, took over 40 minutes before background staining became problematic, and amplification was much weaker than either Danscher's or Newman and Jasani's. In all cases, no improvement in sensitivity was observed, suggesting that the limit of sensitivity of the particular secondary antibody conjugate had been reached.

The choice of technique for covalently coupling enzymes to antibodies can influence both enzyme activity and immunohistochemical sensitivity (Boorsma et al, 1976). In addition, the results indicated that the choice of commercial source can also dramatically affect the final immunohistochemical sensitivity, making comparisons between coupling methods difficult, if not impossible. Peroxidase conjugates from Santa Cruz and Sigma-Aldrich are both coupled by the periodate method, yet that of the former was five-fold more sensitive than the latter. Furthermore, Dako's conjugate is coupled by the glutaraldehyde method and might have been expected to perform better (Boorsma et al, 1976), but was the worst of all. It has been noted, however, that the periodate conjugation method, by linking larger numbers of enzyme molecules to the antibody, gives greater sensitivity at low antigen concentrations (Tsang et al, 1984). In contrast, Dako's Envision™ polymeric conjugate performed almost as well as colloidal gold. This improvement in sensitivity may, in part, reflect the greater quantity of polyDAB that the system deposits. The proprietary coupling method may also have contributed, but it seems

unlikely that this alone could account for an improvement of nearly two orders of magnitude. It is conceivable that the proximity of enzymes to the antibody that have been coupled by either the glutaraldehyde or periodate method, or proprietary variations, cause steric interference with the antibody-antigen interaction and this might not pertain in the case of the Envision™ system, where enzymes might be at some distance from the antibody. In principle, it is possible to evaluate the contribution of secondary antibody affinity to the final result by indirect methods, such as (1) detection of the secondary antibody conjugate by a tertiary anti-goat or anti-peroxidase colloidal gold conjugate or (2) adsorption of colloidal gold onto the peroxidase conjugates. Either system could then be visualised by silver development. Preparation of reagents for both techniques are expensive and time consuming, particularly the latter, and were not attempted.

Colloidal gold/silver remained the most sensitive system and may, in part, have reflected the nature of conjugation, namely adsorption onto the metal particles without any covalent modification. Under these conditions, the antibody is probably in its most native state and thus exhibited the greatest sensitivity. In addition, the initial marker is solid metal rather than a deposit composed mostly of organic polymer with complexed metal, and this may confer greater catalytic potency with regard to silver reduction.

### 3.6 Summary and Conclusions

At the limits of immunohistochemical sensitivity, the colloidal gold/silver system is the simplest method and outperforms all peroxidase/DAB amplification techniques. The high cost of colloidal gold conjugates and the need for silver development, however, have restricted its use to research laboratories.

Current marker amplification technology, while achieving up to a 10-fold improvement in sensitivity, is far too complicated to be routinely employed, and a more rationalised approach is required if the various problems are to be surmounted.

The rational design of novel marker systems that exploit current technologies can adopt two approaches, namely (1) novel enzyme substrates that do not result in the deposition of enzyme-inhibiting markers and/or (2) the development of directly amplifiable markers. The design of both would be aided by knowledge of the structure and co-ordination chemistry of polyDAB together with an understanding of the mechanistic chemistry underlying the marker amplification process, particularly the effects of sulfide on both the amount of metal sulfide formed/remaining and the final amount of silver reduced.

### 3.7 References

- AVRAMEAS, S. & URIEL, J. 1966. [Method of antigen and antibody labelling with enzymes and its immunodiffusion application]. *Comptes Rendus Hebdomadaires des Seances de l'Academie des Sciences - D: Sciences Naturelles*, 262, 2543-2545.
- BOORSMA, D. M., STREEFKERK, J. G. & KORS, N. 1976. Peroxidase and fluorescein isothiocyanate as antibody markers - quantitative comparison of 2 peroxidase conjugates prepared with glutaraldehyde or periodate and a fluorescein conjugate. *Journal of Histochemistry & Cytochemistry*, 24, 1017-1025.
- DANSCHER, G. 1981a. Histochemical demonstration of heavy metals - a revised version of the sulfide silver method suitable for both light and electron microscopy. *Histochemistry*, 71, 1-16.
- DANSCHER, G. 1981b. Localization of gold in biological tissue - a photochemical method for light and electron-microscopy. *Histochemistry*, 71, 81-88.
- DE BRUIJN, W., VAN DER MEULEN, C. J., BREDEROO, P. & DAES, W. T. 1986. Pt-staining of peroxidatic reaction products at the ultrastructural level. *Histochemistry*, 84, 492-500.
- GALLYAS, F. 1979a. Factors affecting the formation of metallic silver and the binding of silver ions by tissue components. *Histochemistry*, 64, 97-109.
- GALLYAS, F. 1979b. Kinetics of formation of metallic silver and binding of silver ions by tissue components. *Histochemistry*, 64, 87-96.
- GALLYAS, F. 1979c. Light insensitive physical developers. *Stain Technology*, 54, 173-175.
- GALLYAS, F. 1982a. Physico-chemical mechanism of the argyrophil I reaction. *Histochemistry*, 74, 393-407.
- GALLYAS, F. 1982b. Physico-chemical mechanism of the argyrophil III reaction. *Histochemistry*, 74, 409-421.

- GALLYAS, F. 2008. Physicochemical mechanisms of histological silver staining and their utilization for rendering individual silver methods selective and reliable. *Biotechnic & Histochemistry*, 83, 221-238.
- GALLYAS, F. & MERCHENTHALER, I. 1988. Copper-H<sub>2</sub>O<sub>2</sub> oxidation strikingly improves silver intensification of the nickel diaminobenzidine (Ni-DAB) end-product of the peroxidase reaction. *Journal of Histochemistry & Cytochemistry*, 36, 807-810.
- GALLYAS, F. & WOLFF, J. R. 1986. Metal-catalyzed oxidation renders silver intensification selective - applications for the histochemistry of diaminobenzidine and neurofibrillary changes. *Journal of Histochemistry & Cytochemistry*, 34, 1667-1672.
- HACKER, G. W., GRAF, A. H. & THURNER, J. 1990. Application of silver acetate autometallography in histopathology - a new detection method for use in immunogold-silver staining, lectin histochemistry and *in situ* hybridisation. *Pathology of the Hematopoietic Stem Cell : Quantative Pathology, Molecular Pathology: Pathologie Der Haematopoietischen Stammzelle : Quantative Pathologie, Molekularpathologie*, 74, 368-372.
- HAYAT, M. A. 1989. Colloidal gold Volume 1. Principles, methods and applications. Hayat, M. a. (Ed.). *Colloidal Gold, Vol. 1. Principles, Methods, and Applications. Xxvii+536p. Academic Press, Inc.: San Diego, California, USA; London, England, Uk. Illus.*
- JASANI, B., WYNFORD-THOMAS, D. THOMAS, N. D. & NEWMAN, G. R. 1986. Broad-spectrum nondeleterious inhibition of endogenous peroxidase - light and electron-microscope immunocytochemical application. *Histochemical Journal*, 18, 56-56.
- KELLY, S. 2010. *The Optimisation of Immunohistochemical Marker Amplification.* Bachelor of Science, University of Wales Institute, Cardiff.



- LI, C. Y., ZIESMER, S. C. & LAZCANOVILLAREAL, O. 1987. Use of azide and hydrogen peroxide as an inhibitor for endogenous peroxidase in the immunoperoxidase method. *Journal of Histochemistry & Cytochemistry*, 35, 1457-1460.
- LIU, G., AMIN, S. OKUHAMA, N. N. LIAO, G. & MINGLE, L. A. 2006). A quantitative evaluation of peroxidase inhibitors for tyramide signal amplification mediated cytochemistry and histochemistry. *Histochemistry and Cell Biology*, 126, 283-291.
- NAKANE, P. K. & KAWAOI, A. 1974. Peroxidase-labeled antibody. A new method of conjugation. *Journal of Histochemistry & Cytochemistry*, 22, 1084-1091.
- NEWMAN, G. R. & JASANI, B. 1998. Silver development in microscopy and bioanalysis: A new versatile formulation for modern needs. *Histochemical Journal*, 30, 635-645.
- NEWMAN, G. R., JASANI, B. & WILLIAMS, E. D. 1983. Metal compound intensification of the electron density of diaminobenzidine. *Journal of Histochemistry & Cytochemistry*, 31, 1430-1434.
- STRAUS, W. 1972. Phenylhydrazine as inhibitor of horseradish peroxidase for use in immunoperoxidase procedure. *Journal of Histochemistry & Cytochemistry*, 20, 949-951.
- STREEFKERK, J. G. 1972. Inhibition of erythrocyte pseudoperoxidase activity by treatment with hydrogen peroxide following methanol. *Journal of Histochemistry & Cytochemistry*, 20, 829-831.
- TSANG, V. C. W., HANCOCK, K. & MADDISON, S. E. 1984. Quantitative capacities of glutaraldehyde and sodium m-periodate coupled peroxidase-anti-human IgG conjugates in enzyme-linked immunoassays. *Journal of Immunological Methods*, 70, 91-100.

- VAN DUIJN, P. 1957. Histochemistry of DOPA factors.3. Inactivation experiments the DOPA factors in neutrophilic and eosinophilic leucocytes and erythrocytes. *Acta Physiologica Et Pharmacologica Neerlandica*, 5, 428-444.
- WYNFORD-THOMAS, D., JASANI, B. & NEWMAN, G. R. 1986. Immunohistochemical localisation of cell surface receptors using a novel method permitting simple, rapid and reliable LM/EM correlation. *Histochemical Journal*, 18, 387 - 396.

# **The Molecular Basis of Modern Marker Chemistry**

## **Part 2**

**By**

**Christopher J. von Ruhland M.Phil.**

**Submitted to the School of Chemistry, Cardiff University for the  
Degree of Doctor of Philosophy**

**October 2011**

# **Chapter 4**

## **Electron Microscopic Immunohistochemistry and Analytical Electron Microscopical Tomography**

## 4.1 Introduction

### *An Ultrastructural Sonnet*

In sombre beauty in her room she broods;  
Tis night-and all her pumps are deathly still,  
And thus she slumbers peacefully, until  
The morn, when unkind amperes end this interlude.

With steady beat her motors wheeze and keen,  
Industrious vapours drain the inner core,  
That Bohr's electrons shortly will explore,  
In headlong torrent downward to her screen.

What truths does she uncover with her beam?  
How much is artefact produced by man,  
And how much really fits into the plan  
Of nature? That believed is easily seen!

But even if she may promote confusion,  
It is at least an elegant illusion.  
(Yeomans, 1975)

The demonstration of antigens at the electron microscopic level has mainly relied on the capacity of the marker to scatter electrons. Early studies, focussing on techniques for use in the TEM, stained the primary antibody with electron opaque elements such as mercury (Pepe, 1961), uranium (Sternberger et al., 1963) and iodine (Mekler et al., 1964), or attached inherently electron opaque particles such as ferritin (Singer, 1959) or colloidal gold (Faulk and Taylor, 1971) to the antibody. The great advantage of the colloidal gold marker system is the ease with which particle size can be manipulated (Slot and Geuze, 1985), which has two distinct benefits, namely (1) particle size can be chosen to suit the magnification at which the specimen is to be examined and (2) multiple antigens can be demonstrated simultaneously by labelling each with a different sized particle.

The precision with which antigens can be localised is dependent upon the distance from the marker to the target. For the most commonly used reporter system, namely a primary antibody plus a secondary antibody conjugate, this can be as much as 30 nm (Huber et al., 1976; Murphy et al., 1988). Attempts to reduce

this value have employed antibody fragments in conjunction with very small gold particles to minimise steric hindrance (Hainfeld, 1987).

The analytical capabilities of the electron microscope have been exploited for detecting antibodies labelled with boron (Bendayan et al., 1989; Malecki et al., 2003) or recombinant antibody fragments hybridised with metal-binding domains (Malecki et al., 2002). In both cases, in-column and post-column electron energy filtering techniques were used, which require expensive instrumentation. Since a variety of techniques already exist for immunohistochemical staining of thin sections, which give comparable results and are far easier to perform, such esoteric procedures are rarely used.

The disadvantage of the most commonly employed IHC marker for TEM, colloidal gold, is that labelling efficiency is inversely proportional to particle size (Slot and Geuze, 1981). A further disadvantage is the inability of colloidal gold-labelled antibodies to penetrate tissue sections (Stierhof et al., 1986; Newman and Hobot, 1987; Stierhof and Schwarz, 1989,) which places constraints on sensitivity, since only antigens at the surface of the section can be detected, and also has important implications for the exploitation of electron tomography.

More recently, attention has been focussed on correlating dynamic events that are observed at the light microscopic level with the greater resolution afforded by the electron microscope in a technique that has come to be known as correlative light and electron microscopy (CLEM). Since many of these dynamic processes are observed by confocal microscopy, the use of tomographic systems at the electron microscopic level becomes a logical extension of this approach.

With the commercial availability of tomographic systems for TEMs, penetrable reporter-marker systems for electron microscopic IHC are clearly required to

advance this technology beyond simple morphological investigations and pre-embedding (immuno)histochemical techniques, since this will allow a greater range of histochemical techniques to be deployed for answering important biological questions.

There is evidence to suggest that enzyme conjugates might penetrate resin-embedded tissue sections to a limited extent (Newman and Hobot, 1987), although this remains controversial; perhaps not surprising given the size of antibody molecules (150 kD). Little, if anything, is known regarding the molecular weight cut-off of resins and tissues embedded therein.

#### **4.1.1 Electron Tomography**

3-dimensional reconstruction from 2-dimensional images of an object can be achieved in two ways; by stacking images of serial sections and by back projection from images taken from a number of different angles.

In light microscopy, the simplest method is to cut serial sections from a sample and reconstruct from images of each, but uncertainty exists regarding the exact thickness of the section after staining and mounting, particularly for paraffin wax-embedded tissue. Confocal microscopy avoids this problem by optically sectioning the sample.

In the electron microscope, reconstruction from serial sections is the simplest, albeit technically demanding, technique (Bruns and Palade, 1968) but mass loss from sections in the instrument is problematic (Aronova et al., 2010), again leading to uncertainties regarding exact specimen thickness. This problem has recently been addressed by using the SEM to image the surface of tissue blocks as serial layers are progressively removed by either ion beam ablation (De Winter et al., 2009) or by



inserting a modified ultramicrotome into the instrument (Denk and Horstmann, 2004). In both cases, however, the process is necessarily destructive.

Transmission electron microscopes often have stages that allow axial rotation, permitting a series of images from different angles to be acquired, and reconstruction by back projection performed. Early studies focussed on highly ordered structures such as viruses (De Rosier and Klug, 1968). The mathematical principles underlying the application of tomography in the electron microscope were subsequently described (Crowther et al., 1970), but it was not until the early 1980s that structures with irregular morphology were successfully reconstructed (Olins et al., 1983). Practical limitations of specimen holder design restrict the angle through which a sample can be rotated.

#### **4.1.2 Immunohistochemical Markers and Electron Opacity**

Since it is preferable to be able to observe immunohistochemical labelling prior to any analysis, marker electron opacity is desirable.

PolyDAB is slightly electron opaque (Newman et al., 1983) but benefits from treatment with d-block metal compounds. Osmium tetroxide has remained the preferred reagent since its early application (Graham and Karnovsky, 1966), probably due to its additional use as a secondary fixative in epoxy resin-embedding. Sodium gold chloride has a number of advantages over Os(VIII)O<sub>4</sub>, in that it binds to polyDAB in greater amounts (Siegesmund et al., 1979), improves immunohistochemical staining intensity in the electron microscope (Newman et al., 1983) and is more compatible with acrylic resin embedding (Wynford-Thomas et al., 1986). Alkaline phosphatase markers have exploited the production of insoluble metal phosphates following hydrolysis of phosphorylated enzyme substrates

(Hanker et al., 1964; Robinson and Karnovsky, 1983; Halbhuber et al., 1988). In electron microscopic immunohistochemistry, cerium appears to be the only metal that has been examined (Rowden and Dean, 1991).

#### **4.1.3 Analytical Instrumentation**

Two principle methods exist for determining elemental composition in the electron microscope; X-ray spectroscopy and electron energy loss spectroscopy. In X-ray spectroscopy, high energy beam electrons ionise atoms within the sample, sometimes by ejecting core shell electrons. Where this occurs, outer shell electrons fill the gap, emitting X-rays in the process. The energy of these transitions, and thus the energy of the resulting X-rays, is characteristic of the particular element. Such transitions can only occur in elements with atomic numbers higher than 2, but limitations imposed by instrument design usually restrict detectability to boron and above.

X-rays can be analysed in two ways; energy dispersion and wavelength dispersion. In energy dispersive spectrometers (EDS or EDX), the charge resulting from ionisation of the detector material (Si(Li), Ge(Li) or Si) is proportional to the energy of the incident X-ray photon. Detection and analysis are thus a single event and multiple elements can be detected simultaneously, but this is at the expense of both energy resolution (and thus analytical precision) and sensitivity. Wavelength dispersive spectrometers (WDS or WDX) separate element-specific X-rays by diffracting them through a specifically selected crystal. Energy resolution and sensitivity (particularly for light elements) are improved by an order of magnitude, but the range of elements that can be simultaneously detected is restricted to 5 per

spectrometer. EDX systems cost approximately £25k, whereas WDX systems are usually twice this price.

Electron energy loss analyses the energies of electrons that have been inelastically scattered by the sample. This can be achieved in two ways; energy loss spectroscopy and energy filtering. Electron energy loss spectroscopy (EELS) utilises a post-column magnetic prism to separate electrons of different energies. It is particularly sensitive for the analysis of light elements (carbon through to the 3d transition elements) and can easily distinguish between allotropes of carbon and oxidation states of 3d elements (Keast et al., 2001). Energy filtering (EF) utilises an in-column Ottensmeyer lens to select/exclude electrons of particular energies for subsequent image acquisition (Ottensmeyer, 1986). In both cases, analytical resolution is limited by the energy spread of the primary electron beam and the requirement to keep interactions to single events, thus restricting sample thickness. In addition, instrumentation is very expensive (e.g. £350k for an entry level EELS system, £1M for an energy-filtered TEM).

Not surprisingly, EDX systems are the most commonly encountered analytical instruments on both SEMs and TEMs and it is with these in mind that the development of novel markers for analytical tomography should be directed.

#### **4.1.4 Analytical Electron Microscopical Tomography**

A limited number of studies have demonstrated the practicality of analytical electron microscopical tomography (AEMT) including the three-dimensional distribution of magnetite in bacteria (Midgley and Weyland, 2003), phosphorus in nematode cells (Leapman et al., 2004) and *Drosophila* larvae (Aronova et al., 2007), and of phosphorus and nitrogen in the nuclei of fibroblasts (Bazett-Jones et al.,

1999) and thymocytes (Aronova et al., 2010). All these, however, have used energy filtering techniques to achieve the highest spatial resolution. Such technologies are expensive and restrict the applicability of this form of AEMT to a few laboratories. In the case of immunohistochemistry, spatial resolution is less of an issue for the reasons given above. Furthermore, subcellular localisation, rather than molecular resolution is all that is often required. Consequently, AEMT may be possible with relatively low cost TEM technology, namely a TEM with beam control and an EDX detector, thus broadening its availability. Development of markers for AEMT entails some important considerations.

#### **4.1.5 Elemental Mapping**

Elemental mapping involves the movement of a focussed electron beam across the specimen in a raster and the collection and analysis of characteristic X-rays. The resulting elemental maps correspond to, and can be overlaid upon, the original image.

The spatial resolution of the analytical image is dictated, primarily, by the minimum size to which the electron beam can be focussed i.e., the spot size. This, in turn, is dictated by the choice of electron source. Tungsten filaments, by far the cheapest and most commonly encountered electron source in the TEM can achieve a spot size of 40 nm whereas LaB<sub>6</sub> produce probes of approximately 5 nm. Field emission guns can produce probes below 0.2 nm (Williams and Carter, 1996).

A further consideration is the image resolution of the elemental map and its consequences upon acquisition time. By way of illustration, figure 4.1 shows the influence of image resolution on image quality. Compared to the original 300 x 300 pixel image (figure 4.1a), figure 4.1b, with an image resolution of 256 x 256 pixels

is, as might be expected, of comparable quality. In the setting of AEMT, with an arbitrary beam dwell time of 1 second per pixel and a single axis tilt series at 1° intervals over +/- 70°, an analytical image of such quality would take 214 days to acquire. The analytical image resolution can be reduced to 128 x 128, which maintains acceptable image quality (figure 4.1c), and the number of images in the tilt series can be lowered (since all that is required is marker identification) but whilst retaining the 1 second dwell time, acquisition time is still unacceptably long (5.5 days).

The only parameter that can now be altered is the dwell time per pixel, since image quality is unacceptably low when reduced to 64 x 64 pixels (figure 4.1d). This can be achieved by either increasing the brightness of the beam, i.e. switching to a LaB<sub>6</sub> or field emission gun (Williams and Carter, 1996, Goldstein et al., 2003), and/or increasing the concentration of specific element in the final marker.

Since PolyDAB could be rendered electron opaque by various d-block metals these might be present in sufficient concentrations to permit AEMT in an acceptable time frame.

#### **4.1.6 Choice of Section Substrate**

In section 2.4.2.3, X-ray spectra of PVDF membrane contained, as expected, a prominent fluorine peak at 0.6768 KeV (Goldstein et al., 2003). While this would not have interfered with the d-block elements under study, the choice of a suitable section support substrate for preliminary scanning electron microscopy should not, ideally, be composed of elements whose X-ray emission spectra contain peaks that

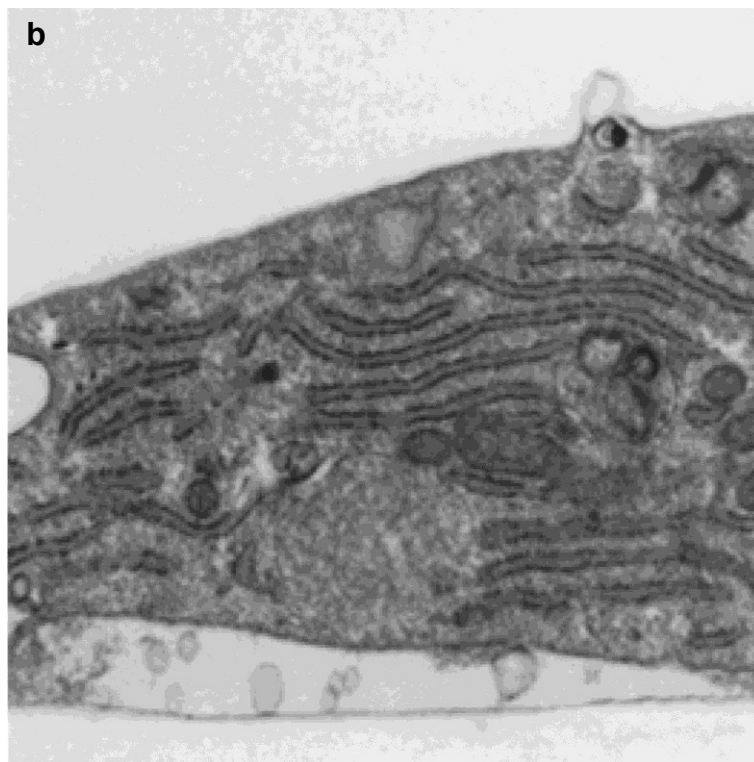
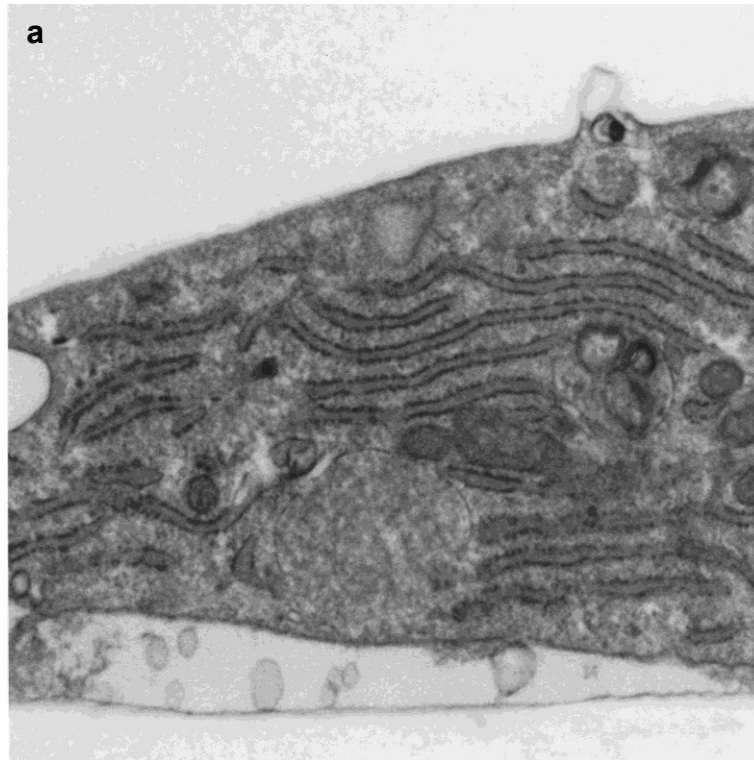


Figure 4.1. Electron micrograph of an 80 nm thick transverse section of an epoxy resin-embedded cultured cell showing the effects of image resolution on image quality. Standard 300 pixel image (a), 256 x 256 pixels (b).

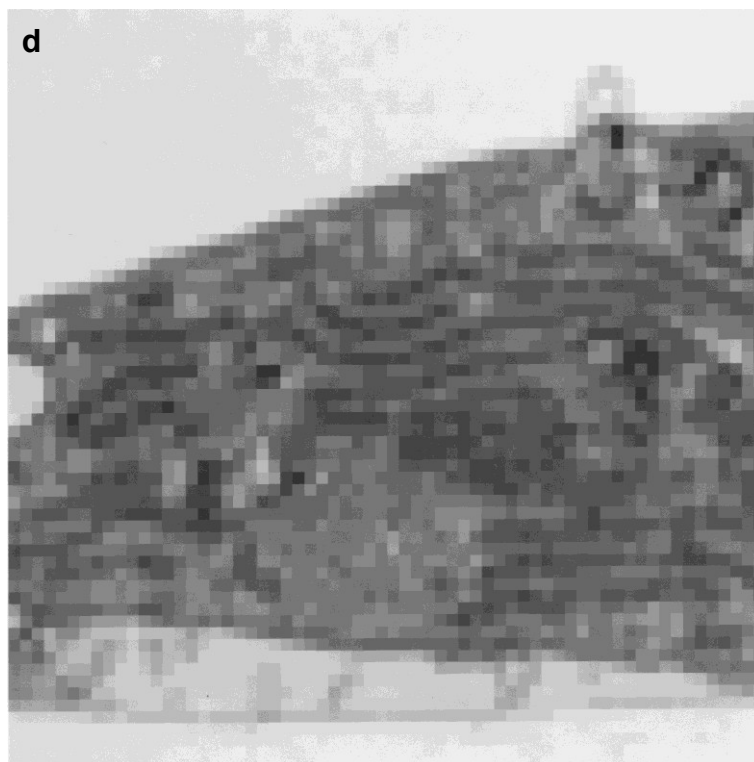
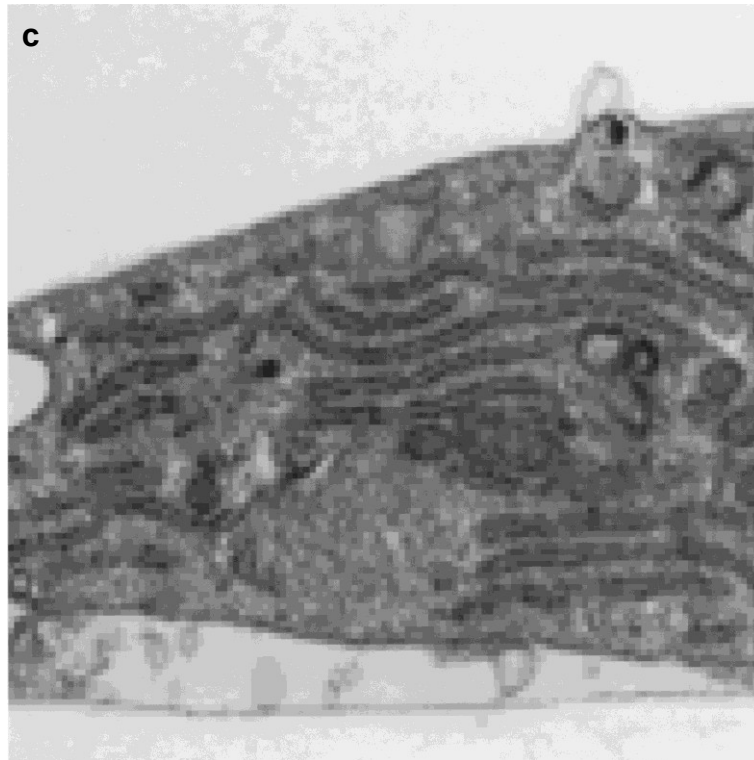


Figure 4.1 (continued). Electron micrograph of an 80 nm thick transverse section of an epoxy resin-embedded cultured cell showing the effects of image resolution on image quality. 128 x 128 pixels (c) and 64 x 64 pixels (d).



might mask, or be confused with peaks of the element under examination. The choice is further constrained by the requirement for adherence of tissue sections and compatibility with rehydration and staining reagents.

#### **4.1.7 Tissue Model Systems**

The development of any novel immunohistochemical staining technique should initially seek to demonstrate an antigen that is present in abundance. At the light microscopic and scanning electron microscopic levels, smooth muscle actin (SMA) provides a suitable target. As the name suggests, SMA is present in (involuntary) smooth muscle, such as the wall of the gut. In addition, it is present in the contractile cells of blood vessels, and thus almost ubiquitous in mammalian tissue.

At the transmission electron microscopic level, exocrine and endocrine granules provide clearly identifiable and discrete structures that contain abundant levels of demonstrable antigen, such as  $\alpha$ -amylase and trypsin in the exocrine granules of the pancreas (Bendayan and Ito, 1979), and various hormones in the endocrine granules of the pituitary (Mirecka and Pearse, 1971; Naik, 1973; Martincomin and Robyn, 1976).

## **4.2 Materials**

### **4.2.1 Reagents**

All reagents and suppliers are listed in section 2.2.1.

### **4.2.2 Model Systems**

Vectabond-treated glass microscope slides were prepared according to section 2.2.5 of Chapter 2. Thermanox™ coverslips were supplied by Nalge Nunc International (Rochester, New York). Nescofilm™ was purchased from Bando Chemical Industries Ltd (Kobe, Japan). Archival normal human peritoneum, fixed for 24 hours in 4% formaldehyde + 0.2% glutaraldehyde in 100 mM Sorensen's phosphate buffer pH 7.4 + 2% sucrose (SPB) and stored at 4°C in SPB was supplied by the Peritoneal Biopsy Study Group. Archival rat pancreas and pituitary, perfusion-fixed with 1% glutaraldehyde and stored at 4°C in 100 mM sodium phosphate buffer pH 7.4, were supplied by Dr. Jan Hobot, Medical Microscopy Sciences, Cardiff University.

### **4.2.3 Antibodies**

Mouse monoclonal anti- $\alpha$ -amylase, anti-adrenocorticotrophic hormone (ACTH), and goat anti-mouse IgG peroxidase conjugate were supplied by Autogen Bioclear (Calne, Wiltshire, U.K.). Mouse monoclonal anti-smooth muscle actin was supplied by Dako (Ely, Cambridgeshire, U.K.).

## **4.3 Methods**

### **4.3.1 Choice of Section Substrate**

Vectabond-treated glass microscope slides and Thermanox™ coverslips were carbon-coated and examined in a JEOL 840A analytical SEM as in section 2.3.3.5. Thermanox coverslips were subsequently selected for use as support substrates for tissue sections.

### **4.3.2 Tissue Model Systems**

#### **4.3.2.1 Preparation of Paraffin Wax-embedded Sections for Preliminary Immunoelectron Microscopy**

Peritoneum was embedded in paraffin wax and sectioned according to section 2.3.4.1 of Chapter 2.

#### **4.3.2.2 Preparation of Acrylic Resin-embedded Sections for Immunoelectron Microscopy**

##### **4.3.2.2.1 Resin Embedding**

Dehydration and resin infiltration were performed at RT on a rotary mixer. 5 x 1 x 1 mm samples were post-fixed for 2 hours in 2% aqueous uranyl acetate, washed for 3 x 10 minutes in ddH<sub>2</sub>O and partially dehydrated through graded ethanol (50% for 10 minutes and 2 x 70% for 10 minutes), infiltrated with LR White acrylic resin (2:1 LR White:70% ethanol for 30 minutes and neat resin for 4 x 20 minutes). Samples were placed into size O gelatine capsules containing 0.64 ml LR White resin + 1.5 µl/ml LR White accelerator in a pre-cooled (0°C) aluminium heat sink and transferred to a 4°C refrigerator to polymerise overnight. Samples were further polymerised at 50°C for 2 hours.

#### 4.3.2.2.2 Microtomy and Ultramicrotomy

Following removal of the gelatine capsule, surplus resin was removed from around the samples (blocks) with a fine coping saw and the faces of the blocks trimmed to trapeziums with a glass knife (prepared with an LKB knife maker (LKB Produkter AB, Bromma, Sweden)). Preliminary 0.35  $\mu\text{m}$  thick sections were cut on an Ultracut E ultramicrotome (Reichert-Jung, Wien, Austria) with a glass knife fitted with a plastic boat and filled with 0.2  $\mu\text{m}$  filtered ddH<sub>2</sub>O. Sections were picked up over the tip of dumoxel number 5 forceps (Dumont, Montignez, Switzerland), placed onto a droplet of water on a glass slide, dried at 60°C on a hot plate and stained for 10 seconds with 0.5% toluidine blue in tetraborate buffer. Following thorough washing with ddH<sub>2</sub>O, the slide was dried on the hot plate and the sections mounted with Gurr's neutral mountant and coverslipped for light microscopical identification of suitable areas for subsequent immunohistochemical staining. For scanning electron microscopy, areas containing blood vessels in sections of normal human peritoneum were identified, the block trimmed down, and 0.35  $\mu\text{m}$  thick sections placed onto droplets of water on 5 mm diameter Thermanox™ coverslip discs and dried at 50°C for 60 minutes. For transmission electron microscopy, exocrine granule-rich areas of pancreas were identified and 80nm thick sections cut and picked up on pre-washed (5 seconds each in acetone, ethanol and 0.2  $\mu\text{m}$  filtered ddH<sub>2</sub>O) 300 mesh nickel grids and allowed to air dry.

To examine the feasibility of immunoelectron tomography, endocrine granule-rich areas of pituitary were identified and 1  $\mu\text{m}$  thick sections collected as above.

#### 4.3.2.3 Immunohistochemical Staining

All immunohistochemical stainings were performed in humidified chambers. For scanning electron microscopy, solutions were applied/removed as droplets directly onto/from the sections with a pipette.

For transmission electron microscopy, grids were transferred through 50  $\mu$ l droplets of solutions on Nescofilm™.

Sections were equilibrated with PBS/BSA for 10 minutes followed by 60 minutes incubation in either mouse monoclonal anti-smooth muscle actin diluted  $1/1000$  in PBS/BSA (for staining of blood vessels in peritoneal sections) or mouse monoclonal anti-amylase diluted  $1/10,000$  in PBS/BSA (for staining of exocrine granules in pancreas sections). Following 3 x 1 minute washes in PBS/BSA, sections were incubated for a further 60 minutes in goat anti-mouse Ig HRP. Sections were washed for 1 minute in PBS/BSA and 2 x 1 minute in either  $\text{PO}_4$  buffer or Tris buffer, as appropriate to the subsequent DAB polymerisation conditions. For SEM, DAB was polymerised in an identical manner for the preparation of dot blots in section 2.3.3 of Chapter 2. Those DAB-metal combinations that resulted in specific immunohistochemical labelling, as seen by BSI were subsequently tested on thin resin sections for TEM.

For electron tomography, staining was performed on rat pituitary sections as above, except that incubation times were extended to 3 hours in  $1/800$  anti-ACTH followed by 3 x 5 minute washes and a further 3 hours in the peroxidase conjugate. Following 3 x 5 minutes washes in  $\text{ddH}_2\text{O}$ , sections were incubated in DAB- $\text{PO}_4$  as above, and polyDAB rendered electron opaque with 2.5 mM  $\text{NaAu(III)Cl}_4$ .

### **4.3.3 Scanning Electron Microscopy**

All preparations were examined in a JEOL 840A analytical scanning electron microscope as in section 2.3.3.5 of Chapter 2 under the following conditions

Accelerating voltage: 20kV Probe current:  $10^{-8}$  amps Magnification x 200

Working distance: 15 mm. Acquisition time 3 hours

### **4.3.4 Analytical Transmission Electron Microscopy**

Thin resin sections were examined in a Philips CM12 transmission electron microscope at 80kV. X-ray spectra were acquired from a 600 nm spot, focused on an exocrine granule, using an EDAX Sapphire X-ray spectrometer and Genesis software (Mahwah, New Jersey, U.S.A.).

### **4.3.5 Electron Tomography**

Sections were examined in a JEOL 2100 tomographic electron microscope at the Rothamsted Research Laboratories, Hertfordshire, U.K. A  $\pm 50^\circ$  tilt series was collected at 200 kV. Image alignment was performed by Dr. Andy Yarwood of JEOL UK Ltd (Welwyn Gardens City, Herts., U.K.). Red-green anaglyphs of serial tilt images were produced with Adobe Photoshop (Adobe Systems Incorporated, San Jose, California, U.S.A.).

## **4.4 Results**

### **4.4.1 Choice of Section Substrate**

Vectabond-treated glass microscope slide contained, in addition to the expected major components of silicon and oxygen, detectable quantities of sodium, magnesium, potassium, calcium and aluminium (figure 4.2a). In contrast, Thermanox™ coverslips contained only carbon and oxygen (figure 4.2b).

### **4.4.2 Scanning Electron Microscopy**

#### **4.4.2.1 Preliminary Studies in Paraffin Wax-embedded Sections**

Immunohistochemical staining of smooth muscle actin in the wall of peritoneal blood vessels could be clearly seen by back-scattered electron imaging, as could the surrounding collagen (figure 4.3a). Elemental mapping revealed the presence of gold both in the smooth muscle cells of the blood vessel wall and in the surrounding collagen fibres (figure 4.3b).



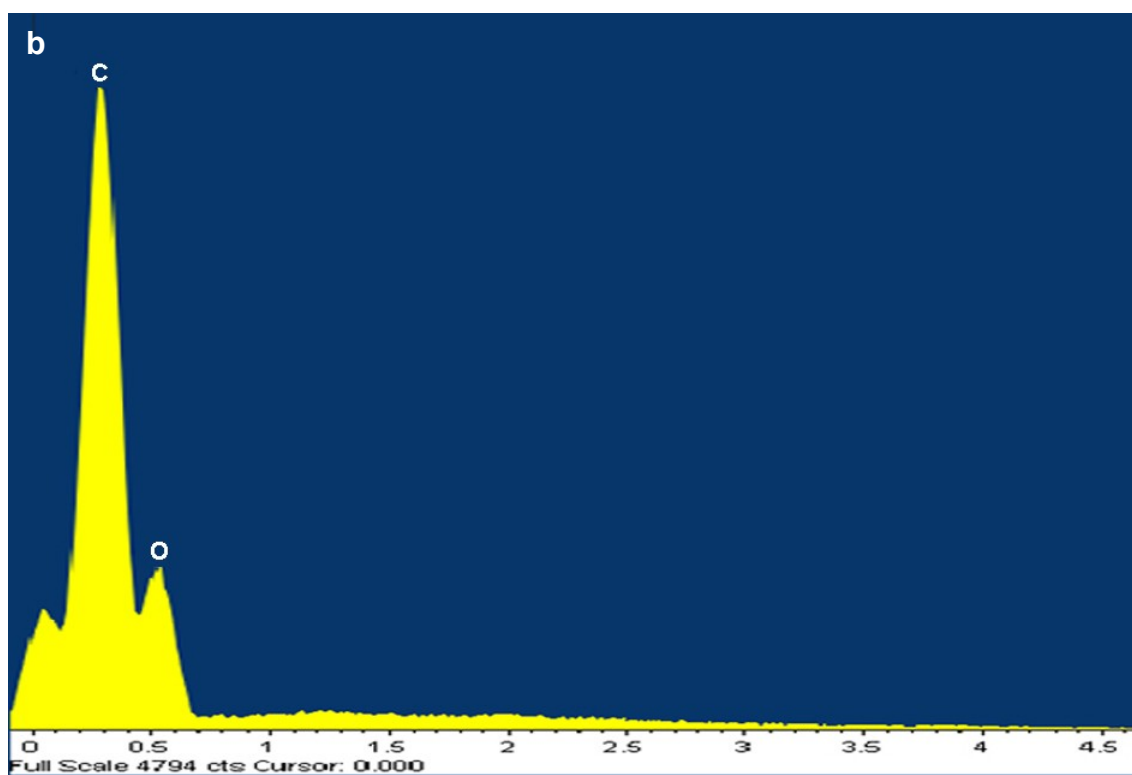
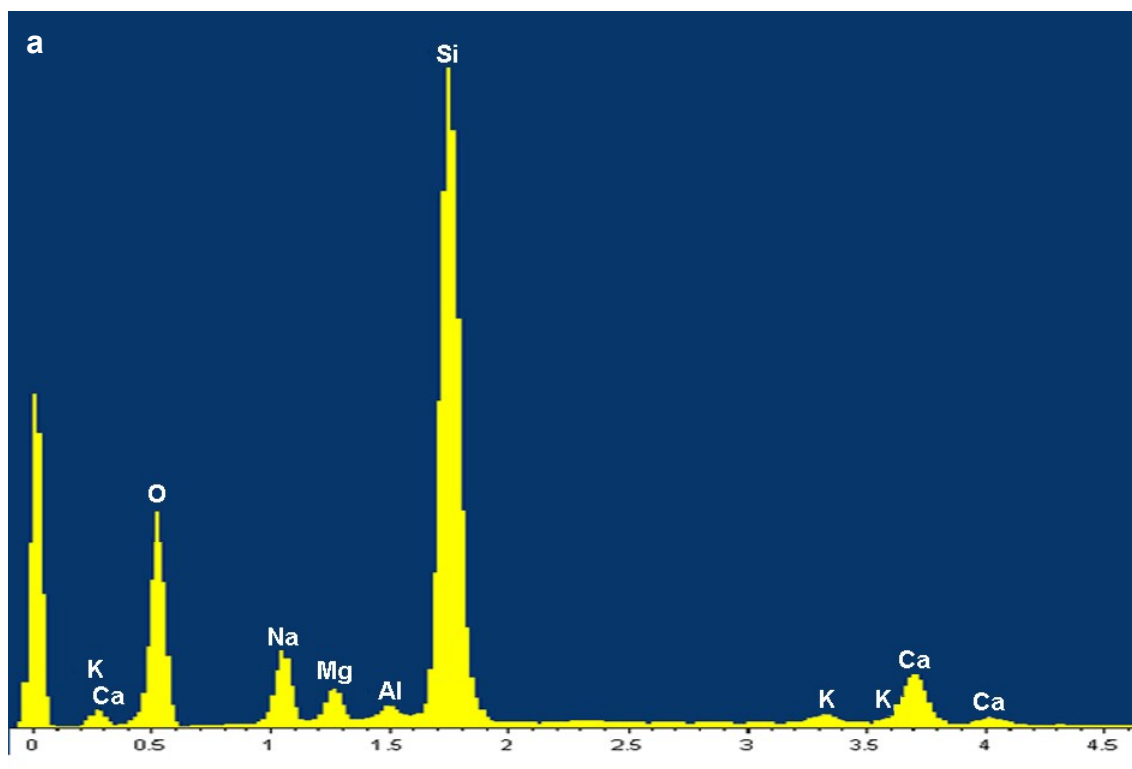


Figure 4.2. X-ray spectra of glass slide (a) and Thermanox coverslips (b)

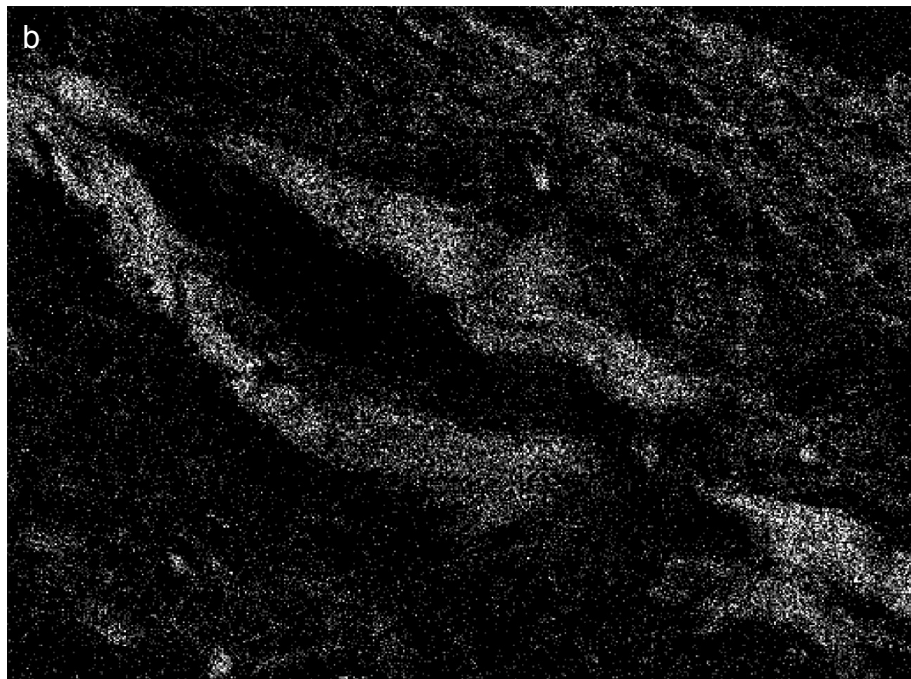
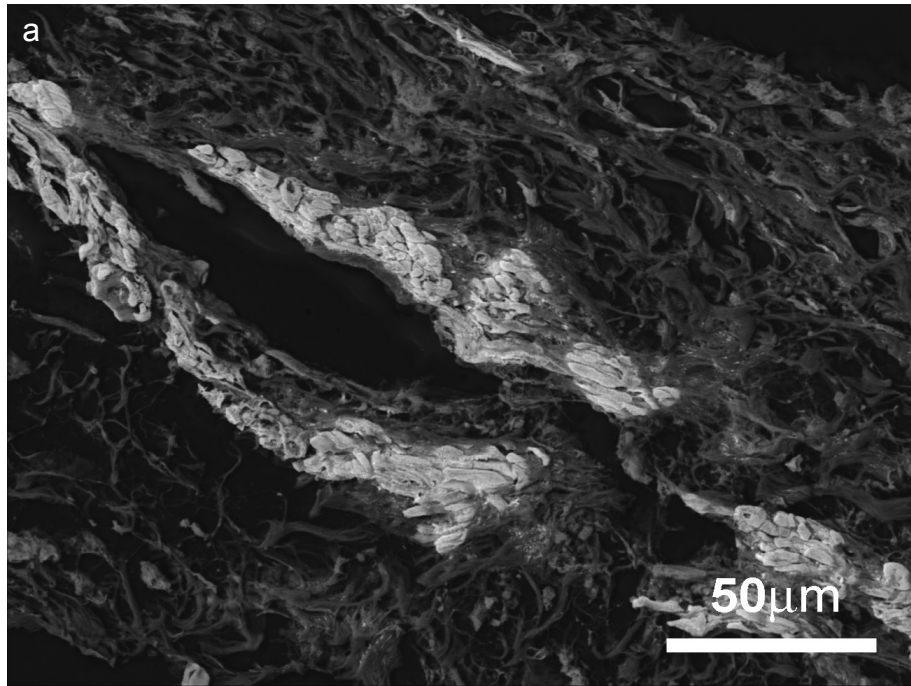


Figure 4.3. Back-scattered electron image (a) and corresponding gold elemental map (b) of a 4  $\mu\text{m}$  thick section of paraffin wax-embedded peritoneal blood vessel immunohistochemically stained for smooth muscle actin and visualised with DAB/NaAu(III)Cl<sub>4</sub>.

#### 4.4.2.2 Resin Sections

Back-scattered electron imaging provided a simple and rapid method for identifying immunopositive staining that contained elements of higher atomic number than the background tissue and resin. In addition, it allowed non-specific staining of tissue to be identified.

Of the 31 d-block metal compounds tested in pre- and post-polymerisation settings, only 8 resulted in specific complexing with polyDAB such that high back-scattered imaging contrast occurred between immunopositive sites and the surrounding tissue, namely; pre-polymerisation with DAB-Tris plus  $\text{Re(III)Cl}_3$  (figure 4.4.a),  $\text{K}_3\text{Ir(III)Cl}_6$  or  $\text{K}_2\text{Pt(IV)Cl}_6$  and DAB- $\text{PO}_4$  plus  $\text{K}_2\text{Pt(IV)Cl}_6$  (figure 4.4.b), and post-polymerisation with  $\text{NaW(VI)O}_4$ ,  $\text{K}_2\text{Os(IV)Cl}_6$  (figure 4.3.c),  $\text{Os(VIII)O}_4$  (figure 4.3.d),  $\text{K}_3\text{Ir(III)Cl}_6$  (slight) (figure 4.4.e),  $\text{K}_2\text{Pt(II)Cl}_4$ ,  $\text{K}_2\text{Pt(IV)Cl}_6$  and  $\text{NaAu(III)Cl}_4$  (figure 4.4.f). Post-polymerisation treatment with  $\text{La(III)Cl}_3$  resulted in light staining of the tissue and strong staining of elastic fibres within the blood vessel walls and between the collagen fibres of the peritoneal membrane (figure 4.4.g).  $\text{H}_3\text{PW(IV)}_{12}\text{O}_{40}$  stained all the tissue with no obviously increased staining of polyDAB (figure 4.4.h).

Elemental mapping was not performed, as resin sections suffered from considerable beam damage during prolonged exposure, which was noted during attempts to acquire high quality images with the instrument in slow scanning mode.

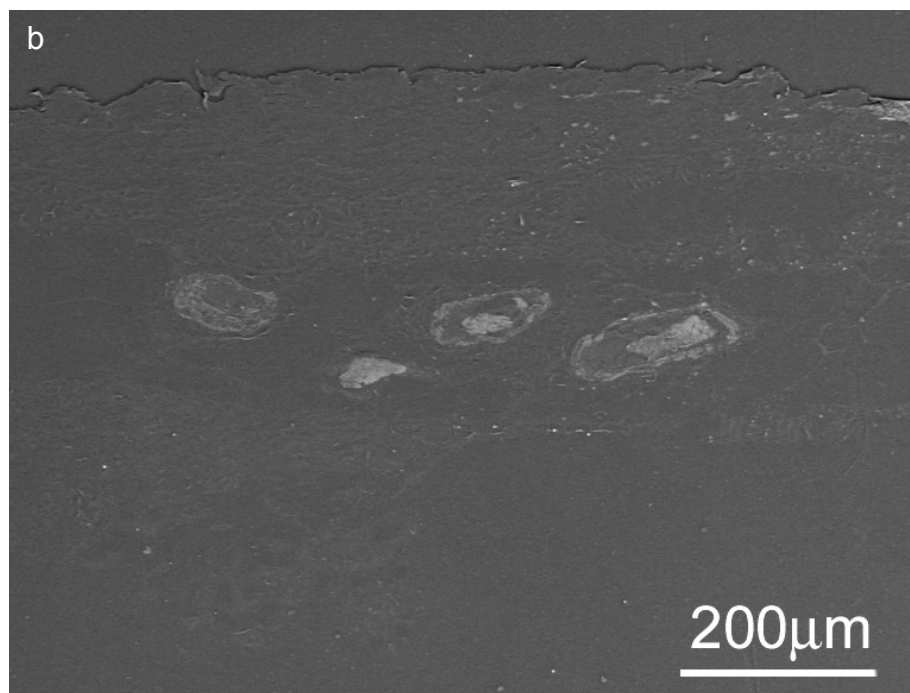
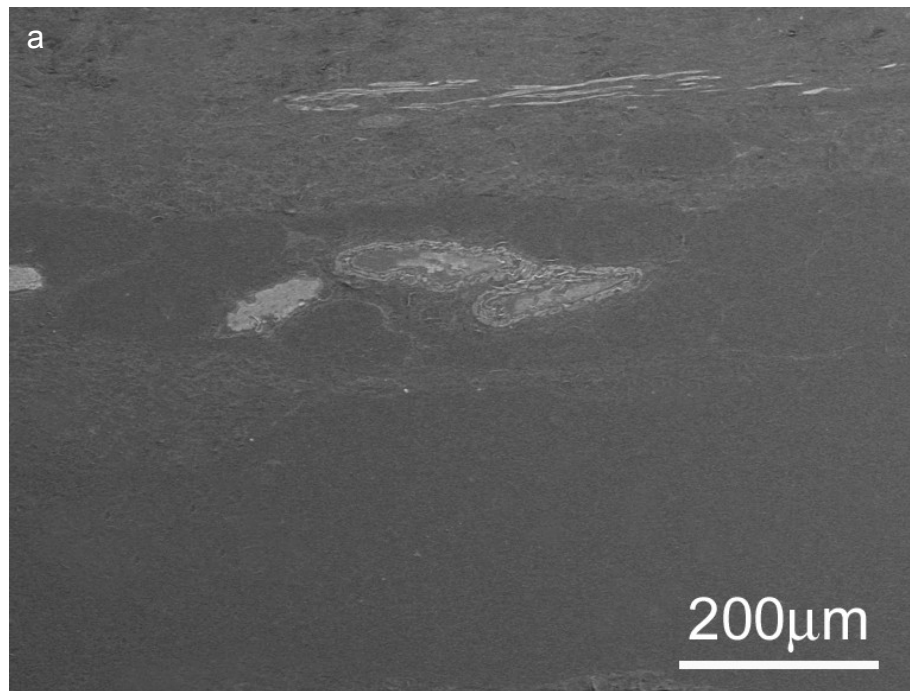


Figure 4.4. Back-scattered electron micrographs of 0.35  $\mu\text{m}$  thick LR White-embedded human peritoneum sections immunohistochemically stained for smooth muscle actin. Pre-polymerisation with  $\text{Re(III)Cl}_3$  (a) and  $\text{K}_2\text{Pt(IV)Cl}_6$  (b).

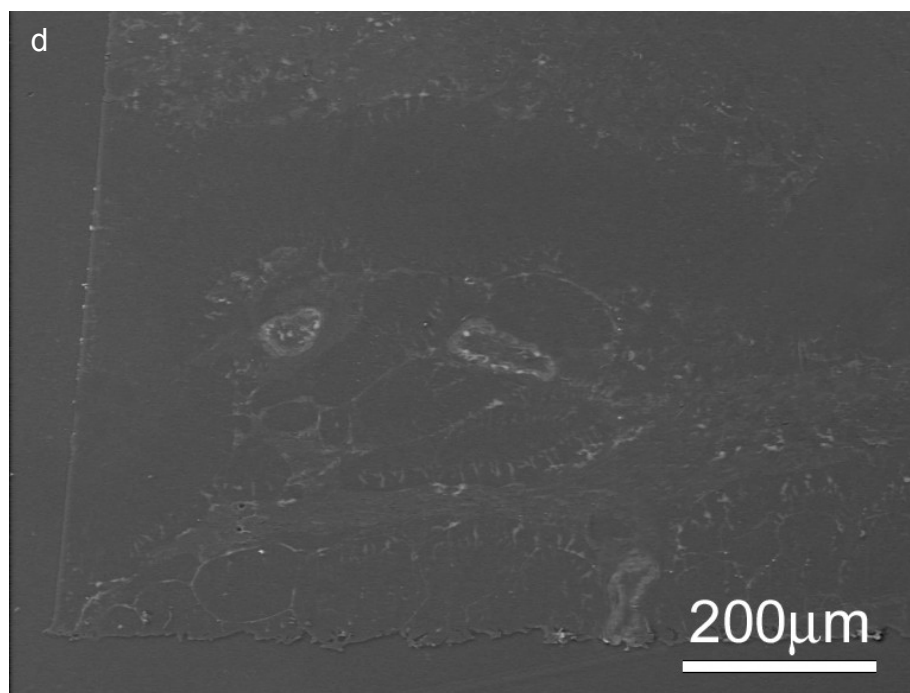
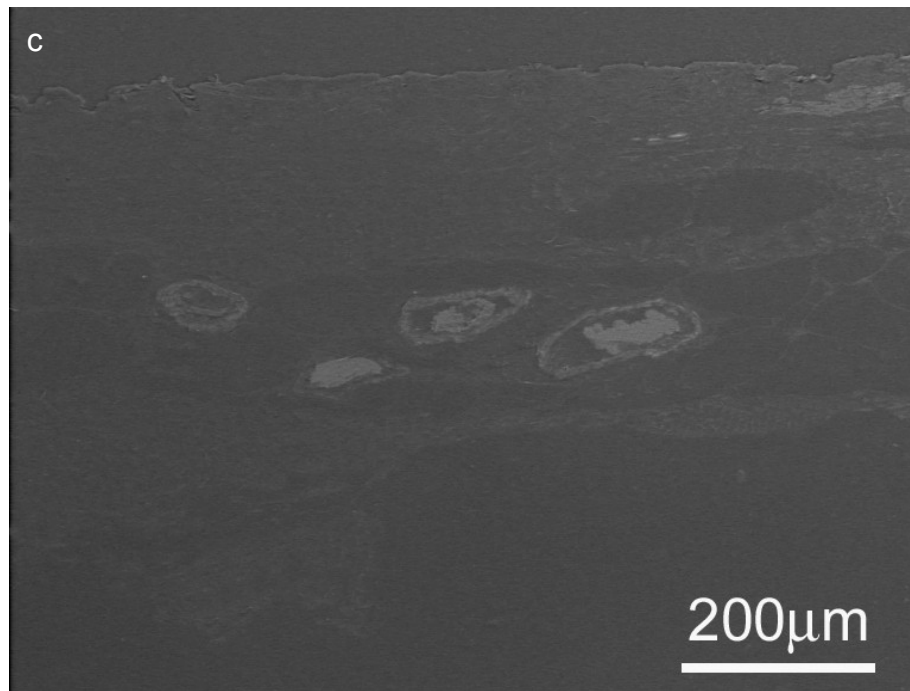


Figure 4.4 (continued). Back-scattered electron micrographs of 0.35  $\mu m$  thick LR White-embedded human peritoneum sections immunohistochemically stained for smooth muscle actin. Post-polymerisation with  $K_2Os(IV)Cl_6$  (c) and  $Os(VIII)O_4$  (d).

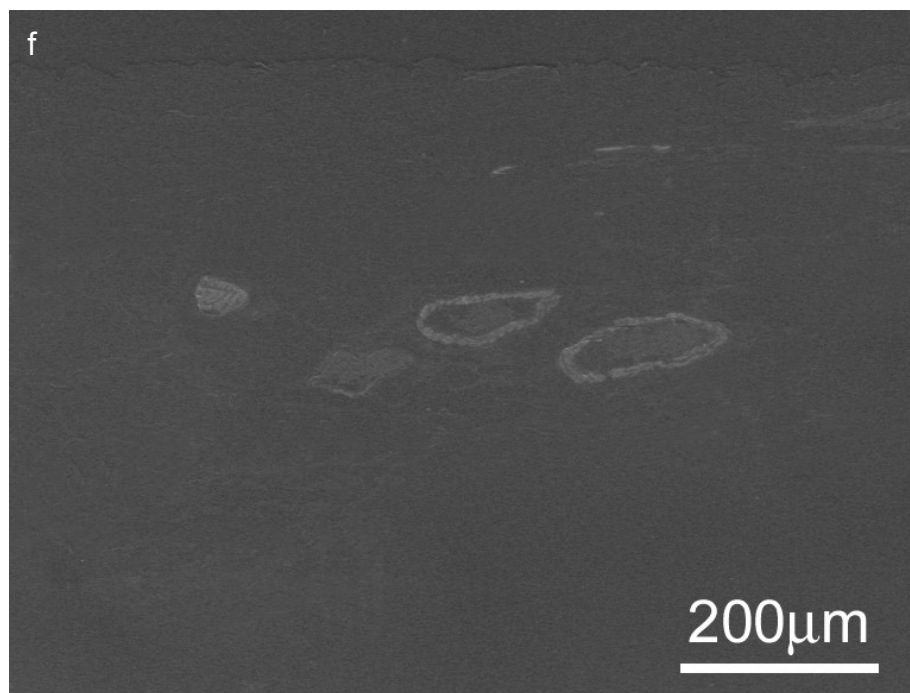
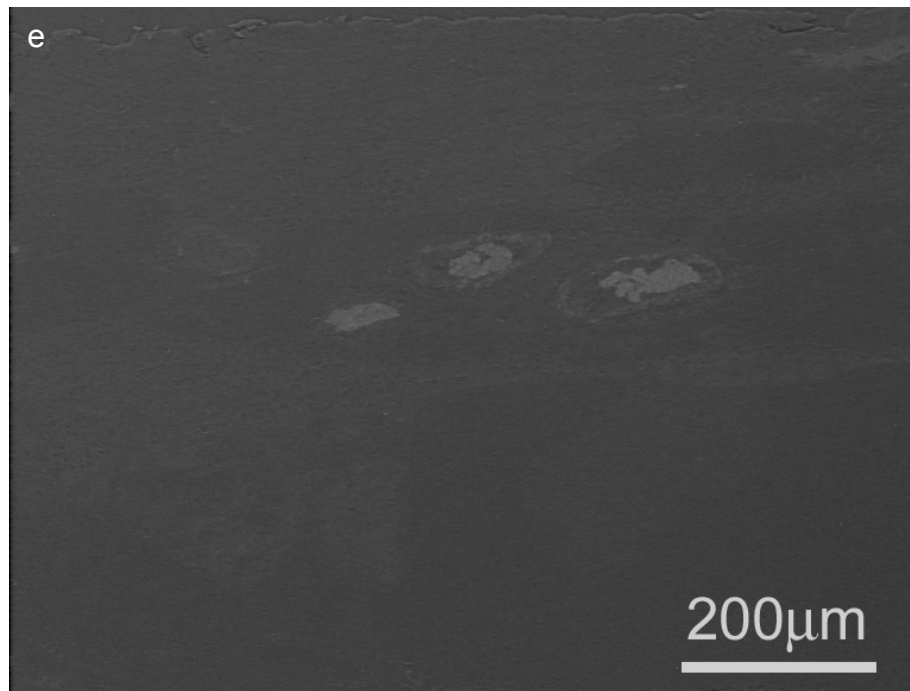


Figure 4.4 (continued). Back-scattered electron micrographs of 0.35  $\mu\text{m}$  thick LR White-embedded human peritoneum sections immunohistochemically stained for smooth muscle actin. Post-polymerisation with  $\text{K}_3\text{Ir(III)Cl}_6$  (e) and  $\text{NaAu(III)Cl}_4$  (f).

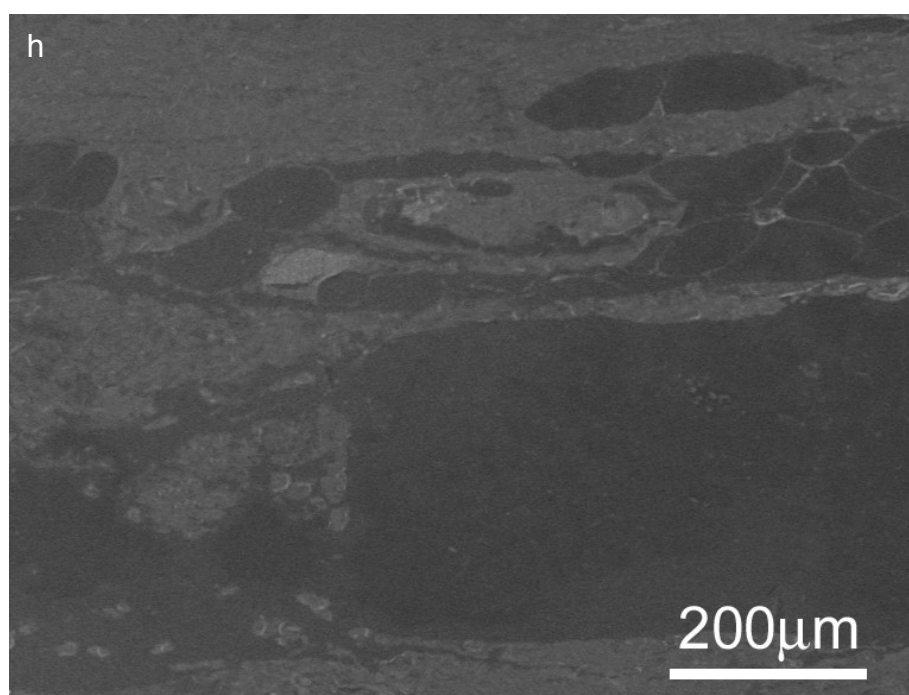
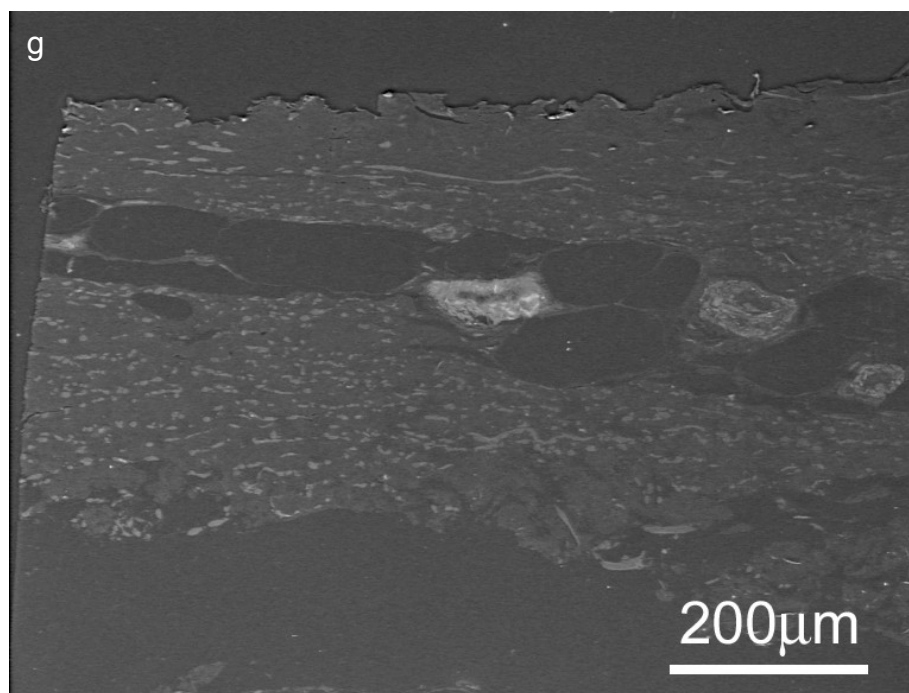


Figure 4.4 (continued). Back-scattered electron micrographs of 0.35  $\mu\text{m}$  thick LR White-embedded human peritoneum sections immunohistochemically stained for smooth muscle actin. Post-polymerisation with,  $\text{La(III)Cl}_3$  (g), and  $\text{H}_3\text{PW(IV)}_{12}\text{O}_{40}$  (h).



#### 4.4.3 Transmission Electron Microscopy

Unstained pancreatic exocrine granules had slight inherent electron opacity (figure 4.5a). Immunohistochemical staining for  $\alpha$ -amylase with DAB alone resulted in specific electron opacity in the exocrine granules (figure 4.5b). In sharp contrast to the results from scanning electron microscopy, d-block metal compounds that were applied pre-polymerisation did not appreciable increase the electron opacity of polyDAB (figure 4.5c-f).

Post-polymerisation application of d-block metal compounds to polyDAB resulted in an increase in electron opacity in some, but not all cases.  $\text{NaW(VI)O}_4$  (figure 4.5g),  $\text{Os(VIII)O}_4$  (figure 4.5i) and  $\text{NaAu(III)Cl}_4$  (figure 4.5n) all increased the electron opacity of polyDAB, and the electron opacity of the surrounding tissue was also elevated to varying degrees,  $\text{NaW(VI)O}_4$  causing the most, and  $\text{Os(VIII)O}_4$  causing the least. The remaining compounds did not affect the electron opacity of either polyDAB or the tissue to any appreciable extent (figure 4.5j, k, l, and m).

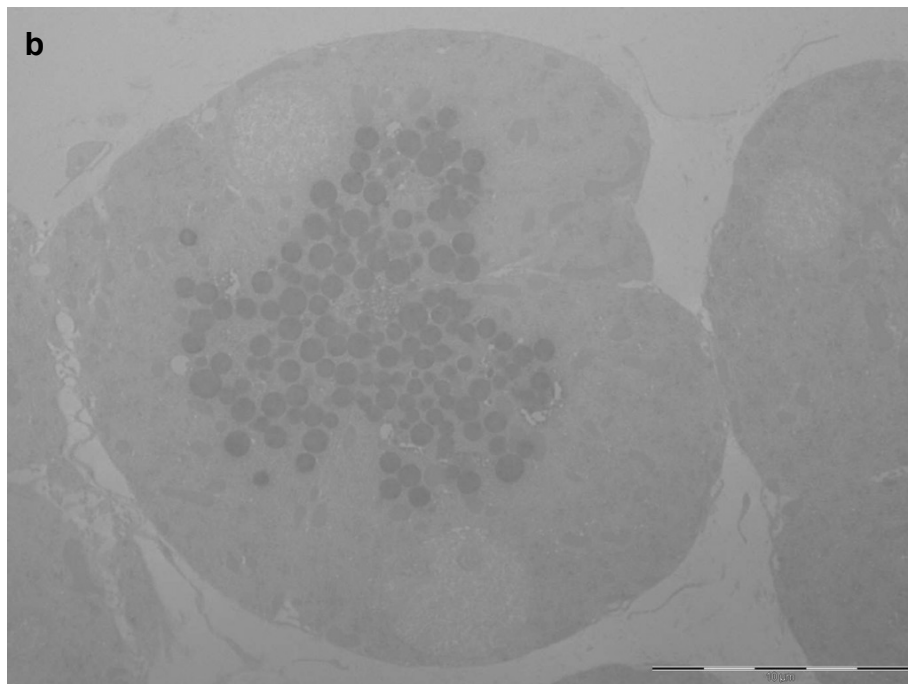
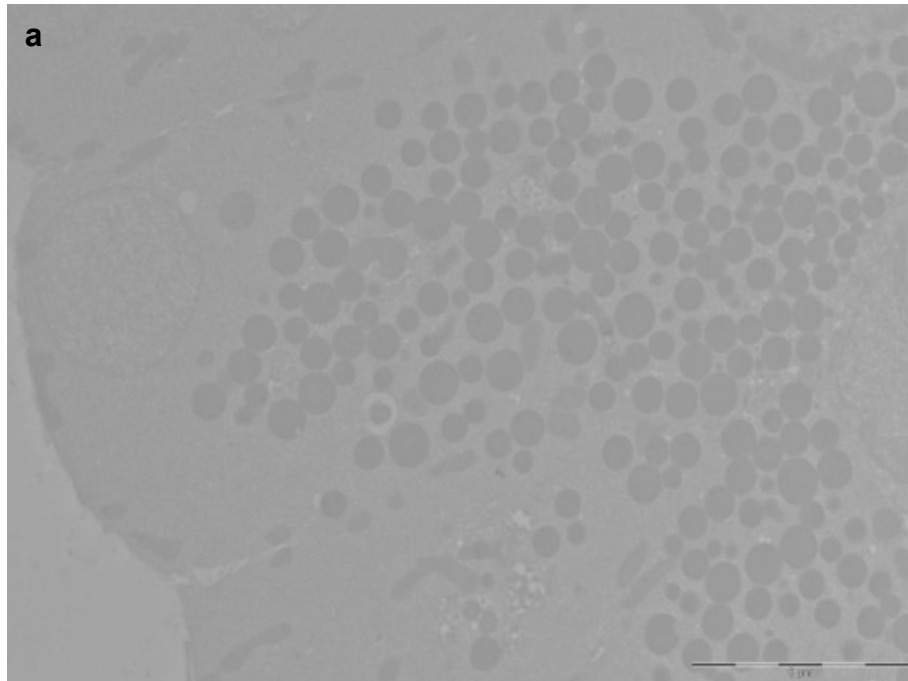


Figure 4.5. Transmission electron micrographs of 80 nm thick LR White-embedded rat pancreas sections immunohistochemically stained for  $\alpha$ -amylase. Unstained (a) and DAB alone (b).

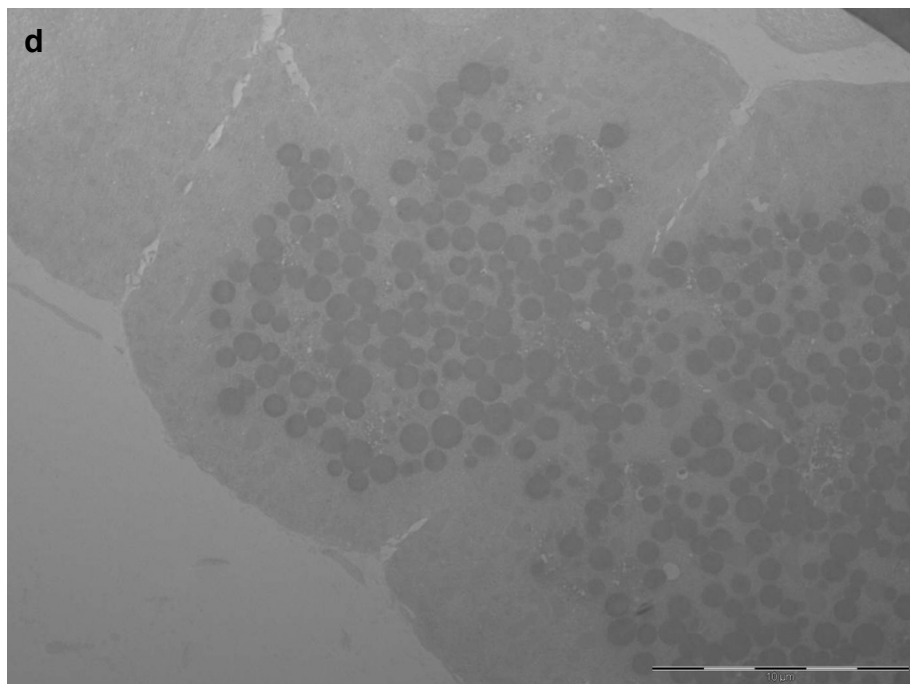
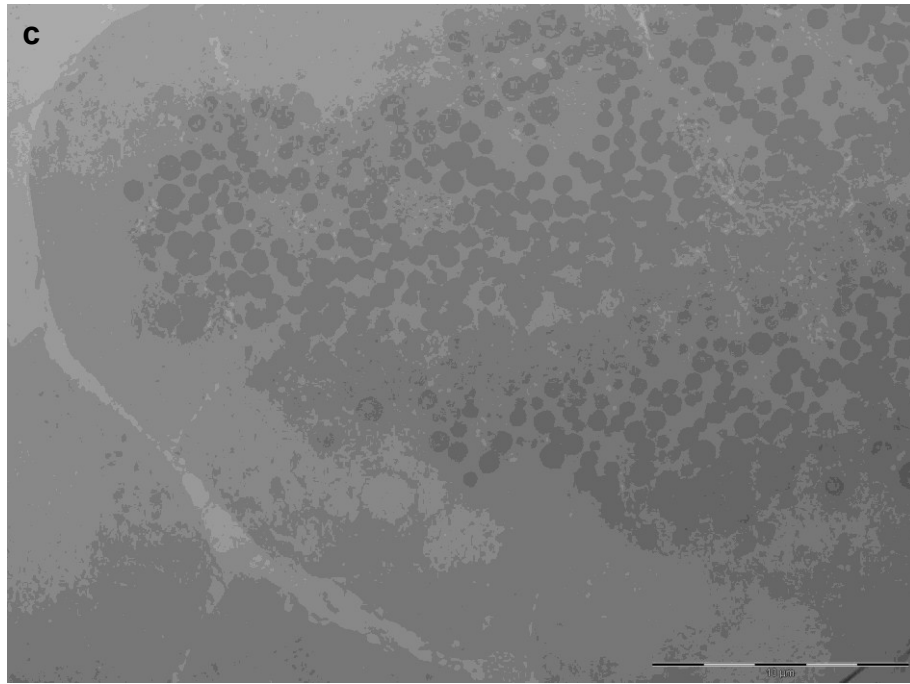


Figure 4.5 (continued). Transmission electron micrographs of 80 nm thick LR White-embedded rat pancreas sections immunohistochemically stained for  $\alpha$ -amylase. Pre-polymerisation in Tris with  $\text{Re(III)Cl}_3$  (c) and  $\text{K}_3\text{Ir(IV)Cl}_6$  (d).

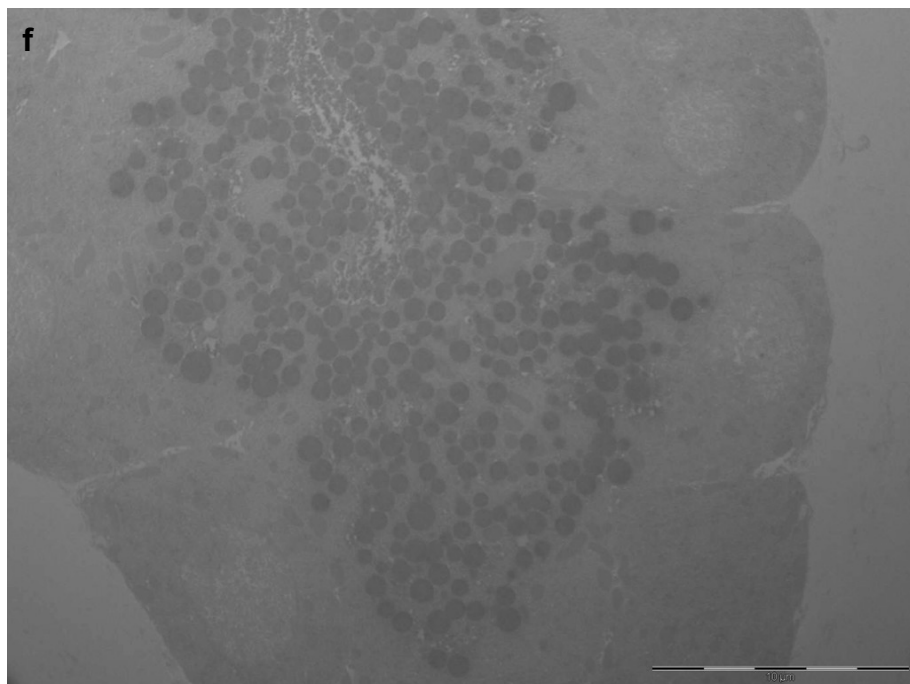
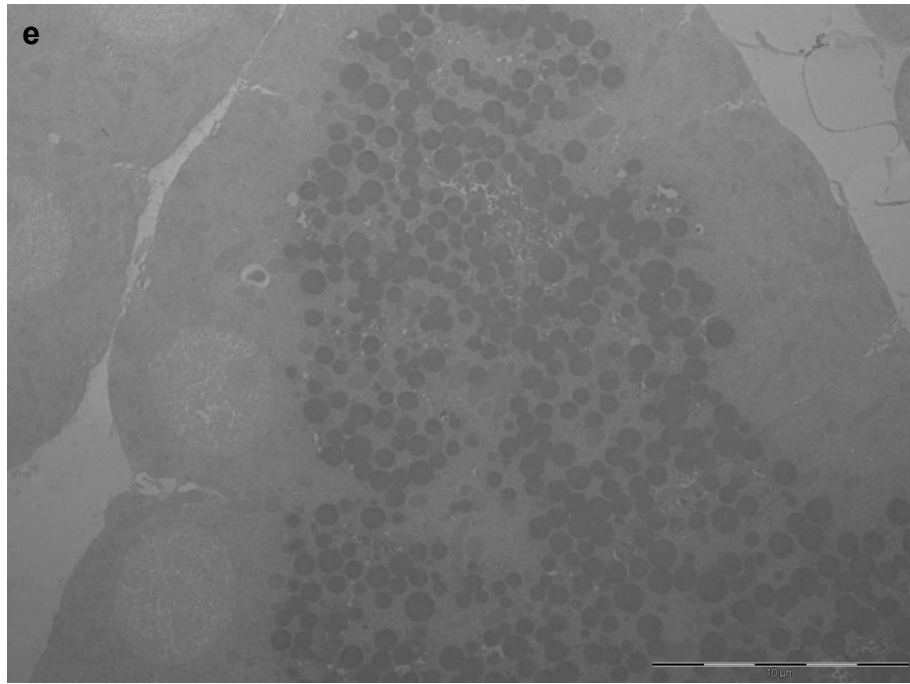


Figure 4.5 (continued). Transmission electron micrographs of 80 nm thick LR White-embedded rat pancreas sections immunohistochemically stained for  $\alpha$ -amylase. Pre-polymerisation in Tris with  $\text{K}_2\text{Pt(IV)Cl}_6$  (e) and in  $\text{PO}_4$  with  $\text{K}_2\text{Pt(IV)Cl}_6$  (f).

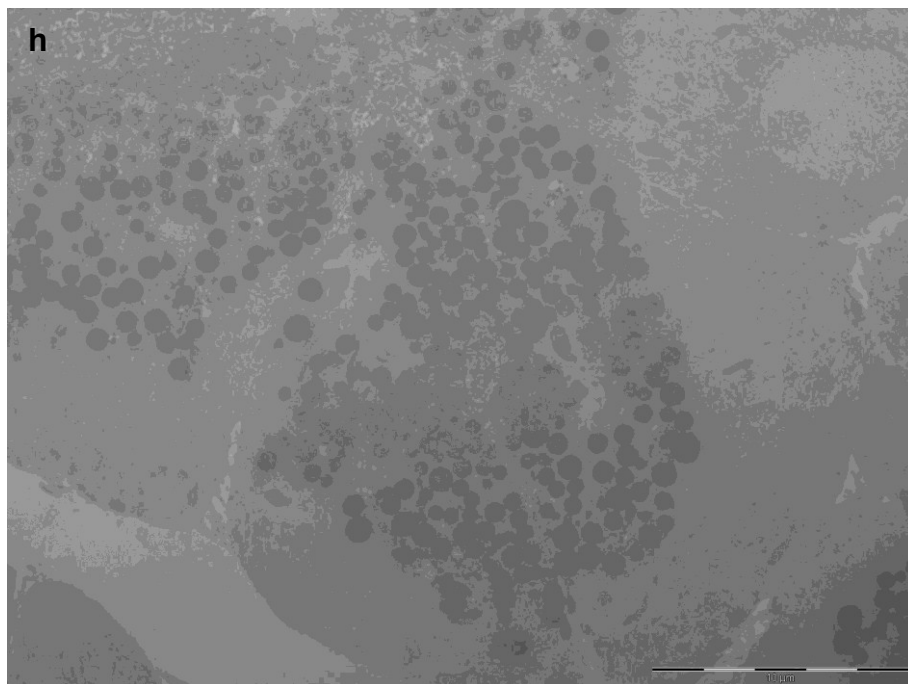
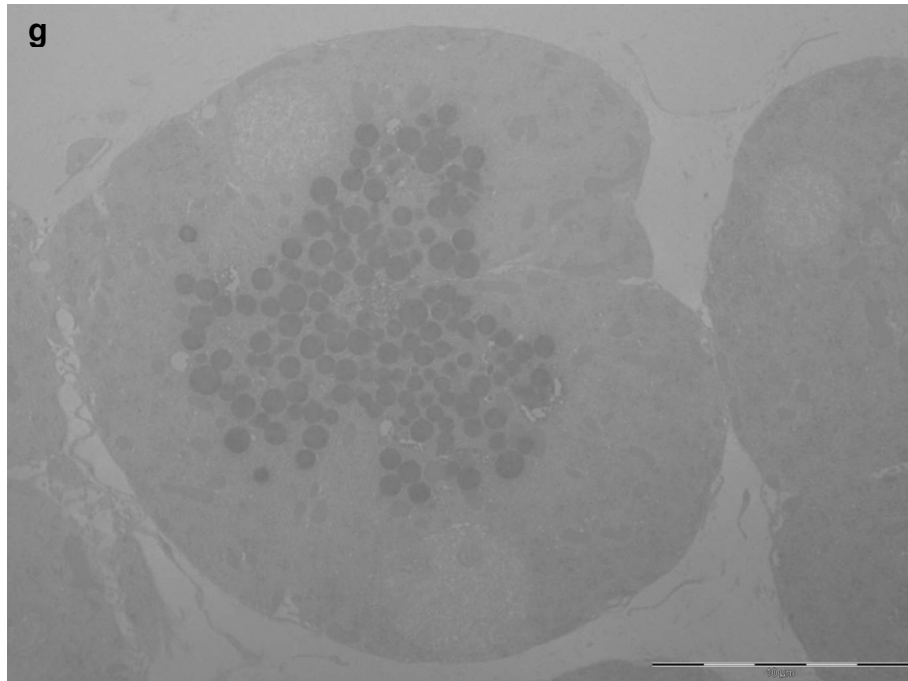


Figure 4.5 (continued). Transmission electron micrographs of 80 nm thick LR White-embedded rat pancreas sections immunohistochemically stained for  $\alpha$ -amylase. DAB alone (g), and post-polymerisation with  $\text{NaW(VI)O}_4$  (h).

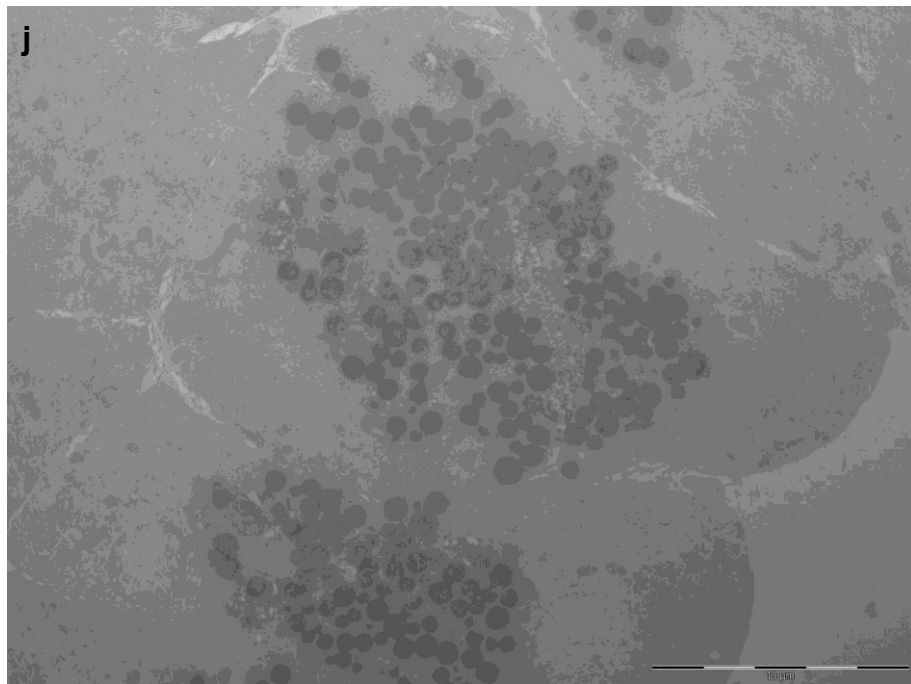
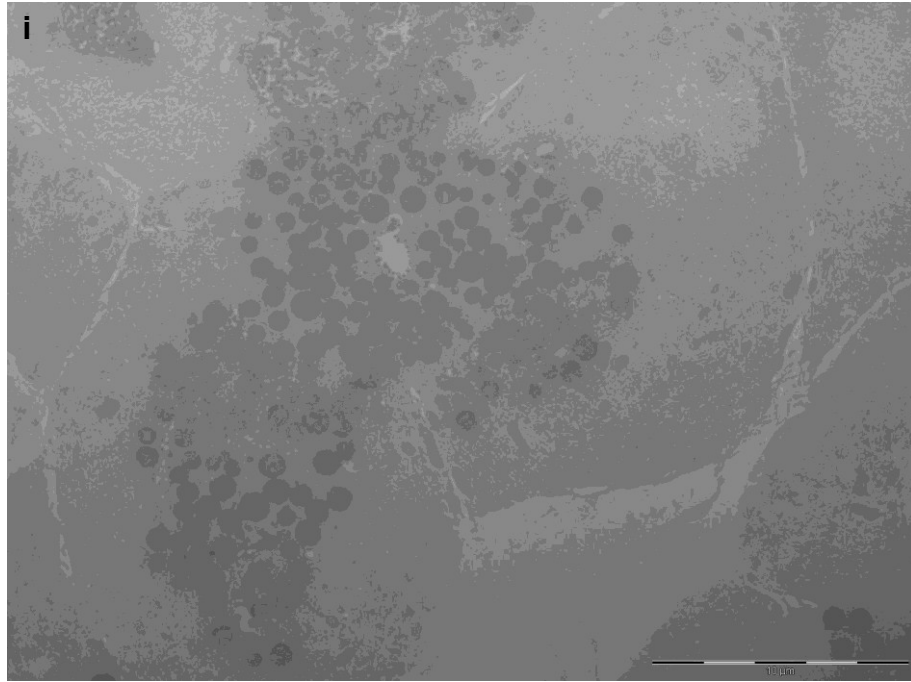


Figure 4.5 (continued). Transmission electron micrographs of 80 nm thick LR White-embedded rat pancreas sections immunohistochemically stained for  $\alpha$ -amylase. Post-polymerisation with  $\text{K}_2\text{Os(IV)Cl}_6$  (i),  $\text{Os(VIII)O}_4$  (j).

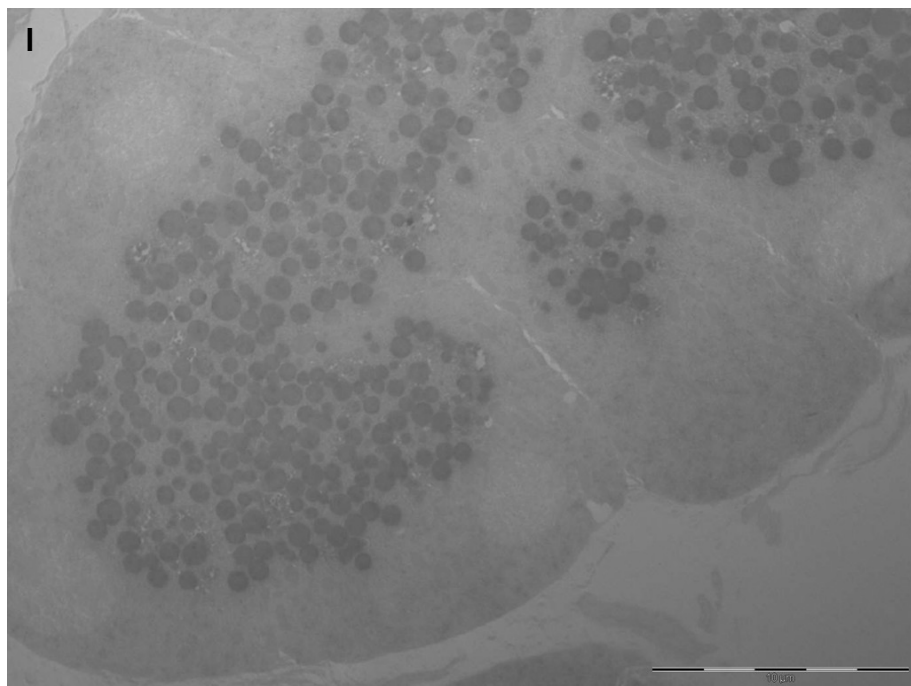
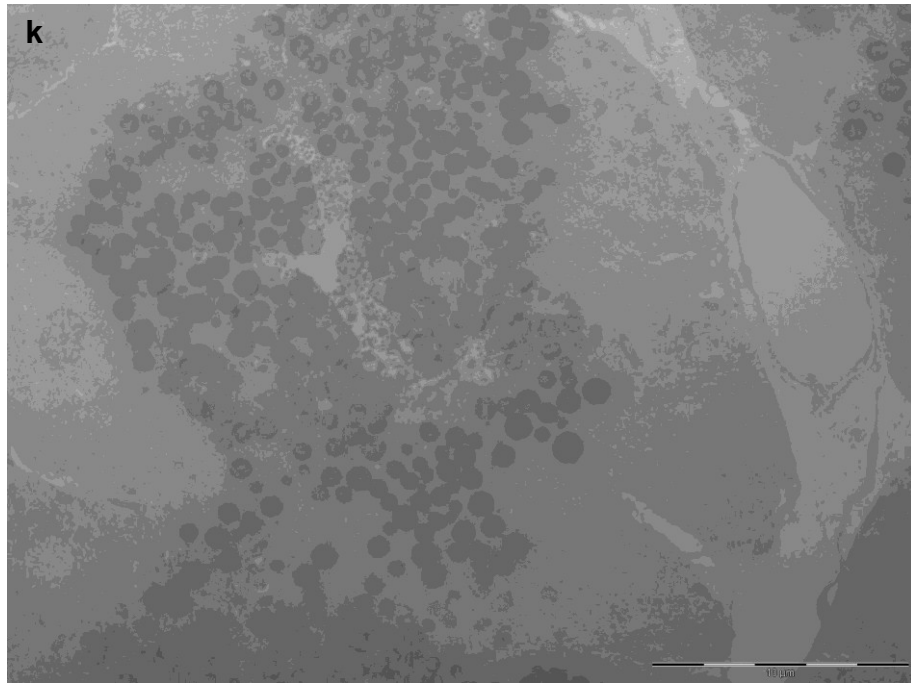


Figure 4.5 (continued). Transmission electron micrographs of 80 nm thick LR White-embedded rat pancreas sections immunohistochemically stained for  $\alpha$ -amylase. Post-polymerisation with  $K_3Ir(III)Cl_6$  (k),  $K_2Pt(II)Cl_4$  (l).



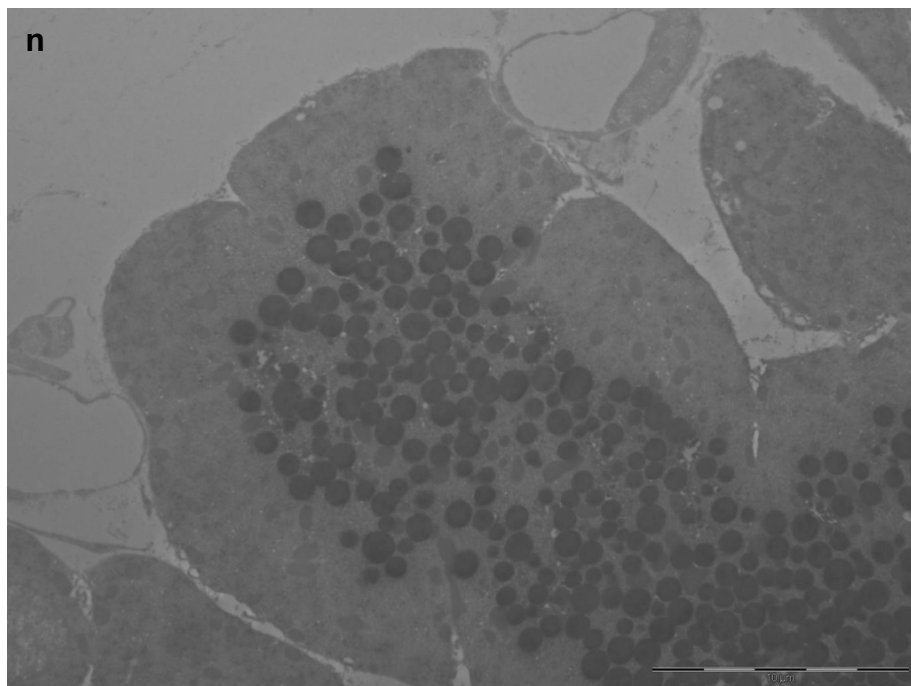
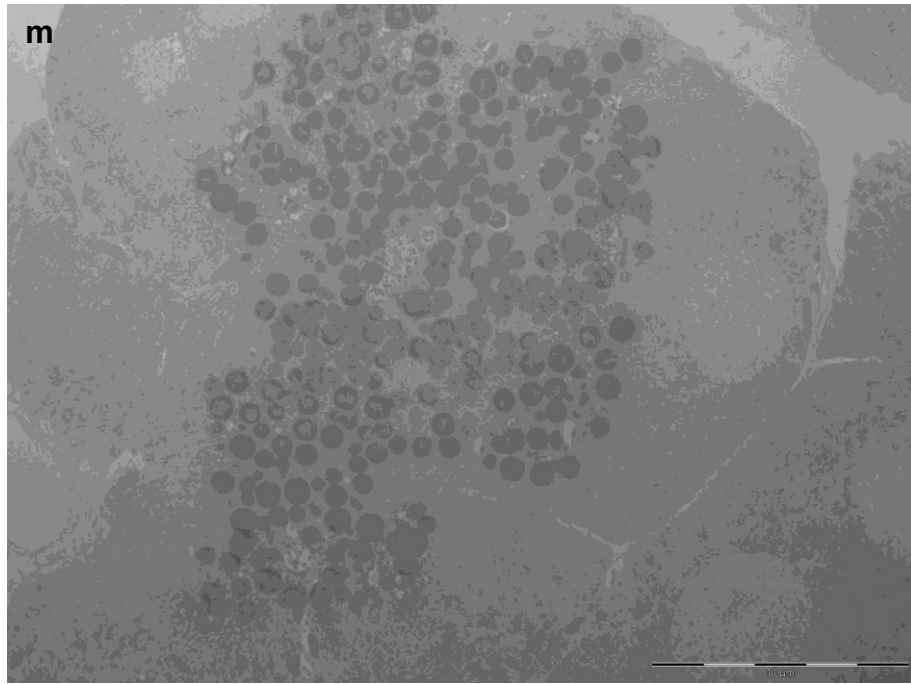


Figure 4.5 (continued). Transmission electron micrographs of 80 nm thick LR White-embedded rat pancreas sections immunohistochemically stained for  $\alpha$ -amylase. Post-polymerisation with  $K_2Pt(IV)Cl_6$  (m), and  $NaAu(III)Cl_4$  (n).

#### 4.4.4 Analytical Transmission Electron Microscopy

X-ray microanalysis demonstrated the presence of metal in some, but not all cases. No signal could be detected in samples that had been treated with  $\text{Re(III)Cl}_3$  or  $\text{K}_3\text{Ir(III)Cl}_6$ , pre-polymerisation. Both platinum compounds could be detected when applied pre-polymerisation but acquisition required a minimum of 10 seconds for unequivocal identification of signal (figure 4.6a).

All metal compounds, when applied post-polymerisation could be detected with a 50 second acquisition time, with the exception of  $\text{K}_3\text{Ir(III)Cl}_6$ , which could not be detected at all. Both  $\text{NaW(VI)O}_4$  (figure 4.6b) and  $\text{Os(VIII)O}_4$  (figure 4.6c) could be identified after just 5 seconds whereas  $\text{K}_2\text{Os(IV)Cl}_6$  required twice as long.

Both platinum compounds and sodium tetrachloraurate (figure 4.6d) could be identified in as little as 2 seconds. In most cases, elements were present at approximately 0.1% by weight, but  $\text{Os(VIII)O}_4$  was measured at 0.3%,  $\text{K}_2\text{Pt(II)Cl}_4$  at 0.6%,  $\text{K}_2\text{Pt(IV)Cl}_6$  at 0.9% and  $\text{NaAu(III)Cl}_4$  at 3.2%. Measurements of background levels of metals indicated that most were present at 0.1%, with the exception of  $\text{K}_2\text{Pt(II)Cl}_4$  (0.2%) and  $\text{NaAu(III)Cl}_4$  (0.5%).

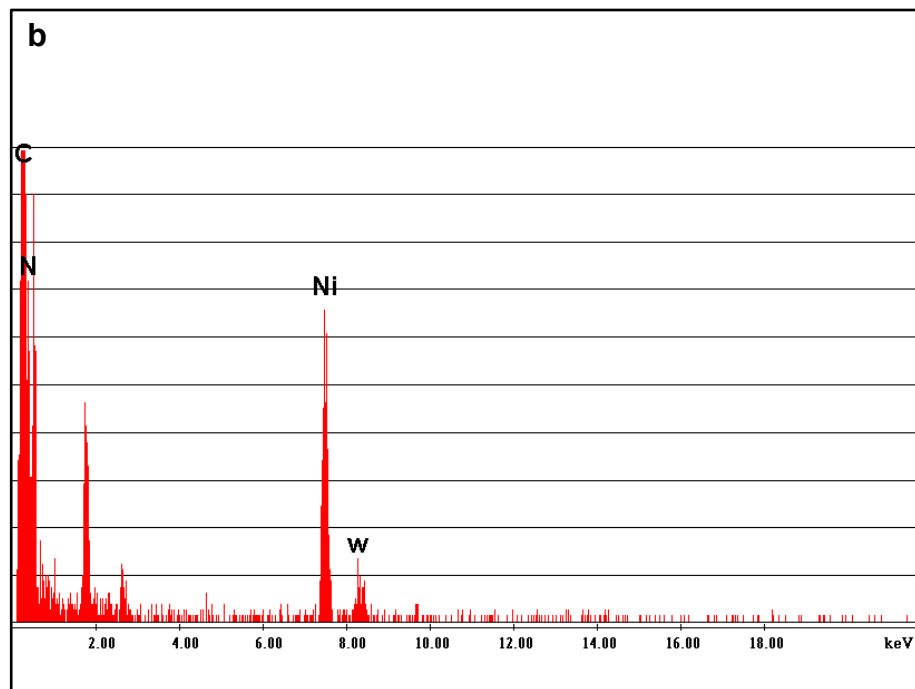
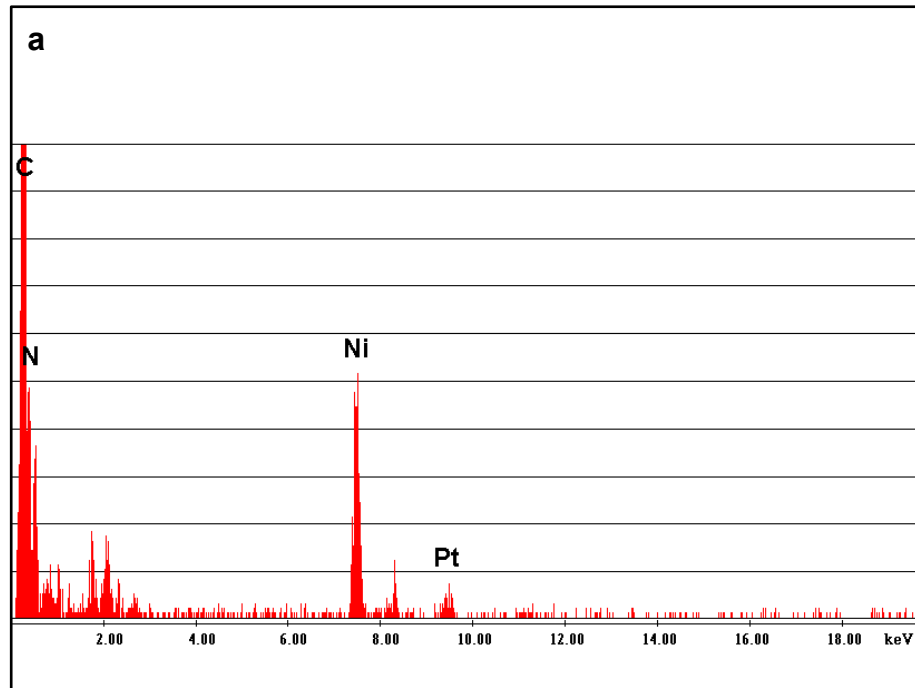


Figure 4.6. X-ray spectra from pancreatic exocrine granules immunohistochemically stained for  $\alpha$ -amylase and developed, pre-polymerisation, with DAB and  $K_2Pt(II)Cl_4$  (a) or post-polymerisation with  $NaW(VI)O_4$  (b).

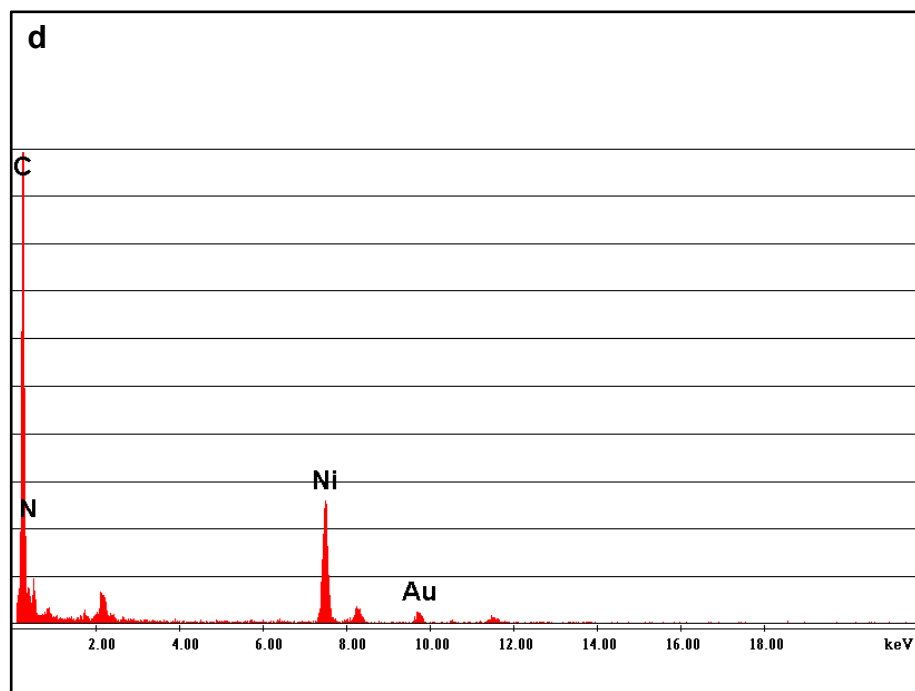
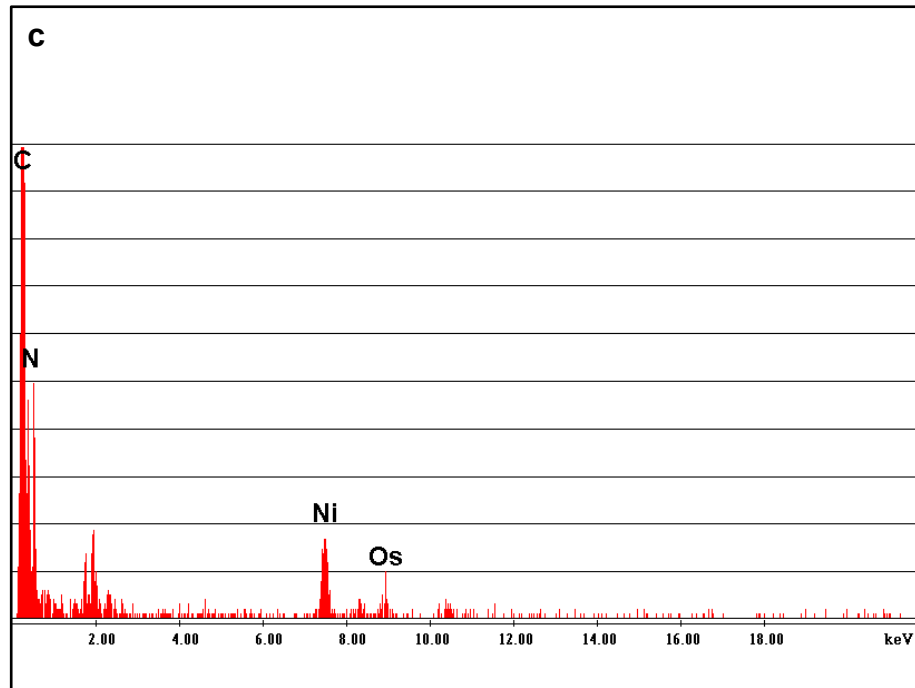


Figure 4.6 (continued). X-ray spectra from pancreatic exocrine granules immunohistochemically stained for  $\alpha$ -amylase. Post-polymerisation with  $\text{Os(VIII)O}_4$  (c) or  $\text{NaAu(III)Cl}_4$  (d).

#### **4.4.5 Electron Tomography**

1  $\mu\text{m}$  thick resin sections were stable throughout the tomographic tilt series acquisition and no serious beam damage was evident. Immunopositivity in endocrine granules of pituitary corticotrophs could be clearly seen, and granules appeared uniformly stained (figure 4.7a). 3-D reconstruction of the tilt series was not performed, but image alignment allowed a stereo anaglyph to be produced from consecutive images (figure 4.7b).

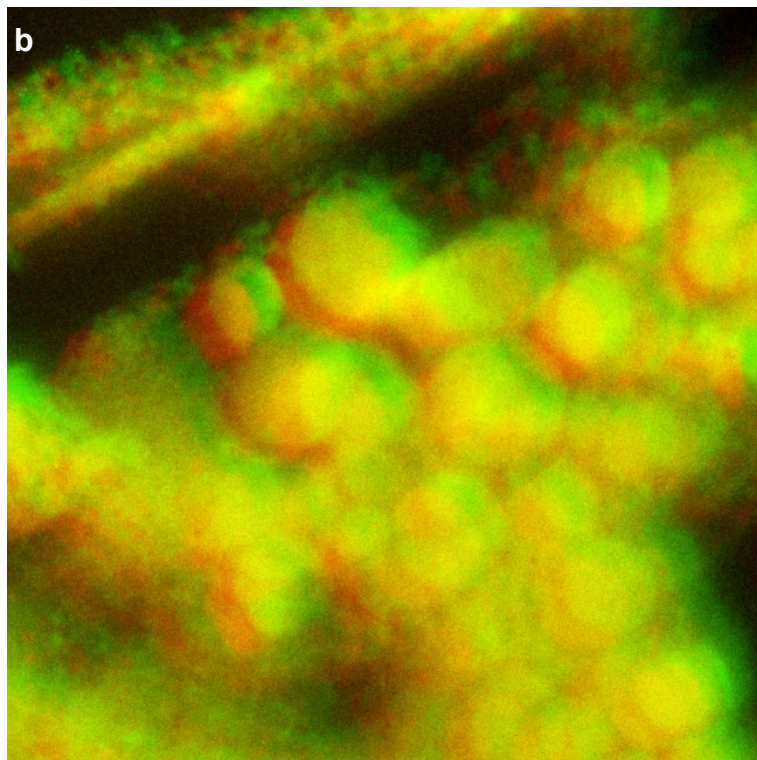
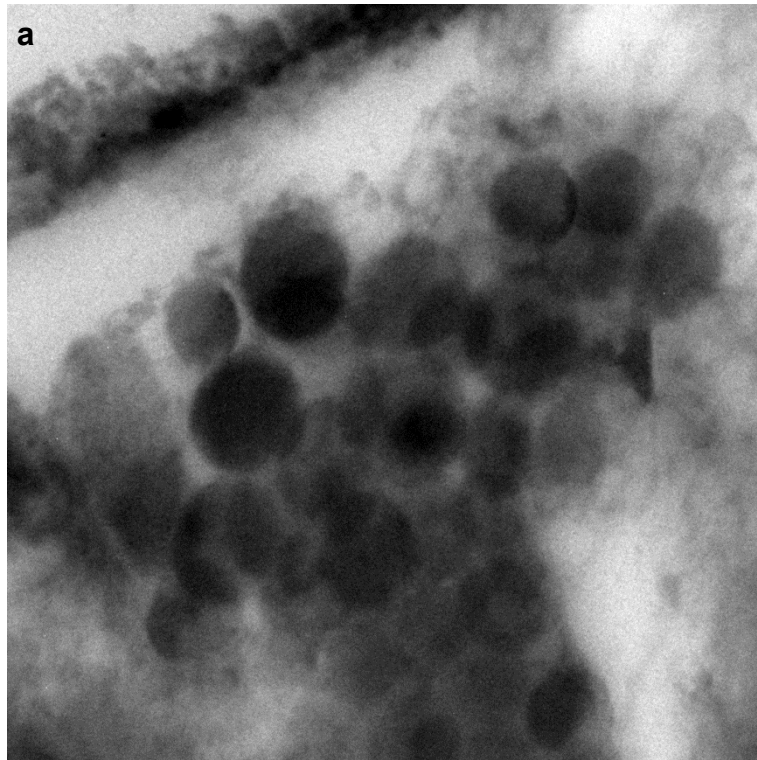


Figure 4.7. Electron tomography images of 1  $\mu\text{m}$  thick section of LR White-embedded pituitary. Corticotroph granules immunohistochemically stained for ACTH and visualised with DAB/NaAu(III)Cl<sub>4</sub>. Bright field image (a) and stereo anaglyph (b). (requires red/green glasses).

## 4.5 Discussion

In preliminary studies, glass microscope slides were rejected as suitable support substrates for tissue sections due to the presence of elements whose X-ray emission peaks were too close to those of the d-block metals under investigation, such as silicon ( $K\alpha$  1.7389 KeV) and tungsten ( $M\alpha$  1.773 KeV). Thermanox™ coverslips provided suitable support surfaces for the immunohistochemically staining of both paraffin wax and acrylic resin sections, since sections adhered to them well without the pre-treatment that is normally required for glass slides. An additional advantage of Thermanox™ coverslips is their lower atomic number composition compared to that of glass, which facilitated back-scattered electron imaging (BSI) of resin sections. BSI exploits average atomic number to achieve contrast, and small amounts of higher atomic number material can easily be overlooked by an overwhelming signal from a much larger amount of lower atomic number substrate.

In preliminary studies, using 4  $\mu\text{m}$  thick sections of paraffin wax-embedded peritoneum immunohistochemically stained for smooth muscle actin, BSI revealed a strong signal from blood vessel walls, and subsequent elemental mapping demonstrated sufficiently large amounts of gold for an analytical image to be produced, although acquisition time was considerable. In both cases, adherence of gold to background tissue, particularly collagen, was evident.

Thermanox™ coverslips, like glass slides, are poor conductors of heat and electricity, and resin sections experienced considerable damage when electron beam dwell time was extended, such as occurred during slow beam scanning for high quality image acquisition. In the SEM, electrons are of lower energy than in the TEM, and consequently interact much more strongly with specimens. A major consequence of this is an increased interaction volume and a subsequent reduction



in the spatial resolution that is achievable. In addition, beam damage can be much more severe, and this was noted in resin sections, even though the resin had been specifically formulated to be electron beam-stable in the TEM. Conditions in the TEM are, however, somewhat different; resin sections are usually supported on a thin metal mesh which dissipates heat and electrons, and high energy electrons result in reduced beam-specimen interaction.

Back-scattered electron imaging revealed a small number of d-block metal compounds that formed complexes with polyDAB, some with considerable specificity, notably those of platinum and gold. General tissue staining was seen with  $\text{La(III)Cl}_3$  and  $\text{H}_3\text{PW(IV)}_{12}\text{O}_{40}$  and this is, perhaps, not surprising since the former has been advocated as a pre-embedding stain for electron microscopy (Leeson and Higgs, 1982) and the latter has been used as a biological TEM stain for a considerable time (Silverman and Glick, 1969). Phosphotungstic acid has been reported to increase the electron opacity of polyDAB (Newman et al., 1983) and this should have been observable by BSI, but no increased signal was seen.

In the TEM, selected d-block metals increased the electron opacity of polyDAB, but not to the same extent as previously reported (Newman et al., 1983). The reason for this is unclear, since development of photographic plates and prints was reported to be identical in the 1983 study, and raw digital images, taken under identical levels of illumination without automatic gamma correction were collected here.

X-ray microanalysis of polyDAB-metal deposits on exocrine granules was able to demonstrate the presence of most metals, and signal was strongest when the d-block compounds were applied post-polymerisation. Few studies have attempted to compare the incorporation of metal into polyDAB, but the results presented here

are in broad agreement with them. In the earliest study, gold(III) was demonstrated to complex with polyDAB in approximately 3-fold greater amounts than osmium(VIII)tetroxide (Siegesmund et al., 1979) but here, proportionately more gold was detected (10-fold). Complexing of hexachloroplatinate with polyDAB has also been compared with Os(VIII)O<sub>4</sub> in histochemically stained preparations, and was shown to impart greater specificity, but absolute values were not reported (de Bruijn et al., 1986). Here, both platinum compounds were present in higher concentrations than Os(VIII)O<sub>4</sub> while background values were comparable.

The minimum acquisition time required to unequivocally demonstrate the presence of metal was 2 seconds in the case of both platinum compounds and tetrachloraurate. Unfortunately, this would be too long for analytical electron tomography to be a practical proposition using this staining technology, since pixel dwell times of less than 50 ms would be necessary to acquire an analytical tomogram in less than 6 hours.

The controversy surrounding antibody penetration into resin-embedded tissue sections was briefly investigated, since this has profound implications for the successful implementation of immunohistochemical staining in a tomographic setting. The polyDAB-gold complex was stable throughout the acquisition period and the resin remained intact. 3-D reconstruction from the tilt series was not performed, but a stereo anaglyph from two consecutive images gave the impression that staining had occurred to some depth. The pre-penultimate line of Yeoman's sonnet, 'that believed is easily seen' is particularly apposite; careful inspection of the individual bright field images of the tilt series suggested staining of the granules to be more consistent with discs, rather than spheres; if staining had penetrated through the entire depth of the section, spherical granules would appear darker in

the central region than at the periphery. There are a number of possible explanations for this, namely (1) antibody penetration does not occur in resin-embedded tissue, (2) antibody penetration occurs, but antibody conjugates do not (3) both primary and secondary antibodies penetrate resin sections, but polyDAB rapidly forms an impenetrable barrier to further diffusion of monomer and (4) endocrine granules are too dense to allow antibodies to penetrate.

#### **4.6 Summary and Conclusions**

A number of d-block metal compounds formed complexes with polyDAB that increased its electron opacity and were demonstrable by analytical TEM. In some cases, notably platinum and gold compounds, they could be identified with short acquisition times. Unfortunately, none could be unequivocally detected in less than 2 seconds, which was still too long for the purposes of AEMT.

The brief investigation of immunohistochemical staining for electron tomography may not have been successful, and suggested that further studies would be required to dissect the reason for the apparent failure of one or more components of the staining system to penetrate resin-embedded tissue sections.

For multiple labelling of tissue constituents to become a realistic proposition in electron tomography, much higher concentration of specific element will be required. These elements cannot be carbon, nitrogen or oxygen, since they are, of course, abundant in biological tissue. Any element with an atomic number higher than 4, and preferably higher than 11 to allow identification by the older detectors, would be adequate for the purpose. The issue of reporter/marker penetration will also have to be addressed.

#### 4.7 References

- ARONOVA, M. A., KIM, Y. C., HARMON, R., SOUSA, A. A., ZHANG, G. & LEAPMAN, R. D. 2007. Three-dimensional elemental mapping of phosphorus by quantitative electron spectroscopic tomography (QuEST). *Journal of Structural Biology*, 160, 35-48.
- ARONOVA, M. A., SOUSA, A. A., ZHANG, G. & LEAPMAN, R. D. 2010. Limitations of beam damage in electron spectroscopic tomography of embedded cells. *Journal of Microscopy-Oxford*, 239, 223-232.
- BAZETT-JONES, D. P., HENDZEL, M. J. & KRUHLAK, M. J. 1999. Stoichiometric analysis of protein- and nucleic acid-based structures in the cell nucleus. *Micron*, 30, 151-157.
- BENDAYAN, M., BARTH, R. F., GINGRAS, D., LONDONO, I., ROBINSON, P. T., ALAM, F., ADAMS, D. M. & MATTIAZZI, L. 1989. Electron spectroscopic imaging for high-resolution immunocytochemistry - Use of boronated protein-A. *Journal of Histochemistry & Cytochemistry*, 37, 573-580.
- BENDAYAN, M. & ITO, S. 1979. Immunohistochemical localization of exocrine enzymes in normal rat pancreas. *Journal of Histochemistry & Cytochemistry*, 27, 1029-1034.
- BRUNS, R. R. & PALADE, G. E. 1968. Studies on blood capillaries 1. General organisation of blood capillaries in muscle. *Journal of Cell Biology*, 37, 244 - 276.
- CROWTHER, R. A., DEROSIER, D. J. & KLUG, A. 1970. The reconstruction of a three-dimensional structure from projections and its application to electron microscopy. *Proceedings of the Royal Society of London Series a-Mathematical and Physical Sciences*, 317, 319-340.
- DE BRUIJN, W. C., VAN DER MEULEN, J., BREDEROO, P. & DAEMS, W. T. 1986. Pt-staining of peroxidatic reaction products at the ultrastructural level. *Histochemistry*, 84, 492-500.

- DE ROSIER, D. J. & KLUG, A. 1968. Reconstruction of three dimensional structures from electron micrographs. *Nature*, 217, 130-134.
- DE WINTER, D. A. M., SCHNEIJDENBERG, C. T. W. M., LEBBINK, M. N., LICH, B., VERKLEIJ, A. J., DRURY, M. R. & HUMBEL, B. M. 2009. Tomography of insulating biological and geological materials using focused ion beam (FIB) sectioning and low-kV BSE imaging. *Journal of Microscopy-Oxford*, 233, 372-383.
- DENK, W. & HORSTMANN, H. 2004. Serial block-face scanning electron microscopy to reconstruct three-dimensional tissue nanostructure. *Plos Biology*, 2, 1900-1909.
- FAULK, W. P. & TAYLOR, G. M. 1971. An immunocolloid method for the electron microscope. *Immunochemistry*, 8, 1081-1083.
- GOLDSTEIN, J., NEWBURY, D., JOY, D., LYMAN, C., ECHLIN, P., LIFSHIN, E., SAWYER, L. & MICHAEL, J. 2003. *Scanning electron microscopy and X-ray microanalysis*, New York, Kluwer Academic/Plenum Press.
- GRAHAM, R. C. & KARNOVSKY, M. J. 1966. The early stages of absorption of injected horseradish peroxidase in the proximal tubules of mouse kidney: ultrastructural cytochemistry by a new technique. *Journal of Histochemistry and Cytochemistry*, 14, 291-302.
- HAINFELD, J. F. 1987. A small gold-conjugated antibody label - improved resolution for electron-microscopy. *Science*, 236, 450-453.
- HALBHUBER, K. J., ZIMMERMANN, N. & LINSS, W. 1988. New, improved lanthanide-based methods for the ultrastructural localisation of acid and alkaline-phosphatase activity. *Histochemistry*, 88, 375-381.
- HANKER, J. S., SEAMAN, A. R., WEISS, L. P., UENO, H., BERGMAN, R. A. & SELIGMAN, A. M. 1964. Osmiophilic reagents: new cytochemical principle for light and electron microscopy. *Science*, 146, 1039-1043.

- HUBER, R., DEISENHOFER, J., COLMAN, P. M., MATSUSHIMA, M. & PALM, W. 1976. Crystallographic structure studies of an IgG molecule and an Fc fragment. *Nature*, 264, 415-420.
- KEAST, V. J., SCOTT, A. J., BRYDSON, R., WILLIAMS, D. B. & BRULEY, J. 2001. Electron energy-loss near-edge structure - a tool for the investigation of electronic structure on the nanometre scale. *Journal of Microscopy*, 203, 135-175.
- LEAPMAN, R. D., KOCSIS, E., ZHANG, G., TALBOT, T. L. & LAQUERRIERE, P. 2004. Three-dimensional distributions of elements in biological samples by energy-filtered electron tomography. *Ultramicroscopy*, 100, 115-125.
- LEESON, T. S. & HIGGS, G. W. 1982. Lanthanum as an intracellular stain for electron microscopy. *Histochemical Journal*, 14, 553-560.
- MALECKI, M., GREASER, M. & ALBRECHT, R. 2003. Bioengineering of antibodies marked with atoms of different elements for simultaneous localization of biomolecules with electron energy loss spectroscopic imaging. *Microscopy and Microanalysis*, 9, 1192-1193.
- MALECKI, M., HSU, A., TRUONG, L. & SANCHEZ, S. 2002. Molecular immunolabeling with recombinant single-chain variable fragment (scFv) antibodies designed with metal-binding domains. *Proceedings of the National Academy of Sciences of the United States of America*, 99, 213-218.
- MARTINCOMIN, J. & ROBYN, C. 1976. Comparative immunoenzymatic localization of prolactin and growth hormone in human and rat pituitaries. *Journal of Histochemistry & Cytochemistry*, 24, 1012-1016.
- MEKLER, L. B., KLIMENKO, S. M., DOBREZOV, G. E., NAUMOVA, V. K., HOFFMAN, Y. P. & ZHDANOV, V. M. 1964. Cytochemical and immunochemical analysis at the electron microscopy level: Obtaining contrasting antibodies by use of iodine. *Nature.*, 203, 717-719.

- MIDGLEY, P. A. & WEYLAND, M. 2003. 3D electron microscopy in the physical sciences: the development of Z-contrast and EFTEM tomography. *Ultramicroscopy*, 96, 413-431.
- MIRECKA, J. & PEARSE, A. G. E. 1971. Localization of follicle stimulating hormone and luteinizing hormone producing cells in the pig adeno hypophysis by an immunohistochemical technique. *Folia Histochemica et Cytochemica*, 9, 365-372.
- MURPHY, R. M., SLAYTER, H., SCHURTENBERGER, P., CHAMBERLIN, R. A., COLTON, C. K. & YARMUSH, M. L. 1988. Size and structure of antigen-antibody complexes - electron microscopy and light-scattering studies. *Biophysical Journal*, 54, 45-56.
- NAIK, D. V. 1973. Immunohistochemical localization of adrenocorticotropin and melanocyte stimulating hormone in pars intermedia of rat hypophysis. *Zeitschrift Fur Zellforschung Und Mikroskopische Anatomie*, 142, 289-304.
- NEWMAN, G. R. & HOBOT, J. A. 1987. Modern acrylics for post - embedding immunostaining techniques. *Journal of Histochemistry and Cytochemistry*, 35, 971 - 981.
- NEWMAN, G. R., JASANI, B. & WILLIAMS, E. D. 1983. Metal compound intensification of the electron density of diaminobenzidine. *Journal of Histochemistry & Cytochemistry*, 31, 1430-1434.
- OLINS, D. E., OLINS, A. L., LEVY, H. A., DURFEE, R. C., MARGLE, S. M., TINNEL, E. P. & DOVER, S. D. 1983. Electron-microscope tomography - transcription in 3-dimensions. *Science*, 220, 498-500.
- OTTENSMEYER, F. P. 1986. Elemental mapping by energy filtration - advantages, limitations, and compromises. *Annals of the New York Academy of Sciences*, 483, 339-353.



- PEPE, F. A. 1961. The use of specific antibody in electron microscopy. I. Preparation of mercury-labeled antibody. *Journal of Biophysical & Biochemical Cytology*, 11, 515-520.
- ROBINSON, J. M. & KARNOVSKY, M. J. 1983. Ultrastructural localisation of several phosphatases with cerium. *Journal of Histochemistry & Cytochemistry*, 31, 1197-1208.
- ROWDEN, G. & DEAN, S. 1991. Immunoalkaline phosphatase with cerium-based cytochemistry for double staining at the transmission electron microscopic level. *Journal of Electron Microscopy Technique*, 18, 121-125.
- SIEGESMUND, K. A., YORDE, D. E. & DRAGEN, R. 1979. A quantitative immunoperoxidase procedure employing energy dispersive x-ray analysis. *Journal of Histochemistry & Cytochemistry*, 27, 1226-1230.
- SILVERMAN, L. & GLICK, D. 1969. Reactivity and staining of tissue proteins with phosphotungstic acid. *Journal of Cell Biology*, 40, 761-767.
- SINGER, S. J. 1959. Preparation of an electron-dense antibody conjugate. *Nature*, 183, 1523-1524.
- SLOT, J. W. & GEUZE, H. J. 1981. Sizing of protein A-colloidal gold probes for immunoelectron microscopy. *Journal of Cell Biology*, 90, 533-536.
- SLOT, J. W. & GEUZE, H. J. 1985. A new method of preparing gold probes for multiple-labeling cytochemistry. *European Journal of Cell Biology*, 38, 87-93.
- STERNBERGER, L. A., DONATTI, J. T. & WILSON, C. E. 1963. Electron microscopic study on specific protection of isolated *Bordetella Bronchiseptica* antibody during exhaustive labelling with uranium. *Journal of Histochemistry and Cytochemistry*, 11, 48 - 58.
- STIERHOF, Y. D. & SCHWARZ, H. 1989. Labeling properties of sucrose-infiltrated cryosections. *Scanning microscopy. Supplement*, 3, 35-46.

- STIERHOF, Y. D., SCHWARZ, H. & FRANK, H. 1986. Transverse sectioning of plastic-embedded immunolabeled cryosections- morphology and permeability to protein A-colloidal gold complexes. *Journal of Ultrastructure and Molecular Structure Research*, 97, 187-196.
- WILLIAMS, D. B. & CARTER, C. B. 1996. *Transmission electron microscopy: a textbook for materials science*, New York, Plenum Press.
- WYNFORD-THOMAS, D., JASANI, B. & NEWMAN, G. R. 1986. Immunohistochemical localisation of cell surface receptors using a novel method permitting simple, rapid and reliable LM/EM correlation. *Histochemical Journal*, 18, 387 - 396.

# **Chapter 5**

## **Halogenated Aromatic Diamine Polymers as Potential Markers for Analytical Electron Microscopical Tomography**

## 5.1 Introduction

From the results of the previous chapter, it was evident that the concentration of metal in polyDAB-metal complexes, while permitting immunohistochemical deposits to be identified by analytical electron microscopy in some cases, was inadequate for practical purposes. The presence of the prominent fluorine peak of the PVDF membrane, in spectra of dot blot preparations that were examined in Chapter 2, suggested that elements other than transition metals might be more fruitfully explored.

Any element, other than those commonly encountered in biological specimens or preparations thereof, in sufficient quantity might serve as an analytical marker. The choice of specific element, to be incorporated into a suitable marker, is dictated by chemistry.

With the exception of the enzyme metallography technique, mentioned in Chapter 2, peroxidase markers are all derived from aromatic amines, including benzidine (Adler and Adler, 1904), 3-amino-9-ethylcarbazole (Graham et al., 1965), 3,3'-diaminobenzidine (Graham and Karnovsky, 1966), p-phenylenediamine (Hanker and Rabin, 1975; Hanker et al., 1977), tetramethylbenzidine (Hardy and Heimer, 1977), o-dianisidine (Carthew, 1978), and o-toluidine (Somogyi et al., 1979). All are rendered electron-opaque by treatment with osmium(VIII)tetroxide.

The simplest method of labelling aromatic compounds with specific elements is halogenation, and a number of methods exist for generating electrophilic halogen species such as fluoroborate (Balz and Schiemann, 1927), acetyl hypofluorite (Lerman et al., 1981), reaction of ferric chloride or bromide with chlorine and bromine, respectively, and iodine with sulfuric acid/iodic acid (Kraszkievicz et al., 2004) or oleum (Symons, 1957a; 1957b).

### **5.1.1 Commercially Available Halogenated Phenylene Diamines**

A brief catalogue survey revealed a number of compounds that might be suitable for investigation (figure 5.1).

### **5.1.2 Synthesis of Halogenated Phenylene 1,2-Diamines**

In addition to the compounds above, a number of synthetic routes exist for preparing halogenated marker precursors. The simplest is reduction of commercially available halogenated nitroanilines with  $\text{SnCl}_2$ /ethanol (Xing and Ogata, 1982) or  $\text{Sn}/\text{HCl}$ . Slightly more complex is the orthonitration of haloanilines and halogenated bis-4-aminophenyls via N-acetylation-protected intermediates. Where suitable precursors are commercially unavailable or prohibitively expensive, synthesis can be achieved by halogenation of nitrobenzenes and subsequent reduction (Stephens and Bower, 1950; Cheeseman, 1962; Youngblood, 2006).

### **5.1.3 Synthesis of Halogenated DAB**

Given the properties of polyDAB, and the suggestion that a labelled analogue might prove a useful marker for analytical electron microscopy (Chandler, 1973), an attempt at halogenated DAB synthesis seems reasonable. Synthesis of the 2,2'-dibromo analogue might be achieved via bromination of commercially available 4,4'-dinitrobiphenyl (Bunnett and Rauhut, 1958), nitration of commercially available 2,2'-dibromobiphenyl or bromination of DAB (Shaffer et al., 1985).

A number of synthetic routes for preparing the iodo analogue were attempted by Shaffer et al, with a view to providing a starting material for the synthesis of

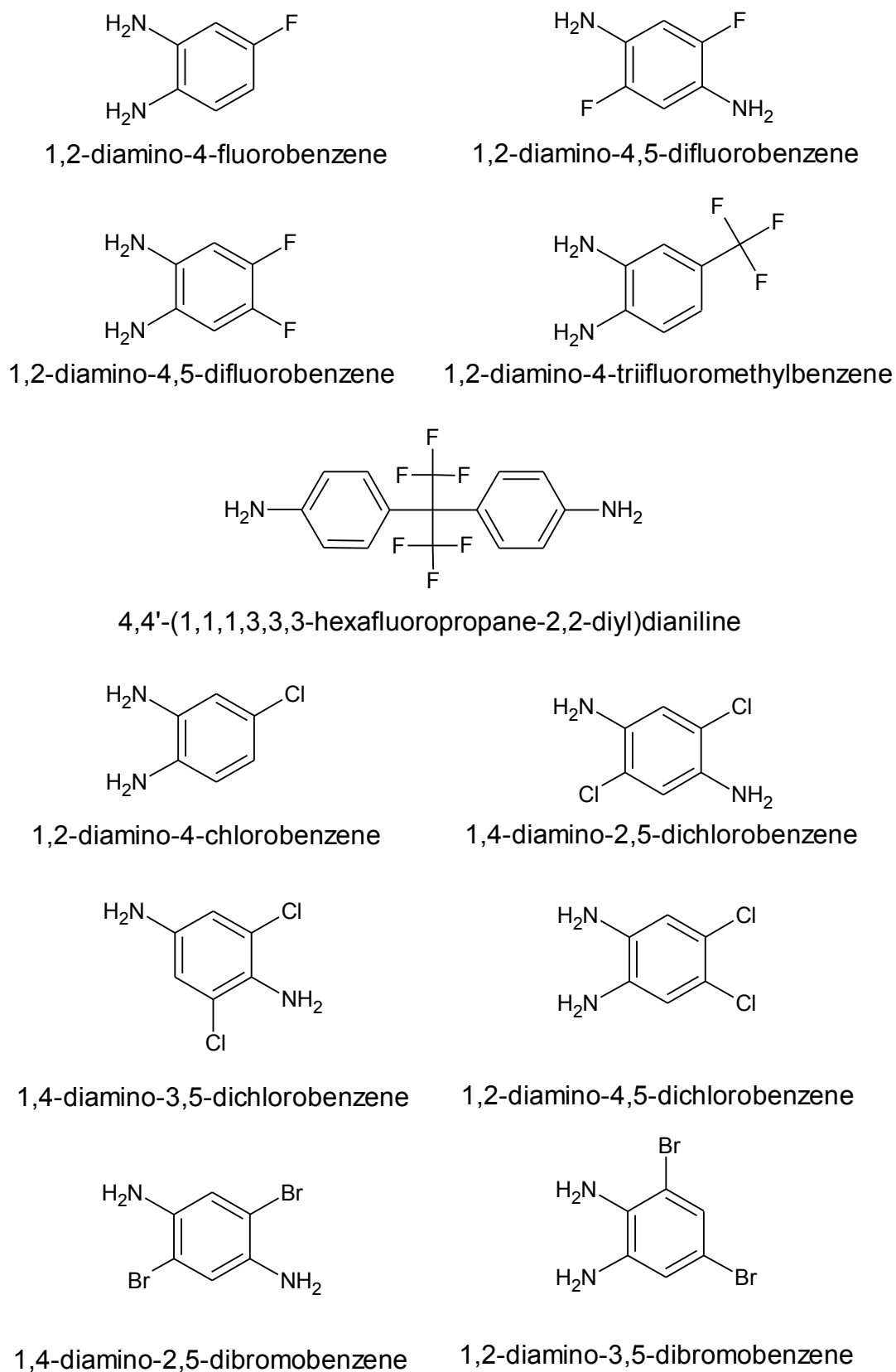


Figure 5.1. Commercially available halogenated phenylene diamines.

lightweight high temperature-resistant composites, including direct iodination of the protected biphenyl tetramine and biaryl coupling of dihalo derivatives of *o*-phenylenediamine, but none of these procedures proved successful (Shaffer et al., 1985). A number of alternative synthetic routes might exist based on (1) direct iodination of aromatic amines (Monnereau et al., 2005), (2) monoiodination of 4-nitrotoluene (Kraszkiwicz et al., 2004; Chaikovskii et al., 2007) (3) iodination of dinitrobenzene (Youngblood) or (4) nitration of commercially available 2,2'-diiodobiphenyl. The starting material in this last approach is prohibitively expensive, but halogen exchange of the dibromo analogue (Klapars and Buchwald, 2002) might provide a cheaper solution.

#### **5.1.4 Selection of Suitable Substrates for Preliminary Dot Blot and Immunohistochemical Staining**

PVDF membrane is clearly unsuitable for use in X-ray analysis of fluorinated aromatic compounds and an alternative is required. Ideally, the substrate should not contain nitrogen in case sufficient marker is deposited that quantitation becomes a possibility i.e. comparison of marker nitrogen with halogen. Two commercially available membranes fulfil these requirements, namely cellulose acetate (CA) and reconstituted cellulose (RC).

In section 4.4.1 of the previous chapter, it was noted that glass microscope slides contained elements whose X-ray peaks interfered with those of some of the d-block elements under study. Similarly, the aluminium  $K\alpha$  peak (1.4866 KeV) is very close to the  $L\alpha$  peak of bromine (1.4805 KeV). For this reason, Thermanox coverslips were again chosen as section support substrates for immunohistochemical staining.

## **5.2 Materials**

### **5.2.1 Reagents**

All reagents were of analytical grade. Tin powder, concentrated hydrochloric acid, concentrated (90%) sulfuric acid, 20% oleum, iodine, potassium nitrate, sodium sulfite, sodium hydroxide, magnesium sulfate, chloroform, ethyl acetate and hexane were supplied by Fisher Scientific (Loughborough, Leicestershire, U.K.). 1-amino-2-nitro-4-bromobenzene, 1-amino-2-nitro-4-iodobenzene, 1-amino-3,4-dibromobenzene, 1-methyl-4-nitrobenzene, 1-methyl-3,4-dinitrobenzene, 4,4'-dinitrobiphenyl, 4,4'-(1,1,1,3,3,3-hexafluoropropane-2,2-diyl)dianiline, 4,4'-methanediyldianiline, triethylamine, dimethylaminopyridine, and acetic anhydride were purchased from Sigma-Aldrich (Poole, Dorset, U.K.). 2,2'-dibromobiphenyl was purchased from Tokyo Chemical Industry UK Ltd (Oxford, Oxfordshire, U.K.). Monoclonal mouse anti-human smooth muscle actin (MAH SMA) was supplied by Dako (Ely, Cambridgeshire, U.K.). Monoclonal mouse anti-human amylase and polyclonal goat anti-mouse Ig HRP conjugate (GAM IgPC) were purchased from Autogen Bioclear (Calne, Wiltshire, U.K.). All antibodies were diluted in TBS/BSA.

### **5.2.2 Tissue**

Archival, post-mortem human adrenal and pancreas tissue were acquired, with consent, prior to the introduction of the Human Tissue Act (2004) and prepared according to section 2.3.4.1. Archival normal human peritoneum and rat pancreas were prepared according to section 4.3.2.2.



## 5.3 Methods

### 5.3.1 Organic Synthesis

The general scheme for synthesis of halogenated aromatic diamines is summarised in figure 5.2.

#### 5.3.1.1 Characterisation of Intermediates and Final Products of Syntheses

Given the structural simplicity of the compounds under investigation, characterisation was performed by  $^1\text{H}$  NMR on a Bruker AMX-400 spectrometer (Bruker UK Ltd., Coventry, U.K.). Where uncertainty existed regarding structure, infra red spectroscopy and/or mass spectrometry (performed by Dr. Rob Jenkins, School of Chemistry, Cardiff University) was performed. Formal names were generated with ChemsSketch and NMR spectra were analysed with NMR Processor freeware (both ACD/Labs Toronto, Ontario, Canada).

Trivial names of compounds are indicated in parentheses. For brevity, derivatives of phenylene-1,2-diamines will be referred to as halo-OPDs and those of 1,4-diamine isomers as halo-PPDs.

#### 5.3.1.2 Synthesis of Halogenated Phenylene 1,2-Diamines

##### 5.3.1.2.1 1,2-Diamino-4-bromobenzene (4-Br-OPD)

1,2-Diamino-4-bromobenzene was prepared by a single step Sn/HCl reduction of 1-amino-2-nitro-4-bromobenzene.

1 g (4.60 mmol) 1-amino-2-nitro-4-bromobenzene was dissolved in 10 ml ethanol and 8 ml conc. HCl added. The mixture was heated under reflux to 110°C and 0.82 g (6.9 mmol, 1.5eq), dispersed in 2 ml of ethanol, added. Reflux was continued until all visible tin had been consumed and the reaction mixture had

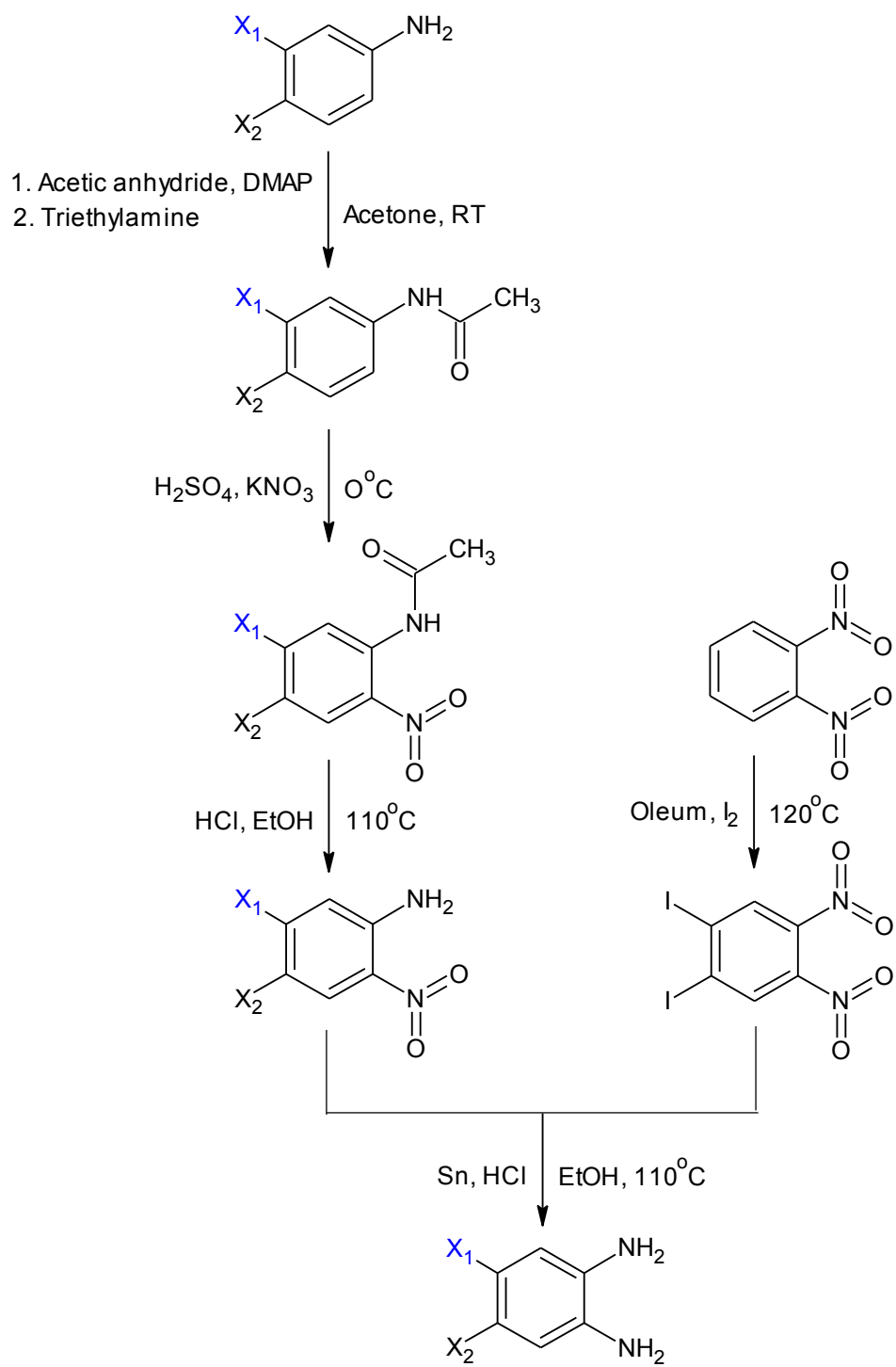


Figure 5.2. Generalised scheme for synthesis of halogenated aromatic diamines.  $X_1$  and  $X_2$  are H, Br or I.

changed from deep red to clear. The mixture was cooled to RT, basified with 2 M NaOH to alkaline pH and extracted with ethyl acetate. The organic phase was dried sequentially with brine and MgSO<sub>4</sub>, and solvent removed by rotary evaporation. 1,2-Diamino-4-bromobenzene was purified by recrystallisation from ethanol/water, yielding 149 mg of white crystals (0.79 mmol) (17.28%). <sup>1</sup>H NMR (400 MHz, CDCl<sub>3</sub>) δ 3.14 (br, s, 4H; NH<sub>2</sub>), 6.49 (d, <sup>3</sup>J<sub>HH</sub> = 8.13, 1H; C6), 7.36 (dd, <sup>3</sup>J<sub>HH</sub> = 8.13, <sup>4</sup>J<sub>HH</sub> = 2.22, 1H; C5) and 8.21 (d, <sup>4</sup>J<sub>HH</sub> = 2.22, 1H; C3) ppm.

#### 5.3.1.2.2 1,2-Diamino-4-iodobenzene (4-I-OPD)

1,2-Diamino-4-iodobenzene was prepared by Sn/HCl reduction of 1 g (4.61 mmol) 1-amino-2-nitro-4-iodobenzene according to section 5.3.1.2.1, above. The organic solvent extract of the basified reaction mixture darkened rapidly and yielded, initially, only a small amount of tarry product. Drying under vacuum resulted in the appearance of crystals that yielded 305 mg (1.30 mmol) (28.2%) pale brown needles of 1,2-diamino-4-iodobenzene upon recrystallisation from ethyl acetate/hexane. <sup>1</sup>H NMR (400 MHz, CDCl<sub>3</sub>) δ 3.40 (br, s, 4H; NH<sub>2</sub>), 6.47 (dd, <sup>3</sup>J<sub>HH</sub> = 7.02, <sup>4</sup>J<sub>HH</sub> = 1.46, 1H; C5), 7.01 (2H, overlapping peaks from C3 and C6 could not be individually resolved, but <sup>3</sup>J<sub>HH</sub> = 7.02 and <sup>3</sup>J<sub>HH</sub> = 1.46 couplings could be identified) ppm.

#### 5.3.1.2.3 1,2-Diamino-4,5-dibromobenzene (4,5-diBr-OPD)

1,2-Diamino-4,5-dibromobenzene was prepared from 1-amino-3,4-dibromobenzene by a four-step procedure; (1) acetylation of the amine, (2) orthonitration, (3) hydrolysis and (4) reduction.

Acetylation was performed according to Yang et al (2009). 3.77 g (12.86 mmol) 1-amino-3,4-dibromobenzene was dissolved in 50 ml acetone on ice, 5 ml (52.90 mmol) acetic anhydride added dropwise and a catalytic quantity (approximately 20 mg) of 4-dimethylaminopyridine (DMAP) (Höfle et al., 1978) added and stirred for 3 hours. The reaction was terminated by the addition of 5 ml triethylamine and the product precipitated by addition of H<sub>2</sub>O (Yang et al., 2009).

The mixture was extracted twice with ethyl acetate and the organic phase dried as above. The product was purified by recrystallisation from both hot ethanol and ethyl acetate/hexane to yield 4.18 g (14.27 mmol) 1-acetamido-3,4-dibromobenzene (95.12%). <sup>1</sup>H NMR (400MHz, CDCl<sub>3</sub>) δ 2.20 (s, 3H; acetyl), 7.34 (dd, <sup>3</sup>J<sub>HH</sub> = 8.77, <sup>4</sup>J<sub>HH</sub> = 2.34, 1H; C6), 7.53 (d, <sup>3</sup>J<sub>HH</sub> = 8.77, 1H; C5), 7.63 (br, s, 1H; NH) and 7.89 (d, <sup>4</sup>J<sub>HH</sub> = 2.34, 1H C2) ppm.

1.8 g (6.14 mmol) 1-acetamido-3,4-dibromobenzene was dissolved in 10 ml conc. H<sub>2</sub>SO<sub>4</sub>, cooled on ice, and 0.27 g (2.73 mmol) KNO<sub>3</sub> added with stirring (Stephens and Bower, 1950). After 3 hours, the mixture was poured onto ice, neutralised with 2 M NaOH and extracted twice with ethyl acetate. Recrystallisation from both hot ethanol and chloroform/hexane yielded 1.61 g (47.64%) of pale yellow 1-acetamido-2-nitro-4,5-dibromobenzene. <sup>1</sup>H NMR (400 MHz, CDCl<sub>3</sub>) δ 2.24 (s, 3H; acetyl), 8.39 (s, 1H; C6), 9.16 (s, 1H; C3) and 10.22 (br, s, 1H; NH) ppm.

1 g (2.96 mmol) 1-acetamido-2-nitro-4,5-dibromobenzene was hydrolysed by dissolving in 10 ml ethanol plus 2 ml conc. HCl and refluxing overnight at 100°C. The mixture was cooled, basified by addition of 2 M NaOH and extracted twice with ethyl acetate. Recrystallisation from chloroform/hexane yielded 0.55 g (1.86

mmol) of red/orange needles; 1-amino-2-nitro-4,5-dibromobenzene (62.81%) <sup>1</sup>H NMR (400 MHz, CDCl<sub>3</sub>) δ 6.08 (br, s, 2H; NH<sub>2</sub>), 7.20 (s, 1H; C6) and 8.38 (s, 1H; C3) ppm.

600 mg (2.03 mmol) 1-amino-2-nitro-4,5-dibromobenzene was reduced with Sn/HCl as above 0.326 g (1.22 mmol) of white crystals of 1,2-diamino-4,5-dibromobenzene (60.38%). <sup>1</sup>H NMR (400 MHz, CDCl<sub>3</sub>) δ 3.42 (br, s, 4H; NH<sub>2</sub>) and 6.95 (s, 2H; C3 & C6) ppm. Overall yield of the preparation was 17.18%.

#### 5.3.1.2.4 1,2-Diamino-4,5-diiodobenzene (4,5-diI-OPD)

Preparation of 1,2-diamino-4,5-diiodobenzene was achieved by a two step reaction; (1) diiodination of 1,2-dinitrobenzene (Youngblood, 2006) and (2) reduction of the resulting dinitro compound to the diamine.

38 ml 20% oleum was heated in an oil bath, with stirring, to 120°C in a three-necked round-bottomed flask fitted with a condenser and nitrogen bubbler. 6.86 g (27.0mmol) I<sub>2</sub> was added and, after 20 minutes, 4.54 g (27 mmol) 1,2-dinitrobenzene. After 75 minutes, the reaction mixture was poured into a 1 l conical flask filled with ice. The mixture was quenched by addition of NaOH until slightly alkaline to pH paper, ice being added as required to keep the mixture cold. The mixture was filtered through Whatman No. 1 filter paper and the filtrate extracted with chloroform. The organic phase was washed with aqueous Na<sub>2</sub>S<sub>2</sub>O<sub>5</sub>, water, and dried as above. The light brown cake was resuspended in 200 ml ddH<sub>2</sub>O and Na<sub>2</sub>S<sub>2</sub>O<sub>5</sub> added until no smell of SO<sub>2</sub> was detectable. The cake was recovered by filtration and extracted with both chloroform and hot ethanol. The organic solvent extracts were combined, the solvent evaporated and the product recrystallised from

chloroform/hexane to yield 2.95 g (7.02 mmol) of pale yellow crystals of 1,2-dinitro-4,5-diiodobenzene (26.02%).  $^1\text{H}$  NMR (400 MHz,  $\text{CDCl}_3$ )  $\delta$  8.34 (s; C3 and C6) ppm.

Sn/HCl reduction of 2 g (4.76 mmol) 1,2-dinitro-4,5-diiodobenzene was performed as above to yield 1.369 g (3.80 mmol) of 1,2-diamino-4,5-diiodobenzene (79.91%).  $^1\text{H}$  NMR (400 MHz,  $\text{CDCl}_3$ )  $\delta$  3.31 (s, 4H;  $\text{NH}_2$ ) and 7.09 (s, 2H; C3 and C6) ppm. The overall yield was 20.79%.

### 5.3.1.3 Synthesis of Halogenated bis-Phenylene 1,2-Diamines

The general scheme for the synthesis of 4,4'-(1,1,1,3,3,3-hexafluoropropane-2,2-diyl)dibenzene-1,2-diamine and 4,4'-methanediyl dibenzene-1,2-diamine is shown in figure 5.3.

#### 5.3.1.3.1 4,4'-(1,1,1,3,3,3-Hexafluoropropane-2,2-diyl)dibenzene-1,2-diamine (F6)

F6 was prepared in an analogous fashion to the synthesis of 4,5-dibromo-OPD in section 5.3.1.2.3, above.

Acetylation of 3 g (8.97 mmol) 4,4'-(1,1,1,3,3,3-hexafluoropropane-2,2-diyl)dianiline yielded 3.50 g (8.37 mmol) of *N,N*-[(1,1,1,3,3,3-hexafluoropropane-2,2-diyl)bis(2-nitrobenzene-4,1-diyl)]diacetamide (93.08%).  $^1\text{H}$  NMR (400 MHz, MeOD)  $\delta$  2.15 (s, 6H; acetyl), 7.32 (d,  $^3J_{\text{HH}} = 8.77$ , 4H; C2, C2', C6 and C6') and 7.62 (m,  $^3J_{\text{HH}} = 8.77$ , 4H; C3, C3, C5 and C5' and  $^5J_{\text{HF}} = 1.75\text{Hz}$ ) ppm.

Nitration of 3.50 g (8.37 mmol) *N,N*-[(1,1,1,3,3,3-hexafluoropropane-2,2-diyl)bis(2-nitrobenzene-4,1-diyl)]diacetamide with 2 equivalents of  $\text{KNO}_3$  yielded

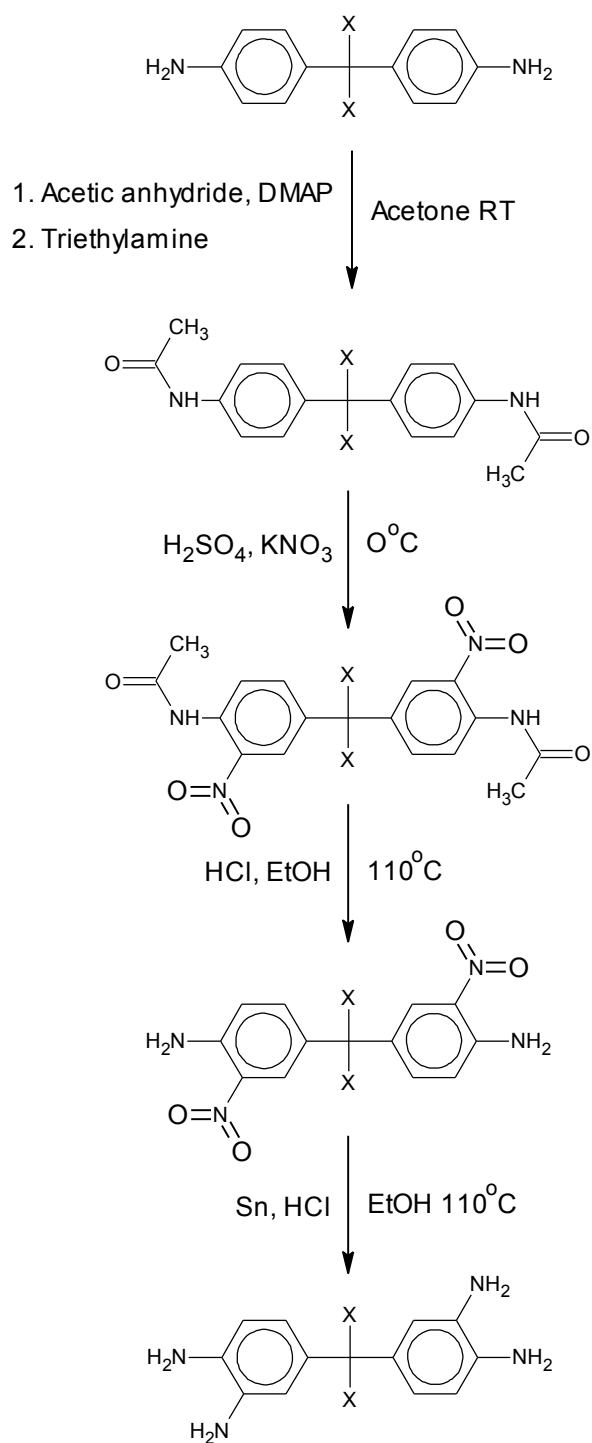


Figure 5.3. Generalised scheme for synthesis of 4,4'-(1,1,1,3,3,3-hexafluoropropane-2,2-diyl)dibenzene-1,2-diamine and 4,4'-methanediyldibenzene-1,2-diamine. X is trifluoromethyl or H respectively.

2.223 g (4.27 mmol) *N,N*-[(1,1,1,3,3,3-hexafluoropropane-2,2-diyl)bis(2-nitrobenzene-4,1-diyl)]diacetamide (52.25%). <sup>1</sup>H NMR (400 MHz, CDCl<sub>3</sub>) δ 2.35 (s, 6H; acetyl), 7.62 (d, <sup>3</sup>J<sub>HH</sub> = 9.06, 2H; C6 and C6'), 8.31 (br, s, 2H; NH), 8.93 (d, <sup>3</sup>J<sub>HH</sub> = 9.06, 2H; C5 and C5') and 10.44 (s, 1H; C3 and C3') ppm.

Hydrolysis of 2.00 g (3.93 mmol) of the above dinitro product gave 4,4'-(1,1,1,3,3,3-hexafluoropropane-2,2-diyl)bis(2-nitroaniline) in good yield; 1.47 g (3.46 mmol) (88.11%). <sup>1</sup>H NMR (400 MHz, CDCl<sub>3</sub>) δ 6.68 (br, s, 4H; NH<sub>2</sub>), 6.92 (d, <sup>3</sup>J<sub>HH</sub> = 9.02, 2H; C6 and C6'), 7.22 (d, <sup>3</sup>J<sub>HH</sub> = 9.02, 2H; C5 and C5') and 8.06 (s, 2H; C3 and C3') ppm.

Sn/HCl reduction of 0.6 g of 4,4'-(1,1,1,3,3,3-hexafluoropropane-2,2-diyl)bis(2-nitroaniline) yielded 0.164 g (0.45 mmol) 4,4'-(1,1,1,3,3,3-hexafluoropropane-2,2-diyl)dibenzene-1,2-diamine (31.93%). <sup>1</sup>H NMR (400 MHz, CD<sub>3</sub>CN) δ 3.83 (br; NH<sub>2</sub>) ppm. Aromatic protons resolved poorly in CD<sub>3</sub>CN and could not be assigned. Overall yield of the synthesis was 15.53%.

#### 5.3.1.3.2 4,4'-Methanediyl-dibenzene-1,2-diamine

The fluorescence of the F6 reaction product following immunohistochemical deposition (section 5.4.2.1, below) prompted an investigation to determine whether this was due to the presence of the methylene bridge in the starting material (since polyDAB does not fluoresce to any appreciable extent) or to the presence of the two trifluoromethyl residues. Synthesis of 4,4'-methanediyl-dibenzene-1,2-diamine from 4,4'-methanediyl-dianiline was performed according to section 5.3.1.3.1, above.

Acetylation of 2.00 g (10.09 mmol) 4,4'-methanediyl-dianiline yielded 0.57 g (2.02 mmol) *N,N*-(methanediyl-dibenzene-4,1-diyl)diacetamide (20.01%). <sup>1</sup>H NMR



(400 MHz, MeOD)  $\delta$  2.11 (s, 6H; acetyl), 3.90 (s, 2H; methylene), 7.14 (d,  $^3J_{\text{HH}} = 8.48$ , 4H; C3, C3', C5 and C5') and 7.45 (d,  $^3J_{\text{HH}} = 8.48$ , 4H; C2, C2', C6 and C6') ppm. Nitration of 400 mg (1.42 mmol) of the acetamide yielded 0.213 g (0.57 mmol), not of *N,N*-[methanediy]bis(2-nitrobenzene-4,1-diyl)]diacetamide as required, but of *N,N*-[(dinitromethanediy]dibenzene-4,1-diyl)]diacetamide (40.28%).  $^1\text{H}$  NMR (400 MHz,  $\text{CDCl}_3$ )  $\delta$  2.27 (s, 6H; acetyl), 7.52 (br, s, 2H; NH), 7.72 (m,  $^3J_{\text{HH}} = 9.06$ ,  $^4J_{\text{HH}} = 2.92$ ,  $^5J_{\text{HH}} = 2.03$ , 4H; C2, C2', C6 and C6') and 8.23 (m,  $^3J_{\text{HH}} = 9.06$ ,  $^4J_{\text{HH}} = 2.92$ ,  $^5J_{\text{HH}} = 2.05$ , 4H; C3, C3', C5 and C5') ppm. No further attempt was made to synthesise this compound.

### 5.3.1.3.3 6,6'-Dibromobiphenyl-3,3',4,4'-tetramine

#### 5.3.1.3.3.1 Bromination of 4,4'-Dinitrobiphenyl

Bromination of was performed according to Bunnet and Rauhut (1958). 1 g (4.09 mmol) 4,4'-dinitrobiphenyl was added to 25 ml glacial acetic acid containing 2 g (8 mmol)  $\text{Br}_2$  and 100 mg Fe powder at  $70^\circ\text{C}$  and refluxed for 2 hours under a nitrogen blanket. The reaction mixture was poured onto ice, neutralised with 2 M NaOH and extracted with chloroform. Only starting material was recovered.

#### 5.3.1.3.3.2 Nitration of 2,2'-Dibromobiphenyl

Nitration of 0.5g (1.60mmol) 2,2'-dibromobiphenyl was performed according to section 5.3.1.2.3, above, and yielded 0.34 g (0.84 mmol) 2,2'-dibromo-4,4'-dinitrobiphenyl (52.78%).  $^1\text{H}$  NMR (400 MHz,  $\text{CDCl}_3$ )  $\delta$  7.95 (d,  $^3J_{\text{HH}} = 8.77$ , 2H; C6 and 6'),  $\delta$  8.17 (d,  $^4J_{\text{HH}} = 2.63$ , 2H; C3 and 3') and  $\delta$  8.22 (dd,  $^3J_{\text{HH}} = 8.77$ ,  $^4J_{\text{HH}} = 2.63$ , 2H; C5 and 5') ppm. This synthesis was not concluded due to lack of time.

#### 5.3.1.3.4 6,6'-Diiodobiphenyl-3,3',4,4'-tetramine

Preliminary syntheses were performed on mono- and dinitrotoluene as cheaper surrogates for mono- and dinitrobiphenyl respectively.

##### 5.3.1.3.4.1 1-Methyl-2-iodo-4-nitrobenzene

1-Methyl-4-nitrobenzene was used a surrogate for 4,4'-dinitrobiphenyl. Monoiodination was performed according to Kraszkiwicz et al (2004). 1.22 g (4.40 mmol) powdered I<sub>2</sub> and 0.39 g (2.20 mmol) HIO<sub>3</sub> were added to 30 ml conc. H<sub>2</sub>SO<sub>4</sub> and stirred for 30 minutes at RT. The mixture was added drop-wise to 1.37 g (10 mmol) 1-methyl-4-nitrobenzene in 20 ml conc. H<sub>2</sub>SO<sub>4</sub> and stirred for a further 15 minutes at RT. The mixture was poured onto ice, extracted with diethyl ether, washed with Na<sub>2</sub>SO<sub>3</sub> solution and recrystallised with chloroform/hexane. The reaction yielded 0.34 g (1.30 mmol) 1-methyl-2-iodo-4-nitrobenzene (13%). <sup>1</sup>H NMR (400 MHz, CDCl<sub>3</sub>) δ 2.57 (d, J<sub>HH</sub> = 4.70, 3H; methyl), 7.41 (dd, <sup>3</sup>J<sub>HH</sub> = 8.18, J<sub>HH</sub> = 4.70, 1H; C6), 8.13 (dd, <sup>3</sup>J<sub>HH</sub> = 8.18, <sup>4</sup>J<sub>HH</sub> = 2.34, 1H; C5) and 8.67 (d, <sup>4</sup>J<sub>HH</sub> = 2.34, 1H; C3) ppm.

##### 5.3.1.3.4.2 1,3-Diiodo-2-methyl-4-nitrobenzene

Diiodination was performed according to Arotzky et al (1970). 8 g (31.54 mmol) I<sub>2</sub> was added to 20 ml 20% oleum and stirred for 30 minutes at RT. 2.16 g (15.77 mmol) 1-methyl-4-nitrobenzene was added and the mixture stirred for 18 hours at RT. The mixture was poured onto ice, extracted with chloroform, washed with Na<sub>2</sub>SO<sub>3</sub> solution and recrystallised from chloroform/hexane. The reaction

yielded 4.98 g (12.80 mmol) 1,3-diiodo-2-methyl-4-nitrobenzene (81.17%). <sup>1</sup>H NMR (400 MHz, CDCl<sub>3</sub>) δ 2.87 (s, 3H; methyl) and 8.68 (s, 2H; C3 and C5) ppm.

#### **5.3.1.3.4.3 1-Methy-2-iodo-4,5-dinitrobenzene**

Monoiodination of 1.46 g (8.0 mmol) 1-methyl-3,4-dinitrobenzene was performed according to section 5.3.1.3.4.1, above, but only starting material was recovered.

Diiodination was performed as in section 5.3.1.3.4.2, using 2 g (11.0 mmol) 1-methyl-3,4-dinitrobenzene. Refluxing for 75 minutes resulted in a small amount of tarry product. Extending the reaction to 4 hours yielded only 100 mg (0.23 mmol) of 1-iodo-2-(iodomethyl)-4,5-dinitrobenzene (2.09%). <sup>1</sup>H NMR (400 MHz CDCl<sub>3</sub>) δ 4.75 (d, J<sub>HH</sub> = 4.68, 2H; iodomethyl), 8.12 (s, 1H; C6) and 8.36 (s, 1H; C3) ppm.

#### **5.3.1.3.5 2,2'-Diiodo-4,4'-dinitrobiphenyl**

Iodination of 0.5 g (4.09 mmol) of 4,4'-dinitrobiphenyl was performed according to section 5.3.1.3.4.2, above. Only 50 mg of gray/brown product was recovered. <sup>1</sup>H NMR indicated the presence of starting material and minor, unidentified, products.

### **5.3.2 Dot-blot model system**

Dot blots were prepared according to section 2.3.3. For preliminary evaluation, dot blots of <sup>1</sup>/<sub>50,000</sub> GAM IgPC were prepared. Where deposit of marker was

evident, further dot blots were prepared from doubling dilutions of GAM IgPC from  $1/50,000$  to  $1/1,600,000$  for visual comparison with polyDAB.

Preliminary attempts to dissolve the compounds in Tris buffer were unsuccessful. This was overcome by initially dissolving 5 mg in 1 ml DMSO followed by addition of 9 ml citrate buffer pH 6.5 and 15  $\mu$ l  $H_2O_2$ . Dot blots were incubated in each solution for 3 minutes, thoroughly washed with ddH<sub>2</sub>O and air dried. Digital images were acquired as previously described.

For analysis by analytical SEM, all dot blots were prepared with GAM IgPC on RC membrane. The peroxidase solution tended to spread over a larger area on RC membrane prior to adsorption, compared to PVDF, thus a higher concentration of GAM IgPC were used, namely  $1/5,000$ . Preparations were attached to 32 mm diameter aluminium stubs with double-sided sticky tape and carbon coated. Those dot blots that contained measureable amounts of halogen were subsequently tested in the tissue model.

### **5.3.3 Tissue model system**

#### **5.3.3.1 Light Microscopy**

Rehydrated sections of either human pancreas or adrenal tissue were equilibrated for 10 minutes with TBS/BSA and incubated for 1 hour in  $1/500$  MAH SMA. Following 3 x 1 minute washes in TBS/BSA, sections were further incubated for 1 hour in  $1/150$  GAM IgPC. Following a 1 minute wash in TBS/BSA, sections were washed twice in either Tris or Citrate buffer, as appropriate to the subsequent marker generating solution. Sections were thoroughly washed in ddH<sub>2</sub>O, dehydrated, cleared in xylene and mounted, initially, in Gurr's neutral mountant.

In cases where the marker dissolved in one of the dehydrating solutions, mounting was performed with the aqueous mountant, Fluorsave™ (Vector Laboratories, Peterborough, U.K.).

### **5.3.3.2 Electron Microscopy**

For SEM, tissue sections were stained in an identical manner as above, and allowed to air dry. Regions containing well stained blood vessels, together with the underlying coverslip, were cut out and mounted on 32 mm diameter aluminium stubs with conductive carbon adhesive discs (TAAB Laboratories Equipment Ltd, Aldermaston, Berks., U.K.) and carbon coated.

For TEM, 80 nm thick sections of either LR White-embedded human peritoneum or rat pancreas were immunohistochemically stained as in section 4.3.2.4 of the previous chapter. Markers were rendered electron dense by a 2 minute wash with either 2.5 mM NaAu(III)Cl<sub>4</sub> or Os(VIII)O<sub>4</sub>, or examined unstained to assess any inherent electron opacity.

### **5.3.3.3 Analytical Electron Microscopy**

For SEM, analytical conditions for examining dot blots were as follows:

Accelerating voltage: 10 kV Probe current:  $10^{-7}$  amps Magnification x 20

Working distance: 15 mm Count time: 100 seconds Processing time 6

For immunohistochemically stained preparations, elemental mapping conditions were as above, except that magnification was set at x 100. Initial mapping was performed at an image resolution of 256 x 192 pixels with 1200  $\mu$ s beam dwell-time per pixel and accumulation of 5 image frames. Where strong signal specific signal was detected, further mapping was performed at 1 frame,

which reduced total acquisition time from 595 seconds to 121 seconds, or pixel dwell time reduced to 100  $\mu$ s and accumulation of 5 or 1 frames, which reduced total acquisition time to 57 or 12 seconds respectively. In some cases, where moderate specific signal was initially detected, accumulation was performed over 10 frames.

TEM acquisition conditions were as described in section 4.3.4.

## 5.4 Results

### 5.4.1 Dot Blot Model System

#### 5.4.1.1 Choice of Dot Blot Substrate for Analytical SEM

Application of GAM IgPC solution to CA membranes resulted in considerable spreading of the solution such that subsequent dot blots covered a much larger area and were more diffuse than those seen in previous experiments using PVDF. In contrast, solutions applied to RC membranes remained focussed, resulting in intense dot blots. One minor problem of the RC membrane was the tendency to curl upon drying. This was overcome by briefly blotting the membranes with filter paper, to remove surplus water, and applying them to double-sided adhesive tape before they fully dried.

#### 5.4.1.2 Polymerisation of Halogenated Compounds on Dot Blots

All halogenated compounds produced visible deposits, although dot blot intensity varied to a greater or lesser extent. Of the fluorinated compounds, 1,2-diamino-4-trifluoromethylbenzene (TriFMe-OPD) produced the faintest dots (figure 5.3a), followed by 1,2-diamino-3,4-difluorobenzene (3,4-diF-OPD) (figure 5.3b). Both 1,2-diamino-4-fluorobenzene (4-F-OPD) (figure 5.3c) and 1,2-diamino-4,5-difluorobenzene (4,5-diF-OPD) (figure 5.3d) produced dots of equal intensity. In all cases, dot colour was yellow-brown.

The chlorinated compounds produced blots of varying colour and intensity; 1,2-diamino-4-chlorobenzene (4-Cl-OPD) was faint and pale yellow brown (figure 5.3e) whereas those of 1,2-diamino-4-fluoro-5-chlorobenzene (4-F-5-Cl-OPD) were intense and dark brown (figure 5.3f). The two chlorinated 1,4-diamines, 1,4-diamino-2,5-dichlorobenzene (2,5-diCl-PPD) (figure 5.3g) and 1,4-diamino-2,6-

dichlorobenzene (2,6-diCl-PPD) (figure 5.3h) were purple-brown and orange-brown respectively, and each produced intense dots. 1,4-diamino-4,5-dichlorobenzene (4,5-diCl-OPD) produced intense orange-brown dots (figure 5.3i).

The brominated compounds were similarly varied, with both 4-Br-OPD (figure 5.3j) and 1,2-diamino-3,5-dibromobenzene (3,5-diBr-OPD) (figure 5.3k) producing yellow-brown dots that were of moderate and low intensity respectively, whilst the dots of 4,5-diBr-OPD were pale and purple-brown (figure 5.3l).

Both iodinated compounds produced intense dots, those of 4-I-OPD being deep purple-brown (figure 5.3m) whereas those of 4,5-diI-OPD were a rather attractive dusky-pink (figure 5.3n).

F6 produced intense yellow dots (figure 5.3o). DAB was included for comparison and produced brown dots (figure 5.3p).



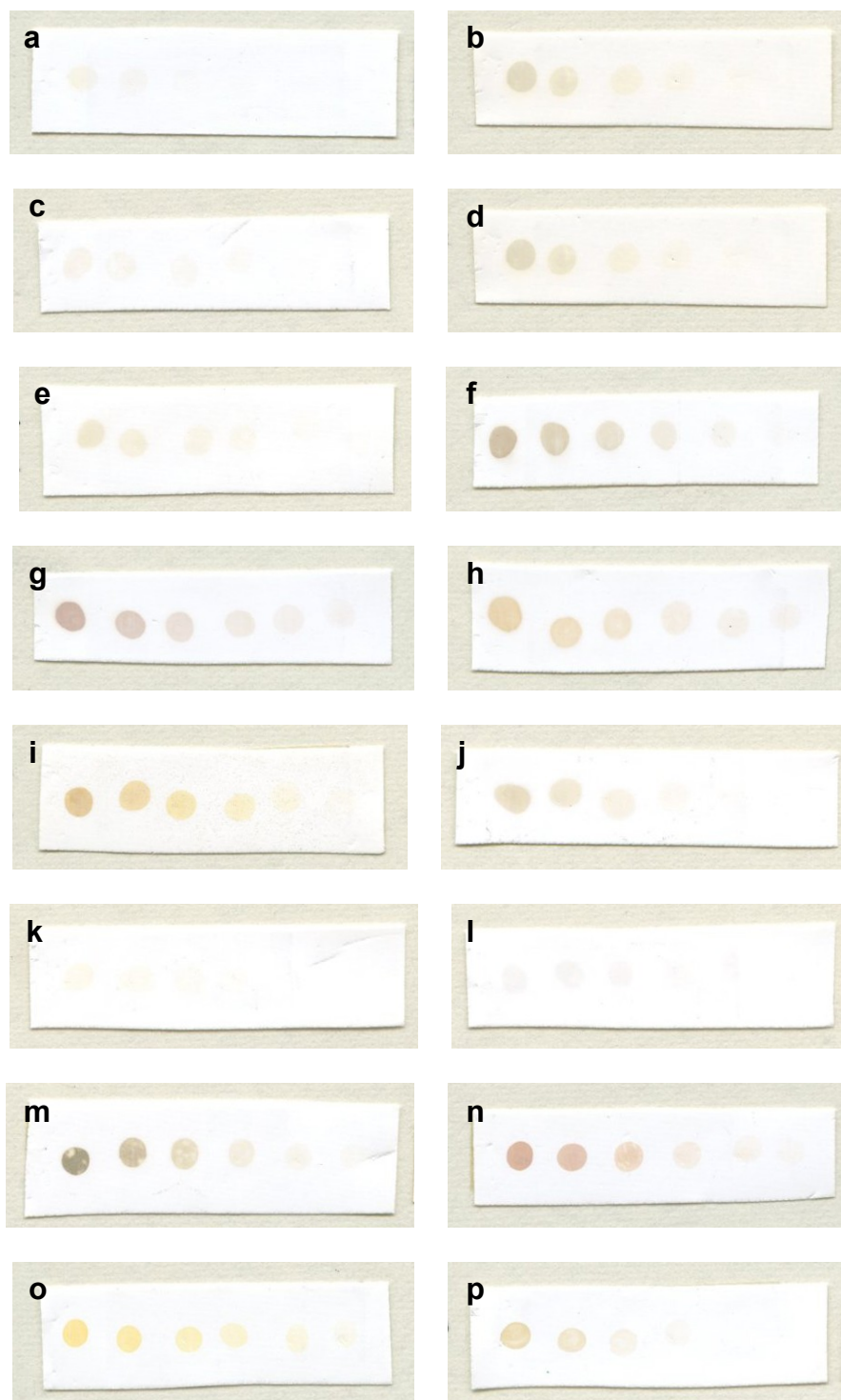


Figure 5.3. Dot blots of polymerised halogenated compounds prepared by incubating PVDF with 2 $\mu$ l drops of doubling dilution of GAM IgPC, from  $1/50,000$  to  $1/1,600,000$ , in 0.5 mg/ml solutions of TriFMe-OPD (a) 4-F-OPD (b), 3,5-diF-OPD (c), 4,5-diF-OPD (d), 4-Cl-OPD (e), 4-F-5-Cl-OPD (f) 2,5-diCl-PPD (g), 3,5-diCl-PPD (h), 4,5-diCl-OPD (i), 4-Br-OPD (j), 3,5-diBr-OPD (k) 4,5-diBr-OPD (l), 4-I-OPD (m), 4,5-diI-OPD (n), F6 (o) and DAB (p).

### 5.4.1.3 Analytical Scanning Electron Microscopy

Even with a high probe current, a long acquisition and long processing time, it was not possible to resolve any polymer nitrogen peak, since it formed part of a broad shoulder of the oxygen signal from the RC membrane. All spectra contained detectable amounts of sulfur, typically 0.1 weight %, 0.35 atomic %, presumably due to residual DMSO solvent.

Of the 5 fluorinated compounds examined, only one, F6, produced a dot blot that contained detectable amounts of fluorine. With the exception of 4-F-5-Cl-OPD, all polymerised chlorinated compounds had measurable levels of chlorine, mostly below 0.25 atomic%. The dot blot of polymerised 4,5-diCl-OPD could just be seen by BSI and had the highest detected concentration of chlorine (figure 5.4a and b). Polymerised 4-Br-OPD could not be discerned by BSI and only had low amounts of detectable bromine (figure 5.4c and d). In contrast, 4,5-Br-OPD produced a dot blot that was both bright by BSI and contained the second highest concentration of halogen of all the compounds tested (figure 5.4e and f). Bromine could not be detected in dot blots produced from either 3,5-diBr-OPD nor 2,5-diBr-PPD.

Both polymerised iodinated compounds produced BSI-bright dot blots and both were detectable by EDX, although, unlike either their chlorinated or brominated analogues, they both contained comparable amounts of iodine (figure 5.4g to j). The results of X-ray microanalysis are summarised in table 5.1.

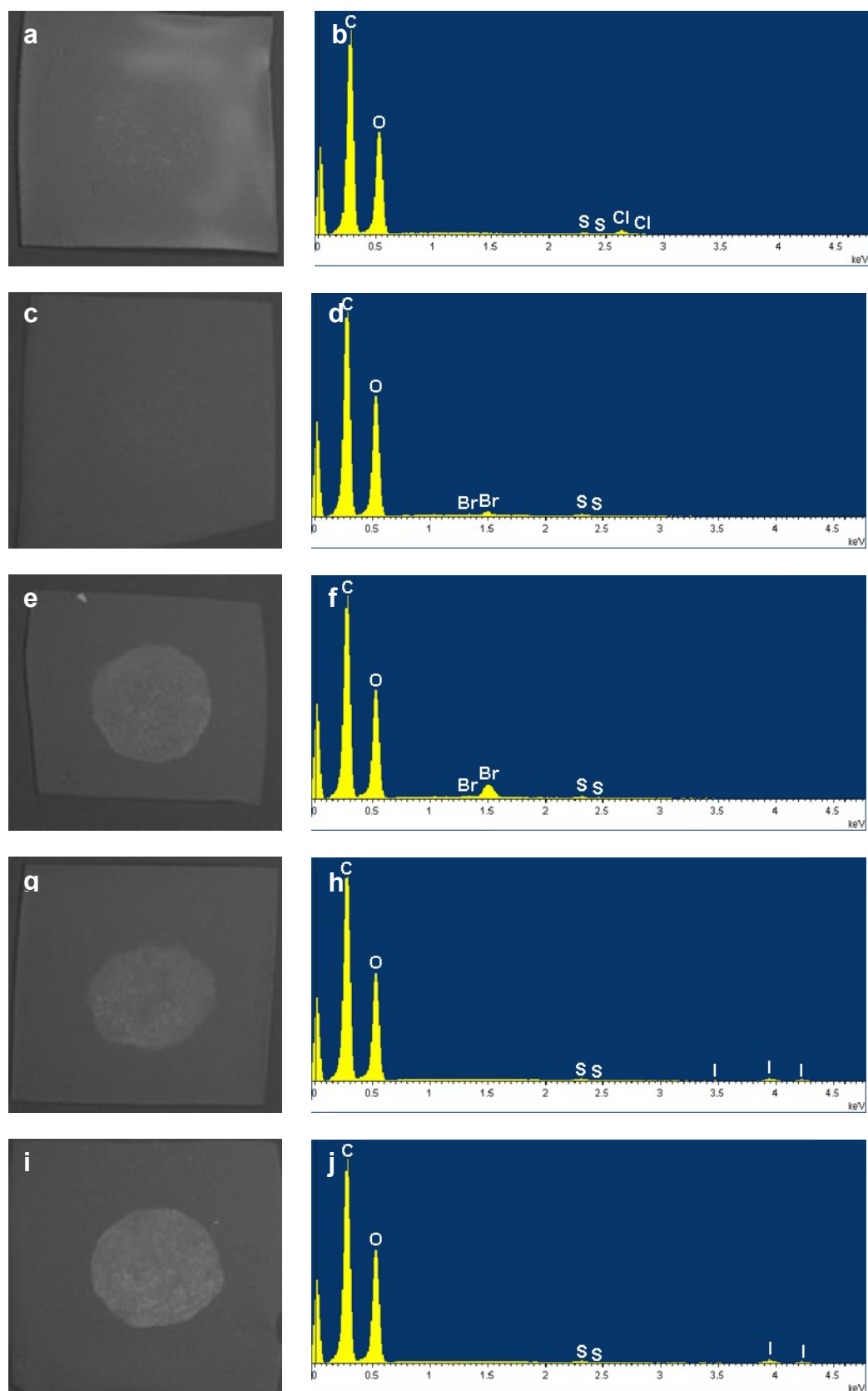


Figure 5.4. Representative back-scattered images and corresponding X-ray spectra of dot blots for halogenated aromatic compounds. 4,5-diCl-OPD (a and b), 4-Br-OPD (c & d), 4,5-diBr-OPD (e & f), 4-I-OPD (g & h) and 4,5-diI-OPD (i & j).

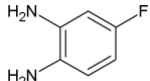
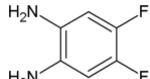
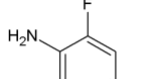
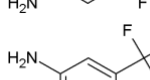
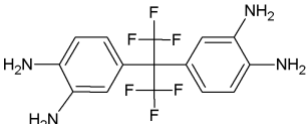
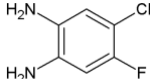
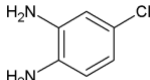
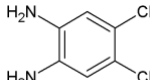
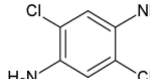
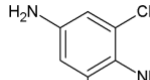
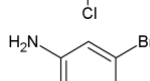
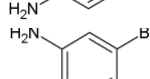
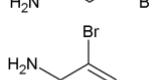
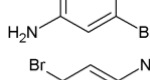
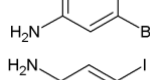
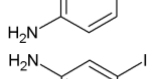
Substrate	Trivial Name	X-ray Analysis	
		Weight %	Atomic %
	4-F-OPD	N/D	N/D
	4,5-diF-OPD	N/D	N/D
	3,5-diF-OPD	N/D	N/D
	4-TriFMe-OPD	N/D	N/D
	F6	6.44	5.5
	4-F-5-Cl-OPD	N/D	N/D
	4-Cl-OPD	0.29	0.13
	4,5-diCl-OPD	2.29	1.05
	2,5-diCl-OPD	0.41	0.19
	2,6-diCl-OPD	0.55	0.25
	4-Br-OPD	2.94	0.61
	4,5-diBr-OPD	12.12	2.7
	3,5-diBr-OPD	N/D	N/D
	2,5-diBr-PPD	N/D	N/D
	4-I-OPD	6.18	0.83
	4,5-diI-OPD	7.24	0.98

Table 5.1 Results of X-ray analysis on halogenated aromatic diamine dot blots.

## 5.4.2 Tissue Model System

### 5.4.2.1 Light Microscopy

All immunohistochemically deposited halogenated polymers were soluble in the dehydrating solvents used for conventional mounting of slides, and it was necessary to use an aqueous mountant instead.

Intensity and colour of staining was broadly similar to what was seen in dot blots, but additional background staining of tissue sections was also noted in many cases.

TriFMe-OPD produced localised yellow staining (figure 5.5a) whereas 4-F-OPD produced deposits that were restricted to background tissue (figure 5.5b). The faint deposits seen in dot blots were mirrored in tissue section in the case of 3,5-diF-OPD (figure 5.5c) as was the intense staining of 4,5-diF-OPD. In this latter case, a yellow background staining, similar to that seen with 4-F-OPD was also evident, and the colour of immunopositive deposits was of a red-brown colour (figure 5.5d).

The chlorinated compounds produced deposits that were consistent in terms of colour and intensity to those seen in dot blots (figures 5.5e to i). In all cases, background staining was evident but generally light, with the exception of 4-Cl-OPD where a yellow background, similar to that seen in some of the fluorinated compounds, was clearly present (figure 5.5e).

The deposits produced from brominated compounds were somewhat different from those of their respective dot blots; those of 4-Br-OPD were orange-brown (figure 5.5j) and those of 4,5-diBr-OPD were intense and orange-red (figure 5.5k). Background staining in both cases was light to moderate respectively.

The iodinated compounds produced deposits that were qualitatively similar to those seen in dot blots, with those of 4-I-OPD being purple-brown (figure 5.5l), and those of 4,5-diI-OPD being dusky pink, although intensity was lower (figure 5.5m).

F6 produced a localised pale yellow deposit similar to that seen in dot blots (figure 5.5n). Again, DAB was included for comparison (figure 5.5o).

To conserve polymerised halogenated compounds for subsequent characterisation, it became common practice to add surplus peroxidase conjugate to the monomer solutions and extract the polymers with ethyl acetate or chloroform. When this was performed on F6, the extracted polymer appeared fluorescent under daylight conditions. Subsequent immunohistochemical staining of a spare section of rat colon with MAH SMA revealed a yellow/orange fluorescence of the marker against the background green autofluorescence of the tissue when irradiated with blue light (figure 5.5p).

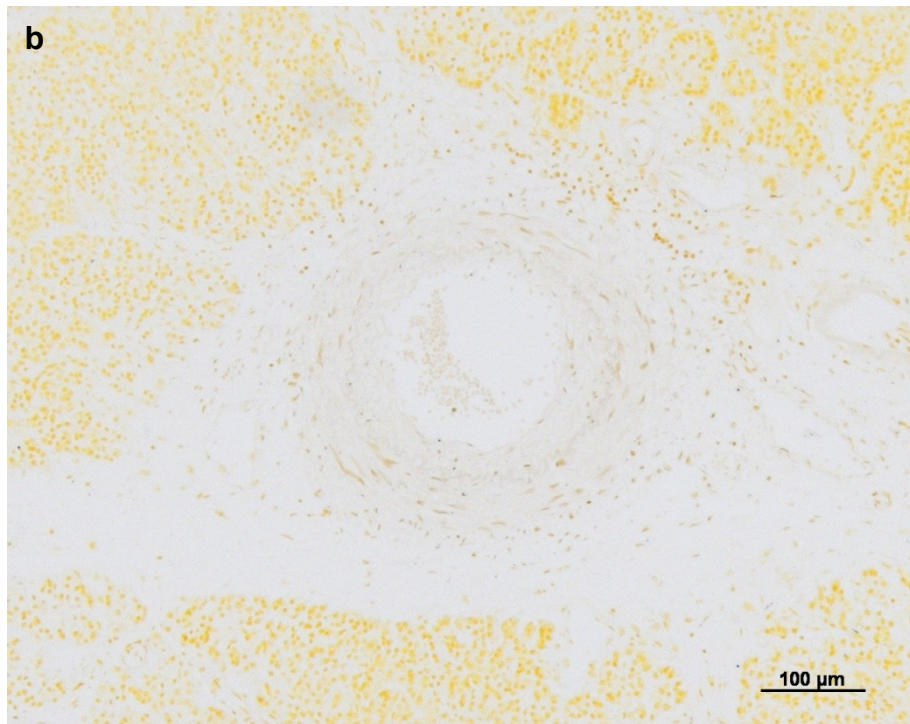
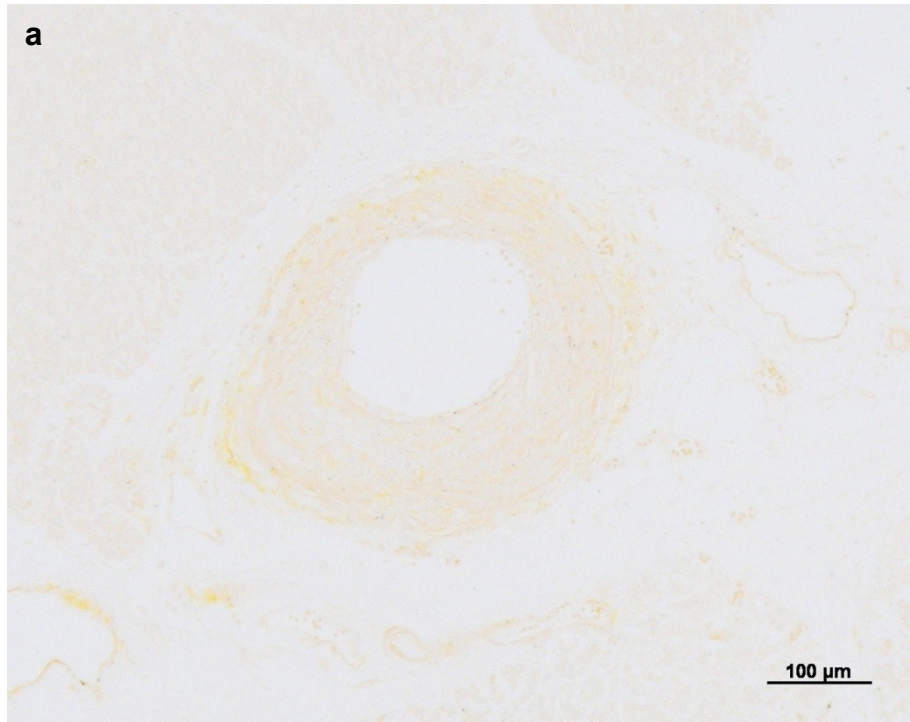


Figure 5.5. 4 μm thick sections of paraffin wax-embedded pancreas. Blood vessel immunohistochemically stained for smooth muscle actin.

TriFMe-OPD (a) and 4-F-OPD (b).



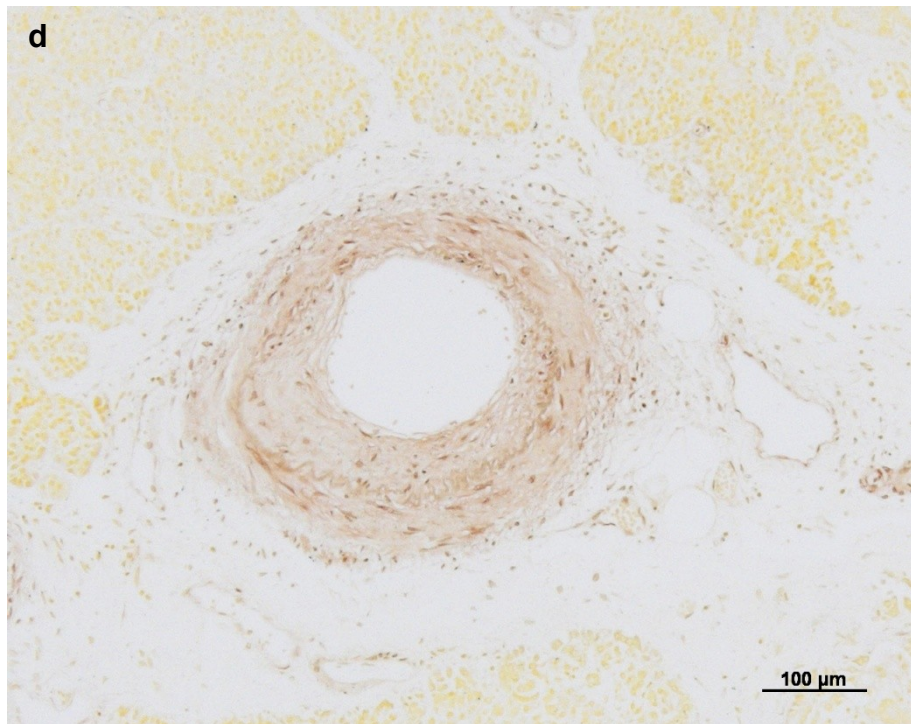
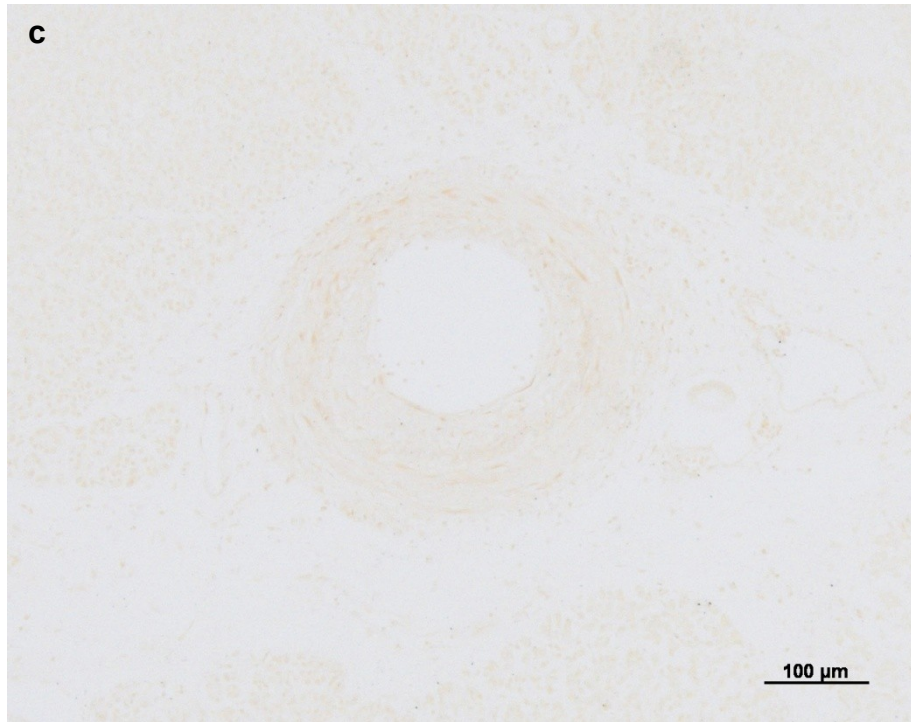


Figure 5.5 (continued). 4  $\mu$ m thick sections of paraffin wax-embedded pancreas.

Blood vessel immunohistochemically stained for smooth muscle actin.

3,5-diF-OPD (c) and 4,5-diF-OPD (d).



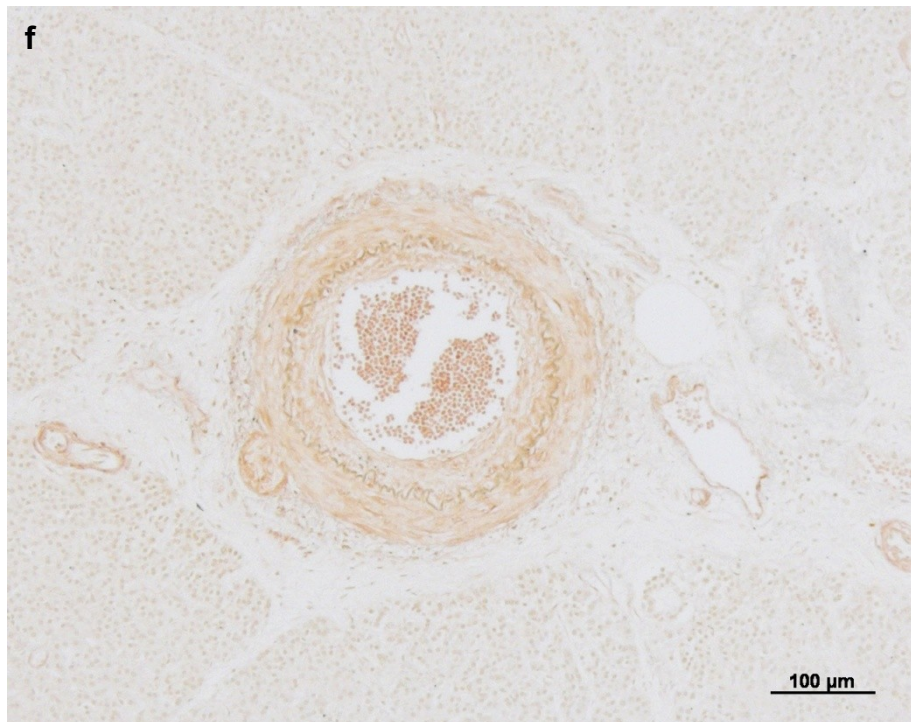
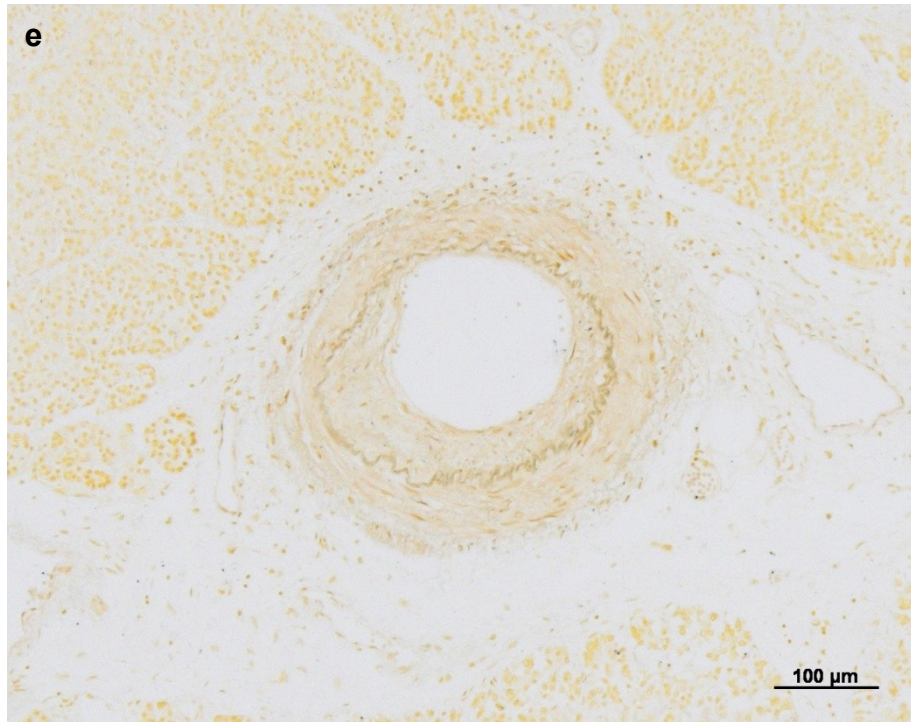


Figure 5.5 (continued). 4 μm thick sections of paraffin wax-embedded pancreas.

Blood vessel immunohistochemically stained for smooth muscle actin.

4-Cl-OPD (e) and 4-F-5Cl-OPD (f).

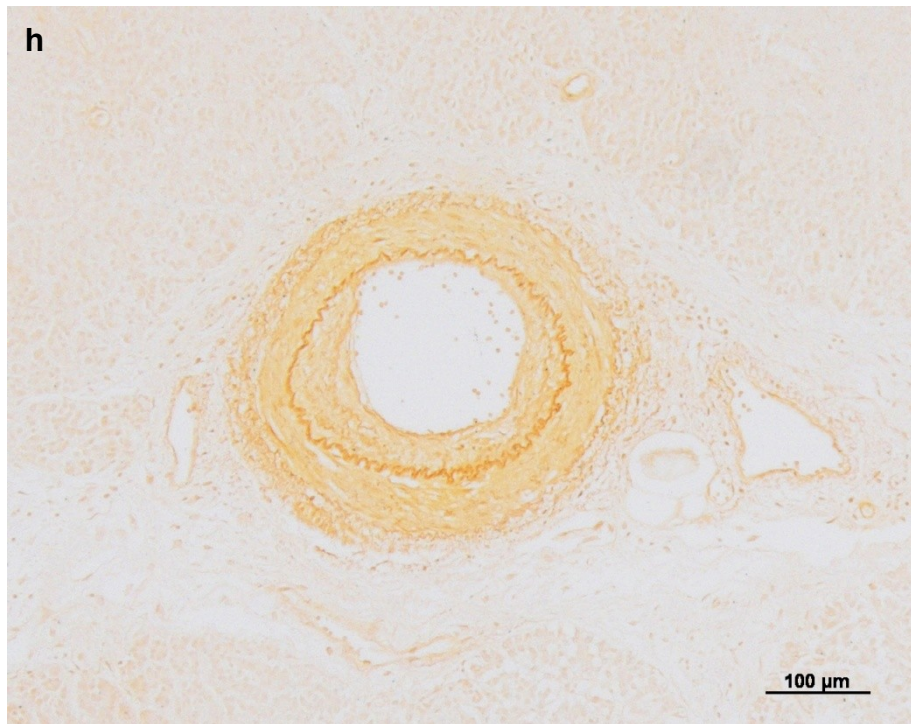
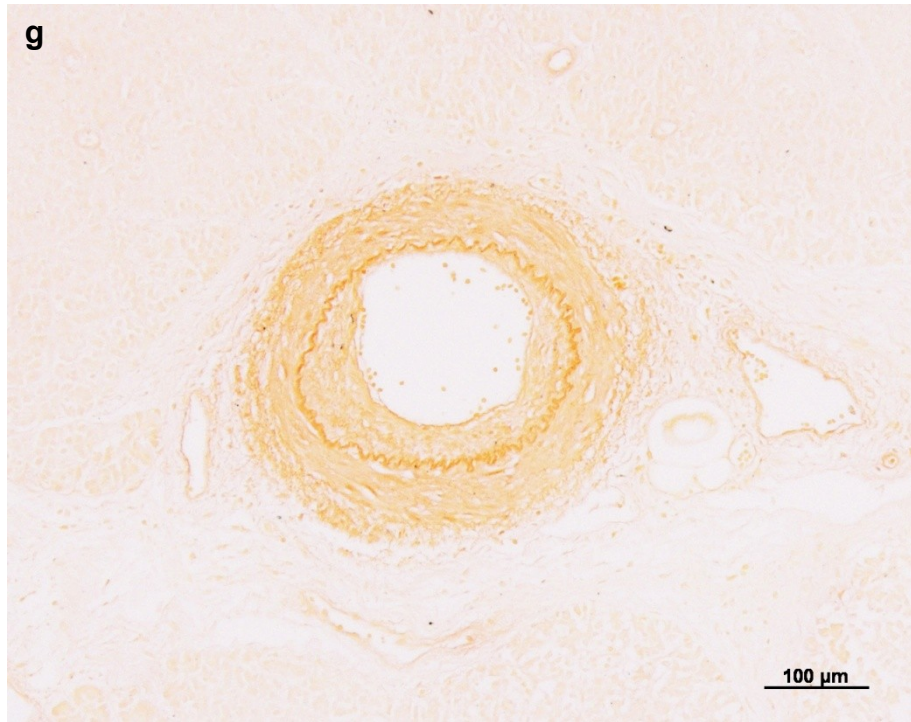


Figure 5.5 (continued). 4 μm thick sections of paraffin wax-embedded pancreas.

Blood vessel immunohistochemically stained for smooth muscle actin.

2,5-diCl-PPD (g) and 2,6-diCl-PPD (h).



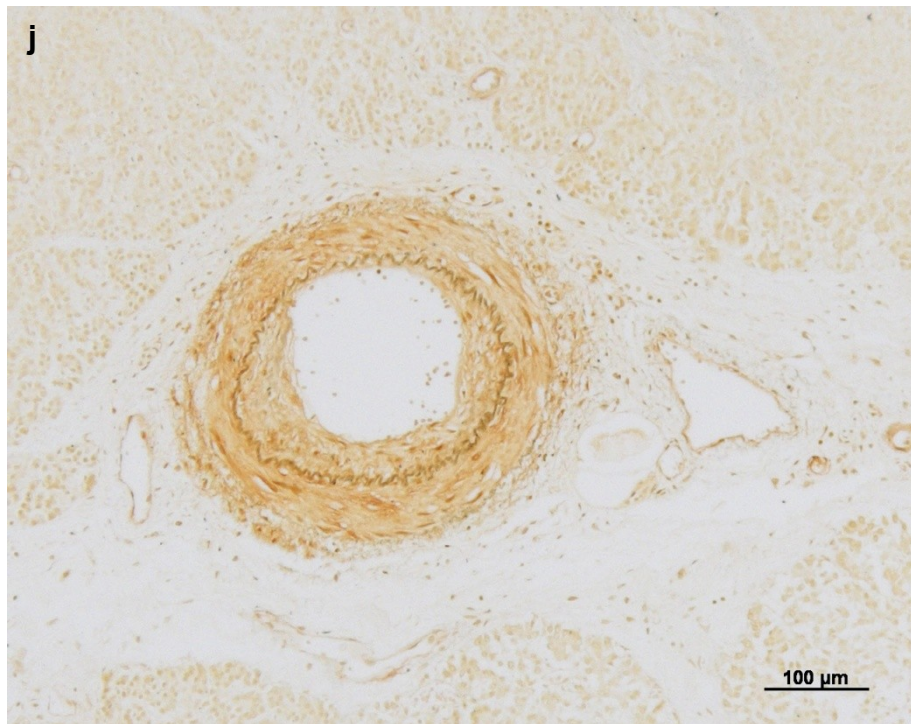
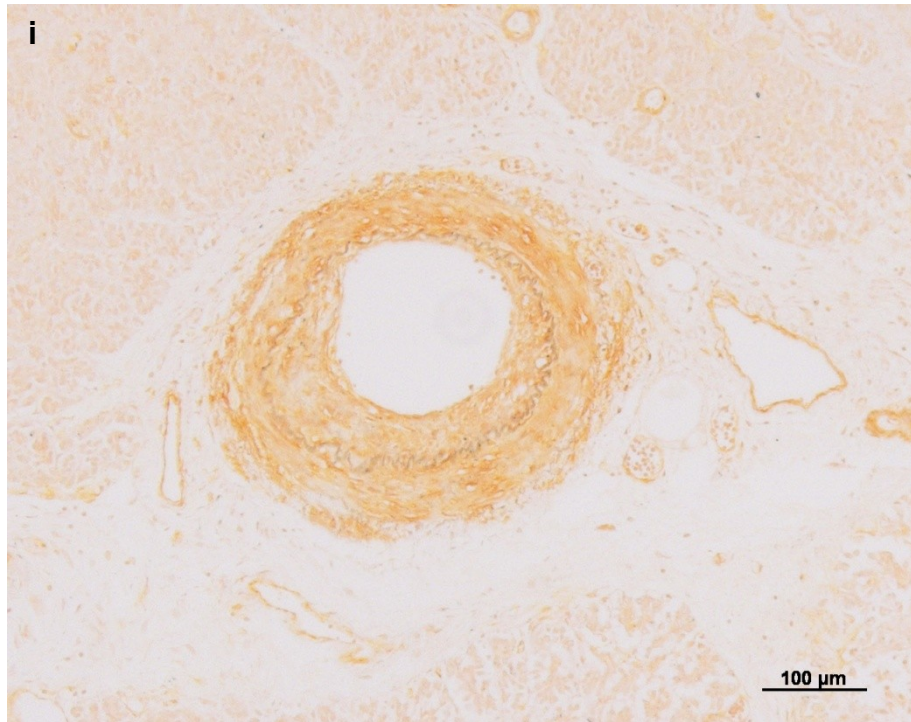


Figure 5.5 (continued). 4 μm thick sections of paraffin wax-embedded pancreas.

Blood vessel immunohistochemically stained for smooth muscle actin.

4,5-diCl-OPD (i) and 4-Br-OPD (j).

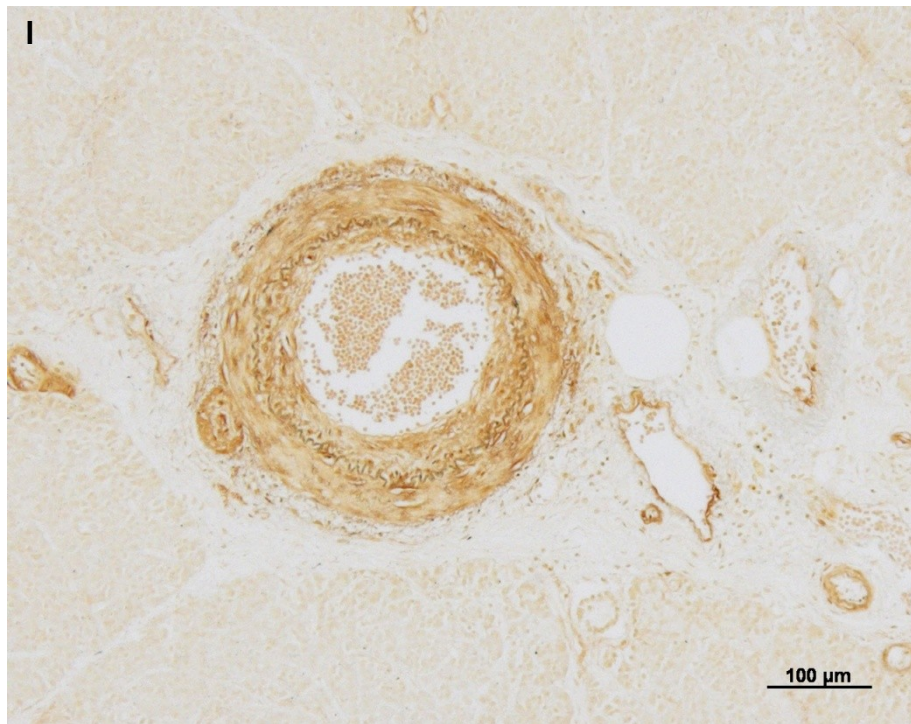
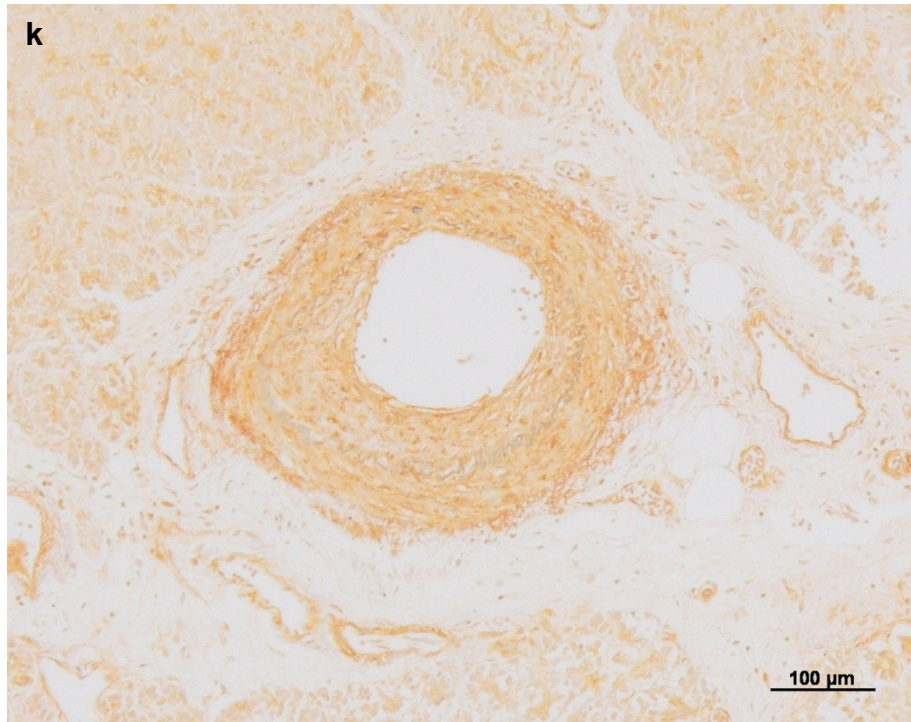


Figure 5.5 (continued). 4 μm thick sections of paraffin wax-embedded pancreas.

Blood vessel immunohistochemically stained for SMA.

4,5-diBr-OPD (k) and 4-I-OPD (l).



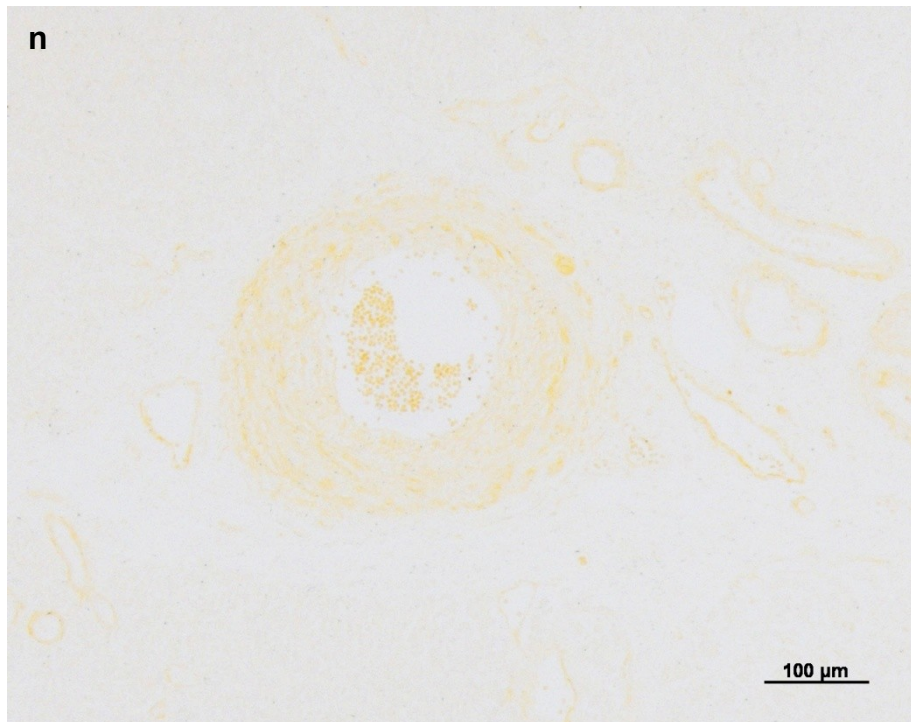
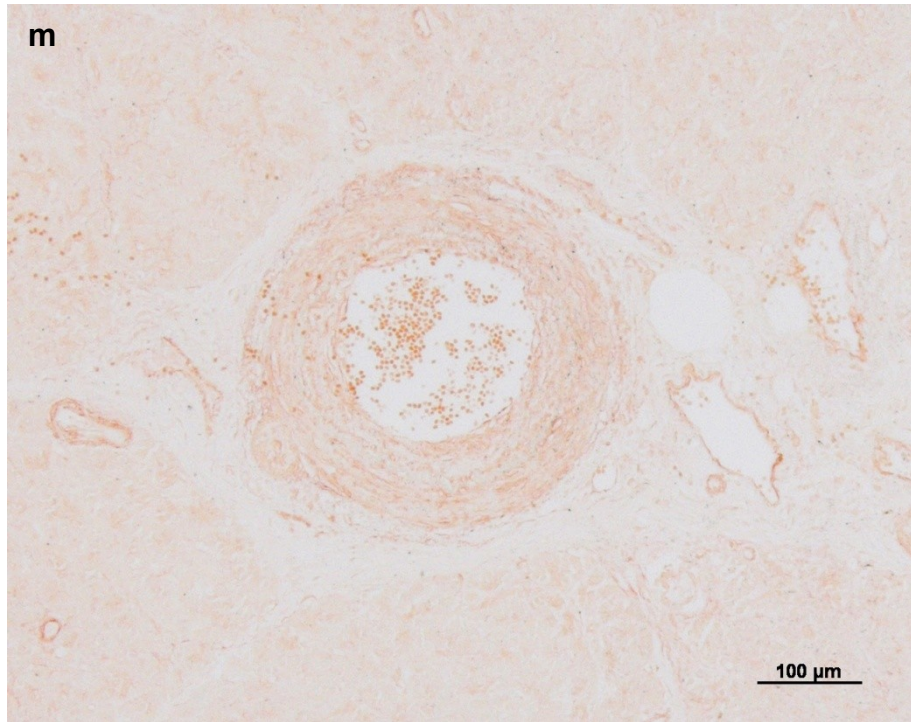


Figure 5.5 (continued). 4 μm thick sections of paraffin wax-embedded pancreas.

Blood vessel immunohistochemically stained for SMA.

4,5-diI-OPD (m) and F6 (n).

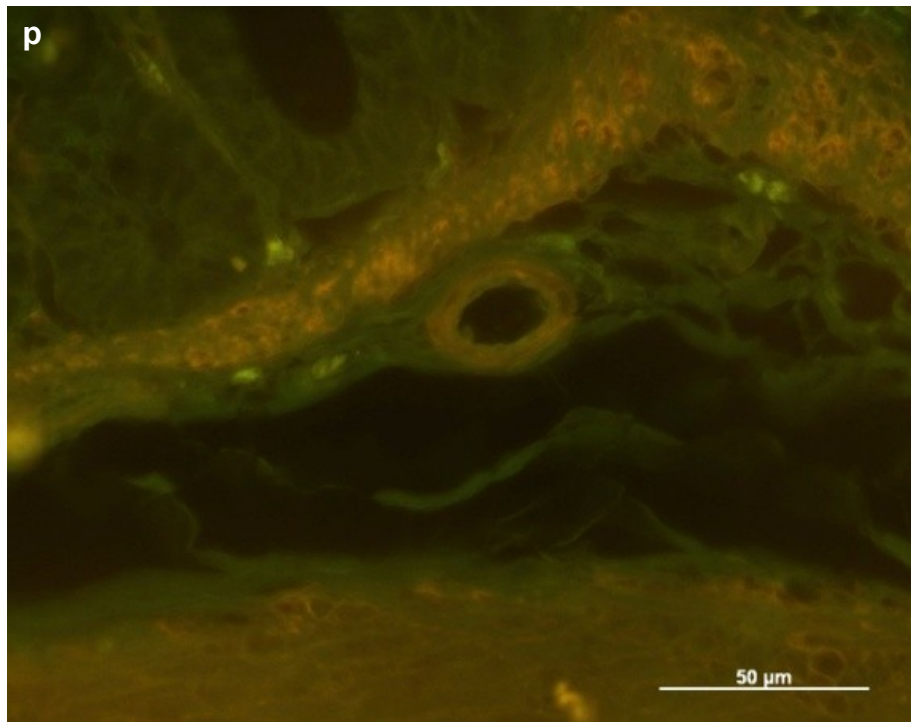
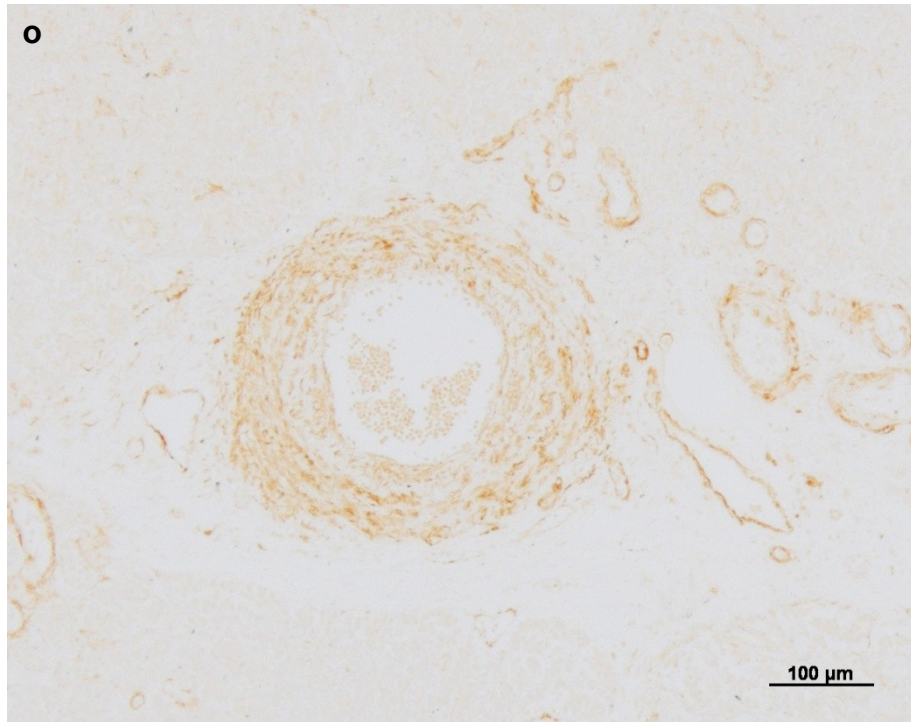


Figure 5.5 (continued). 4  $\mu\text{m}$  thick section of paraffin wax-embedded pancreas.

Blood vessel immunohistochemically stained for SMA. DAB (o) and F6 fluorescence in 4  $\mu\text{m}$  thick section of paraffin wax-embedded colon. Blood vessel immunohistochemically stained for SMA (p).

#### 5.4.2.2 Analytical Scanning Electron Microscopy

Preliminary elemental mapping of pancreatic blood vessels on Thermanox cover slips took 595 seconds. Total beam dwell-time on the samples was 295 seconds, but acquisition time was considerably extended due to the long signal processing time.

In agreement with the result from the dot blot model system, F6 did not generate any observable back-scattered signal but, in contrast to the high concentration of fluorine that was detected in the dot blot, F6 in immunohistochemically stained blood vessel (figure 5.6a) produced only a poor signal in the tissue model, which could only just be discerned against the relatively high background noise (figure 5.6b).

Of the four chlorinated compounds that produced detectable levels of chlorine in the dot blot model, three (4-Cl-OPD, 2,5-diCl-PPD and 2,6-diCl-PPD) could not be detected by BSI and were either undetectable (4-Cl-OPD (figures 5.6c and d)), or only just demonstrable by elemental mapping (figures 5.6e to h respectively). In contrast, the blood vessel that was developed with 4,5-diCl-OPD (figure 5.6i) could just be seen by BSI (figure 5.6j) and was clearly detectable by elemental mapping (5.6k). Furthermore, the polymer was still detectable when the number of accumulated frames was reduced to 1 (figure 5.6l), when the pixel dwell-time was reduced to 100 ms with 5 accumulated frames (figure 5.6m) and just detectable with 1 frame (figure 5.6n).

Both 4-Br-OPD and 4,5-diBr-OPD produced polymers that could be clearly seen by BSI and elemental mapping. In the case of 4-Br-OPD, immunohistochemical staining could be seen as bright areas in the secondary electron (SE) image (figure 5.7a). The back-scattered electron (BSI) signal (figure

5.7b) was much more easily seen than was the case for the dot blot but the X-ray signal, like that of the dot blot, was not particularly strong (figure 5.7c), but improved when the signal was accumulated over 10 frames (figure 5.7d), although this extended total acquisition time to 1187 seconds. The SE image of 4,5-diBr-OPD did not display the same bright specific staining that was seen with its monohalogenated analogue (figure 5.7e) even though the BSE signal, like that seen with the dot blots, was dramatically brighter (figure 5.7f). Similarly, the X-ray signal was strong and the corresponding map showed clear localisation of stain with little background noise (figure 5.6g) and could still be detected when the frame number was reduced to 1, or pixel dwell-time reduced to 100  $\mu$ s with accumulation over 5 frames (figure 5.6h), but not 1 frame.

In contrast to the brominated compounds, the iodinated analogues, while producing bright BSIs, gave rather poor X-ray signals. 4-iodo-OPD could not be seen in the SE image (figure 5.6i) but produced very good contrast in the BSI (figure 5.6j). The X-ray signal strength, like that of its brominated analogue, was not very strong (figure 5.6k) but was, again, improved by extending the number of accumulated frames to 10 (5.6l). Similar results were seen with 4,5-diI-OPD, where no staining could be seen in the SE image (figure 5.6m), but the BSI had higher contrast (figure 5.6n) and a stronger X-ray signal was produced (figure 5.6o) that improved slightly when frame accumulation was increased to 10 (figure 5.6p). In both cases, background noise was problematic.



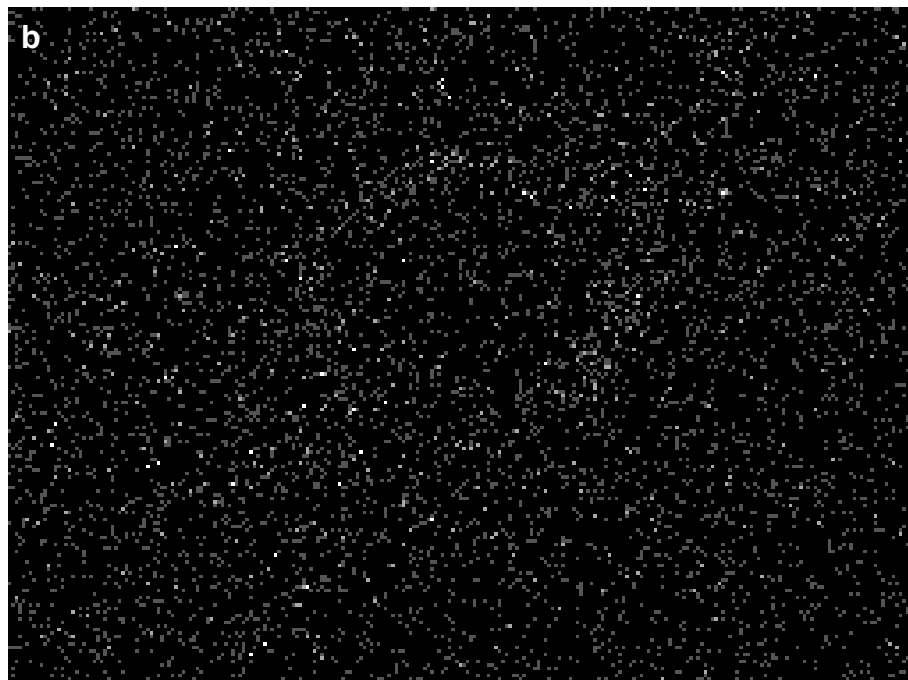
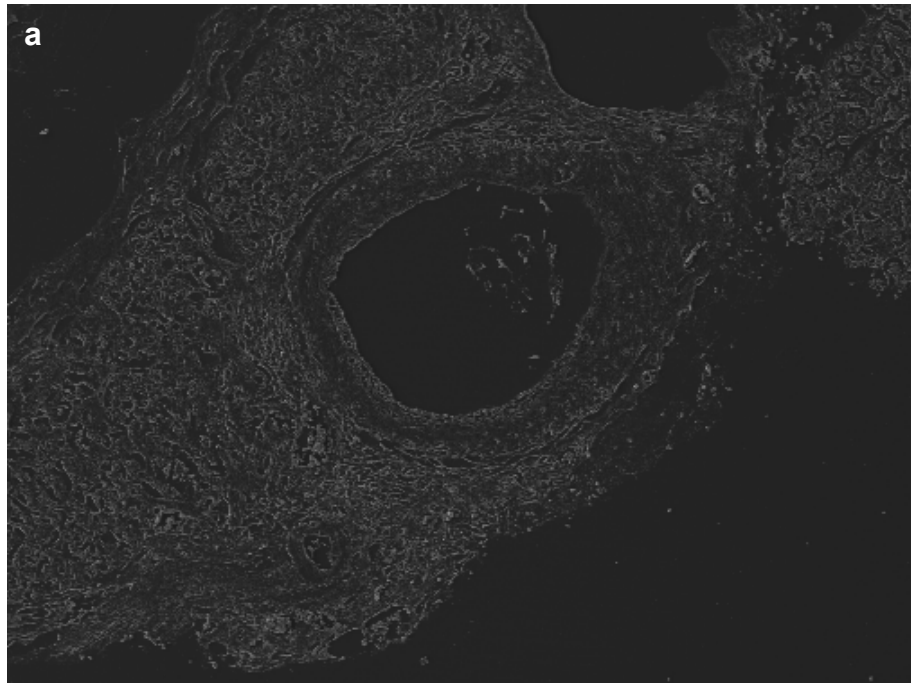


Figure 5.6. Secondary electron (a) and corresponding elemental map (b) of 4  $\mu\text{m}$  thick section of paraffin wax-embedded pancreatic blood vessels immunohistochemically stained for SMA and developed with F6.

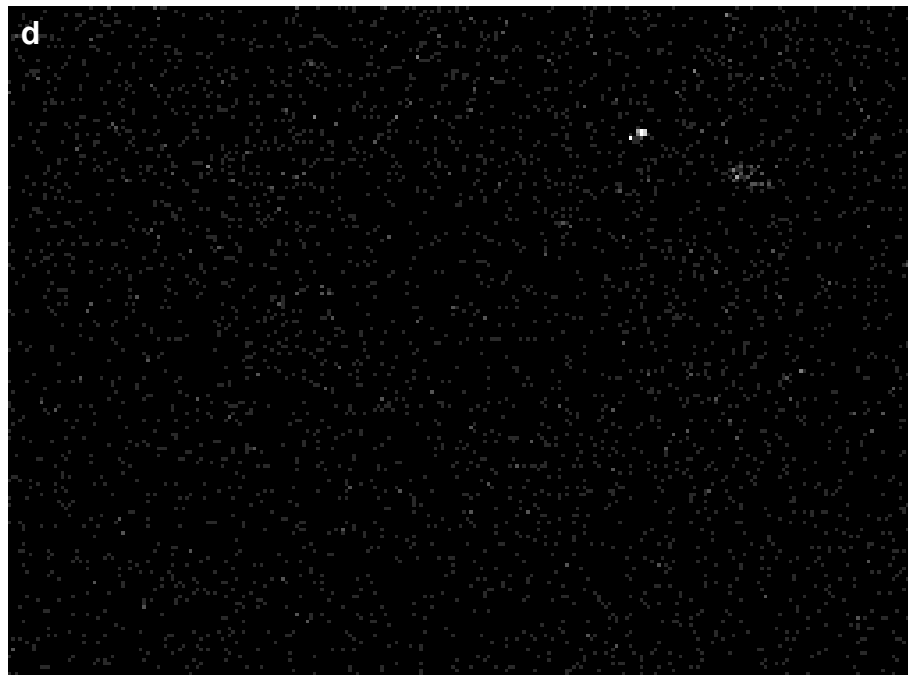
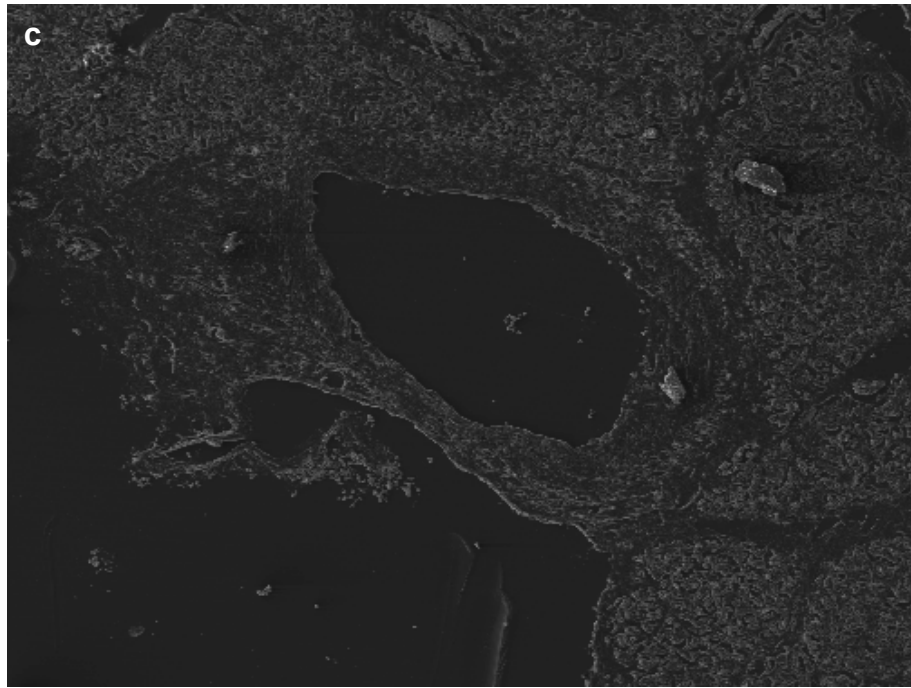


Figure 5.6 (continued). Secondary electron image (c) and corresponding elemental map (d) of 4  $\mu\text{m}$  thick section of paraffin wax-embedded pancreatic blood vessels immunohistochemically stained for SMA and developed with 4-Cl-OPD.

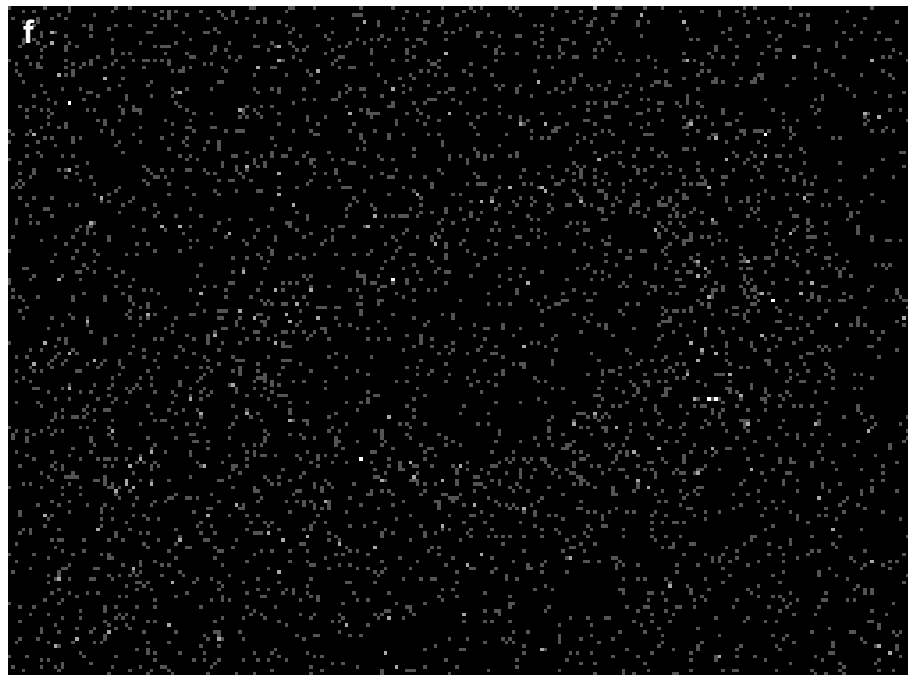
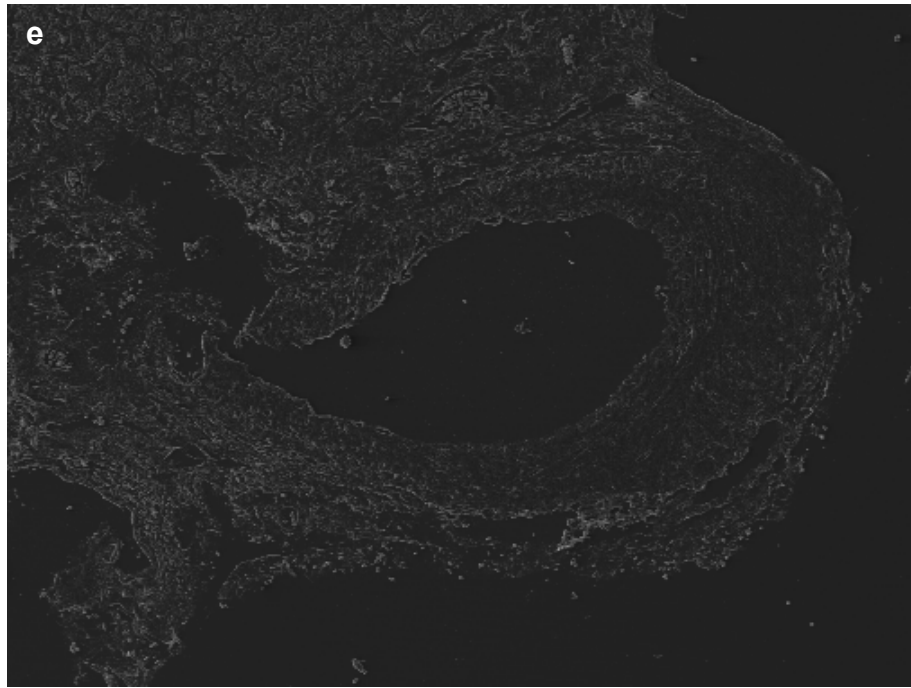


Figure 5.6 (continued). Secondary electron image (e) and corresponding elemental map (f) of 4  $\mu\text{m}$  thick section of paraffin wax-embedded pancreatic blood vessels immunohistochemically stained for SMA and developed with 2,5-diCl-OPD.

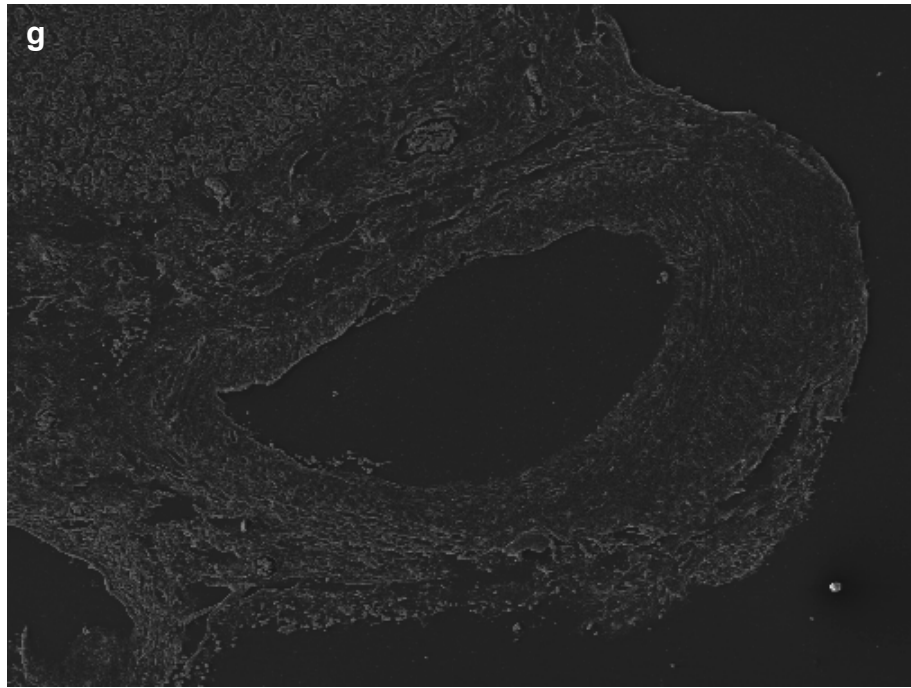


Figure 5.6 (continued). Secondary electron image (g) and corresponding elemental map (h) of 4  $\mu\text{m}$  thick section of paraffin wax-embedded pancreatic blood vessels immunohistochemically stained for SMA and developed with 2,6-diCl-OPD.

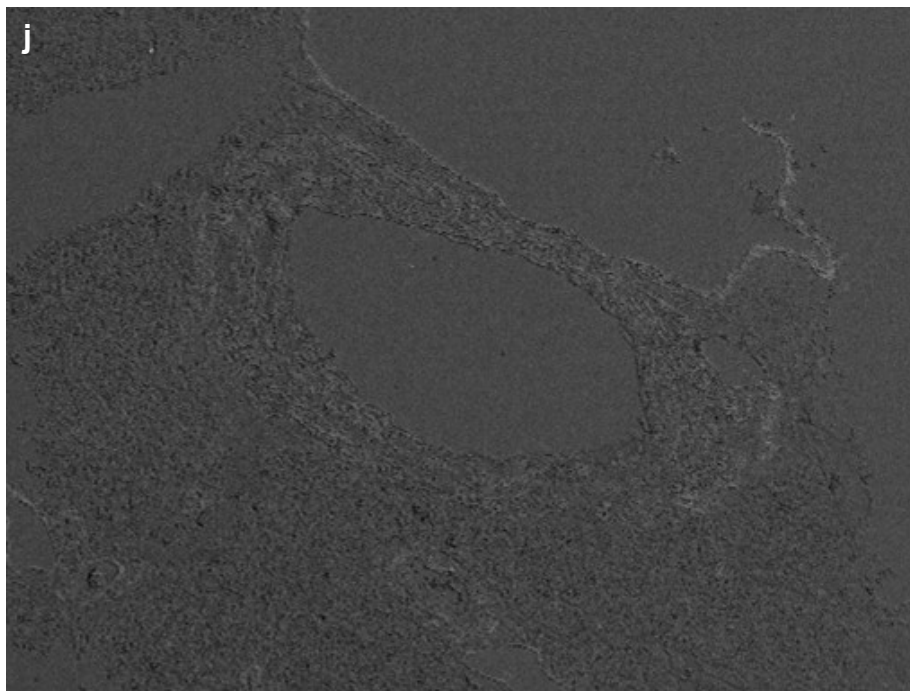
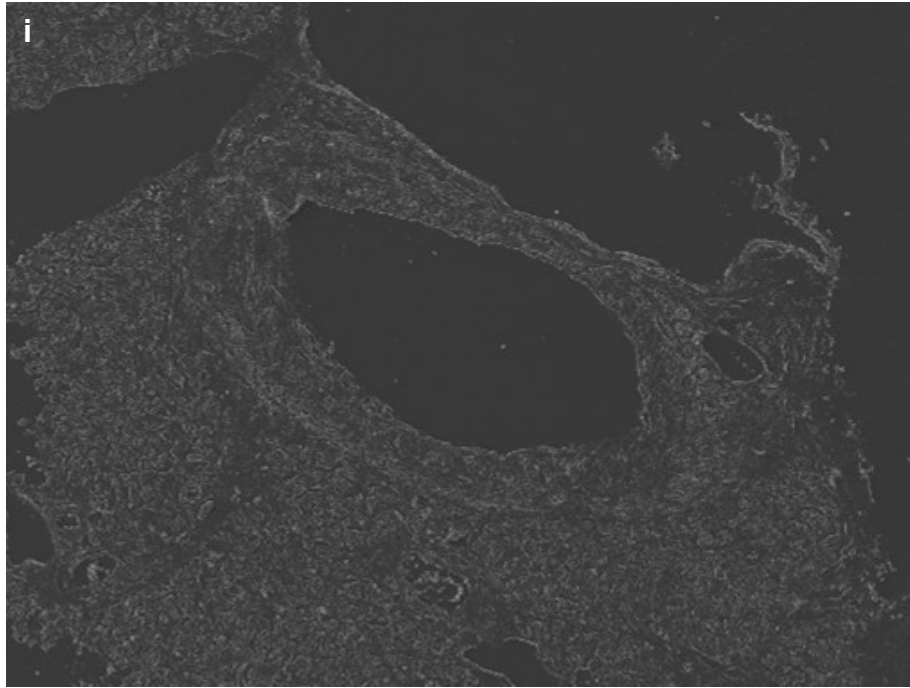


Figure 5.6 (continued). Secondary electron (i) and back-scattered electron (j) images of 4  $\mu\text{m}$  thick section of paraffin wax-embedded pancreatic blood vessels immunohistochemically stained for SMA and developed with 4,5-dichloro-OPD.

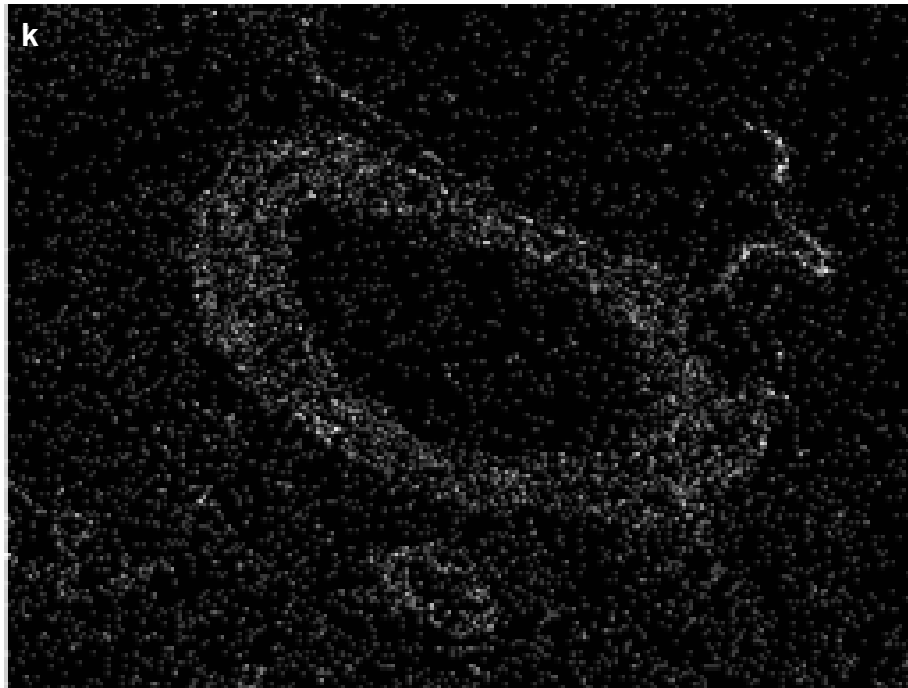


Figure 5.6 (continued). Elemental maps of 4  $\mu\text{m}$  thick section of paraffin wax-embedded pancreatic blood vessels immunohistochemically stained for SMA and developed with 4,5-dichloro-OPD. Pixel dwell-times of 1200  $\mu\text{s}$  and either 5 frames (k) or 1 frame (l).

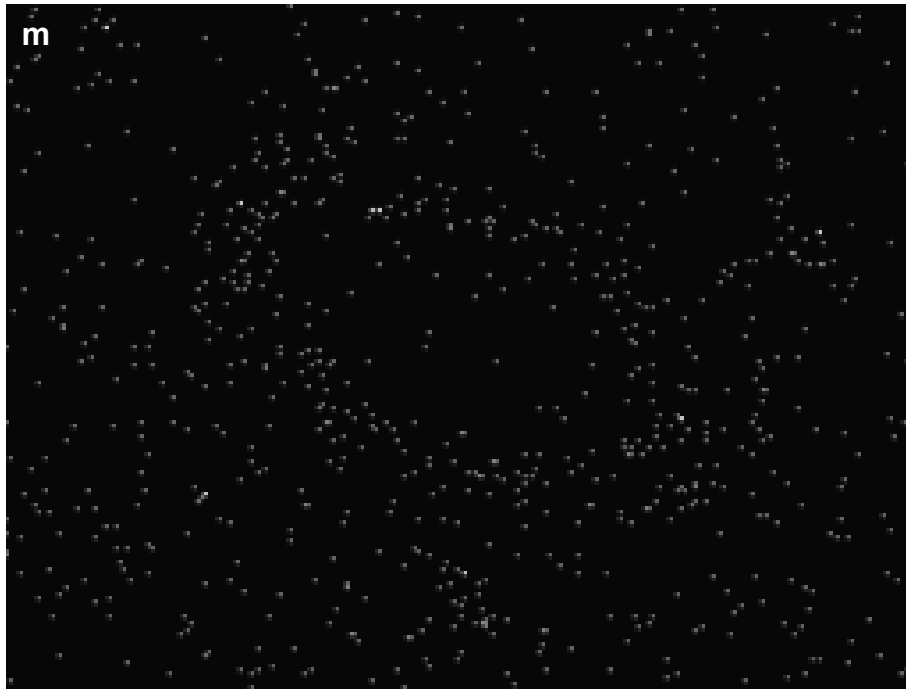


Figure 5.6 (continued). Elemental maps of 4  $\mu\text{m}$  thick section of paraffin wax-embedded pancreatic blood vessels immunohistochemically stained for SMA and developed with 4,5-dichloro-OPD. Pixel dwell-time of 100  $\mu\text{s}$  and either 5 frames (m) or 1 frame (n).

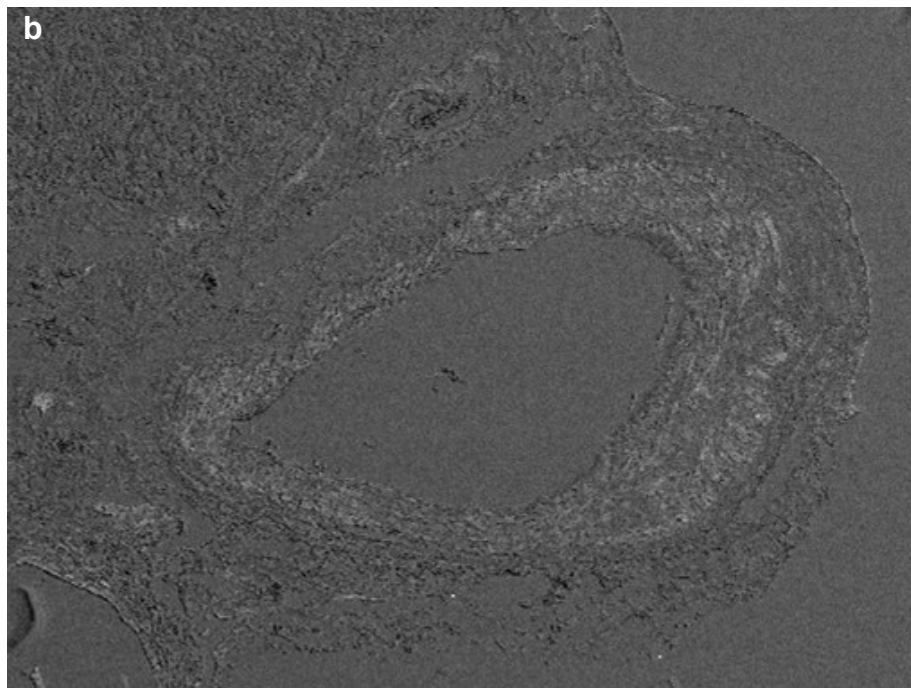
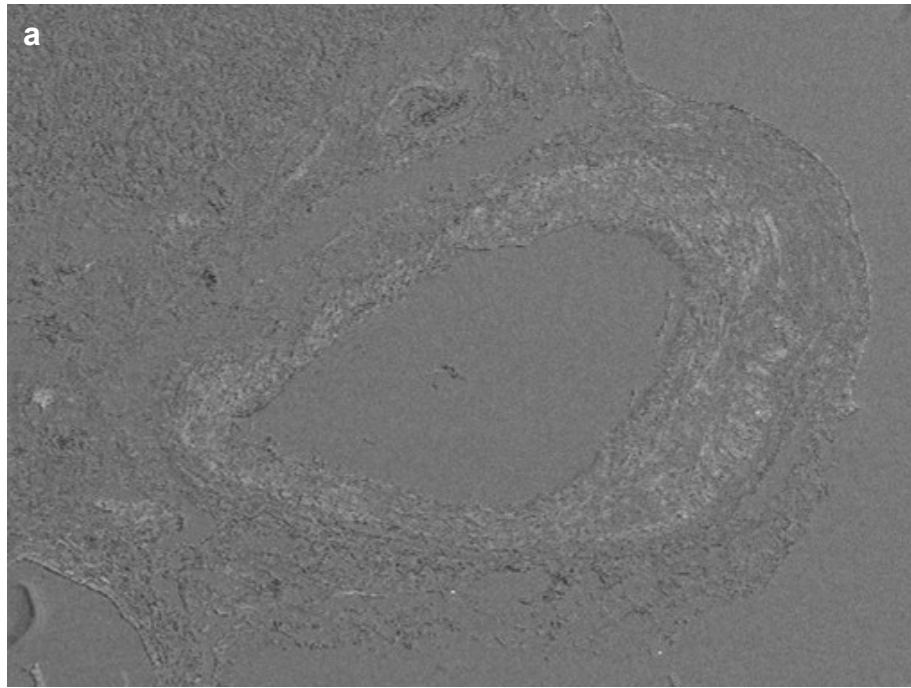


Figure 5.7. Secondary electron (a) and back-scattered electron (b) images of 4  $\mu\text{m}$  thick section of paraffin wax-embedded pancreatic blood vessels immunohistochemically stained for SMA and developed with 4-Br-OPD.



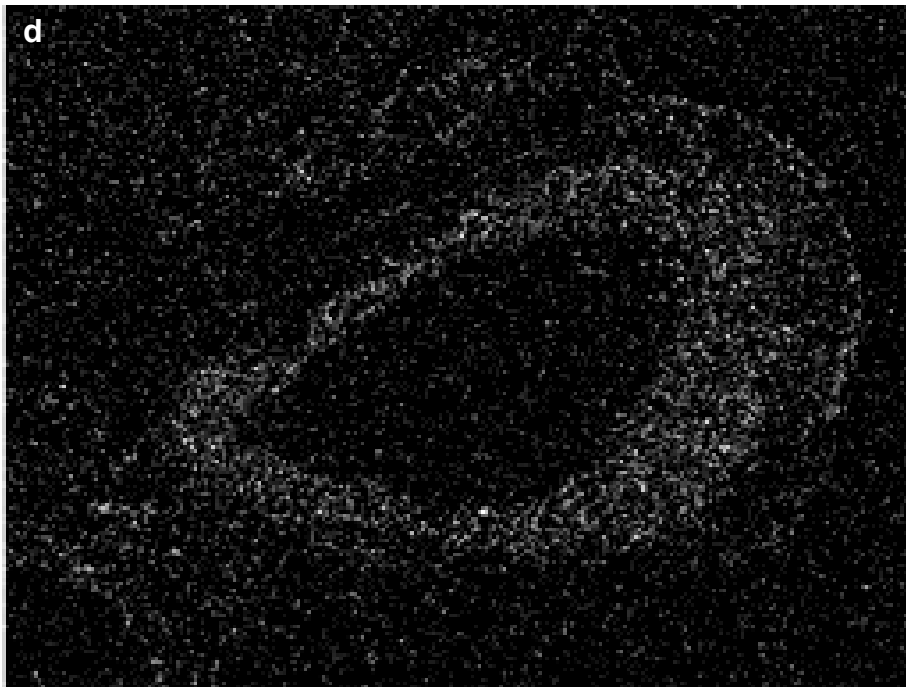
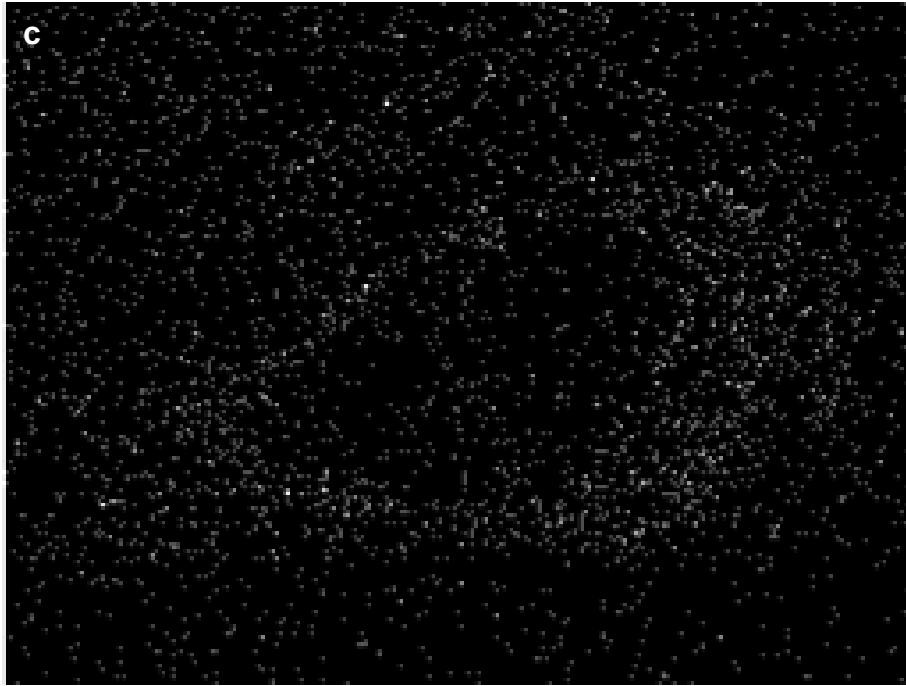


Figure 5.7 (continued). 4  $\mu\text{m}$  thick section of paraffin wax-embedded pancreatic blood vessels immunohistochemically stained for SMA and developed with 4-Br-OPD. Elemental maps with accumulation over either 5 (c) or 10 frames (d).

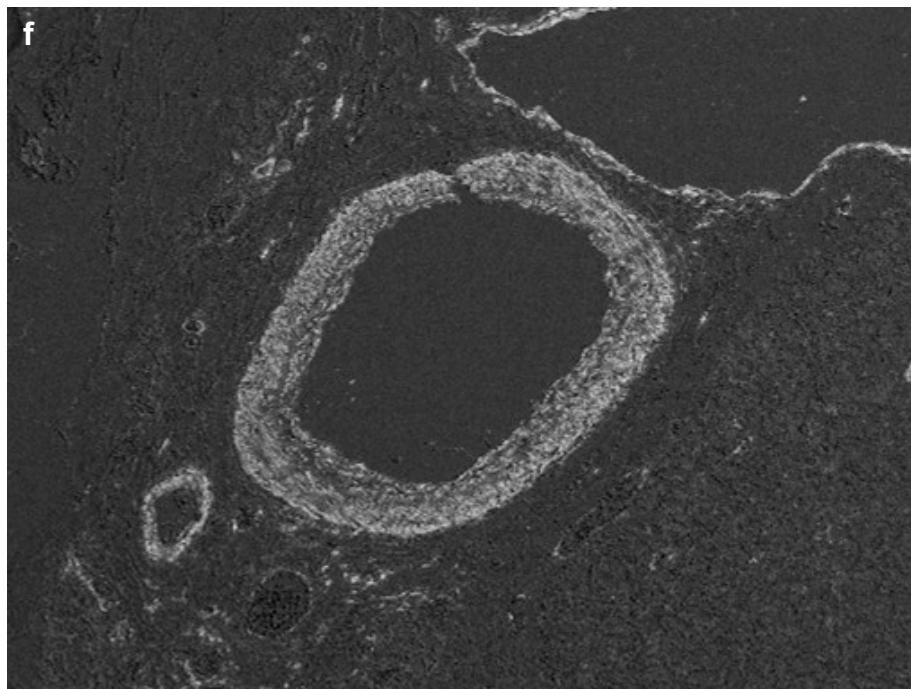
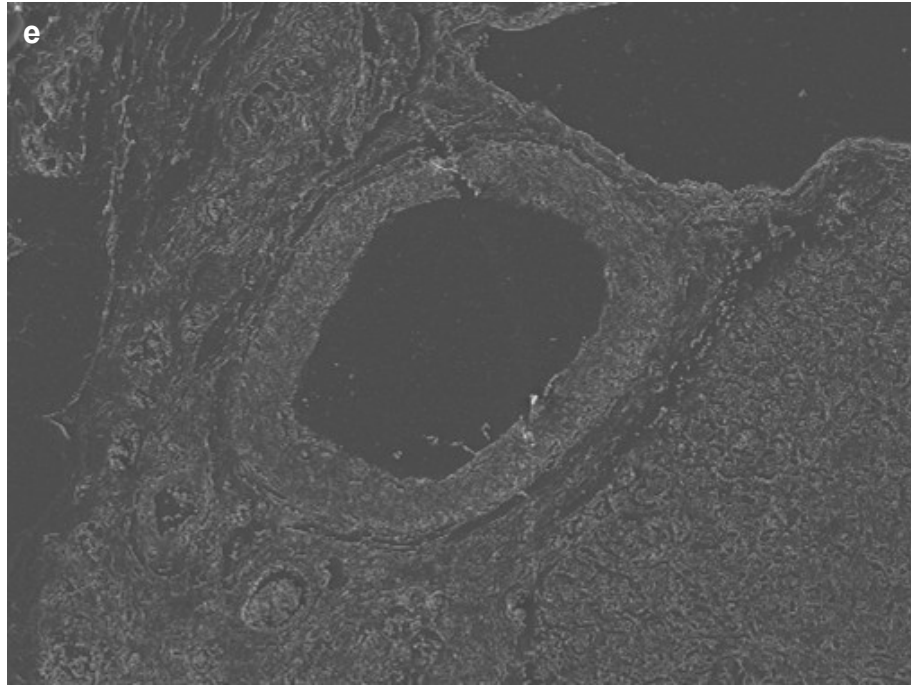


Figure 5.7 (continued). Secondary electron (e) and back-scattered electron (f) images of 4  $\mu\text{m}$  thick section of paraffin wax-embedded pancreatic blood vessels immunohistochemically stained for SMA and developed with 4,5-diBr-OPD.

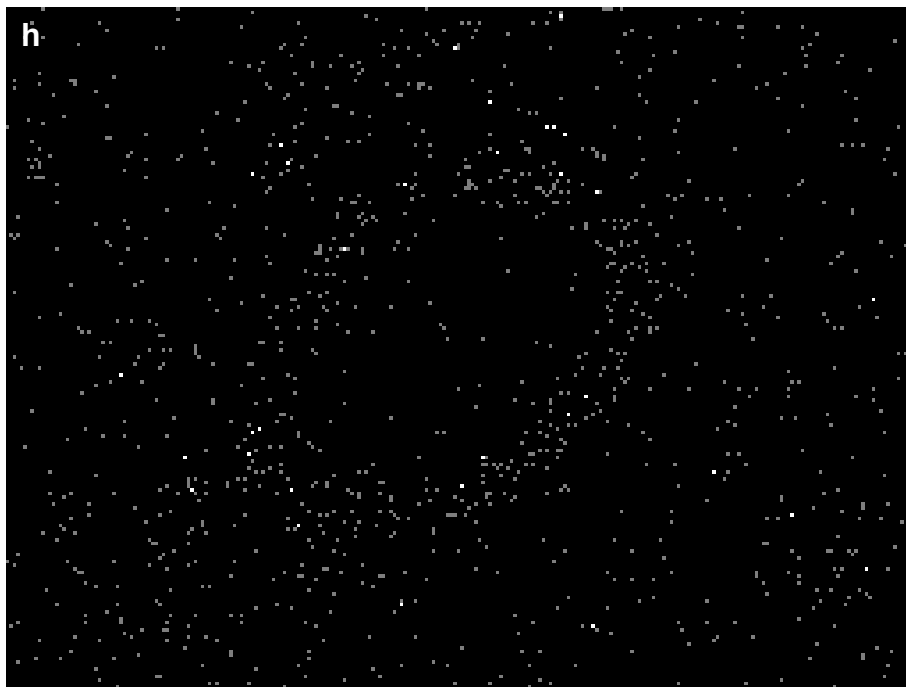
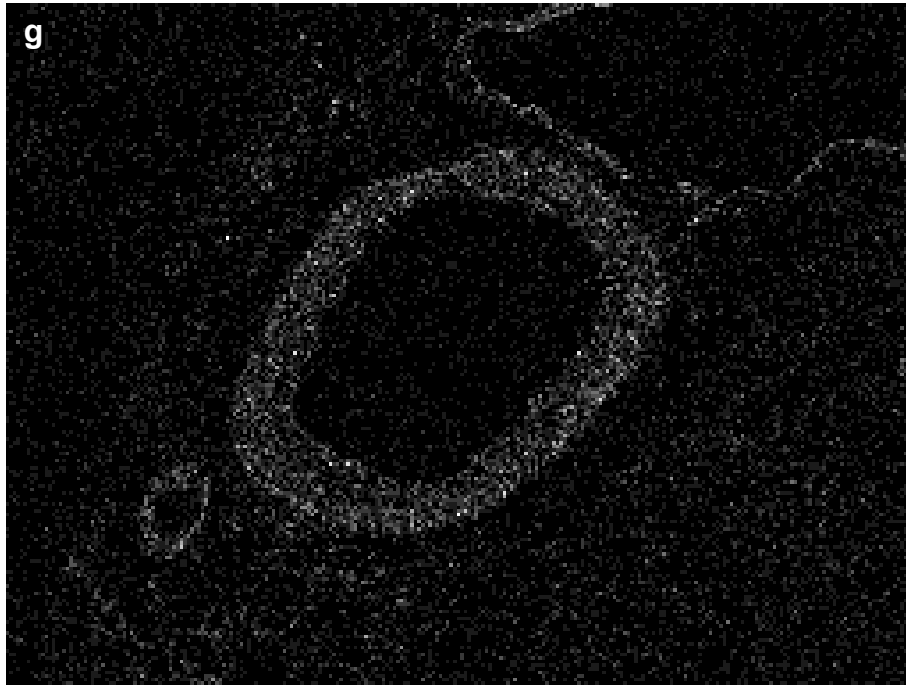


Figure 5.7 (continued). 4  $\mu\text{m}$  thick section of paraffin wax-embedded pancreatic blood vessels immunohistochemically stained for SMA and developed with 4,5-diBr-OPD. Elemental maps accumulated over 5 frames with pixel dwell-times of either 1200  $\mu\text{s}$  (g) or 100  $\mu\text{s}$  (h).

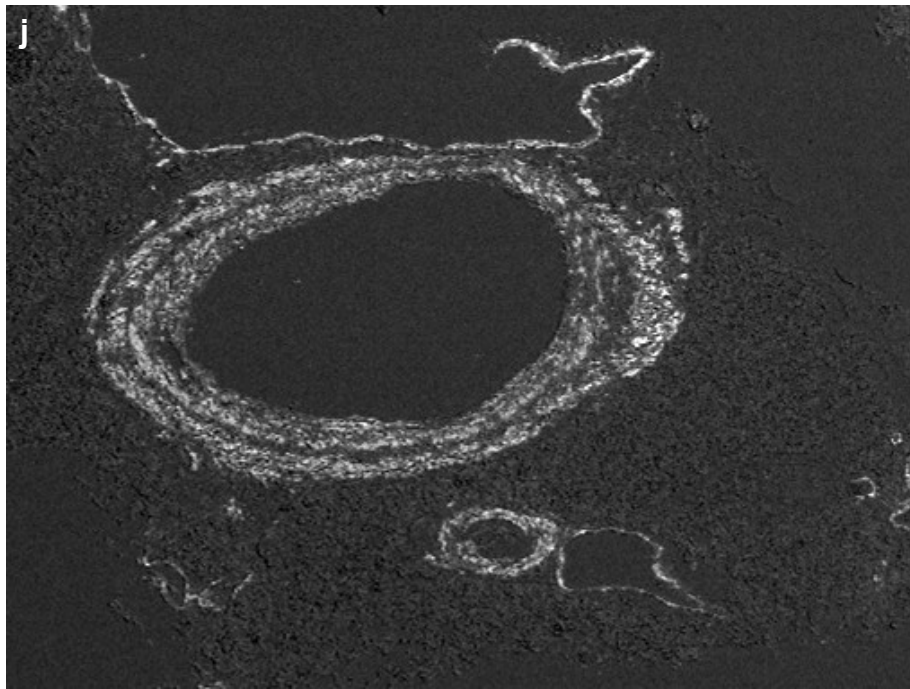
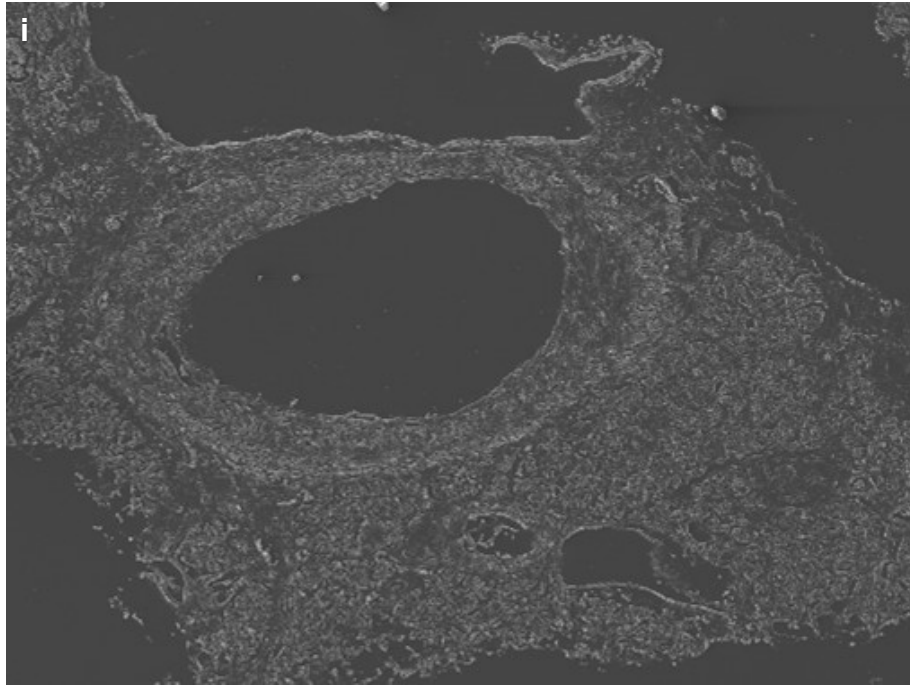


Figure 5.7 (continued). Secondary electron (i) and back-scattered electron (j) images of 4  $\mu\text{m}$  thick section of paraffin wax-embedded pancreatic blood vessels immunohistochemically stained for SMA and developed with 4-I-OPD.

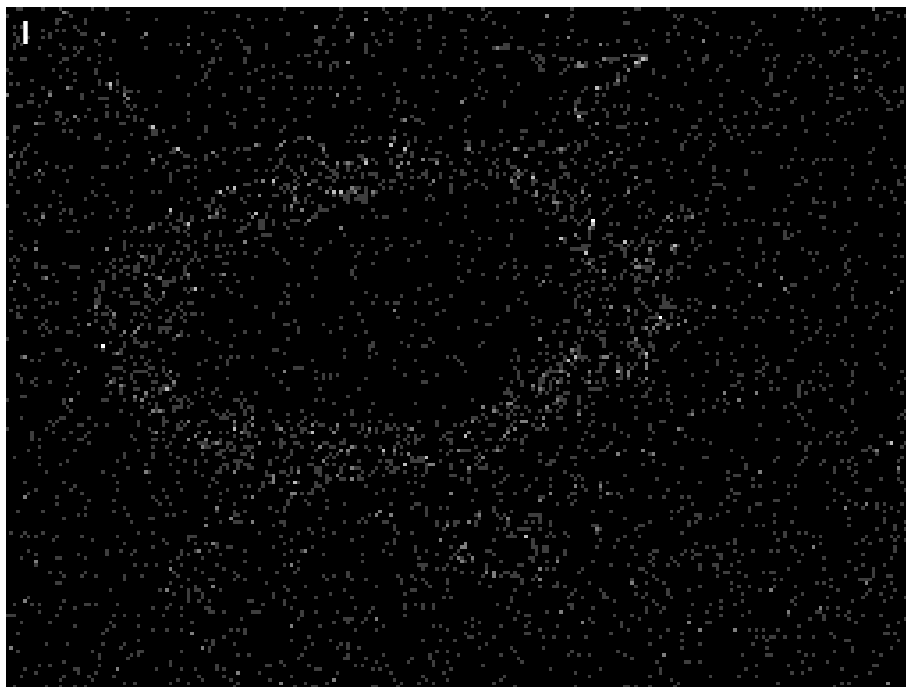
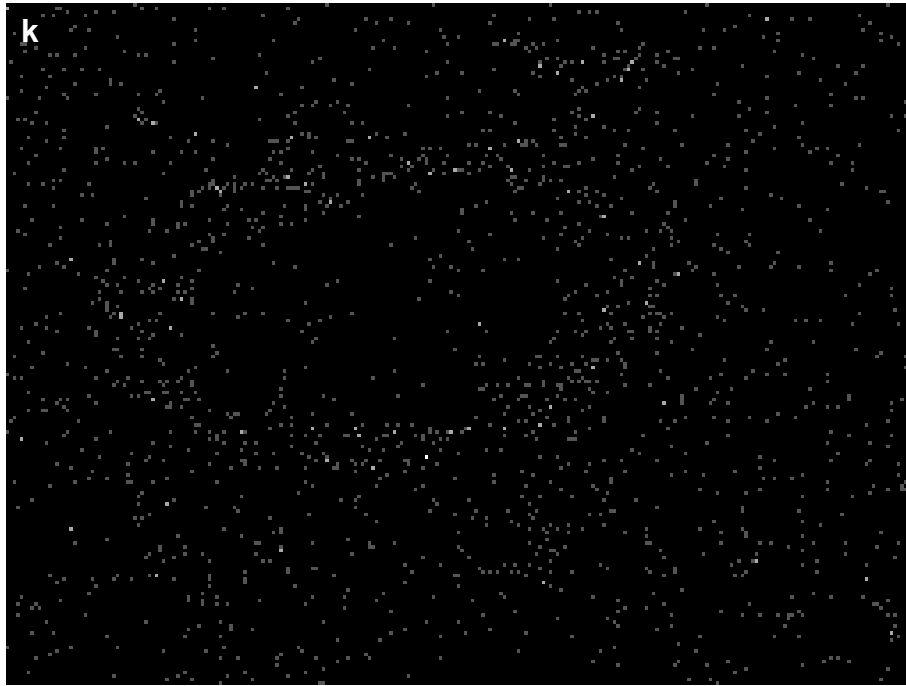


Figure 5.7 (continued). 4  $\mu\text{m}$  thick section of paraffin wax-embedded pancreatic blood vessels immunohistochemically stained for SMA and developed with 4-I-OPD. Elemental maps accumulated over 5 (k) or 10 (l) frames.

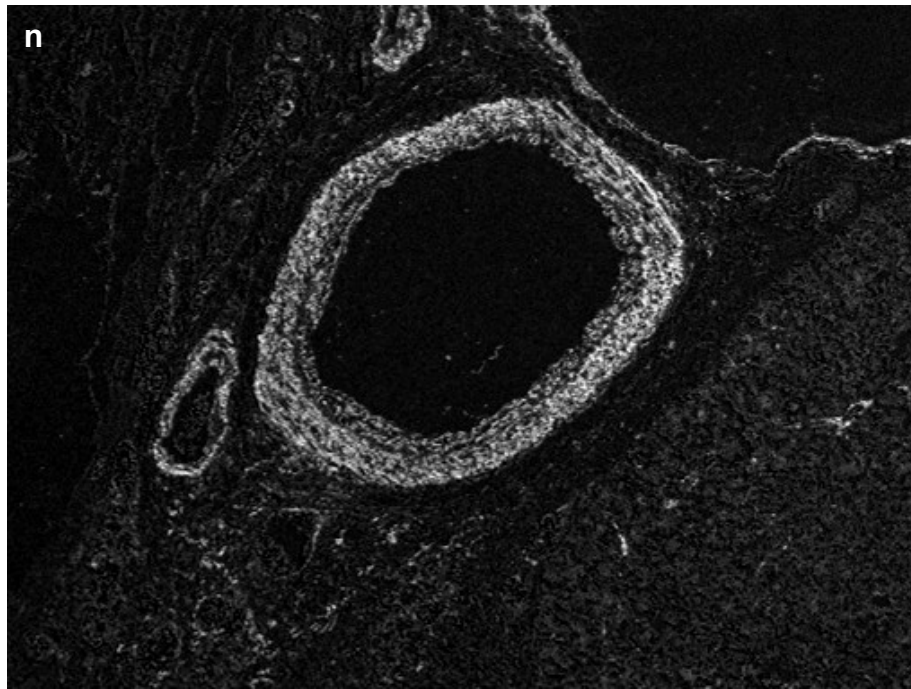
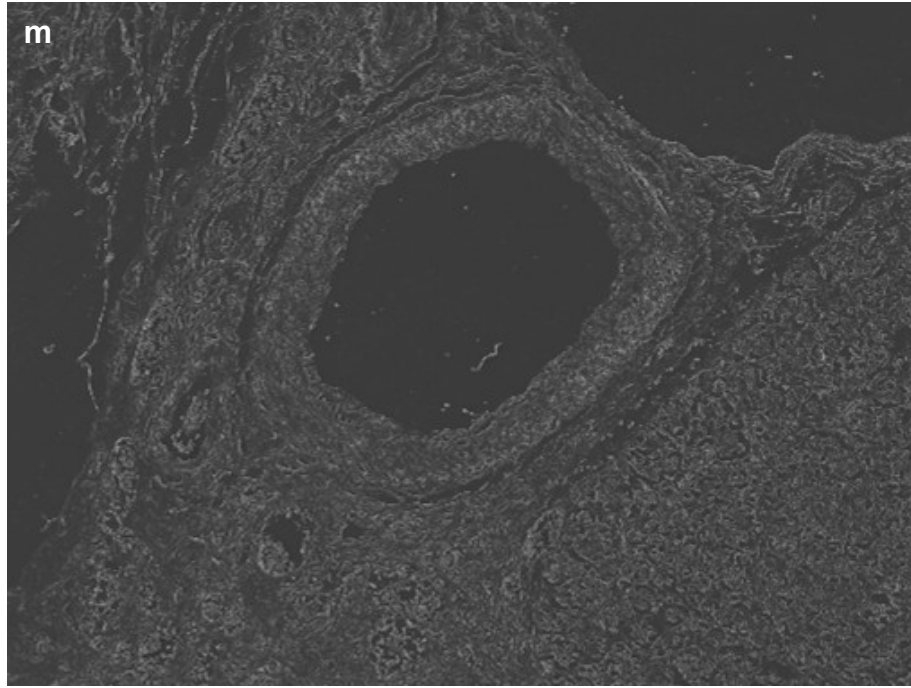


Figure 5.7 (continued). Secondary electron (m) and back-scattered electron (n) images of 4  $\mu\text{m}$  thick section of paraffin wax-embedded pancreatic blood vessels immunohistochemically stained for SMA and developed with 4,5-diI-OPD.

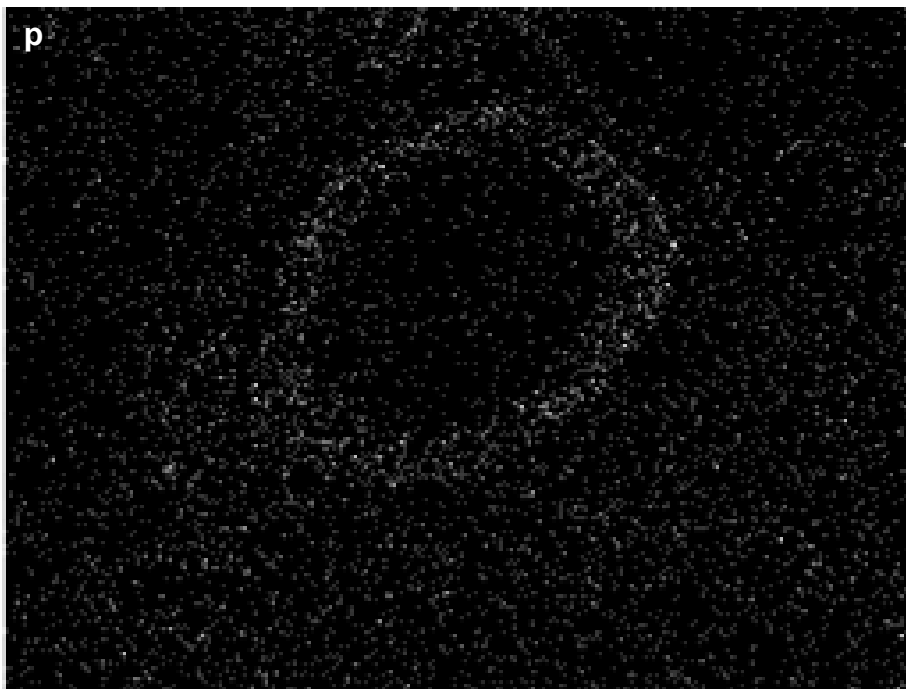
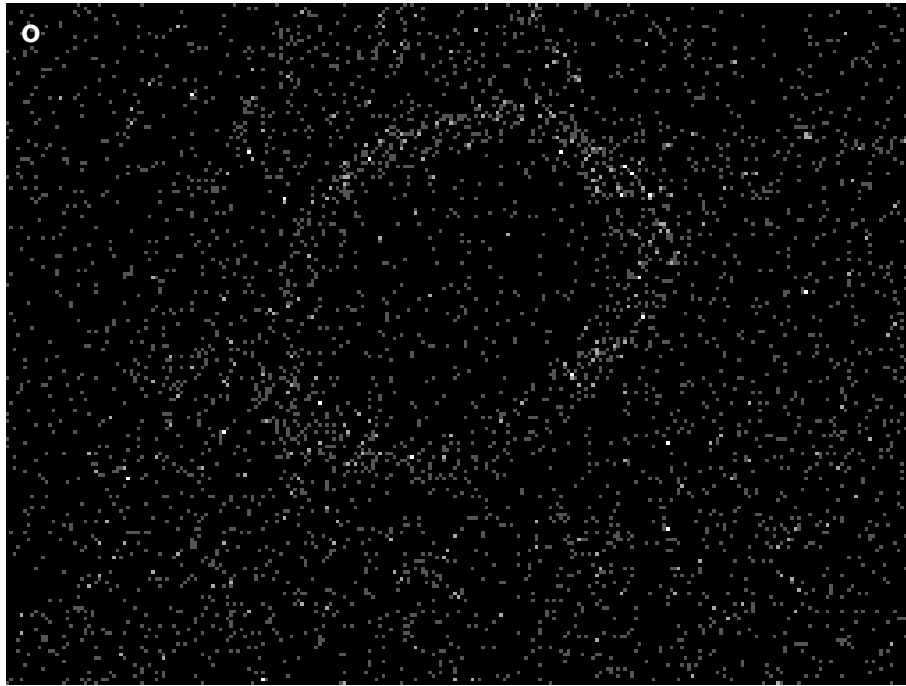


Figure 5.7 (continued). 4  $\mu\text{m}$  thick section of paraffin wax-embedded pancreatic blood vessels immunohistochemically stained for SMA and developed with 4,5-diI-OPD. Elemental maps accumulated over 5 (o) or 10 (p) frames.

### 5.4.2.3 Transmission Electron Microscopy

Preliminary examination of 4,5-diCl-OPD in the TEM on similarly stained LR White-embedded normal human peritoneal blood vessels revealed the resulting marker to be fibrillary in appearance. Where individual fibres could be clearly seen, e.g. in sparsely staining areas such as red blood cells, they were at least 2  $\mu\text{m}$  in length (figure 5.7a and b). When staining was repeated on pancreatic exocrine granules, using 4,5-diCl-OPD from a different supplier (Sigma), the morphology of the deposit was dramatically different, being more granular in appearance. In addition, numerous, randomly distributed pleomorphic deposits were also seen (figures 5.7c and d). No electron diffraction pattern was seen, suggesting that these deposits were not crystalline in nature.

4-Br-OPD produced a well localised finely granular deposit (figure 5.7e), but inherent electron opacity was revealed to be low in the absence of automatic gamma correction (figure 5.7f). In contrast, 4,5-diBr-OPD produced only a moderately well localised deposit (figure 5.7g), the appearance of which can reasonably be described as bizarre (figure 5.7h).

Staining with 4-I-OPD was localised, in that it occurred largely over the exocrine granule-rich areas of the cells (figure 5.7i), but deposits were large (400 – 600 nm diameter) and tended to coalesce. In addition, the high inherent electron opacity of these large granules obscured underlying structure (figure 5.7j). The appearance of 4,5-diI-OPD was close to that of an ideal marker in that it was finely granular, remained localised to the sites of immunopositivity, and was inherently electron opaque (figures 5.7k and l). Occasionally, pleomorphic deposits, similar to those seen with 4,5-diCl-OPD, were observed (figures 5.7m and n). Again, no electron diffraction pattern was noted, indicating a non-crystalline nature.



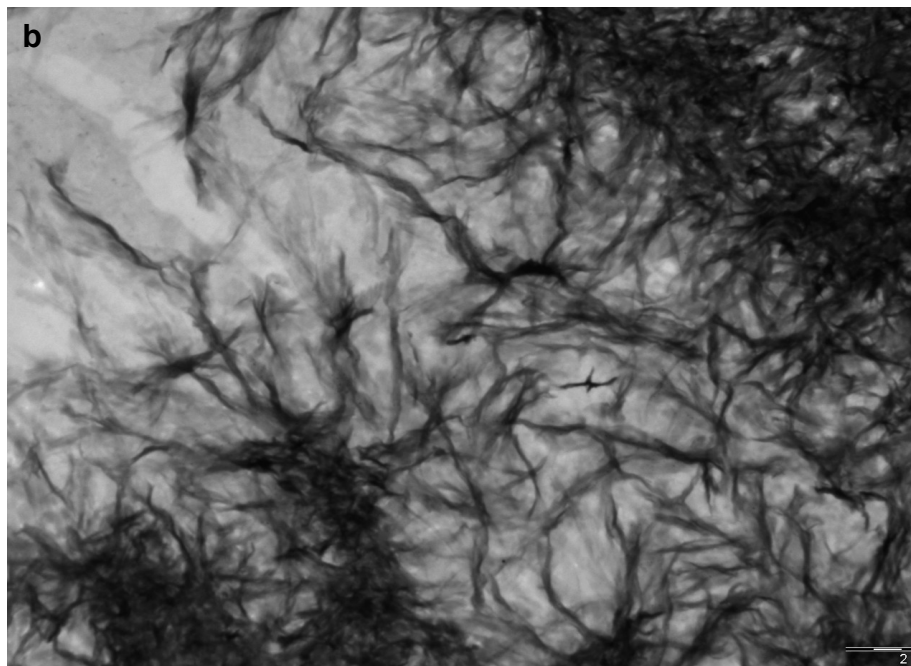
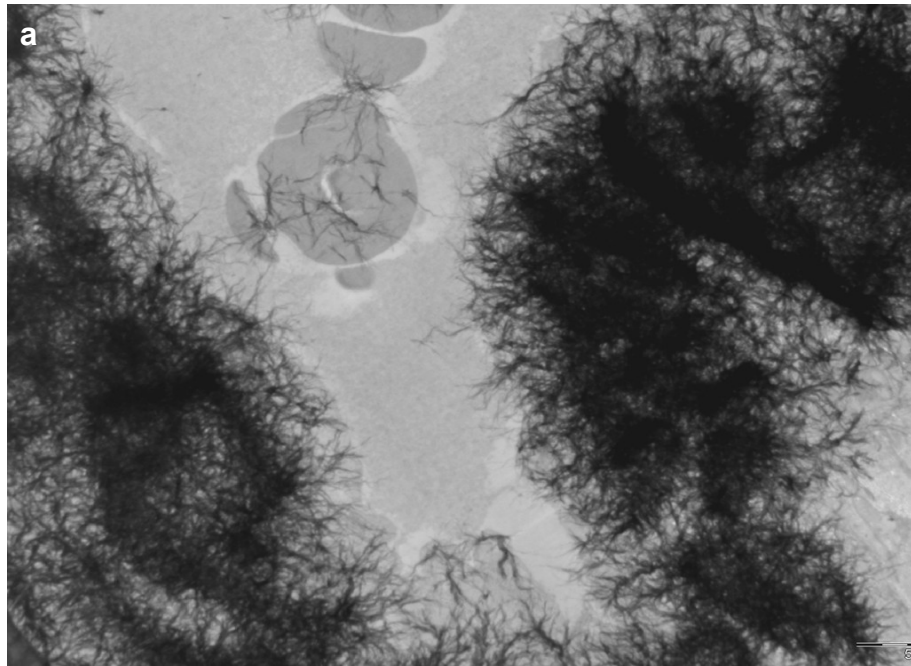


Figure 5.8. 80 nm thick section of LR White-embedded peritoneum. Blood vessel immunohistochemically stained for SMA. Polymerised 4,5-diCl-OPD, supplied by Acros, in preliminary studies (a and b).

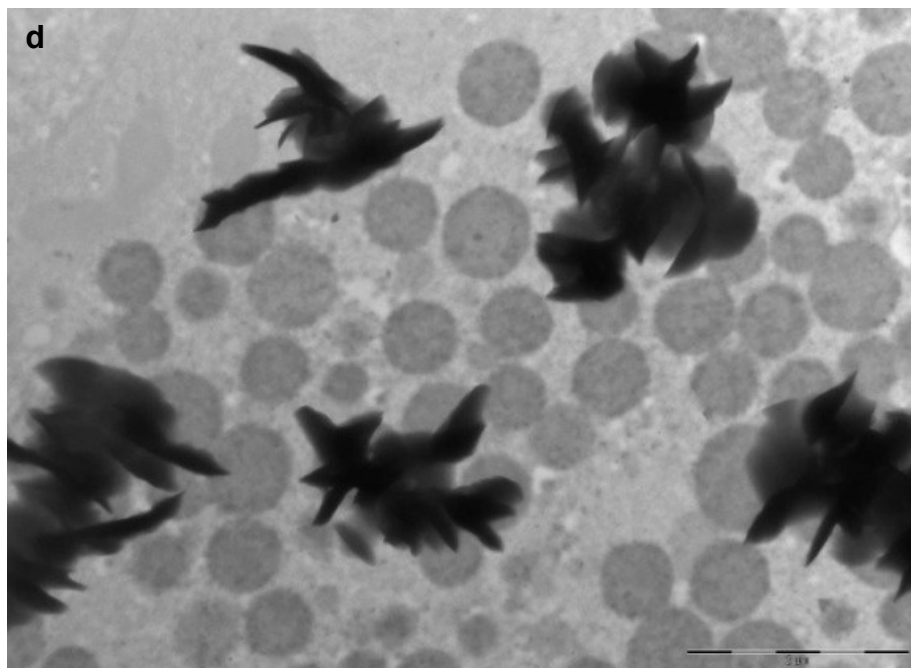
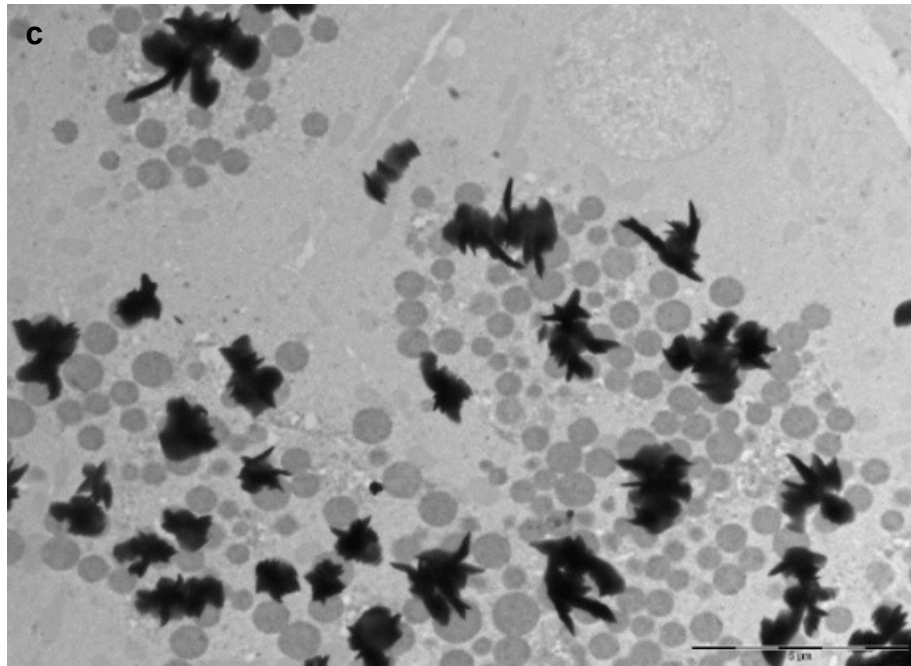


Figure 5.8 (continued). 80 nm thick sections of LR White-embedded rat pancreas. Exocrine granules immunohistochemically stained for  $\alpha$ -amylase. Polymerised 4,5-diCl-OPD, supplied by Sigma (c and d).

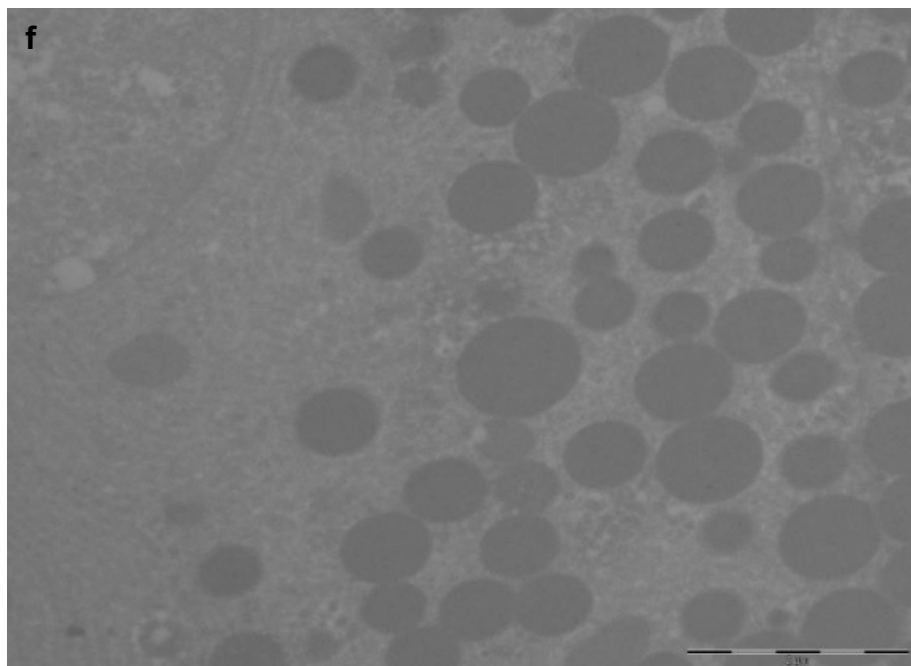
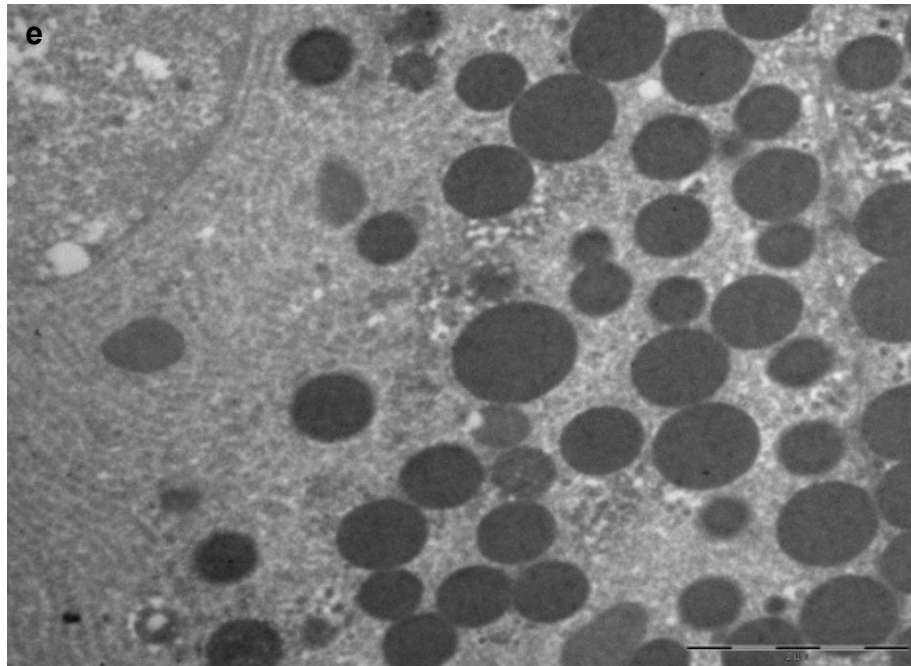


Figure 5.8 (continued). 80 nm thick sections of LR White-embedded rat pancreas. Exocrine granules immunohistochemically stained for  $\alpha$ -amylase. Polymerised 4-Br-OPD with automatic gamma-correction (e) and without (f).

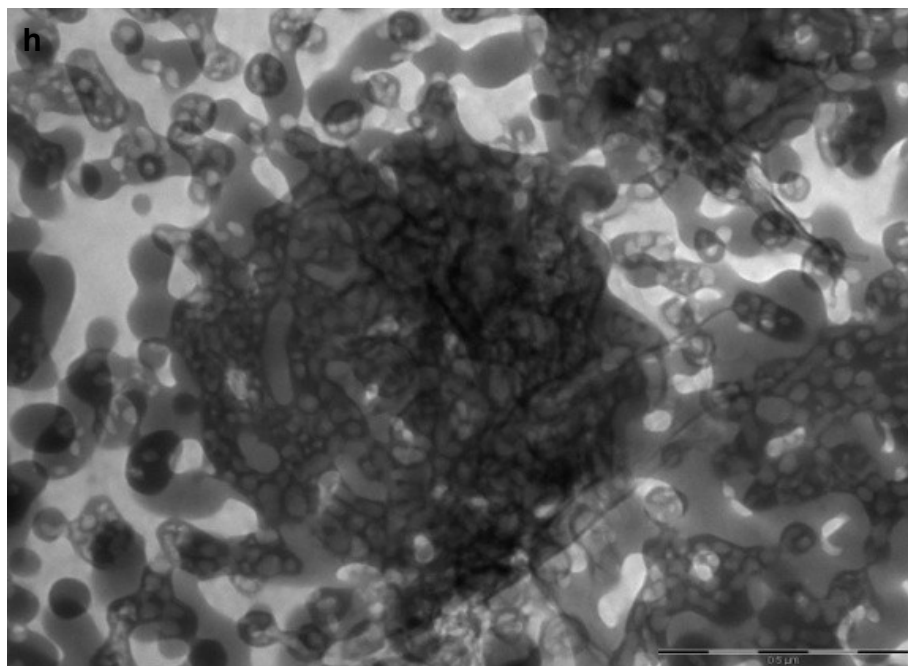
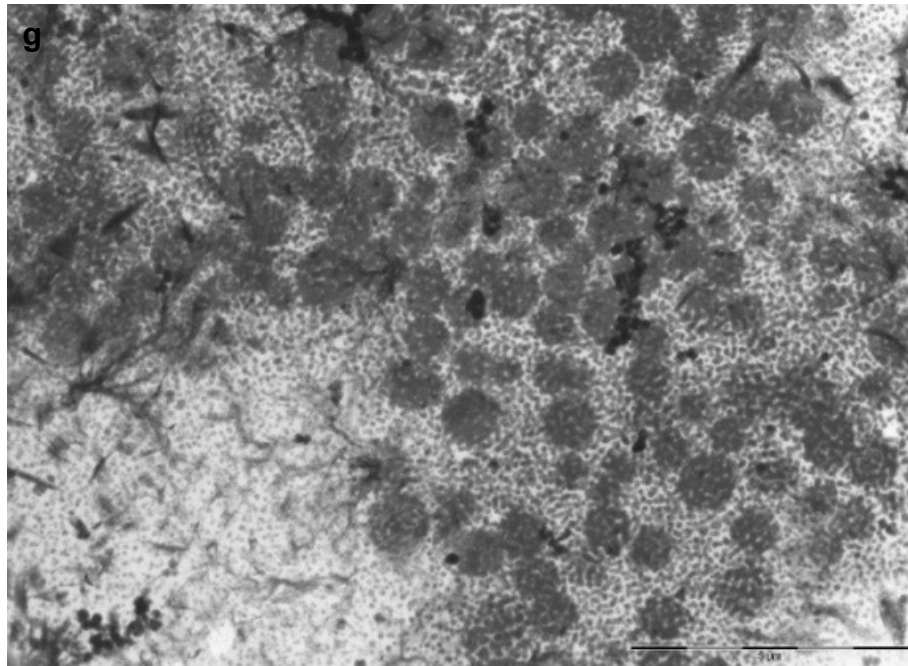


Figure 5.8 (continued). 80 nm thick sections of LR White-embedded rat pancreas. Exocrine granules immunohistochemically stained for  $\alpha$ -amylase. Polymerised 4,5-diBr-OPD at low (g) and high power (h), both without gamma correction.

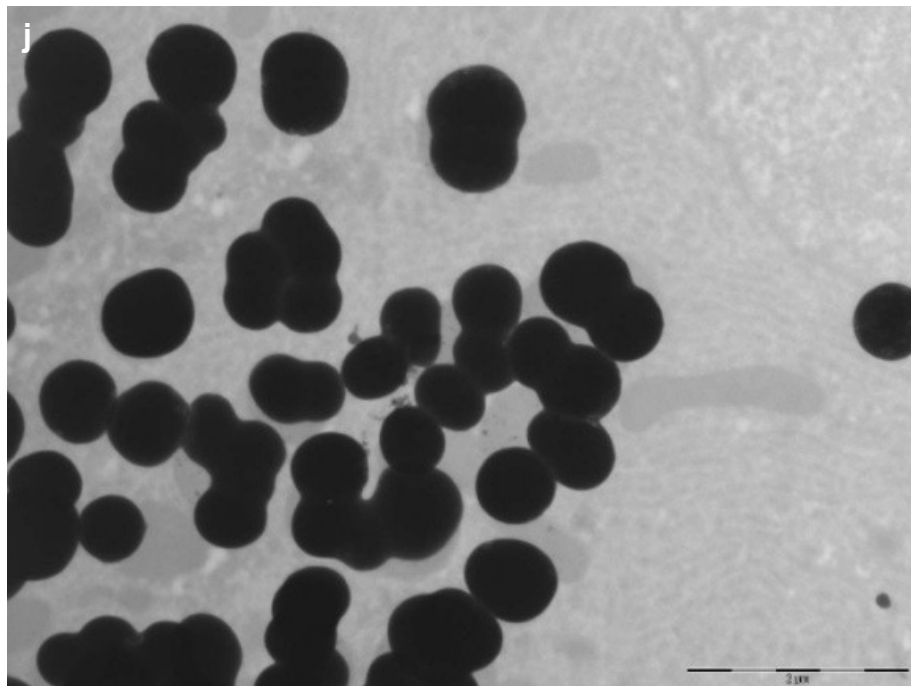
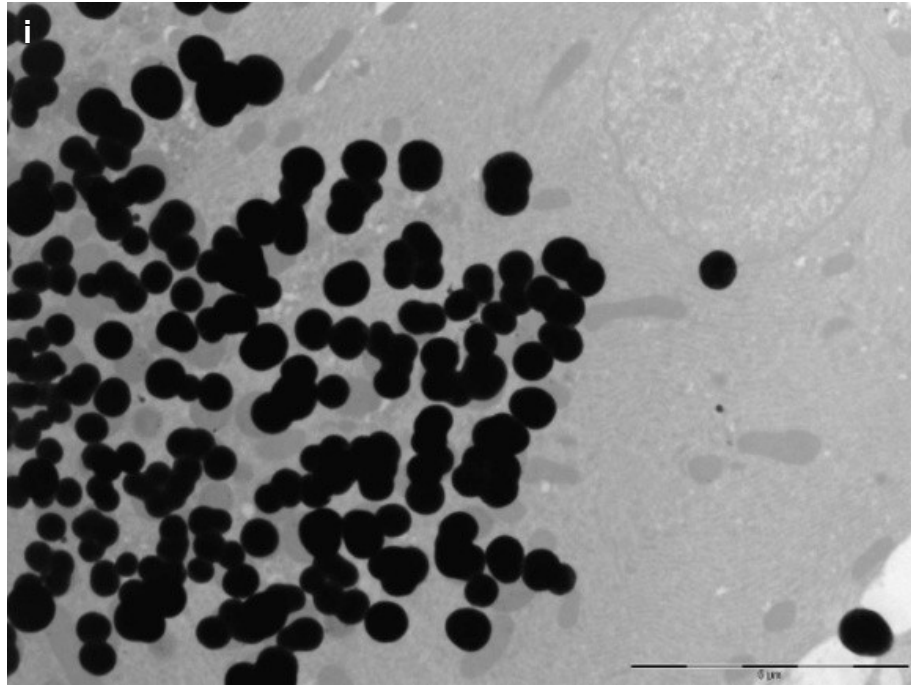


Figure 5.8 (continued). 80 nm thick sections of LR White-embedded rat pancreas. Exocrine granules immunohistochemically stained for  $\alpha$ -amylase. Polymerised 4-I-OPD at low (i) and high power (j), both without gamma correction, showing inherent electron opacity.

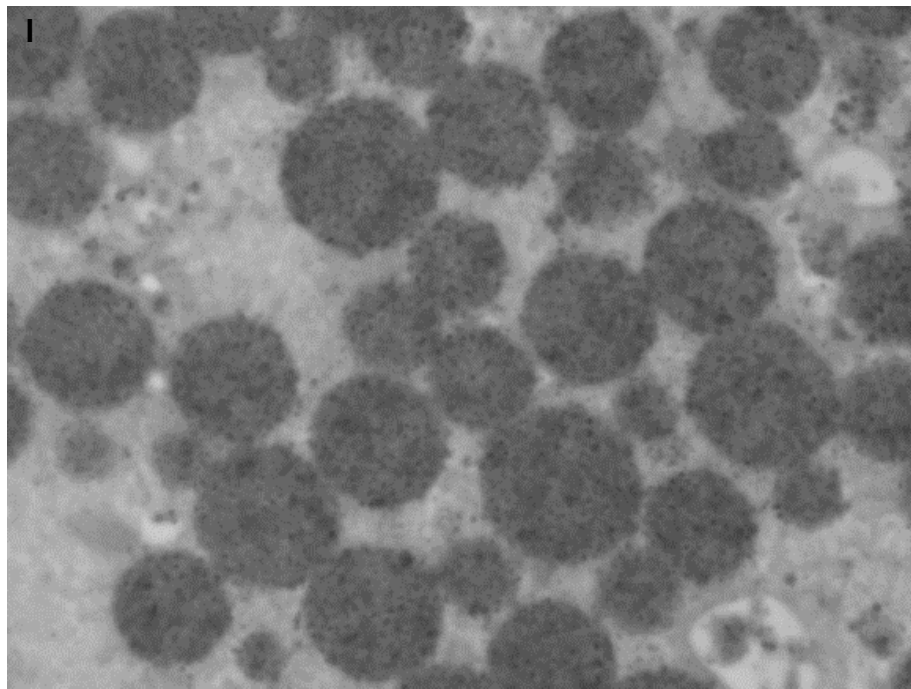
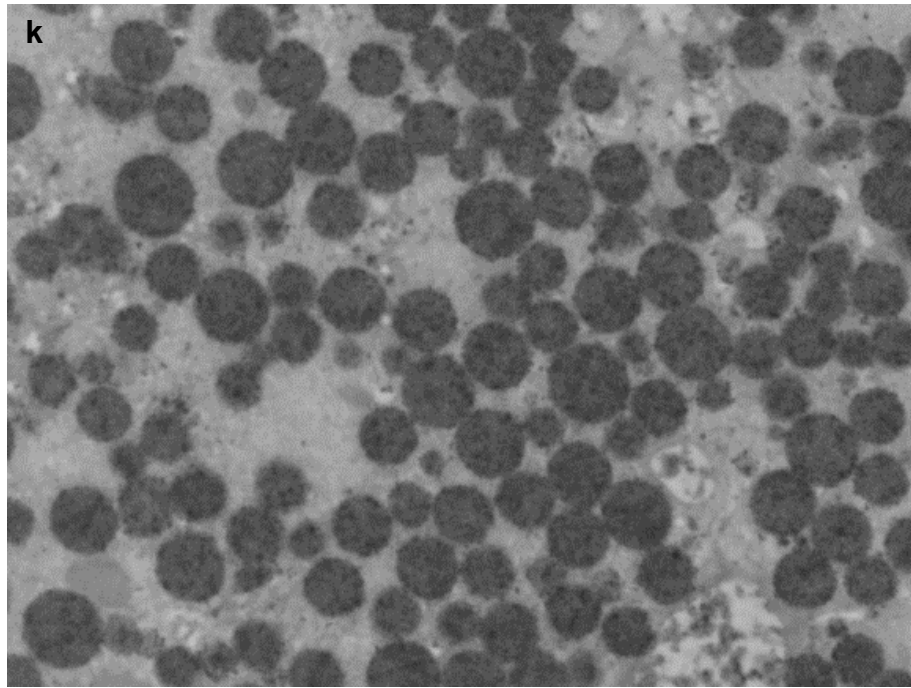


Figure 5.8 (continued). 80 nm thick sections of LR White-embedded rat pancreas. Exocrine granules immunohistochemically stained for  $\alpha$ -amylase. Polymerised 4,5-diI-OPD at low (k) and high power (l), both without gamma correction, showing inherent electron opacity.

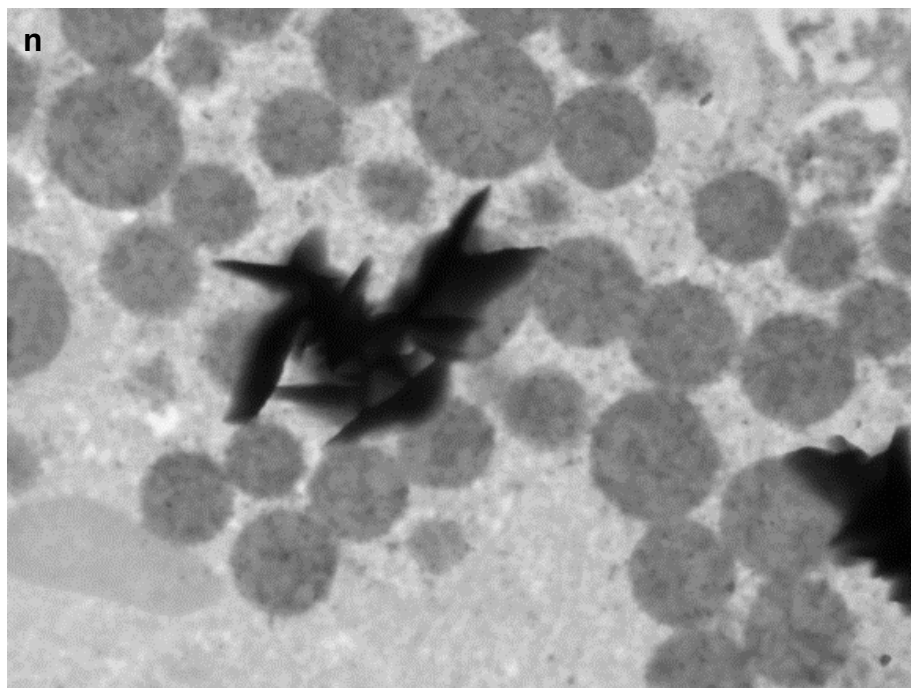
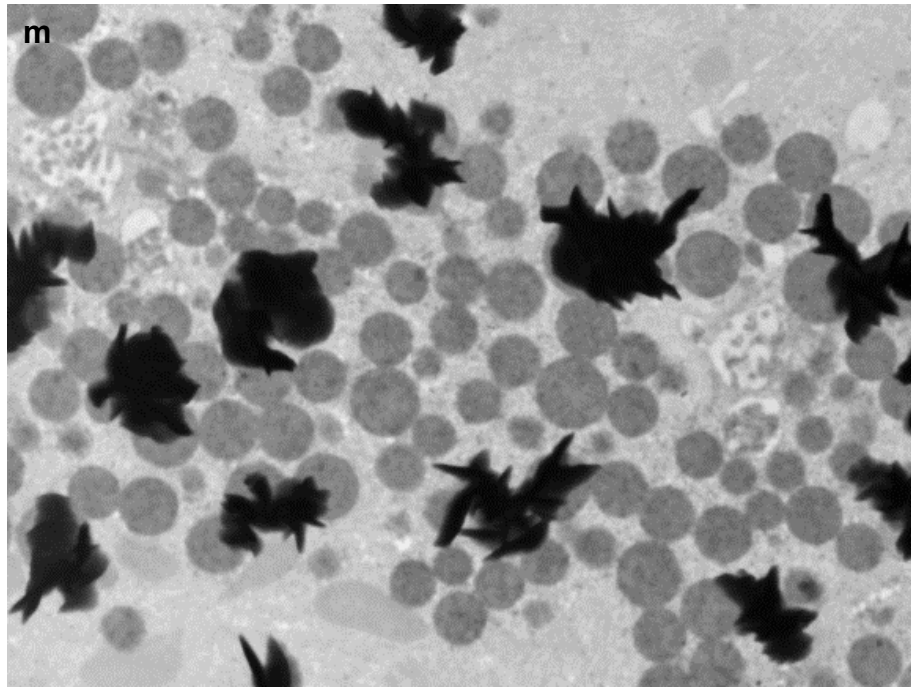


Figure 5.8 (continued). 80 nm thick sections of LR White-embedded rat pancreas. Exocrine granules immunohistochemically stained for  $\alpha$ -amylase. Polymerised 4,5-diI-OPD showing occasional background deposits at low power (m) and high power (n), both images without automatic gamma correction.

#### 5.4.2.4 Analytical Transmission Electron Microscopy

Of the 5 halogenated compounds that were examined by TEM, only two appeared suitable as potential markers for AEMT, namely 4-Br-OPD and 4,5-diI-OPD (4,5-diCl-OPD was excluded until the reason for the variable morphology of deposits produced by different sources of the monomer was understood).

When TEM spot size was 600 nm, 4-Br-OPD was easily detected in 5 seconds (figure 5.8a) and when spot size was reduced to 40 nm, it could just be detected within 2 seconds (figure 5.8b).

Iodine in deposits of 4,5-diI-OPD could be detected within just 1 second, with a 600 nm spot size (figure 5.8c). When spot size was reduced to 40 nm, I could just be detected within 1 second (figure 5.8d).



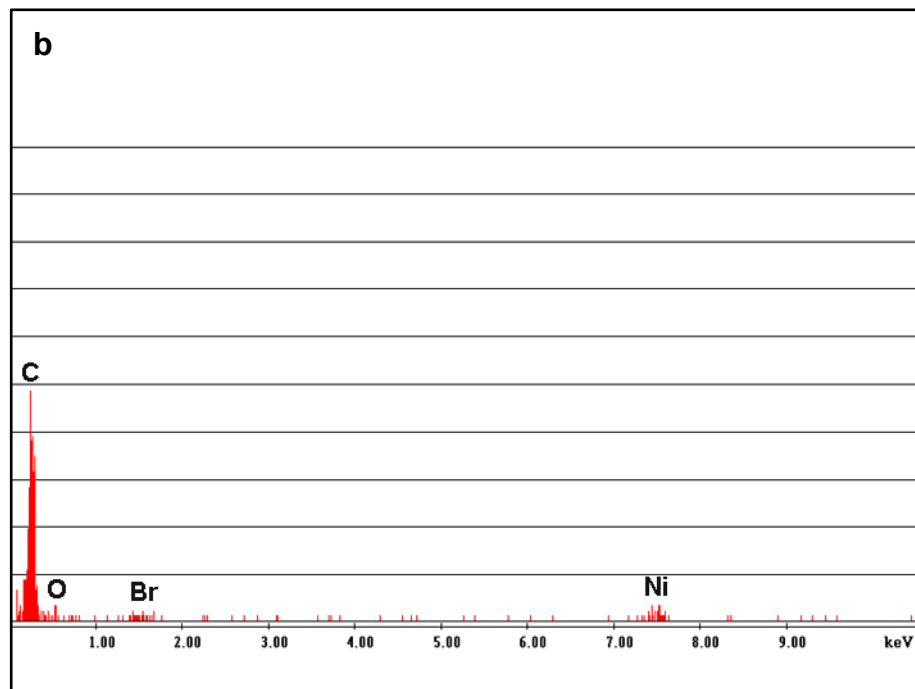
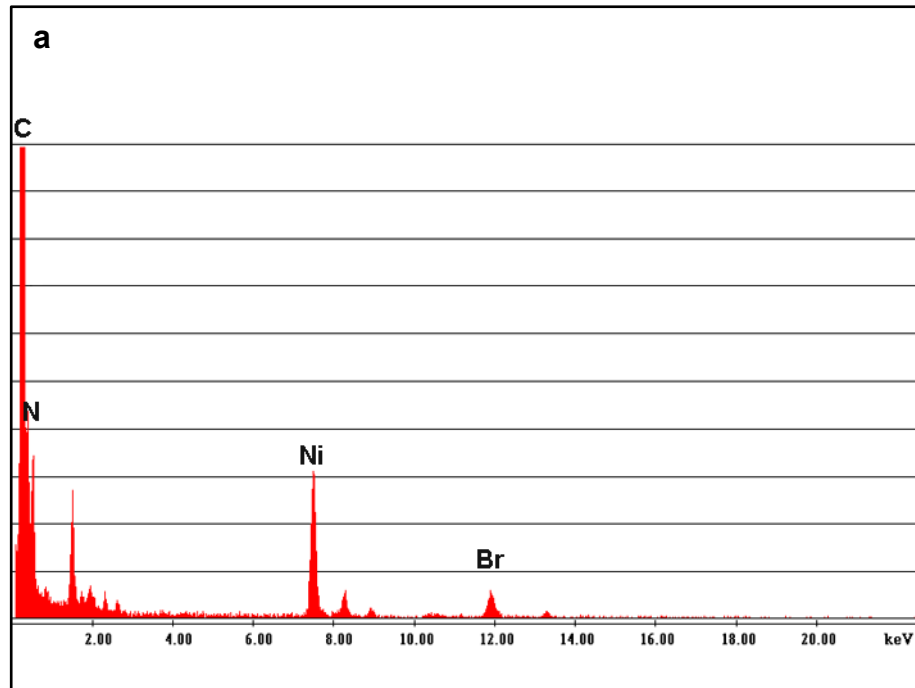


Figure 5.8. X-ray spectra of polymerised halogenated compounds on 80 nm thick sections of LR-White-embedded rat pancreas. Exocrine granules immunohistochemically stained for  $\alpha$ -amylase. Polymerised 4-Br-OPD signal from 600 nm spot with 5 seconds acquisition (a), and 40 nm spot with 2 seconds acquisition (b).

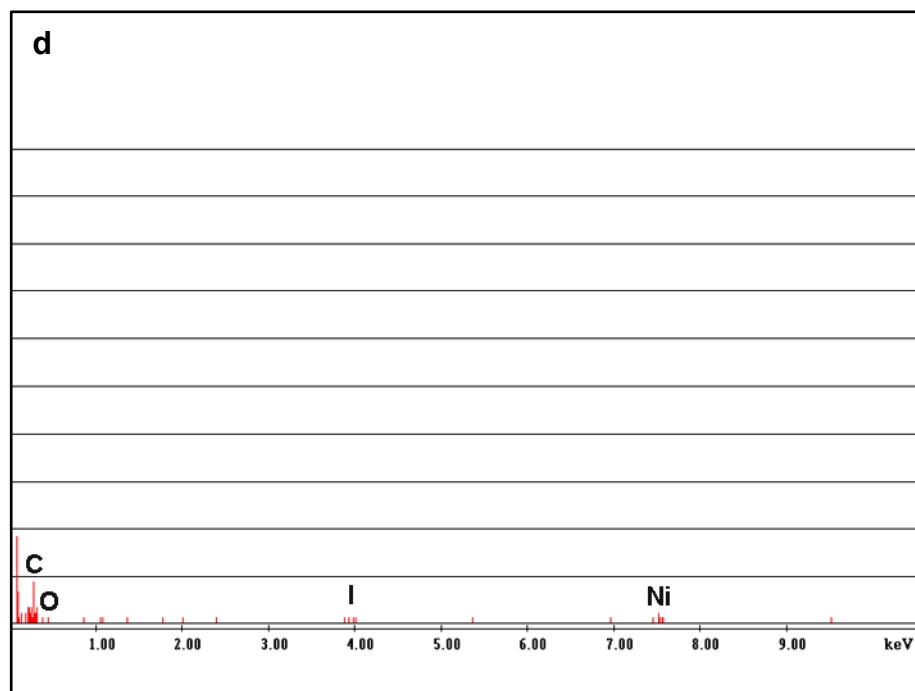
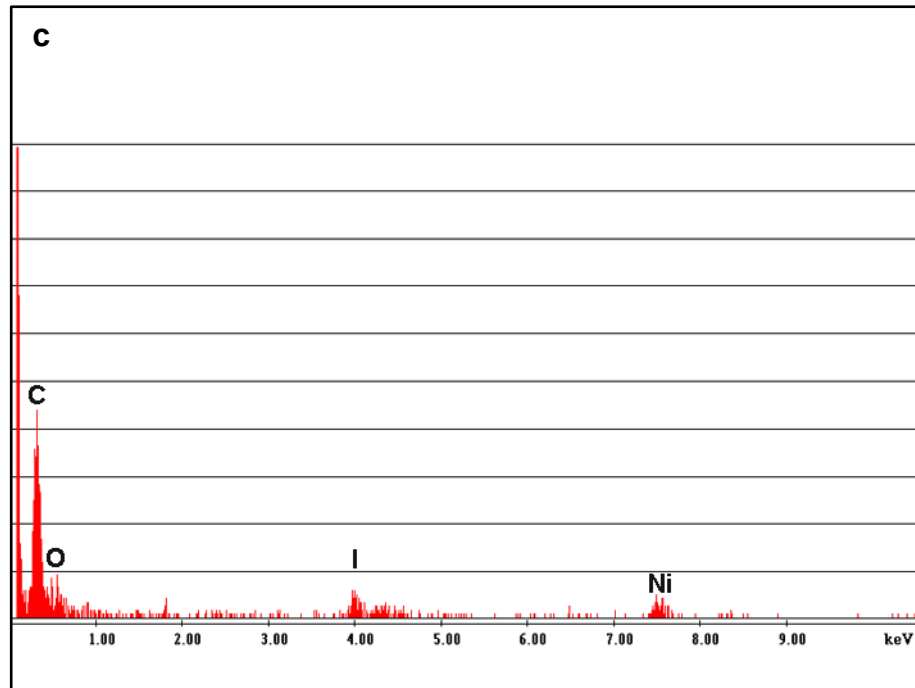


Figure 5.8 (continued). X-ray spectra of polymerised halogenated compounds on 80 nm thick sections of LR-White-embedded rat pancreas. Exocrine granules immunohistochemically stained for  $\alpha$ -amylase. Polymerised 4,5-diI-OPD signal from 600 nm spot with 1 second acquisition (c), and 40 nm spot with 1 seconds acquisition (d).

## 5.5 Discussion

Synthesis of halogenated compounds presented few problems, and where these occurred, they were mainly centred on the instability of iodinated products, particularly 4-I-OPD, which appeared to be particularly air/light sensitive. Other problems were associated with low overall yield, and these could usually be traced to poor extraction of N-acetylated derivatives, the low solubility of which were not fully appreciated at the time.

Purity of product, rather than maximisation of yield, was considered of greater importance and the inclusion of additional re-crystallisation steps at each stage of the syntheses lowered overall yield to values below those published elsewhere e.g. the yields of 4-Br-OPD and 4,5-diBr-OPD were 17% compared with 94% (uncharacterised) (Rangarajan et al., 2000) and 63% (Moje, 1964) respectively. 4,5-diI-OPD was, however, recovered in better yield (26.8% cf. 20.78%) than those of Youngblood (2006).

Attempts to prepare 2,2' diiodo derivatives of 4,4'-dinitrobiphenyl by direct iodination were unsuccessful, even though preliminary results using toluene surrogates gave encouraging results, and steric hindrance from the bulky phenyl ring was the most likely explanation. Unfortunately, time did not allow for completion of the synthesis of the 2,2' dibromo analogue, since this might have provided not only another compound for examination, but also an alternative route to the synthesis of the diiodo compound via halogen exchange. Both compounds might be expected to have properties similar to those of DAB and thus form more insoluble and localised derivatives.

That all halogenated compounds produced visible deposits in preliminary dot blot and light microscopical immunohistochemistry experiments was particularly

encouraging, since 1,2-diaminobenzene (OPD) does not; it is for this reason that it is widely used as a colorimetric reagent in enzyme immunoassay (Wolters et al., 1976). Their solubility in organic solvents was disappointing, however, since this limits their applicability. There was a general trend in the colour of the final polymerised deposits, from yellow-brown, in the case of the fluorinated compounds, through orange-brown and red-brown for the chlorinated compounds, to red-brown for the brominated analogues and finally purple-brown and red-purple (dusky pink) in the case of the iodinated compounds.

Analytical SEM produced some surprising results, particularly for the fluorinated products; no fluorine could be detected in any, with the exception of F6, which produced a particularly strong signal. The chlorinated compounds could be demonstrated in varying amounts which showed little relationship to the intensity of the dot blots that they produced. Similarly, 4-Br-OPD, which produced moderately intense dots, had considerably lower amounts of detectable bromine than that of 4,5-diBr-OPD, which only produced pale dots. Both iodinated compounds produced intense dots and strong X-ray signals for iodine. X-ray signal strength appeared roughly equivalent to BSI signal, as might be expected.

Light microscopy produced generally similar results to those seen on dot blots, with a few notable exceptions and this probably reflects the difference in the nature of the material to which the polymerised products adhered, as well as some influence from the aqueous mountant. In some cases, unexpected background staining was present, which may have reflected problems of substrate solubility as well as additional and unexpected catalytic effects of tissue components on some, but not all of the halogenated compounds. The discovery of fluorescence associated with polymerised F6 was surprising, but attempts to determine whether this was

related to the presence of the two trifluoromethyl residues or the methylene bridge separating the two phenyl rings, by synthesising the non-halogenated analogue were unsuccessful.

Analytical SEM provided a useful and rapid tool for evaluating immunohistochemically deposited products, since shorter pixel-dwell times could be achieved than in the TEM. In addition, several samples could be inserted into the instrument at one time and rapidly examined. 4,5-diCl-OPD, both brominated and both iodinated compounds produced striking results, with bright BSI images and strong X-ray signals which could all be detected in short time frames.

It is the TEM, however, that is the final arbiter for evaluating the utility of the halogenated substrates, and of the 5 compounds that were selected for examination, only 2 approached the requirements for use in AEMT, namely 4-Br-OPD and 4,5-diI-OPD. The software used for the analytical instrumentation on the TEM did not allow acquisition times shorter than 1 second, but the spectra suggested that 4,5-diI-OPD might be detectable in sub-second acquisitions.

## **5.6 Summary and conclusions**

The successive application of progressively more stringent technologies facilitated the rapid selection of promising compounds whilst, at the same time, excluding those that performed poorly.

Of the 16 halogenated compounds that were tested, only 1 compound, 4,5-diI-OPD, approached the requirements for AEMT, namely good localisation of immunohistochemically deposited product, inherent electron opacity, and a sufficiently high concentration of specific element to permit sub-second detection of X-ray signal.

## 5.7 References

- ADLER, O. & ADLER, R. 1904. Concerning the amount of quasi organic bond of blood with especial consideration of veracity of blood. *Hoppe-Seylers Zeitschrift Fur Physiologische Chemie*, 41, 59-67.
- BALZ, G. & SCHIEMANN, G. 1927. On aromatic fluoric compounds. I. A new method for its representation. *Berichte Der Deutschen Chemischen Gesellschaft*, 60, 1186-1190.
- BUNNETT, J. F. & RAUHUT, M. M. 1958. 2-Bromo-3-methylbenzoic acid. *Organic Syntheses*, 38, 11-13.
- CARTHEW, P. 1978. Peroxidase-labelled antibody technique for rapid detection of mouse hepatitis virus in cases of natural outbreaks. *Journal of Infectious Diseases*, 138, 410-413.
- CHAIKOVSKII, V. K., FILIMONOV, V. D., SKOROKHODOV, V. I. & OGORODNIKOV, V. D. 2007. Superactivity and dual reactivity of the system N-iodosuccinimide-H<sub>2</sub>SO<sub>4</sub> in the iodination of deactivated arenes. *Russian Journal of Organic Chemistry*, 43, 1278-1281.
- CHANDLER, J. A. The use of wavelength dispersive X-ray microanalysis in cytochemistry. In: WISSE, E., DAEMS, W. TH., MOLENAAR, L. AND VON DUIJN, P., ed. *Electron Microscopy and Cytochemistry*, 1973 Drienerlo, The Netherlands. North Holland Publishing Company, 203-222.
- CHEESEMAN, G. W. 1962. Quinoxalines and related compounds. Part 6. Substitution of 2,3-dihydroxyquinoxaline and its 1,4-dimethyl derivative. *Journal of the Chemical Society*, 1170-1176.
- GRAHAM, R. C. & KARNOVSKY, M. J. 1966. The early stages of absorption of injected horseradish peroxidase in the proximal tubules of mouse kidney: ultrastructural cytochemistry by a new technique. *Journal of Histochemistry and Cytochemistry*, 14, 291-302.

- GRAHAM, R. C., LUNDHOLM, U. & KARNOVSKY, M. J. 1965. Cytochemical demonstration of peroxidase activity with 3-amino-9-ethylcarbazole. *Journal of Histochemistry & Cytochemistry*, 13, 150-152.
- HANKER, J. S. & RABIN, A. N. 1975. Color-reaction streak test for catalase-positive microorganisms. *Journal of Clinical Microbiology*, 2, 463-464.
- HANKER, J. S., YATES, P. E., METZ, C. B. & RUSTIONI, A. 1977. New specific, sensitive and non-carcinogenic reagent for demonstration of horseradish-peroxidase. *Histochemical Journal*, 9, 789-792.
- HARDY, H. & HEIMER, L. 1977. Safer and more sensitive substitute for diaminobenzidine in light microscopic demonstration of retrograde and anterograde axonal transport of HRP. *Neuroscience Letters*, 5, 235-240.
- HÖFLE, G., STEGLICH, W. & VORBRÜGGEN, H. 1978. 4-Dialkylaminopyridines as highly active acylation catalysts. *Angewandte Chemie International Edition in English*, 17, 569-583.
- KLAPARS, A. & BUCHWALD, S. L. 2002. Copper-catalyzed halogen exchange in aryl halides: An aromatic Finkelstein reaction. *Journal of the American Chemical Society*, 124, 14844-14845.
- KRASZKIEWICZ, L., SOSNOWSKI, M. & SKULSKI, L. 2004. Easy, inexpensive and effective oxidative iodination of deactivated arenes in sulfuric acid. *Tetrahedron*, 60, 9113-9119.
- LERMAN, O., TOR, Y. & ROZEN, S. 1981. Acetyl hypofluorite as a taming carrier of elemental fluorine for novel electrophilic fluorination of activated aromatic rings. *Journal of Organic Chemistry*, 46, 4629-4631.
- MOJE, W. 1964. Structure of 2 new dibromobenzofurazan oxides from dehydrobromination of tetrabromotetrahydrobenzofurazan oxide. *Journal of Organic Chemistry*, 29, 3722-&.

- MONNEREAU, C., BLART, E. & ODOBEL, F. 2005. A cheap and efficient method for selective para-iodination of aniline derivatives. *Tetrahedron Letters*, 46, 5421-5423.
- RANGARAJAN, M., KIM, J. S., SIM, S. P., LIU, A., LIU, L. F. & LAVOIE, E. J. 2000. Topoisomerase I inhibition and cytotoxicity of 5-bromo- and 5-phenylterbenzimidazoles. *Bioorganic & Medicinal Chemistry*, 8, 2591-2600.
- SHAFFER, A., A, LINDLEY, P., M & HEDBERG, F. L. 1985. An Investigation of alternate synthesis for 2,2'-bis(phenylethynyl)-5,5'-diaminobenzidine. Wright-Patterson Air Force Base.
- SOMOGYI, P., HODGSON, A. J. & SMITH, A. D. 1979. An approach to tracing neuron networks in the cerebral cortex and basal ganglia. Combination of Golgi staining, retrograde transport of horseradish peroxidase and anterograde degeneration of synaptic boutons in the same material. *Neuroscience*, 4, 1805-1852.
- STEPHENS, F. F. & BOWER, J. D. 1950. The Preparation of benzimidazoles and benzoxazoles from Schiff's bases. Part 2. *Journal of the Chemical Society*, 1722-1726.
- SYMONS, M. C. R. 1957a. The formation of iodine cations. Part 1. Magnetic evidence. *Journal of the Chemical Society*, 387-392.
- SYMONS, M. C. R. 1957b. The formation of iodine cations. Part 2. Spectroscopic evidence. *Journal of the Chemical Society*, 2186-2190.
- WOLTERS, G., KUIJPERS, L., KACAKI, J. & SCHUURS, A. 1976. Solid-phase enzyme-immunoassay for detection of hepatitis-B surface-antigen. *Journal of Clinical Pathology*, 29, 873-879.
- XING, W. K. & OGATA, Y. 1982. Steric acceleration by ortho substituents of the stannous chloride reduction of nitrobenzenes in aqueous ethanol. *Journal of Organic Chemistry*, 47, 3577-3581.



YANG, Y. H., CHENG, M. S., WANG, Q. H., NIE, H., LIAO, N., WANG, J. & CHEN, H. 2009. Design, synthesis, and anti-tumor evaluation of novel symmetrical bis-benzimidazoles. *European Journal of Medicinal Chemistry*, 44, 1808-1812.

YOUNGBLOOD, W. J. 2006. Synthesis of a new trans-A(2)B(2) phthalocyanine motif as a building block for rodlike phthalocyanine polymers. *Journal of Organic Chemistry*, 71, 3345-3356.

# **Chapter 6**

## **Electron Microscopical Visualisation of Fluorochromes**

## 6.1 Introduction

Previous chapters have focussed on the immunohistochemical aspects of marker chemistry, but DAB can also be polymerised by the action of excited fluorochromes in a process called photooxidation (Maranto, 1982) or photoconversion (Sandell and Masland, 1988). This has facilitated fluorescent markers, used at the light microscopic level, to be visualised in the TEM, a technique that has recently come to be known as correlative light and electron microscopy (CLEM). Correlating fluorescence microscopy with TEM examination is not, of course, new; in the late 1970s, the cytoskeletons of single cells were visualised for light microscopy by immunofluorescence labelling and subsequently identified in the TEM, albeit by morphological criteria (Osborn et al., 1978). For the majority of CLEM studies, however, unequivocal localisation in the EM can only be achieved by rendering the fluorochrome electron opaque.

Early studies examined injected fluorescent dyes (Maranto, 1982), but later techniques employed fluorescent antibody and streptavidin conjugates for electron microscopical localisation by immunohistochemical and *in-situ* hybridisation methods (Deerinck et al., 1994). A refinement of this technique coupled both fluorochromes and gold particles to the same antibody (Powell et al., 1997).

For live cell studies, immunocytochemical techniques are impractical. Commonly available antibodies are bivalent, leading to concerns about the perturbing effects of cross-linking their respective antigens, and are difficult to introduce into cells. It is more usual to employ molecular biological techniques to generate cellular proteins with either a fluorescent tag, i.e. a fluorescent protein, or a shorter peptide sequence that acts as a coordination host for metal-fluorochrome complexes.

Since the introduction of fluorescent proteins, initially as markers of gene expression (Chalfie et al., 1994) and subsequently as cytochemical markers (Kaether and Gerdes, 1995; Marshall et al., 1995; Rizzuto et al., 1995) in the mid 1990s, attempts to localise them at the ultrastructural level by photoconversion of DAB have proved difficult. It was eventually achieved and employed in electron tomography (Grabenbauer et al., 2005), but alternative systems, using metal-fluorochrome complexes have been more successful. An arsenic-fluorescein complex, binding to tetracysteine motifs of proteins in transfected cells (Griffin et al., 1998), has been used in the photoconversion of DAB for electron microscopical localisation (Gaietta et al., 2002). Fluorochromes labelled with tris-nitrilotriacetic acid-Ni complexes have been successfully employed for localising proteins in cells (Lata et al., 2006) but do not appear to have been used to visualise proteins at the ultrastructural level.

The observation that nanocrystalline semiconductor materials have narrow emission spectra (Hines and Guyot-Sionnest, 1996) and that this is size-dependent (Dabbousi et al., 1997) prompted the development of a novel class of fluorescent labels for light microscopic immunocytochemistry (Bruchez et al., 1998; Chan and Nie, 1998). Their inherent electron opacity has made them compatible with subsequent electron microscopical localisation, either alone (Giepmans et al., 2005) or following silver enhancement (Dahan et al., 2003; Danscher and Stoltenberg, 2006). Furthermore, differences in their size and morphology have permitted multiple labels to be identified in thin sections in the TEM (Giepmans et al., 2005). Problems associated with toxicity, conjugation, size and high cost have limited their broad applicability. In addition, broad and overlapping excitation spectra preclude

selective excitation and thus marker deposition and subsequent facile differentiation by analytical electron tomography.

Multiple labelling by immunohistochemical techniques in an analytical tomographic setting can be achieved by utilising different enzyme conjugates to deposit different markers, or by sequential immunohistochemical staining with different markers using the same enzyme, where product inhibition occurs. Alternatively, selective marker deposition can be achieved by histochemical techniques. Since photoconversion of DAB has been successfully applied in a wide range of contexts, it is reasonable to suppose that similar compounds might be selectively polymerised by excitation of specific fluorochromes. The mechanism of photooxidation is unknown, but does not appear to require  $H_2O_2$  in the reaction mixture. It may, however, utilise molecular oxygen as a radical source (Sandell and Masland, 1988).

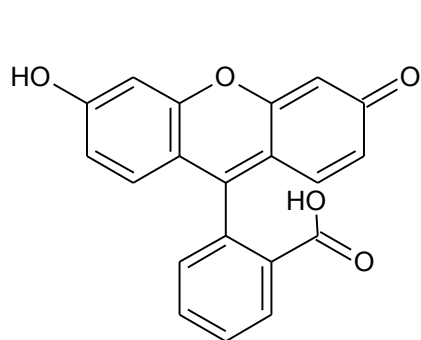
The immunohistochemical reduction and deposition of silver has been achieved by the action of horseradish peroxidase (Hainfeld et al., 2002) in conjunction with a proprietary physical developer (Professor Bharat Jasani, personal communication). This technique, coupled with the polymerisation of DAB by both enzymatic and photoconversion pathways, suggests the possibility of a common link between the two. This is further supported, albeit indirectly, by the observation that common reagents can suppress both the unwanted reduction of silver by tissue (type 1 argyrophilia (Gallyas, 1982)) (Gallyas and Wolff, 1986) and tissue autofluorescence (Kelly, 2010). Thus, the intriguing possibility exists of reducing silver from a physical developer by the photoconversion process, a technique predicted by the late Dr. Geoff Newman.

### 6.1.1 Model Systems

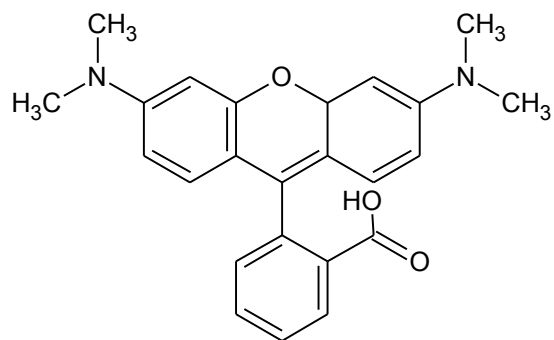
Tissue culture chamber slides provide a convenient system for preliminary evaluation of the photoconversion process. They comprise a series of wells that are sealed to a glass microscope slide with a silicone gasket. Ordinarily, the plastic wells are removed for staining, the gasket forming a reservoir for staining solutions. Once stained, the gasket is removed and the cell culture preparation is mounted for microscopic examination. The gasket presents a shallow well of uniform depth and, once covered with a thin glass window such as a glass cover slip, allows solutions to be tested and examined under comparable conditions; the microscopical equivalent of the spectrophotometer cuvette.

Fluorescein and tetramethylrhodamine are both xanthene dyes with absorption/emission maxima, in water, at 494 nm/521 nm and 557 nm/576 nm, respectively (figure 6.1). They have been used as fluorescent markers for many years and are both cheap and readily available. Furthermore, their structural similarity improves the comparability of results compared to chemically dissimilar fluorochromes.

Immunofluorescent staining for SMA provides a simple tissue model system for the reasons mentioned in Chapter 4, namely ubiquity and abundance.



Fluorescein



Tetramethylrhodamine

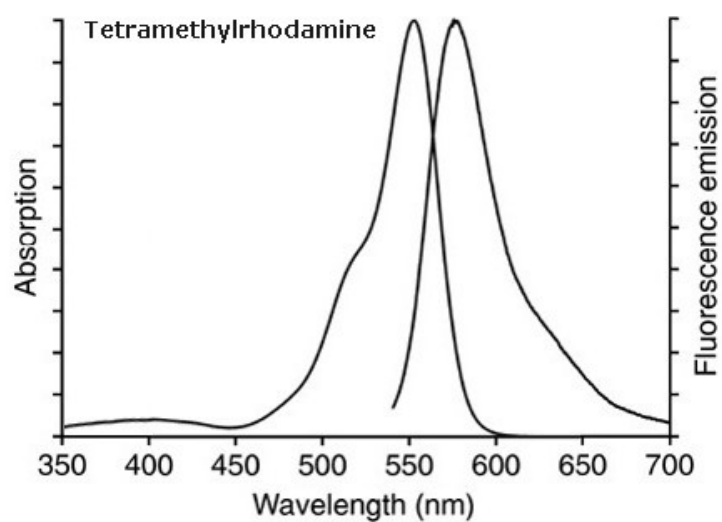
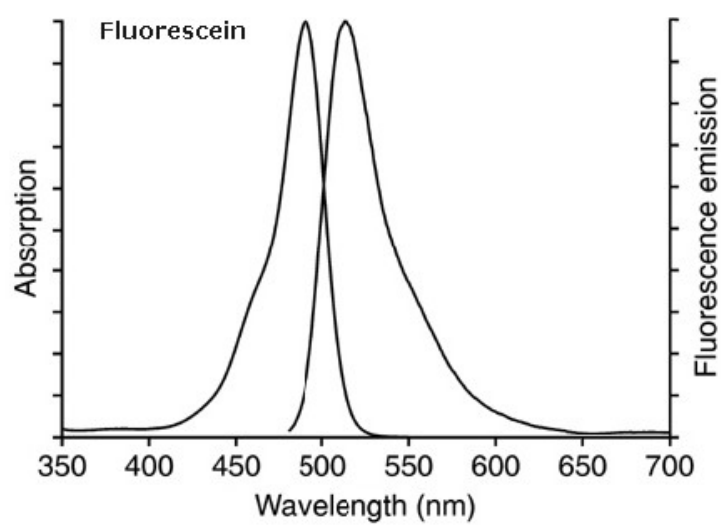


Figure 6.1. Structures and absorption/emission spectra of fluorescein and tetramethylrhodamine.

## **6.2 Materials**

Lab-Tek® Chamber slides™ were supplied by Nalge Nunc International (Rochester, New York, U.S.A). Goat anti-mouse Ig fluorescein isothiocyanate (GAM IgFITC) and goat anti-mouse Ig tetramethylrhodamine isothiocyanate (GAM IgTRITC) conjugates were supplied by Autogen Bioclear (Calne, Wiltshire, U.K.). Fluorescein and tetramethylrhodamine were purchased from BDH (Lutterworth, Leicestershire, U.K.) and Sigma-Aldrich (Poole, Dorset, U.K.), respectively. Newman and Jasani's developer was prepared according to sections 2.2.3.2 of Chapter 2.

## **6.3 Methods**

### **6.3.1 Model Systems**

#### **6.3.1.1 Homogeneous Model System**

The plastic wells from Lab-Tek® Chamber slide™ were removed to leave the silicone gasket.

Fluorescein or tetramethylrhodamine was added to DAB-Tris and Newman and Jasani's developer to a final concentration of 0.005%. Chamber slide wells were filled with test solutions and covered with a piece of glass coverslip (cut to size by scoring with a diamond pen and gently applying pressure) before being irradiated with either green (520-550 nm) or blue (460-490 nm) light, for tetramethylrhodamine or fluorescein excitation respectively, from a 100W mercury lamp through the x2 (0.05 N.A.) objective lens of an Olympus BX51 light microscope (Olympus Optical Co. (U.K.) Ltd, London, U.K.).

Progress was monitored at 5 minute intervals, up to 30 minutes, by capturing digital images through a x10 (0.3 N.A.) objective lens, under ordinary bright field



conditions, with an Zeiss Axiocam digital camera and Axiovision software (Carl Zeiss Vision GmbH, Hallbergmoos, Germany) without white background colour correction, so that images could be easily seen when printed. Control solutions of DAB and developer, with or without fluorochromes were kept in the dark for 30 minutes for comparison with green and blue light-exposed solutions.

#### **6.3.1.2 Tissue Model System**

4 µm thick sections of archival, paraffin wax-embedded, normal human kidney (collected prior to the introduction of the Human Tissue Act, 2004), were immunohistochemically stained for smooth muscle actin as previously described, but with the primary antibody applied at  $1/50$  to achieve clear positivity, and visualised with either GAM IgFITC or GAM IgTRITC conjugates. Sections were irradiated with green and blue light, respectively, in the presence of DAB-PO<sub>4</sub> or Newman and Jasani's developer.

## **6.4 Results**

### **6.4.1 Homogeneous Model System**

#### **6.4.1.1 DAB**

##### **6.4.1.1.1 Fluorescein**

Exposure of the DAB solution to blue light for up to 30 minutes did not cause the formation of any observable polymer (figures 6.1a and b). The presence of 0.005% fluorescein imparted a slight yellow/green tint to the DAB solution (figure 6.1c). Exposure of this solution to blue light (460–490 nm) caused the formation of polyDAB, that could just be discerned as a darkening of the solution by 5 minutes (figure 6.1d) and clearly seen by 10 minutes (figure 6.1e). After this time, the solution became progressively darker and the size and number of particles increased (figures 6.1f – h).

##### **6.4.1.1.2 Tetramethylrhodamine**

Exposure of DAB solution to green light for up to 30 minutes did not cause the formation of any observable polymer (figures 6.2a and b). The presence of 0.005% tetramethylrhodamine imparted a slight pink tint to the DAB solution (figure 6.2c). Exposure of this solution to green light (520–550 nm) for up to 30 minutes failed to produce any discernable deposit (figure 6.2d).



Figure 6.1. Effects of exposure to blue light on solutions of DAB. DAB alone at 0 (a) and 30 minutes (b).

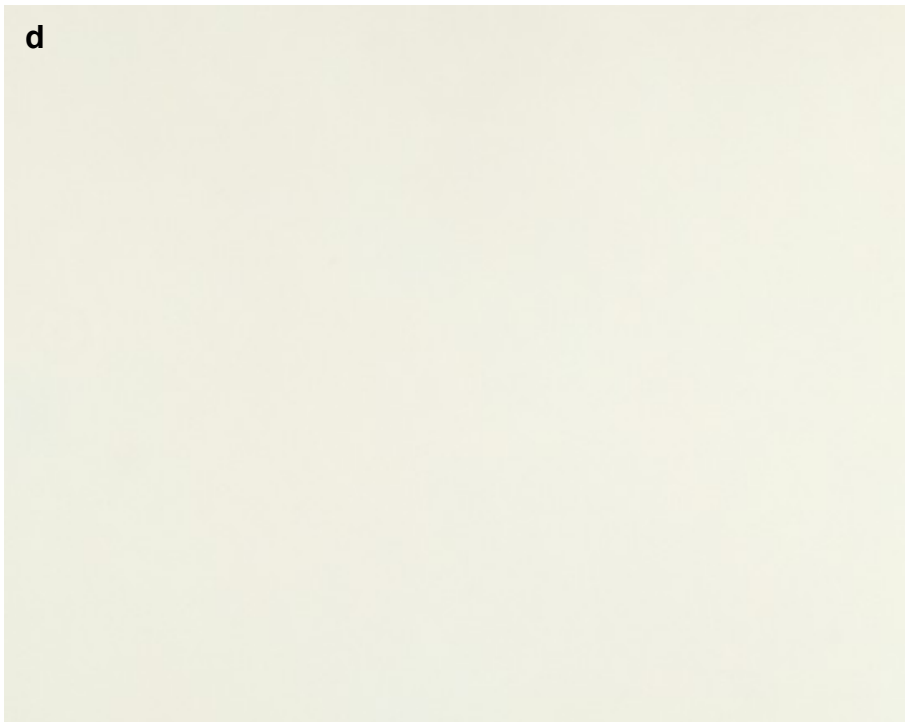


Figure 6.1 (continued). Effects of exposure to blue light on solutions of DAB.  
DAB + 0.005% fluorescein at 0 (c) and 5 minutes (d).



Figure 6.1 (continued). Effects of exposure to blue light on solutions of DAB.  
DAB + 0.005% fluorescein at 10 (e) and 15 minutes (f).

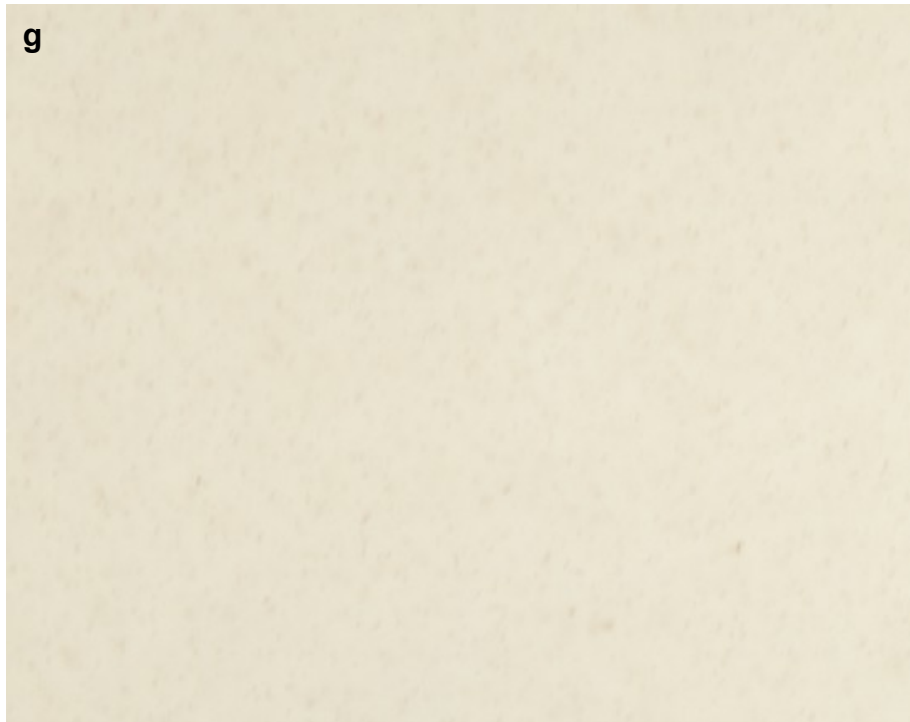


Figure 6.1 (continued). Effects of exposure to blue light on solutions of DAB.  
DAB + 0.005% fluorescein at 20 (c) and 30 minutes (d).



Figure 6.2. Effects of exposure to green light on solutions of DAB. DAB alone at 0 (a) and 30 minutes (b).

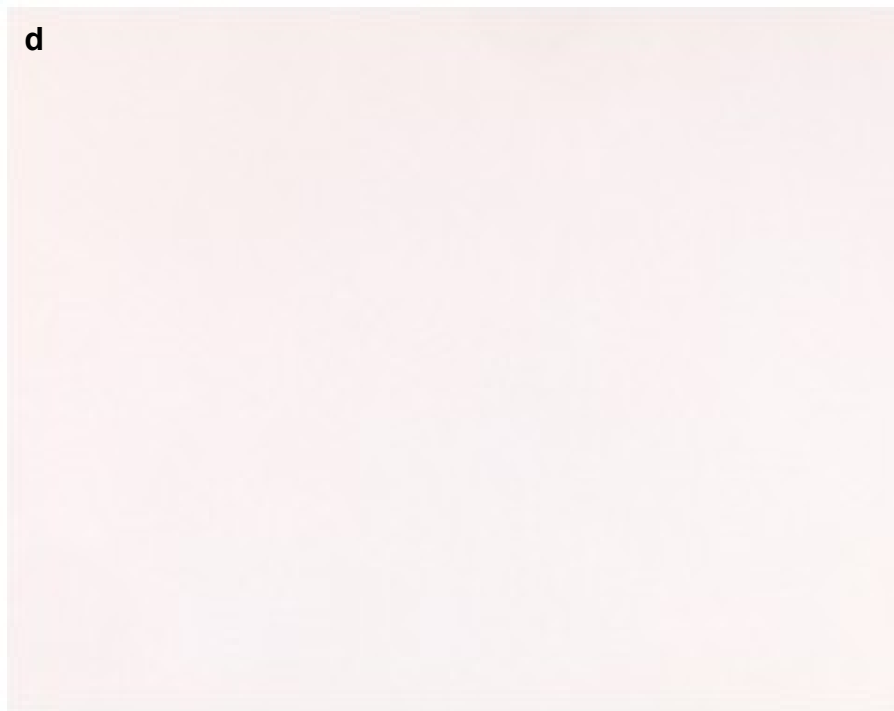


Figure 6.2 (continued). Effects of exposure to green light on solutions of DAB.  
DAB + 0.005% tetramethylrhodamine for 0 (c), and 30 minutes (d).



## **6.4.1.2 Newman and Jasani's Physical Developer**

### **6.4.1.2.1 Fluorescein**

Exposure of Newman and Jasani's physical developer to blue light caused a slight but noticeable darkening of the solution by 5 minutes (figures 6.3a and b). The solution became progressively darker with time until, by 20 minutes, the solution had taken on a grey appearance (figure 6.3c). Individual silver grains became apparent by 25 minutes and were clearly visible and numerous by 30 minutes (figure 6.3d). In the case of solutions containing fluorescein, a similar tint to that seen with DAB was present (figure 6.3e). Exposure to blue light (460–490 nm) caused a darkening of the solution within 5 minutes (figure 6.3f). The solution progressively darkened with increasing exposure time, as silver grains became larger and more numerous (figures 6.3g and h).

### **6.4.1.2.2 Tetramethylrhodamine**

The developer solution appeared slightly brighter than that containing DAB in the previous sections due to the higher refractive index of the former (figure 6.4a). Exposure of Newman and Jasani's physical developer to green light (520-550 nm) for 30 minutes did not cause any noticeable darkening of the solution (figures 6.4b). The presence of tetramethylrhodamine in the developer solution imparted a slight reddish tint (figure 6.4c) Illumination of the solution resulted in the appearance of silver grains by 10 minutes (figure 6.4d) that became progressively more abundant and larger with time (figures 6.4e – h).

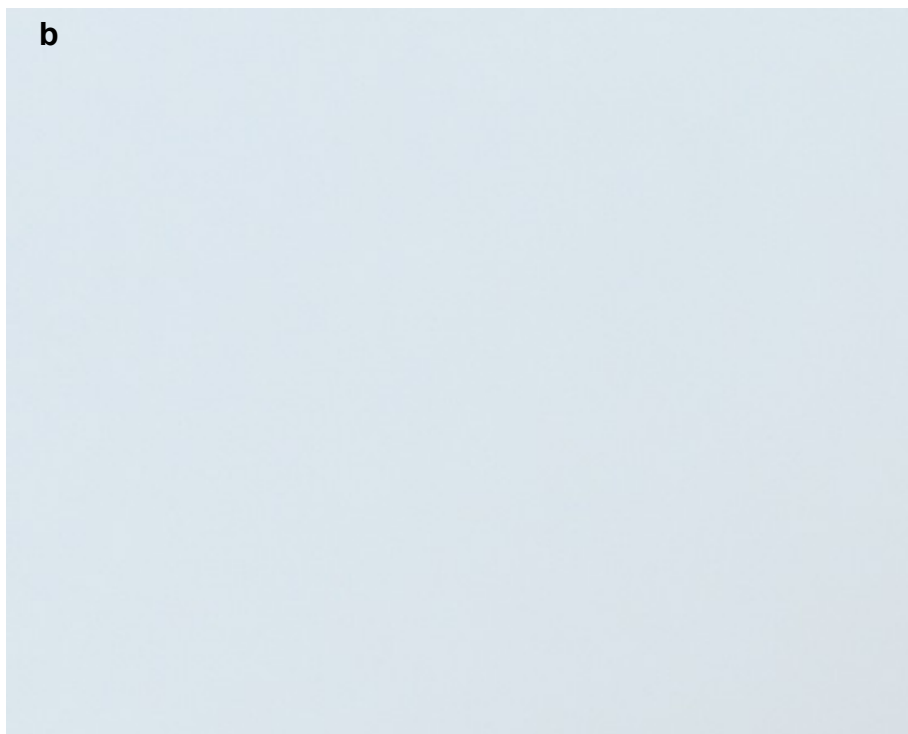
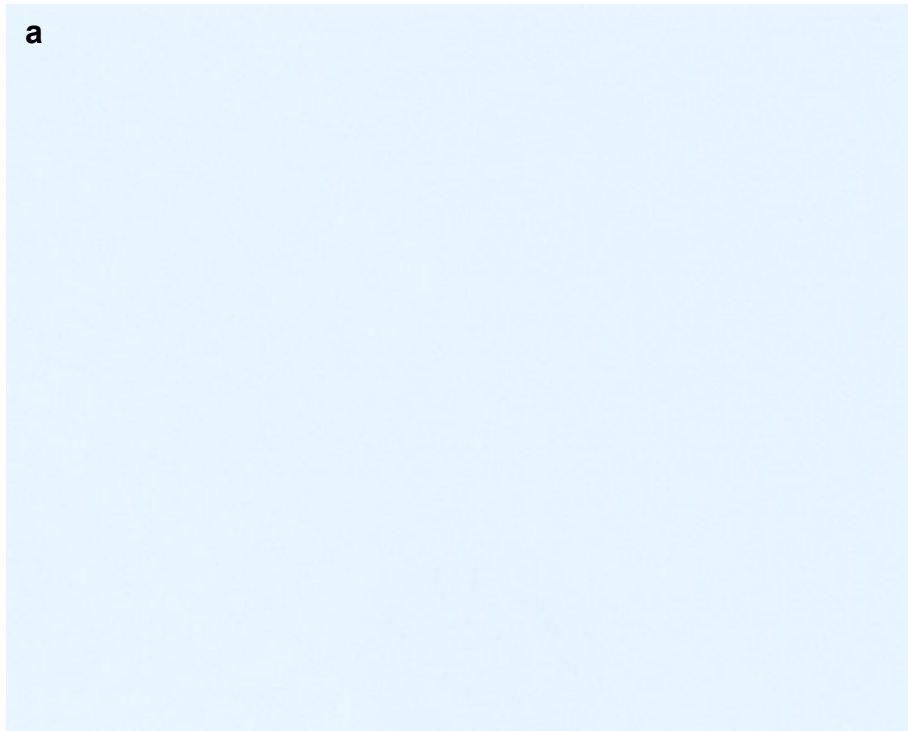


Figure 6.3. Effects of exposure to blue light on Newman & Jasani's developer.

Developer alone at 0 (a) and 5 minutes (b).



Figure 6.3 (continued). Effects of exposure to blue light on Newman & Jasani's developer. Developer at 20 (c) and 30minutes (d).



Figure 6.3 (continued). Effects of exposure to blue light on Newman & Jasani's developer. Developer + 0.005% fluorescein at 0 (e) and 5 minutes (f).



Figure 6.3 (continued). Effects of exposure to blue light on Newman & Jasani's developer. Developer + 0.005% fluorescein at 20 (g) and 30 minutes (h).



Figure 6.4. Effects of exposure to green light on Newman & Jasani's developer.

Developer at 0 (a) and 30 minutes (b).



Figure 6.4 (continued). Effects of exposure to green light on Newman & Jasani's developer. Developer + 0.005% tetramethylrhodamine at 0 (c) and 10 minutes (d).



Figure 6.4 (continued). Effects of exposure to green light on Newman & Jasani's developer. Developer + 0.005% tetramethylrhodamine at 15 (e) and 20 minutes (f).



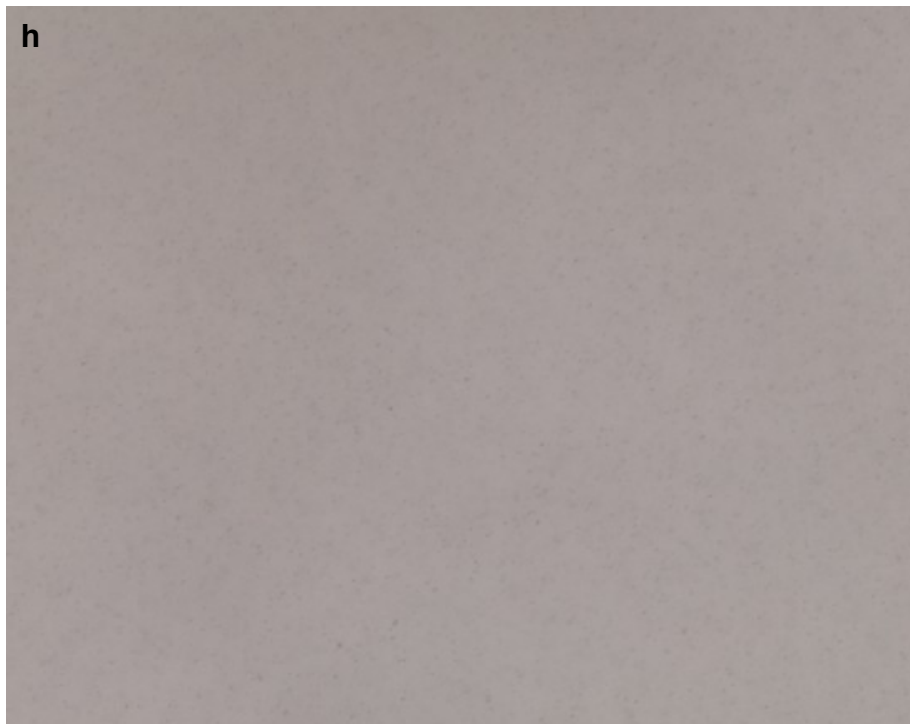
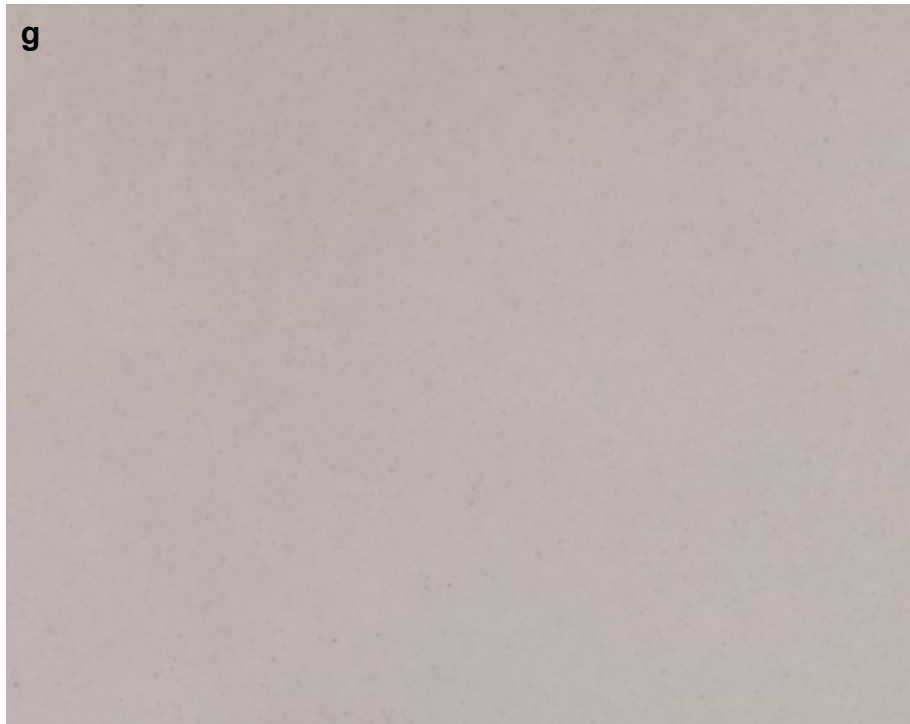


Figure 6.4 (continued). Effects of exposure to green light on Newman & Jasani's developer. Developer + 0.005% tetramethylrhodamine at 25 (g) and 30 minutes (h).

### **6.4.1.3 Control Solutions**

Solutions of either DAB or developer, with or without fluorochromes, which were kept in the dark for 30 minutes were identical in appearance to corresponding solutions at the beginning of light-exposure experiments.

## **6.4.2 Tissue Model System**

### **6.4.2.1 DAB**

#### **6.4.2.1.1 Fluorescein**

Immunofluorescence staining of kidney blood vessels was clear and localised, although background autofluorescence was evident (figure 6.5a). Compared to tissue at the beginning of the experiment (figure 6.5b), irradiation of the section with blue light (460–490 nm) for up to 30 minutes resulted in visible deposits of polyDAB in the background tissue and barely noticeable deposition of polyDAB in the immunopositive areas (figure 6.5c).

#### **6.4.2.1.2 Tetramethylrhodamine**

In the case of tissue sections that had been immunofluorescently stained using the tetramethylrhodamine conjugate, immunopositivity was clearly visible and background autofluorescence was present (figure 6.6a). No deposition of polyDAB in any part of the section was visible after irradiation with green light (520-550 nm) for 30 minutes (figures 6.6b and c).

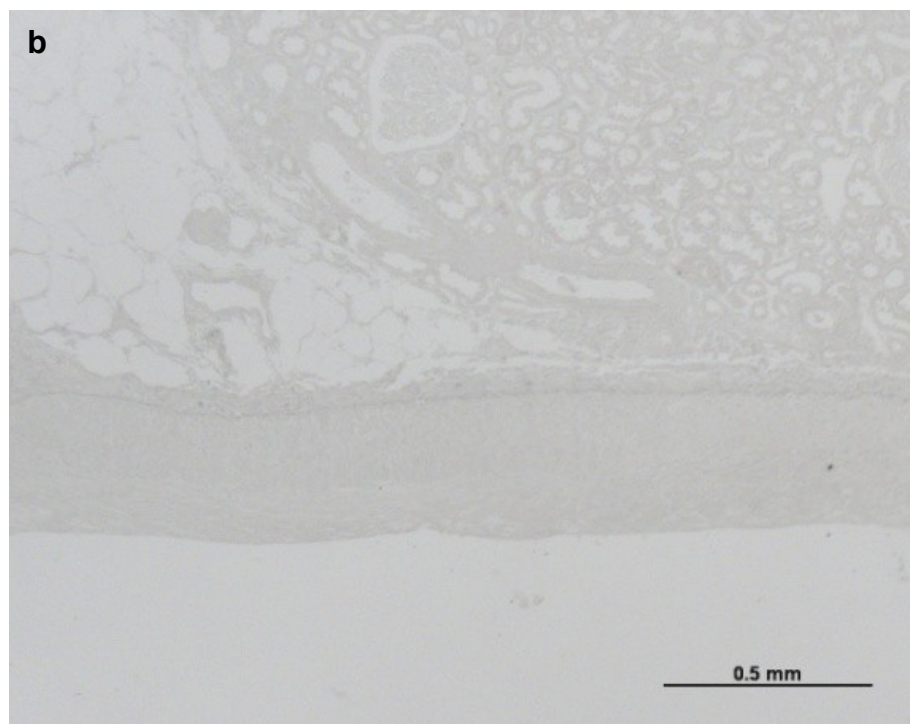
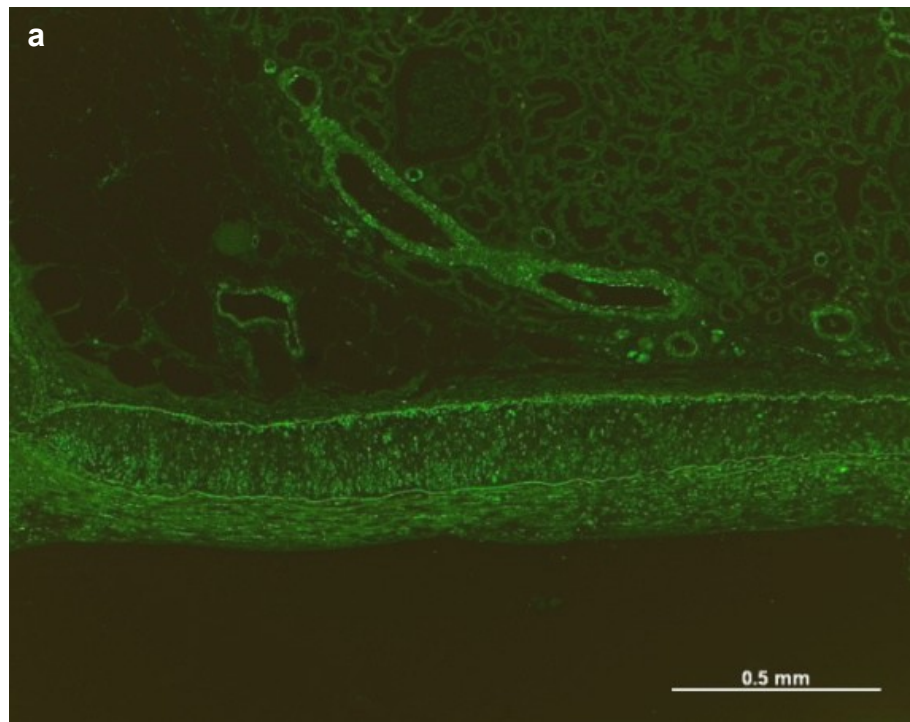


Figure 6.5. Effects of blue light on the deposition of polyDAB on 4  $\mu\text{m}$  thick sections of paraffin wax-embedded kidney immunofluorescently stained for SMA. Fluorescence micrograph of fluorescein-labelled blood vessels (a) and bright field images, in the presence of DAB solution at  $t = 0$  (b).

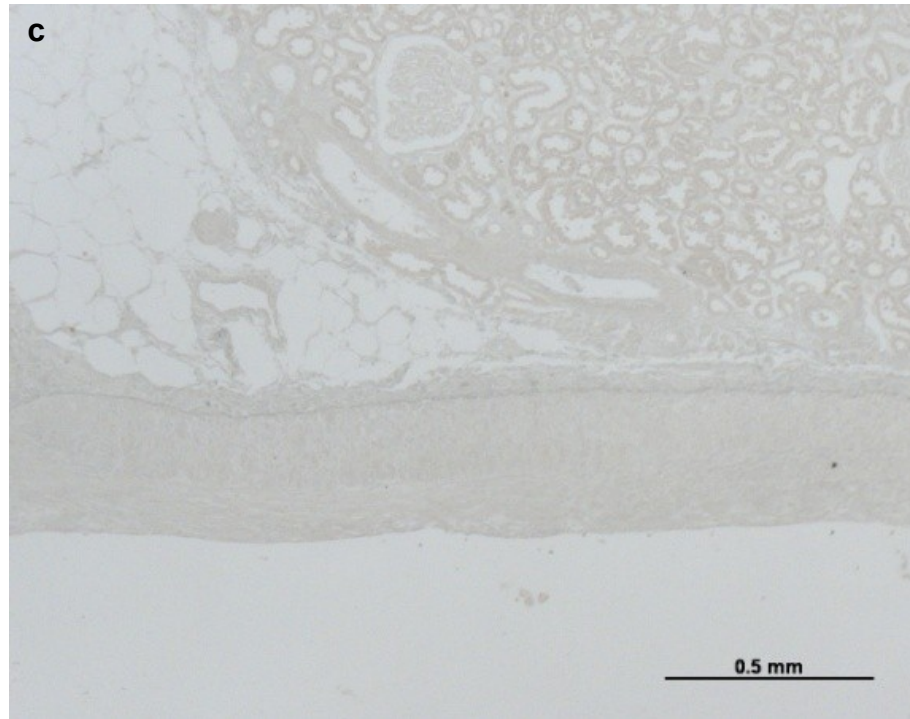


Figure 6.5 (continued). Effects of blue light on the deposition of polyDAB on 4  $\mu\text{m}$  thick sections of paraffin wax-embedded kidney immunofluorescently stained for SMA. Bright field images, in the presence of DAB solution after 30 minutes irradiation with blue light (c).

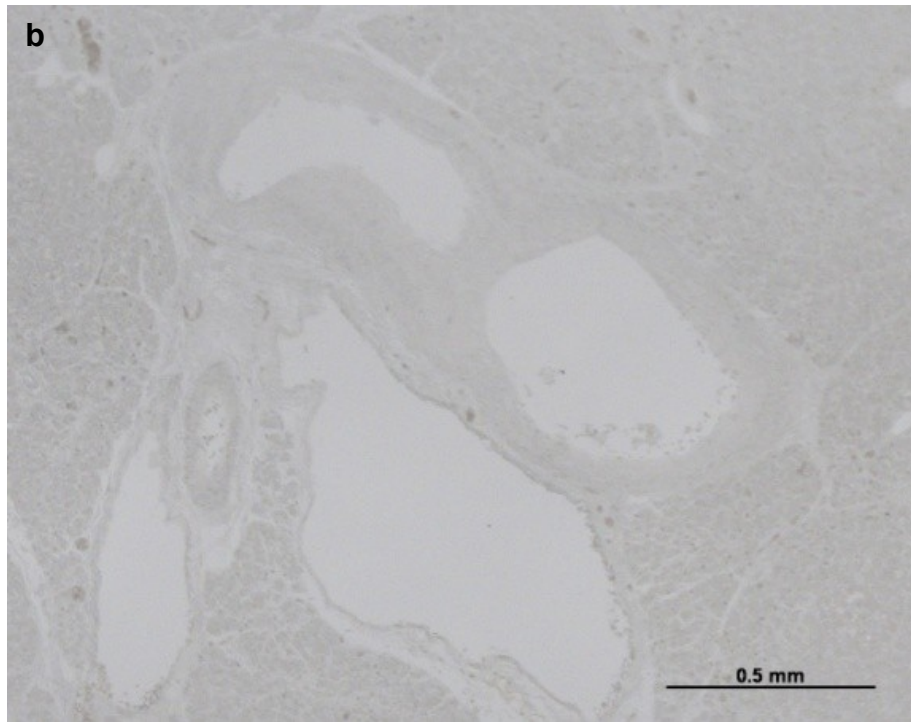
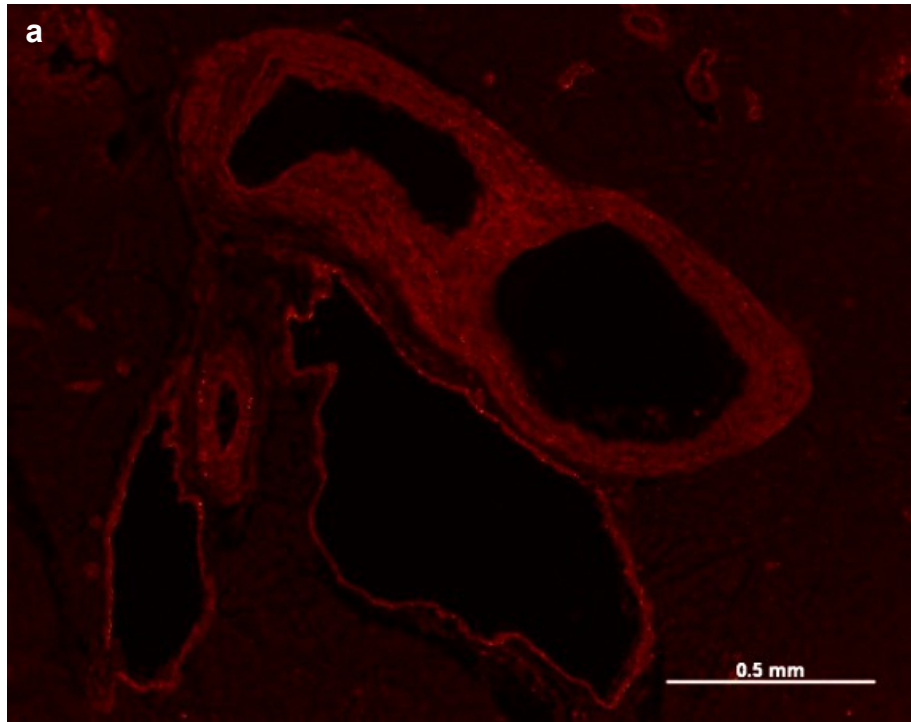


Figure 6.6. Effects of green light on the deposition of polyDAB on 4  $\mu\text{m}$  thick sections of paraffin wax-embedded kidney immunofluorescently stained for SMA. Fluorescence micrograph of tetramethylrhodamine-labelled blood vessels (a) and bright field images, in the presence of DAB solution at  $t = 0$  (b).

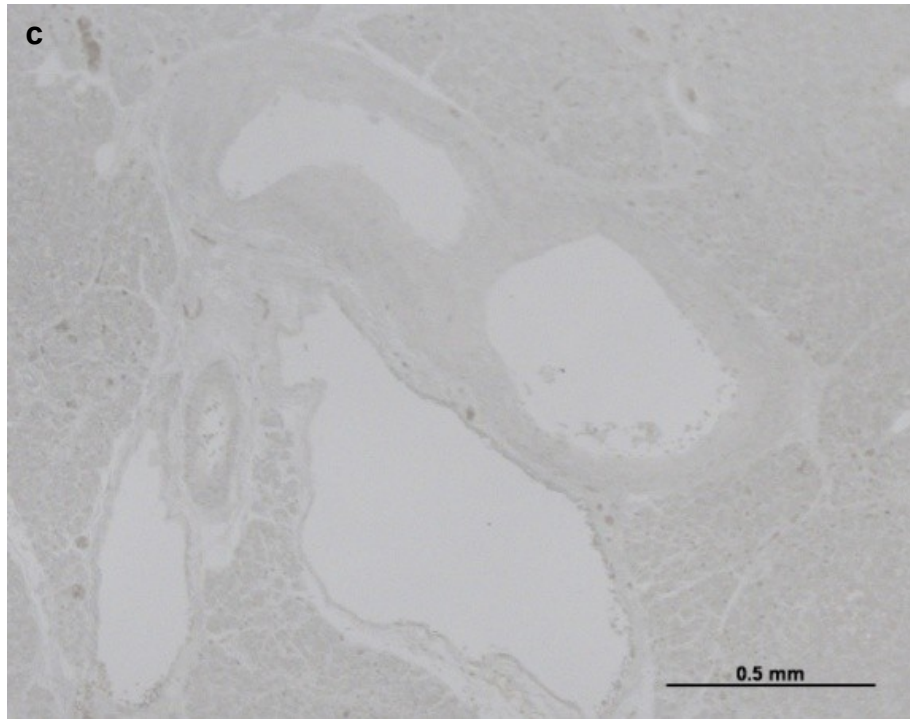


Figure 6.6 (continued). Effects of green light on the deposition of polyDAB on 4  $\mu\text{m}$  thick sections of paraffin wax-embedded kidney immunofluorescently stained for SMA. Bright field images, in the presence of DAB solution after 30 minutes irradiation with green light (c).

## **6.4.2.2 Newman and Jasani's Developer**

### **6.4.2.2.1 Fluorescein**

Immunofluorescence staining was clearly visible against a yellow-green tissue autofluorescence (figure 6.7a). Irradiation of the tissue section with blue light (460–490 nm) in the presence of Newman & Jasani's developer resulted in a progressive darkening of the tissue which was clearly evident by 10 minutes (figure 6.7b), and intense by 15 minutes (figure 6.7c). Specific deposition of silver at the immunopositive sites could be discerned, but background staining was strong.

### **6.4.2.2.2 Tetramethylrhodamine**

Immunofluorescent staining of kidney blood vessels was clearly visible against the pale red autofluorescence of the tissue (figure 6.8a), and after just 5 minutes irradiation with green light (520-550 nm) in the presence of Newman & Jasani's developer, clear and intense deposition of silver was evident at immunopositive sites. A light background deposit in the tissue was also evident (figure 6.8b).



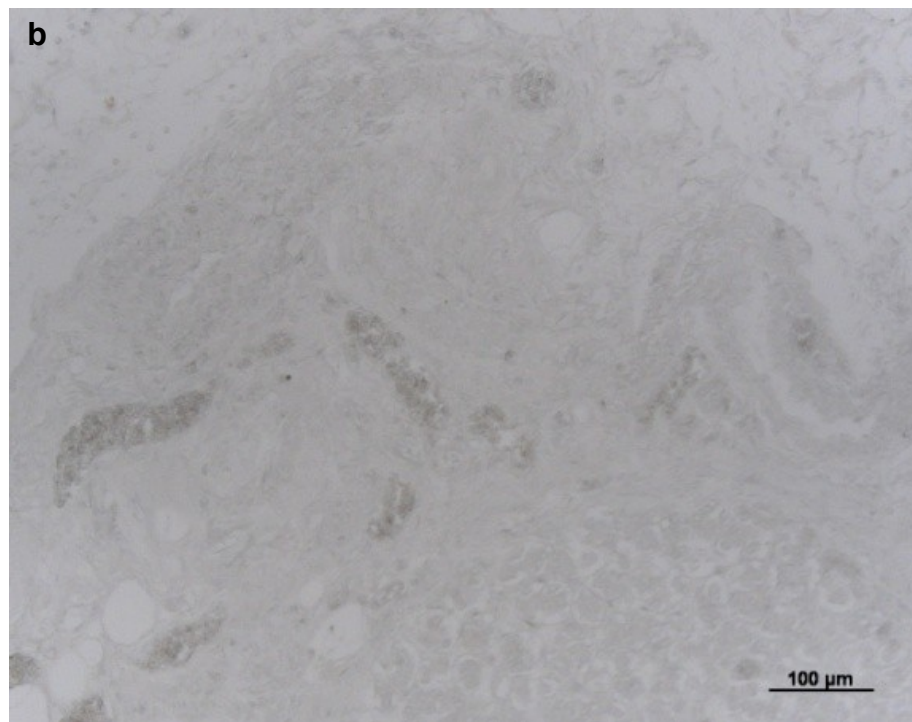
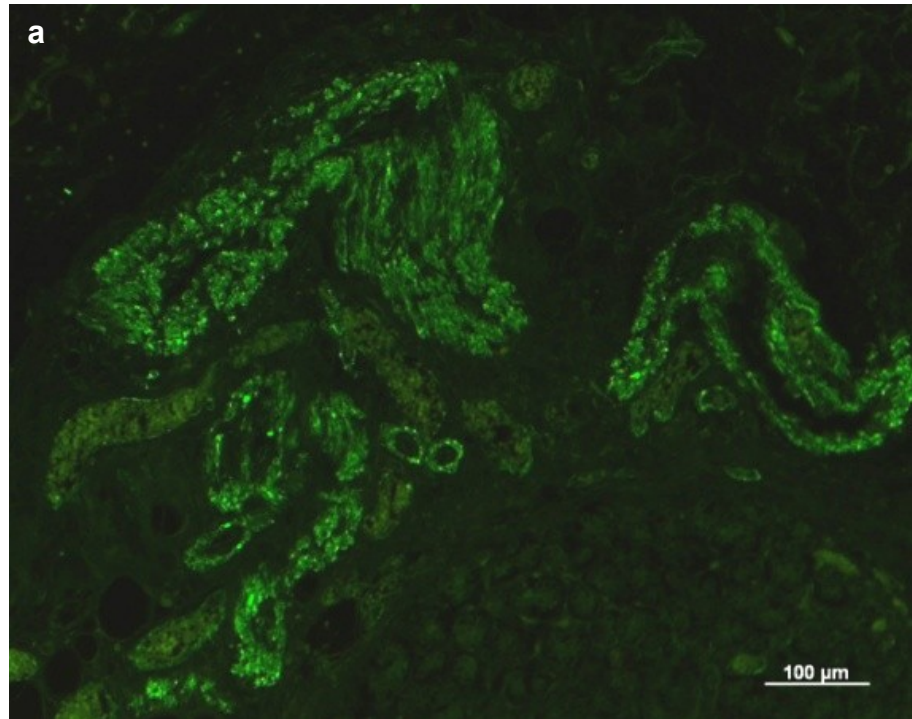


Figure 6.7. Effects of blue light on the deposition of silver on 4  $\mu\text{m}$  thick sections of paraffin wax-embedded kidney immunofluorescently stained for SMA. Fluorescence micrograph of fluorescein-labelled blood vessels (a) and bright field images, in the presence of Newman and Jasani's developer, at  $t = 0$  (b).



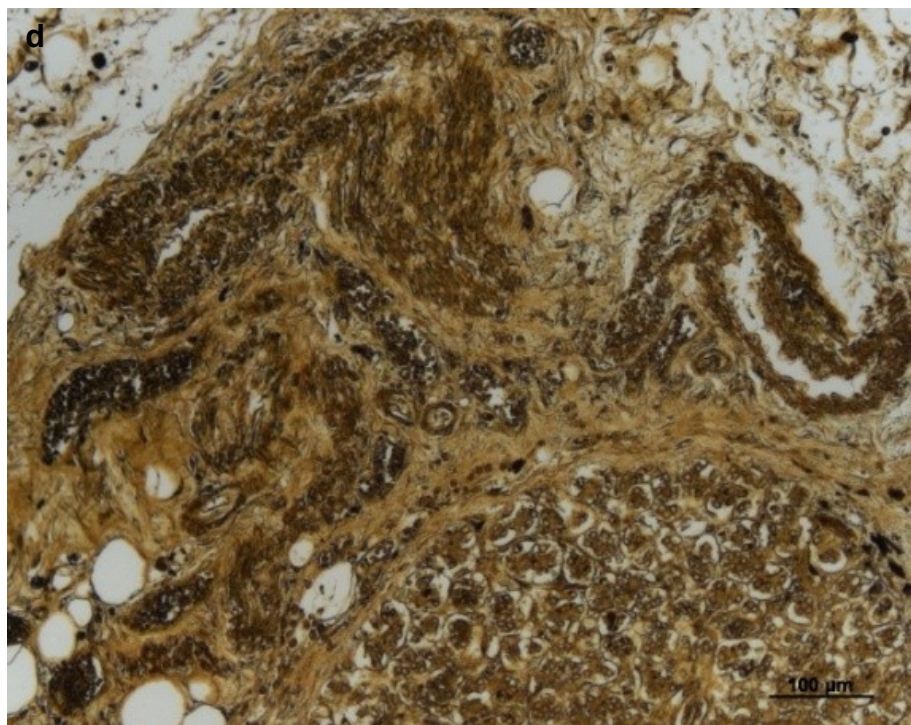
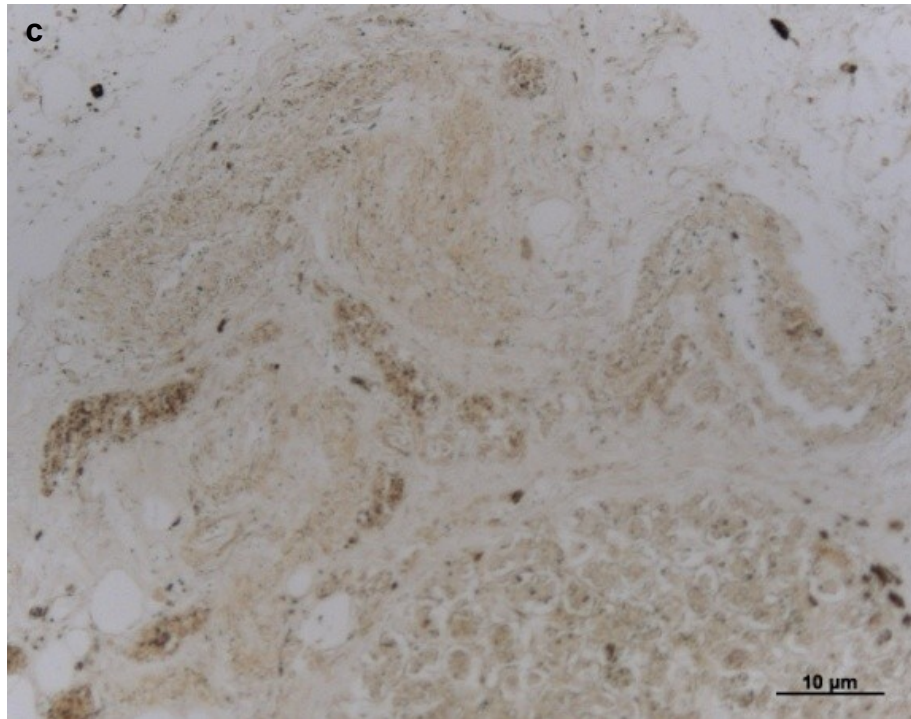


Figure 6.7 (continued). Effects of blue light on the deposition of silver on 4 μm thick sections of paraffin wax-embedded kidney immunofluorescently stained for SMA. Bright field images, in the presence of Newman and Jasani's developer, after irradiation with blue light for 10 minutes (c) and 15 minutes (d).

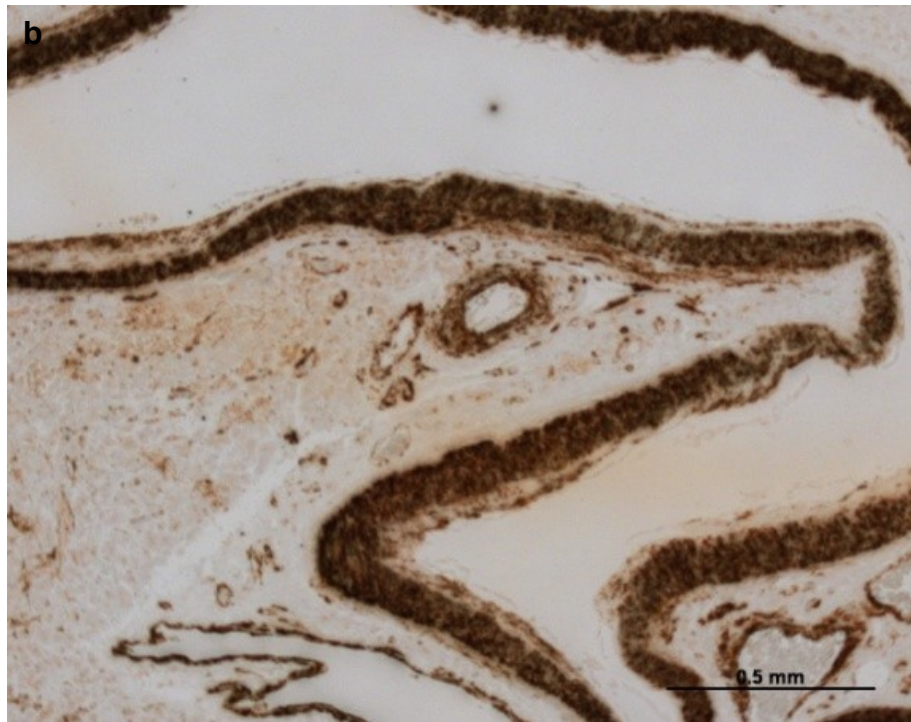
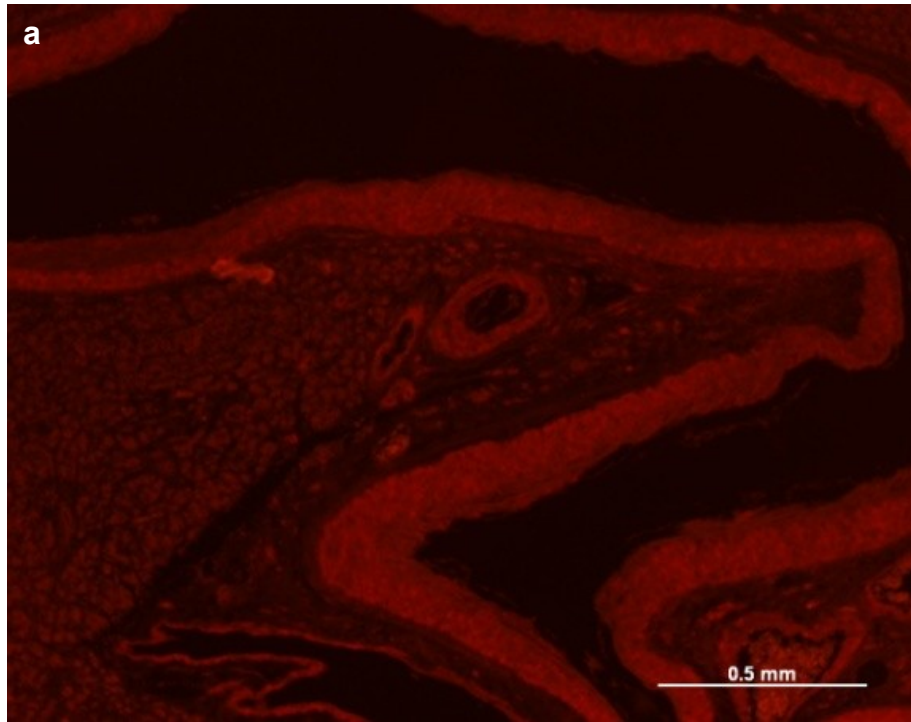


Figure 6.8. Effects of green light on the deposition of silver on 4  $\mu\text{m}$  thick sections of paraffin wax-embedded kidney immunofluorescently stained for SMA. Fluorescence micrograph of tetramethylrhodamine-labelled blood vessels (a), and bright field images, in the presence of Newman and Jasani's developer, after irradiation with green light for 5 minutes (b).

## 6.5 Discussion

Photoconversion of DAB was clearly demonstrated in the homogeneous model system, when conducted in the presence of fluorescein and irradiation with blue light. In contrast, no photoconversion was seen when the same technique was applied to tetramethylrhodamine. In the tissue model system, only a very slight deposition of polyDAB was observed in the fluorescein-labelled tissue, together with a stronger background staining, whereas no deposition was seen at all in the tetramethylrhodamine-labelled preparation. This failure of DAB to undergo photoconversion in the tissue model system was disappointing, and postponed further exploration of this process with halogenated compounds until the cause had been elucidated. The solubility of the polymerised halogenated 1,2-diamines in organic solvents would preclude their application in pre-embedding photoconversion techniques, but they should, in principle, work well in post-embedding, i.e. on-section, techniques.

Photoconversion of DAB by both fluorescein and tetramethylrhodamine, in a tissue model system, has been reported to occur on similar timescales (30 minutes) (Sandell and Masland, 1988). The reason for the discrepancy seen here might be due to the choice of buffer system; in the homogeneous model, and in Sandell and Masland's study, DAB-Tris was used, whereas in the tissue model here, DAB-PO<sub>4</sub> was employed. This was not expected to have any major influence on the photoconversion process, but a recent report indicates that the two buffer systems can have different effects on fluorophore photochemistry, at high concentrations (>20 mM), PO<sub>4</sub> engages in excited-state proton transfer that competes with radiative decay, whereas Tris does not (Peredes et al, 2011).

In contrast to the poor results for DAB, the photoconversion of silver from Newman & Jasani's developer was much more consistent. In the case of blue light irradiation, both control and experimental solutions began to darken within 5 minutes. The number and size of silver grains increased progressively in both cases, but occurred more rapidly in the solution containing fluorescein. In the tissue model system, a similar result was seen, with silver being clearly deposited on the tissue section within 10 minutes. The specificity of the reaction was poor and background staining was clearly present, presumably due to both blue light-catalysed reduction of silver and photoconversion due to tissue autofluorescence. In the homogeneous system, irradiation of the developer with green light caused no obvious reduction of silver in the control experiment, and required 10 minutes for visible darkening of the solution to occur when tetramethylrhodamine was present. There thus existed a short temporal window in which photoconversion of silver might be selectively achieved, and this was borne out in the tissue model system, where silver was deposited in large amounts at specific sites within just 5 minutes. Background staining was still problematic and may have reflected tissue autofluorescence-induced photoconversion. Better temporal control of silver deposition might be achieved by manipulating the composition of the developer, such as lowering the concentration of the reducing agent, pyrogallol.

The specificity of any photoconversion process in tissue is restricted by autofluorescence, which is particularly problematic in aldehyde-fixed tissue. It has also been reported to occur in some embedding resins (Haraguchi and Yokota, 2002; Singhrao et al., 2009,) and this might restrict the circumstances under which photoconversion can be performed i.e. prior to resin embedding.

The suppression of tissue autofluorescence has been achieved with a number of agents, such as sodium borohydride (Weber et al., 1978), Cu(II) (Schnell et al., 1999) and Cu(II) + H<sub>2</sub>O<sub>2</sub> (Kelly, 2010), and such techniques might have some utility here. Treatment of tissue sections with Cu(II) had been shown to catalyse the polymerisation of DAB when combined with H<sub>2</sub>O<sub>2</sub> (Kelly, 2010), but whether the same occurs without H<sub>2</sub>O<sub>2</sub> remains to be determined. That Cu(II) does not catalyse silver reduction, unless treated with sulfide, was described in Chapter 2. It is possible, then, that the specificity of the photoconversion process might be enhanced by a number of simple manoeuvres.

The underlying mechanism of the photoconversion process by fluorochromes has not been described, and the results presented here suggest a paradox; on the one hand, polymerisation of aromatic diamines is generally believed to be an oxidative process (Li et al., 2002), but the deposition of metallic silver from the physical developer is clearly reductive.

Photobleaching of fluorochromes, associated with the triplet state, can be suppressed by reducing agents such as p-phenylenediamine (Johnson and Nogueira-Araujo, 1981) or thiols (Song et al, 1996) and this might provide an explanation for the polymerisation of DAB by the photoconversion process; reduction of the fluorophore is accompanied by the oxidation, and subsequent polymerisation, of DAB.

The reduction of silver, in contrast, might be achieved by electron donation by fluorophores in the excited state by virtue of having a higher reduction potential than in the ground state i.e. an electron transfer process, possibly following coordination of Ag(I) to the fluorophore or via the reducing agent, pyrogallol.

Whether DAB, or indeed any aromatic diamine, can be reductively polymerised remains to be determined, but the existence of the autometallographic technique, for depositing silver with HRP (Hainfeld et al., 2002) lends some support to this.

The application of the photoconversion process has been circumvented, to a certain extent, by the introduction of quantum dots, which have been discriminated in the TEM based on morphological criteria (Giepmans et al., 2005). That quantum dots can be prepared with different elemental compositions, such as CdSe and CdTe, suggests that analytical approaches can be applied to facilitate their discrimination in a tomographic setting, but this does not appear to have been undertaken.

## **6.6 Summary and Conclusions**

While the photoconversion of DAB was largely unsuccessful, the photoconversion of silver from a physical developer gave very encouraging results that deserve further exploration. Since the final deposit is pure metal, identification by analytical TEM should prove facile. Once the problem associated with DAB is resolved, multiple demonstration of fluorochromes by analytical TEM and, ultimately, AEMT may become a practical and affordable reality.



## 6.7 References

- BRUCHEZ, M., MORONNE, M., GIN, P., WEISS, S. & ALIVISATOS, A. P. 1998. Semiconductor nanocrystals as fluorescent biological labels. *Science*, 281, 2013-2016.
- CHALFIE, M., TU, Y., EUSKIRCHEN, G., WARD, W. & PRASHER, D. 1994. Green fluorescent protein as a marker for gene expression. *Science*, 263, 802-805.
- CHAN, W. C. W. & NIE, S. M. 1998. Quantum dot bioconjugates for ultrasensitive nonisotopic detection. *Science*, 281, 2016-2018.
- DABBOUSI, B. O., RODRIGUEZVIEJO, J., MIKULEC, F. V., HEINE, J. R., MATTOUSSI, H., OBER, R., JENSEN, K. F. & BAWENDI, M. G. 1997. (CdSe)ZnS core-shell quantum dots: Synthesis and characterization of a size series of highly luminescent nanocrystallites. *Journal of Physical Chemistry B*, 101, 9463-9475.
- DAHAN, M., LEVI, S., LUCCARDINI, C., ROSTAING, P., RIVEAU, B. & TRILLER, A. 2003. Diffusion dynamics of glycine receptors revealed by single-quantum dot tracking. *Science*, 302, 442-445.
- DANSCHER, G. & STOLTENBERG, M. 2006. Autometallography (AMG) - Silver enhancement of quantum dots resulting from (1) metabolism of toxic metals in animals and humans, (2) in vivo, in vitro and immersion created zinc-sulphur/zinc-selenium nanocrystals, (3) metal ions liberated from metal implants and particles. *Progress in Histochemistry and Cytochemistry*, 41, 57-139.
- DEERINCK, T. J., MARTONE, M. E., LEV-RAM, V., GREEN, D. P., TSIEN, R. Y., SPECTOR, D. L., HUANG, S. & ELLISMAN, M. H. 1994. Fluorescence photooxidation with eosin: a method for high resolution immunolocalization and in situ hybridization detection for light and electron microscopy. *Journal of Cell Biology*, 126, 901-910.

- GAIETTA, G., DEERINCK, T. J., ADAMS, S. R., BOUWER, J., TOUR, O., LAIRD, D. W., SOSINSKY, G. E., TSIEN, R. Y. & ELLISMAN, M. H. 2002. Multicolor and electron microscopic imaging of connexin trafficking. *Science*, 296, 503-507.
- GALLYAS, F. 1982. Physico-chemical mechanism of the argyrophil I reaction. *Histochemistry*, 74, 393-407.
- GALLYAS, F. & WOLFF, J. R. 1986. Metal-catalyzed oxidation renders silver intensification selective - applications for the histochemistry of diaminobenzidine and neurofibrillary changes. *Journal of Histochemistry & Cytochemistry*, 34, 1667-1672.
- GIEPMANS, B. N. G., DEERINCK, T. J., SMARR, B. L., JONES, Y. Z. & ELLISMAN, M. H. 2005. Correlated light and electron microscopic imaging of multiple endogenous proteins using Quantum dots. *Nature Methods*, 2, 743-749.
- GRABENBAUER, M., GEERTS, W. J. C., FERNADEZ-RODRIGUEZ, J., HOENGER, A., KOSTER, A. J. & NILSSON, T. 2005. Correlative microscopy and electron tomography of GFP through photooxidation. *Nature Methods*, 2, 857-862.
- GRIFFIN, B. A., ADAMS, S. R. & TSIEN, R. Y. 1998. Specific covalent labeling of recombinant protein molecules inside live cells. *Science*, 281, 269-272.
- HAINFELD, J. F., EISEN, R. N., TUBBS, R. R. & D., P. R. 2002. Enzymatic metallography: A simple new staining method. *Microscopy and Microanalysis*, 8, 926-917.
- HARAGUCHI, C. M. & YOKOTA, S. 2002. Immunofluorescence technique for 100-nm-thick semithin sections of Epon-embedded tissues. *Histochemistry and Cell Biology*, 117, 81-85.



- HINES, M. A. & GUYOT-SIONNEST, P. 1996. Synthesis and characterization of strongly luminescing ZnS-capped CdSe nanocrystals. *Journal of Physical Chemistry*, 100, 468-471.
- JOHNSON, G.D. AND NOGUEIRA-ARAÚJO, G.M. (1981) A simple method of reducing the fading of immunofluorescence during microscopy. *Journal of Immunological Methods*, 43, 349-350.
- KAETHER, C. & GERDES, H. H. 1995. Visualisation of protein transport along the secretory pathway using green fluorescent protein. *Febs Letters*, 369, 267-271.
- KELLY, S. 2010. *The Optimisation of Immunohistochemical Marker Amplification*. Bachelor of Science, University of Wales Institute, Cardiff.
- LATA, S., GAVUTIS, M., TAMPE, R. & PIEHLER, J. 2006. Specific and stable fluorescence labeling of histidine-tagged proteins for dissecting multi-protein complex formation. *Journal of the American Chemical Society*, 128, 2365-2372.
- LI, X.-G., HUANG, M.-R. & DUAN, W. 2002. Novel multifunctional polymers from aromatic diamines by oxidative polymerizations. *Chemical Reviews*, 102, 2925 - 3030.
- MAGDE, D., WONG, R. & SEYBOLD, P. G. 2002. Fluorescence quantum yields and their relation to lifetimes of rhodamine 6G and fluorescein in nine solvents: Improved absolute standards for quantum yields. *Photochemistry and Photobiology*, 75, 327-334.
- MARANTO, A. R. 1982. Neuronal mapping: a photooxidation reaction makes Lucifer yellow useful for electron microscopy. *Science*, 217, 953-5.
- MARSHALL, J., MOLLOY, R., MOSS, G. W. J., HOWE, J. R. & HUGHES, T. E. 1995. The jellyfish green fluorescent protein; a new tool for studying ion channel expression and function. *Neuron*, 14, 211-215.

- OSBORN, M., WEBSTER, R. E. & WEBER, K. 1978. Individual microtubules viewed by immunofluorescence and electron microscopy in the same PtK2 cell. *Journal of Cell Biology*, 77, R27-R34.
- POWELL, R. D., HALSEY, C. M. R., SPECTOR, D. L., KAURIN, S. L., MCCANN, J. & HAINFELD, J. F. 1997. A covalent fluorescent-gold immunoprobe: Simultaneous detection of a pre-mRNA splicing factor by light and electron microscopy. *Journal of Histochemistry & Cytochemistry*, 45, 947-956.
- PAREDES, J. M., CROVETTO, L., ORTE, A., ALVAREZ-PEZ, J. M. and TALVERA, E. M. 2011. Influence of the solvent on the ground- and excited-state buffer-mediated proton-transfer reactions of a xanthenic dye. *Physical Chemistry Chemical Physics*, 13, 1685-1694.
- RIZZUTO, R., BRINI, M., PIZZO, P., MURGIA, M. & POZZAN, T. 1995. Chimeric green fluorescent protein as a tool for visualising subcellular organelles in living cells. *Current Biology*, 5, 635-642.
- SANDELL, J. H. & MASLAND, R. H. 1988. Photoconversion of some fluorescent markers to a diaminobenzidine product. *Journal of Histochemistry & Cytochemistry*, 36, 555-559.
- SCHNELL, S. A., STAINES, W. A. & WESSENDORF, M. W. 1999. Reduction of lipofuscin-like autofluorescence in fluorescently labeled tissue. *Journal of Histochemistry & Cytochemistry*, 47, 719-730.
- SINGHRAO, S. K., MULLER, C. T., GILBERT, S. J., DUANCE, V. C. & ARCHER, C. W. 2009. An immunofluorescence method for post-embedded tissue in acrylic resin Technovit 9100 New (R) using fluorescein isothiocyanate secondary detection marker. *International Journal of Experimental Pathology*, 90, A129.
- SONG, L., VARMA, C. A. G. O., VERHOEVEN, A. J. W. AND TANKE, H. J. 1996. Influence of the triplet excited state on the photobleaching kinetics of fluorescein in microscopy. *Biophysical Journal*, 70, 2959-2968.

WEBER, K., RATHKE, P. C. & OSBORN, M. 1978. Cytoplasmic microtubular images in glutaraldehyde-fixed tissue-culture cells by electron-microscopy and by immunofluorescence microscopy. *Proceedings of the National Academy of Sciences of the United States of America*, 75, 1820-1824.

# **Chapter 7**

## **Polymer Characterisation**

## 7.1 Introduction

The complexity of the most powerful marker amplification techniques, as explored and developed in Chapters 2 and 3, preclude their use in high throughput automated laboratories and are unattractive even to workers in research laboratories.

For the full potential of marker amplification to be realised, when combined with other amplification techniques, there is a need for considerable simplification. This can be aided by an understanding of the structure of polyDAB and the coordination chemistry of its d-block metal complexes, which might provide useful insights into the rational design of novel catalytic markers. As noted in Chapter 1, however, current knowledge regarding the nature of polyDAB is confined to a single infra-red spectrum (Seligman et al. 1968).

A number of complementary analytical techniques exist that might provide sufficient information, including mass spectrometry, gel permeation chromatography, various spectroscopic methods and quantitative elemental analysis.

## 7.2 Materials

Mesitylene, chlorobenzene, toluene, ethyl acetate, dichloromethane (DCM), acetonitrile, dimethylsulfoxide (DMSO), dimethylformamide (DMF), conc. HCl, H<sub>2</sub>SO<sub>4</sub>, tetrahydrofuran (THF), KOAc, Pd(OAc)<sub>2</sub>,  $\alpha$ -cyano-4-hydroxycinnamic acid (CHCA), PEG 1000, 2000 and 3000, trifluoroacetic acid (TFA) and glacial acetic acid were supplied by Fisher Scientific (Loughborough, Leicestershire, U.K.). [<sup>15</sup>N] KNO<sub>3</sub>, CDCl<sub>3</sub> and D<sub>6</sub>-DMSO were supplied by Goss Scientific (Nantwich,

Cheshire, U.K.). *N,N'*-biphenyl-4,4'-diyl diacetamide was purchased from Tokyo Chemical Industry UK Ltd (Oxford, Oxfordshire, U.K.).

### **7.3 Methods**

#### **7.3.1 Preparation of PolyDAB**

##### **7.3.1.1 Determination of Optimum Conditions for DAB Polymerisation**

In initial experiments, to determine the optimum concentration of peroxidase needed to deposit polyDAB in an acceptable timeframe, 10  $\mu$ l 10-fold dilutions of GAM IgPC, from neat to  $1/10,000$  in ddH<sub>2</sub>O, were added to 1 ml aliquots of DAB-Tris + 15  $\mu$ l/ml 30% H<sub>2</sub>O<sub>2</sub> and the time taken for the solution to darken and the appearance of a polymer precipitate noted. Scaling up the preparation to determine yield, 1.5 ml 30% H<sub>2</sub>O<sub>2</sub> was added to 1 l of DAB-Tris followed by 10 ml  $1/100$  GAM IgPC. After 40 minutes, the preparation was filtered through Whatman No.1 filter paper, the cake thoroughly washed with ddH<sub>2</sub>O and dried in an oven at 150°C.

##### **7.3.1.2 Determination of the Solubility of PolyDAB**

The solubility of dry polyDAB was examined in the following solvents: mesitylene, chlorobenzene, toluene, ethyl acetate, acetonitrile, DMSO, DMF, THF, DCM, conc. HCl, conc. H<sub>2</sub>SO<sub>4</sub> and glacial acetic acid.

##### **7.3.1.3 Polymerisation of DAB in DMSO**

Given the poor solubility of polyDAB in the various solvents tested above, an attempt was made to enzymatically polymerise polyDAB in DMSO. 5 mg DAB

was dissolved in 10 ml DMSO and 15  $\mu$ l 30% H<sub>2</sub>O<sub>2</sub> added followed by 100 ml <sup>1</sup>/<sub>100</sub> GAM IgPC.

#### **7.3.1.4 Solubility of Wet PolyDAB in Polar Solvents**

In a preliminary experiment, the possibility of dissolving freshly prepared wet polyDAB in polar solvents was examined. PolyDAB from a 100 ml 0.05% solution was prepared as above and the precipitate recovered by initial centrifugation at 200 g for 2 minutes. The pellet was washed 3 times by resuspension in ddH<sub>2</sub>O and centrifugation at 1000 g. The pellet was resuspended in 1 ml DMSO and ultrasonicated for 5 minutes in an ultrasonic bath followed by centrifugation at 10,000 g for 10 minutes.

PolyDAB was prepared from 1 l of DAB-Tris as above and resuspended in 10 ml DMSO. 4 ml of the suspension was centrifuged at 10,000 g for 10 minutes and 2 ml supernatant dried in a pre-weighed glass vial at 150°C. The experiment was repeated using DMF as solvent. For gel permeation chromatography, polymer solutions need to be dry. In a further experiment, standing a solution of wet polymer over pre-dried molecular sieve was explored. Solvent was evaporated from the supernatant as above.

#### **7.3.1.5 Solubility of Freeze-Dried polyDAB in Polar Solvents**

PolyDAB was prepared as above, resuspended by ultrasonication in ddH<sub>2</sub>O, and rapidly frozen in liquid nitrogen. The preparation was freeze-dried at -40°C and dissolved in DMSO, DMF and conc. H<sub>2</sub>SO<sub>4</sub>. Solubility was determined as above. In the case of conc. H<sub>2</sub>SO<sub>4</sub>, polyDAB was precipitated by addition of ddH<sub>2</sub>O.

## 7.3.2 Characterisation of polyDAB

### 7.3.2.1 Infra-red Spectroscopy

For infra-red spectroscopy, oven-dried polyDAB was prepared as KBr discs.

### 7.3.2.2 MALDI-TOF

A final concentration of 1 pM is recommended for analysis by MALDI-TOF but since the molecular weight of polyDAB is unknown, a preliminary assumption of 10 kD was chosen. A stock solution of approximately 10 mg/ml polyDAB in DMSO was diluted with 0.1% aqueous TFA to a 10-fold dilution series of 2 nM to 200 fM. Each dilution was mixed 1:1 with 5 mg/ml  $\alpha$ -cyano-4-hydroxycinnamic acid (CHCA) in 1:1 acetonitrile:methanol. 1  $\mu$ l of each solution was applied to a MALDI-TOF plate and allowed to air dry at RT.

To compare polyDAB produced from solution with that deposited *in situ*, a MALDI-TOF plate was glow discharged for 30 seconds in a Balzers vacuum coater (Oerlikon Balzers Coating UK Ltd, Milton Keynes, U.K.) and 1  $\mu$ l droplets of GAM IgPC applied as 10-fold dilutions in ddH<sub>2</sub>O from neat to  $1/_{10,000,000}$ . After 1 minute, surplus solution was removed with a pipette, and 1  $\mu$ l drops of DAB-Tris applied for 3 minutes. The plate was thoroughly washed with de-ionised water and allowed to air dry. 1  $\mu$ l 1:1 with 5 mg/ml CHCA in 1:1 acetonitrile:methanol + 1 pM each of PEG 1000, 2000 and 3000 was applied to each preparation and air dried.



### 7.3.2.3 Gel Permeation Chromatography

For molecular weight characterisation, samples of polyDAB (both molecular sieve-dried and freeze-dried) were dissolved in DMSO and analysed by Dr. Steve Holden (Smithers RAPRA, Shrewsbury, Shropshire, U.K.) by gel permeation chromatography with pullulan polysaccharides as molecular weight standards.

### 7.3.2.4 $^1\text{H}$ , $^{13}\text{C}$ and $^{15}\text{N}$ NMR Spectroscopy

PolyDAB was dissolved in  $\text{D}_6$ -DMSO by ultrasonication for 15 minutes. Following centrifugation in a glass eppendorf vial (to avoid solution of polypropylene) at 10,000 g for 10 minutes, the supernatant was removed for subsequent analysis.

### 7.3.3 Synthesis of $^{15}\text{N}$ -labelled 3,3'-4,4'-tetraaminobiphenyl (DAB)

The relatively high cost of *N,N*-biphenyl-4,4'-diyldiacetamide prompted an attempt to prepare 4,4'-dinitrobiphenyl by biaryl coupling of 4-nitro-iodobenzene (Yu, Tang and Li 2009). 1 g (4.00 mmol) 4-nitro-iodobenzene was dissolved in 20 ml acetone and 0.089 g (0.4 mmol)  $\text{Pd}(\text{OAc})_2$  and 1.96 g (10.8 mmol) KOAc added. The mixture was refluxed under a nitrogen blanket at  $100^\circ\text{C}$  over night. The cooled mixture was extracted twice with diethyl ether, and the product recrystallised from chloroform/hexane.  $^1\text{H}$  NMR was not consistent with the expected product, which should have produced two doublets. Instead, an additional peak was seen, and interpretation was more consistent with 2,6-dinitrobiphenylene.  $^1\text{H}$  NMR (400 MHz,  $\text{CDCl}_3$ )  $\delta$  7.32 (d,  $^3J_{\text{HH}} = 8.48$ , 2H; C4 and C8), 8.05 (dd,  $^3J_{\text{HH}} = 8.48$ ,  $^4J_{\text{HH}} = 2.34$ , 2H; C3 and C7), 8.58 (d,  $^4J_{\text{HH}} = 2.34$ , 2H; C1 and C5) ppm.

0.5 g (1.877 mmol) *N,N*-biphenyl-4,4'-diyldiacetamide was dissolved in 10 ml conc. H<sub>2</sub>SO<sub>4</sub>, cooled on ice, and 0.38 g (3.77 mmol) 50% [<sup>15</sup>N] KNO<sub>3</sub> added with stirring for 2 hours. Work-up was performed as previously described. 0.5 g (1.877 mmol) *N,N*-biphenyl-4,4'-diyldiacetamide yielded 0.438 g (1.22 mmol) *N,N*-(3,3'-dinitrobiphenyl-4,4'-diyldiacetamide (64.99%). <sup>1</sup>H NMR (400 MHz, CDCl<sub>3</sub>) δ 2.18 (s, 6H; acetyl), 2.28 (s, 6H; acetyl), 7.58 (d, <sup>3</sup>J<sub>HH</sub> = 8.48, 2H), 7.70 (dd, <sup>3</sup>J<sub>HH</sub> = 8.77, <sup>4</sup>J<sub>HH</sub> = 2.05, 2H), 7.93 (td, <sup>3</sup>J<sub>HH</sub> = 8.48, <sup>4</sup>J<sub>HH</sub> = 2.05, <sup>5</sup>J<sub>HH</sub> = 1.46, 2H) 8.13 (d, <sup>5</sup>J<sub>HH</sub> = 1.17, 2H), 8.51 (d, <sup>5</sup>J<sub>HH</sub> = 1.46, 2H), 8.54 (dd, <sup>3</sup>J<sub>HH</sub> = 8.77, <sup>4</sup>J<sub>HH</sub> = 4.97, 2H), 9.71 (s, broad, 1H) and 10.07 (s, broad, 1H) ppm. The <sup>1</sup>H NMR spectrum indicated either the presence of at least two species or, possibly, mononitration. TLC with 20% hexane in ethyl acetate resolved only a single species. Mass spectroscopy confirmed successful dinitration (clear triple peaks (differing by 1 mass unit) centred on 359 (mass ion), 317 (the monoacetamide) and 275 (the dinitrodianiline)). The <sup>1</sup>H NMR spectrum was difficult to reconcile with the other data, even if considerable <sup>15</sup>N - <sup>1</sup>H coupling was invoked (more than occurs between <sup>15</sup>N amine nitrogen and amine protons; usually around 95Hz). Time did not allow further investigation of this phenomenon.

## 7.4 Results

### 7.4.1 Preparation of PolyDAB

#### 7.4.1.1 Determination of Optimum Conditions for DAB Polymerisation

Following addition of H<sub>2</sub>O<sub>2</sub> to DAB solutions, a slight darkening was evident, prior to addition of GAM IgPC. Results of the optimisation experiment are summarised in Table 7.1, below:

Table 7.1. DAB solution darkening and precipitation times following addition of varying concentrations of GAM IgPC.

Concentration of GAM IgPC	Time until solution darkened (minutes)	Time until precipitate appeared (minutes)
Neat	Immediate	2
<sup>1</sup> / <sub>10</sub>	Immediate	5
<sup>1</sup> / <sub>100</sub>	Immediate	35
<sup>1</sup> / <sub>1000</sub>	3	>180
<sup>1</sup> / <sub>10,000</sub>	20	>180
<sup>1</sup> / <sub>100,000</sub>	>180	>180

<sup>1</sup>/<sub>100</sub> GAM IgPC was chosen for subsequent preparations, and produced polyDAB in moderate yield (34%).

#### **7.4.1.2 Determination of the Solubility of PolyDAB**

PolyDAB was insoluble, as judged by the colour of supernatants in almost all the solvents tested, with the exception of DMSO and DMF, where only a pale colouration was evident.

#### **7.4.1.3 Polymerisation of DAB in DMSO**

No polymerisation was observed, as judged by darkening on the solution, even after 60 minutes.

#### **7.4.1.4 Solubility of Wet PolyDAB in Polar Solvents**

Wet polyDAB dissolved to a concentration of 9.45 mg/ml in DMSO and 6.45 mg/ml in DMF. After storage over molecular sieve, however, final concentration of polyDAB were reduced to 0.9 mg/ml and 0.4 mg/ml respectively.

#### **7.4.1.5 Solubility of Freeze-dried PolyDAB in Polar Solvents**

Freeze-drying of polyDAB increased the polymer's solubility to 12.35 mg/ml in DMSO and to 8.66 mg/ml for DMF. Solubility in conc. H<sub>2</sub>SO<sub>4</sub> was 11.25 mg/ml.

### **7.4.2 Characterisation of polyDAB**

#### **7.4.2.1 Infra Red Spectroscopy**

PolyDAB exhibited broad absorption bands centred on 1621 cm<sup>-1</sup> (C-N or C=N stretch) and 3433 cm<sup>-1</sup> (broad; N-H stretch), and additional, narrower bands at 803 cm<sup>-1</sup>, 1099 cm<sup>-1</sup>, 1261 cm<sup>-1</sup> and 1500 cm<sup>-1</sup> (N=N stretch).

Prominent absorption bands of DAB.4HCl were 2566  $\text{cm}^{-1}$ , 2846  $\text{cm}^{-1}$  and 3389  $\text{cm}^{-1}$  (broad; N-H stretch), and 1498  $\text{cm}^{-1}$  (narrow; C=C stretch). In addition, there were a number of smaller, narrow bands at 543  $\text{cm}^{-1}$ , 827  $\text{cm}^{-1}$ , 868  $\text{cm}^{-1}$ , 1108  $\text{cm}^{-1}$  (N-H wag), 1193  $\text{cm}^{-1}$ , 1248  $\text{cm}^{-1}$  (C-N stretch), 1336  $\text{cm}^{-1}$  (C-N stretch), 1398  $\text{cm}^{-1}$  and 1618  $\text{cm}^{-1}$ . Assignments are tentative.

#### **7.3.2.2 MALDI-TOF**

Preliminary attempts to acquire spectra by MALDI-TOF revealed a larger series of peaks that were separated by 44 mass units, and consistent with polypropylene fragments derived from the eppendorf tube in which polyDAB solution had been prepared. Repetition of the preparative procedure using glass tubes failed to produce any signal that was consistent with DAB polymer.

#### **7.4.2.3 Gel Permeation Chromatography**

Gel permeation chromatography indicated that polyDAB, prepared as molecular sieve-dried samples, had a molecular weight range of approximately 600 (trimer) to 130,000, with an average molecular weight calculated at 9180. Ultrasonicated, freeze-dried samples gave less reproducible results than the initial preparations, and had lower molecular weight values (mean 2210).

#### **7.4.2.4 $^1\text{H}$ and $^{13}\text{C}$ NMR Spectroscopy**

$^1\text{H}$  NMR of polyDAB revealed a complex spectrum of peaks between  $\delta$  6.3 and 7.5 which could not be interpreted. No peaks could be identified with  $^{13}\text{C}$  NMR.

## 7.5 Discussion

In preliminary optimisation experiments, darkening of the DAB solution upon addition of  $\text{H}_2\text{O}_2$  was noted. Ordinarily, this goes unnoticed, since small volumes of solution are employed for immunohistochemical staining. A similar phenomenon has been observed during the early stages of melanin bleaching by  $\text{H}_2\text{O}_2$ , where oxidation was postulated to lead to a quinone-type intermediate (Korytowski and Sarna, 1990) (figure 7.1a). Whether DAB undergoes conversion to an imine intermediate remains to be determined (figure 7.1b).

Characterisation of polyDAB presented a number of challenges, mainly centred on solubility. Dry polyDAB was remarkably insoluble in a wide number of solvents, and even when wet, only dissolved in high polarity compounds or strong acid. It is both the insolubility and 'stickiness' of polyDAB that makes it so attractive a marker and it was this latter property that was probably responsible for the failure of the MALDI-TOF experiments. The limited solubility precluded separation of the mixture of polymers that gel permeation chromatography revealed. The use of ultrasonication to facilitate the solution of polyDAB in polar solvents resulted in poor reproducibility, but this problem might be overcome by avoiding ultrasonication prior to freeze-drying of samples.

The results from molecular weight characterisation should be interpreted with a certain amount of caution, since the molecular weight standards were chemically dissimilar and unpredictable adsorption effects of polyDAB may have occurred.

That a mixture of polymers was being examined placed constraints on the amount of data that infrared spectroscopy could reveal. Tentative assignment of absorption bands suggested the presence of azo or azine linkages. The results are

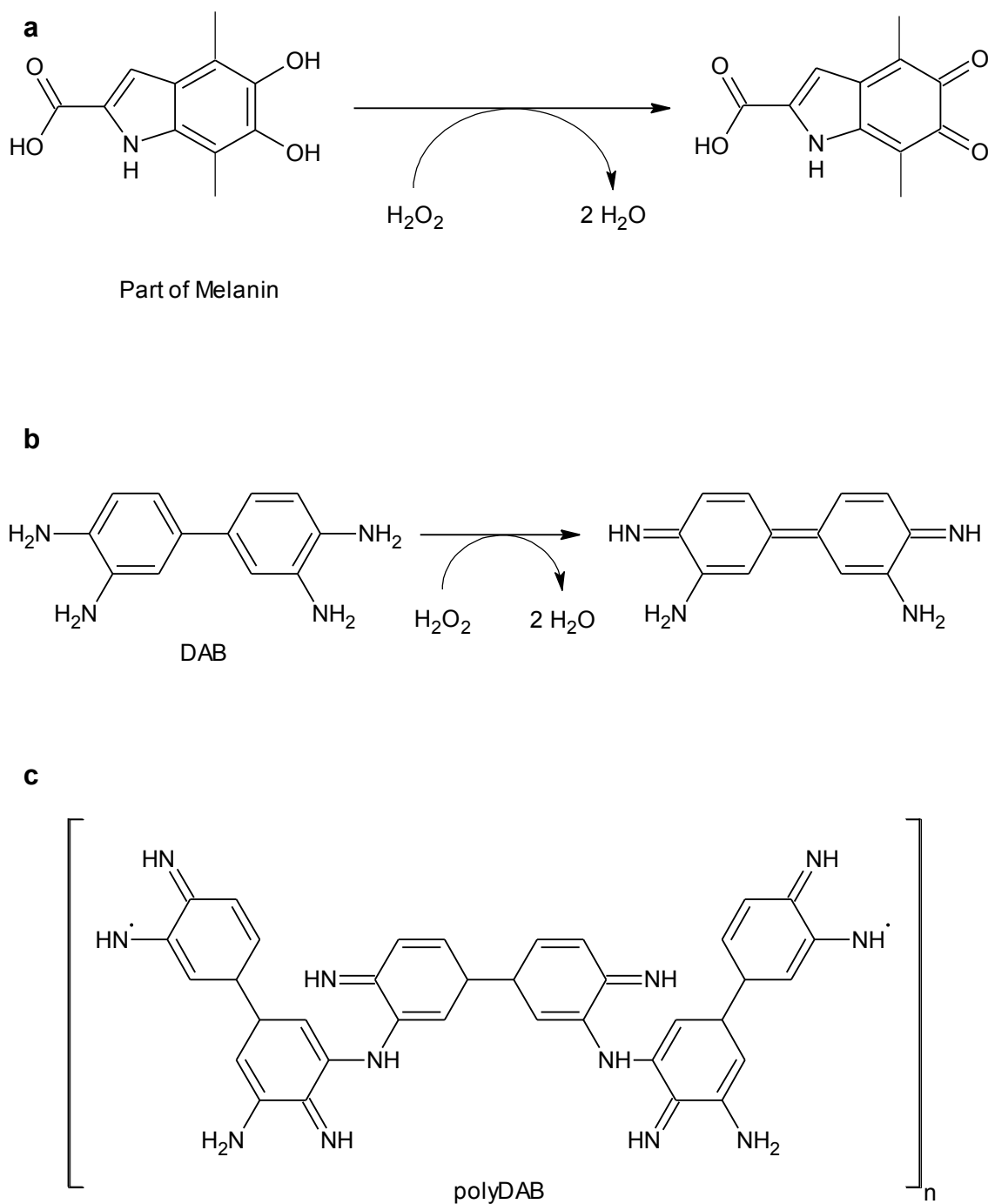


Figure 7.1. Proposed mechanism for the early stages of melanin bleaching by  $\text{H}_2\text{O}_2$  (Korytowski and Sarna, 1990) (a), a suggested mechanism for the darkening of DAB solution following addition of  $\text{H}_2\text{O}_2$  (b), and a proposed indamines structure for polyDAB (Seligman et al, 1968) (c).

broadly similar to, and not inconsistent with the formation of an indamines-type polymer, as suggested by Seligman et al (1968) (figure 7.1c). The purchase or preparation of standard compounds, such as azobenzene, phenazine etc., might provide some useful information in this regard.

Given the limited information that the various techniques supplied, an attempt to prepare  $^{15}\text{N}$ -enriched DAB was made. The unexpected results from the initial attempt to prepare 4,4'-dinitrobiphenyl necessitated the purchase of acetylated benzidine from a commercial source. Benzidine, which would have been an intermediate in the synthesis, is a known carcinogen and is best avoided if possible. Alternative synthetic routes might be possible via  $^{15}\text{N}$ -enriched 1,2-dinitro-4-halobenzene precursors.  $^{15}\text{N}$ -enrichment might thus be achieved at either the 3,3' or 4,4' position of the final product, which might provide some useful insights into the structure of the final polymer. The preparation of  $^{13}\text{C}$ -enriched DAB would also be useful, given the poor solubility of the final polymer, but the cost would be very high since such compounds would have to be prepared from either  $^{13}\text{C}$ -enriched benzene or aniline.

Nitration had not presented any difficulties in previous syntheses, but the  $^1\text{H}$  NMR spectrum was difficult to interpret, even though TLC and mass spectrometry suggested the presence of a single compound of expected molecular weights (un-, mono-, and doubly  $^{15}\text{N}$  nitrated). Time limitations did not permit an investigation of these conflicting results, nor the eventual preparation of  $^{15}\text{N}$ -labelled polyDAB.

The low solubility of polyDAB, together with the existence of a wide range of sizes, ranging from trimers to <100,000 mw polymers placed constraints on the information that could be gleaned from the various analytical techniques. The low



molecular weight oligomers may be more soluble in a greater range of organic solvents and might be prepared by stopping the polymerisation reaction by addition of either strong acid or base. The latter would be expected to deprotonate the oligomer and increase its solubility in organic solvents such as ethyl acetate. Alternatively, far greater control of polymerisation may be achieved by the photoconversion process (once the problems that were encountered in Chapter 6 have been resolved), since all that is required is an intense light source, such as a mercury lamp.

Characterisation of polyDAB-metal complexes was not undertaken, since many of the techniques used for characterising polyDAB provided only limited information. CHN-metal and CHN-metal-sulfide analysis would have been useful, but was prohibitively expensive, particularly when the influence of different concentrations of metal and sulfide on marker amplification was considered. CHN-halide analysis would have been similarly useful for characterising the various halogenated aromatic amine polymers, but, again, the cost was prohibitive. The solubility of the halogenated polymers in organic solvents, such as ethyl acetate and chloroform, might provide a means of chromatographic separation prior to characterisation by various spectroscopic techniques such as NMR, UV/visible and infrared spectroscopy. Synthesis of substrates from halonitroaniline precursors would supply material of higher purity than those that are commercially available, all of which have suffered from some degree of oxidation, as judged by their brown/black appearance. Preparation of  $^{15}\text{N}$ -enriched substrates could similarly be prepared from haloaniline precursors.

## 7.6 Summary and Conclusions

The mechanism of aromatic diamine polymerisation and the subsequent characterisation of the polymers has been the preserve of material scientists, since a wide variety of useful composites can be derived from them (Li et al, 2002). That polyDAB has remained largely uncharacterised since its introduction (Graham and Karnovsky, 1966), is perhaps surprising. This paucity of information might be explained in two ways, namely its poor solubility in a wide variety of solvents, and the fact that biologists are much more interested in the information that (immuno)histochemically deposited polyDAB reveals than they are in the polymer itself.

The attempt to characterise polyDAB was driven by a desire to apply the knowledge of its structure and coordination chemistry to the design of novel markers, but the results of this limited study were more instructive than revelatory, in that they indicated what might be more fruitful avenues for exploration rather than providing many insights. Clearly, much work still needs to be done.

## 7.7 References

- Graham, R. C. & M. J. Karnovsky (1966) The early stages of absorption of injected horseradish peroxidase in the proximal tubules of mouse kidney: ultrastructural cytochemistry by a new technique. *Journal of Histochemistry and Cytochemistry*, 14, 291-302.
- Korytowski, W. & T. Sarna (1990) Bleaching of melanin pigments - role of copper ions and hydrogen peroxide in auto-oxidation and photo-oxidation of synthetic DOPA-melanin. *Journal of Biological Chemistry*, 265, 12410-12416.
- Li, X.-G., M.-R. Huang & W. Duan (2002) Novel multifunctional polymers from aromatic diamines by oxidative polymerizations. *Chemical Reviews*, 102, 2925 - 3030.
- Seligman, A. M., M. J. Karnovsky, H. L. Wasserkrug & J. S. Hanker (1968) Nondroplet ultrastructural demonstration of cytochrome oxidase activity with a polymerising osmiophilic reagent, diaminobenzidine (DAB). *Journal of Cell Biology*, 38, 1-14.
- Yu, M., R.-Y. Tang & J.-H. Li (2009) Synthesis of 6,7-dihydro-5H-dibenzo c,e azepines and biaryls by palladium-catalyzed Ullmann reaction. *Tetrahedron*, 65, 3409-3416.

# **Chapter 8**

## **Additional Applications of Halogenated Aromatic Diamines**

## 8.1 Introduction

One of the major weaknesses of the peroxidase/DAB system at the light microscopic level, as mentioned in Chapter 2, is that the reaction ceases after about 3 minutes, making the visualisation of very small amounts of target molecule impossible without recourse to either reporter or marker amplification.

As seen in Chapter 5, 4,5-diCl-OPD, from one commercial source at least, produced a polymer of fibrillary appearance. The morphology suggested that the fibres might continue to grow from the site of enzyme-catalysed reaction for some time before enzyme inhibition occurred. While clearly unsuitable for use in AEMT, this phenomenon might have some utility as an alternative light microscopical marker to polyDAB, and possibly obviate the need for either reporter or marker amplification. If successful, such a technology would greatly simplify current immunohistochemical staining procedures, particularly where extremely small quantities of target molecule required demonstration and localisation.

Polymer growth might occur from either the proximal (enzyme-catalysed) or distal end (autocatalytic) of the fibre, or both. Inhibition of HRP, following an initial period of polymerisation would allow dissection of this process. A number of inhibitors of endogenous peroxidase have been described including  $H_2O_2$  (Van Duijn, 1957), phenylhydrazine (Straus, 1972), sodium azide (Li et al., 1987; Klapper and Hackett, 1963), phenol (Baynton et al., 1994) and cyanide (Klapper and Hackett, 1963). The inclusion of aromatic compounds in the reaction mixture is probably best avoided since there exists the possibility of copolymer formation.

The solubility of the polymer in organic solvents necessitates the use of aqueous mountants, the use of which does not fit easily into high-throughput automated procedures. This restriction might be addressed by fixation with, for example,

glutaraldehyde, since free amines on adjacent polymer fibres could be cross-linked. An alternative might be air-, or heat-drying, since the latter was noted, in Chapter 7, to severely reduce the solubility of polyDAB compared to wet, or freeze dried preparations. Some proprietary automated procedures use air drying of slides, rather than solvent dehydration, prior to mounting, so this latter technique may well be preferable.

## 8.2 Materials

4,5-diCl-OPD was purchased from Acros (Fisher Scientific, Loughborough, Leicester, U.K.). The sources of other materials are as previously described.

## 8.3 Methods

### 8.3.1 Determination of the Sensitivity of Poly4,5-diCl-OPD

Sections of paraffin wax-embedded pancreatic or adrenal tissue were prepared and immunohistochemically stained with MAH SMA at  $1/5000$ ,  $1/10,000$ ,  $1/20,000$  and  $1/50,000$  as previously described, and incubated in 0.05% solutions of 4,5-diCl-OPD for 3, 10, 20 and 60 minutes. Following thorough washing in ddH<sub>2</sub>O, sections were mounted in Fluorsave™. Similarly immunohistochemically stained sections were prepared using DAB as substrate for comparison.

### 8.3.2 Inhibition of Horseradish Peroxidase

Preliminary studies, to determine the optimum inhibitor concentration, were performed with MAH SMA at  $1/500$  and DAB as substrate. Inhibitors were used for the following times and concentrations:

H<sub>2</sub>O<sub>2</sub> 0.3% for 5 minutes prior to addition of DAB-Tris

NaN<sub>3</sub> 0.02%, 0.2% and 2% both prior to (5 minutes application) and during incubation with DAB-Tris

NaCN 0.1 μM to 1 mM in 10-fold increments, as for NaN<sub>3</sub>

Further sections were stained with  $1/20,000$  MAH SMA and incubated in 4,5-diCl-OPD solution for 3 minutes followed by thorough washing and further

incubation in the 4,5-diCl-OPD solution with or without 1 mM NaCN for 7, 27 or 57 minutes.

### **8.3.3 Fixation of Poly4,5-diCl-OPD**

Sections, immunohistochemically stained with MAH SMA at  $1/5000$  and incubated in 4,5-diCl-OPD for 3 minutes, were fixed with either 0.5% glutaraldehyde as for immunocolloidal gold in Chapter 2, or air dried, and dehydrated and mounted as previously described.



## **8.4 Results**

### **8.4.1 Determination of the Sensitivity of Poly4,5-diCl-OPD**

In blood vessels that were immunohistochemically stained with MAH SMA at  $1/5000$ , staining was clearly seen by 3 minutes (figure 8.1a) and intensity increased further by 10 minutes (figure 8.1b). No further increase in staining intensity was observed at 20 minutes (figure 8.1c) or 60 minutes. At  $1/10,000$  (figures 8.1d - f) and  $1/20,000$  (figures 8.1g - i) MAH SMA, staining intensity continued to increase until the full 60 minutes, whereas at  $1/50,000$  maximum staining was complete by 20 minutes (figures 8.1j - l). In contrast, staining with DAB as substrate could be clearly seen by 3 minutes at  $1/500$  and  $1/1,000$  (figure 8.1m) but no further increase in staining intensity was observed after 60 minutes (figure 8.1n). Similarly, at  $1/2,000$ , only the faintest staining could be discerned (figure 8.1o), which did not improve with prolonged incubation (figure 8.1p). No staining could be seen at  $1/5,000$  SMA.

### **8.4.2 Inhibition of Horseradish Peroxidase**

#### **8.4.2.1 Preliminary Studies with DAB**

##### **8.4.2.1.1 H<sub>2</sub>O<sub>2</sub>**

In untreated sections, deposits of polyDAB were seen in both the smooth muscle cells of the arterioles and venules, and in the erythrocytes (figure 8.2a). Pre-incubation with 0.3% H<sub>2</sub>O<sub>2</sub> for 5 minutes abolished erythrocyte staining but only resulted in minor inhibition of HRP (figure 8.2b).

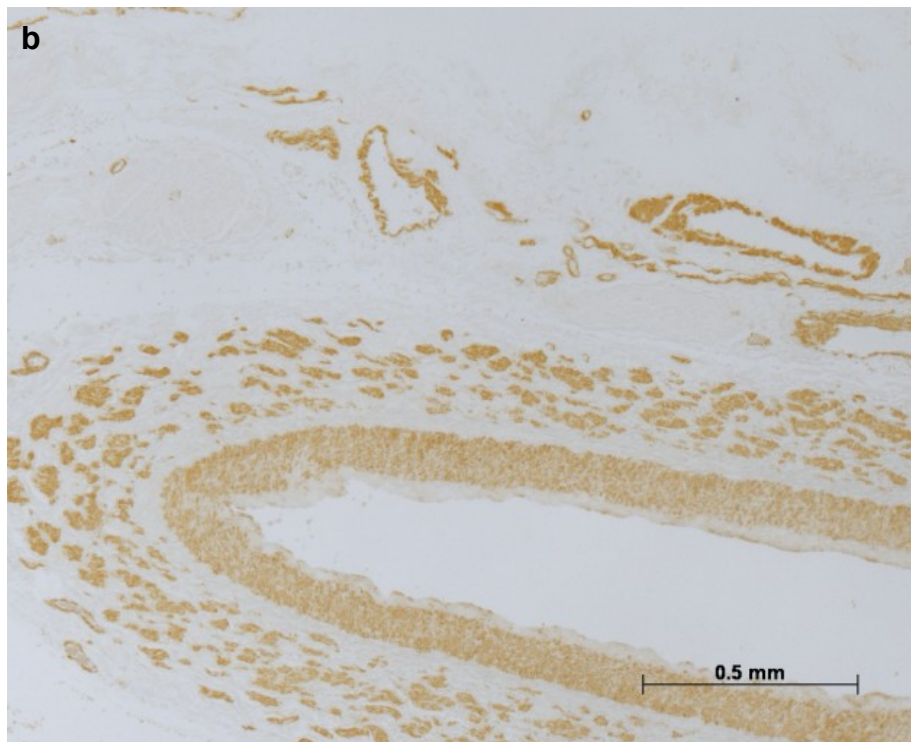
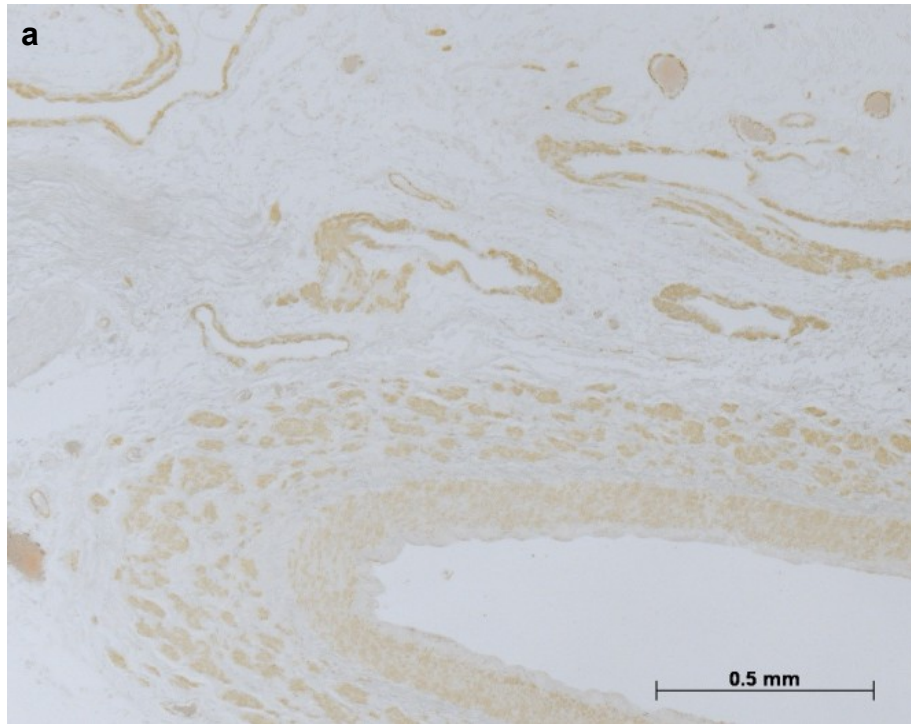


Figure 8.1. 4  $\mu\text{m}$  thick sections of paraffin wax-embedded pancreas immunohistochemically stained for SMA using MAH SMA at  $1/5,000$  and incubating in 4,5-diCl-OPD for 3 minutes (a) and 10 minutes (b).

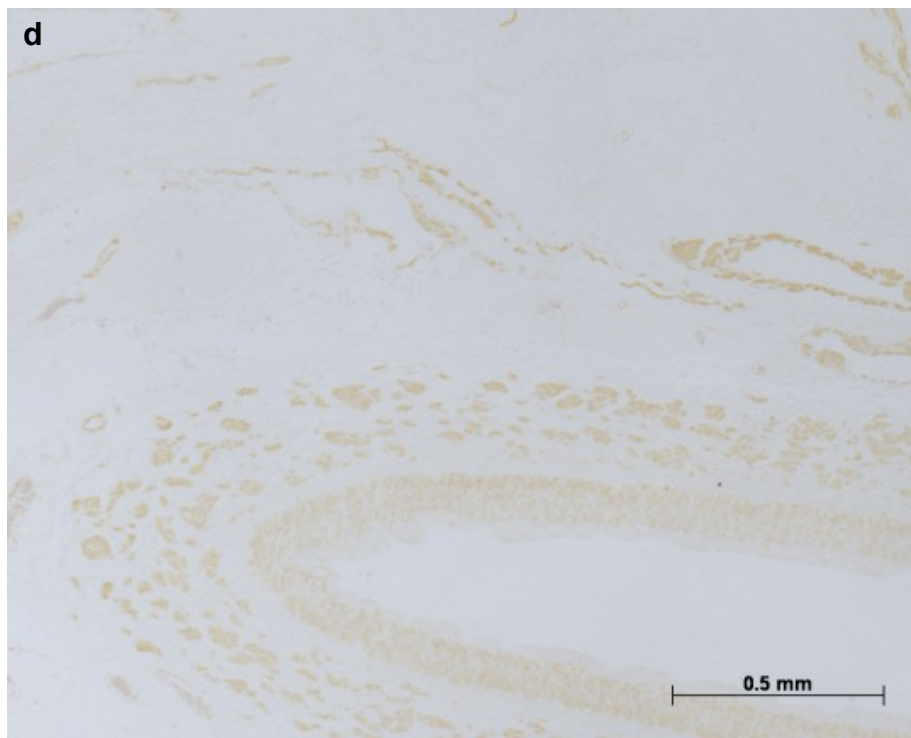
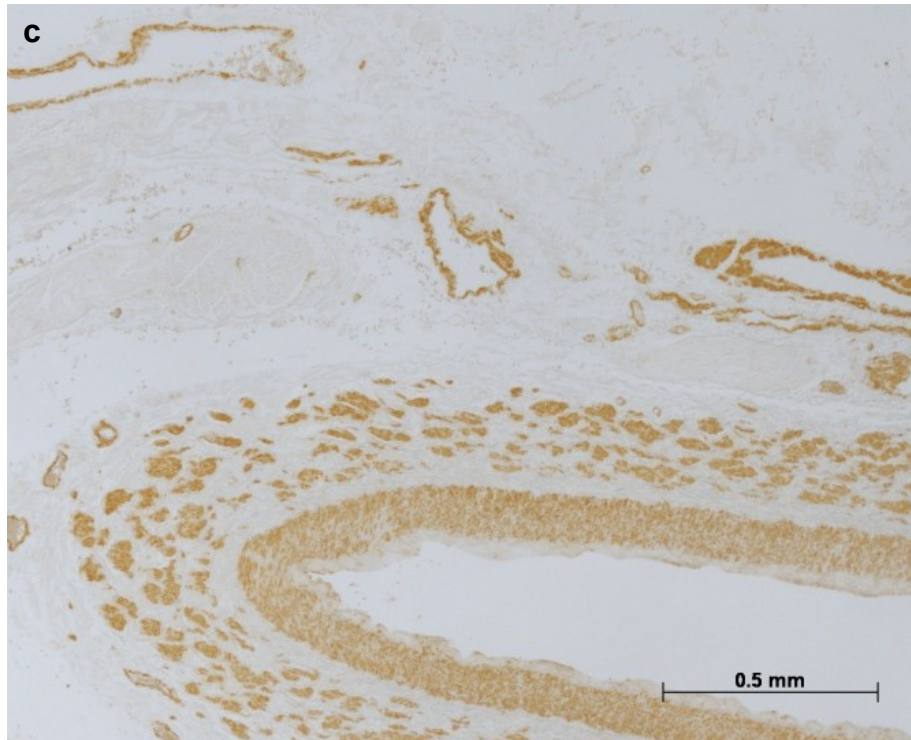


Figure 8.1 (continued). 4  $\mu$ m thick sections of paraffin wax-embedded pancreas immunohistochemically stained for SMA using MAH SMA at  $1/5,000$  and incubating in 4,5-diCl-OPD for 20 minutes (c) or at  $1/10,000$  and incubating in 4,5di-Cl-OPD for 3 minutes (d).

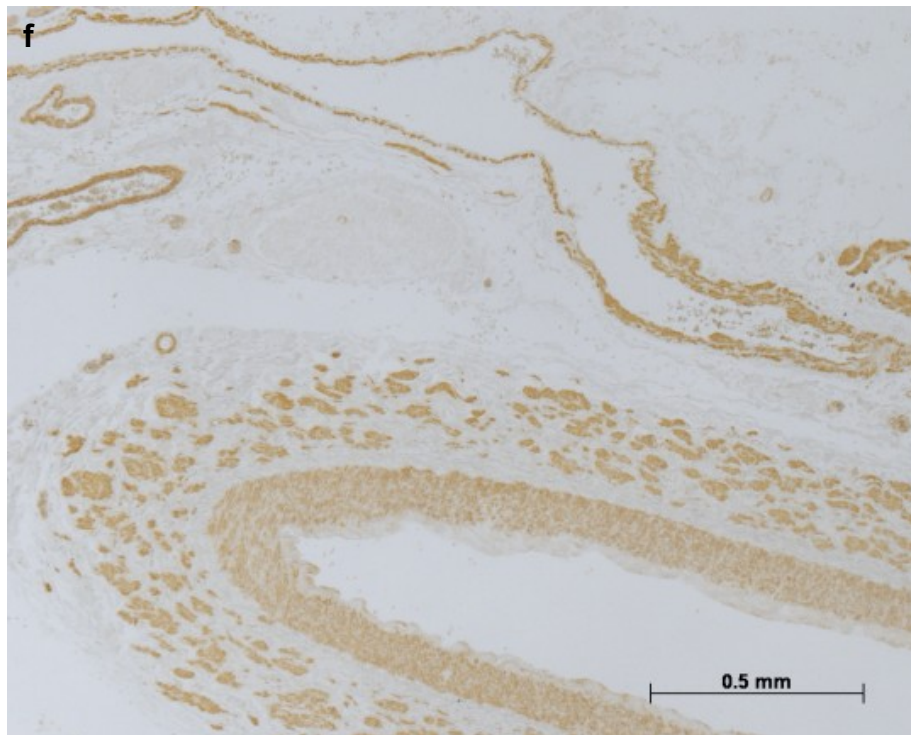
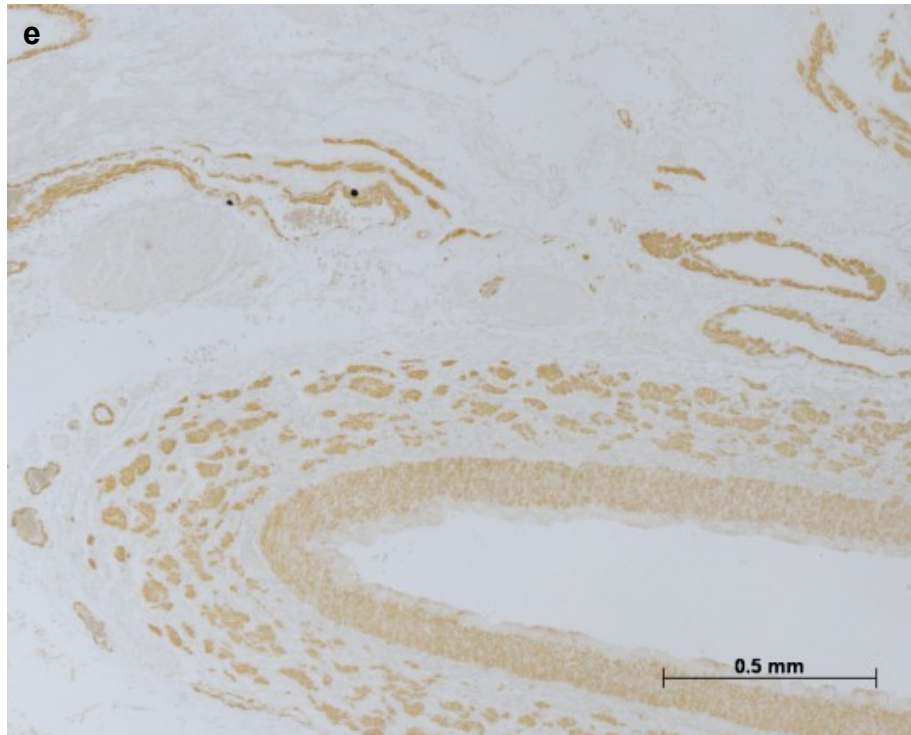


Figure 8.1 (continued). 4  $\mu$ m thick sections of paraffin wax-embedded pancreas immunohistochemically stained for SMA using MAH SMA at  $1/10,000$  and incubating in 4,5-diCl-OPD for 20 minutes (e) and 60 minutes (f).



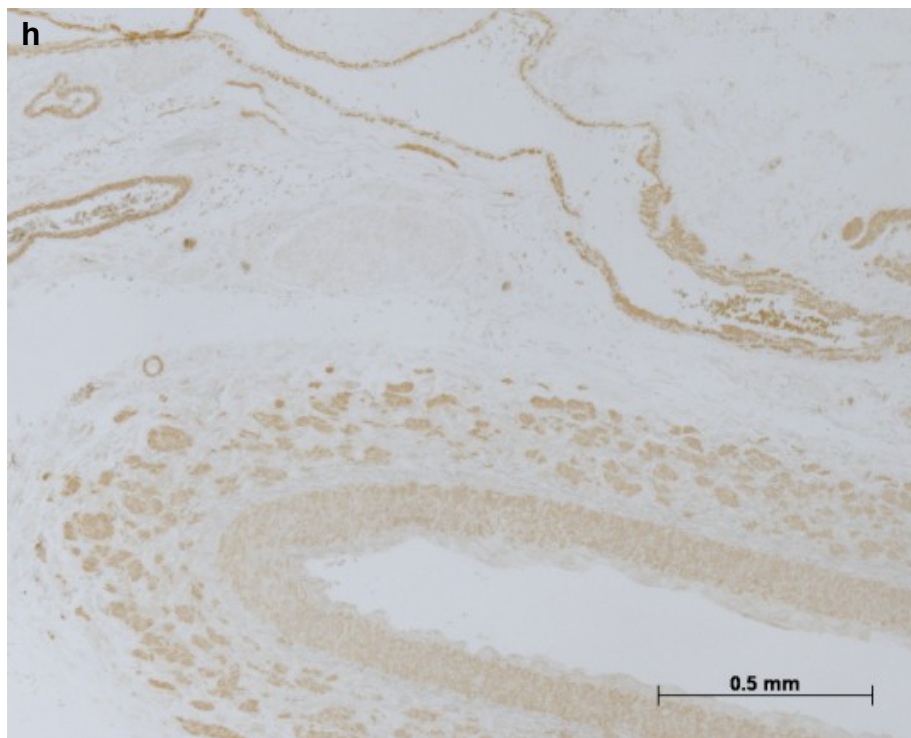
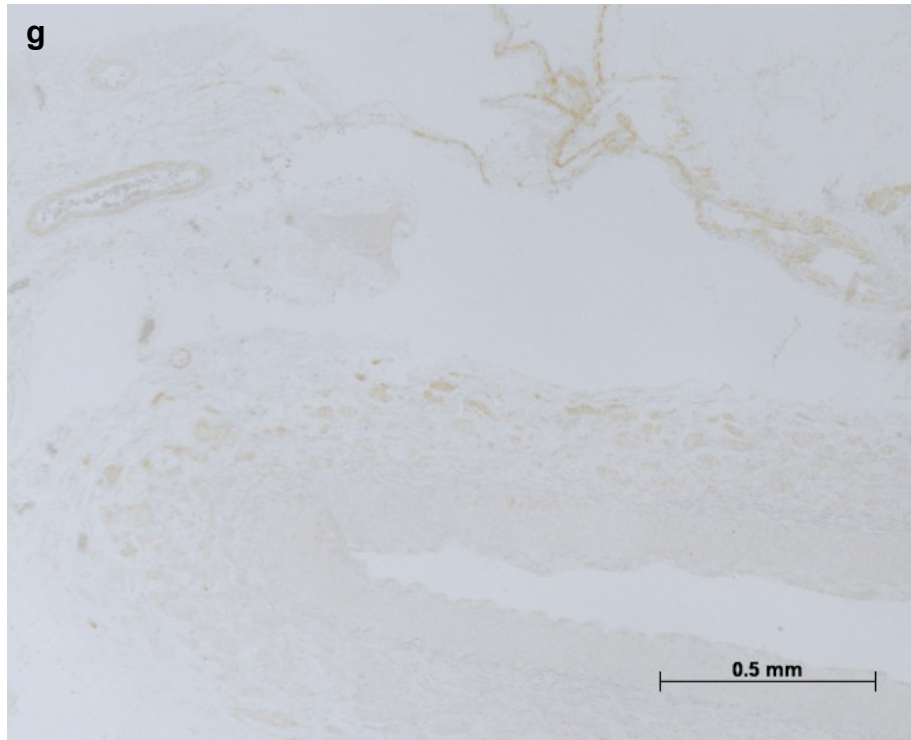


Figure 8.1 (continued). 4  $\mu\text{m}$  thick sections of paraffin wax-embedded pancreas immunohistochemically stained for SMA using MAH SMA at  $1/20,000$  and incubating in 4,5-diCl-OPD for 3 minutes (g) and 20 minutes (h).

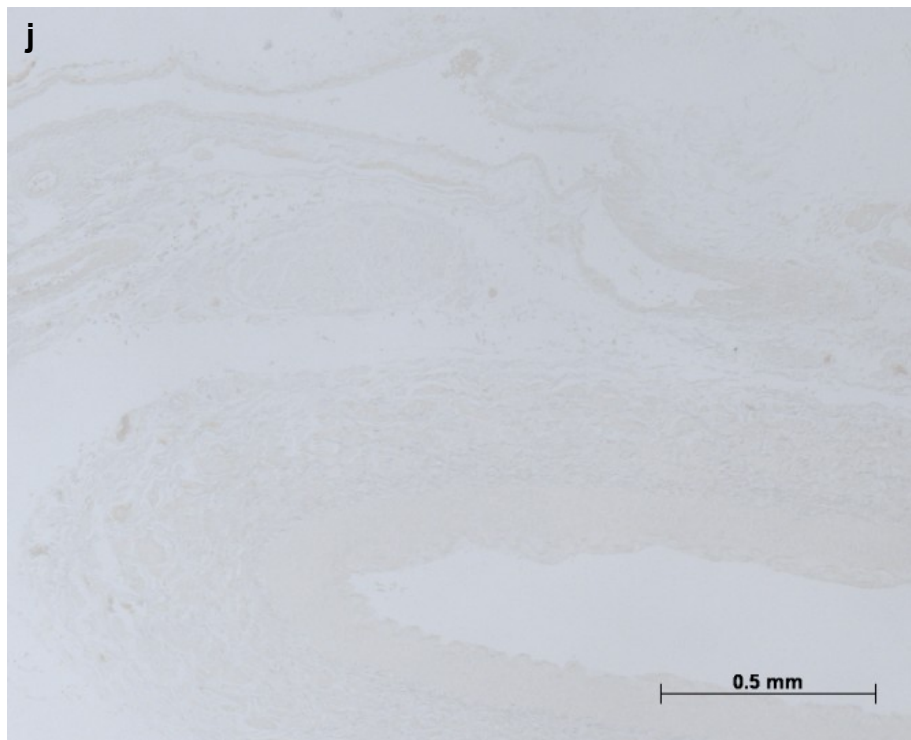
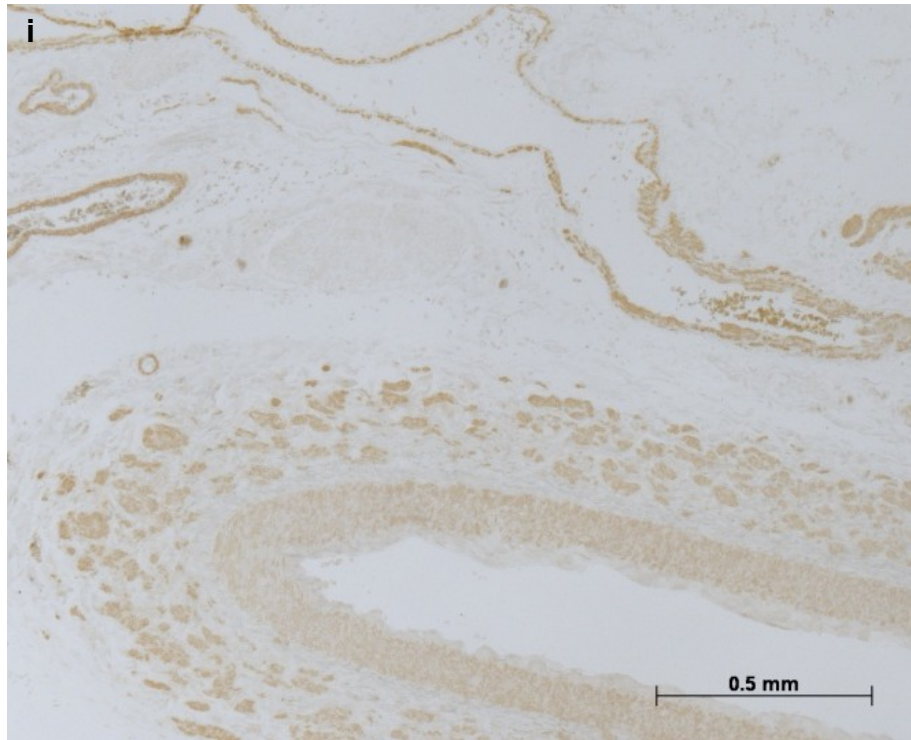


Figure 8.1 (continued). 4  $\mu$ m thick sections of paraffin wax-embedded pancreas immunohistochemically stained for SMA using MAH SMA at  $1/20,000$  and incubating in 4,5-diCl-OPD for 60 minutes (i), or at  $1/50,000$  and incubating in 4,5-diCl-OPD for 3 minutes (j).

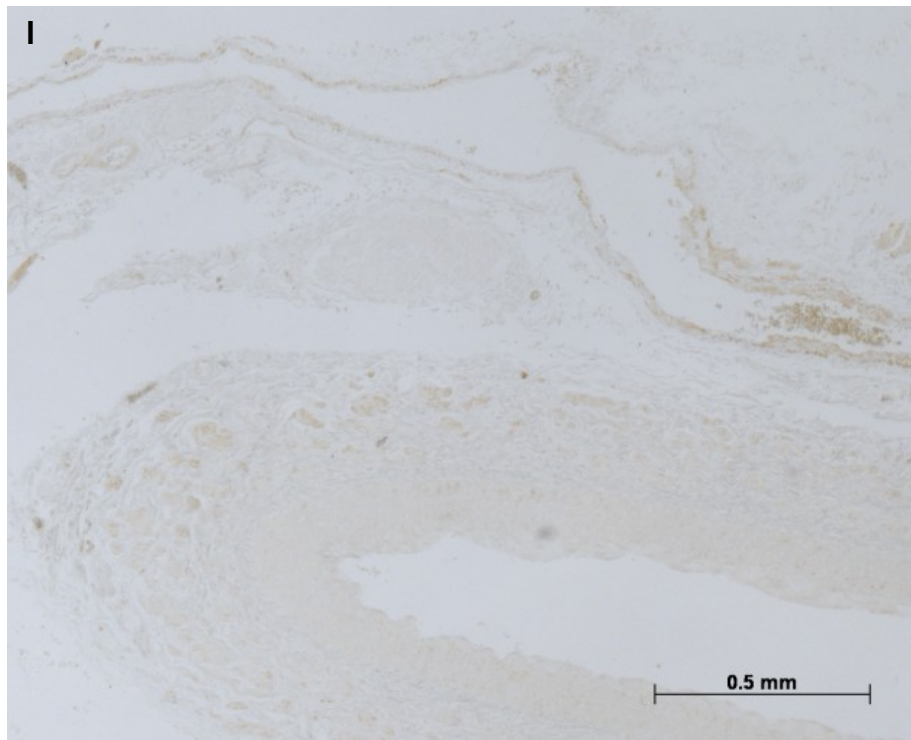
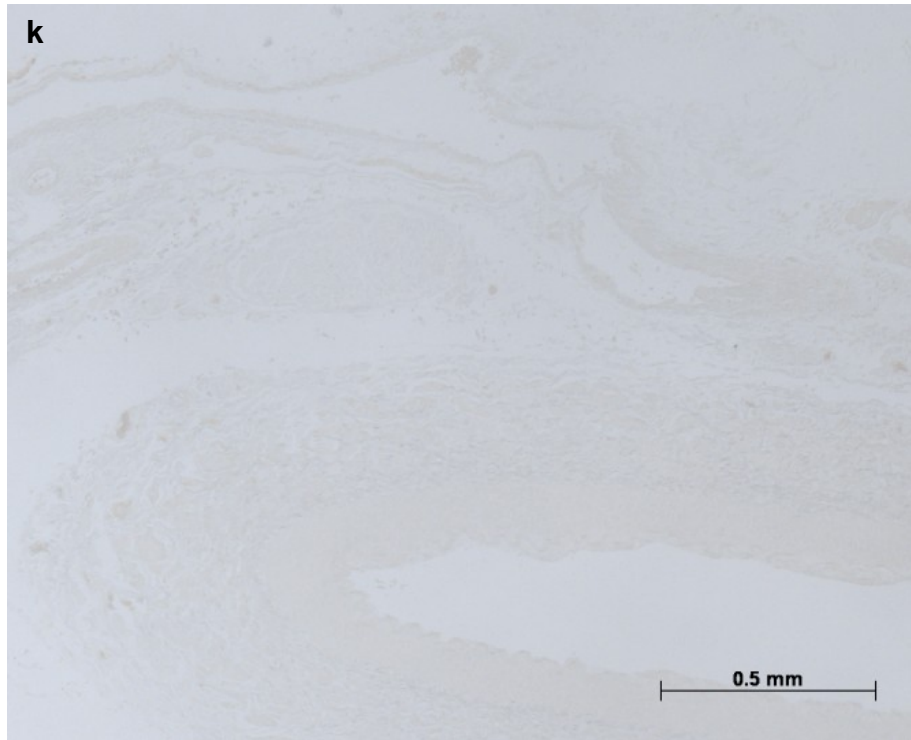


Figure 8.1 (continued). 4  $\mu\text{m}$  thick sections of paraffin wax-embedded pancreas immunohistochemically stained for SMA using MAH SMA at  $1/50,000$  and incubating in 4,5-diCl-OPD for 3 minutes (k) and 20 minutes (l).

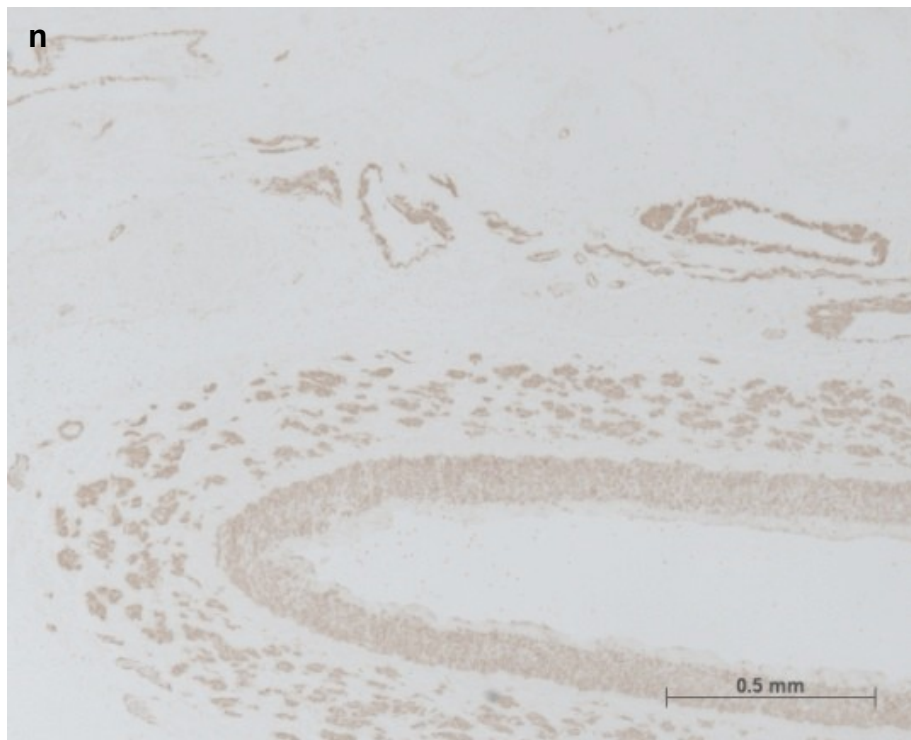
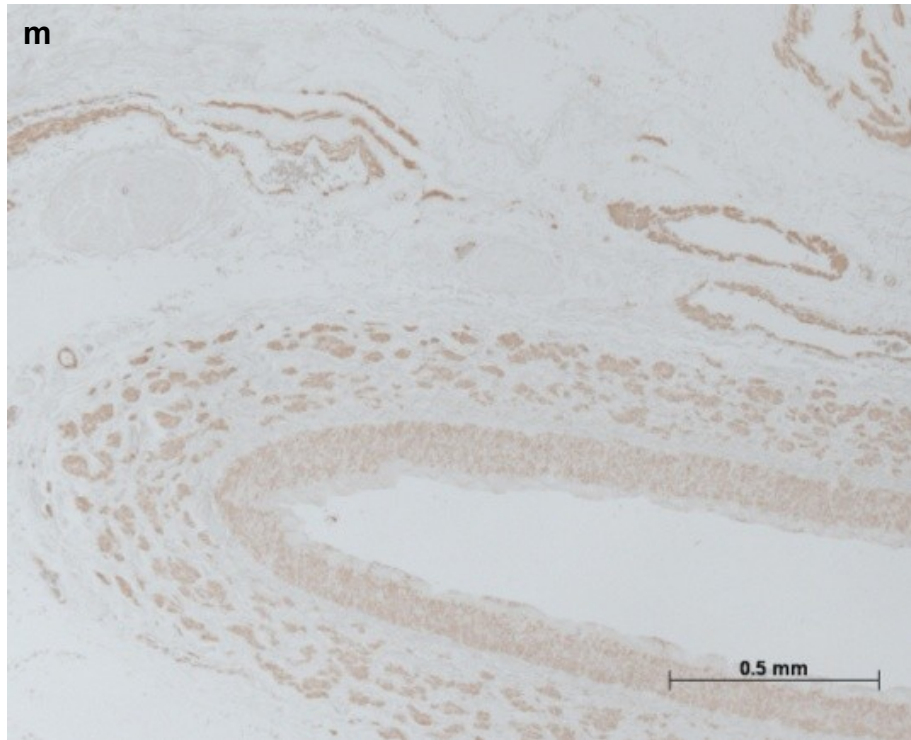


Figure 8.1 (continued). 4  $\mu\text{m}$  thick sections of paraffin wax-embedded pancreas immunohistochemically stained for SMA using MAH SMA at  $1/500$  and incubating in DAB for 3 minutes (m) and 60 minutes (n).



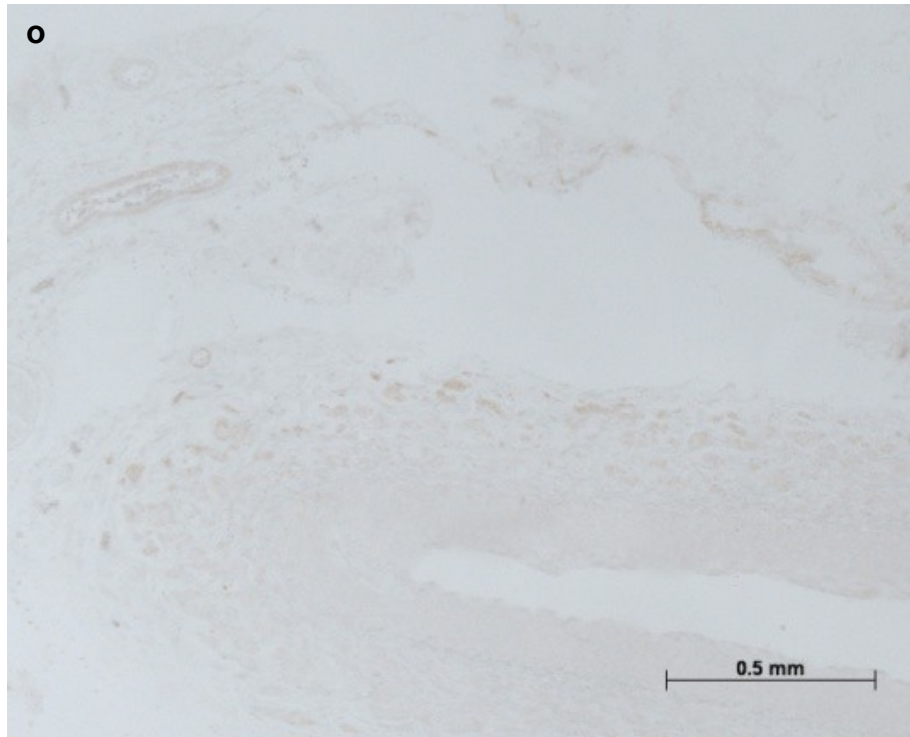


Figure 8.1 (continued). 4  $\mu\text{m}$  thick sections of paraffin wax-embedded pancreas immunohistochemically stained for SMA using MAH SMA at  $1/1,000$  and incubating in DAB for 3 minutes (o) and 60 minutes (p).

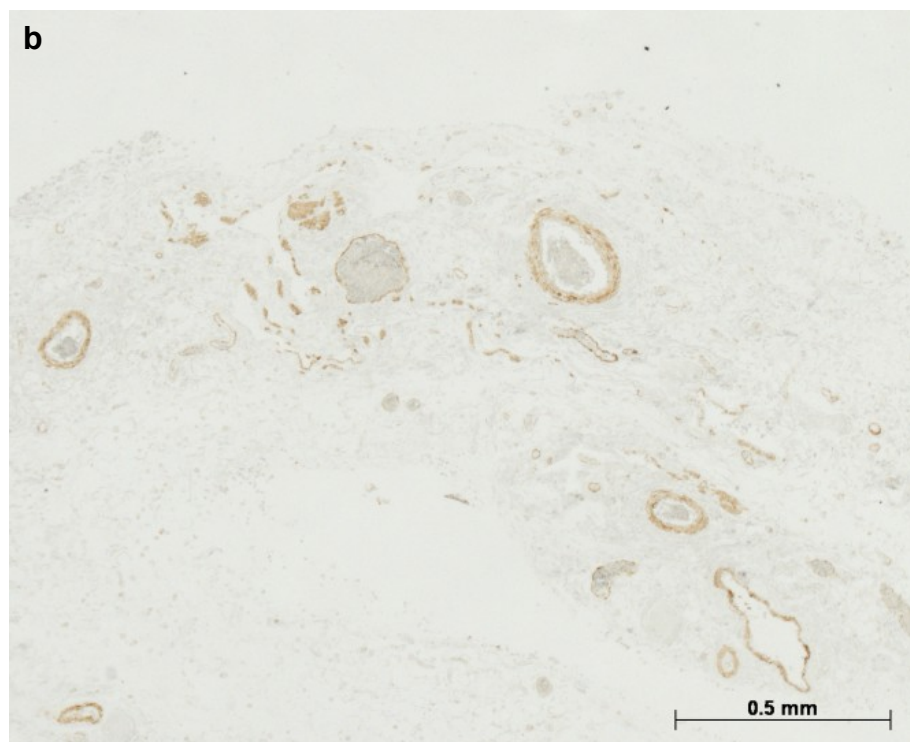
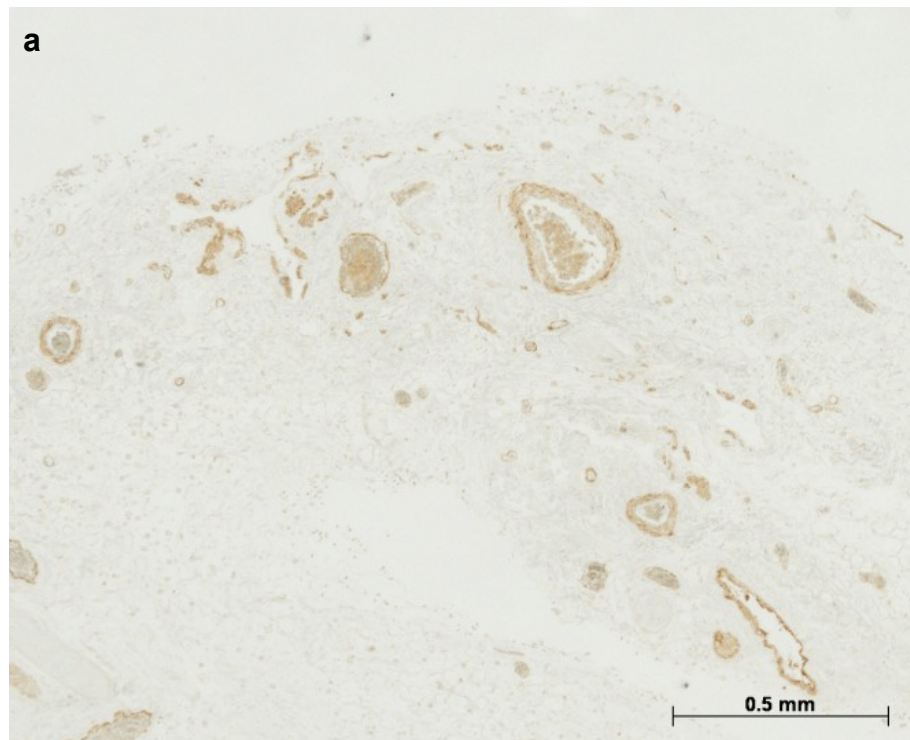


Figure 8.2. 4  $\mu$ m thick sections of paraffin wax-embedded adrenal cortex immunohistochemically stained for SMA using  $1/500$  MAH SMA followed by DAB alone (a) or following 5 minutes pre-treatment with 0.3%  $H_2O_2$  for 5 minutes (b).

#### **8.4.2.1.2 NaN<sub>3</sub>**

Compared to untreated controls (figure 8.3a), pre-treatment of sections with NaN<sub>3</sub> at 0.02% resulted in partial inhibition of both HRP activity and erythrocyte staining (figure 8.3b). No further inhibition was observed at higher (0.2% and 2%) concentrations of NaN<sub>3</sub> (figure 8.3c and d respectively), even when included in the DAB-Tris incubation mixture (Figure 8.4a - d).

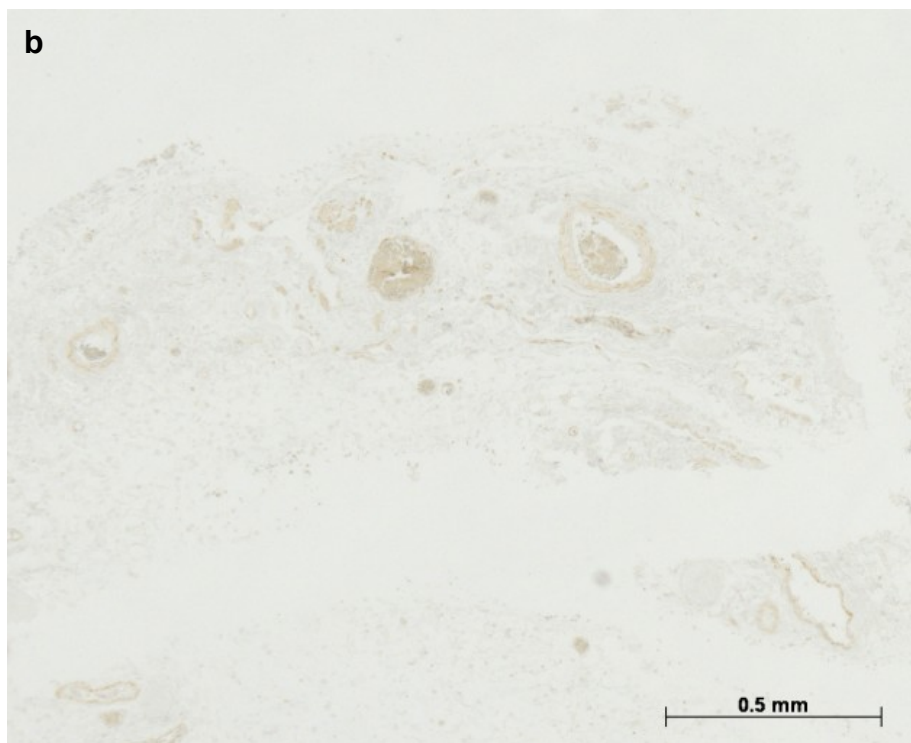
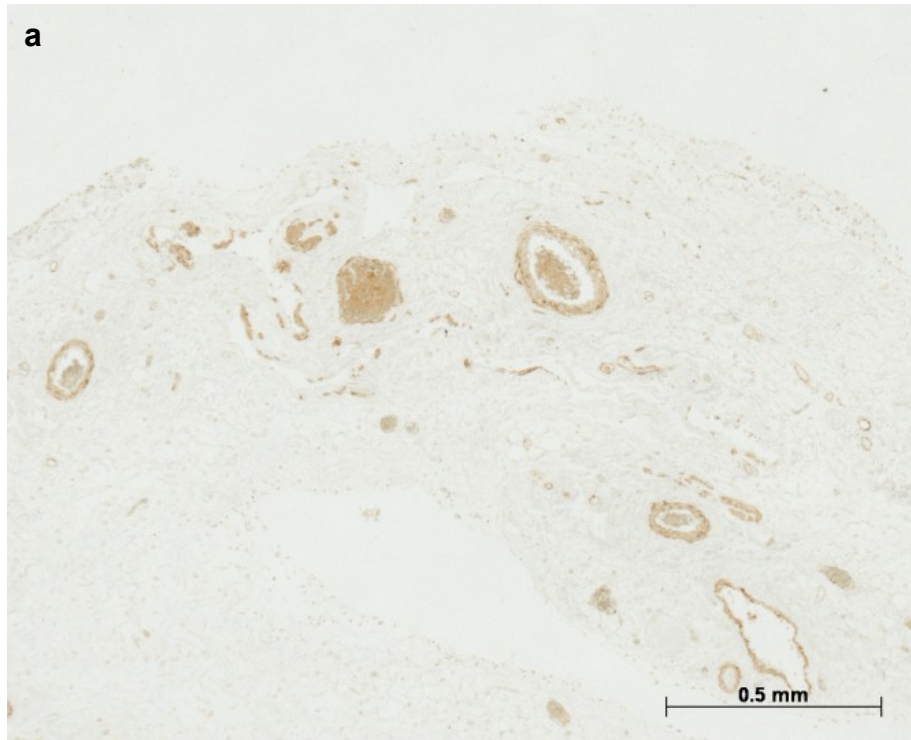


Figure 8.3. 4  $\mu\text{m}$  thick sections of paraffin wax-embedded adrenal cortex immunohistochemically stained for SMA using  $1/500$  MAH SMA followed by DAB alone (a) or following 5 minutes pre-treatment with  $\text{NaN}_3$  at 0.02% (b).

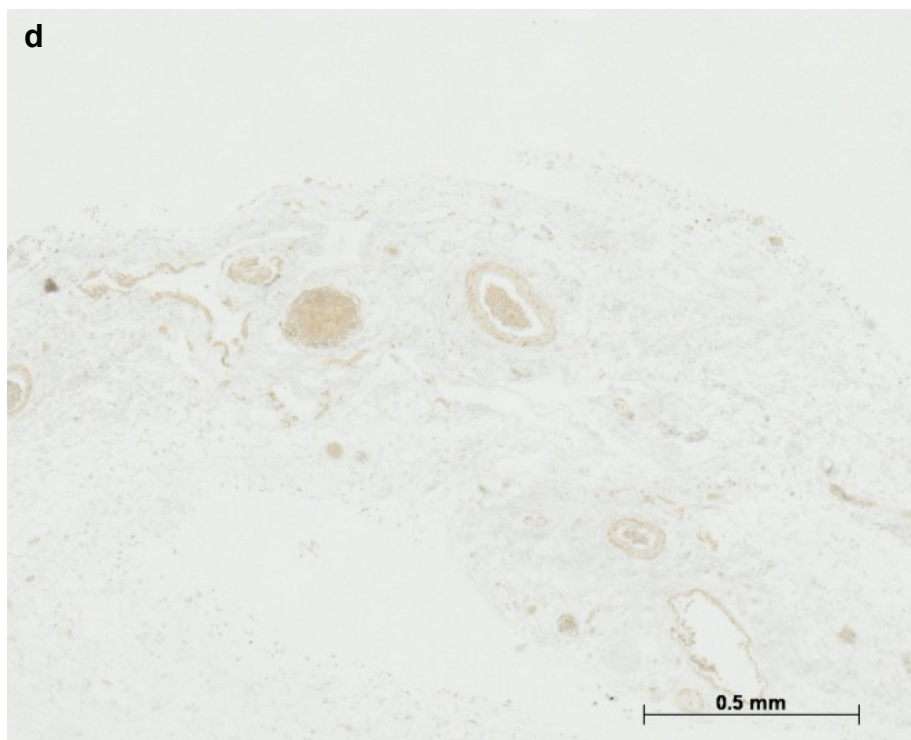
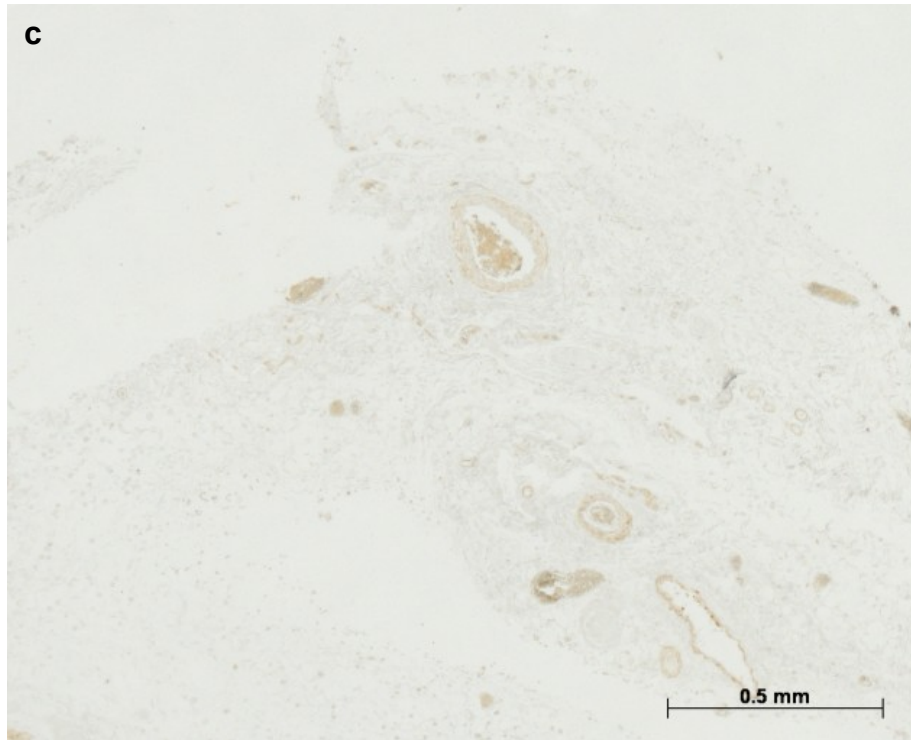


Figure 8.3 (continued). 4  $\mu$ m thick sections of paraffin wax-embedded adrenal cortex immunohistochemically stained for SMA using  $1/500$  MAH SMA following 5 minutes pre-treatment with  $\text{NaN}_3$  at 0.2% (c) or 2% (d).



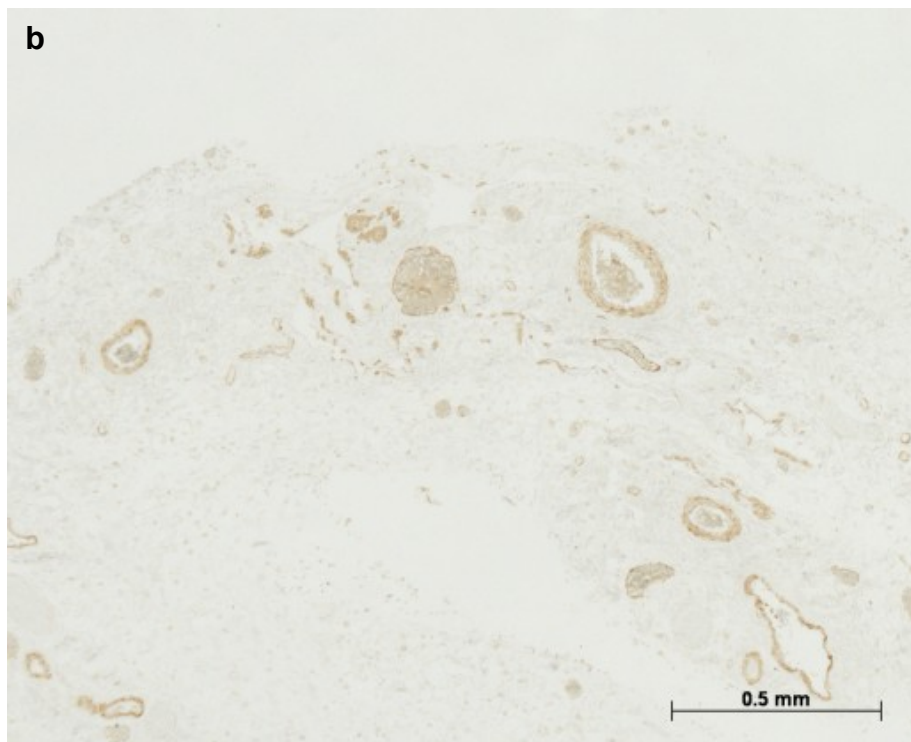
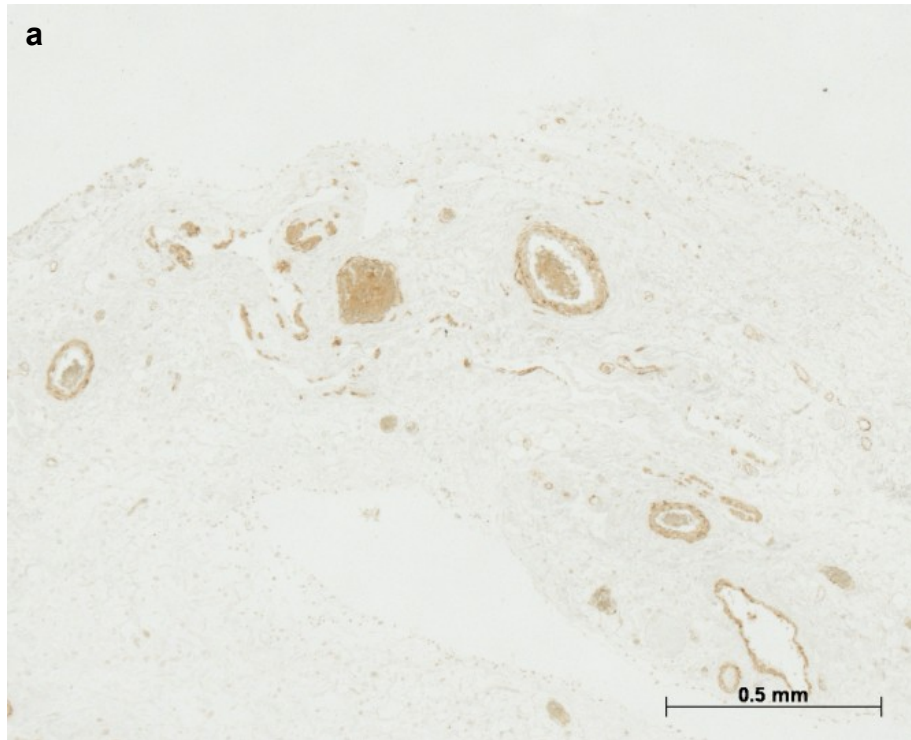


Figure 8.4. 4  $\mu\text{m}$  thick sections of paraffin wax-embedded adrenal cortex immunohistochemically stained for SMA using  $1/500$  MAH SMA followed by DAB alone (a) or following 5 minutes pre-treatment and including  $\text{NaN}_3$  in the DAB-Tris at 0.02% (b).

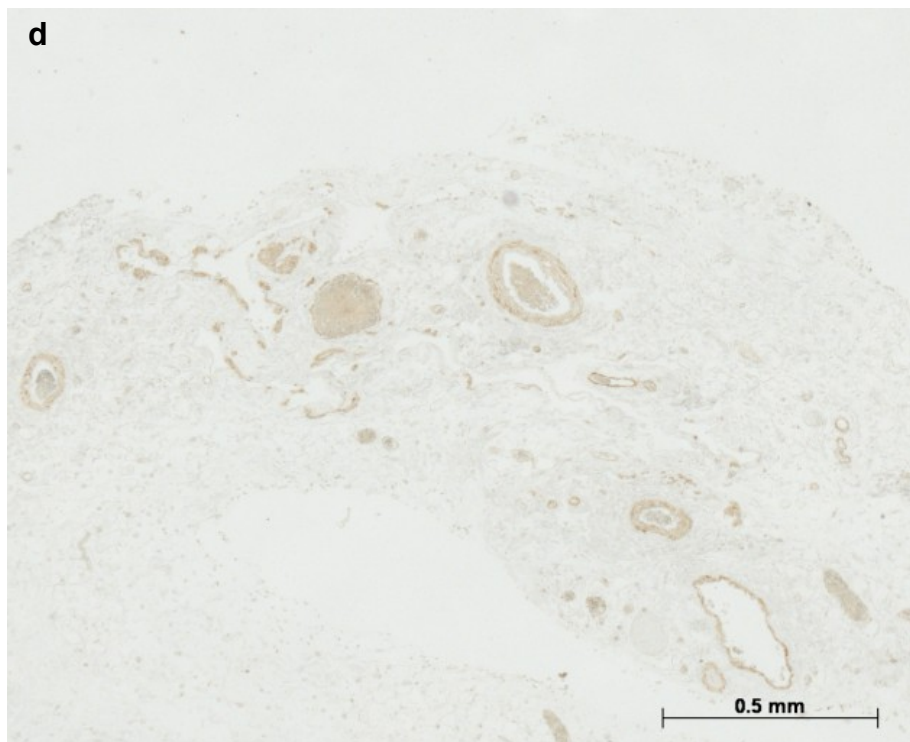
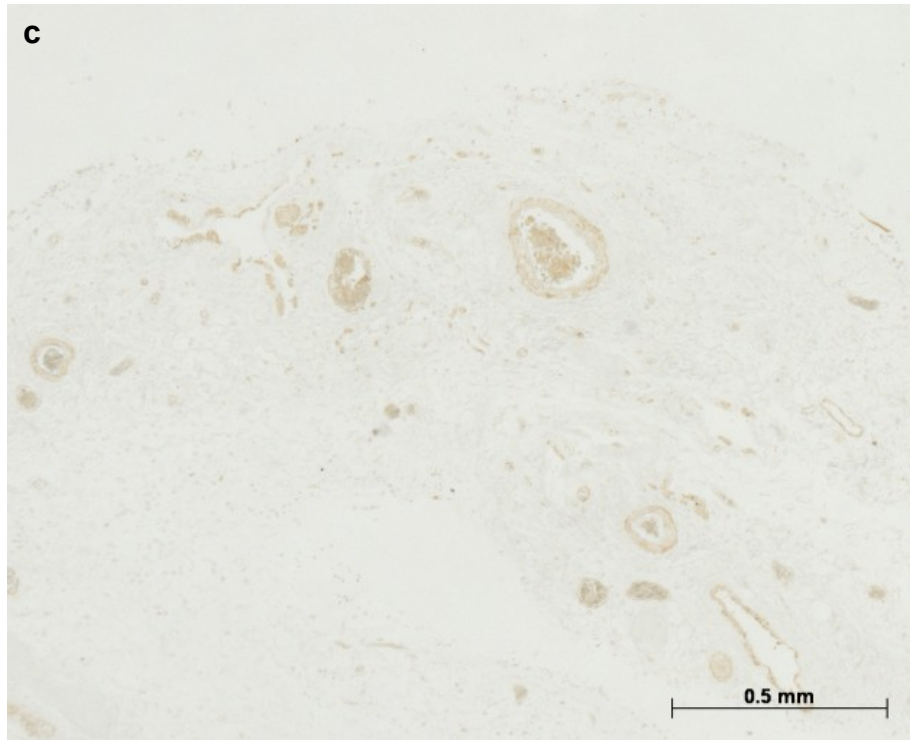


Figure 8.4 (continued). 4  $\mu\text{m}$  thick sections of paraffin wax-embedded adrenal cortex immunohistochemically stained for SMA using  $1/500$  MAH SMA followed by 5 minutes pre-treatment and including  $\text{NaN}_3$  in the DAB-Tris at 0.2% (c) or 2% (d).

#### **8.4.2.1.3 NaCN**

Compared to untreated controls (figure 8.5a), pre-treatment of sections with NaCN at either 1 mM (figure 8.5b) or 10 mM (figure 8.5c) caused only slight inhibition of both HRP and erythrocyte staining. Including NaCN in the reaction mixture slightly inhibited HRP at  $10^{-4}$  M, and almost completely abolished HRP activity at  $10^{-3}$  M, although erythrocyte staining remained (Figure 8.6a - f).



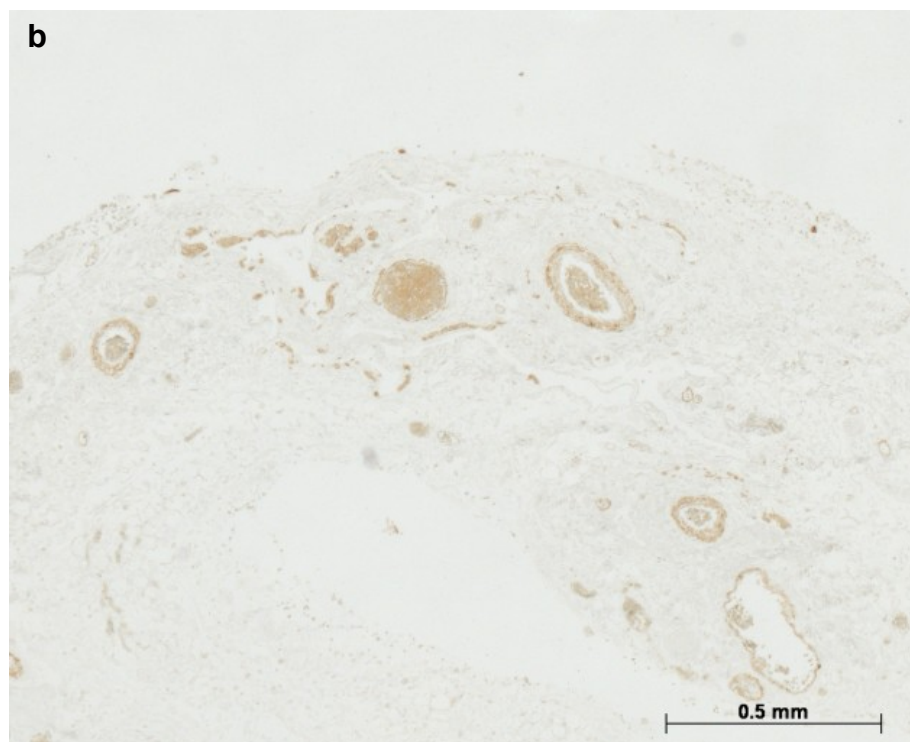
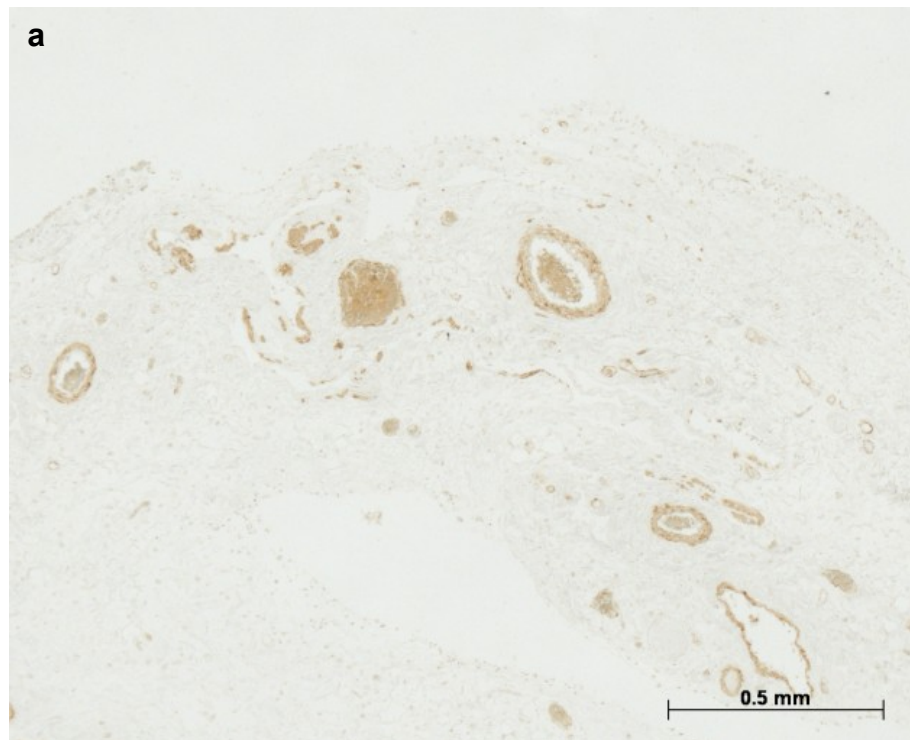


Figure 8.5. 4  $\mu$ m thick sections of paraffin wax-embedded adrenal cortex immunohistochemically stained for SMA using  $1/500$  MAH SMA followed by DAB alone (a) or following 5 minutes pre-treatment with NaCN at 1 mM (b).

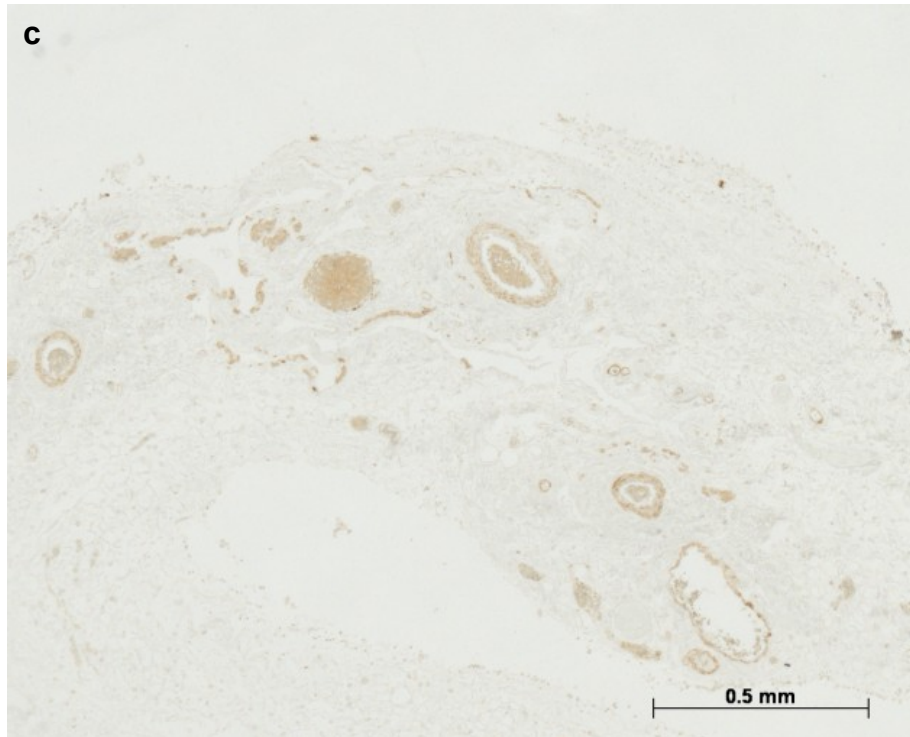


Figure 8.5 (continued). 4  $\mu\text{m}$  thick sections of paraffin wax-embedded adrenal cortex immunohistochemically stained for SMA using  $1/500$  MAH SMA followed by 5 minutes pre-treatment with NaCN at 10 mM (c).

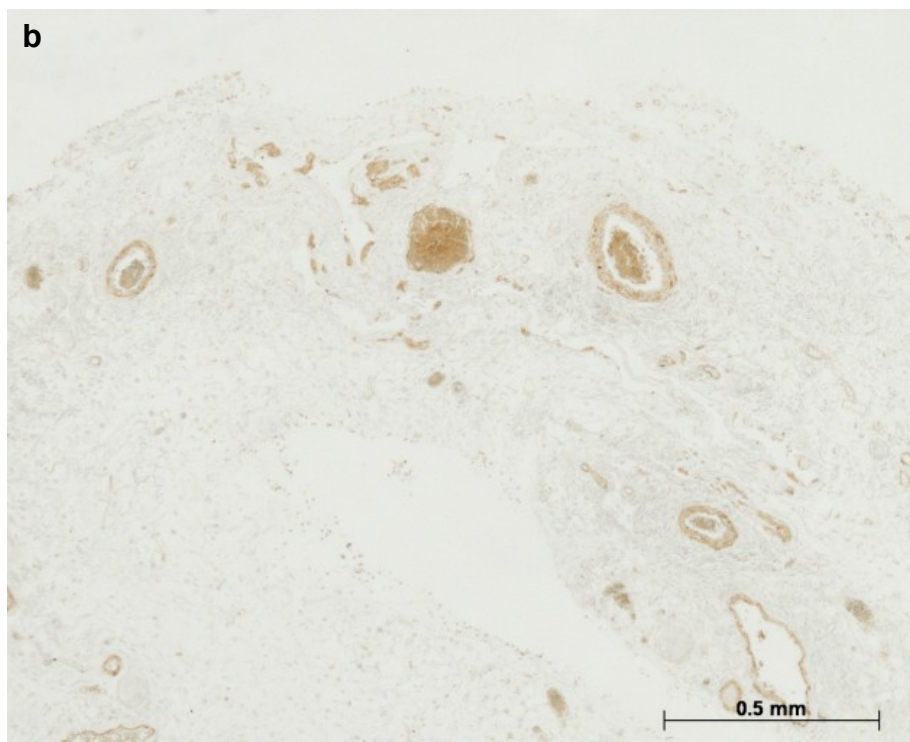
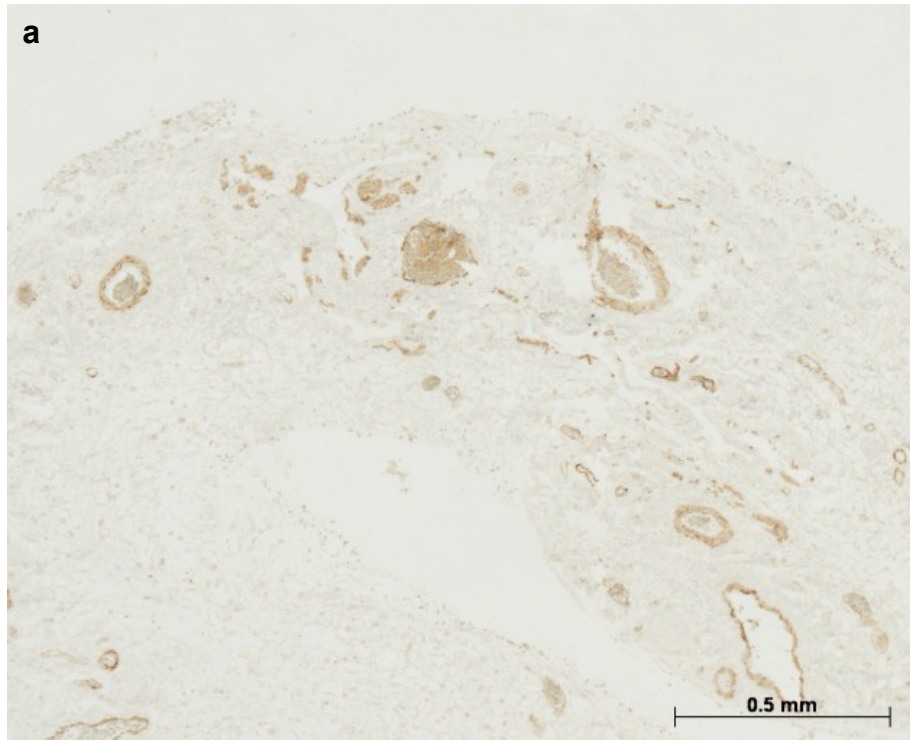


Figure 8.6. 4  $\mu\text{m}$  thick sections of paraffin wax-embedded adrenal cortex immunohistochemically stained for SMA using  $1/500$  MAH SMA followed by DAB alone (a) or including NaCN in the reaction mixture at  $10^{-7}$  M (b).

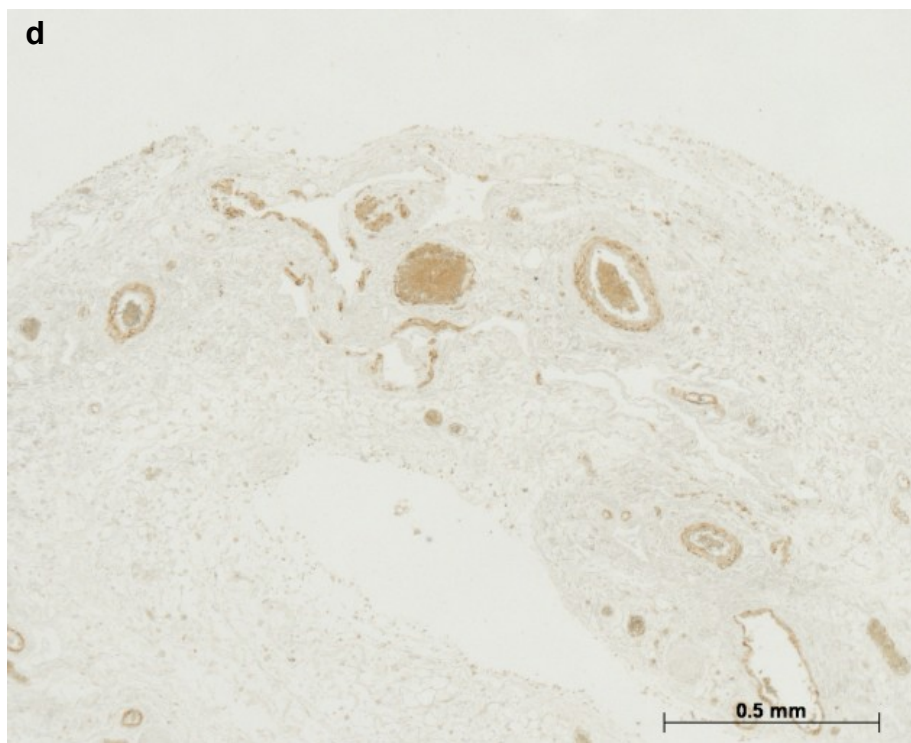
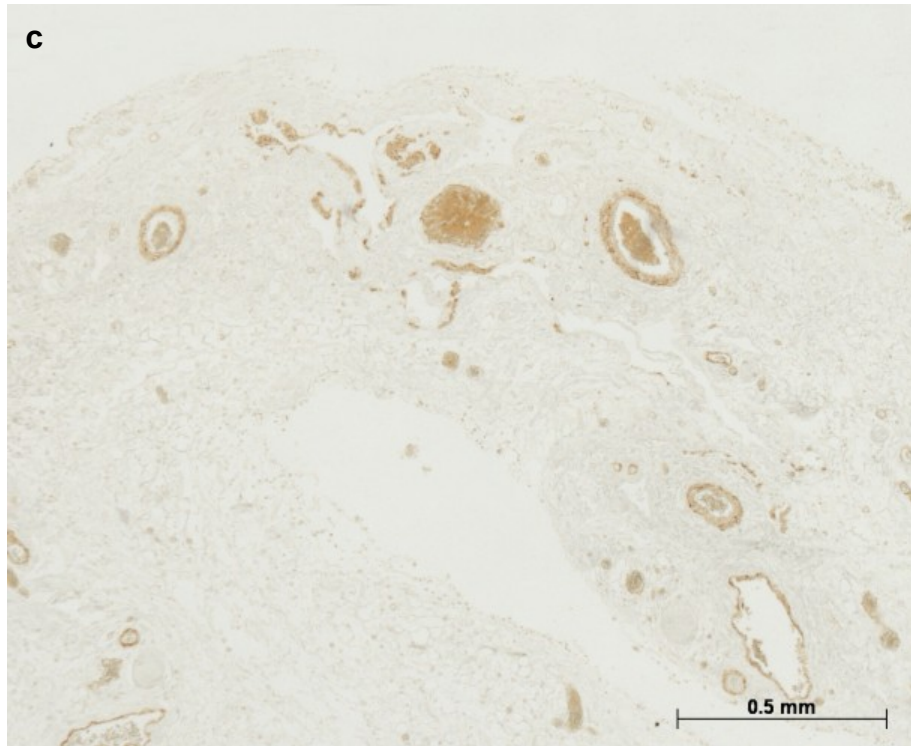


Figure 8.6 (continued). 4  $\mu\text{m}$  thick sections of paraffin wax-embedded adrenal cortex immunohistochemically stained for SMA using  $1/500$  MAH SMA and including NaCN in the reaction mixture at  $10^{-6}$  M (c) or  $10^{-5}$  M (d).



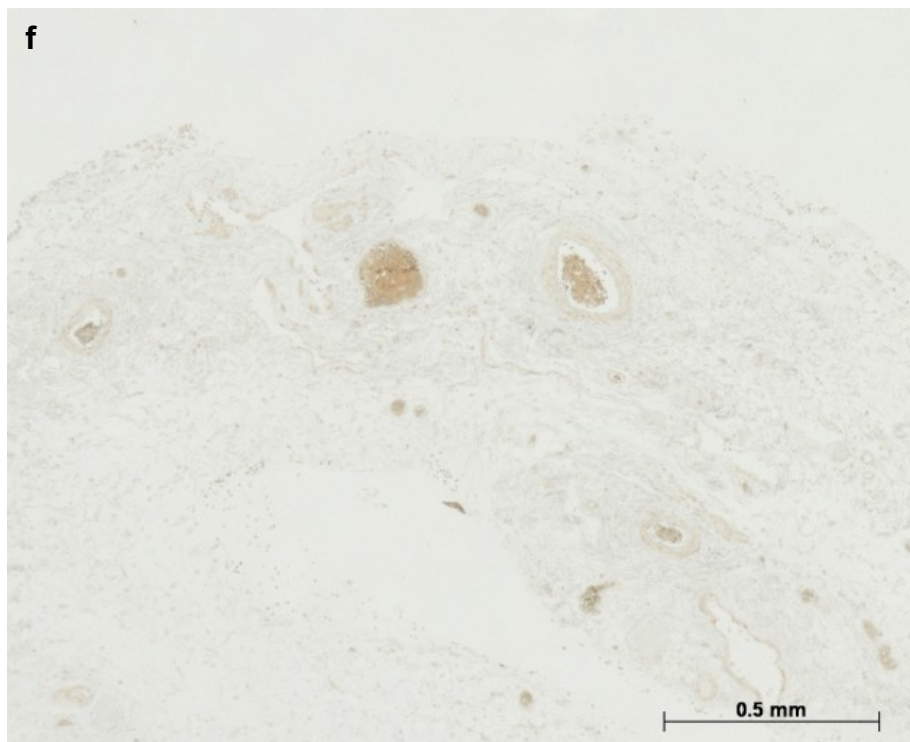
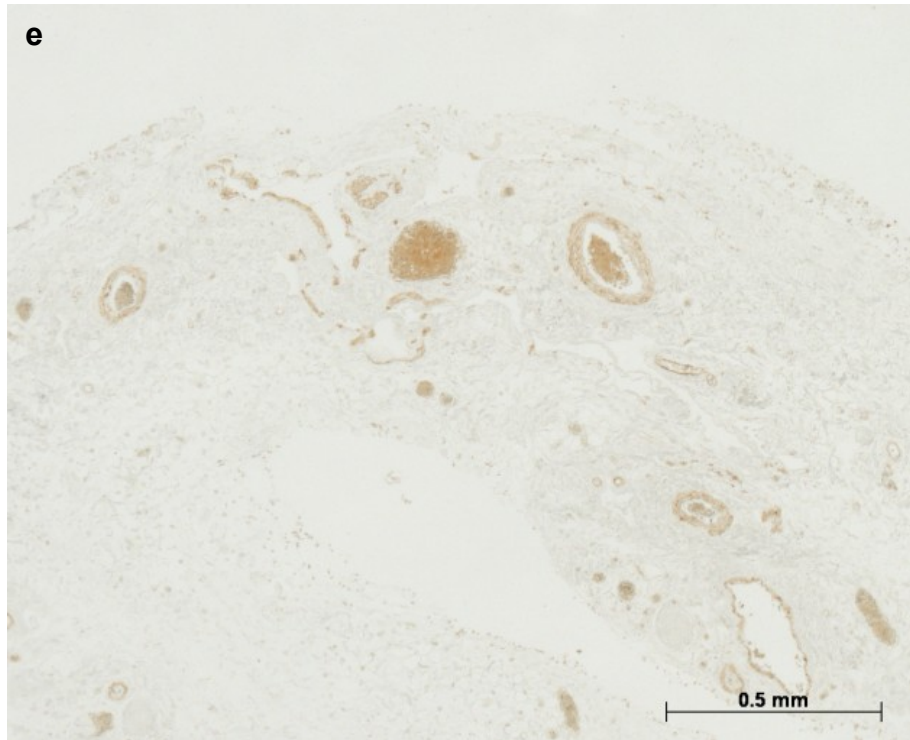


Figure 8.6 (continued). 4  $\mu\text{m}$  thick sections of paraffin wax-embedded adrenal cortex immunohistochemically stained for SMA using  $1/500$  MAH SMA and including NaCN in the reaction mixture at  $10^{-4}$  M (e) or  $10^{-3}$  M (f).

## **8.4.2.2 Studies with 4,5-diCl-OPD**

### **8.4.2.2.1 Preliminary Studies of Inhibition with NaCN**

In the absence of inhibition, incubation in 4,5-diCl-OPD for 3 minutes resulted in intense staining in smooth muscle cells of arterioles and venules along with light staining of erythrocytes (figure 8.7a). Slight inhibition of immunohistochemical staining was observed when NaCN was included in the reaction mixture at  $10^{-4}$  M (figure 8.7b) and complete inhibition of staining occurred at  $10^{-3}$  M and  $10^{-2}$  M (Figure 8.7c and d).

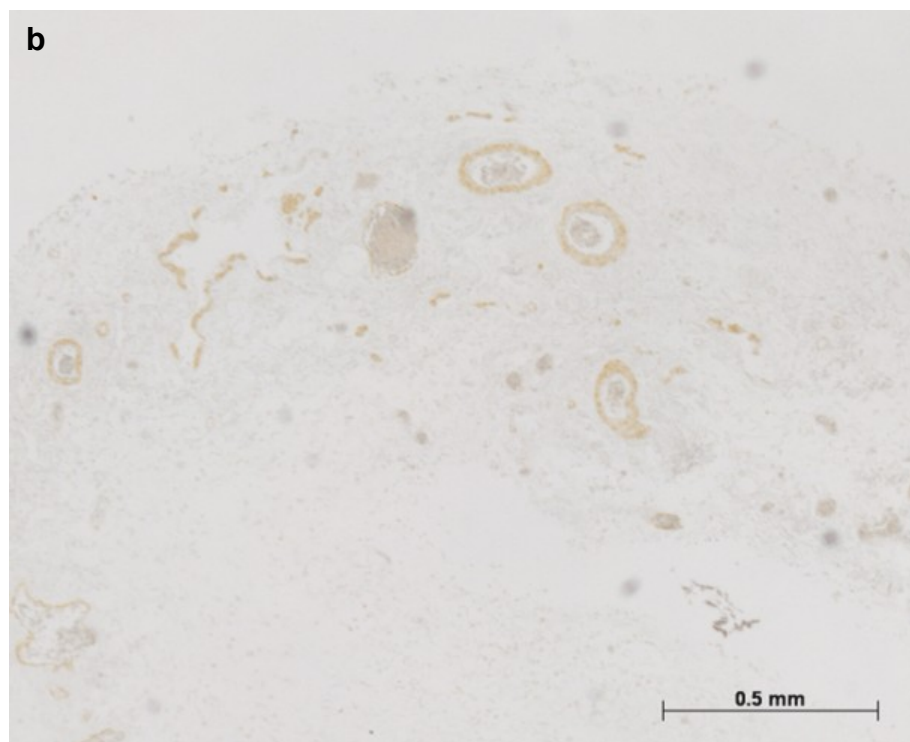
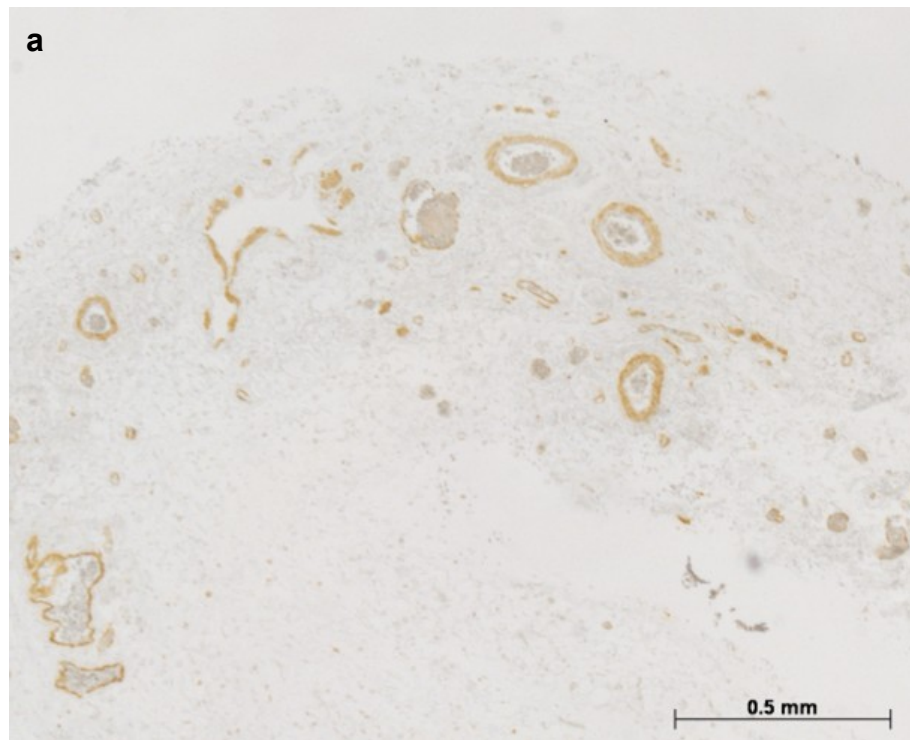


Figure 8.7. 4  $\mu\text{m}$  thick sections of paraffin wax-embedded adrenal cortex immunohistochemically stained for SMA using  $1/500$  MAH SMA followed by 4,5-diCl-OPD for 3 minutes either alone (a), or including NaCN in the reaction mixture at  $10^{-4}\text{M}$  (b).

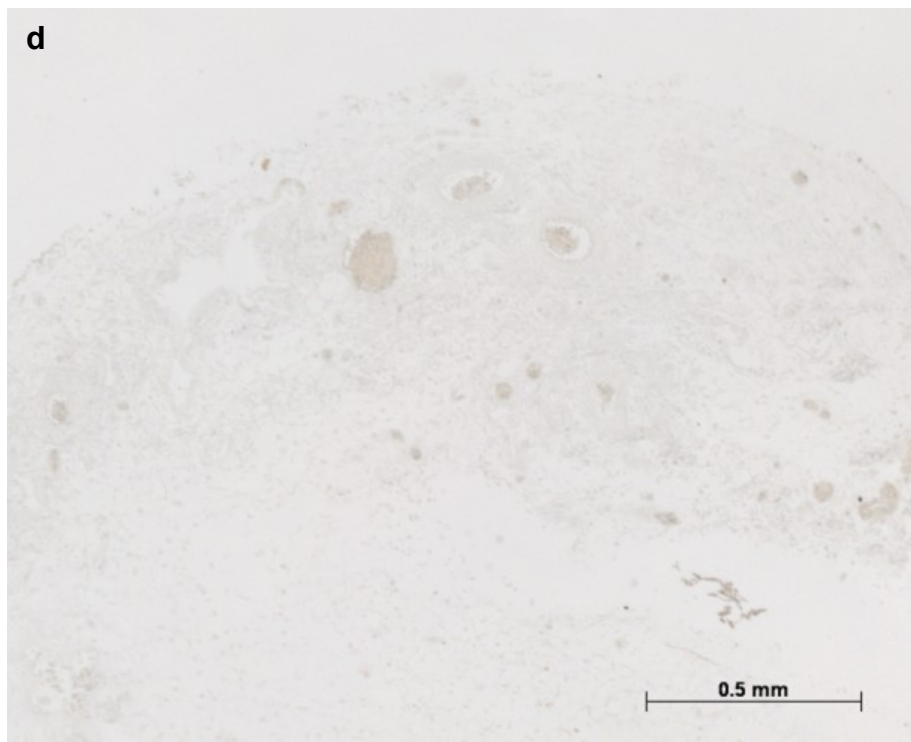
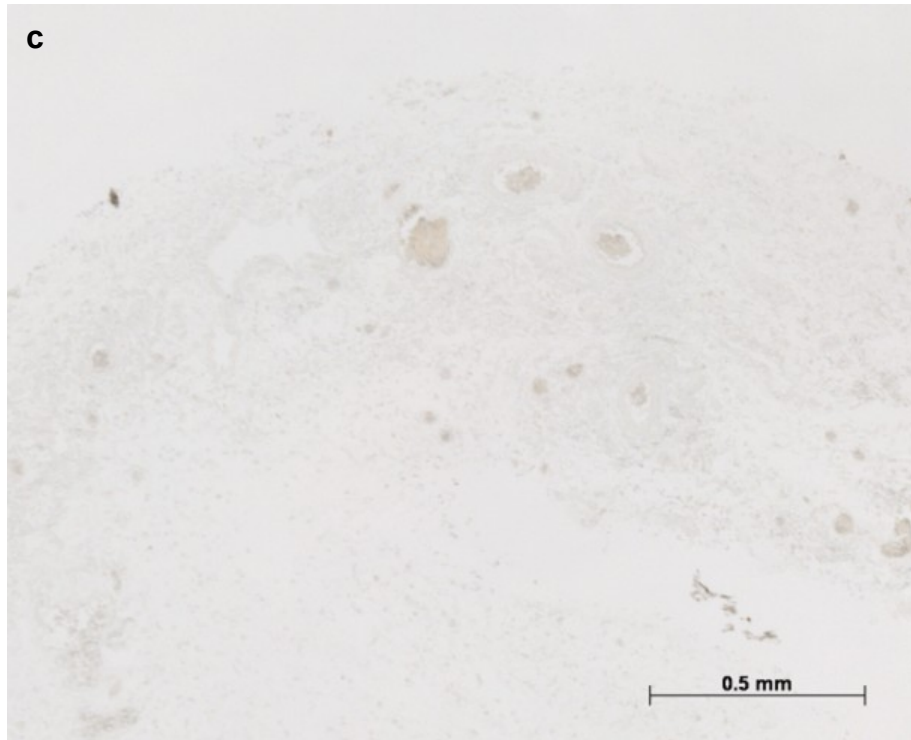


Figure 8.7 (continued). 4  $\mu\text{m}$  thick sections of paraffin wax-embedded adrenal cortex immunohistochemically stained for SMA using  $1/500$  MAH SMA followed by 4,5-diCl-OPD for 3 minutes, including NaCN in the reaction mixture at  $10^{-3}$  M (c) or  $10^{-2}$  M (d).



#### **8.4.2.2.2 Effects of HRP Inhibition with NaCN Following Re-incubation in Staining Solution**

Re-incubation of immunohistochemically stained sections, that had been pre-incubated in 4,5-diCl-OPD solution for 3 minutes (figure 8.8a), for a further 7, 27 or 57 minutes resulted in a progressive increase in staining intensity (figures 8.8b – d). A similar effect was observed when re-incubation was performed with 4,5-diCl-OPD solution containing 1 mM NaCN, although staining intensity was slightly lessened (Figure 8.8e - g).

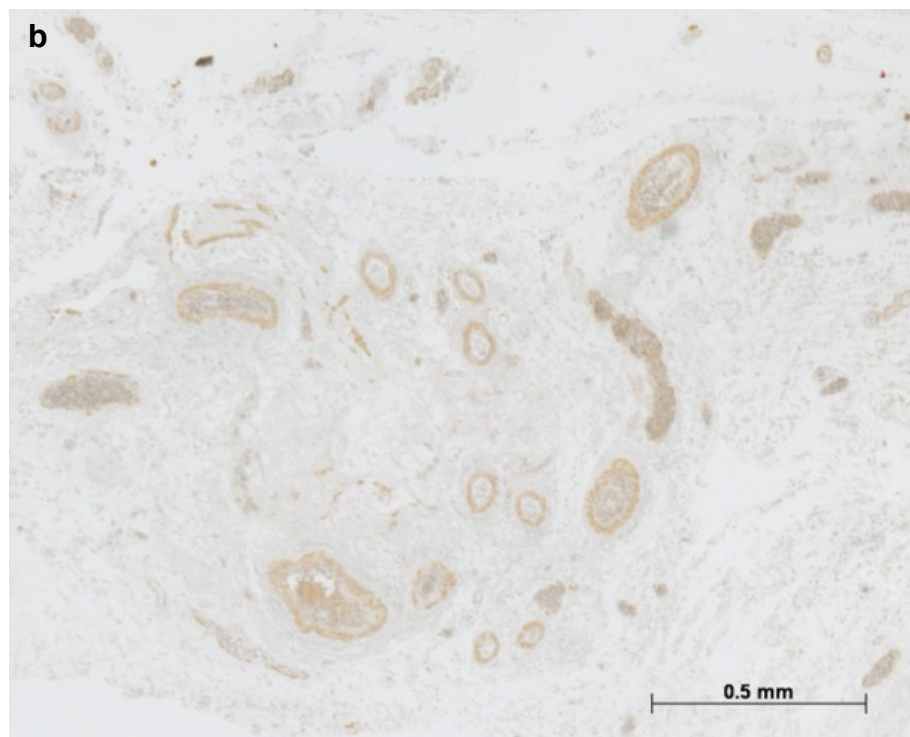
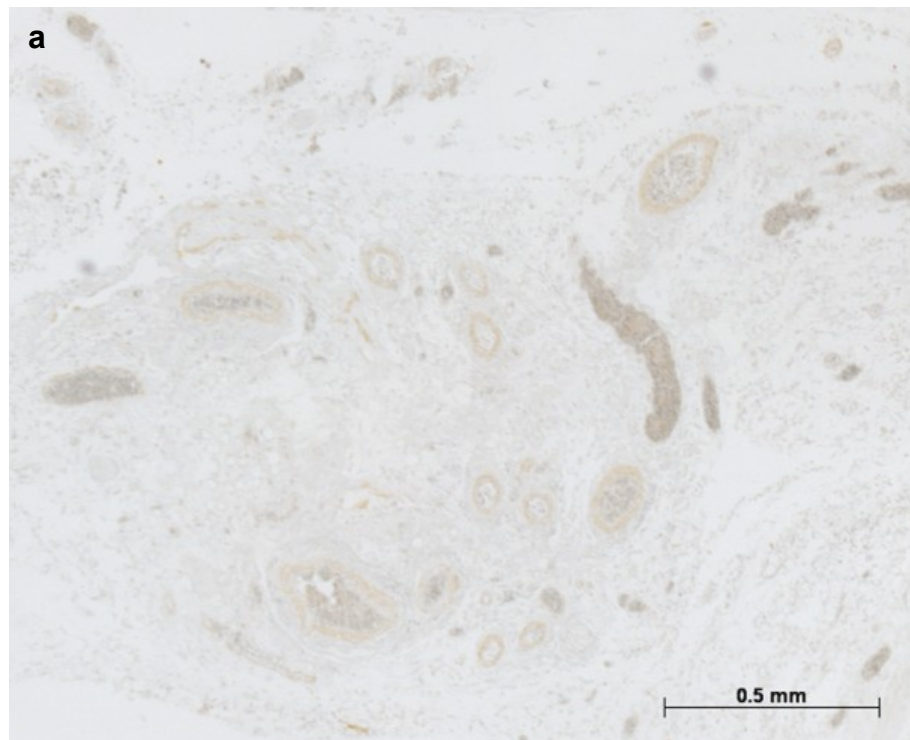


Figure 8.8. 4  $\mu\text{m}$  thick sections of paraffin wax-embedded adrenal cortex immunohistochemically stained for SMA using  $1/20,000$  MAH SMA followed by 4,5-diCl-OPD for 3 minutes (a) and further incubated in 4,5-diCl-OPD for a further 7 minutes (b).

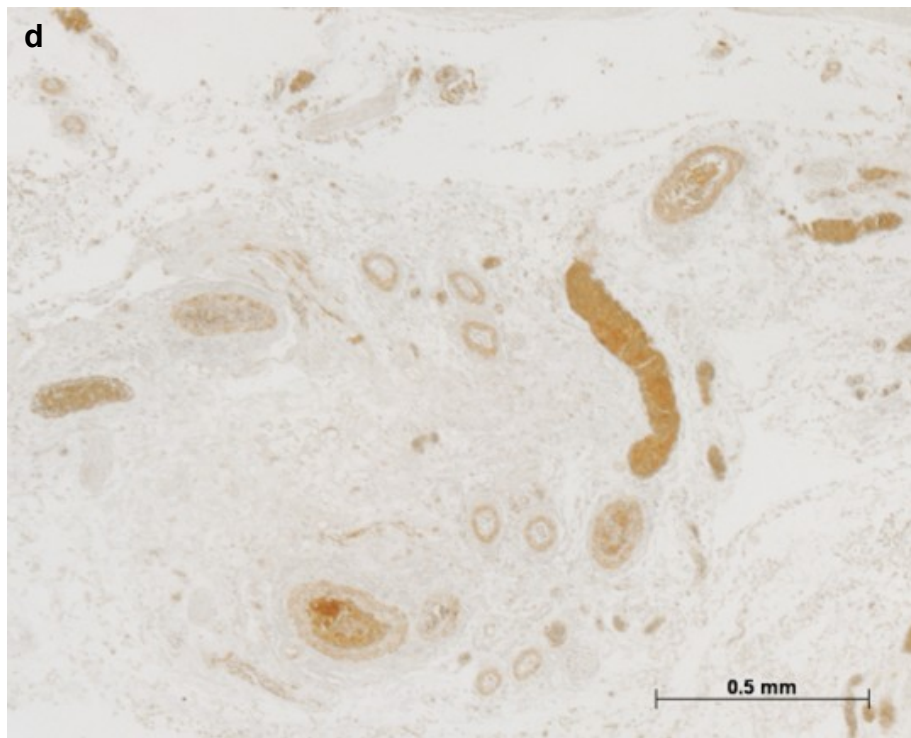
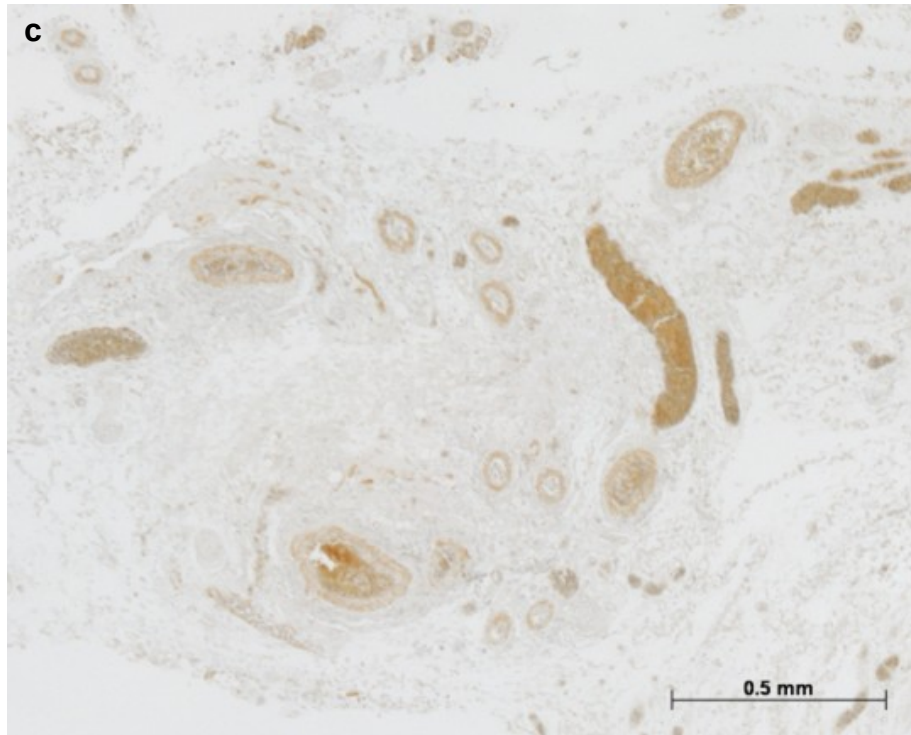


Figure 8.8 (continued). 4  $\mu\text{m}$  thick sections of paraffin wax-embedded adrenal cortex immunohistochemically stained for SMA using  $1/20,000$  MAH SMA followed by 4,5-diCl-OPD for 3 minutes and further incubated in 4,5-diCl-OPD for 27 minutes (c) or 57 minutes (d).

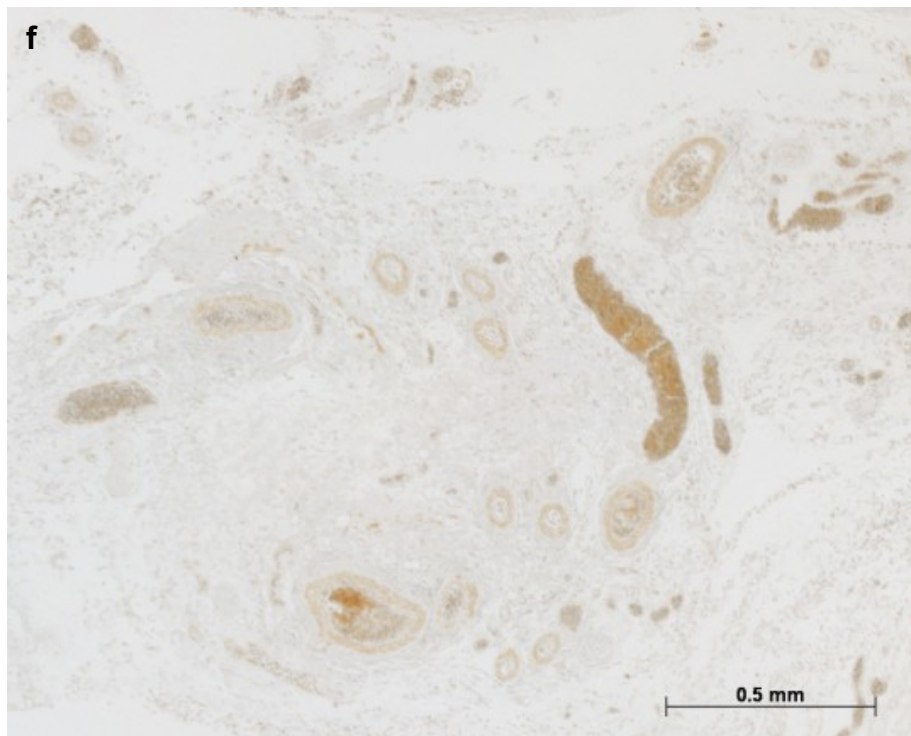
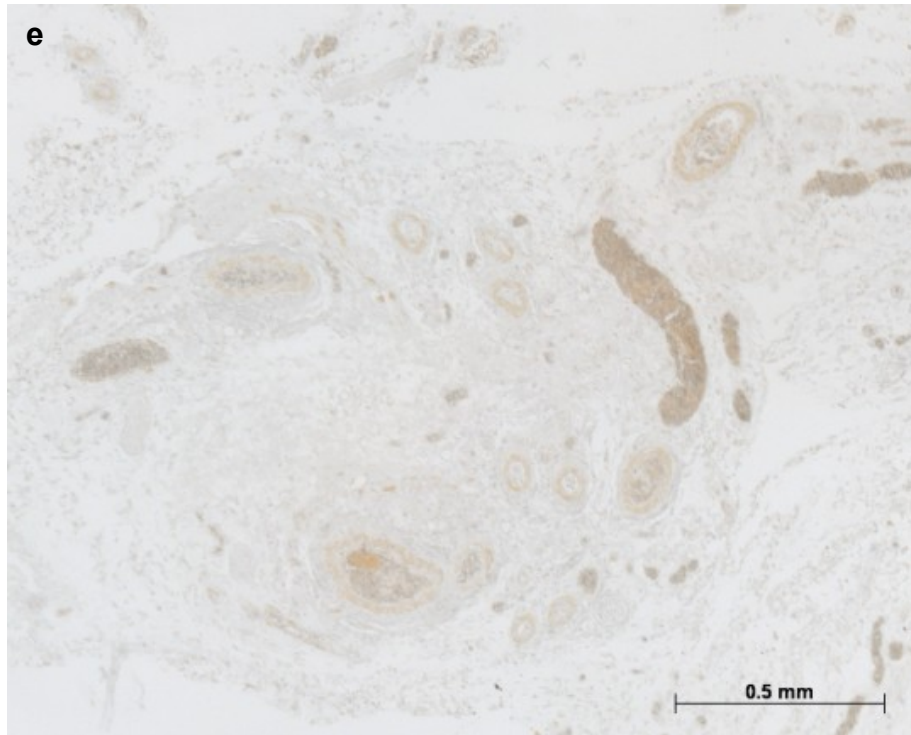


Figure 8.8 (continued). 4  $\mu\text{m}$  thick sections of paraffin wax-embedded adrenal cortex immunohistochemically stained for SMA using  $1/20,000$  MAH SMA followed by 4,5-diCl-OPD for 3 minutes and further incubated in 4,5-diCl-OPD with  $10^{-3}$  M NaCN in the reaction mixture for 7 minutes (e) or 27 minutes (f).

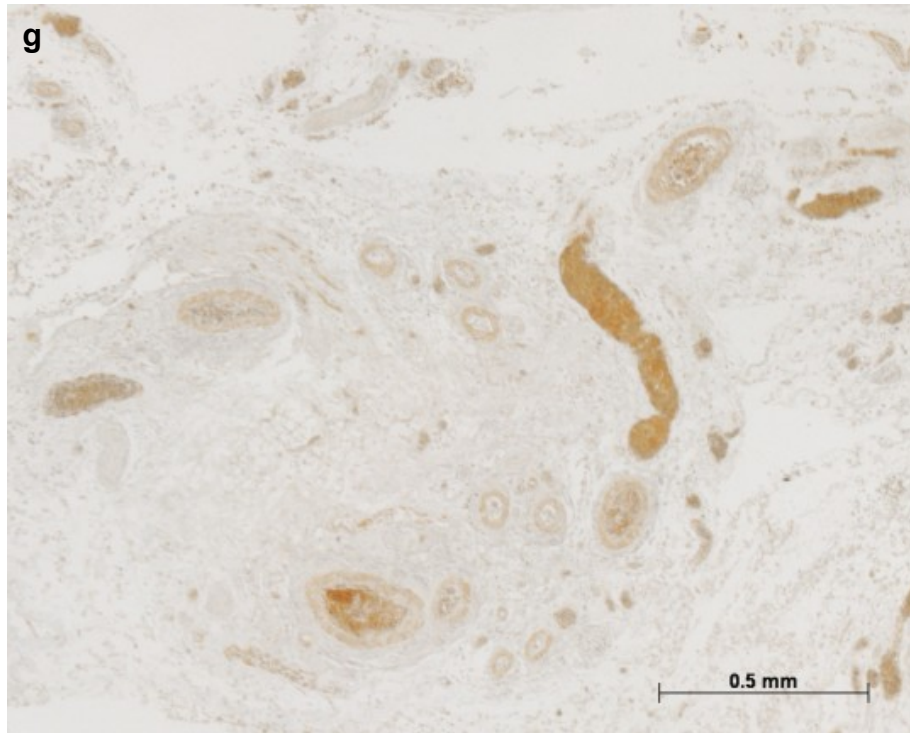


Figure 8.8 (continued). 4  $\mu\text{m}$  thick sections of paraffin wax-embedded adrenal cortex immunohistochemically stained for SMA using  $1/_{20,000}$  MAH SMA followed by 4,5-diCl-OPD for 3 minutes and further incubated in 4,5-diCl-OPD with  $10^{-3}$  M NaCN in the reaction mixture for 57 minutes (g).

#### **8.4.2.2.3 Determination of the Concentration of NaCN Required to Inhibit HRP for 60 Minutes**

The inclusion of NaCN in the 4,5-diCl-OPD reaction mixture caused a concentration-dependent reduction in staining intensity that only completely abolished immunohistochemical staining at 50 mM (figure 8.9a-f).



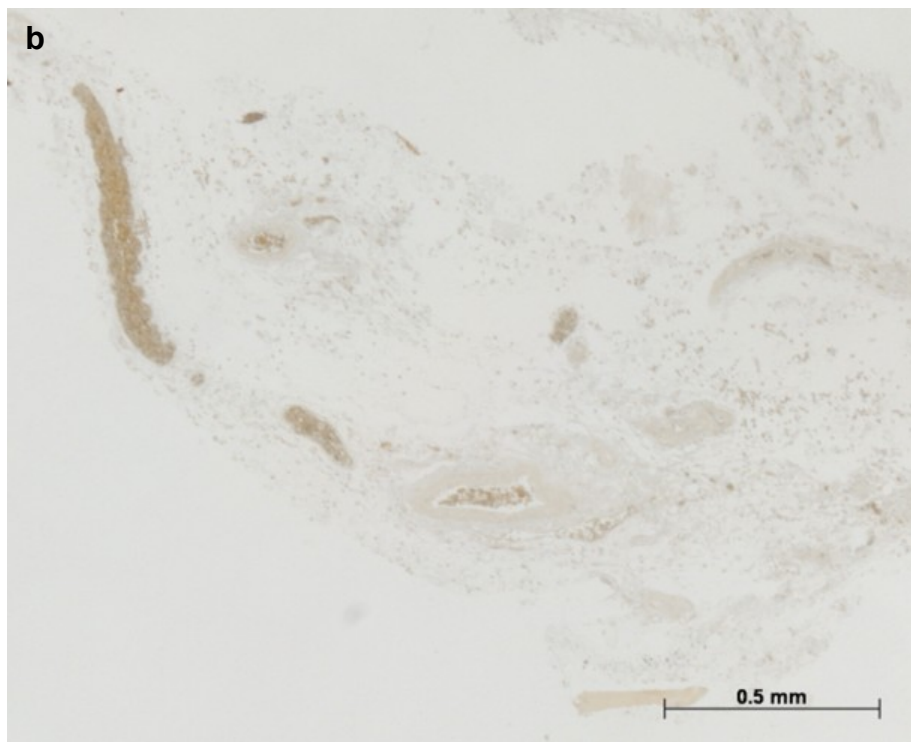
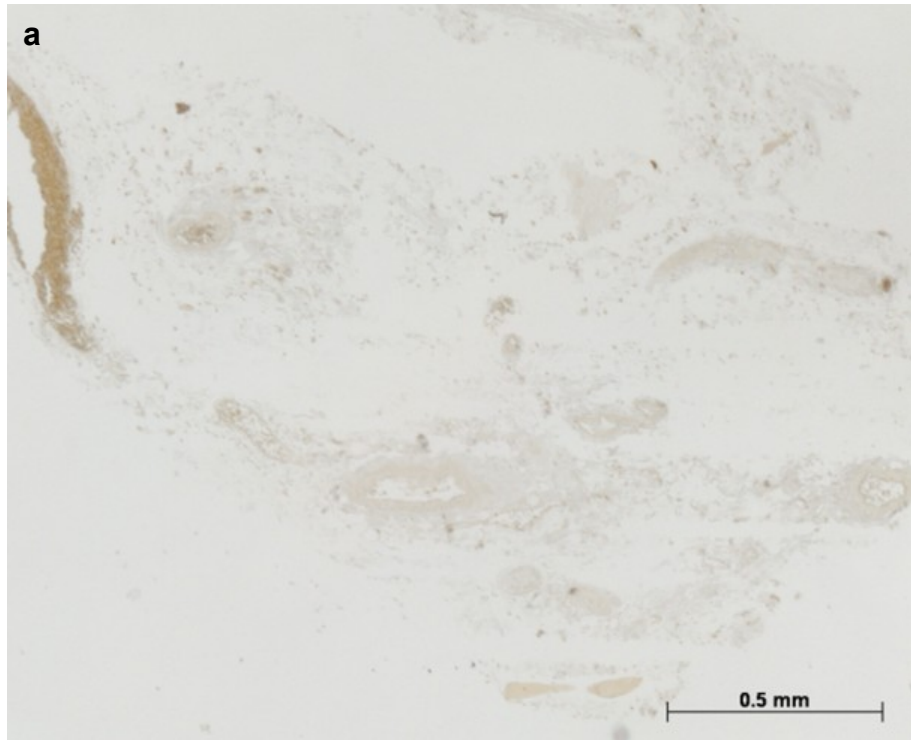


Figure 8.9. 4  $\mu\text{m}$  thick sections of paraffin wax-embedded adrenal cortex immunohistochemically stained for SMA using  $1/20,000$  MAH SMA followed by 4,5-diCl-OPD for 60 minutes containing NaCN at 1 mM (a) or 2 mM (b).

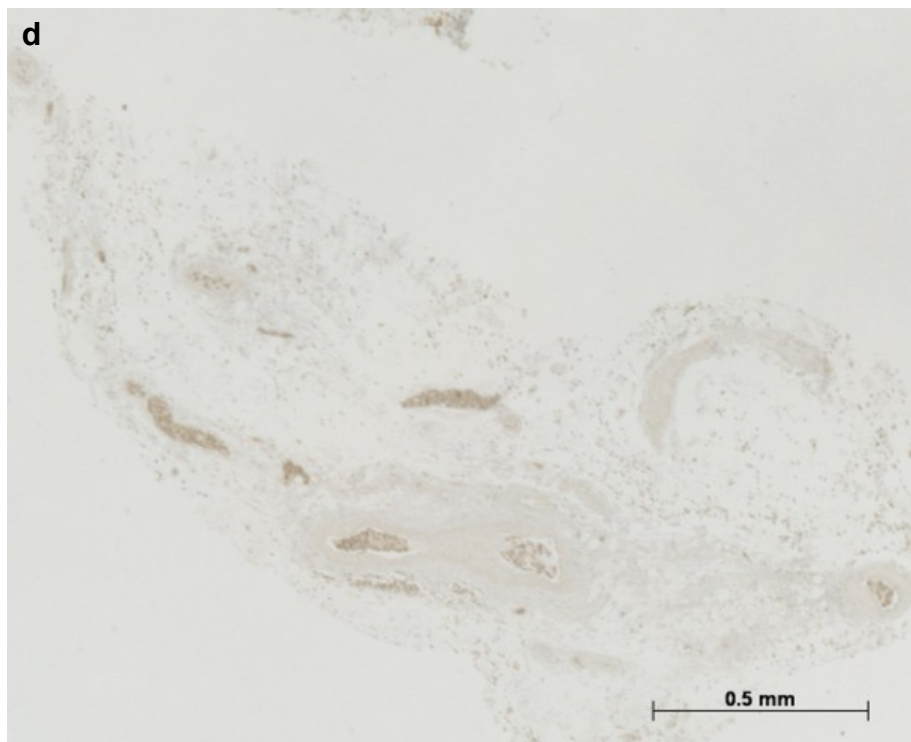
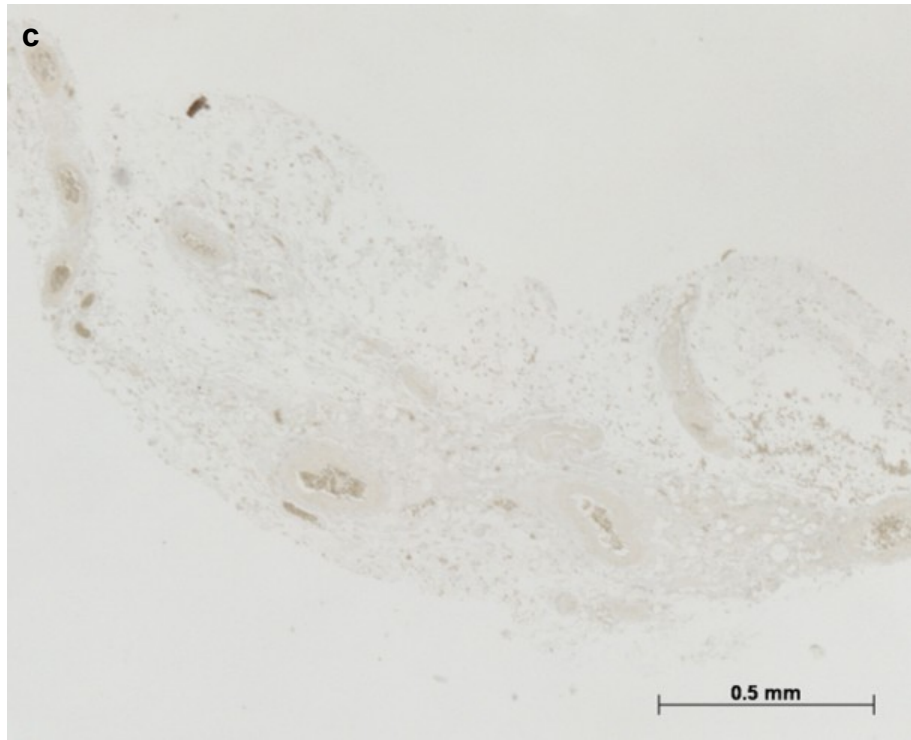


Figure 8.9 (continued). 4  $\mu\text{m}$  thick sections of paraffin wax-embedded adrenal cortex immunohistochemically stained for SMA using  $1/20,000$  MAH SMA followed by 4,5-diCl-OPD for 60 minutes containing NaCN at 5 mM (c) or 10 mM (d).



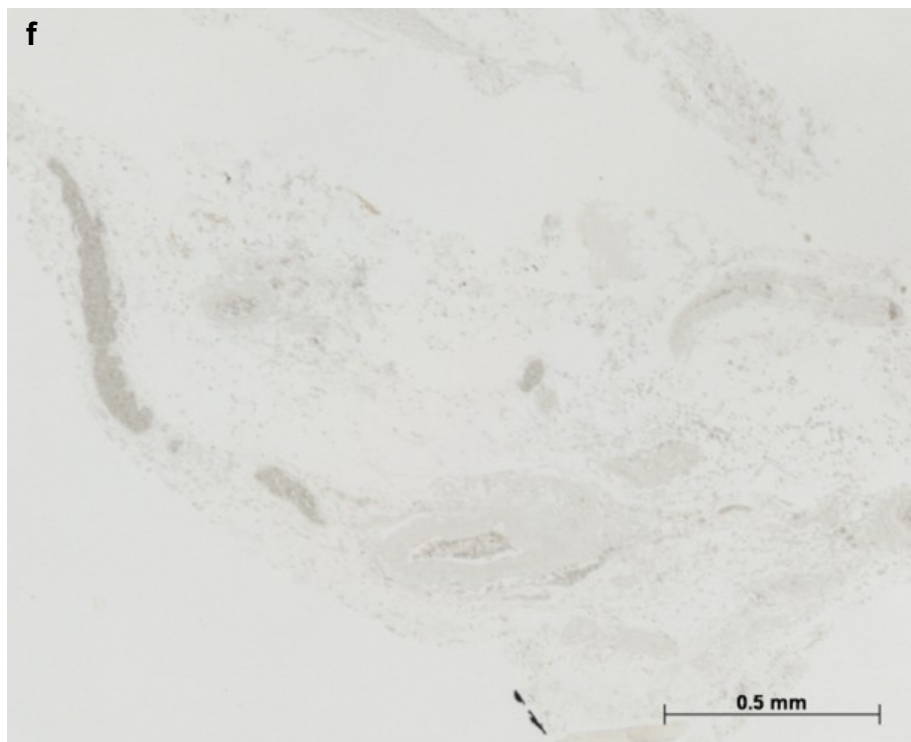
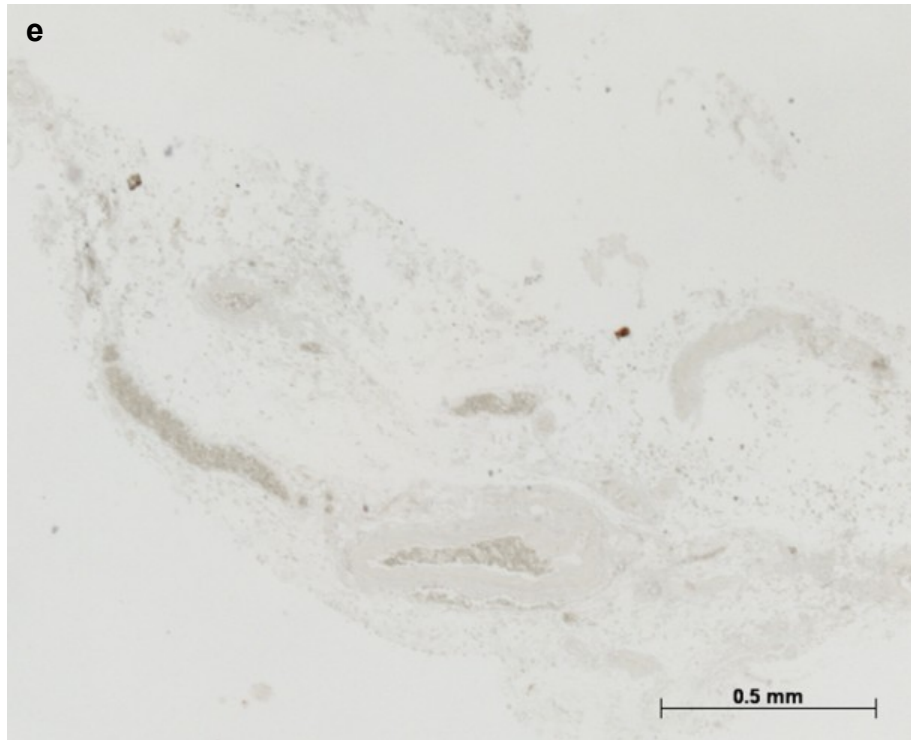


Figure 8.9 (continued). 4  $\mu$ m thick sections of paraffin wax-embedded adrenal cortex immunohistochemically stained for SMA using  $1/_{20,000}$  MAH SMA followed by 4,5-diCl-OPD for 60 minutes containing NaCN at 20 mM (e) or 50 mM (f).

#### **8.4.2.2.4 Effects of HRP Inhibition Following Re-incubation in Staining Solution containing 50 mM NaCN**

Following an initial 3 minute incubation in 4,5-diCl-OPD solution (figure 8.10a), subsequent incubation in the same solution resulted in a progressive increase in staining intensity that was similar to that observed in section 8.4.2.2.2, above (figure 8.10b – d). Inclusion of 50 mM NaCN in the re-incubation solution completely inhibited any further increase in staining intensity (figure 8.10e – g).

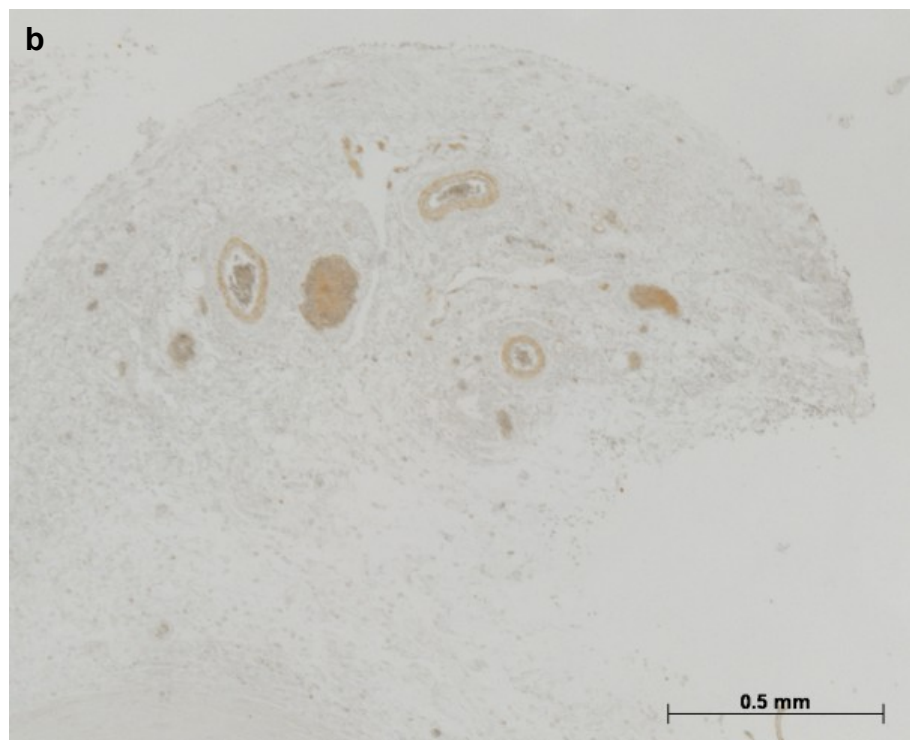
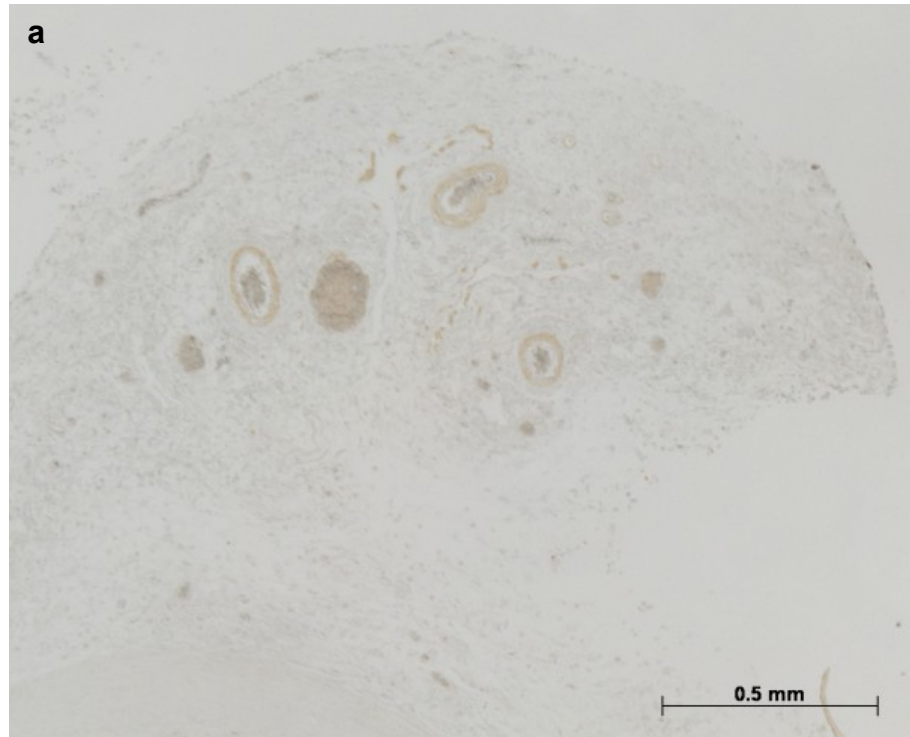


Figure 8.10. 4  $\mu\text{m}$  thick sections of paraffin wax-embedded adrenal cortex immunohistochemically stained for SMA using  $1/20,000$  MAH SMA followed by 4,5-diCl-OPD for 3 minutes (a) and further incubation for 7 minutes in 4,5-diCl-OPD (b).

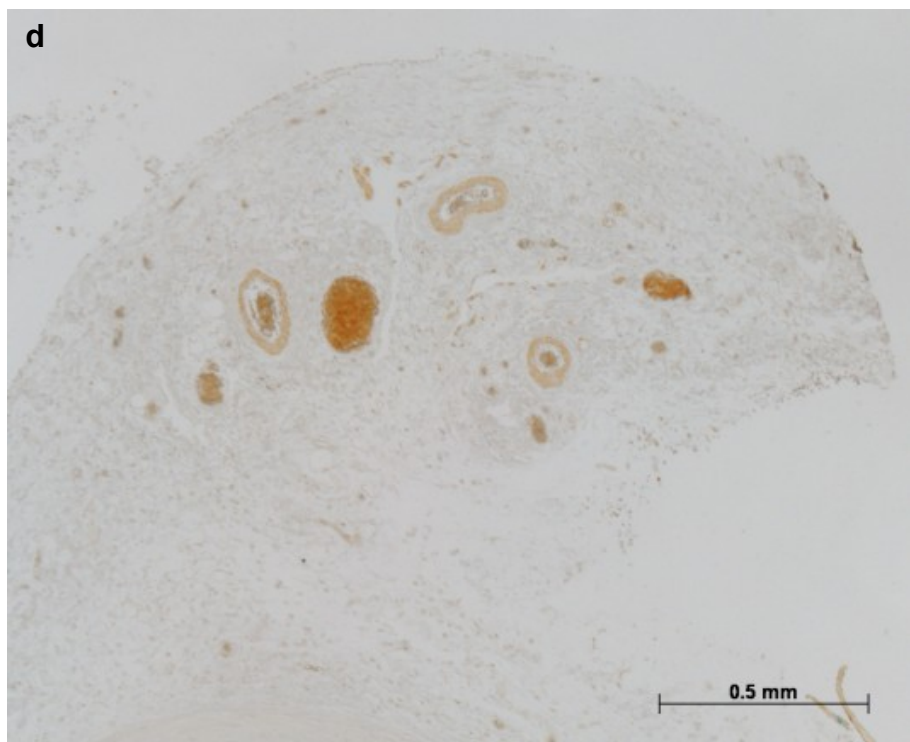
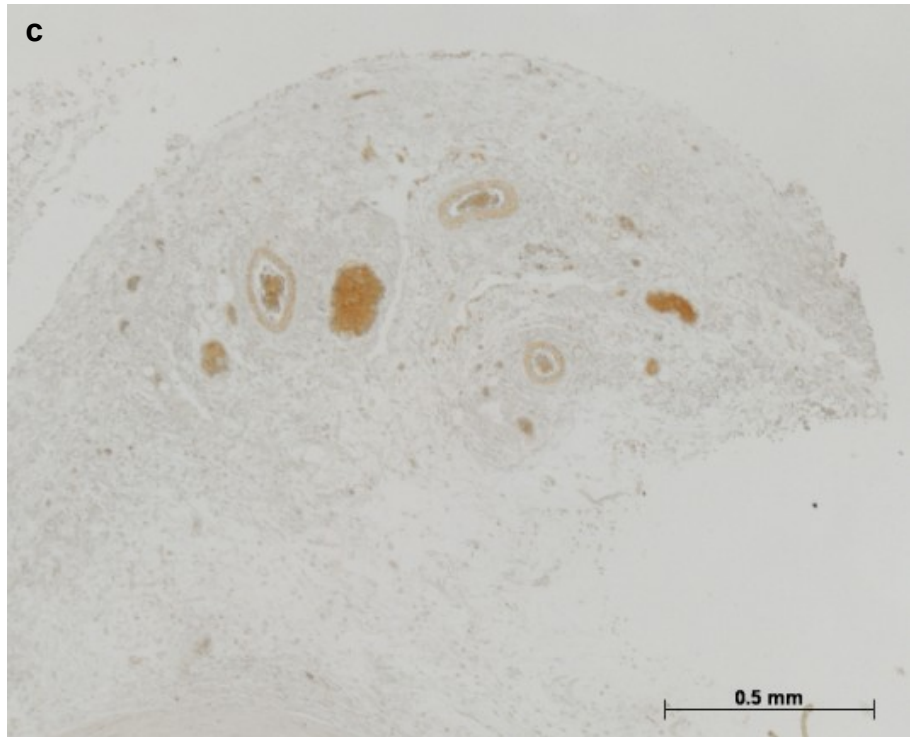


Figure 8.10 (continued). 4  $\mu$ m thick sections of paraffin wax-embedded adrenal cortex immunohistochemically stained for SMA using  $1/20,000$  MAH SMA followed by 4,5-diCl-OPD for 3 minutes and further incubated for 27 minutes (c) or 57 minutes in 4,5-diCl-OPD (d).

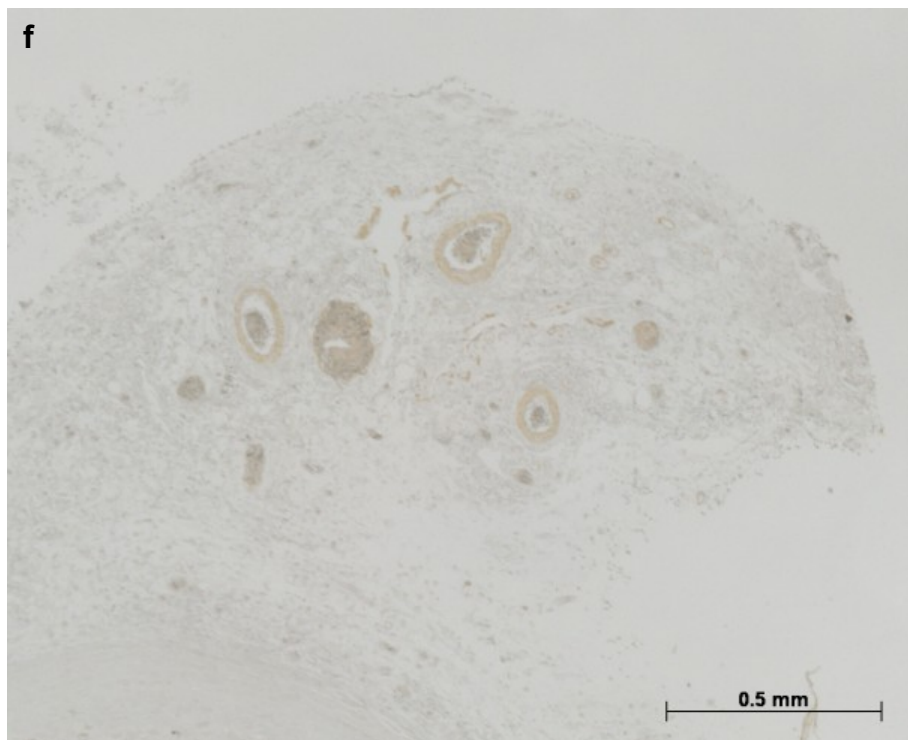
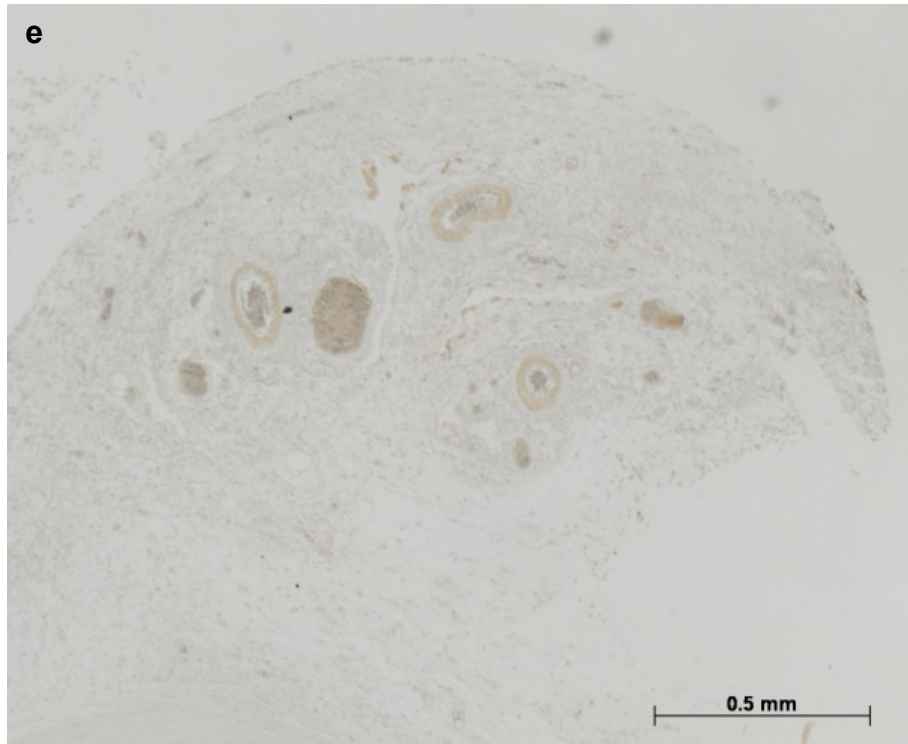


Figure 8.10 (continued). 4  $\mu\text{m}$  thick sections of paraffin wax-embedded adrenal cortex immunohistochemically stained for SMA using  $1/20,000$  MAH SMA followed by 4,5-diCl-OPD for 3 minutes and further incubated in 4,5-diCl-OPD with 50 mM NaCN for 7 minutes (e) or 27 minutes (f).

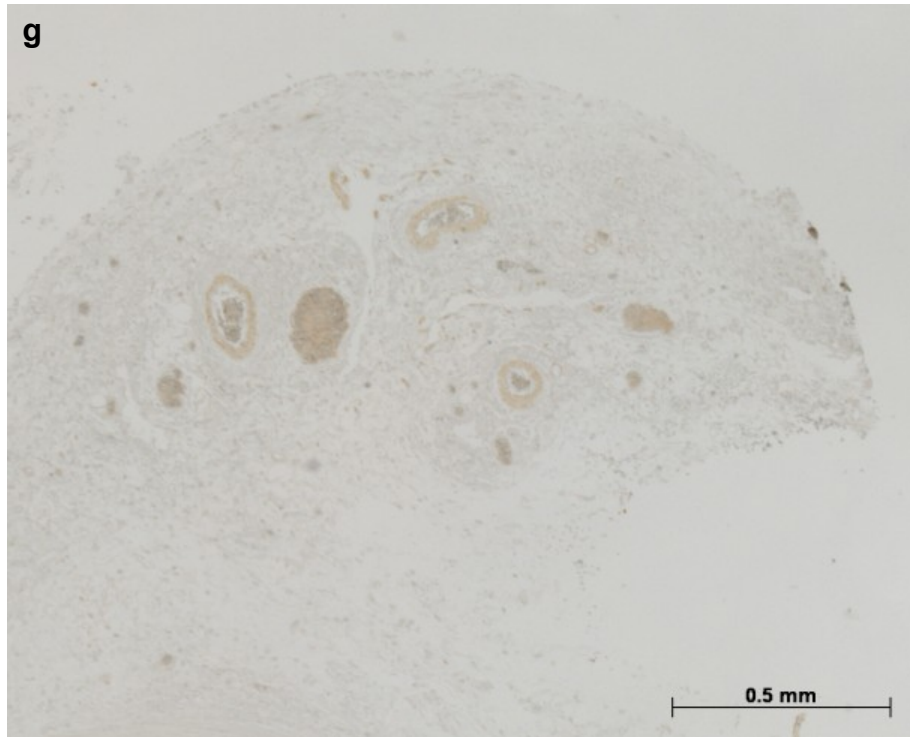


Figure 8.10 (continued). 4  $\mu\text{m}$  thick sections of paraffin wax-embedded adrenal cortex immunohistochemically stained for SMA using  $1/_{20,000}$  MAH SMA followed by 4,5diCl-OPD for 3 minutes and further incubated in 4,5-diCl-OPD with 50 mM NaCN for 57 minutes (g).

### **8.4.3 Fixation of Poly4,5-diCl-OPD**

The intense staining that was preserved by mounting in Fluorsave (figure 8.11a) was almost completely lost following dehydration and mounting (figure 8.11b). What little that was retained, slowly faded over the following few hours until no staining could be seen. Fixation with glutaraldehyde had no effect on this (figure 8.11c), whereas air drying resulted in retention of the majority of staining intensity (figure 8.11d). At higher dilutions of antibody, however, this affect was lost.



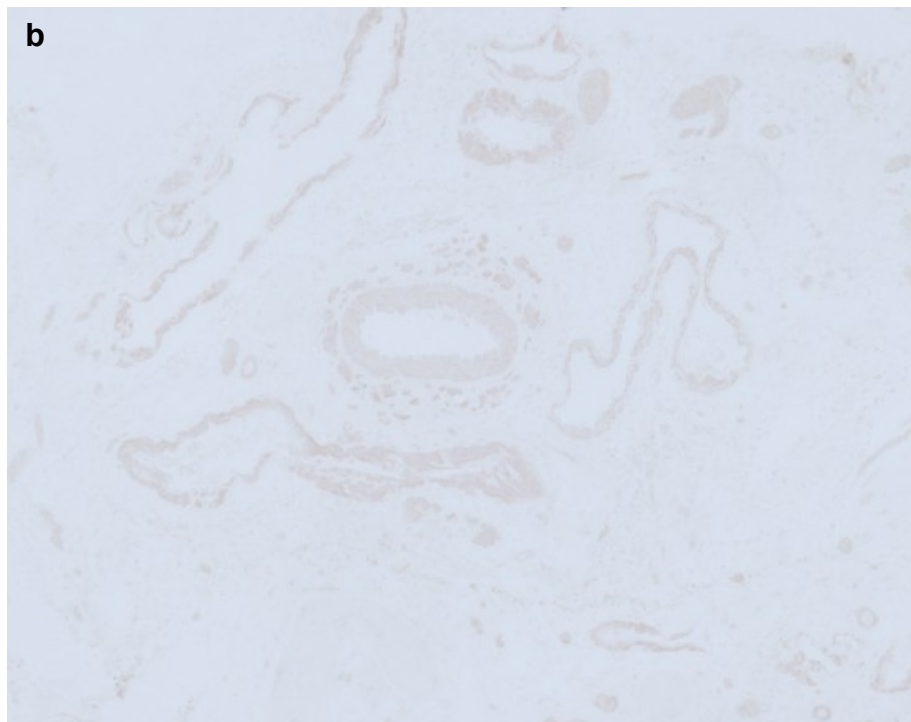
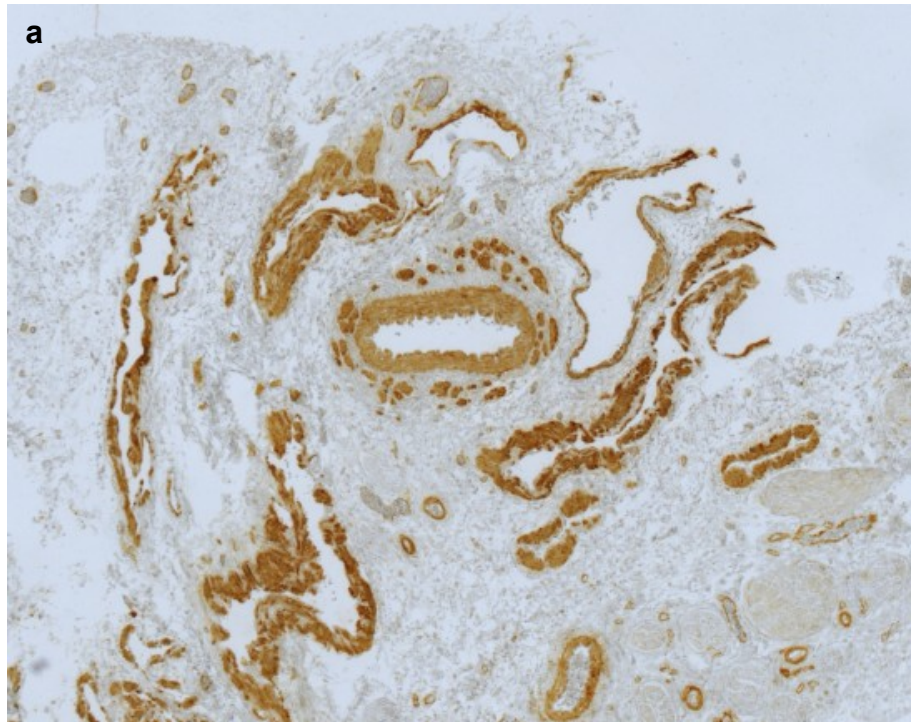


Figure 8.11. 4  $\mu$ m thick sections of paraffin wax-embedded adrenal cortex immunohistochemically stained for SMA using  $1/5,000$  MAH SMA followed by 4,5-diCl-OPD for 3 minutes and mounted in Fluorsave (a) or dehydrated, cleared and mounted in Gurr's neutral mountant (b).



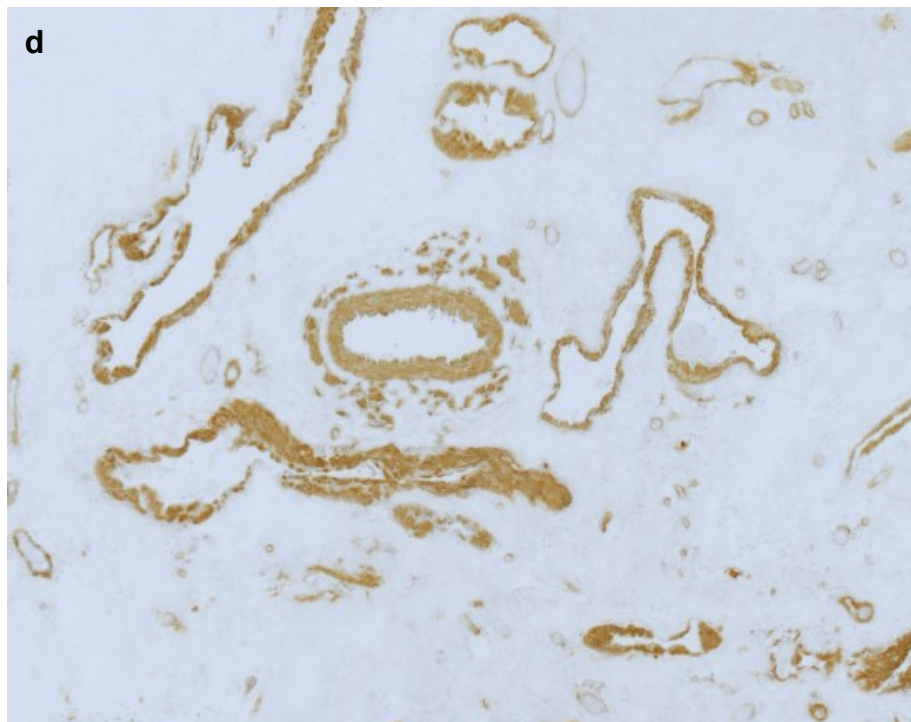
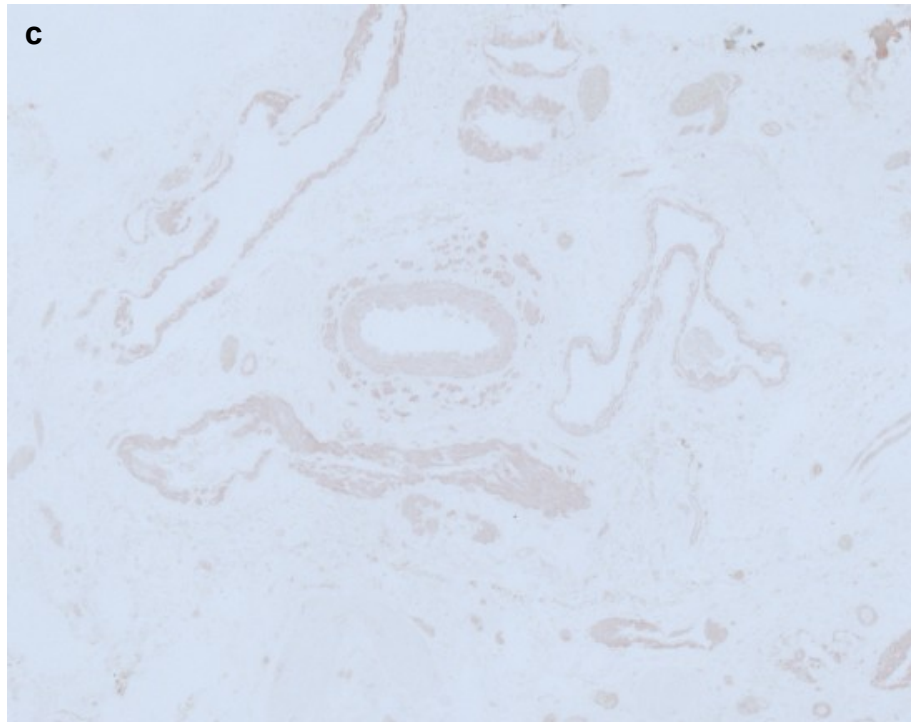


Figure 8.11 (continued). 4  $\mu\text{m}$  thick sections of paraffin wax-embedded adrenal cortex immunohistochemically stained for SMA using  $1/5,000$  MAH SMA followed by 4,5-diCl-OPD for 3 minutes followed by fixation with 0.5% glutaraldehyde (c), or air-dried (d) and dehydrated, cleared and mounted in Gurr's neutral mountant.

## 8.5 Discussion

The possibility of exploiting the progressive growth of poly4,5-diCl-OPD fibres, suggested by transmission electron micrographs, for light microscopical immunohistochemistry was successful, with sensitivity being increased by nearly an order of magnitude compared to DAB. That this improvement mirrored what was achieved in Chapter 3 may, again, have reflected the practical limits of sensitivity of the peroxidase system.

That little increase in staining intensity was observed beyond 20 minutes at the highest primary antibody dilution was surprising, given that this did not occur at slightly lower dilutions.

Attempts to inhibit HRP indicated that the enzyme was surprisingly resilient, and very high concentrations of either  $\text{H}_2\text{O}_2$  or  $\text{NaN}_3$  would probably be required to achieve complete inhibition, and only when included in the reaction mixture. Only NaCN was able to completely inhibit HRP for the full 60 minutes, and only when included in the substrate solution at a final concentration of 50 mM, a nearly 20-fold higher concentration than 4,5-diCl-OPD. Inhibition of HRP has been reported to be 95% with  $10^{-4}$  M cyanide, an order of magnitude lower than required here (Klapper and Hackett, 1963) but conjugation to an antibody may affect the enzyme in an analogous way to that observed for the antibody in Chapter 3. The reversibility of HRP inhibition by peroxide, azide and cyanide has also been reported (Keilin et al., 1951). The results suggested that enzymatic activity was required for fibre growth, and that the polymerisation of 4,5-diCl-OPD was not autocatalytic, although interference from such a high concentration of inhibitor cannot be ruled out. Fibre growth from the proximal end raises the question of how the fibre remains attached to the enzyme, since dissociation of product molecule

from the enzyme must occur for the catalytic cycle to continue. Given the solubility of the polymer, it is possible that the fibre becomes loosely adsorbed onto a non-catalytic part of the enzyme and only briefly dissociates when fresh product reacts with it, only becoming attached, itself. Another site of adsorption might be adjacent fibres, and this might explain why increased staining was not seen beyond 20 minutes at the highest primary antibody titre in the preliminary experiments. The insolubility and 'stickiness' of polyDAB lends some support to this; adsorption is stronger, but the presence of two aromatic rings allows reaction at more sites without the need for dissociation, thus the enzyme becomes rapidly buried in polymer product, and eventually the substrates are unable to gain access to the catalytic site.

Attempts to reduce the solubility of poly4,5-diCl-OPD with glutaraldehyde were unsuccessful, suggesting that the polymer may be predominantly phenazine-like in structure, with few available amines. Air drying was more successful, but only when high concentrations of primary antibody were used and thus large amounts of fibre were present. At low primary antibody titres, air drying did not prevent solution of the polymer. These results can be accounted for by invoking entanglement of fibres and interaction, in the absence of solvent, by dispersive forces. At low fibre concentrations, interaction is substantially reduced or absent, and fibres are more amenable to solvation.

The formation of the fibrillary form of poly4,5-diCl-OPD was only observed with one commercial source and suggested that a minor contaminant or oxidation product might be responsible. Identification of this substance or substances and the mechanism of fibrillary polymer formation might prove extremely useful in developing novel immunohistochemical markers for use at the light microscopic

level, since staining intensity and sensitivity could be controlled by simple manipulation of incubation time or substrate concentration. Such technology would be easily incorporated into high throughput automated procedures and might largely obviate the need for reporter and marker amplification. Target retrieval would probably still have some utility, however, since it has broadened the range of antibodies that can be used in immunohistochemical staining.

An additional, albeit specialised, application of halogenated diamines would be the visualisation of carbohydrates (specifically 1,2-diols) in the TEM. Currently, this is achieved using periodic acid and thiocarbohydrazide, followed by either osmium (Seligman et al., 1965) or silver (Seligman et al., 1965; Thiery, 1967; Neiss, 1988,). Thiocarbohydrazide is highly toxic and the multi-step procedures require prolonged staining times. N,N-dimethyl-p-phenylenediamine has been successfully used as a substitute (Spicer and Jarrels, 1961) for the more commonly employed pararosaniline (Hotchkiss, 1948) at the light microscopic level, and thus provides additional support to the proposition. The substitution of iodinated aromatic diamines as the nucleophile should impart electron opacity and greatly simplify this procedure.

## **8.6 Summary and Conclusions**

The potential for developing a simple alternative to current marker amplification technology has been demonstrated. The technique suffers from marker solubility, but identification of substance(s) responsible for producing the fibrillary polymer may provide a means of generating living polymers with greater insolubility. Such technology could be easily incorporated into automated procedures and might also render reporter amplification obsolete.

## 8.8 References

- BAYNTON, K. J., BEWTRA, J. K., BISWAS, N. & TAYLOR, K. E. 1994. Inactivation of horseradish peroxidase by phenol and hydrogen peroxide: a kinetic investigation. *Biochimica et Biophysica Acta*, 1206, 272-278.
- HOTCHKISS, R. D. 1948. A microscopical reaction resulting in the staining of polysaccharide structures in fixed tissue preparations. *Archives of Biochemistry*, 16, 131-141.
- KEILIN, D., HARTREE, E. F., CECIL, R. & OGSTON, A. G. 1951. Purification of horse-radish peroxidase and comparison of its properties with those of catalase and methaemoglobin. *Biochemical Journal*, 49, 88-106.
- KLAPPER, M. H. & HACKETT, D. P. 1963. Oxidatic activity of horseradish peroxidase.1. oxidation of hydro- and naphthohydroquinones. *Journal of Biological Chemistry*, 238, 3736-3742.
- LI, C. Y., ZIESMER, S. C. & LAZCANOVILLAREAL, O. 1987. Use of azide and hydrogen peroxide as an inhibitor for endogenous peroxidase in the immunoperoxidase method. *Journal of Histochemistry & Cytochemistry*, 35, 1457-1460.
- NEISS, W. F. 1988. Enhancement of the periodic acid - Schiff (PAS) and periodic acid - thiocarbohydrazide - silver proteinate (PA-TCH-SP) reaction in LR White sections. *Histochemistry*, 88, 603-612.
- SELIGMAN, A. M., HANKER, J. S., WASSERKRUG, H., DMOCHOWSKI, H. & LATZOFF, L. 1965. Histochemical demonstration of some oxidised macromolecules with thiocarbohydrazide (TCH) or thiosemicarbazide (TSH) and osmium tetroxide. *Journal of Histochemistry and Cytochemistry*, 13, 629-639.
- SPIKER, S. S. & JARRELS, M. H. 1961. Histochemical reaction of an aromatic diamine with acid groups and periodate engendered aldehydes in mucopolysaccharides. *Journal of Histochemistry*, 9, 368-379.

- STRAUS, W. 1972. Phenylhydrazine as inhibitor of horseradish peroxidase for use in immunoperoxidase procedure. *Journal of Histochemistry & Cytochemistry*, 20, 949-951.
- THIERY, J. P. 1967. Mise en évidence des polysaccharides sur coupes fines en microscopie électronique. *J. Microscopie* 6, 987-1018.
- VAN DUIJN, P. 1957. Histochemistry of DOPA factors.3. Inactivation experiments the DOPA factors in neutrophilic and eosinophilic leucocytes and erythrocytes. *Acta Physiologica Et Pharmacologica Neerlandica*, 5, 428-444.

# **Chapter 9**

## **General Discussion and Conclusions**

## 9.1 General Discussion

Light and electron microscopy have traditionally been regarded as separate technologies, but the development of fixatives (Karnovsky, 1965), embedding media (Newman and Hobot, 2001) and staining techniques (Hanker et al., 1964; 1966; Graham and Karnovsky, 1966; Holgate et al., 1983; Wynford-Thomas et al., 1986; Bowdler et al., 1989) that are applicable to both are testament to the artificiality of this distinction, in the biological sciences, at least.

The work presented in this thesis has, for practical purposes, been broadly divided along traditional lines i.e. into the visualisation of trace amounts of target by marker amplification at the light microscopic level and the demonstration of multiple markers, by analytical methods, in the electron microscope. The capacity of polyDAB to form catalytic complexes with d-block metal compounds, for the former purpose, led logically to an exploration of this phenomenon for discriminating multiple markers using analytical electron microscopy, thus reinforcing the link between the two microscopy modes.

In practical terms, the approach for refining existing marker technologies, as well as developing novel ones, has been one of empiricism, or what might be called 'applied ignorance'. This has, to a certain extent, been unavoidable, since almost nothing is known regarding the co-ordination chemistry of polyDAB, and the success or failure of novel marker chemistries, when applied to biological systems, is largely unpredictable.

This unpredictability was particularly evident in Chapter 2, where, for example, Fe(II) and Cu(II) both produced encouraging results in the dot blot model system but when applied in the tissue model system, catalysed the rapid and widespread background deposition of silver. What was also surprising was the extraction of



probably all complex-forming metals from polyDAB by Newman and Jasani's developer. That ethylenediamine is displaced from Ni(II) complexes by pyrogallol has been known for some time (Patel and Bhattach, 1971) and a similar mechanism presumably occurs in the case of polyDAB. Another surprise was that the gold/sulfide/silver method (Newman et al., 1983) remained the most powerful and controllable system of all. Had other metals, like platinum, not been subject to extraction by the developer, more powerful amplification may have been observed.

Manipulation of this particular amplification system, together with the application of additional methods for suppressing background staining, extended the limit of immunohistochemical sensitivity by an order of magnitude, when compared with polyDAB alone. While this, in itself, was impressive, the colloidal gold/silver method still outperformed the peroxidase system by a further order of magnitude. This was probably due, in part, to the presence of solid metal as the catalytic surface, but also to the antibody being in a more native state. This observation raised an important issue regarding the ultimate sensitivity of reporter-marker systems, namely, that current conjugation methods might lower antibody affinity to a considerable extent.

The capacity of polyDAB to form d-block metal complexes allowed their demonstration in both the SEM and TEM within relatively short time frames. Furthermore, immunohistochemical deposits were also demonstrated by elemental mapping in the SEM. Unfortunately, the concentrations of metals were too low for AEMT to be realistically achievable in the majority of laboratories using this method. AEMT, using polyDAB-metal complexes, may well be possible in laboratories with sufficiently sophisticated equipment such as field emission guns, electron energy loss spectrometers or in-column energy filters and it surprising that

such technologies have not been applied to quantum dots. It is possible that it already has, and was unsuccessful. Alternatively, the belief that sections thicker than about 50 nm are unsuitable for energy filtering techniques, since such techniques rely on single electron-atom interaction events, may have dissuaded worker from exploring this possibility, even though analytical tomography has been successfully demonstrated in 70 nm sections at high tilts at only 120 kV (Leapman et al., 2004).

It was not, however, the purpose of these investigation to develop technologies that could only be exploited in the best equipped laboratories, but to broaden the applicability of marker systems. The limitations imposed by polyDAB-metal complexes in AEMT led to an exploration of the utility of halogenated compounds as potential AEMT markers. By the process of elimination, using progressively more stringent technologies, the range of potential markers was narrowed to just one compound, namely 4,5-diI-OPD, which was demonstrable within the shortest timeframe that was achievable with the available analytical equipment.

Once again, a number of unexpected results were obtained with the halogenated compounds, not least the loss of fluorine from all the fluorinated diamines upon polymerisation. The C-F bond is one of the strongest, but the high electronegativity of fluorine may have allowed it to behave as a leaving group if the electron density of the aromatic system increased sufficiently. This proposition is lent tentative support by the observation that both DAB (Maranto, 1982; Sandell and Masland, 1988; Gaietta et al., 2002; Grabenbauer et al., 2005) and silver are deposited by the photoconversion process, a process that may, in part, be reductive. The appearance of some of the polymers, notably the fibrillary poly4,5-diCl-OPD and the bizarre poly4,5-diBr-OPD was, again, unexpected and an investigation of

this phenomenon would be of academic interest, at least. The fibrillary nature of poly4,5-diCl-OPD was only observed from one commercial source of the substrate. Identification of the substance(s) that caused this phenomenon might prove useful in developing an alternative to DAB at the light microscopic level. Product inhibition is the major restriction of the peroxidase/DAB system and has driven the development of both reporter and marker amplification technologies. These would be largely obviated should a living polymer be developed, and such a novel substrate could easily be incorporated into the high throughput systems that are used in both diagnostic histopathology and industry; all that would be required would be the manipulation of the incubation time for a given level of sensitivity.

The investigations in Chapters 4 and 5 were based on the supposition that antibodies could penetrate acrylic resin sections. The evidence for this phenomenon (Newman and Hobot, 1987) remains controversial and the results of the brief investigation in Chapter 4 lend support to the generally held belief that antibodies are simply too large. The behaviour of LR White acrylic resin has changed slightly over the last couple of decades; early personal observations indicated that it swelled to a considerable extent when hydrated, but more recent formulations do not. The composition of the resin has not been altered (Dr. Brian Causton, London Resin Company, personal communication), but subtle variations in the composition, such as a change in the commercial source of one of the components or an improvement in purity, might alter the behaviour of the final resin. The lowicryl resin, K4M, also swells when hydrated (Newman and Hobot, 2001) and its composition, unlike that of the LR resins, is published (Carlemalm et al., 1982). It is not, however, compatible with the peroxidase/DAB system, suffering from serious background

staining (Newman and Hobot, 2001), but manipulation of its composition might overcome this drawback.

Antibodies are probably too large to penetrate resin sections, and even the smallest active fragments are in the order of 15 kD (Sheriff and Constantine, 1996). The molecular weight cut-off of acrylic resins and tissues that are embedded therein is unknown, but manipulation of resin formulation may improve reporter penetration. Failing this, two approaches exist for preparing low molecular weight reporters, namely (1) design of ligands with a high specificity for selected epitopes and (2) synthesis of a scaffold with randomly attached functional groups followed by screening. The former technique requires detailed information concerning the 3-dimensional structure of the target epitope, extensive mathematical modelling to determine an appropriate complementary structure and subsequent synthesis and evaluation. The latter approach mimics the process underlying antibody production *in vivo*. Both approaches would involve a huge amount of work.

In Chapter 6, the possibility of depositing silver from a physical developer by the photoconversion process was explored. The results were extremely encouraging and raised questions regarding the nature of the photoconversion process, with particular regard to the polymerisation of DAB. Refinement of this technique, together with the application of appropriate methodologies for suppressing tissue autofluorescence, may well lead to an alternative approach for illustrating fluorochromes at the electron microscopic level and, ultimately, to the development of an AEMT marker, since metallic silver is inherently electron opaque and should produce a strong X-ray signal.

Current technologies for CLEM exploit the photoconversion process to deposit electron-opaque markers for examination in the TEM. This might be circumvented,

and the problems associated with tissue and resin autofluorescence avoided, by the development of fluorescent reporters with catalytic properties. The introduction of such catalytic moieties into live cells would probably have unforeseen consequences, but the masking of such sites may overcome this. Such unmasking might be achieved by photoisomerisation of stilbene (Waldeck, 1991) and azobenzene compounds (Schultz et al., 2003). An additional advantage to this approach would be the avoidance of problems associated with overlapping excitation spectra of organic and inorganic fluorochromes. In the light microscope, a wide variety of optical and digital techniques exist for separating their emission spectra, but these cannot be applied, of course, to the photoconversion process. In some ways, this brings the thesis full-circle to the first experimental chapter where the catalytic action of polyDAB-metal complexes was empirically investigated.

The characterisation of polyDAB was less extensive than initially hoped, but provided some useful insights into the direction that more fruitful investigation might be directed. The resolution of some of the conflicting results, together with the application of more informative technologies, should hopefully reveal the coordination chemistry of polyDAB and thus lead to the development to novel catalytic markers. In addition, such techniques could aid an understanding of the polymerisation of the halogenated compounds.

This thesis has focussed, primarily on the peroxidase/DAB system for generating markers, but this inevitably places constraints on the chemistries that might be available. There is no reason, in principle, why enzymes should not be replaced by more stable, non-enzymatic catalysts. This might not only allow for the rational development of new classes of markers, but also avoid the problems associated with existing immunohistochemical techniques e.g. endogenous

enzymatic and non-enzymatic activities. In addition, the coupling of non-enzymatic catalysts to antibodies would reduce the overall size of the molecule and would contribute to the development of penetrable reporters.

The recent commercial introduction of SEM tomography (SEMT) (Zankel et al., 2009) represents an exciting development in 3-D reconstruction of biological samples, since much larger specimens can be examined than in the TTEM. Currently, an ESEM is required to overcome the problems associated with electrostatic charging of uncoated, non-conducting resins. Electrically conducting resins are commercially available, but achieve conductivity by the incorporation of metal particles, which preclude ultramicrotomy. In addition, such particles would probably fail to penetrate biological samples and thus any advantage that such resins might offer would be lost. Electrostatic charging can be overcome by operating the SEM at low voltages e.g. 0.1 kV, but this restricts the technology to those laboratories with high vacuum SEMs fitted with field emission guns. An alternative approach would be the development of electrically conducting organic resins, since this would broaden the availability of SEMT to the majority of laboratories. An additional advantage of conducting resins would be improved stability in the TEM, which would be of particular importance in AEMT.

## **9.2 Summary and Conclusion**

The study of dynamic processes in live cells has led to the introduction of a wide range of cytochemical markers to exploit the numerous optical techniques that have been developed over the last couple of decades. In sharp contrast, immunohistochemical and CLEM marker chemistries have not progressed significantly since the 1980s, even though considerable advances have been made in both instrument design and capability. The rational design of novel marker chemistries for visualising the smallest amounts of target molecule at the light microscopic level and for discriminating marker deposits at the electron microscopic level is long overdue, and simplicity of application, to ensure the broadest applicability, should be the guiding principle.

### 9.3 References

- BOWDLER, A. L., GRIFFITHS, D. R. & NEWMAN, G. R. 1989. The morphological and immunohistochemical analysis of renal biopsies by light and electron microscopy using a single processing method. *Histochemical Journal*, 21, 393 - 402.
- CARLEMALM, E., GARAVITO, R. M. & VILLIGER, W. 1982. Resin development for electron microscopy and an analysis of embedding at low temperature. *Journal of Microscopy-Oxford*, 126, 123-143.
- GAIETTA, G., DEERINCK, T. J., ADAMS, S. R., BOUWER, J., TOUR, O., LAIRD, D. W., SOSINSKY, G. E., TSIEN, R. Y. & ELLISMAN, M. H. 2002. Multicolor and electron microscopic imaging of connexin trafficking. *Science*, 296, 503-507.
- GRABENBAUER, M., GEERTS, W. J. C., FERNADEZ-RODRIGUEZ, J., HOENGER, A., KOSTER, A. J. & NILSSON, T. 2005. Correlative microscopy and electron tomography of GFP through photooxidation. *Nature Methods*, 2, 857-862.
- GRAHAM, R. C. & KARNOVSKY, M. J. 1966. The early stages of absorption of injected horseradish peroxidase in the proximal tubules of mouse kidney: ultrastructural cytochemistry by a new technique. *Journal of Histochemistry and Cytochemistry*, 14, 291-302.
- HANKER, J. S., DEB, C., WASSERKRUG, H. L. & SELIGMAN, A. M. 1966. Staining tissue for light and electron microscopy by bridging metals with multidentate ligands. *Science*, 152, 1631-1634.
- HANKER, J. S., SEAMAN, A. R., WEISS, L. P., UENO, H., BERGMAN, R. A. & SELIGMAN, A. M. 1964. Osmiophilic reagents: new cytochemical principle for light and electron microscopy. *Science*, 146, 1039-1043.
- HOLGATE, C. S., JACKSON, P., COWEN, P. N. & BIRD, C. C. 1983. Immunogold silver staining - new method of immunostaining with enhanced sensitivity. *Journal of Histochemistry & Cytochemistry*, 31, 938-944.



- KARNOVSKY, M. J. 1965. A formaldehyde-glutaraldehyde fixative of high osmolarity for use in electron microscopy. *Journal of Cell Biology*, 27, 137A.
- LEAPMAN, R. D., KOCSIS, E., ZHANG, G., TALBOT, T. L. & LAQUERRIERE, P. 2004. Three-dimensional distributions of elements in biological samples by energy-filtered electron tomography. *Ultramicroscopy*, 100, 115-125.
- MARANTO, A. R. 1982. Neuronal mapping: a photooxidation reaction makes Lucifer yellow useful for electron microscopy. *Science*, 217, 953-955.
- NEWMAN, G. R. & HOBOT, J. A. 1987. Modern acrylics for post-embedding immunostaining techniques. *Journal of Histochemistry and Cytochemistry*, 35, 971 - 981.
- NEWMAN, G. R. & HOBOT, J. A. 2001. *Resin microscopy and on-section immunocytochemistry*, Springer-Verlag.
- NEWMAN, G. R., JASANI, B. & WILLIAMS, E. D. 1983. The visualization of trace amounts of diaminobenzidine (DAB) polymer by a novel gold-sulfide-silver method. *Journal of Microscopy-Oxford*, 132, RP1-RP2.
- PATEL, D. C. & BHATTACH, P. K. 1971. A study of ligand exchange in some nickel complexes. *Journal of Inorganic & Nuclear Chemistry*, 33, 529-533.
- SANDELL, J. H. & MASLAND, R. H. 1988. Photoconversion of some fluorescent markers to a diaminobenzidine product. *Journal of Histochemistry & Cytochemistry*, 36, 555-559.
- SCHULTZ, T., QUENNEVILLE, J., LEVINE, B., TONIOLO, A., MARTINEZ, T. J., LOCHBRUNNER, S., SCHMITT, M., SHAFFER, J. P., ZGIERSKI, M. Z. & STOLOW, A. 2003. Mechanism and dynamics of azobenzene photoisomerization. *Journal of the American Chemical Society*, 125, 8098-8099.
- SHERIFF, S. & CONSTANTINE, K. L. 1996. Redefining the minimal antigen-binding fragment. *Nature Structural Biology*, 3, 733-736.

- WALDECK, D. H. 1991. Photoisomerization dynamics of stilbenes. *Chemical Reviews*, 91, 415-436.
- WYNFORD-THOMAS, D., JASANI, B. & NEWMAN, G. R. 1986. Immunohistochemical localisation of cell surface receptors using a novel method permitting simple, rapid and reliable LM/EM correlation. *Histochemical Journal*, 18, 387 - 396.
- ZANKEL, A., KRAUS, B., POELT, P., SCHAFFER, M. & INGOLIC, E. 2009. Ultramicrotomy in the ESEM, a versatile method for materials and life sciences. *Journal of Microscopy-Oxford*, 233, 140-148.